COMPOSITIONAL STUDIES OF THE RESIDUAL LATERITIC PROFILES OVER MINERALISED AND BARREN PEGMATITES IN PARTS OF THE PRECAMBRIAN BASEMENT COMPLEX OF SOUTHWESTERN NIGERIA

BY

OLAWALE KAYODE AROMOLARAN
B.Sc. (Hons.) Geology; M.Sc. Mineral Exploration (Ibadan)
(Matric No.: 100311)

A Thesis in the Department of Geology

Submitted to the Faculty of Science

In partial fulfilment of the requirements for the Degree of

DOCTOR OF PHILOSOPHY

of the

UNIVERSITY OF IBADAN

MAY, 2019

ABSTRACT

Pegmatites (mineralised and barren) occur as intrusive bodies within the basement rocks of southwestern Nigeria. They are overlain by residual lateritic profiles which hinder access to the rocks thus making the discrimination between barren and mineralised pegmatites difficult. Geological information on lateritic profiles over mineralised and barren pegmatites in Nigeria is rare. The aim of this study was to determine the mineralogical and geochemical indicators in the overlying residual lateritic profiles that could be used to discriminate between barren and mineralised pegmatites.

One hundred and twenty-three lateritic profile samples were collected from five selected vertical profiles over mineralised (Ijero, Komu, Ofiki and Iwere) and non-mineralised (Osu) pegmatites. Thirty mineralised and seven barren bedrock pegmatite samples were collected directly from exposed rocks underlying the profiles using standard geological method. Discrete mineral phases in the pegmatite samples were isolated and identified using standard methods. The mineralogy of the whole-rock and lateritic samples was determined using petrographic and X-ray diffraction techniques. The mineral chemistry of discrete phases in the pegmatites was determined by electron microprobe and laser-ablation-inductively coupled plasma-mass spectrometry. Elemental compositions of the pegmatites and their lateritic profile samples were determined, using X-ray fluorescenceand inductively coupled plasma-mass spectrometry. Data were analysed using descriptive statistics.

The essential minerals in the barren pegmatite were microcline-perthite, quartz and muscovite, with accessory biotite, garnet and schorl; while the mineralised pegmatites contained accessory beryl, lepidolite, tourmalines, topaz, tantalo-columbite, rutile, ilmenite and magnetite in addition to the essential minerals. The lateritic profile over barren pegmatite was dominated by quartz and kaolinite with minor amounts of microcline, albite and muscovite. The mineralised pegmatite profiles contained quartz, kaolinite, muscovite, microcline and albite, with minor amounts of schorl, magnetite, dilithium tungstate, rutile and ilmenorutile. K-feldspar and muscovite showed low K/Rb(45.00-143.00 and 15.20-29.80), K/Cs(123.00-448.00 and 20.12-77.42) and Nb/Ta(1.30-1.50 and 1.10-1.56) ratios, reflecting moderate degree of fractionation and rare-metal enrichment of the mineralised pegmatites; whereas higher K/Rb(911.00 and 368.00), K/Cs (4456.00 and 2378.00) and Nb/Ta (3.70 and 1.64) ratios indicated very low fractionation and

poor rare metal-bearing potential of the barren pegmatite. Immobile trace elements including Nb, Ta, Sn, YandTh were enriched in the mineralised pegmatite profiles, relative to the barren pegmatite. The mineralised pegmatite profiles showed low Nb/Ta (0.9-3.9) and high Th/U (0.5-3.6) ratios, while the barren pegmatite profile had high Nb/Ta (>6.0) and low Th/U (0.3-0.7) ratios. The residual profiles were clearly differentiated into their respective clusters on the Zr-Th, Y-Nb, Nb-Ta-Sn and Hf-Th-Ta discrimination plots. These geochemical patterns reflected the varying abundances of accessory minerals hosting the immobile elements in the respective pegmatite protoliths and the differential susceptibility of the mineral phases to intensive weathering conditions.

Mineralogical indicators, including schorl, rutile, ilmenorutile, dilithium tungstate and magnetite, and geochemical indicators (niobium, tantalum, tin, yttrium and thorium) which showed abundance in the mineralised pegmatite profiles clearly distinguished them from the barren pegmatite profile. These mineralogical and geochemical indicators can be used as exploration guides for mineralised pegmatites underneath lateritic profiles.

Keywords: Geochemical and mineralogical indicators, Residual lateritic profiles, Pegmatite protoliths.

Word Count: 492

CERTIFICATION

I certify that this work was carried out by OlawaleKayode AROMOLARAN, in the Department of Geology, University of Ibadan.

……..

Supervisor

Anthony TemidayoBolarinwa
B.Sc. (Ilorin), M.Sc., Ph.D., PGDTHE (Ibadan)
Reader, Department of Geology
University of Ibadan, Ibadan

DEDICATION

This research project is affectionately dedicated to the loving memory of my beloved father, **Samuel OladipoAROMOLARAN** (1928-2000), who gave the earliest motivation and invaluable support towards my academic pursuit;

and

In a very special way to the loving memory of my beloved and cherished teacher, **Professor Anthony AzubuikeELUEZE,***FGS, FNMGS, FSEG* (1949-2017), who, for many years, provided inspirational and outstanding academic mentoring.

ACKNOWLEDGEMENTS

I would like to express my sincere appreciation to my supervisor, Dr A. T. Bolarinwa, for his thorough supervision, excellent mentoring and amazing encouragement throughout my PhD candidature. Your patience, expert guidance and timely acceptance to continue with the supervision of this research made this thesis a possibility. Professor Anthony AzubuikeElueze, *FGS, FNMGS, FSEG* was a mentor *par excellence*; he taught me to think freely and critically. He suggested this study, and was my PhD guide until his demise on the 25th June, 2017. I feel very elated to have had the opportunity to be mentored by such an exceptional geoscientist.

I want to specially appreciate the Head of Department, Prof. O. A. Ehinolafor his profound support during critical periods of my postgraduate training; while Professors M. E. Nton, A. C. Ajibade and A. A. Adedapo were very helpful in facilitating sustenance for my PhD training. My special gratitude goes to Professors A. I. Olayinka, G. O. Adeyemi, M. N. Tijani, and O. A. Okunlola with DrsA. S. Olatunji, O. C. Adeigbe, O. A. Boboye, M.A. Oladunjoye, A. Osinnowo, I. A. Oyediran and M. A. Adeleye for their contributions to my present status.

This research project benefitted from the scholarship award of the *PromotionsteilstipendiumausInstitutsmitteln, Rheinische Friedrich-Wilhelms, Universitat Bonn* and the outstanding analytical support of Steinmann Institute, University of Bonn, Germany. My deep appreciation goes to Prof. Dr. Thorsten Geisler-Wierwille, who generously agreed to host the analytical aspect of this research in Bonn, Germany. He also facilitated a research award for this PhD project, and graciously consented to read drafts of this thesis. Prof. Dr. Martin Langer (Bonn, Germany) and Dr O. T. Fajemila are deeply thanked for facilitating appropriate research linkages; while Dr O. M. Bankole (Potiers, France) is immensely appreciated for the expert guidance and patience exhibited during XRD data interpretation.I owe a special debt of gratitude to the good people of Nigeria, whose taxes were accrued into the coffers of the Tertiary Education Trust Fund (TETFund). TETFund's sponsorship took care of my subsistence and travel expenses during the analytical component of this research, while Osun State University is thanked for granting study leave for my visiting fellowship to Bonn, Germany.

Outstanding analytical assistance were provided by Dr F. Tomaschek (U-Pb LA-ICP-MS dating and Raman Spectrometry), Dr H. Euler (X-Ray Diffractometry), Dr S. O. Franz (XRF Spectrometry), Dr R. Fonseca (Mineral LA-ICP-MS analyses), Dr Ruth Keppler (EMPA), Nils

Jung (thin/polished section preparation), Ms Pahsmann, and Mrs. B. Schuttle (XRF fused beads preparation) and MessrsT. Andreas and Friedrich (XRD sample preparation and interpretation). Drs David van Acken, Fellippe Leitzke and C.Lenting were helpful during statistical analyses. Professors Ambre Luguet and Chris Ballhaus made my stay in Steinmann Institute a blissful one.

This research work benefitted from stimulating discussions with Prof. Dr. H. E. Frimmel (Wurzburg, Germany) and Dr O. O. Ocan (Ife, Nigeria). Profs. T. R. Ajayi and I. A. Tunbosun and Dr A. V. Akwinga are thanked for inspirational discussions that gave clearer insights into this work. The invaluable motivations of highly esteemed colleagues in Geological Sciences, Osun State University are particularly noteworthy and warmly appreciated. These include Drs T.O. Kolawole (gave expert guidance during statistical analyses), A. O. Ojo, A. C. Oyelami, A. G. Oluwadebi and Mrs. F. O. Akinyele. Mr. Olarewaju Nassir is thanked for pulverising my soilsamples at the Geology Department, OAU, Ile-Ife, Nigeria; while John Mbanefo, DamilolaBabatunde, SikiruAzeez, and OluwatobilobaAiyetigbo were very helpful during the field studies.HRM Oba Nicholas Oyelami Folaranmi (Onidiko of Idiko-Ile), Pastor David Yakubu, Engr. Wasiu Adegoke and Mr. Abiodun Aminu for their warm hospitality during the field trips.

I want to say a big thank you to Rev. and Rev. (Mrs.) OlusolaAreogun, whose valuable instructions and sound teachings constantly keep me on the path of success. I appreciate, with much thanks, the concerns and prayers of my mother-in-law, Mrs. Mary Moyosore Taiwo (*Sisimi*) and my brother-in-law, Mr. OlufunsoOlawaleTaiwo. I sincerely acknowledge your being there for me through thick and thin. To my sweet and supportive mother, Evang. (Mrs.) Ruth EbunOluwaAromolaran and my amiable siblings, Adebayo and Oladiran, I owe my deep gratitude. Thank you for your love, encouragement and unflinching support in diverse ways.

To my treasured wife, DrOlukemiAromolaran, with whom I have shared much joy and anxiety, I would like to express my heartfelt thanks. Olukemi graciously tolerated my periodic long stays in the field and the eleven months visiting fellowship to Bonn, Germany. Many thanks for your indescribable understanding, unequalled perseverance, encouraging assistance and unfeigned support. You are indeed a rare gem of inestimable value.

Above all, I appreciate the Almighty God (The Source of My Inspiration), Whose love knows no bound. I am grateful to Him for the gift of life and for His grace and mercy in the entire endeavour. Indeed,I can say, “Faithful is He that had promised and He has also done it”

TABLE OF CONTENTS

LIST OF TABLES

LIST OF FIGURES

	Caption	Page
4.15:	Photomicrographs of massive and foliated amphibolites of Komu area	81
4.16:	Photomicrograph of tonalite of Komu area	82
4.17:	Field photographs of pegmatites of Komu area	84
4.18:	Photomicrograph of pegmatites of Komu area showingintergranular texture of microcline, albite, quartz and muscovite.	86
4.19:	Geological map of Ofiki area showing sample locations.	88
4.20:	Photomicrographs of banded gneiss in Ofiki area showing preferred alignment of the long axes of biotite laths, alternating with feldspar and quartz-rich bands	90
4.21:	Photomicrographs of massive and foliated amphibolites in Ofiki area	91
4.22:	Photomicrographs of the coarse porphyritic biotite granite in Ofiki area.	93
4.23:	Photomicrograph of the fine-grained granite in Ofiki area	94
4.24:	Field photographs of pegmatites of Ofiki area	95
4.25:	Photomicrograph of pegmatites of Komu area, showingintergranular texture of microcline, albite, quartz and muscovite.	97
4.26:	Geological map of Iwere-Ile area showing mining points and sample locations	99
4.27:	Photomicrographs of biotite granite gneiss in Iwere-Ile area showing alignment of long axes of biotite lathsalternating with quartzofeldspathic bands	100

Caption **Page**

Caption **Page**

Caption **Page**

Caption **Page**

Caption **Page**

Caption	Page

LIST OF ABBREVIATIONS

ACC – AutomotiveCatalytic Converters

BSE – Back Scattered Electron

CFL – Compact fluorescent lamp

CIA – Chemical Index of Alteration

DVD – Digital video disc

EDS – Energy dispersive spectrometer

EMPA – Electron microprobe analyser

FCC – Fluid-Cracking Catalyst

GPS – Global Positioning System

HFSEs - High field strength elements

HLSA – High strength low alloy

HREEs – Heavy rare-earth elements

ICDD – International Centre for Diffraction Data

ICP-AES – Inductively Coupled Plasma-Atomic Emission Spectrometry

ICP-M S– Inductively Coupled Plasma-Mass Spectrometry

ITO – Indium tin Oxide

LA-ICP-MS – Laser Ablation – Inductively Coupled Plasma-Mass Spectrometry

LCD – Liquid crystal display

LCT – Lithium-Cesium-Tantalum

LCT+NYF - Lithium-Cesium-Tantalum+ Niobium-Yttrium-Fluorine

LED – Light emitting diodes

LILEs – Large ion lithophile elements

LOI – Loss on ignition

LREEs – Light rare-earth elements

MPP – Mineralised pegmatite profile

NanoSIMS – Nano Secondary ion mass spectrometry

NMPP – Non mineralised pegmatite profile

NYF – Niobium-Yttrium-Fluorine

PVC – PolyVinyl-Chloride

REE – Rare-earth elements

SPSS –Statistical Package for Social Sciences

STS – Standard Topographic Sheet

TEM – Transmission electron microscopy

UHP – Ultra-high purity

WDS – Wavelength dispersive spectrometer

WIC – Weathering Index of Colman

WIG – Weathering Index of Granite

WIP – Weathering Index of Parker

WIS – Weathering Intensity Side

XRD – X-Ray diffraction

XRF – X-ray Fluorescence Spectrometry

CHAPTER ONE

INTRODUCTION

1.1 General Statement

Pegmatites are generally emplaced as intrusive dykes, sills, flat-lying sheets, irregularly shaped pods and lenses, fracture-filling veins and small stocks into the pre-existing gneisses, migmatites, metasediments, metaigneous rocks and various granitic suites of the Basement Complex. In most places, they are observed to be structurally controlled, invariably conforming to the regional foliation; whereas other occurrences essentially exhibit cross-cutting relationship with the older rock units of the Basement Complex (Elueze and Aromolaran, 2014). Pegmatites are generally of very restricted extents within the host lithologies, and are often poorly outcropping.

Depending on the magmatic sources, the extent of geochemical enrichment and the degree of chemical fractionation, residual pegmatite melts can crystallise to form either simple (barren) or rare-element (mineralised) pegmatites. The barren pegmatites are marked by homogenous distribution of K-feldspar, albite, quartz, muscovite and/or biotite (Cerny, 1991a; London, 2005a). They are essentially products of pegmatite melts devoid of fluxing components, and lack chemical fractionations and other postmagmatic alteration processes. As a result, they are marked by very low levels of rare-metal accessory mineral phases, with rare-element contents sometimes similar to that of the bulk upper continental crust (Sun and McDonough, 1989; McDonough and Sun, 1995; Taylor and McLennan, 1995; Wedepohl, 1995; Linnen and Cuney, 2005; Linnen, *et al*., 2014; Rudnick and Gao, 2014). The rare-element pegmatites, on the other hand, are generally formed from flux-rich (Li, F, P, B) and fluid-dominated residual melts at relatively low temperature (Cerny, 1991; London, 2005b; Simmons, 2007a; Anderson *et al.,* 2012), during which the incompatible high field strength elements (HFSEs; Ti, Zr, Hf, Sn, Nb, Ta, W, Y, Ga, Th, and U), some large ion lithophile elements (LILEs; Rb, Cs, Ba, Sr,) and rare-earth elements (REEs) are preferentially

concentrated in trace amounts in the residual melts towards the late phase of pegmatite crystallisation. This process results in economic concentration of these rare metals into the late accessory mineral phases, such as, tantalite, columbite, apatite, zircon, monazite, microlite, tapiolite, pyrochlore, wodginite, struverite, spodumene, allanite, pollucite, gadolite, zinnwaldite, lepidocrocite, fergusonite, xenotime, amblygonite, petalite, cassiterite, ixiolite and fluorite (London, 2005b; London and Kontak, 2012; London and Morgan, 2012, Linnen *et al*., 2012; Cerny *et al*., 2012; Linnen *et al*., 2014; Dill, 2015; Melcher *et al.*, 2015). Similar late stage residual process has also been documented to facilitate unusual gem mineralisations in pegmatites (London, 1986a; Morgan and London, 1999; Groat *et al.,* 2007; Simmons *et al*., 2003; Simmons, 2007b; London, 2008; Simmons *et al.*, 2012).

Mineralogical studies and geochemical characterisation of pegmatites within the Basement Complex units have invariably indicated the occurrences of both barren and mineralised varieties, with the former being much more prevalent over the latter (Kinnaird, 1984; Matheis, 1987; Woakes *et al*., 1987; Matheis and Caen Vachette, 1988; Kuster, 1990; Garba, 2002; 2003; Okunlola, 2005; Okunlola and Jimba, 2006; Okunlola and Somorin, 2006; Adekeye and Akintola, 2007; Akintola and Adekeye, 2008; Aromolaran, 2007; Okunlola and Ocan, 2009; Elueze and Aromolaran, 2009,2013, 2014; Omada *et al.,* 2015). This assertion is equally supported by the exploration for rare-element pegmatites in different pegmatite districts and provinces around the world, where only a small population (< 1.0 %) of the pegmatites possess assemblages enriched in rare metals (Ginsburg *et al*., 1979; Cerny, 1989; 1991; London and Eversen, 2002, London, 2005a; Linnen *et al*., 2012; London and Kontak, 2012; London and Morgan, 2012). For instance, Page *et al.* (1953) reported that only 32 beryl-bearing and seven lithium-rich pegmatites could be isolated out of about 24,000 pegmatite bodies investigated in the Black Hill, South Dakota, USA. Rare-element pegmatites are the major primary hosts of Li, Rb, Cs, Be, Ga, Ta, Nb, Sn, W and REEs, which are of profound interest and applications in modern-day electronic, aerospace, maritime, chemical and oil industries, as well as in the building of green technology facilities, military hardwares and medical equipment among others (Sorensen, 1992; Pollard, 1995; Selway *et al*., 2005; Kuster, 2009; London and Kontak, 2012; Linnen *et al*., 2012; 2014; Skirrow *et al*., 2013; Mackay and Simandl, 2014; Dill, 2015; Melcher *et al.*, 2015).

The Precambrian basement terrain of Nigeria falls within the humid tropical region, where the rock units have been subjected to varying degrees of chemical decomposition, leaching and desiccation, resulting in the formation of deep residual weathering profiles, which hinder access to fresh outcrops. Therefore, in prospecting and exploring for rare-element pegmatites in this terrain, there are challenges of extensive lateritic covers over pegmatites, the occurrences of both barren and mineralised pegmatites within the laterite-mantled basement rocks, poor outcrop conditions, the restricted extents of pegmatite bodies, as well as the limited alteration haloes and geochemical signatures of pegmatites (Brown, 2004; Aromolaran *et al.*, 2017). The above presents profound impediment to geochemical characterisation of pegmatites underneath the residual lateritic covers.

Most exploration efforts, in recent times, are focused on using geochemistry as a tool to unravel hidden deposits underneath thick residual and transported overburdens (Clark, 1993; Brand *et al.*, 1996; Brand, 1997, 1999; Xianrong *et al.*, 1999; Anand, 2000; Butt *et al*., 2000; Brand and Butt, 2001; Cameron *et al.*, 2002,2004,2005; Singh and Cornelius, 2006; Smith and Singh, 2007; Cornelius *et al.,* 2008; Arhin and Nude, 2009; Hattori *et al*., 2009; Broster *et al*., 2009; Fabris *et al*., 2009; Mokhtari, *et al.*, 2009; Nelson *et al.*, 2009; Sarala *et al*., 2009; Cameron *et al.*, 2010; Coker, 2010, Mumm *et al*., 2013; Kyser, 2017). Accordingly, the present investigation on compositional characterisation of pegmatites and their overlying weathering profiles in the Precambrian Basement Complex of southwestern Nigeria, was undertaken to identify the mineralogical indicators and the geochemical trends within the residual weathering profiles, which may possibly reflect the secondary geochemical dispersion patterns of the underlying parent pegmatites.

1.2 Justification for the research

Prospecting, exploration and mining of mineralised pegmatites in southwestern Nigeria are by the traditional invasive excavation methods, without any definite scientific exploration guides. The economic prospects of these pegmatites are often extrapolated from the presence of varieties of indicator minerals, such asmuscovite, lepidolite and schorl,which have been interpreted to indicate the occurrence of gem-bearing pegmatites. However, studies have shown that such indication parameters and extrapolations are not sufficient guides to distinguishing between mineralised and barren pegmatites (Cerny, 1989; London

and Eversen, 2002; London and Morgan, 2012).

Pegmatite bodies are generally very restricted in extents and commonly poorly outcropped due to their ease of decomposition in the acidic and oxidising conditions of the tropical environment. The extensive lateritic covers developed above the pegmatites also prevent direct access and adequate compositional studies of these pegmatites. Also, pegmatites do not contain sufficient metallic mineral to be conductive or magnetic and are characterised by deficient density-mass ratio to allow for their differentiation from the host lithologies using gravity geophysical method (Trueman and Cerny, 1982),therefore,it is expedient to explore for rare-metal pegmatite deposits through compositional studies of the lateritic horizons overlying pegmatites as well as the bedrocks. This would assist in locating concealed mineralised pegmatites and complement other rare-metal pegmatite exploration techniques.

1.3 Objectives of the investigation

The present investigation is aimed at using geochemical data of weathering profiles over pegmatites as viable exploration tools in locating mineralised pegmatites within the Basement Complex of southwestern Nigeria. The main objectives of this investigation include:

(i) mapping of the field relationships of pegmatites and the host rocks in parts of southwestern Nigeria;
(ii) determination of the mineralogical and geochemical compositions of the pegmatites, their *in situ*-derived weathering profiles and characterisation of the pegmatites into barren and mineralised types;
(iii) comparison of the mineralogical and geochemical dispersion patterns of the residual profiles with the chemical composition of the fresh unaltered underlying pegmatites;
(iv) evaluation of the geochemical enrichment and depletion patterns of the pegmatite petrogenetic elements in the weathering profiles and the underlying pegmatites, for possible distinction of mineralised and barrenpegmatites beneath lateritic overburdens.

1.4 Scope of investigation

Geological field mapping was carried out at Ijero, Komu, Ofiki, Iwere, and Osu mining districts between 2013 and 2015. The field characteristics and relationships among the rock units of the areas were studied. Rock samples were collected and prepared into thin sections for petrographic examination. Geological maps of the areas were produced from the field and petrographic data. Lateritic samples were collected from profiles developed above known mineralised and barren pegmatites bedrocks of the areas of investigation.

Rock and lateritic profile samples were pulverised to fine powder, while discrete mineral phases in the pegmatites were prepared into polished sections. Mineralogical analyses of the powdered lateritic samples were undertaken using the X-ray diffraction (XRD) technique, while the pulverised rock and lateritic profile samples were analysed for major, minor and trace elements, usingX-ray fluorescence spectrometery (XRF), inductively coupled plasma-atomic emission spectrometry (ICP-AES) and inductively coupled plasma-mass spectrometry (ICP-MS) techniques. Mineral chemistry of the discrete mineral phases in the polished sections was determined, using an electron probe microanalyser (EPMA) and a laser ablation-inductively coupled plasma-mass spectrometry (LA-ICP-MS) system.

1.5 Location and accessibility of the areas of investigation

The study areas are within the Precambrian Basement Complex of southwestern Nigeria (Fig 1.1). The descriptions of specific locations are highlighted below:

(i) the mineralised pegmatites of Ijero area are located within the northwestern part of Ado-Ekiti Standard Topographic Sheet (STS) 278;
(ii) the mineralised pegmatites of Komu area and their host rocks occur in the eastern part of Akande STS 219 and the western part of Ikomu STS 220, respectively;
(iii) the mineralised pegmatites of Ofiki area and their host lithologies are located within Ikomu STS 220;
(iv) the mineralised pegmatites of Iwere-Ile area and their associated rock units are obtained from Igangan STS 240; and
(v) the barren Osu pegmatites are located within the Ilesha Schist Belt. Samples were collected from Ilesha STS 243;

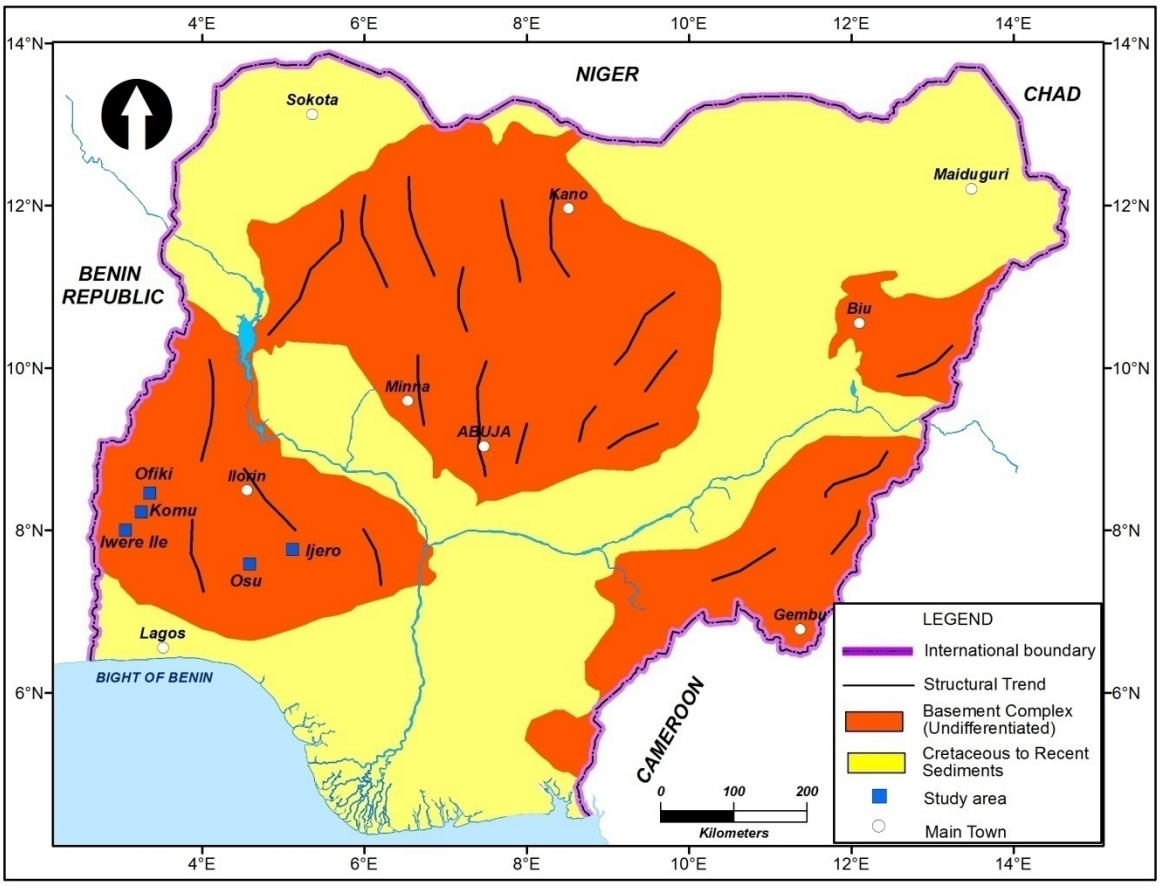

Fig. 1.1: Generalised geological map of Nigeria showing the location of the study areas (modified after Malomo, 2004).

Ijero and Osu towns are respectively the Administrative Headquarters of Ijero and Atakunmosa West Local Government Areas; and as such, they are well connected by good network of tarred and untarred roads, linking their respective neighbouring towns, villagesand farm settlements. Komu, Ofiki and Iwere-Ile areas are located towards the northwest of Iseyin, Oke-Ogun District, southwestern Nigeria. These areas are well known for agricultural and informal mining activities. They are well connected with good network of tarred and untarred roads. Notable among these are the Iseyin-Iganna-Iwere-Ijio and the Iseyin-Ipapo-Saki Roads.

During geological mapping and sampling, traverses were made through major-minor roads and footpaths linking important geological features of the areas of study.

1.6 Physiography

The areas of investigation are underlain by the crystalline Basement Complex rocks, which are essentially migmatites, gneisses, granites, quartzites, quartz-schists, mica schists, amphibolites, amphibole schists and pegmatites. The characteristic relief features of the areas can be explained in terms of differential weathering of these rock types.

The Ijero area displays prominent undulating topography, mainly resulting from the underlying resistant gneisses, migmatites and granites. In between the rock units are topographic highs of pegmatites of about 800 m above the mean sea level. The Osu area is equally marked by undulating terrain with elevations approximately 450 m to 900 m. This landscape is typified by lowland terrain, mainly underlain by biotite schist, amphibolites and pegmatites, and more or less dotted with few continuous ridges of quartzite/quartz schist and granitic rocks.

The resistant granitoids form the topographic highs around Iwere-Ile and Ofiki areas in Oke-Ogun District, while the gneisses, amphibolites and pegmatites constitute the intervening lowlands. These topographic highs of granites are mostly ridges that stretch to hundreds of metres and inselbergs of various shapes. Elevations range from about 350 to 850 m above the mean sea level.

1.7 Climate and vegetation

The study areas are located within the humid tropical belt, which is characterised by two alternate climatic seasons, which are a wet season that occurs from early March to mid-November and a distinct dry season that stretches from mid-November to February. Peak rainfall is usually from May to August, with average annual precipitation of between 1720 and 2100mm.Relative humidity across the areas varies from about 30% in January-March to about 70% in April-December. Temperature is fairly constant and varies between 24^{o}C and 34^{o}C, with maximum values occurring in the months of January and February(Iloeje, 1981). Vegetation cover in the areas is that of tropical rain forest, which is marked by dense vegetation with tall perennial trees, shrubs, climbers and bushy undergrowths. However, anthropogenic activities, such as settlements, shifting cultivation, cattle grazing, lumbering, road construction, bush burning and informal mining have modified the vegetation into a secondary forest around Ijero and Osu areas and derived savannah in Oke-Ogun District.

1.8 Drainage

The areas of investigation are well drained by some major rivers and their tributaries. These rivers include Oyan and Ofiki (Oke-Ogun District)and Osun in Osu area. These major rivers are well connected to dense network of other smaller rivers and streams, which usually dry off during the dry season. Oyan and Ofiki Rivers generally flow southwards and debouch into the Ogun River. Ogun River and the aforementioned rivers eventually empty into the Lagos-Badagry Lagoons (Iloeje, 1981).

The direction of flow of these rivers and streams are influenced by the lithologic character of the underlying basement rocks. Trellis and dendritic drainage patterns are observed in these areas, which generally reflect the structural control of the underlying basement rocks.

CHAPTER TWO

LITERATURE REVIEW

2.1 Review of the Geology of the Nigerian Basement Complex

The Nigerian Basement Complex forms a part of the Pan-African (*ca*. 750 - 450 Ma) mobile belt, which lies between the Archaean to Palaeoproterozic (*ca*. 3800 - 1600 Ma) West African Craton to the west and the Archaean to Mesoproterozoic (*ca*. 3800-1000 Ma) Congo-Gabon Craton to the southeast(Kennedy, 1964; Clifford, 1970; Kroner, 1977; Black *et al*., 1979; Caby *et al*., 1981; Caby, 1989; Gubernov and Mooney, 2009) (Fig. 2.1). It is intruded by the Jurassic (*ca*.180 - 170 Ma) calc-alkaline ring complexes (Younger Granites) of the Jos Plateau area, and unconformably overlain by Cretaceous to Recent sedimentary sequences (Figs. 2.2 and 2.3).

The Basement Complex is polycyclic in nature, having witnessed at least four major tectono-metamorphic events, corresponding to the Liberian (*ca*. 2700 ± 200 Ma), Eburnean (*ca*. 2000 ± 200 Ma), Kibaran (*ca*. 1100 ± 200 Ma) and Pan-African (*ca*. 600 ± 150 Ma) (Cooray, 1974; Odeyemi, 1981). The Pan-African orogenic event was accompanied by deformation, regional metamorphism, migmatisation and extensive granitisation, and produced syntectonic to late tectonic granites and homogenous gneisses (McCurry, 1976; Abaa, 1983; Turner, 1983).

The Precambrian Basement Complex rocks in Nigeria (Fig. 2.4) have been categorised into six major lithologic units (McCurry, 1976; Rahaman,1976; McCurry and Wright, 1977; Rahaman, 1988), viz:

1. The Migmatite-Gneiss-Quartzite Complex
2. The Schist Belts (Metasedimentary and metavolcanic rocks)
3. Charnockitic, Gabbroic and Dioritic Rocks
4. The Pan-African Granitoids (Older Granites)

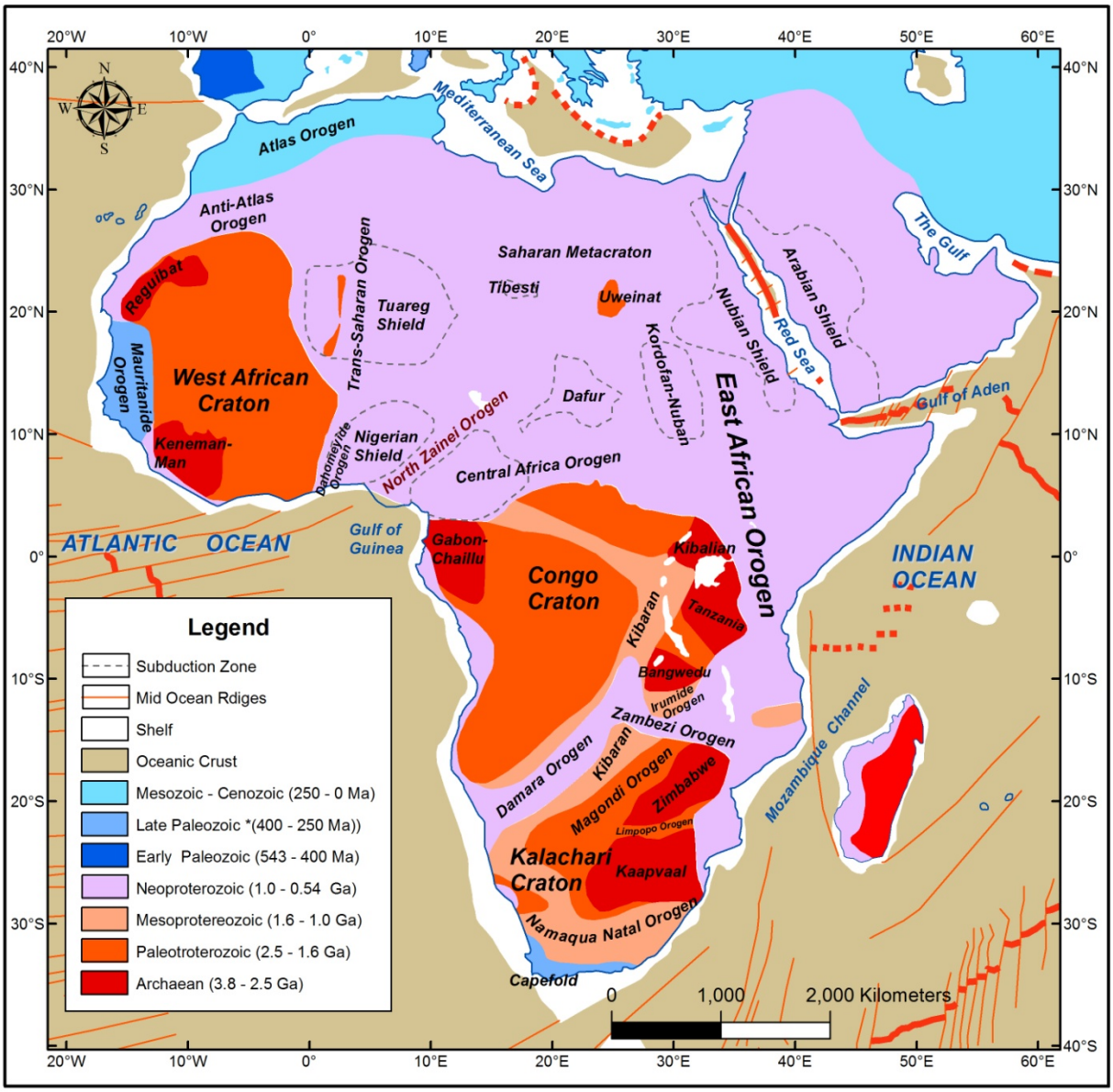

Fig. 2.1: Geological map of Africa showing the cratonic zones and mobile belts with their respective ages of crustal formation (modified after Kennedy, 1966; Clifford, 1970 and Gubanov and Mooney, 2009).

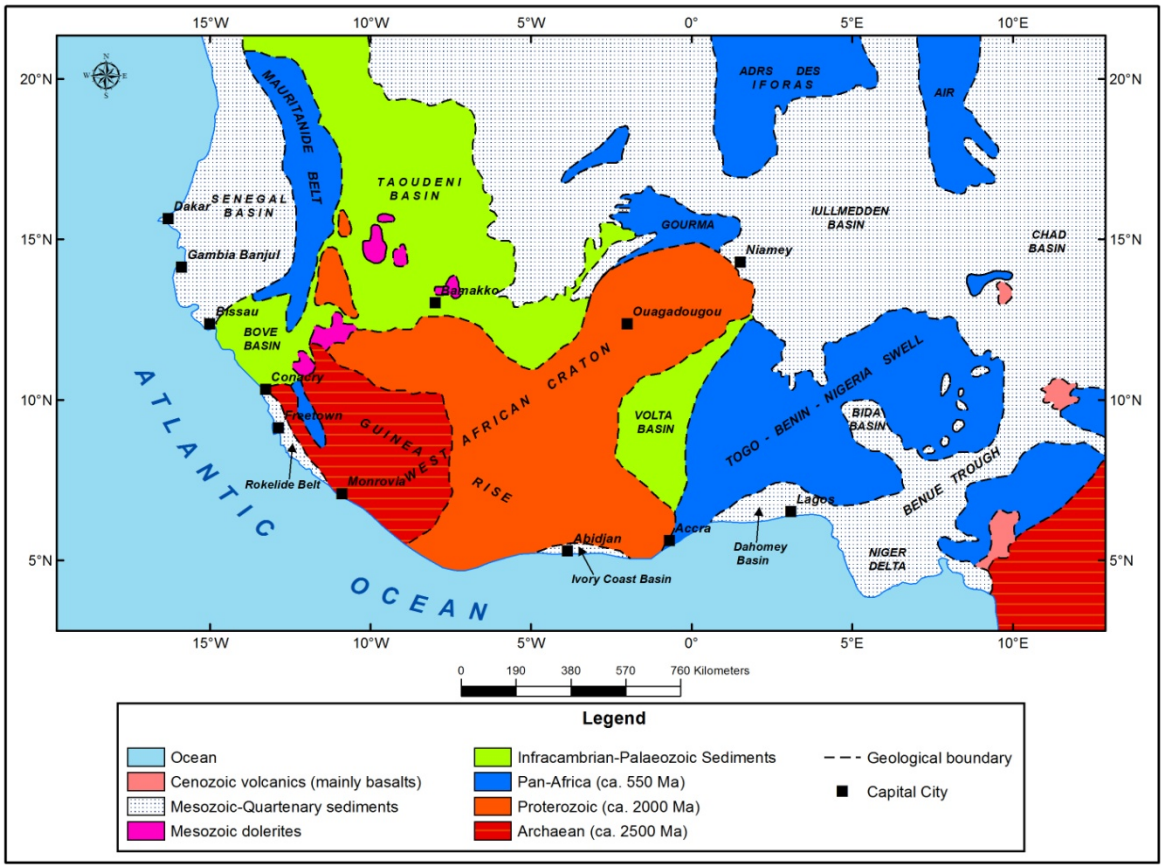

Fig. 2.2: Simplified geological map of West Africa showing the principal geological units iv

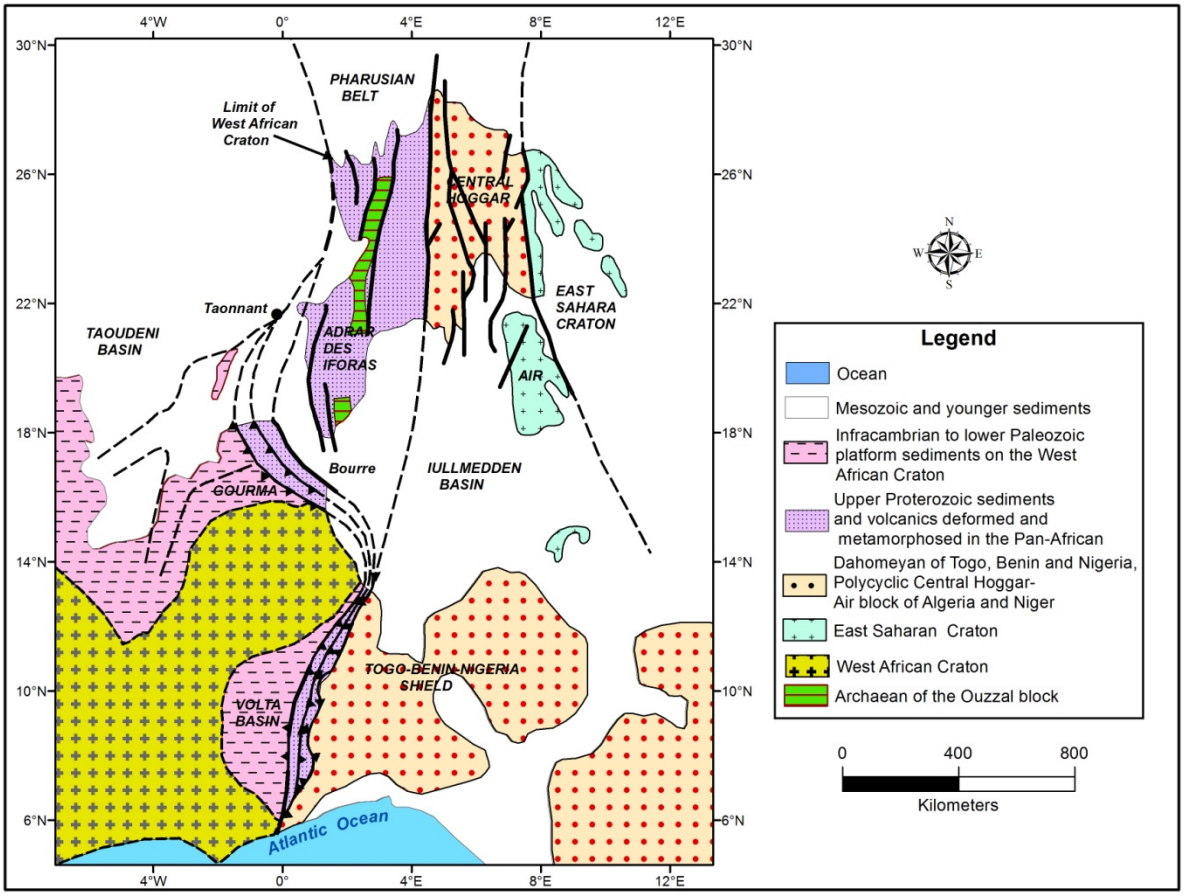

Fig. 2.3: Simplified geological map of the Pan-African Province east of the West African Craton, showing correlation between the northern Hoggar Shield and the southern Togo-Benin-Nigeria Shield (modified after *Caby et al.*, 1981).

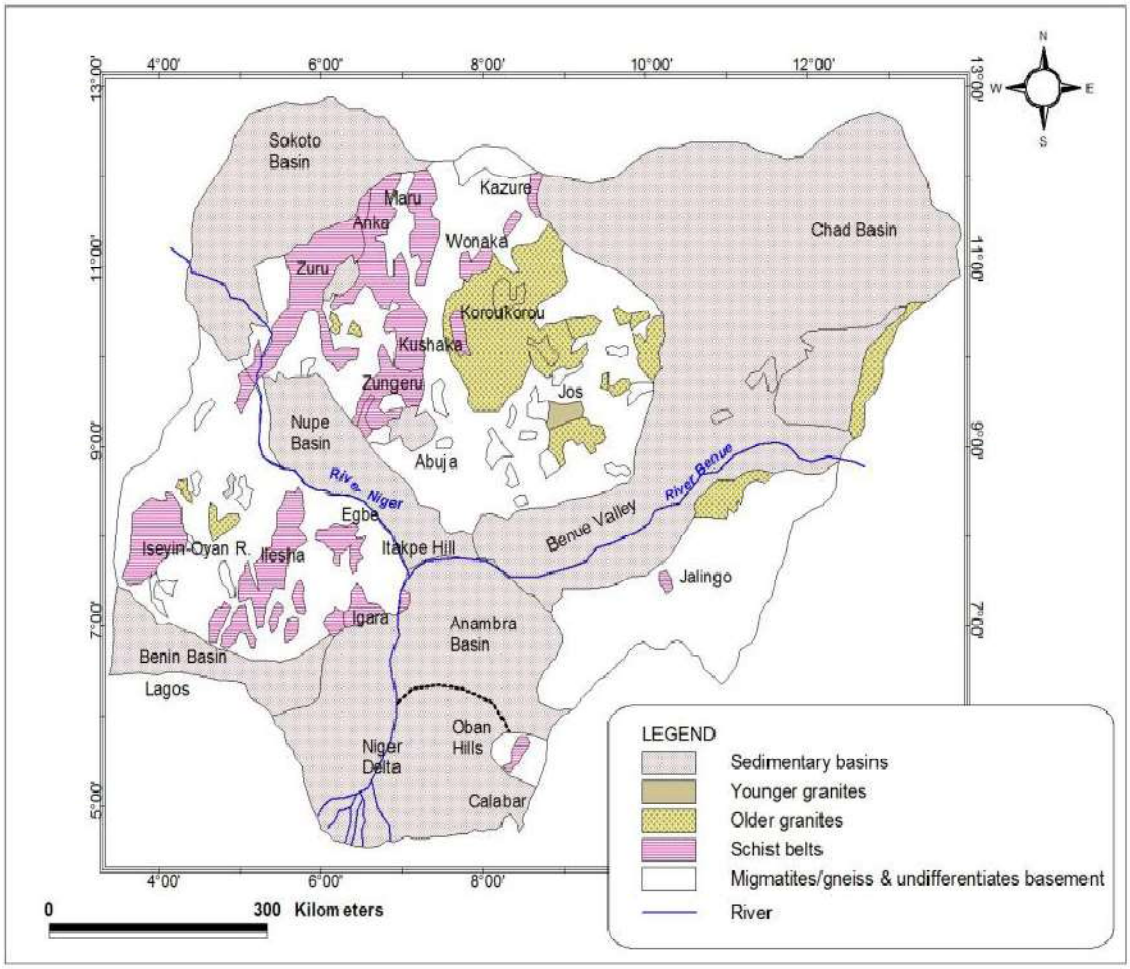

Fig 2.4: Simplified geological map of Nigeria (modified after Woakes *et al.*, 1987).

5. Metamorphosed and unmetamorphosed calcalkaline volcanic and hypabyssal rocks
6. Unmetamorphosed dolerite dykes, basic dykes and syenitedykes*etc.*

2.1.1 Migmatite-gneiss-quartzite complex

The migmatite-gneiss-quartzite complex (Fig. 2.4) is the oldest rock unit of the Basement Complex (Rahaman, 1976, 1988; Rahaman and Ocan, 1978). It consists of high grade metamorphic assemblages that have been subdivided into three main components (Rahaman, 1976; Rahaman and Ocan, 1978; Elueze, 1980, 1982; Rahaman, 1988). These include the early gneiss, mafic-ultramafic units and the felsic components. The early gneissis a grey melanocratic foliated biotite and biotite-hornblende quartzofeldspathic gneiss of tonalitic to dioritic composition. The mafic-ultramafic units are made up of mafic amphibolites gneiss, biotite-rich and biotite-hornblende schists, which often occur as concordant lenses, bands and sheets in the migmatite gneisses. The felsic components are essentially of granitic composition, varying in texture from aplitic to granitic to pegmatitic, and are commonly found to have largely modified the pre-existing structures in the other two components. Depending on the relationships between the aforelisted components, different types of gneisses can be distinguished. These include banded gneisss, granite gneisss, transition gneiss, augen gneiss, agmatite, nebulitic gneiss, porphyroblastic gneiss and cataclasic gneiss.

Associated with the gneisses and migmatittes are the Ancient Metasediments (McCurry, 1976), which are mainly represented by refolded quartzites and quartz schists, lenses and sheets of amphibolites and amphibole schists, marbles and calc-silicate rocks. These are found as relict rafts within the gneisses and migmatites, and are possibly of earlier Leonian and/or Liberian ages.

Geochronological data on the rocks of the migmatite-gneiss-quartzite complex from different districts in Nigeria have indicated their evolution through at least three and possibly four main tectono-metamorphic cycles of deformation, metamorphism and remobilisation in the Liberian *(ca*. 2700 ± Ma, Grant, 1970; Oversby, 1975, Rahaman, 1976, 1988; Rahaman and Lancelot, 1984; Ogezi, 1988; Dada *et al*., 1993;Annor, 1995); Eburnean (*ca*. 2000 ± 200 Ma, Hurley, *et al*., 1966; Grant, 1970; Grant *et al.*, 1972;

Cooray, 1974, Ogezi, 1977; Rahaman, 1983; Rahaman, 1988, Ocan, 1991; Annor, 1995),Kibaran (*ca.*1100 ± 200 Ma, Grant, 1972, Ogezi, 1977; Ferre, *et al*., 1996), though highly disputed; and the Pan-African (*ca.* 600 ± 150 Ma, Grant, 1970; Oversby, 1975; Ogezi, 1977; Ferre *et al*., 1998). However, Ekwueme and Kroner (1993), Bruguier *et al*. (1994), Dada (1998), Dada *et al*. (1998)and Kroner *et al.* (2001) have obtained Early Archaean (≥ 3.56 Ga) Sm-Nd model ages and Mid Archaean (≥ 3.46 Ga) U-Pb zircon ages for granodioritic orthogneiss in Kaduna area, northern Nigeria. These ages have been interpreted to indicate the initial crust-forming processes for the Nigerian Basement Complex, while the comparatively lower ages, varying from 3.1 Ga to 2.5 Ga, have been suggested to represent subsequent metamorphic events.

2.1.2 Schist Belts (Metasedimentary and metavolcanic rocks)

The Schist Belts are north-south trending synformal troughs of dominantly low-medium grade metasedimentary and minor mafic-ultramafic assemblages. They are extensive volcanic and sedimentary supracrustal covers over the migmatite-gneiss basement,that were subsequently deformed and metamorphosed during the Pan-African Orogeny. The Schist Belts were reported to be largely confined to the western half of the country, particularly the west of 8^{O} E Longitude (Oyawoye, 1972; Ajibade, 1976; Ajibade *et al*., 1976; Ajibade and Fitches, 1976; McCuurry, 1976; Fitches *et al*., 1985). However, other schist belts havebeen delineated in central Nigeria (Oluyide and Okunlola, 1995) and the eastern part of the country (Okezie, 1974; Ekwueme and Onyeagocha, 1986; Muotoh *et al*., 1988; Nwabufo-Ene and Mbonu, 1988; Ekwueme and Kroner, 1997).

The Schist Belts are predominantly of pelitic and semipelitic assemblages, with subordinate psammitic facies (Elueze, 1980, 1981b, 1982; Annor, 1983, Fitches *et al*., 1985; Elueze, 1988; Elueze and Okunlola, 2003a). The pelitic and semipelitic lithologies consist essentially of argillaceous compositions and are mainly represented by phyllites, biotite schists, muscovite schists and graphitic schists; while the psammitic assemblages are largely of greywacke and arkosic affinities typified by quartzites and quartz schists. Associated with these major petrological units are other minor rocks which are variably distributed and frequently applied in discriminating the belts (Elueze, 2002). These comprise of ferruginous

and carbonate rocks, which are commonly banded iron-formations (BIFs), calcitic and dolomitic marbles, as well as calc-silicate rocks (Odeyemi, 1977, 1988;Emofurieta, 1984; Adekoya, 1988, 1995, 1996; Okunlola, 2001; Ibrahim, 2008; Elueze *et al*., 2015). Amphibolites and amphibole schists, talc-bearing schists, serpentinites, and pyroxenites, as well as metaconglomerates, have been reported in parts of some of the Schist Belts (Wright and Ogezi, 1977; Olade and Elueze, 1979; Ajayi, 1980; Elueze, 1981b, 1982, 1985, 2000; Muotoh *et al*., 1988; Ige and Asubiojo, 1991; Elueze and Akin-Ojo, 1993; Elueze and Emofurieta, 1995; Olobaniyi *et al*., 2001; Elueze and Okunlola, 2003b; Olobaniyi and Annor, 2003; Danbatta and Garba, 2007; Olobaniyi and Mucke, 2011). Metamorphic grades are slightly variable among the Schist Belts, ranging from greenschist facies to lower amphibolite facies.

The contact relationship between the Schist Belts and the ancient migmatite-gneiss complex are commonly gradational or sheared due to faulting and thrusting. Variations observed in lithologic assemblages of the schist belts have been ascribed to the disparities in the depths of depositional basins: hence two generations of the Schist Belts have been suggested (Grants, 1978; Holt *et al*., 1978; Turner, 1983; Fitches *et al*., 1985). They may also be responsible for the variation in ages, which cut across Kibaran and Pan-Afican (Ogezi, 1977; Ajibade, 1980; Tuner, 1983 and Rahaman, 1988).

Two tectonic models have been postulated for the evolution of the Nigerian Schist Belts. These include ensialic model which emphasizes crustal thickening in response to crustal extension and continental rifting at the cratonic margin leading to the deposition of sediments in graben-like troughs floored by continental crust (Ogezi, 1977; Holt *et al*., 1978; Olade and Elueze, 1979; Ajibade, 1980; Turner, 1983); while ensimatic model favours the formation of back-arc marginal basins with subsequent sediment deposition (Holt, 1982; Fitches *et al.,* 1985; Rahaman, 1988; Ajibade, *et al.,* 1987; Ajibade and Wright, 1989).However, theabsence of subduction-related mineral deposits invariably suggeststhe limited role of the ensimatic processes in the evolution of the Schist Belts (Elueze, 1992; Obaje, 2009). Olade and Elueze (1979) and Elueze (1992) have suggested tectonic evolution characterised by rifting of back arc basins and island arcs formation for the Nigerian Schist Belts.

2.1.3 Charnockitic, Gabbroic and Dioritic Rocks

Hypersthene-bearing rocks, commonly known as charnockites, constitute one of the important petrological units within the Basement Complex of Nigeria (Cooray, 1972, 1975, Rahaman, 1976, 1988; Rahman, 1981; Annor and Freeth, 1985; Olerewaju, 1987, 1988; Umeji, 1988; Ocan, 1991; Ekwueme *et al.*, 1995). These rocks are commonly observed to be associated with porphyritic and non-porphyritic coarse grained biotite-hornblende granites (Rahaman, 1976, 1988; Olarewaju, 1981, 1988; Kayode, 1988). They are generally recognised by their dark green to greenish gray appearance in hand samples.

Charnockitic rocks occur as discrete (dyke-like) bodies within gneisses and migmatites and as cores and along margins of granitic suites. They show rounded bouldery outcrops in most places, but with few isolated hills marked in some areas. Metamorphic and igneous charnockites have been recognised within the Basement Complex of Nigeria (Olarewaju, 1981; Rahaman and Ocan, 1988; Olarewaju, 2006). While the former shows strong foliation and owns its charnockitic attributes to granulite facies metamorphism, the latter generally shows weak magmatic foliation and acquires its charnockitic character during crystallization form magma (Olarewaju, 1981, 1987, 1988; Dada *et al*., 1989).

Petrographically, charnockites range in composition from norite to hypersthene diorite, enderbite, true charnockites, monzonites and hypersthenes syenite (Cooray, 1975; Olarewaju, 2006); and generally show mineralogical assemblages of perthitic alkaline feldspar, quartz, plagioclase, orthopyroxenes, clinopyroxenes, fayalite,hornblende, biotite with accessory zircon, apatite and opaque ores (Olarewaju, 1981, 1988; Kayode, 1988).

The contact relationships between charnockitic rocks and their closely associated Older Granite suites vary from gradational to cross-cutting. Charnockites broken up into xenolithic blocks by porphyritic granites also occur in few places (Olarewaju, 1987).

Radiometric data on charnockitic complexes in different districts in Nigeria have indicateda Pan-African (ca. 600 ± 150 Ma) age for their emplacement, and thus showing their spatial relationship with the Older Granite suites (Van Breeman *et al*., 1977; Tubosun *et al.*, 1984; Dada *et al*., 1989).

2.1.4. Pan-African Granitoids (Older Granites)

The syntectonic to late tectonic Pan-African granitoids, commonly referred to as the Older Granites, are quite ubiquitous within the Nigerian Basement Complex. They are the obvious manifestations of the Pan-African orogenic event, and represent significant additions to the continental crust (Rahaman, 1988). The term "Older Granites" essentially distinguishes the deepseated, often concordant to semi-concordant late Precambrian (*ca*. 600 ± 150 Ma) granitoids of the Basement Complex from the high level and highly discordant epeirogenic alkali tin-bearing Jurassic (*ca*. 180 Ma) granites of central Nigeria, referred to as Younger Granites (Woakes *et al*., 1987; Ajibade *et al.*, 1989).

The Pan-African granitoids commonly range in size from small sub-circular cross-cutting stocks to large elongate concordant batholiths, and are predominantly of granitic to granodioritic compositions. The Pan-African intrusives mainly crop out as isolated hills, inselbergs, low whalebacks and granite pavements (Ogezi, 1988), and intruded both migmatite-gneiss complex and the low-grade metasedimentary belts. The contact relationships of these granitoids with the migmatites and gneisses, where exposed, are commonly concordant, sharp, contact metamorphosed, sheared or migmatised (Ogezi, 1988); while sharp and cross-cutting (discordant) contact relationships are commonly observed within the Schist Belts.

The Pan-African granitoids include rocks of a wide range of compositions, namely granites, granodiorites, diorites, adamellites, quartz monzonites, tonalites, syenites, and pegmatites, with granitic-granodioritic compositions displaying the widest occurrences. Textural varieties of the Pan-African intrusives suites include coarse porphyritic, medium-coarse grained, medium-grained and fine-grained granitic rocks, with the coarse porphyritic alkaline granites predominating (McCurry, 1976; Olarewaju, 1981, 1987, 1988; Olarewaju and Rahaman, 1982; Ocan, 1991). The coarse porphyritic variety is generally weakly foliated, showing preferred alignment of alkali feldspar phenocrysts and biotite flakes.

Geochronological data indicated the emplacement of the Older Granites between 750 and 450 Ma (Ogezi, 1977; Van Breenman, 1977; Grant, 1978; Rahaman *et al.*, 1983; Tubosun

et al., 1984; Umeji and Caen Vachette, 1984; Matheis and Caen-Vachette, 1988;Ekwueme and Kroner, 1998; Ferre *et al*., 1998; Goodenough, 2014, Adetunji *et al*., 2015, 2018), thus linking their origin to Pan-African tectono-magmatic episode.

2.1.5 Metamorphosed to unmetamorphosed calc-alkaline volcanic and hypabyssal rocks

Volcanic and hypabyssal rocks of possibly late Pan-African age are emplaced in differentdistricts, particularly in the northwestern and northeastern parts of Nigeria. They are mostly represented by unmetamorphosed volcanic aggregates, tuffs, rhyolites, rhyodacites and dacites and by partly deformed porphyry dikes, microgranites, felsite dykes, trachyte dykes and lamprophyre dykes (McCurry, 1976; Rahaman, 1988). These rocks are generally associated with faults which controlled their emplacement (McCurry, 1976); and are agreed to be emplaced during epeirogenic uplift and fracturing that mark the waning phase of Pan-African orogeny.

Geochronological data on the volcanic and hypabyssal rocks have largely confirmed their emplacement towards the closing stage of the Pan-African orogeny, as indicated in the whole-rock K/Ar age of 507 ± 20 Ma for the Kisemi porphyritic dacite and Rb/Sr biotite ages in the range of 480-509 Ma for the Igarra potassic syenite (McCurry, 1976).

2.1.6 Unmetamorphosed dolerite dykes, basic dykes and syenite dykes

These are represented by concordant and discordant dykes, veins and irregular bodies of pegmatites, aplites, vein quartz, syenite, microgranites, dolerites, gabbro, pyroxenites, serpentinites and lamprophyres (Adekoya *et al*., 2003; Dada, 2006). These intruded all the pre-existing rocks of the Basement Complex, including the migmatite-gneiss-quartzite complex, the Schist Belts and the Pan-African intrusive suites. They are thus the youngest member of the Basement Complex of Nigeria(Adekoya *et al*., 2003; Dada, 2006).

Radiometric age determinations of the minor felsic dykes have largely indicated their emplacements between 580 and 535 Ma (Matheis and Caen-Vachette, 1988; Dada, 2006); while the mafic dykes have given a much lower age of 500 Ma (478 ± 19 Ma, Grant, 1970; Dada, 2006). These indicate that they are late to post tectonic Pan-African in age.

2.2 Review of the mineralogy, geochemistry and petrogenesis of pegmatites

Pegmatites are very coarse-grained intrusive igneous rocks that are generally associated with granites and contain the major granite rock-forming minerals (Simmons and Webber, 2008; Philpotts and Ague, 2009; Robb, 2011; London and Kontak, 2012). Pegmatite bodies are characterised by a variety of sizes, shapes, orientations and structural relationships to their host lithologies (Brisbin, 1986). These include simple and multiple tabular bodieswhich are essentially dykes and sills; small stocks; ellipsoidal, lenticular and amoeboid forms; irregularly shaped pods and bulbous masses (Brisbin, 1986; Cerny *et al*., 2005). Contacts with host rocks are commonly sharp, and may be gradational when pegmatites are in contact with their plutonic parent rock. The position, shape, orientation, and to some extent, the size of pegmatite bodies are controlled by a complex interplay of pegmatite fluid pressure, rheological state of the host rocks, lithostatic and directional stresses, pore-water pressure, strength and ductility anisotropies and dilational directions (Brisbin, 1986; Cerny *et al.*, 2005).

Pegmatites are loosely categorised into simple and complex types. Simple pegmatites have simple mineralogy and generally lack internal zoning, while complex pegmatites have complex mineralogy, marked by many rare minerals in zonal sequences from contact inwards (Cerny, 1991b; Evans, 1993; London and Morgan, 2012). Microcline-perthite and quartz are the main minerals in simple pegmatites, while micas, albite, garnet, tourmaline (schorl), apatite, zircon, Fe-Ti oxides are of very minor abundances. The complex pegmatites contain, in addition to the rock-forming minerals in simple pegmatites, other exotic mineral phases, including tantalite, columbite, fergusonite, wodginite, microlite, tapiolite, cassiterite, zinnwaldite, lepidolite, montebrasite, amblygonite, lithiophilite, petalite, spodumene, allanite, xenotime, gadolinite, sphene, anatase, ilmenite, magnetite, fluorite, bastnasite, lepidocrocite, hafnon and bertrandite.

Complex pegmatites are principally marked by inwardly coarsening crystals, concentric layerings and sharp/gradational mineralogical zoning (Cerny, 1991b; Evans, 1993; London and Kontak, 2012). The mineralogical zoning progresses from the fine-grained border zone of more or less granitic composition to inner zone that exhibits enrichment in rare-element

mineralogy and textural diversity and to near monomineralic quartz-rich zone (Cerny *et al.*, 1991) (Fig. 2.5). The mineralogical zoning and rare-element mineralisation in the wall zone through the inner zone to the core zone, amply demonstrate the inward increasing geochemical fractionation in rock-forming minerals, as well as increasingconcentration of fluxes and volatiles (Cerny *et al*., 1985; Cerny, 2005; Cerny *et al*., 2005; London, 2005a; Selway *et al*., 2005; Wise and Brown, 2010), which provide excellent exploration guide for rare-metal pegmatites (Cerny, 1992).

London (2009) suggested that the outer zone of pegmatite bodies which is commonly marked by fine-grained, graphic and highly anisotropic fabric of pegmatites is dominated by the effect of undercooling on the crystallisation response of the pegmatite melt; while the inner zone typified by exceedingly coarse-grained and blocky textures of pegmatites results from the build-up of fluxing components in a boundary layer of melt that advances into the pegmatite along the crystal growth front.

The vast majority of pegmatites are granitic in composition and mineralogically simple, indicating bulk composition of the minimum-temperature melt in the natural granite system $NaAlSiO_3$ - $KAlSiO_3$ - Al_2O_3- SiO_2 (London and Kontak, 2012; London and Morgan, 2012). The rare-element pegmatites, also called rare-metal pegmatites, in addition to above, differslightly by portraying high concentration levels of lithophile elements. This differenceinvariably stems from the relatively higher modal abundances of rare element-bearingaccessory mineral phases in rare-metal pegmatites. The lithophile elements arepredominantly either large ion lithophile elements (LILEs), Li, Rb, Cs, Ba, Sr or highfield strength elements (HFSEs), Ti, Y, Zr, Hf, Nb, Ta, Sn, W, Mo, P, REEs (Linnen andCuney, 2005; Linnen *et al*., 2012; Linnen *et al.*, 2014). Large ion lithophile elements are marked by large ionicradii to low charges, while HFSEs are typified by high ionic charges to small ionic radii (Krauskopf and Bird, 1995; Albarede, 2003; Linnen and Cuney, 2005; Linnen *et al.,* 2014).

Rare-element pegmatites are formed by disequilibrium crystallisation and undercooling of pegmatite residual melts at temperature well below the liquidus, and indicate unusual concentrations of incompatible components, fluxes, volatiles and rare-elements (Simmon

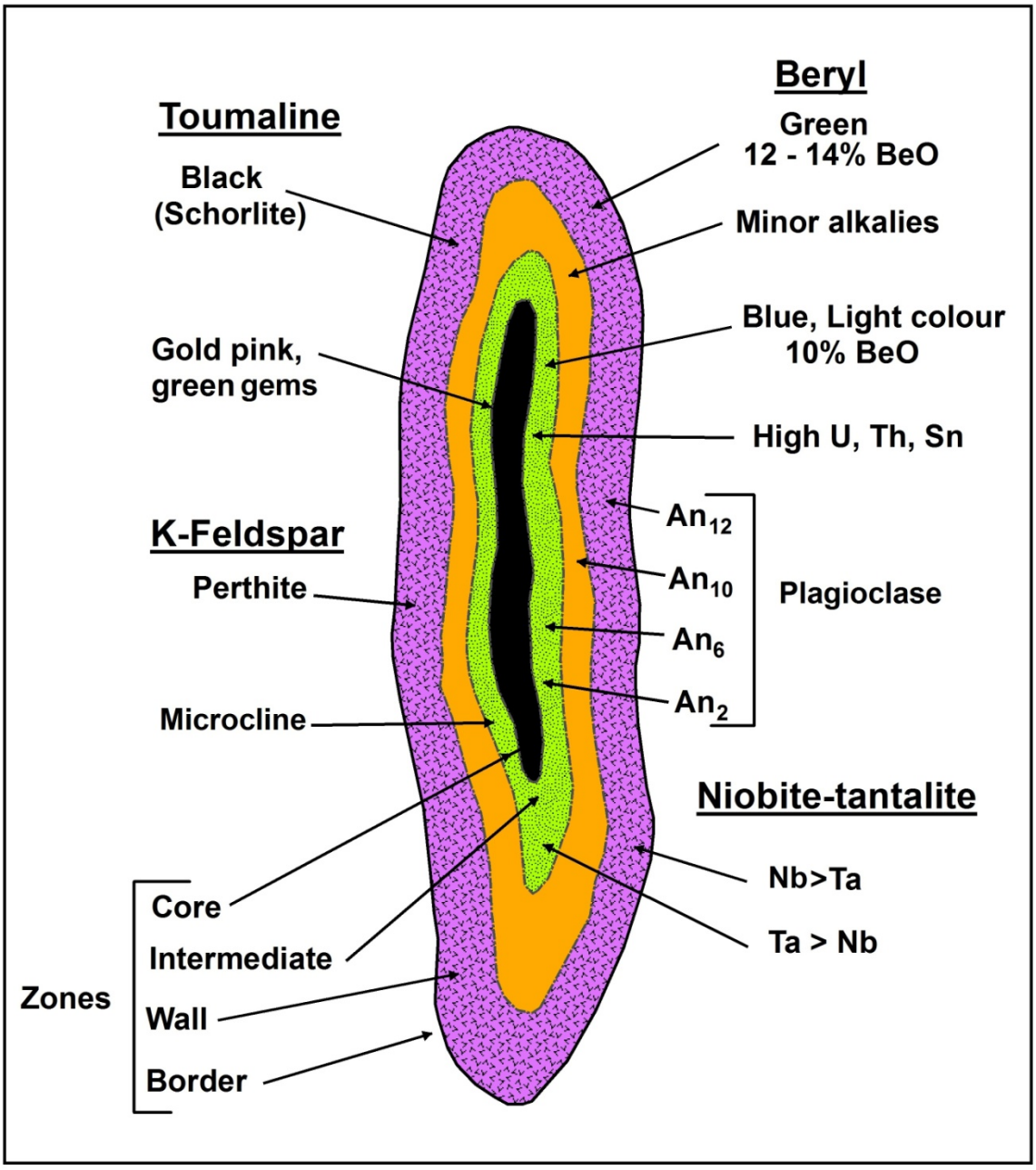

Fig. 2.5: Schematic section through a complex pegmatite showing mineralogical and geochemical zoning and rare-element mineralisation from the aplitic boarder zone to the quartz-rich core zone (modified after Cerny *et al*., 1991)

and Webber, 2008). The geochemical attributes of the lithophile elements make them toprefer being enriched inpegmatite melts rather than being partitioned into the common rock-forming minerals of pegmatites. The presence of flux components (Li, F, B and P) and volatiles in residual pegmatite melts sufficiently alter the melt structures by appreciably lowering the crystallisation temperature, suppressing nucleation rates, reducing meltpolymerisation, decreasing viscosity and density, but increasing diffusion rates and solubility of water (Pichavant, 1981; London, 1987; 1992; 2005a; 2005b, London *et al*., 1989; 1993; Simmon *et al*., 2003; Linnen and Cuney, 2005; Simmons, 2007b; Simmons and Webber, 2008). The foregoing result in extended fractionation, the development of large crystals, pegmatitic textures, as well as enigmatic rare-element mineralisation in rare metal-bearing pegmatites (Simmon and Webber, 2008; Cerny *et al.*, 2005).

Multiple intrusions of pegmatite melts resulting in different generations of pegmatites have been reported in some terranes (Baadsgard *et al.*, 1984; Scharer *et al.*, 1996; Henderson and Ihlen, 2004). They are generally recognised by their mutual spatial and cross-cutting relationships. Henderson and Ihlen (2004) have suggested a progressive ductile deformation punctuated by multiple but relatively short cycles of brittle deformation and the eventual multiple pegmatite injections for the Haukemyrliene polygeneration pegmatites located within fault-bounded Bamble region, southern Norway.

Trace elements generally show varying degrees of incompatibility between the melt and the crystal phases in granite-pegmatite systems, with pegmatite petrogenetically important trace-elements partitioning more strongly into the late residual accessory mineral phases*vis-à-vis* the major rock-forming minerals (Noval *et al*., 2012, Linnen and Cuney, 2005). The above results in pegmatites accentuating the trace element signatures of their granitic sources (Cerny *et al.*, 2012), in showing their (protoliths) pre-enrichment extents and possible geotectonic environment of emplacement. Therefore, the trace element characteristics in pegmatites are commonly employed in identifying the granitic parentage, whose source characteristics are known and distinctive (Cerny, 1991; Cerny and Ercit, 2005; Cerny *et al*., 2012).

Three petrogenetic-geochemical families are commonly distinguished within the rare-element class of granitic pegmatites, based on tectonic affiliations and elemental associations (Cerny, 1991, 1992; Cerny and Ercit, 2005; Martin and De Vito, 2005). These are the lithium, cesium and tantalum (LCT)-pegmatites, the niobium, yttrium and fluorine (NYF)-pegmatites and the mixed-signature (cross-bred LCT and NYF)-pegmatites. The LCT-pegmatites show enrichment in Li, Cs and Ta (with Rb, Cs, Be, Ga, Sn, B, P) as diagnostic signatures, and are mostly generated by anatexis of undepleted middle to lower crustal protoliths (supracrustals and/or basement) undergoing their first melting event (Cerny, 1991; Cerny *et al*., 2005). They are strongly correlated with extremely peraluminous S-type granites with their provenance commonly linked to chemically matured sedimentary sources (Shelley, 1993) and post collisional geotectonic environment (Martin and De Vito, 2005; Tkachev, 2011). The NYF-pegmatites are marked by elevated contents of Nb (Nb>Ta), Y, F, Be, REEs, Sc, Ti, Zr, U, and Th, commonly showing proximity to anorogenic peralkaline A-type and I-type granites (Eby, 1990; 1992; Cerny and Ercit, 2005; Marin and De Vito, 2005). They are suggested to be derived from the anatexis of depleted middle to lower crustal protoliths that have witnessed a previous melting episode or by partial melting of undepleted juvenile igneous rocks (Cerny *et al*., 2005; Cerny and Erict, 2005; Linnen and Cuney, 2005; Martin and De Vito, 2005; Selwa*y et al.*, 2005). The mixed LCT+NYF pegmatites are generally of minor occurrences and marked by composite origin. They are essentially derived from the contamination of NYF-granites by digestion of undepleted supracrustal rocks (Van Breemen *et al.*, 1975 Cerny and Ercit, 2005; Cerny *et al*., 2005; Simmon, 2007).

Pegmatites have been classified based on the geological environments of the host rocks, depths of emplacements, internal structures, paragenetic relationships, bulk chemical composition, petrogenesis and trace-element geochemical signatures (Solodov, 1971,; Zou and Xu, 1975; Ginsburg *et al*., 1979; Cerny, 1982; Zou *et al*., 1985; Cerny, 1990; Cerny and Kyellman, 1999; Hanson *et al*., 1991, Zagorskyi *et al*., 2003). These classifications are, however, not without few contradictions, ambiguities, misgivings and misconceptions (TKachev, 2012). For instance, Ginsburg *et al.* (1979) categorised pegmatites into pegmatite classes based on metamorphic environment of their host lithologies (the abyssal

class), mineralogy (the muscovite class), elemental composition (rare-element class) and texture (the miarolitic class). This classification, however, suffered some drawbacks and proved to be of little relevance due to the fact that pegmatites generally postdate the metamorphic conditions of their host rocks, while their depths of emplacements are not easily extrapolated from their chemical and textural attributes (Cerny *et al*., 2012; Tkachev, 2011).

Cerny's (1991) pegmatite classification employs a combination of emplacement depths, metamorphic grade and minor element contents (Table 2.1). This classification provides insight into the origin of melts and relative degree of fractionation (Simmon, 2007). Cerny and Ercit (2005) provided a modified classification of Cerny (1991) by expanding the pegmatite classes into subclasses, types and subtypes (Table 2.2). This classification, which utilises petrological affiliations, tectonic settings and trace element geochemical signatures of pegmatites, as reflected in their mineralogy and mineral chemistry, enjoys the widest acceptability. It is quite applicable in the evaluation of ore- and gem-bearing potentials of pegmatites from diverse geological environments (Cerny *et al*., 2005; Cerny and Ercit, 2005). The rare-element class pegmatites (Appendix 1) are the most common and show significant enrichments in rare-elements (Cerny *et al*., 2005). These are further categorised into petrogenetic families (Appendix 1), so as to amplify their geochemical and exploration applicability.

2.3 Review of the economic potentials of pegmatites

Pegmatites are economic sources of important minerals, which are of common applications in materials ranging from simple glasswares to various high-tech devices. The extreme chemical fractionation that produces pegmatites refines the pegmatite constituent minerals to a purity level that is not achieved in other geologic environments (London and Morgan, 2012; Glover *et al.*, 2012). The exceptionally large crystals of pegmatites which facilitate ease of extraction and the high chemical purity of some its mineral phasesmakes pegmatites amenable to low-cost open-pit mining and efficient and economic sources of rare metals, industrial minerals and gem-quality crystals (Glover *et al.*, 2012).

The accessory mineral phases in rare-element (mineralised) pegmatites are geochemical

Table 2.1:Depth classification of pegmatites (Cerny 1991; modified from Simmons *et al.* 2003)

Class	Family	Typical Minor Elements (mineralisation)	Pressure-Temperature conditions (metamorphic environment)	Relation to Granite	Examples
Miarolitic	NYF	Be, Y, REE, Ti, U, Th, Zr, Nb>Ta, F (poor mineralisation, gemstock)	Shallow to subvolcanic ~1-2 kb	Interior to marginal	Pikes Peak, Colorado; Sawtooth Batholith, Idaho; Korosten Pluton, Ukraine
Rare-Elements	LCT	Li, Rb, Cs, Be, Ga, Nb<Ta, Sn, Hf, B, P, F (poor to abundant mineralisation, gemstock industrial minerals)	Low-pressure, Abukuma amphibolite to upper greenschist facies (andalusite-sillimanite) ~2-4 kb	Interior to marginal to exterior	Yelloknife field, NWT; Black Hills, South Dakota; Cat Lake-Winnipeg River field, Manitoba
	NYF	Y, REE, Ti, U, Th, Zr, Nb>Ta, F (poor to abundant mineralisation, ceramic minerals)	~ 650°-500°C	Interior to marginal	Llano Co., Texas; South Platte district, Colorado; Western Keivy, Kola, USSR
Muscovite Rare -Element	_	Be, Y, REE, Ti, U, Th, Nb-Ta, Li	Moderate to high pressure, amphibolite facies: ~3-7 kb ~ 650°-520°C	Interior to exterior; locally poorly defined	Spruce Pine and Hickory, North Carolina
Muscovite	_	Li, Be, Y, REE, Ti, U, Th, Nb>Ta (poor to moderate mineralisation, micas and ceramic minerals)	High pressure, Barrovian amphibolite facies (kyanite-sillimanite) ~5-8 kb ~ 650°-580°C	None; direct melting to lower crustal rocks (anatexis) to marginal and exterior	White Sea region, USSR; Appalachian Province; Rajahstan, India
Abyssal	_	U, Th, Zr, Nb, Ti, Y, REE, Mo (poor to moderate mineralisation)	(upper amphibolite to) low to high-pressure granulite facies ~4-9 kb ~ 700°-800°C	None; direct melting of lower crustal rocks	Rae-Hearne provinces, Saskatchewan; Aldan and Anabar shields, Siberia; Eastern Baltic Shield

Table 2.2: Classification of pegmatites

Class	Subclass	Type	Subtype	Family
Abyssal	HREE			NYF
	LREE			
	U			NYF
	Be			LCT
Muscovite				
Muscovite-Rare element	REE			NYF
	Li			LCT
Rare element	REE	Allanite-monazite		
		Euxenite		NYF
		Gadolinite		
	Li	Beryl	Beryl-columbite	
			Beryl-columbite-phosphate	
		Complex	Spodumene	
			Petalite	
			Lepidolite	LCT
			Elbaite	
			Amblygonite	
		Albite-spodumene		
		Albite		
Miarolitic	REE	Topaz-beryl		
		Gadolinite-fergusonite		NYF
	Li	Beryl-topaz		
		Spodumene		LCT
		Petalite		
		Lepidolite		

NYF – Niobium-yttrium-fluorine family; LCT – Lithium-cesium-tantalum family; HREE – Heavy rare earth elements; LREE – Light rare earth elements.

reservoirs of rare-metals and rare-earths and the elements extracted from these minerals find specialised applications in high-tech and green energy industries.Some of these metals have been designated critical metals, as they show high risk to supply disruption (Skirrow *et al.*, 2013; European Commision, 2014). The critical metals in pegmatites indicate moderate to high criticality index (Appendix 2).

In considering the economic values of some of these ore elements, it is important to note that there some areas of overlapping metallurgical and industrial applications.

Tantalite-columbite-cassiterite

Tantalum finds major application in the electronic industry, particularly in the manufacture of micro-capacitors,which are essential components in portable electronic devices, including smart phones, digital cameras, laptop computers, GPS navigator systems in cars and airplanes and airbag activation devices. Superalloys of Ta are employed in the manufacture of jet engines, rocket nozzles and turbine blades (Tantalum-Niobium International Study Centre, 2013a; Papp, 2013a; European Commission, 2014). Tantalum is applied in the manufacture of cutting tools (Ta carbide), furnace equipment and heat crucibles. It is also used in corrosion prevention in chemical and nuclear plantsdue to its chemical inertness. Tantalum is used in producing glasses and electronic filters. It is also employed as medical implants due to its chemical inertness and biocompatibility with body tissues.

The dominant use of niobium alloys is in the production of micro-alloy or high strength low-alloy (HSLA) steel, containing approximately 0.03% Nb (Mackay and Simandl, 2014; European Commission, 2011; Tantalum-Niobium International Study Centre, 2013b). The HSLA steels are used extensively in building vehicle bodies, railway tracks, ship hulls, pipeline tubes, and offshore petroleum drilling platforms (Roskill, 2013 Linnen *et al.*, 2014). Niobium-base alloys equally have high temperature applications in gas turbines and space vehicles and as superconductors in high field magnets. Niobium-bearing chemical are utilised in acoustic wave filters, camera lenses, coating on glass for computer screens, and ceramic capacitors (Linnen *et al.*, 2014). Niobium carbide is also engaged in some specialised cutting tools. The low neutron absorption coefficient, high temperature strength and extreme

corrosion resistance to liquid metals make niobium suitable as cladding materials for fuel elements in nuclear reactors (Papp, 2013b).

Tin is used in the production of water stills, organ pipes, brewery piping and costume jewelries. It is also applied as sheets in the construction of building and roofs. It equally provides non-toxic, hygienic and corrosion-free coatings for domestic hardwares, food packaging cans, containers and boxes. Other specialised applications of tin are in flat and touch screen technologies, most notably as indium tin oxide (ITO) (Skirrow *et al.*, 2013)

Lithium

Lithium is essentially sourced from spodumene [$LiAlSi_2O_6$), petalite [$LiAlSi_4O_{10}$], lepidolite [$K(Li,Al)_3(Si,Al)_4O_{10}(F,OH)$] and amblygonite-montebrasite [$LiAlPO_4(F,OH)$] in rare-element pegmatites. These lithium aluminosilicates have both metallurgical and industrial applications (Glover *et al*., 2012). Technical-grade Li is utilised in glass and ceramics manufacturing processes as a flux, while ceramic grade spodumene and petalite can also be applied directly without processing. Lithia [Li_2O] is a very potent flux, particularly when used with potassium and sodium feldspars (Selway *et al*., 2005), as it lowers thermal expansion and reduces the firing temperature. It also reduces the viscosity of the molten glass, thereby providing excellent fluidity and substantially bringing down the melting point of the glass.

Chemical-grade Li is valued in lubricants and in the production of Li-ion rechargeable batteries, which are important components of electric vehicles, digital cameras and smart phones. Lithium carbonate and other organic salts of Li are the active ingredients in antidepressant drugs, which help in reducing the severity of bipolar depression in psychiatric patients (Glover *et al*., 2012). The anti-inflammatory attribute of Li compound is equally exploited in orthopedics in treating gout in skeletal joints (Glover e*t al.,* 2012).

Cesium

Cesium is mainly extracted from pollucite [$Cs(Si_2Al)O_6 .nH_2O$]. It can be converted to cesium formate and applied as a high density specialty drilling and completion fluid for high temperature and high pressure hydrocarbon exploration and development wells

(www.cabot-corp.com, accessed June 2017). Cesium formate is environmentally friendly, as it is non-toxic, biodegradable and water soluble (Selway *et al,* 2005). Cesium's photoemissive characteristic is exploited in solar photovoltaic cells.

Beryllium

Non-gem beryls are valuable as ores of the light metal Be and have immense metallurgical applications. Beryllium is a potent strengthener of Cu, Ni, Fe, Mo, Ti and a host of other metals. The application of beryllium for alloying has important engineering properties, including elasticity, lightness, stiffness, machinability, good formability and great strength. Beryllium and Cu alloys are essential components of aerospace, automotive and electronic devices. The nuclear properties of Be are exploited in beryllium X-ray windows, nuclear reactors and other radiation measuring equipment. Beryl can also be used as additives to kaolin and talc for application in refractory.

Tungsten

Tungsten superalloys are utilised in turbine blades, aerospace and automotive industries. Tungsten retains its strength at high temperature, and this makes it valuable in high temperature applications, such as light bulbs and halogen lamps, cathode-ray tubes, vacuum tube filaments, rocket engine nozzle, electrical heatings and welding equipment. The electronic structure of tungsten enables it to be used as a source of X-ray (both as filaments and targets) in X-ray tubes and also for shielding high-energy radiations. Tungsten carbide, a product of high temperature chemical reaction of tungsten and carbon, is noted for its exceptional hardness, and it is utilised in industrial machinery, abrasives and cutting tools (knives, drilling bits, circular saw, millings and turning tools).

Rare-earths

Rare-earths exhibit a range of special electronic, magnetic, optical and catalytic properties, which are critical in modern day high technologies (Hatch, 2012). The electronic applications of the rare-earths (Eu, Y, Tb and Ce) include its being used as phosphorous materials in the modern day energy-efficient liquid crystal display (LCDs), plasma screen displays, light emitting diodes (LEDs) and compact fluorescent lamps (CFLs); while Nd, Er and other REEs are valued in various laser and fibre-optic applications (Linnen *et al.*, 2014). The high

strength and relatively small sizes of REEs are exploited in electronic devices, including hard disks, digital video disc (DVD) and high performance speakers (Linnen *et al*., 2014)

The magnetic applications of rare-earths (Nd, Pr, Sm, Dy and Tb) are quite apparent as superalloys in permanent magnets, which are important components of wind turbines and electric motors. Lanthenum and Ce impact stability to fluid-cracking catalysts (FCCs) during the catalytic cracking of petroleum, thereby transforming heavy petroleum molecules to refined diesel fuel and gasoline (Linnen *et al*., 2014). They are used as automotive catalytic converters (ACCs) to reduce the emission of pollutant that comes from internal combustion systems. They are also utilised as polishing powders for glasses, mirrors, TV screens, computer display and other high-class finishes (Hatch, 2012; Linnen *et al*., 2014).

Pegmatite-derived industrial minerals are very few but their industrial applications are many and diverse (Glover *et al.,* 2012).

Feldspar

Powdered feldspar is used as flux in producing ceramic tiles, China wares, enamels and high-voltage electrical insulators. Granular feldspar facilitates batch melting of alumina- or silica-rich reagents, and also makes glass more amenable to forming, more durable and resistant to devitrification (Glover *et al*., 2012). Finely pulverised feldspars are suitable as fillers in paints, poly vinyl-chloride (PVC) plastics and welding rods. Feldspar facilitates resistance to chemical attacks and abrasion and ultimately improves the durability of paint film, while in plastics it improves resistance to staining and chemical attacks (Glover *et al.*, 2012). Feldspars are also exploited as slag former in metallurgical industry and as a binder for abrasive wheels. Crushed and powdered feldspars are used as abrasive in scouring soaps, as well as non-skid dusting agent for oily floors and concretes.

Quartz

Crushed quartz from pegmatite is used in glass, ceramics, abrasives and refractories. Pegmatites are the principal sources of high purity (<100 ppm total impurities by weight)

or ultrahigh-purity (UHP) (<10 ppm total impurities by weight) quartz (Glover *et al*., 2012). Pulverised high-purity quartz is utilised in producing high-quality fused silica that is

employed in producing chemically and thermally resistant vessels and tubes (high performance halogen bulbs). Ultra high-purity quartz powders are used in making quartz glass apparatus for the manufacture of semiconductor chips, silicon-based solar cells, mirrors and specialised ceramics (Glover *et al*., 2012). Quartz crystals, especially the oriented slice derivatives, are applied as resonators and oscillators in radiotelephoning microphones and depth-measuring instruments in submarines. These important applications are largely due to the pyroelectric and piezoelectric properties of quartz crystals.

Muscovite

Muscovite finds diverse industrial applications as fillers, lubricants, coatings, electrical insulators and cosmetics. It is used as electrical insulators in high voltage lamps, aircraft, spark plugs, heating elements, electric soldering irons and other heat containment household appliances. Mica is used in the production of diaphragms (oxygen breathing equipment), quarter-wave (optical instrument), stove window, sight glasses (used in furnaces and ovens), lamp chimneys and base for platinum wire resistance thermometers.

Ground micasare utilised as fillers in automotive plastic parts (mica-filled bumpers, facia, fenders, wheel covers, windshield components, underhood components and some selected interior parts), where it impacts heat resistance, strength and improved dielectric properties(Glover *et al*., 2012). Micasalso perform functional role as fillers in asphalt products, pipeline enamels, ceiling tiles and in various rubber products. Pulverised muscovite is employed as important additive when compounding specialised oil drilling fluids. It helps in overcoming lost circulation of drilling fluids, as it quickly fills the cracks in bore holes and seal them.

Pulverised mica is used as decorative finishes in concretes, stone and bricks. It is also used as weather-proof materials in the manufacture of roll roofing and shingle. Premium-quality, wet-ground muscovite is used in cosmetics, as it adds sheen, cohesion and moisture to nail polish, eye shadow, lipsticks, barrier creams and other products of personal hygiene(Glover *et al*., 2012).

Kaolin

High grade kaolin is extremely white and cohesive, and finds important industrial applications as fillers, lubricants, sealants, refractories and in ceramics. Kaolin is added to feldspar, quartz and sand and fused at high temperature to produce ceramic, pottery products and sanitary wares. Kaolin-made ceramics are employed as catalyst in catalytic cracking of petroleum and as catalytic converter for automobiles. Kaolin, as filler, increases the strength of plastics, rubber, sealant and adhesives, while reducing the amount of more expensive resins and latex in the formulations. Processed kaolin impacts better appearance and add heft to papers

Gemstones

Gem-quality crystals of exceptionally high commercial values are largely derived from exsolved products of the late-stage volatile and flux–rich residual pegmatite melts. They crystallise when the concentration of water in the residual melt exceeds its solubility limits and thus facilitate the formation of miaroles (London, 1986a; Simmons *et al*. 2003; London, 2008; Simmon *et al*., 2012). Gem stocks materials are commonly localised in the core margin of zoned pegmatites and in miarolitic cavities, as well as in the reaction zones surrounding pegmatites that intrude into mafic and ultramafic rocks (London, 1987; Simmons *et al*., 2012; Groat *et al*., 2014).

Beryls (emerald, acquamarime, alexandrite, heliodor and morganite), tourmalines (elbaite, indicolite, perdot, verdelite and liddicoalite), topaz, spodumene, spessartine garnet, apatite and zircon are common gems found in complex pegmatites. Others include coloured and gemmy quartz (amethyst, citrine, rose and smoky) and feldspar (moonstone and amazonite) crystals. These gemstocks can be polished, cut and shaped into desired shapes and sizes, and can also be heated and irradiated to enhance their aesthetic features and ultimately increase their economic worth. Polishedgems are used as pendants in rings, earrings and necklaces.

2.4 Review on exploration for rare metal-bearing pegmatites

As the commonly outcropping and easily worked rare-metal pegmatites within the Basement Complex units are being rapidly depleted, there is a need to focus exploration efforts on

locating new pegmatite ore deposits underneath lateritic covers. A number of investigations have been carried out on the compositional attributes of pegmatites and weathering profiles of different economic deposits, but very few studies have actually been channeled towards unraveling the mineralogical indicators and geochemical criteria in the residual weathering profiles of pegmatites that can be employed in discriminating between barren and mineralised pegmatites under lateritic covers.

Exploration for rare metal-bearing pegmatites commonly begins with the examination of regional geological maps, as they are generally confined to deep-seated regional faults in greenschist and amphibolite metamorphosed terranes, pre-existing batholithic contacts or lithologic boundaries (Cerny, 1982; 1989; Trueman and Cerny, 1982; Moller and Morteani, 1987; Selway *et al.*, 2005). Rare-metal pegmatites are commonly found within mafic metavolcanics and metasedimentary rocks in Archaean shields, granite-greenstone terranes, metasedimentary gneissic troughs, and metasedimentary-metavolcanic basins, typically showing spatial relationship with extremely evolved and mostly peraluminous granitic plutons (Cerny, 1989; Moller and Morteani, 1987; Selway *et al.*, 2005).

In areas marked by intensive surface erosion and adequate drainage, weathering-resistant minerals that bear the geochemical signatures of rare-metal pegmatites (Ta-Nb oxides, zircon, apatite, rutile, anatase, magnetite, beryl, tourmaline, and garnet) are conventionally panned along stream channels to explore for rare-metal pegmatites at reconnaissance level (Matheis, 1979, Fletcher *et al.*, 1987; Matheis and Kuster, 1989). Where used, this approach has invariably indicated fairly large pegmatite dykes (Matheis, 1979; Lapworth *et al.*, 2012), as smaller mineralised pegmatite bodies could only make meager contributions of indicator minerals to the receiving fluvial channels. The short distances of transportation by seasonal streams have been reported to result in inconsistent patterns of heavy mineral deposition (Matheis and Kuster, 1989). The possibility of many barren to very few mineralised pegmatites in most pegmatite districts, also shows the limitation of

heavy mineral concentrate approach to exploring for unexposed rare-metal pegmatites.

With the identification of regional deep-seated faults and fertile peraluminous granitic batholiths, exploration for mineralised pegmatites continues with basement geological

mapping and lithogeochemical studies, as they are generally known to occur with simple (barren) pegmatites in different pegmatite fields. Mineralised (rare-element) pegmatites are generally reported to constitute far less than 1% of pegmatite population in a typical pegmatite field (Cerny 1989; 1991; London and Eversen, 2002; London, 2005; Linnen *et al*., 2012; London and Kontak, 2012; London and Morgan, 2012). Pegmatite fields containing LCT-pegmatites generally show regional zoning around source granitoids (Fig. 2.6), with the highly fractionated progeny pegmatites, enriched in rare-metals and volatile components, commonly found at great distances from the parent granitoids. The flux components (Li, F, B, P) generally facilitate low viscosity, and the flux-rich pegmatite melt can travel very far from the source granitoid (Linnen *et al*., 2012). The evolved LCT-pegmatites equally indicate consecutive mineralogical and geochemical zoning from barren to Be-Nb-rich to Be-Nb-Ta-rich to Li-Be-Ta-Nb-rich and ultimately to Li-Cs-Be-Ta-Nb-Sn-rich complex pegmatites (Cerny, 1989; Linnen *et al*., 2012; London and Kontak, 2012) (Fig. 2.6).

Lithogeochemical techniques, such as the evaluation of the degree of specialisation of pegmatites from the whole-rocks and mineral samples (Tisdendoff, 1977; Moller and Morteani, 1987; Emofurieta *et al.*, 1988; Cerny, 1989; Morteani and Gaupp, 1989; Okunlola, 2005; Okunlola and Jimba, 2006; Aromolaran, 2007; Kuster, *et al*., 2009; Elueze and Aromolaran, 2014), as well as the detection of primary dispersion halos of mineralised pegmatites using highly mobile (Li, Rb, Cs, B) andvolatile components (Shearer *et al*., 1984; 1986; London, 1986b; 2008), are commonly employed in discriminating between barren and mineralised pegmatites at outcrop scale. Key mineralisation indices, such as high concentration levels of Li, Rb, Cs, Nb, Ta, Sn and Be, as well as fractionation indicators, including low K/Rb, K/Cs, Nb/Ta and Mg/Li ratios in whole-rocks, K-feldspar, albite and muscovite samples, have been highlighted to indicate significant rare-alkali fractionation and rare-metal mineralisation in pegmatites (Cerny *et al*., 1985; Morteani and Gaupp, 1987; Moller and Morteani, 1987; Foord *et al.*, 1995;

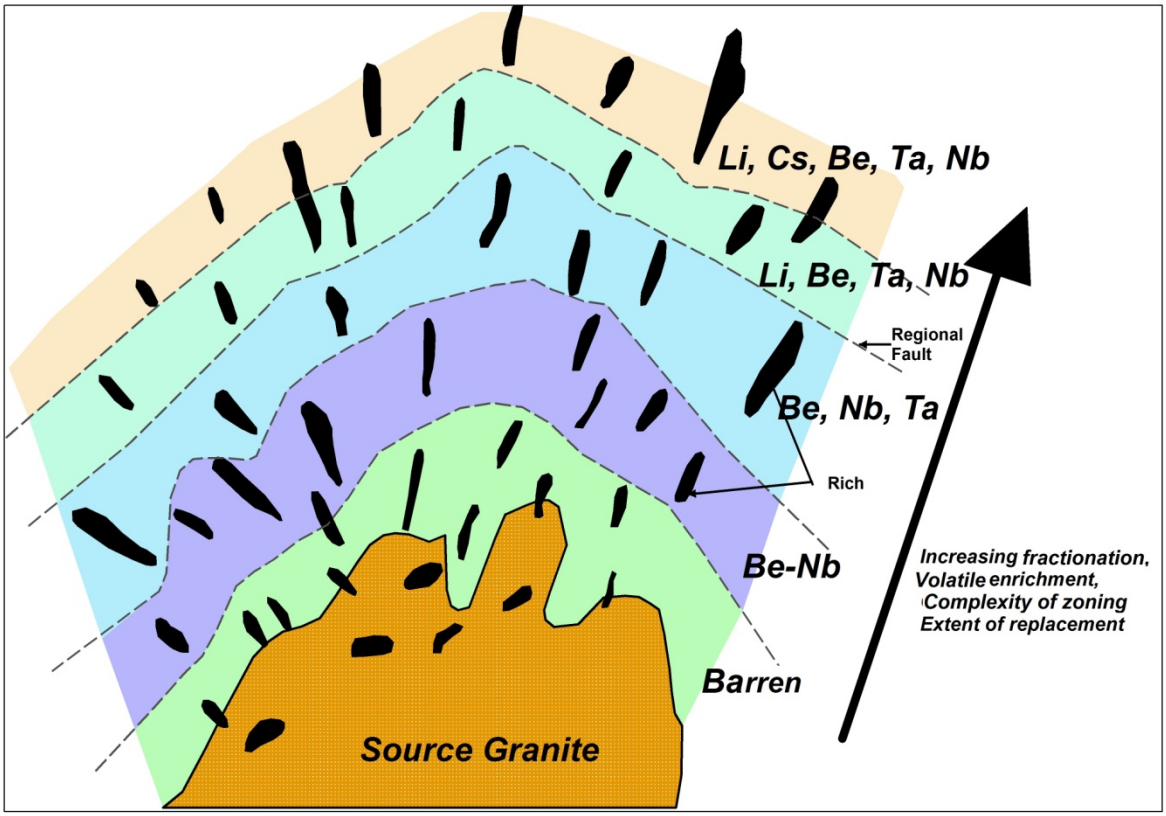

Fig: 2.6: Schematic section of a zoned pegmatite field, showing geochemical fractionation and evolution of rare-element pegmatite around a source granitoids (modified after Cerny, 1989)

Morteani *et al*., 1995; 2000; Wise, 1995; Alfonso *et al*., 2003; Okunlola, 2005; Okunlola and Jimba, 2006; Selway *et al.*, 2005; Kuster *et al*., 2009; Wise and Brown, 2010; Elueze and Aromolaran, 2014). The occurrences of Li-rich minerals (lepidolite, amblygonite, petalite, lithiophilite, spodumene, lithian muscovite and zinnwaldite), Cs-rich minerals (pollucite, Cs-rich beryl) and Ta-Nb ores (manganotantalite, manganocolumbite, microlite, tapiolite, wodginite), Mn-rich spessartine garnet, Li-rich tourmalines (elbaite) and blue or green fluorapatite in pegmatites are consistent with their rare-metal mineralisation (Joliffe *et al*., 1986; Selway *et al*, 2005; Linnen *et al.*, 2012; Neiva, 2013); while exormorphic assemblages of (Rb-Cs)-enriched biotite, bityite, tourmaline, holmquistite (Li-amphibole), muscovite, and chlorite in metasomatic host rocks proximal to pegmatites (Shearer *et al*., 1984; 1986; London, 1986b; Morgan and London, 1987) are also employed to locating rare-metal pegmatites.

In comparison to some other deposits (e.g. base and precious metal deposits), mineralised pegmatites are relatively small and commonly impact limited alteration halos and geochemical signatures on their host lithologies (Morgan and London, 1987; Brown, 2004), thereby making them a difficult deposit type to locate and access for economic potential even at outcrop scale (Brown, 2004). The above are largely due to their relatively small volume and low heat contents of pegmatite melts (Shearer *et al.*, 1984; Morgan and London, 1987). It is noteworthy to state that the limited alteration envelops around pegmatites are particularly difficult to preclude under deep lateritic covers.

Tropical and subtropical belts around the world are marked by intense physico-chemical decomposition of rocks, resulting in relatively very few outcrops and considerable thickness of lateritic profiles (Butt and Zeegers, 1992; Nahon and Tardy, 1992; Anand and Paine, 2002; Tardy, 1996; Butt *et al*., 2000; Freyssinet *et al.*, 2005). The mantling of the basement rocks by deep residual profiles has presented certain exploration challenges, which affect geological, geophysical and geochemical mapping and exploration techniques (Butt *et al*., 2000). For mineralised pegmatites under residual lateritic covers, some of these challenges are commonly not easily resolve using geophysical techniques. This is largely due to their small extents and limited geochemical alteration halos around pegmatite deposits.

Despite the economic significance of mineralised pegmatites, there are very few investigations of their exploration under lateritic covers. Matheis (1981) conducted a regional geochemical soil survey around Sn-Ta-Nb pegmatites of Iregun, Ijero and Egbe areas, within the SW-NE trending mineralised pegmatite belt of Nigeria. Lithium, Be, Rb and Cs concentrations and Mg/Li ratio in the B-horizon of the lateritic soils were investigated to outline pegmatites of these areas. Marshall and Herman (1986), using the sequential extraction of the 20.0 cm B-horizon soil samples above some deeply weathered pegmatites, were able to decipher the restricted lateral dispersion of certain trace elements that delineate the contact between complex pegmatite and the host quartz-biotite gneisses in the Piedmont district, central Virginia, USA. The elements Sn, Be, La, Li and U were observed to be associated with the B-horizon above the complex pegmatites. The susceptibility of the 20.0 cm sampling depth to heavy transportation by meteoric agents, shows the restricted applicability of this approach in deciphering rare-metal pagmatites underneath lateritic profiles.

Using lateritic residuum (ferruginous upper zone of lateritic profile) in a regional geochemical soil survey, Cornelius *et al* (2008) delineated the world-class Archaean Sn-Ta pegmatite ore body at Greenbushes in southwestern Yilgarn Craton, Western Australia. The anomalous Sb, Sn, Ta and Nb concntrations that essentially trend along NW direction parallel to the regional fault system indicated the ore-rich pegmatite. Smith *et al.* (1987), based on the multi-element analysis of pisolitic lateritic duricrust overlying the same pegmatite, delineated the geochemical dispersion anomaly around it from As, Sn, Be, Sb, Nb, B, Ta and Li concentrations. Pegmatophile index was empirically derived for the Greenbushes pegmatite system, which is 0.09As+1.33Sb+Sn+0.6Nb+Ta; while its rare-metal trends were also highlighted (Smith *et al*., 1987). Pegmatophile index is a weighted sum of element abundances that are particularly critical to identifying multi-element anomalies associated with Sn-Ta pegmatites (Smith *et al.*, 1987; Cornelius *et al*. 2008). Galeschuk and Vanstone (2005) have utilised enzyme leach technique to preferentially dissolve amorphous MnO_2 in B-horizon soil samples over pegmatites in Bernic Lake area, southern Manitoba, Canada; and they delineated rare metal-rich LCT-pegmatites. MnO_2 is generally believed to be excellent ionic traps for trace elements that emanate from the LCT-pegmatites.Thehighlighted studies

indicate the possibility of delineating large concealed pegmatite deposits beneath lateritic mantles on a regional scale.

Notable contributions on the exploration for rare-element pegmatites in Nigeria were initially that of Jacobson and Webb (1946), who appraised the pegmatites of central Nigeria for ore mineralisation potential. They acknowledged two distinct stages of tin mineralisation within the crystalline rocks of Nigeria: Sn-Ta-Nb productive pegmatites (Older Tin Fields) and the anorogenic calc-alkaline ring complex of the Jos-Plateau area (Younger Tin Province). Rare-metal bearing pegmatites have earlier been known to be strictly confined to the well-defined ENE-WSW trending belt (Fig. 2.7) from Abeokuta area in southwest to Jos Plateau area in northcentral Nigeria (Wright, 1970; Kinnaird, 1984; Matheis and Caen-Vachette, 1983, Matheis, 1987; Emofurieta *et al.,* 1988; Kuster, 1990). However, there have been reported occurrences of other rare-metal pegmatites away from this belt in Obudu and Obaliku areas (Oban massifs), southeastern Nigeria (Jacobson and Webb, 1946; Ekwueme and Schlag, 1989; Ekwueme and Matheis, 1995; Okunlola, 1998; Ero and Ekwueme, 2009) and in Oke-Ogun district, southwestern Nigeria (Okunlola, 2005; Okunlola and Ofonime, 2006; Aromolaran, 2007; Okunlola and Oyedokun, 2009; Adetunji and Ocan, 2010; Elueze and Aromolaran, 2009; 2013; 2014).

Okunlola (2005) and MMSD (2012), based on trace element geochemistry of muscovite samples, have described the Ta-Nb metallogeny of the Nigerian pegmatites, and outlined seven distinct pegmatite fields within the Basement Complex of Nigeria. These include Oke-Ogun, Ibadan-Osogbo, Kabba-Isanlu, Ijero-Aramoko, Lema-Ndeji in southwestern Nigeria, and Nassarawa-Keffi and Kushaka-Birni-Gwari in the northcentral and northwestern Nigeria, respectively. The pegmatites are reported to be intrusive into pelitic to semi-pelitic schists with minor associated amphibolites and gneisses, granites and metavolcanics (Okunlola, 2005).

Garba (2002) has indicated the localisation/alignment of rare-metal pegmatites and hydrothermal gold mineralisations with the regional NE-SW and NNE-SSW trending faults and their subsidiaries. He attributed these mineralisations to the deformational cum metamorphic-magmatic processes that typified the waning stage of Pan-African crustal

`

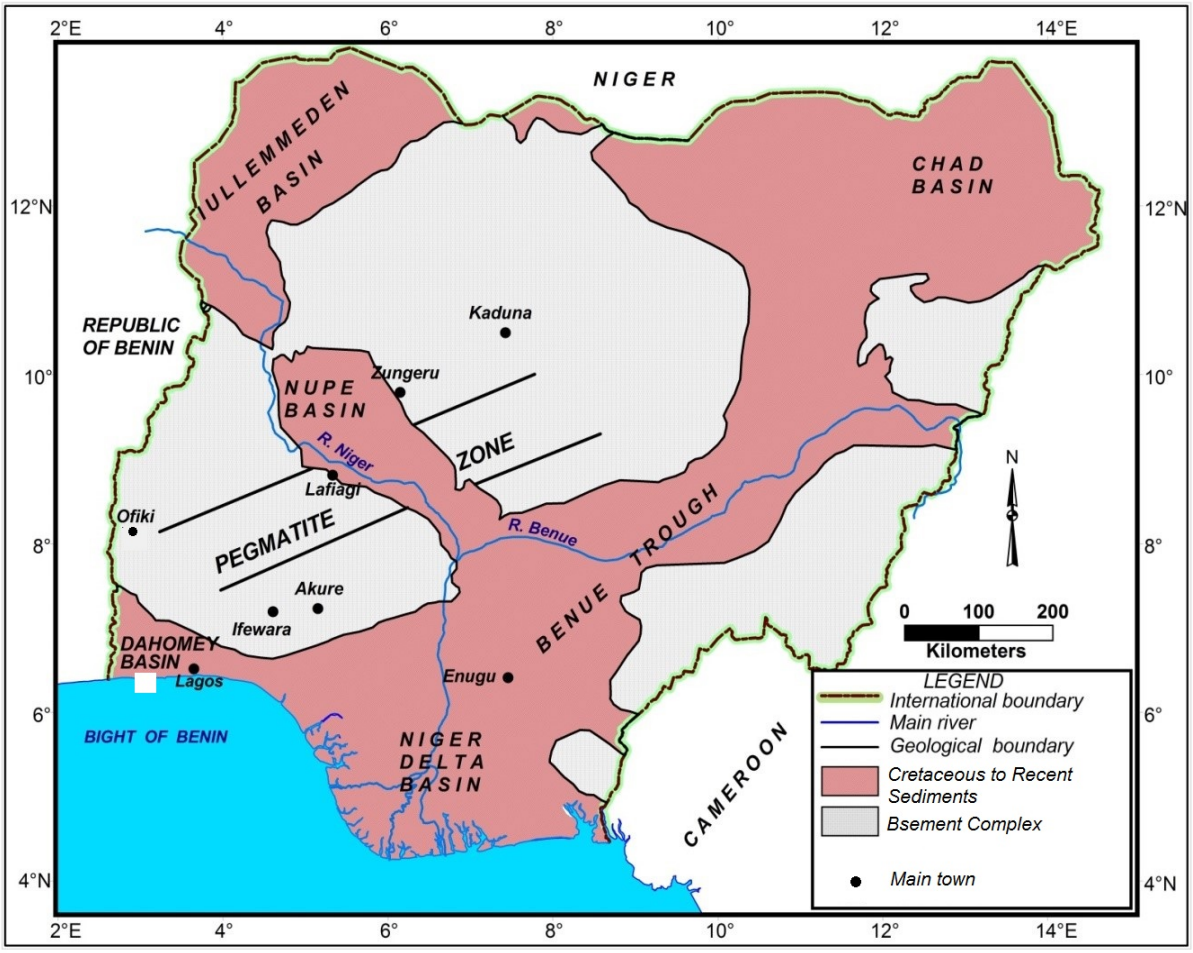

Fig. 2.7: Generalised geological map of Nigeria showing the rare metal-bearing pegmatite zone (modified after Odeyemi *et al.,* 1999)

convergence between microplates, with the generated conjugate faults and shears facilitating the fluid pathways for the rare-metal pegmatite melts and the gold mineralising-fluids. Matheis and Caen Vachette (1988), using Rb-Sr whole-rock isochron data, have indicated that the emplacement of the Nigerian pegmatites occurred mainly after the wanning phase of the Pan-African tectono-magmatic event around 562-534 Ma, with the associated granitoids showing emplacement age of 632 Ma.

Exploration for mineralised pegmatites has essentially relied on solid geological mapping and lithogeochemical approach, with very little efforts geared towards locating them under thick lateritic covers. The presence of deep residual profiles over pegmatites, the occurrences of both barren and mineralised pegmatites within laterite-mantled Basement Complex units and the need to locate deeply buried rare-metal pegmatite deposits have invariably constrained exploration for rare-metal pegmatites to rather less direct approach (Galeschuk and Vanstone, 2005). Therefore, this research work largely seeks to understand the elemental mobility of pegmatite petrogenetic elements within residual profiles by comparing the chemistry and mineralogy of the bedrock pegmatites with their corresponding overlying residual weathering profiles. This is anticipated to show the mineralogical indicators and geochemical signatures that point to rare-metal bearing pegmatites underneath lateritic covers.

2.5 Review of pegmatite weathering and elements mobility in lateritic profiles

Thick lateritic profiles are widespread in inter-tropical regions of the world (Butt *et al*., 2000), and have been estimated to cover about one-third of the earth's continents (Fig. 2.8) (Bardossy and Aleva, 1990; Tardy, 1996; Smith *et al.*, 1997; Dequincey *et al*., 2002).

Although laterites are generally applied as geomaterials for construction purposes, the supergene metal enrichments of lateritic deposits have been noted to significantly contribute to the global mineral resource of Fe, Al, Cu, Ni, Mn, Co, Au, U, Zn, and Nb (Tardy, 1997; Elueze, 2003; Freyssinet, *et al.*, 2005; Robb, 2005).

In an attempt to replace the basic cations from various exchange sites of primary mineralphases of crystalline rocks with the hydrogen ions (H^+) from the meteoric agents,thermodynamic instability of the primary constituents in the crystalline rocks and their

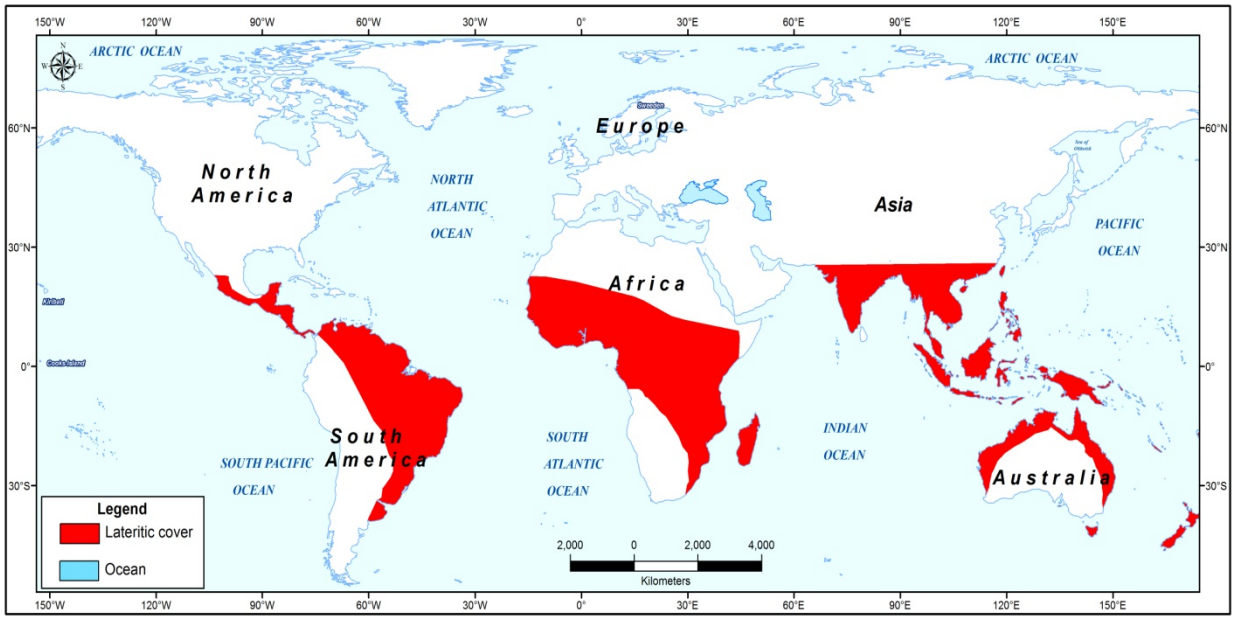

Fig. 2.8: Zone of development and preservation of lateritic cover across the world (modified after Bardossy and Aleva, 1990; Tardy *et al*., 1997)

possible associated proto-ores are invariably initiated in the surficial environment (Pierson-Wickman *et al*., 2009). This reaction initiates lateritisation processes in primary rocks, which essentially involve the dissolution of most soluble elements (especially basic cations), such as K, Na, Mg, Ca, Sr, Zn and some Si, and accumulation of less soluble elements, including Fe, Al, Ti, V, Cr, Zr, Ta, Nb, REEs (sometimes Mn, Ba, Co),notably as oxides, hydroxides and oxyhydroxides (Tardy, 1997; Freyssinet *et al.,* 2005). The chemical and mineralogical composition and the nature of petrological facies of the resulting laterites are indicative of the relative intensity/interplay of the principal controlsand mechanisms of formation of the laterite (Tardy, 1997; Butt *et al*., 2000, Giorgis *et al.,* 2014).

In situ chemical weathering of rock materials generally results in the sequential layering of regolith materials into differing compositional horizons, called lateritic profile. A lateritic profile represents the complete sequence of weathered rock material from the unweathered parent rock to the soil surface, which can generally be distinguished into five principal horizons: the weakly and isovolumentrically weathered saprock; the partially alteredsaprolitic layer, which still retains the fabric and structure of the parent rock; the clay-rich and mostly concretionary mottled zone; the loosely consolidated ferruginised lateritic layer and the organic matter-rich topsoil. In this thesis, the investigated profiles are represented by three principal horizons. These are the C, B and A horizons. The basal C-horizon comprises the saprock and the saprolite; the intermediate B-horizon (illuvial zone), which is made up of the mottled and lateritic layers; while the topmost A-horizon (eluvial zone) represents the organic matter-rich topsoil.

During lateritisation, rock-forming minerals and accessory phases show differential stability, solubility and chemical transformation from one phase to another. The susceptibility of different minerals to chemical dissolution is a complex phenomenon, but the principal controls include crystal lattice stability, the geochemical behavior of the constituting ions, surface chemical reaction of the mineral, degree of openness of the microsystems (cleavages, intermineral joints, microfractures and cracks) and the physico-chemical characters of the aqueous media (Afifa *et al*., 1985; Marshall and Herman, 1986; Krauskopf and Bird, 1995;

Nasraoui *et al*., 2000). The chemistry of the aqueous media exercises a greater control on the alterability of the individual mineral phases and the eventual weatherability of the crystalline rocks (Faure, 1991). Its effectiveness is largely influenced by the prevailing redox condition and its capacity to form complexes with ligands.

The interaction of the aqueous solution with crystalline rock constituents produces soluble labiles (commonly basic cations), slightly soluble solids (essentially Al and Fe-Mn oxides, hydroxides and oxyhydroxides) and insoluble residue (mostly quartz and other resistate accessory phases, such as zircon, rutile, monazite *etc*). During lateritisation, the weathered mantle acts as ionic exchange column, enhancing contemporaneous mixing of materials and ion exchange processes that eventually leads to geochemical fractionation of elements along weathering profiles. Here, water plays a critical role in the mobilisation, remobilisation and redistribution of elements, as it facilitates recrystallisation, geochemical readjustment, precipitation and co-precipitation and transport of materials at all scales (Kehinde-Phillip, 1991; Tardy, 1997). The principal controls on the mobility of elements in solution within regolith profiles include ability to form complexes with clays, Al and Fe-Mn oxides and oxy-hydroxides, Eh-pH condition and ambient temperature.

The late residual pegmatite melts show enrichment in HFSEs (Ti, Zr, Hf, Th, Y, U, Sn, Nb, Ta, W, Ga and REEs) and the LILEs (Rb, Sr, Cs, Ba). The HFSEs are essentially concentrated in the late exotic accessory minerals, such as cassiterite, (SnO_2), tourmalines, columbite $[Fe,Mn][Nb,Ta]_2O_6$, tantalite $[Fe,Mn][Ta,Nb]_2O_6$, euxenite $[Y,Ca,Ce,U,Th][Nb,Ta,Ti]_2O_6$, tapiolite $Fe(Ta,Nb)_2O_6$, wodginite $(Ta,Nb,Sn,Mn,Fe)_{16}O_{32}$, pyrochlore $([Ca,Na]_2[Nb,Ti,Ta]_2O_6[O,OH,F]$, beryl $(Be_3Al_2[Si_3O_{18})$, lepidolite $K(Li,Al)_{2-3}(AlSi_3O_{10})(O,OH,F)_2$, zinnwaldite $[KLiFe^{2+}\ Al(AlSi_3)O_{10}(F,OH)_2]$, zircon ($ZrSiO_4$),rutile ($TiO_2$), anatase ($TiO_2$), xenotime (HREE)$PO_4$, monazite ((Ce,La,Y,Nd,Th) PO_4}, and garnet, and show relative immobility in secondary geochemical environment. On the other hand, the feldspars and other essentially rock-forming minerals (except quartz and muscovite) of pegmatites are highly susceptible to chemical weathering processes. The bulk chemistry and the mineralogy of the fractionated horizons in pegmatite-derived weathering profiles will, amongst others controls, be essentially a reflection of the chemistry of the pegmatite

crystallising melts, the relative abundances of the essentially rock-forming minerals to the exotic accessory phases and the differential dissolution/weathering susceptibility of the various trace element host mineral phases.

Element behaviours during weathering are commonly described and evaluated, based on weathering indices and geochemical mass balance values (Nesbitt and Young, 1982; Nesbitt and Young, 1984; Nesbitt and Wilson, 1992; Ng, *et al*., 2001; Duzgoren-Aydin, 2002; Aristizabal *et al.*, 2005; Ohta and Arai, 2007; Braun *et al.*, 2009; Li and Yang, 2010; Braun *et al.*, 2012; Gong *et al.*, 2013). Weathering indices are evaluated based on major oxide components of the bulk chemical data of the lateritic profile, while geochemical mass balance (expressed as percentage gain or loss and commonly denoted by X_{gp} or τ) estimation utilises the major and trace element components.

To quantitatively evaluate the chemical weathering intensity of lateritic profiles, different weathering indices have been proposed, based on bulk chemical data of weathering profiles. These range from parent-normalised index, such as weathering intensity scale (WIS) (Meunier *et al*., 2013) to non-normalised indices, including chemical index of alteration (CIA) (Nesbitt and Young, 1982), weathering index of Colman (WIC) (Colman, 1982) and weathering index of Parker (WIP) (Parker, 1970). However, Gong *et al*. (2013) proposed and applied weathering index of granite (WIG) to distinguish between normal trace-element enrichments in regoliths, which usually accompany lateritisation processes and the anomalous trace element contents that emanate from the presence of orebodies in bedrocks, which can be utilised as exploration targets.

Owing to their relative immobility and conservative geochemical behaviour in weathering systems, Zr, Hf, Sc, Ti, Nb, Ta, and Th are generally employed to evaluate geochemicalmass balance (elemental depletion and enhancement or elemental loss or gain) of other elements in lateritic profile (Taylor and Mclennan, 1985; Braun *et al*., 1990; Brimhall *et al*., 1991; Beauvais and Colin, 1993; Braun *et al*., 1993; Mathieu *et al*., 1995; Koppi *et al*., 1996; Braun *et al*., 1998; Sheldon and Tabor, 2009; Gong *et al*., 2011; Du, 2012; Du *et al*., 2012 and Nardi *et al*., 2013; Xiao, 2013). Geochemical mass balance calculation assumes a genetic

relationship between the lateritic profile and the parent bedrock, as well as fully conservative reference element (Brimhall *et al.* 1991; Du, 2012)

In this thesis, chemical index of alteration (CIA) (Nesbitt and Young, 1982) was utilised to evaluate weathering intensity and the degree of lateritisation of the investigated lateritic profiles.

CHAPTER THREE

METHODOLOGY

3.1. Geological field mapping

The geological field investigations of the study areas were carried out at various times between 2013 and 2015. Topographic maps produced by the Federal Surveys of Nigeria on a scale of 1:50,000 were used for the geological mapping. These included Ado-Ekiti Standard Topographic Sheet (STS) 278, Akande STS 219, Ikomu STS 220, Igangan STS 240 and Ilesha STS 262. Traverses were made on foot using available footpaths and lateritised roads.

Outcrops, sampling sites and important geological features were located using global positioning system (GPS). Digital camera was employed to obtain photographs of the various geological features observed in the field; while compass/clinometer was used for measurement of strikesand dips of planar structures and directions and plunge of linear features.Fresh rock samples were chipped from outcrops with the useof sledge hammer, while laterite samples were collected from selected pegmatite weathering profiles. The samples collected were labeled according to their sampling locations, while brief descriptions of the sampled lateritic profiles were made to enhance proper interpretation of the compositional data.

3.2 Sampling and sample preparation

One hundred and twenty-three (123) fresh representative lateritic samples, each weighing 1.0 kg, were collected from horizons of selected vertical weathering profiles over mineralised and barren (simple) pegmatitebedrocks. These samples were collected using hand auger at regular intervals of 20.0 cm in freshly opened mine workings and hand-dug pits. The depths of collection vary between 4.0 and 6.4 m. The first 0-20.0 cm top soil layers were not sampled to avoid extraneous dry organic matter and coarse quartz

fractions from interfering with the sample quality. Thirty-seven (37) bedrock pegmatite samples (>5.0 kg) were collected from exposed outcrops directly underlying the profiles, while 2.0 kg each of associated rock samples were also collected.

The lateritic profile samples were air-dried, disaggregated and homogenised in a porcelain bowl. These were sieved through 2.0 mm mesh to eliminate waste and quartered by a rotary divider. Representative fractions for X-ray diffraction (XRD) studies were pulverised using an agate mortar and pestle; while the fractions for other geochemical analyses were pulverised to <2 μm in a tungsten carbide mill. Thirty-seven (37) selected bedrock pegmatite samples were crushed using a steel jaw crusher and powdered in a tungsten carbide mill. Samples of feldspars, muscovite, and columbo-tantalites wereseparated manually from the whole-rock pegmatites. Binocular microscope was used to ascertain that they were unaltered and inclusion free. The parent rock types and their localities, as well as the representative lateritic samples and mineral separates analysed are summarised in Table 3.1.

3.3 Mineralogical analyses

3.3.1 Petrographic analysis

Pegmatites and associated rock types in the study areas were selected and cut into thin sections at the Steinmann Institute for Geology, Mineralogy and Palaeontology, University of Bonn, Germany and at the Department of Geology, Obafemi Awolowo University, Ile-Ife, Nigeria. The procedure involves cutting the rocks into small chips. The chips were grinded on carborundum (silicon carbide) to produce smooth surface and placed on a hot plate to dry. The dried chip was glued to a glass slide and allowed to dry overnight. The grinding of the rock chip continued with carborundum until a uniform thin slice of about 0.03 mm was achieved. The obtained thin slice was washed to remove the grinding powder and dried. The rock slice was then covered with Canadian balsam, and placed on a hot plate to dry. Excess Canadian balsam was washed off with acetone to obtain a clean thin section. A cover slip was then placed over the thin section.

The thin sections were observed in transmitted light, using a Nilkon ECLIPSE E600 POL microscope with a Nilkon Digital Sight DS-U1 camera installed with an NIS-Element-D

Table 3.1: Distribution of samples collected for analyses

SN	Rock type	Locality	Profile No	Parent rock samples	Laterite samples	K-feldspar	Muscovite	Tantalo-columbite
1	Pegmatite (mineralised)	Ijero	1	5	27	5	5	5
2	Pegmatite (mineralised)	Komu	2	5	23	5	5	5
3	Pegmatite (mineralised)	Ofiki	3	10	32	5	5	4
4	Pegmatite (mineralised)	Iwere	4	10	20	5	5	4
5	Pegmatite (Non-mineralised)	Osu	5	7	21	5	5	-
		Total	5	37	123	25	25	18

Total number of samples =228

software, for photomicrograph production. Petrographical and mineralogical examinations of the thin sections were made under plane and cross polarised light. The optical characteristics, such as colour, pleochroism, relief, cleavage, twinning, interference colour and other pertinent optical properties of the minerals were used in identifying mineral grains in the thin sections.

3.3.2. X-ray Diffraction (XRD) analysis

The mineralogical composition of selected one hundred and twenty-three (123) powdered lateritic samples was determined by routine XRD analysis at the Steinmann Institute for Geology, Mineralogy and Palaeontology, University of Bonn, Germany. The instrument utilised was a Siemens D 5000 Bragg-Brentano diffractometer with a scintillation detector, using Ni-filtered CuKα radiation at 40 kV and 40 mA. Diffraction patterns were collected at room temperature (298 K) in the angular range of 4º to 70º 2θ with a step size of 0.02/s.

Qualitative identification of the mineral phases in the diffraction pattern data was achieved, using the Bruker AXS DIFFRAC EVA 4.0 software; while the quantitative estimation of the mineral phases was performed by Rietveld method, following Hill and Howard (1987), using DIFFRAC TOPAS 4.2 software from Bruker AXS. X'pert High Score software was employed for further examination of diffraction peaks and identification of mineral phases by comparison with International Centre for Diffraction Data (ICDD) files (Brindley and Brown, 1980; Moore and Reynolds, 1997).

3.4 Geochemical analyses

The chemical compositions of the whole-rock pegmatites and their respective *in situ*-derived lateritic profiles were established by a combination of determinative techniques. The mineral chemistry of some selected discrete mineral phases in the pegmatites was also investigated, in order to determine their mineralisation potential for possible distinction between mineralised and barren pegmatites. Chemical Index of Alteration (CIA) of the weathering profiles was determined from their bulk chemical data to quantitatively evaluate the degree of chemical weathering (Appendix 3).

3.4.1 Bulk chemical analyses

3.4.1.1 Loss on Ignition (LOI)

Thirty-seven(37) whole-rocks and one hundred and twenty-three (123) soil samples were crushed in a steel jaw crusher and subsequently pulverised in an ethanol precleaned tungsten carbide mill. Contamination of trace elements during the crushing and pulverising processes were restricted to tungsten and cobalt. The powdered samples were dehydrated at 105ºC in an oven for about eighteen hours to eliminate the intergranular water (H_2O^-). 3.0 g of each of the dehydrated sample powder was ignited for one hour in a furnace at 1100ºC to expel the structural water (H_2O^+) and other volatiles. Each sample was left to cool in a desiccator for about forty-five minutes, after which loss on ignition values were determined gravimetrically.

3.4.1.2 X-ray Fluorescence (XRF) Spectrometry

The concentrations of the major (Si, Al, Fe, Mn, Ti, Mg, Ca, Na, K, and P) and trace (Ga, Rb, Sr, Y, Nb, Cs, Ba, Th, U, La, Ce, Nd, Zn, Zr, and Sm) elements in the pulverised whole-rocks and lateritic samples were determined by XRF method. The procedure involves the preparation of fused glass discs by mixing 0.40 g of each sample powder with 4.0 g of the flux (Hoechst-Wachs Spectroflux, 66 % di-lithium tetraborate and 34 % lithium metaborate) and 1.0 g of oxidant ($LiNO_3$), and melted in platinium crucibles in a PANalytical Eagon 2 fusion machines at 1100ºC. The respective melts were cast into platinium molds and allowed to cool for about five minutes to form stable glass beads. The pressed powder pellets were obtained by mixing 1.0 g of respective sample powder with 5.0 g of the flux (Hoechst-Wachs spectroflux); these were thoroughly homogenised and prepared into mechanically pressed pellet samples.

The resultant fused glass discs and the pressed powder tablets were respectively analysed for major and trace element contents, using a PANalytical AXIOS wavelength-dispersive X-ray fluorescence spectrometer at the Steinmann Institute for Geology, Mineralogy and Palaeontology, University of Bonn, Germany. The instrument works with a side-window Rh-tube with max 30 kV, max 1 mA and max 9 W, a wavelength dispersive Si-drift detectors and a sample chamber with He-flush for better detection limits and low

analytical errors. Measurement conditions were 9 kV, 350μA, no filter, 600 s measurement time for Na, Mg, Al, Si, P,K, Ca, and 14 kV, 250μA, thin Al-filter, 300 s measurement time for Ti, Mn and Fe. Forty-four international standards were utilised for calibrations for the major elements, while three PANalytical standards were employed for trace element calibrations. The raw data were processed with the IQ+ software for the major elements, while ProTrace software was used for the trace elements. These softwares were also utilised to screen the standards and the unknown. The SuperQ qualitative software control programme was employed for interpretations. The lower limit of detection is better than 0.004 wt. % for the major elements, while that of the trace elements is generally below 0.5 ppm. The relative analytical error is generally below 0.4 % for major elements, while that of trace elements is generally below 5 %.

3.4.1.3 Inductively Coupled Plasma-Atomic Emission Spectrometry (ICP-AES) and Inductively Coupled Plasma-Mass Spectrometry (ICP-MS) Analyses

Determination of the major (Si, Al, Fe, Mn, Ti, Mg, Ca, Na, K, and P), trace (Zn, Ba, Sr, Li, Be, Rb, Cs, Sn, Nb, Ta, Y, Ga, Zr, Hf, U, Th) and rare-earth (La, Ce, Pr, Nd, Sm, Eu, Gd, Tb, Dy, Ho, Er, Tm, Yb and Lu) element compositions of the pulverised whole-rock pegmatite and lateritic samples was undertaken at ACME Laboratories, Vancouver, Canada, using a combination of ICP-AES and ICP-MS, respectively. The applicable fusion and decomposition procedures, as outlined in the 4A+4B (ICP-AES and ICP-MS) analytical package of the Laboratory (www.acmelabs.com, accessed March, 2016), involve the fusion of 0.2 g of each powdered sample with lithium metaborate / lithium tetraborate (flux reagents) plus the subsequent digestion of the fused aliquots in hot concentrated nitric acid for the eventual simultaneous ICP-AES and ICP-MS analyses. Replicate analyses were respectively performed, using six STD DS9, six STD SO-18 and four OREAS45CA certified reference materials. The uncertainty on the external reproducibility of the analysis was within ±5 relative %; while the detection limit for the major elements is 0.01 % and that of the trace elements ranges between 0.1 and 5 ppm.

For the trace element determination of the laterite samples, ultra trace ICP-MS (MA250 analytical package) of ACME laboratories was employed for complete dissolution of the

refractory minerals (zircon, rutile, columbite, tantalite, tourmaline, magnetite, monazite *etc*). This involved the digestion of 0.25 g of each sample powder in a mixture of fluoric (HF), nitric (HNO_3), perchloric ($HClO_4$) acids. The obtained digestates were each heated to incipient dryness and the residues were respectively dissolved in hot concentrated hydrochloric (HCl) acid. The resultant solutions were subsequently subjected to ultra trace ICP-MS analysis. Replicate analyses of fifteen prepared international standards (STD OREAS25A) were performed during the trace element determination. The detection limit for the trace elements ranges from 0.1 ppb to 1 ppm.

3.4.2 Microchemical Analyses

The K-feldspar and muscovite mineral separates were obtained by disaggregation of the representative whole-rock pegmatite samples, while the columbo-tantalite ore samples were collected from surface exposures, pegmatite weathering crust and from fresh whole-rock samples. Due to the composite nature of most mineral phases in pegmatites, accurate and sensitive micro-analytical techniques are required to precisely determine the mineral chemistry of the discrete mineral phases in pegmatites. As a result, representative K-feldspar, muscovite and tantalo-columbite mineral samples for microchemical analyses were screened with the aid of stereoscopic microscope to avoid contamination, such as albitic, perthitic lamellae and microscopic sericite alteration in K-feldspar and some metallic oxide inclusions in muscovite samples. The unaltered and inclusion-free mineral separates were subsequently mounted in epoxy resin before being polished for the EMPA and LA-ICP-MS microchemical analyses.

3.4.2.1 Electron Microprobe Analysis (EMPA)

Polished sections were cleaned in deionised water and ethanol using ultrasonic baths. These were subsequently carbon-coated and subjected to EMPA analysis. The concentrations of SiO_2, Al_2O_3, MgO, Na_2O, K_2O, FeO, MnO, CaO, TiO_2 and P_2O_5 were determined in the K-feldspar and muscovite samples; while WO_3, Ta_2O_5, Nb_2O_5, SnO_2, TiO_2, FeO, MnO, UO_2 and ThO_2 were analysed in the columbo-tantalite ore samples, using a JEOL JXA-8200 superprobe electron microprobe analyser fitted with five wavelength-dispersive spectrometers (WDS) and one energy-dispersive spectrometer

(EDS) at the Steinman Institute for Geology, Mineralogy and Palaeontology, University of Bonn, Germany. Backscattered electron (BSE) images were used to select analytical points to avoid intergrown phases. Fifty to seventy spots per grain were analysed using accelerating voltage of 15 keV, beam current of 20 nA and a beam diameter of 1 μm. Counting time for background and peak determinations were 10 s and 40 s, respectively for the various analysed elements.JEOL set of synthetic and natural minerals and USGS VG-2 glasswere employed as standards. Data reduction was achieved using standard ZAF correction.Detection limits (3σ) above mean background were less than 0.03 wt. % for most oxides.

3.4.2.2 Laser Ablation-Inductively Coupled Plasma-Mass Spectrometry (LA-ICP-MS)

The polished mounts were screened using EMPA to identify suitable analytical spots for trace element determinations by LA-ICP-MS. *In situ* trace element concentrations of the K-feldspar and muscovitesamples were measured by LA-ICP-MS, using a M50-E Resonetics 193 nm Excimer laser attached to a Thermo Element XR single-collector ICP-MS at the Steinmann Institute for Geology, Mineralogy and Palaeontology, University of Bonn, Germany. The analyses were carried out using spot size of 100 μm, with a laser repetition rate set at 15 Hz, while energy density or fluence was measured at 7-8 J/cm^2. Count rates were normalised using ^{29}Si as the internal standard and were converted to concentrations using the reference materials NIST-SRM 610 silicate glass as external standard. During analyses the concentrations of the following isotopes were measured: ^{7}Li, ^{9}Be, ^{11}B, ^{29}Si, ^{43}Ca, ^{66}Zn, ^{69}Ga, ^{85}Rb, ^{88}Sr, ^{89}Y, ^{90}Zr, ^{91}Zr, ^{93}Nb, ^{118}Sn, ^{133}Cs, ^{137}Ba, ^{138}Ba, ^{139}La, ^{140}Ce, ^{141}Pr, ^{143}Nd, ^{146}Nd, ^{147}Sm, ^{151}Eu, ^{153}Eu, ^{157}Gd, ^{159}Tb, ^{163}Dy, ^{165}Ho, ^{166}Er, ^{172}Yb, ^{175}Lu, ^{178}Hf, ^{180}Hf, ^{181}Ta, ^{182}W, ^{232}Th and ^{238}U.

3.5 pH and Eh determinations

The pH and Eh of the pulverised representative bedrock and residual lateritic soil samples were determined, following the procedures specified in the Compendium of the German Soil Science Society. 10 g of dried soil sample (at 22.5 ºC) was each mixed with 50 ml of water in transparent plastic bottles. These 1:5 mixtures were placed in a shaker for one hour. Sample bottles were allowed to stand for one hour before pH and Eh measurements.

The pH meter was calibrated with buffer solutions of pH 4 and pH 7, respectively. The pH and Eh determinations were then performed with standard pH and Eh probes. Replicates of each sample were within ± 0.05 pH unit and ± 0.02 Eh unit, respectively.

The pH measurement of the residual profiles was undertaken in order to observe the variation in pH with depth and also to infer the geochemical behavior of elements with changes in the pH. The Eh determination was essentially carried out to evaluate oxidation and reduction potentials of some selected charged ions in response to oxidising and reducing characteristics of the weathering environment.

3.6 Statistical analyses

3.6.1 Descriptive statistical techniques

The bulk chemical and mineralogical data of rock and lateritic soil samples in this study were subjected to various basic statistical methods. These include mean, ranges and bar charts employed for comparison of values; while bivariate plots were utilised to identify important geochemical trends and ternary plots explored to amplify subtle variation trends amongst key plotting geochemical parameters. The bivariate plots were accomplished using Microsoft EXCEL 2010; while the ternary plots were drawn with Tridraw 2.6.

3.6.2 Statistical technique of correlation

Correlation analysis is widely used in geochemical data treatment for estimating interelement associations in a vast array of geochemical data sets. It essentially measures the strength of the linear relationship between two elements in a population, without any suggestion that one of the elements is dependent on the other (Rollinson, 1993; Ogunleye *et al*., 2004). The degree of interelement associations in a given geochemical data set may be quantified, using the Pearson product-moment coefficient of linear correlation, *r*.

As indicated by Rollinson (1993), cases of numerous values of some given elements, which are commonly expressed as *n* values of variable x ($x_1 \ldots x_n$) and of variable y ($y_1 \ldots y_n$), generally have *r* statistically computed as:

$$r = CSCP/\sqrt{(CSSX \,.\, CSSY)}$$

where CSCP (corrected sum of cross products) = $\sum(xy) - \sum(x).\sum(y)/n$

CSSX (corrected sum of squares for x) = $\sum(x^2) - \sum(x).\sum(y/n$

CSSY (corrected sum of squares for y) = $\sum(y^2) - \sum(y).\sum(y)/n$

The underlying assumption of the correlation coefficient is that the values of *r* vary between -1 and +1. When r value is closer to1, strong positive correlation is indicated by any two given element pairs. Values of *r* meandering around 0.5 and 0.6 reveal moderately correlated element pairs, while *r* = 0 signifies no relationship between any two given elements. Values of *r* approaching -1 is an indication of strong negative correlation between any two given element pairs.

The bulk geochemical data obtained from the respective pegmatite residual profiles were subjected to Pearson product-moment coefficient of linear correlation, using the Statistical Package for Social Sciences (SPSS 10 for Window ®). The significance of correlation coefficient was drawn at 0.05 level, which indicates 5% or less chance that the result could have been obtained if null hypothesis was true. The null hypothesis in this case would be that two particular elements are not related (Hill *et al.*, 2000).

The derived correlation coefficients for major, minor and trace elements are presented as correlation matrices, which provide useful statistical information employed to: (1) unravel geochemical patterns related to enrichment/depletion of the constituent elements within the respective weathering profiles; (2) identify and isolate consistent and highly correlative element pairs (as discriminating variables) that can be explored in deriving suitable geochemical ratios and in plotting relevant discrimination diagrams, to distinguish between rare metal-bearing and barren pegmatite bedrocks beneath lateritic covers.

CHAPTER FOUR

RESULTS AND DISCUSSION

4.1 Geology of the study areas

The areas of investigation were selected within the reactivated Precambrian Basement Complex of southwestern Nigeria (Fig. 1.1). These areas include Ijero, Komu, Ofiki, and Iwere-Ile, which are located within pegmatite mining districts; while Osu area is non-pegmatite mining area but marked by extensive occurrence of barren pegmatite bodies.

4.1.1 Osu area

The Osu area is located between Latitude 7º 32' - 7º 41' N and Longitude 4º 35' - 4º40' E, towards the western segment of the Ilesa schist belt. The rocks in Osu area are biotite schist, quartzite/quartz schist, amphibolites, chlorite schist, biotite granites and pegmatites (Fig. 4.1). These rocks are cut across by pegmatites, dolerite dykes and quartz veins.

Biotite schist

Fresh outcrops of biotite schist are rare dueto their high susceptibility to weathering. However, the relict schistose structure of the rock is commonly found preserved *in situ* in different localities in the area. The rock is dark coloured and medium to coarse-grained. The biotite schist grades into garnet-staurolite-biotite schist, as revealed by the preponderance of euhedral garnet and staurolite crystals in outcrop samples. Under the microscope, lepidoblastic laths of biotite are prominent (Fig. 4.2), while quartz, plagioclase and muscovite are other essential minerals. Porphyroblasts of garnet and staurolite are also evident in some thin sections (Fig. 4.3). Accessory minerals include apatite, zircon and opaques.

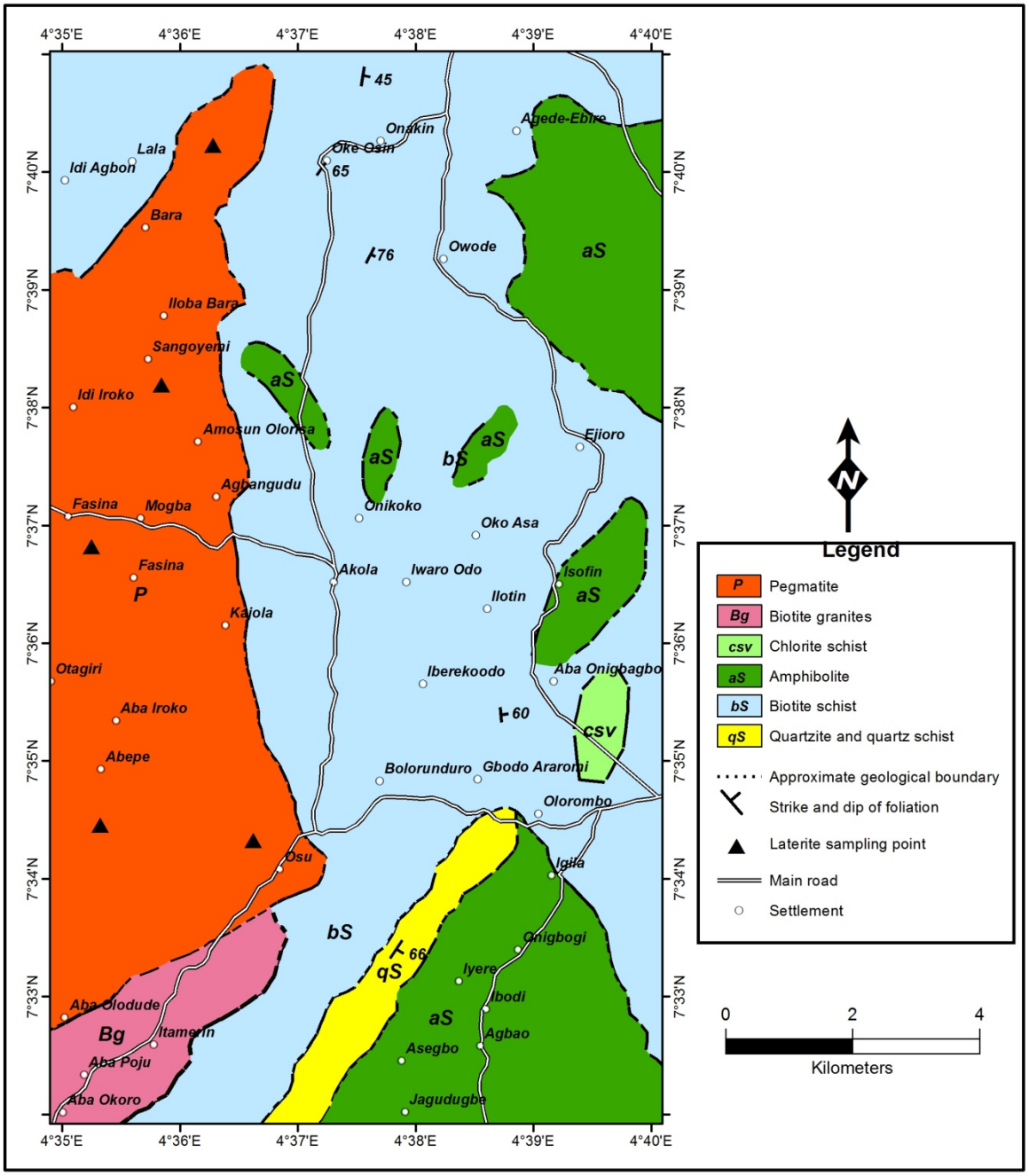

Fig. 4.1: Geological map of Osu area showing sample locations (modified after Elueze, 1986 and Kehinde-Phillips, 1991).

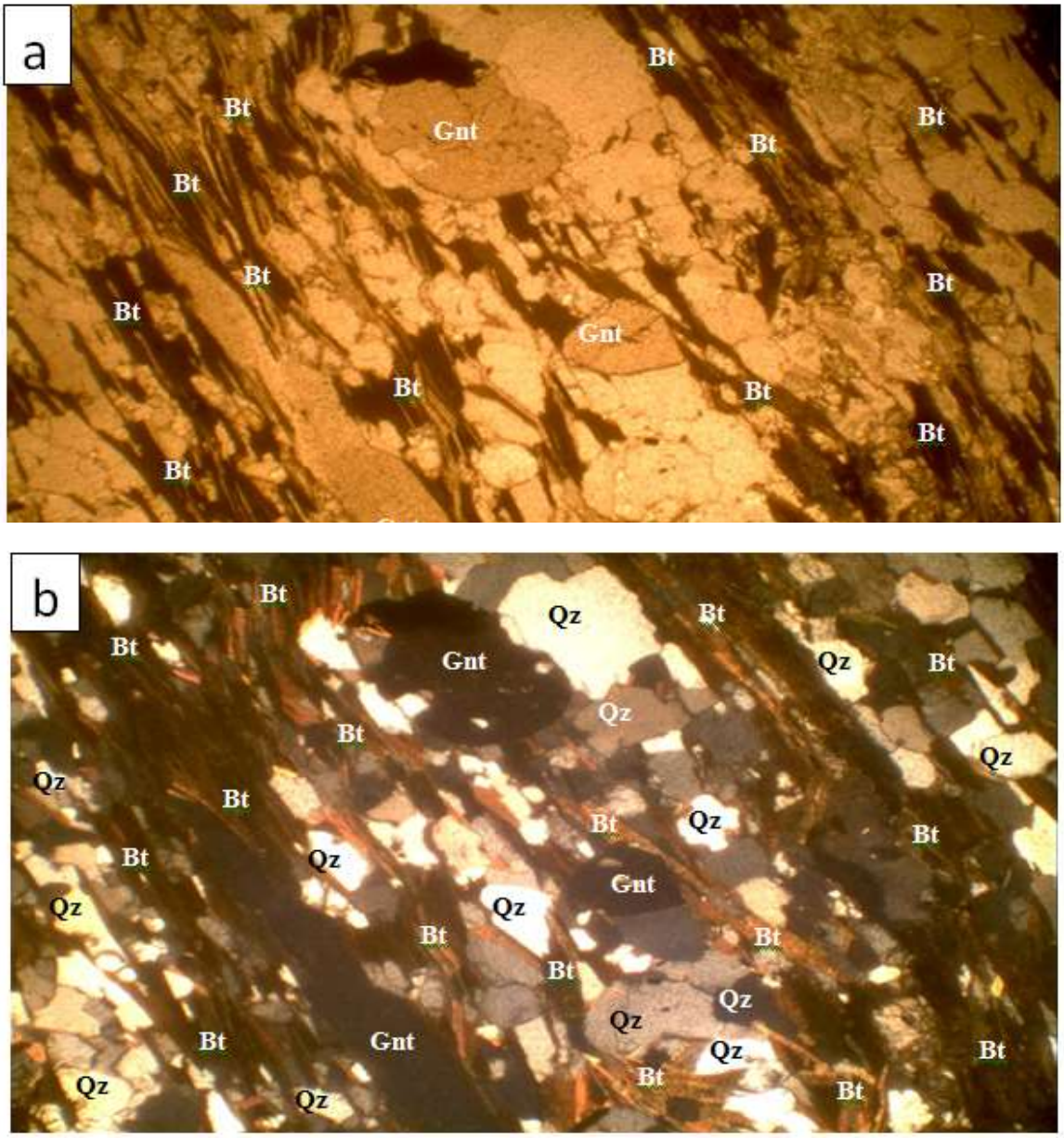

Fig 4.2: Photomicrographs of garnet-staurolite-biotite schist of Osu area, showing schistosity defined by lepidoblastic segregations of biotite laths, alternating with quartzofeldspathic-rich layers in (a) plane-polarised light and (b) under crossed nicols(Mag. x40). Note that quartz grains show subtle flattening parallel to the schistosity of the rock and also note the garnet porphyroblasts (Bt = biotite; Qz = quartz; Gnt = garnet).

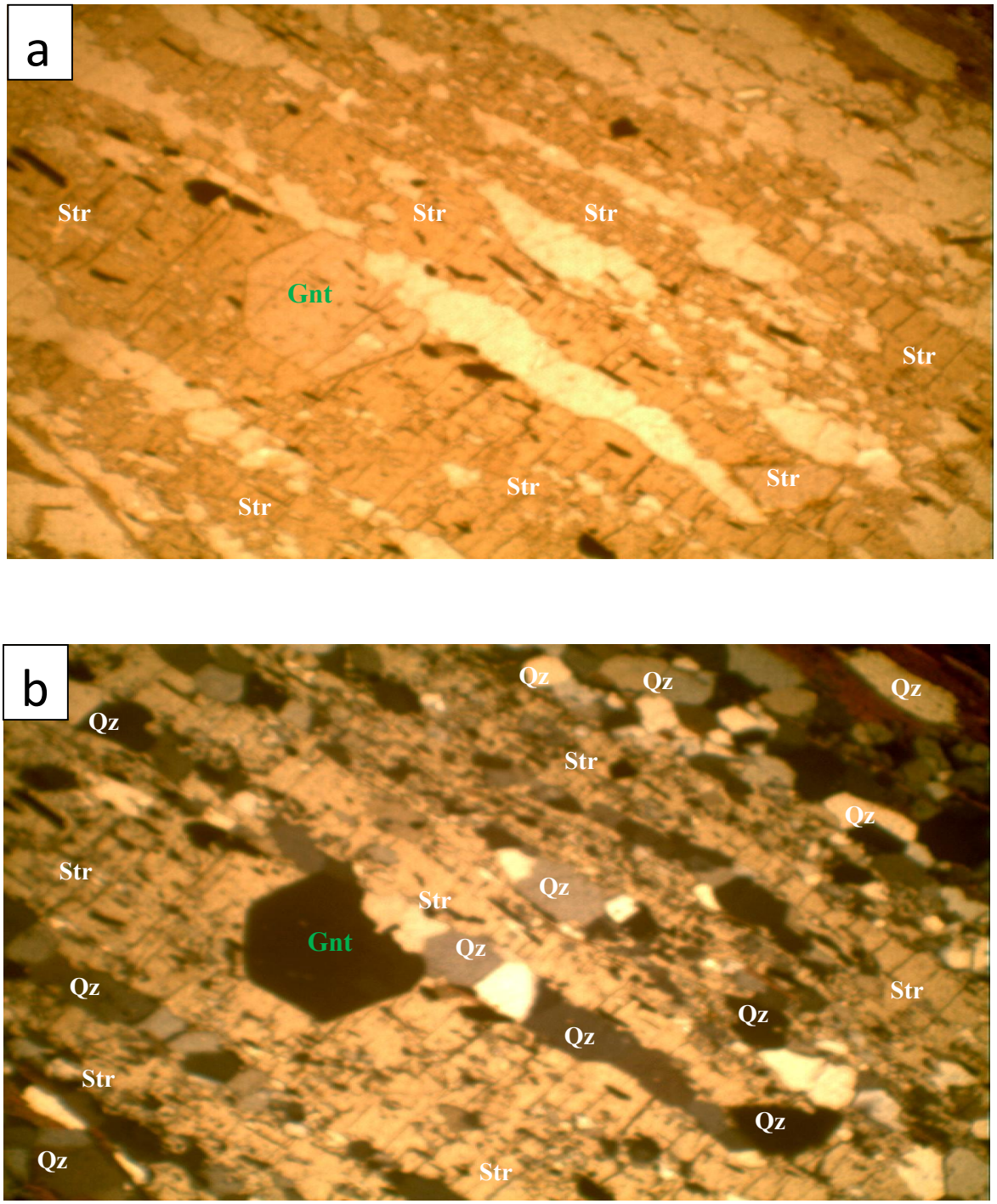

Fig 4.3: Photomicrographs of garnet-staurolite-biotite schist of Osu area showing poikiloblastic texture of staurolite in (a) plane-polarised light and (b) under crossed polars (Mag. x40). Note the inclusions of euhedral garnet crystal and some quartz grains within staurolite crystal (Mag. x40) (Bt = biotite; Qz = quartz; Gnt = garnet; and Str = staurolite).

Quartzite

Quartzite forms high topographic features, trending NE-SW in the south central part of the area. It is white to light yellow in colour and medium to coarse-grained. In places, quartzite shows intercalations with quartz schist. The quartz schist is fine to medium-grained, indicating alternate bands of granular quartz and thin layers of muscovite and biotite. Petrograhpic examination of the quartzite shows granoblastic texture of predominantly (95%) quartz crystals with minor muscovite grains and accessory opaque ores. Quartz grains indicate weak birefringence and very low relief, with characteristic undulose extinction.

Amphibolites

Amphibolites occur as ovoid-shaped bodies in the biotite schist of the area. Two textural varieties can be readily distinguished, which are the massive and foliated types. The massive amphibolite is dark coloured, medium to coarse-grained and massive in texture. The massive amphibolite with decussate texture is composed of hornblende and plagioclase feldspar, with subordinate amounts of quartz, accessory sphene, apatite and magnetite (Fig. 4.4a). The foliated amphibolite is dark grey in colour, fine to medium-grained and weakly foliated. The foliation is marked by separation of thick mafic layer and thin felsic bands. Petrographic studies indicate that the mafic layers are composed of nematoblastic plates of hornblende, while the felsic bands are mainly plagioclase feldspar with subordinate amount of quartz (Fig. 4.4b).

Chlorite schist is of restricted occurrence in the area. It is commonly found as bouldery exposures with very few outcrops preserved *in situ*. It is greenish in colour, weakly foliated and composed largely of chlorite with subordinate amount of quartz.

Biotite granites

Few granitic outcrops in the area showed fairly hilly topographic features. Two textural and mineralogical varieties can be distinguished, which are the medium to coarse-grained biotite granite and the fine to medium-grained biotite-muscovite granite. The granites are weakly foliated, and the foliation is marked by the orientation of mica foliae in generally northeasterly direction. Xenolithic inclusions of biotite schist and intrusive dolerite and

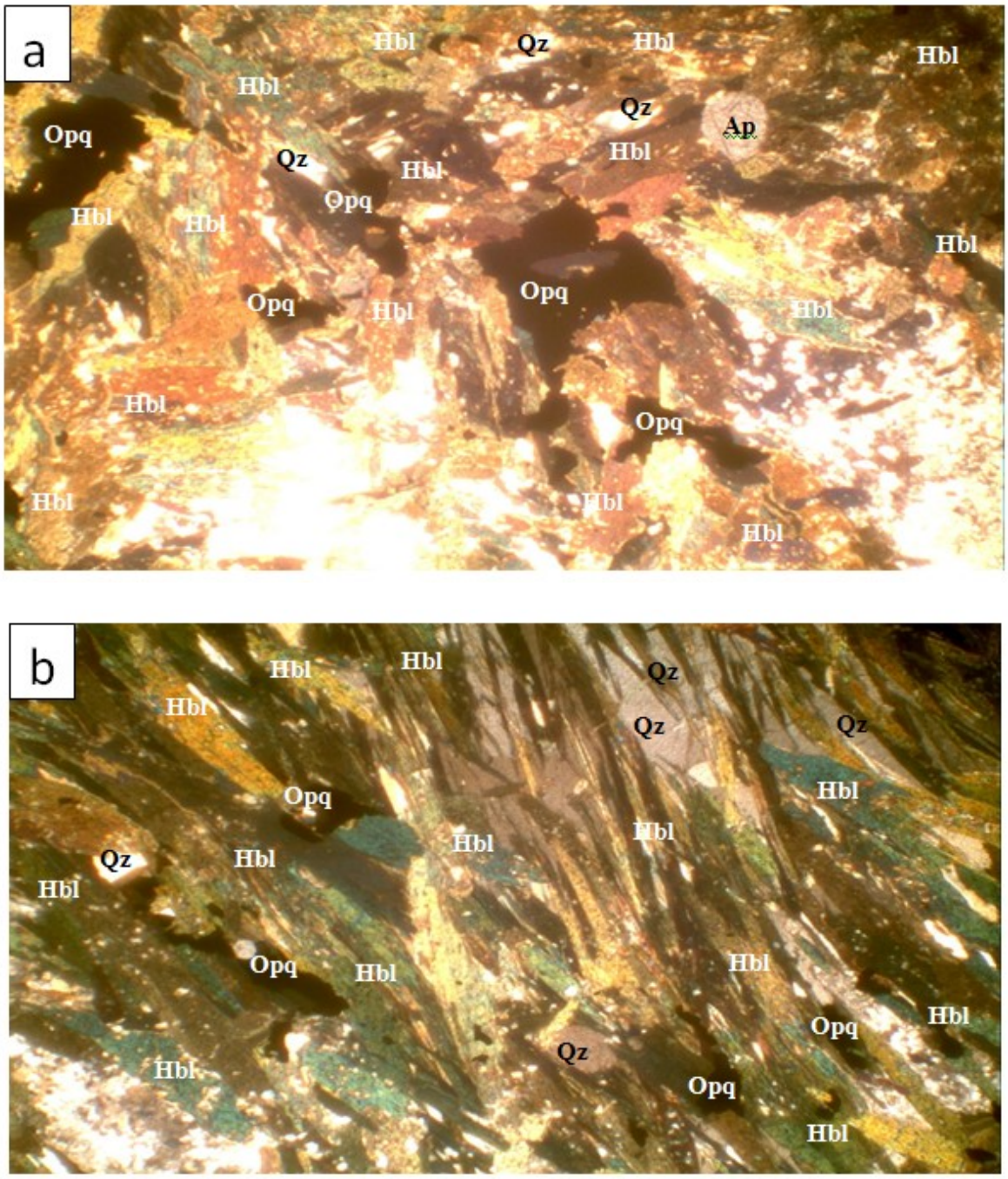

Fig. 4.4: Photomicrograph of (a) massive amphibolite of Osu area showing decussate texture of dominantly hornblende grains with minor amount of quartz, apatite and opaques; (b) foliated amphibolite of Osu area showing preferred dimensional orientation of the long axes of bladed and acicular hornblende grains in crossed-polarised light (Mag. x40) (Hbl = hornblende; Qz = quartz; Ap = apatite; and Opq = opaque)

pegmatite dykes are commonly found in the granites. Petrographic studies of the granites indicate allotriomorphic granular texture of mainly microcline, quartz, biotite, muscovite, and plagioclase (Fig. 4.5). Zircon, apatite, garnet, black tourmaline (schorl) and opaques are in accessory quantities. Microcline crystals show the characteristics tartan twinning and blebby inclusions of exsolved sodic feldspar. Partial seritic alteration is evident, while zircon and apatite inclusions are common in few microline grains (Fig. 4.5). Plagioclase display combined Carlsbad and albite twinning, while apatite inclusions are common in few grains. The plagioclase grains are of albite (An_{10}) to oligoclase (An_{15}) composition. Biotite occurs as subhedral to anhedral plates, showing pleochroism from brown to deep brown. Zircon inclusions are evident in some biotite crystals. Myrmekitic intergrowths are present at contacts of plagioclase and microcline grains.

Pegmatites

The pegmatite in Osuarea occurs as a north-south elongated massive body, intruding the biotite schist of the area (Fig. 4.1). It is restricted to the western part of the area. The pegmatite is a simple pegmatite composed mainly of microcline perthite, albite and quartz, with lesser amounts of muscovite and biotite (Fig. 4.6 and Table 4.1). Accessory minerals include garnet, black tourmaline (schorl), zircon and apatite. Graphic intergrowth of microcline perthite and quartz is preponderant in the pegmatite. The pegmatite is a barren type, as it lacks rare metal and gem minerals, and no mining activity is going on in the area. This is consistent with the views of Matheis and Caen-Vachette (1983) and Emofurieta *et al*. (1988).

Other pegmatite occurrences are mainly in form of small dykes and veins, intruding other rock types in the area.

Dolerite

Dolerite occurs as dykes cross-cutting the host lithologies of the area. It ranges in thickness from few centimetres to about 0.85 m. Petrographic studies of the dolerite revealed olivine, pyroxene and plagioclase crystals in finer matrix of pale brown pyroxene grains, plagioclase laths and opaques (Fig. 4.7). The olivine crystals are colourless, idiomorphic to sub-idiomorphic in shape, showing very high relief and high

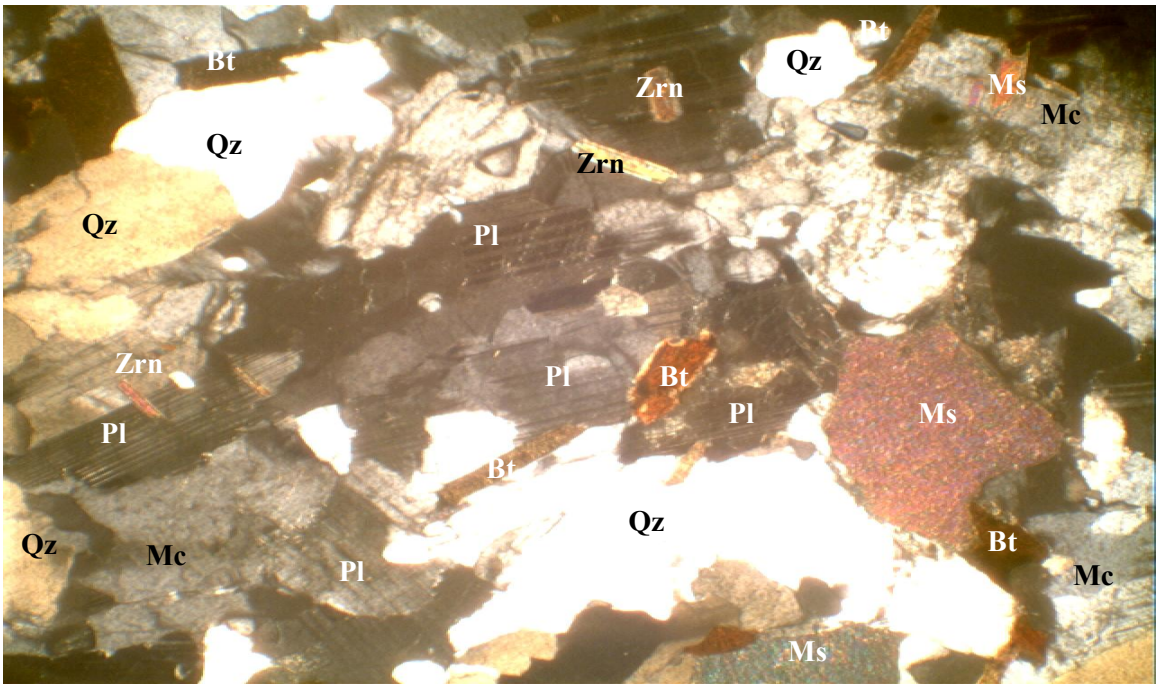

Fig. 4.5: Photomicrograph of the biotite-muscovite granite at Itamerin, Osu area, showing allotriomorphic granular texture of microcline, plagioclase, biotite, muscovite and quartz under crossed nicols (Mag. x40). Note the inclusions of euhedral and oscillatory zoned zircon crystals in the plagioclase crystal (Mc=Microcline; Pl= plagioclase; Qz= quartz; Bt=biotite; Ms = muscovite; and Zrn = zircon).

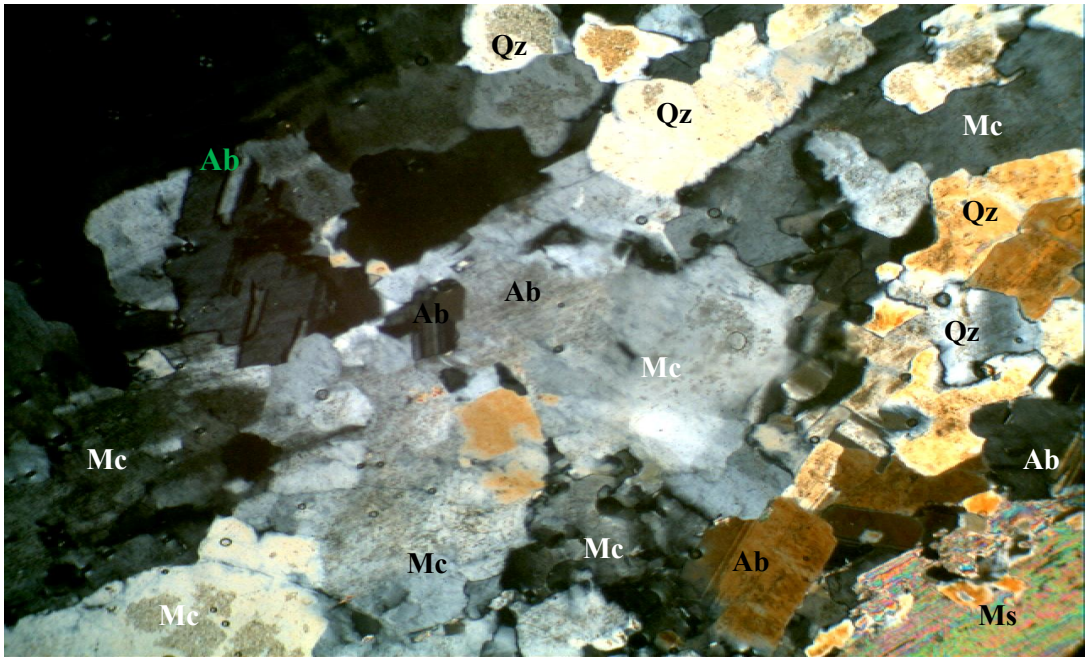

Fig. 4.6: Photomicrograph of pegmatite of Osu area, showing microcline-perthite, albite and quartz (Mag. x40). (Mc = Microcline; Qz = quartz; Ab = albite; Ms = muscovite).

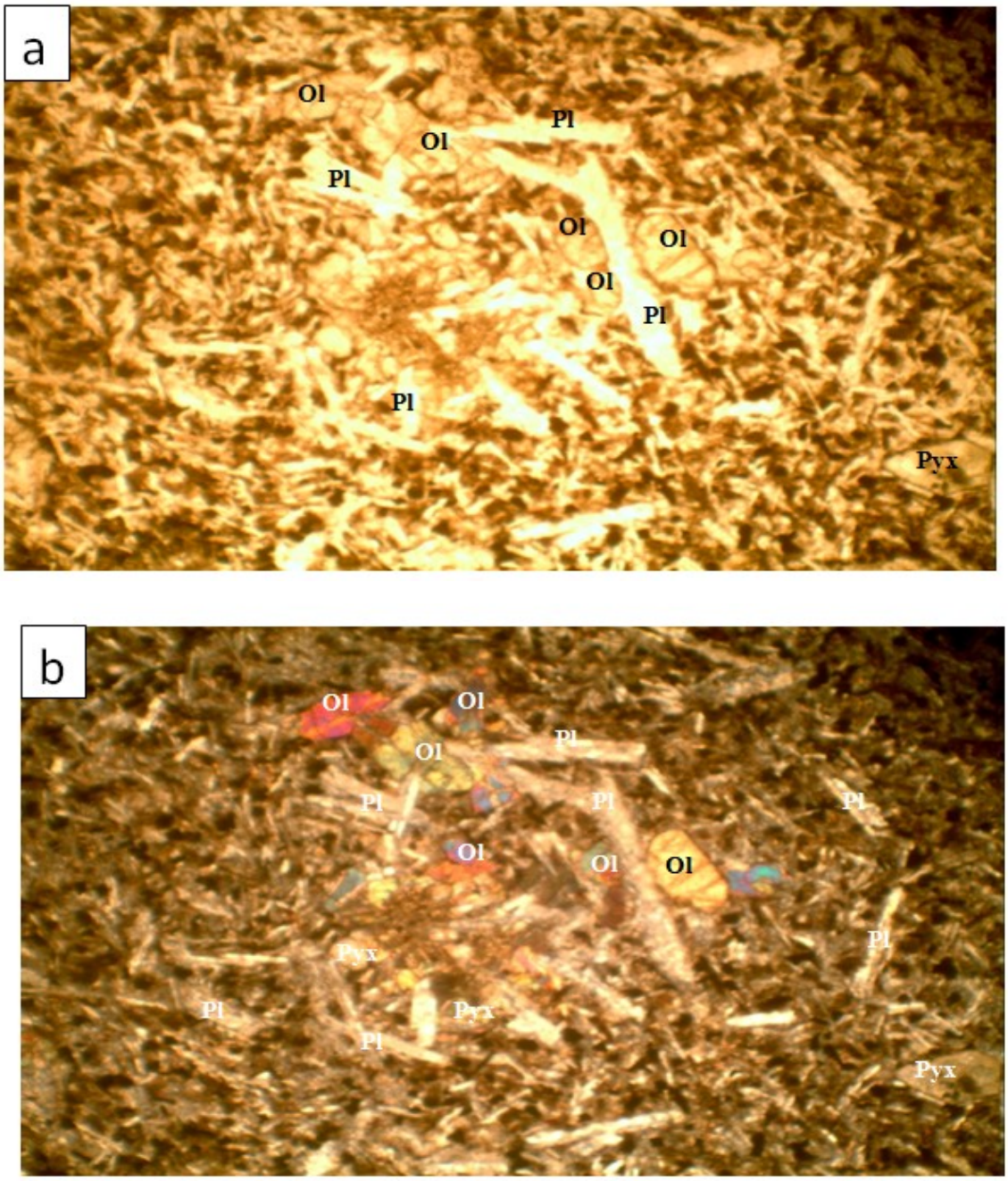

Fig. 4.7: Photomicrographs of dolerite at Osu area, showing porphyritic texture of subhedral olivine and pyroxene crystals and plagioclase laths in finer-grained matrix of pyroxene and plagioclase grains and opaques in (a) plane-polarised light and (b) under crossed-polarised light (Mag. x100). Note that the olivine crystal is thinly mantled by dark brownish iddingstite, a characteristic alteration product of the olivines. (Ol = olivine; Pl = plagioclase; and Pyx = pyroxene)

Table 4.1: Modal composition of the Osu barren pegmatite samples

	OS1	OS2	OS3	OS4	OS5	OS6	OS7
Microcline-pertithe	54	50	57	52	54	51	56
Albite	8	6	10	5	8	8	10
Quartz	26	32	28	32	27	30	26
Muscovite	6	5	2	6	5	6	4
Biotite	1	2	1	2	2	1	2
Schorl	2	2	1	-	1	1	-
Garnet	1	2	1	2	1	2	1
Total	98.0	99.0	100.0	98.0	98.0	99.0	99.0

birefringence. The rims of the olivines are altered. Plagioclase grains are lath-shaped. Both clino (augite) and ortho- (pigeonite) pyroxene were recognised in thin sections. The plagioclase is labradorite (An_{60}) in composition. Accessory constituents include magnetite, ilmenite and pyrite.

4.1.2 Ijero area

This area is delimited by Latitude 7º 46' and 7º 51' and Longitude 5º 01' and 5º 06', covering major towns, such as Ijero, Ikoro and Oke-Oro. Migmatitic gneiss, biotite gneiss and biotite schist dominate the basement rocks of the area, while amphibolite and quartzite constitute the minor exposures (Fig. 4.8). Intruding these rocks are pegmatite dykes and veins as well as vein quartz.

Migmatitic gneiss

Migmatitic gneiss outcrops towards the eastern part of the area. It is dark grey in colour, medium to coarse-grained and marked by alternate segregation of leucocratic and melanocratic bands. The feldspar and quartz-rich leucocratic layers form stringers (1 cm – 6cm wide) or bands that are locally up to 35 cm in width. These alternate with dark grey gneissic biotite-hornblende bands (locally up to 65cm wide), which are generally strongly foliated. Microscopic studies reveal biotite, hornblende, microcline, plagioclase feldspars (oligoclase to andesitic composition) and quartz as the essential minerals. Accessory constituents include garnet, zircon, epidote and magnetite.

Biotite gneiss

Biotite gneiss occurs mainly around Ikoro and Ijero areas. They are generally low-lying relative to the hilly and steeply dipping pegmatite bodies and migmatite gneiss of the area. The strike of the prevalent foliation, which is consistent with the regional trends, is generally NE-SW often with gentle dips to the east. The biotite gneiss is generally medium to coarse-grained. Light pinkish to grayish and weakly foliated variety is prevalent around Ikoro; while dark grey (biotite-rich) and strongly foliated type marks the occurrences towards the west of Ijero.

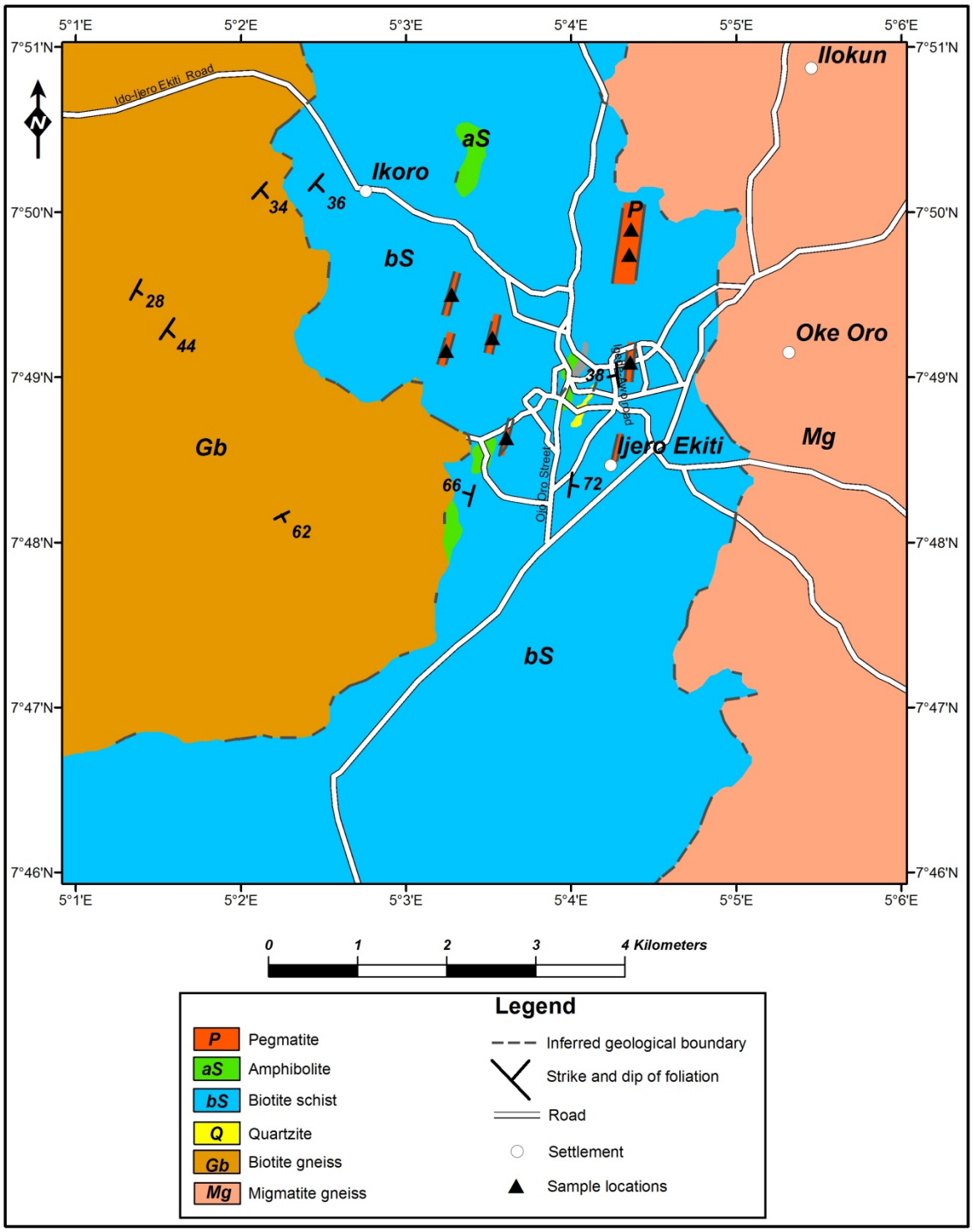

Fig.4.8: Geological map of Ijero area showing sample locations.

Thin section shows alignment of biotite laths and hornblende grains alternating with microcline, quartz and plagioclase (Fig. 4.9). Minor amount of orthoclase and muscovite with accessory garnet, zircon, apatite, sphene and opaques are also present. The biotite laths are pleochroic from brown to yellowish brown, while xenoblastic hornblende grains arepleochroic from green to yellowish green. Plagioclase crystals show polysynthetic twinning, alteration to sericite and zoned zircon inclusions. Microcline exhibits the characteristic cross-hatched twinning, with some of the crystals showing blebby exsolution lamellae of sodic feldspar. Apatite occurs as inclusions in some microcline crystals. Orthoclase is xenoblastic in shape and shows the marked Carlsbad twinning. Xenoblastic quartz shows undulose extinction and the characteristic first order yellow, white and gray interference colours. Euhedral sphene crystals are pleochroic from greenish yellow to pale green.

Biotite schist

Biotite schist occurrence is restricted to the central part of the study area, and is generally low-lying relative to other associated gneisses. The rock has suffered varying degree of weathering, and fresh rock exposures could not be observed. However, the relict schistose structure invariably indicates that it is medium-grained and marked by fair segregation of bands. The altered leucocratic bands are thin and whitish in appearance, indicating alteration of felsic components to kaolinite. These show alternation with relict thicker reddish brown melanocratic bands. The bands are concordant to the regional foliation trends, indicating NE-SW structural trends. Tabular pegmatites dykes intrude the biotite schist of the area.

Amphibolites

Amphibolite occurs as bands and lenses within the biotite schist of the area. In the central part of Ijero town (Fig. 4.8), bands of felsic and weakly foliated amphibolites were traced for several metres, while occurrences elsewhere are essentially dark grey and massive in texture and generally of bouldery exposures with few outcrops preserved *in situ*. Thin section of the felsic amphibolite reveals hornblende-rich bands alternating with plagioclase-quartz-rich bands (Fig. 4.10). Xenoblastic hornblende grains are pale green to

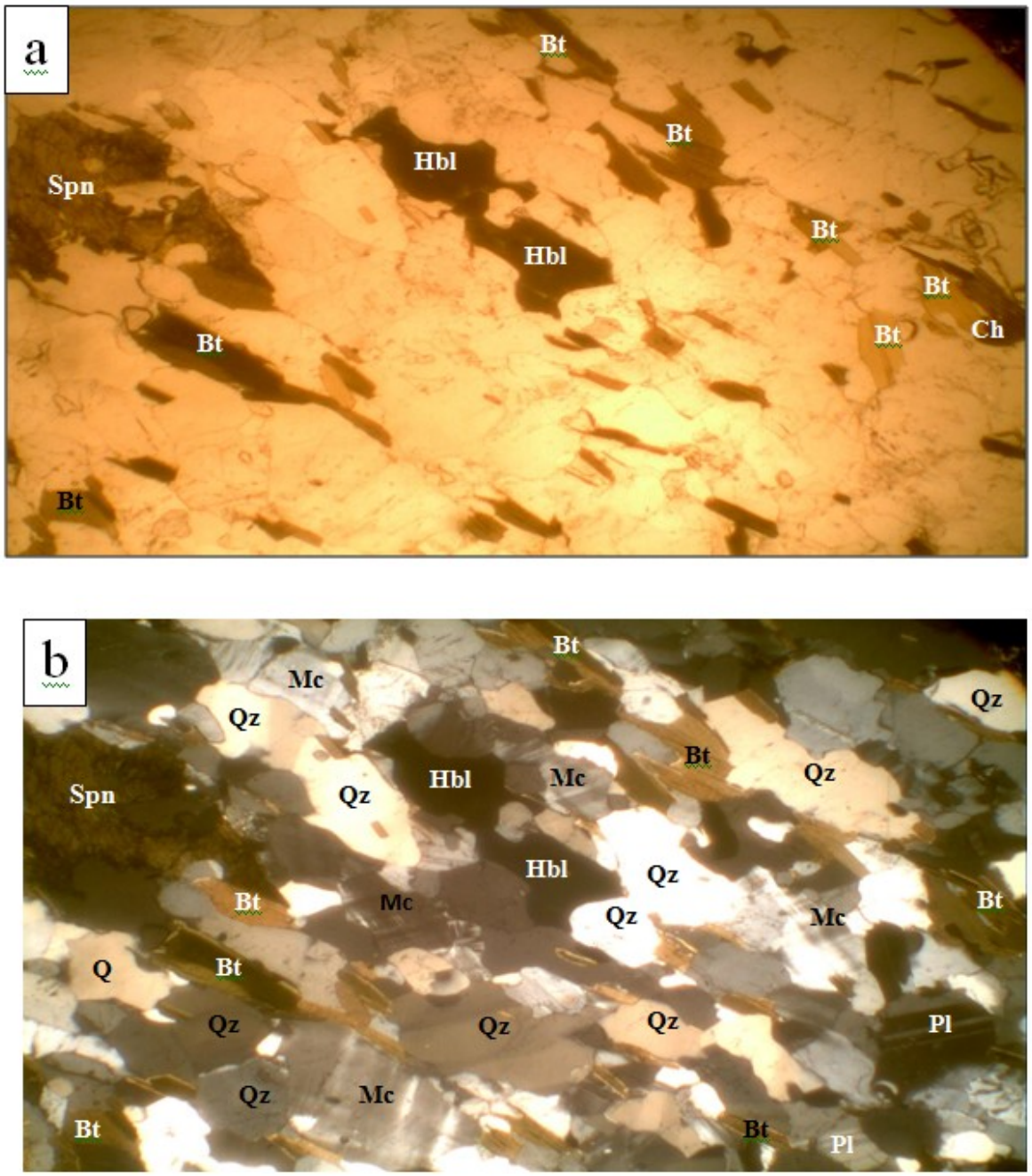

Fig. 4.9: Photomicrograph of biotite gneiss in Ijero area showing biotite laths and hornblende alternating with feldspar and quartz-rich bands under (a) plane polarized-light and (b) under crossed nicols (Mag. x40). (Bt = biotite; Hbl= hornblende; Sph = sphene; Qz=quartz, Pl=plagioclase, Mc=microcline, Ch = chlorite).

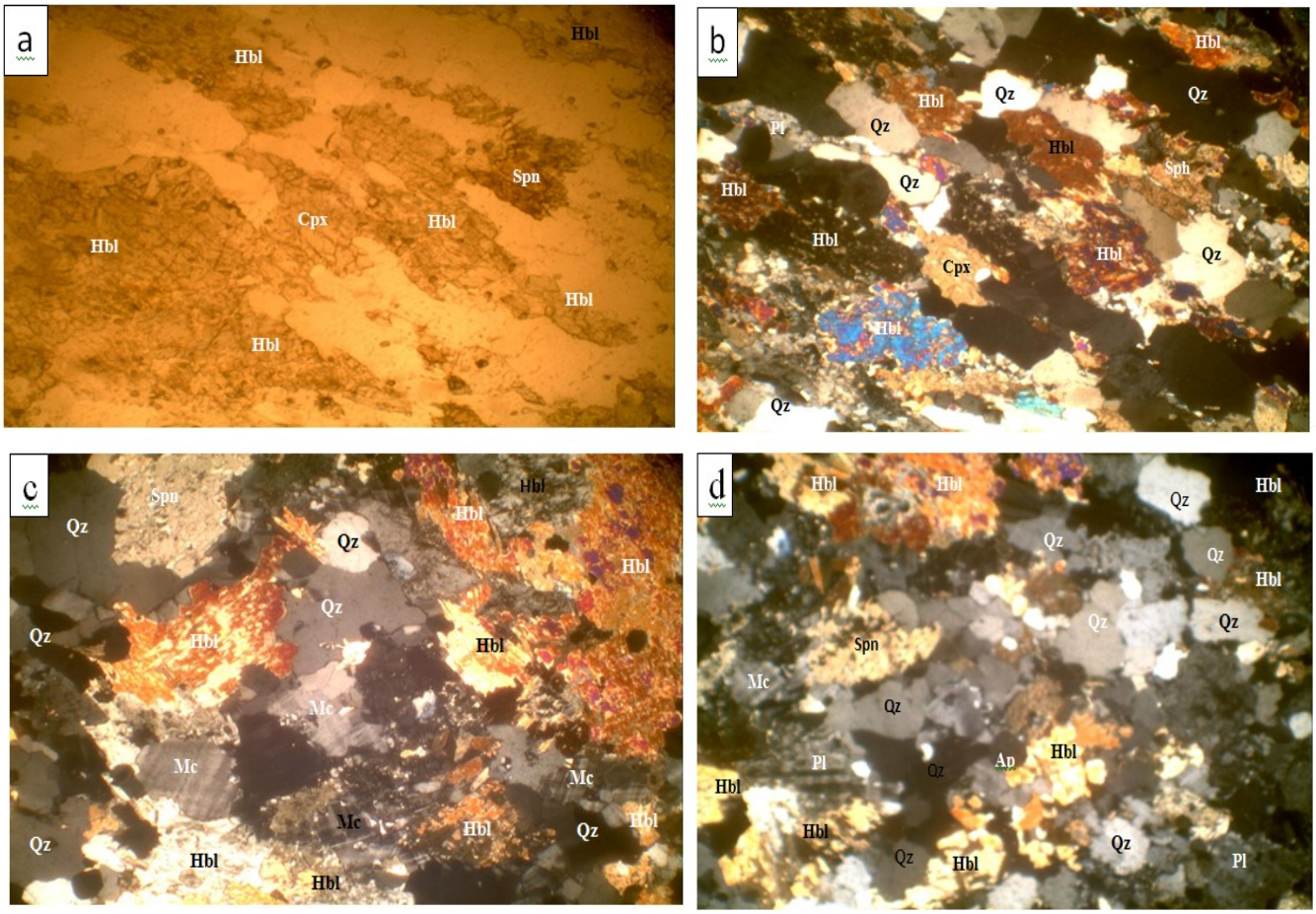

Fig. 4.10: Photomicrographs of (a) foliated amphibolite in Ijero area showingpreferred dimensional orientation of hornblende grains with minor clinopyroxene and sphene (a) in plane-polarised light; (b)under crossed-polars; with (c) and (d) showingdecussate texture of hornblende grains, microcline, plagioclase, quartz, sphene and apatite under crossed-polars(Mag. x40) (Hbl=hornblende; Sph=sphene, Qz=quartz, Pl=plagioclase, Cpx=clinopyroxene; Mc = microcline; Ap = apatite).

.

brownish green in colour. Chloritic alteration is evident in some grains. Plagioclase grains are of subordinate amount, xenoblastic in shape and showing characteristic multiple twinning. Quartz grains are flattened, ribbon-like and strong undulose extinction indicates straining of deformation that resulted in weak foliation. The massive amphibolite consists of hornblende with minor amount of plagioclase, microcline and quartz with accessory sphene, apatite, epidote and magnetite (Fig. 4.10).

Quartzites

Quartzites occur as thin bands within the biotite schist. The quartzite shows granoblastic texture of anhedral quartz grains with the characteristic undulose extinction. Minor amount of muscovite crystals define parallel cleavage in the rock.

Pegmatites

Extensive tabular pegmatite dykes, sheets and veinlets intrude the major rock types of the area. The pegmatites are exposed as flat-lying bodies around Ikoro, whereas they occur as low hills and steeply dipping dykes in Ijero. The contact relationships between intrusive pegmatites and the host biotite schist are commonly transitional but sharp to diffuse in the gneisses (Fig. 4.11a). The sharp contacts, in places, are marked evidence of late-forming tourmalinalizing fluids. Few pegmatite bodies show xenolithic inclusions of the host biotite schist (Fig. 4.11b). The pegmatites are light to pinkish in colour and show graphic intergrowths of coarse-grained microcline perthites, quartz, and muscovite. Field relationships and mineralogical characteristics of the pegmatites have indicated both simple and complex pegmatites in the area.

The simple pegmatites are generally of small dimensions and show simple mineralogy. They are mainly composedof microcline-perthite, quartz, and muscovite, with minor amount of albite and biotite. Accessory constituents include garnet, schorl, apatite and zircon.

The complex pegmatites are commonly well zoned, with distinct mineralogical assemblages characterising each compositional zoning (Fig. 4.11c and 4.11d).The core zone is mainly represented by nearly pure quartz (Fig. 4. 11c) with few large books of

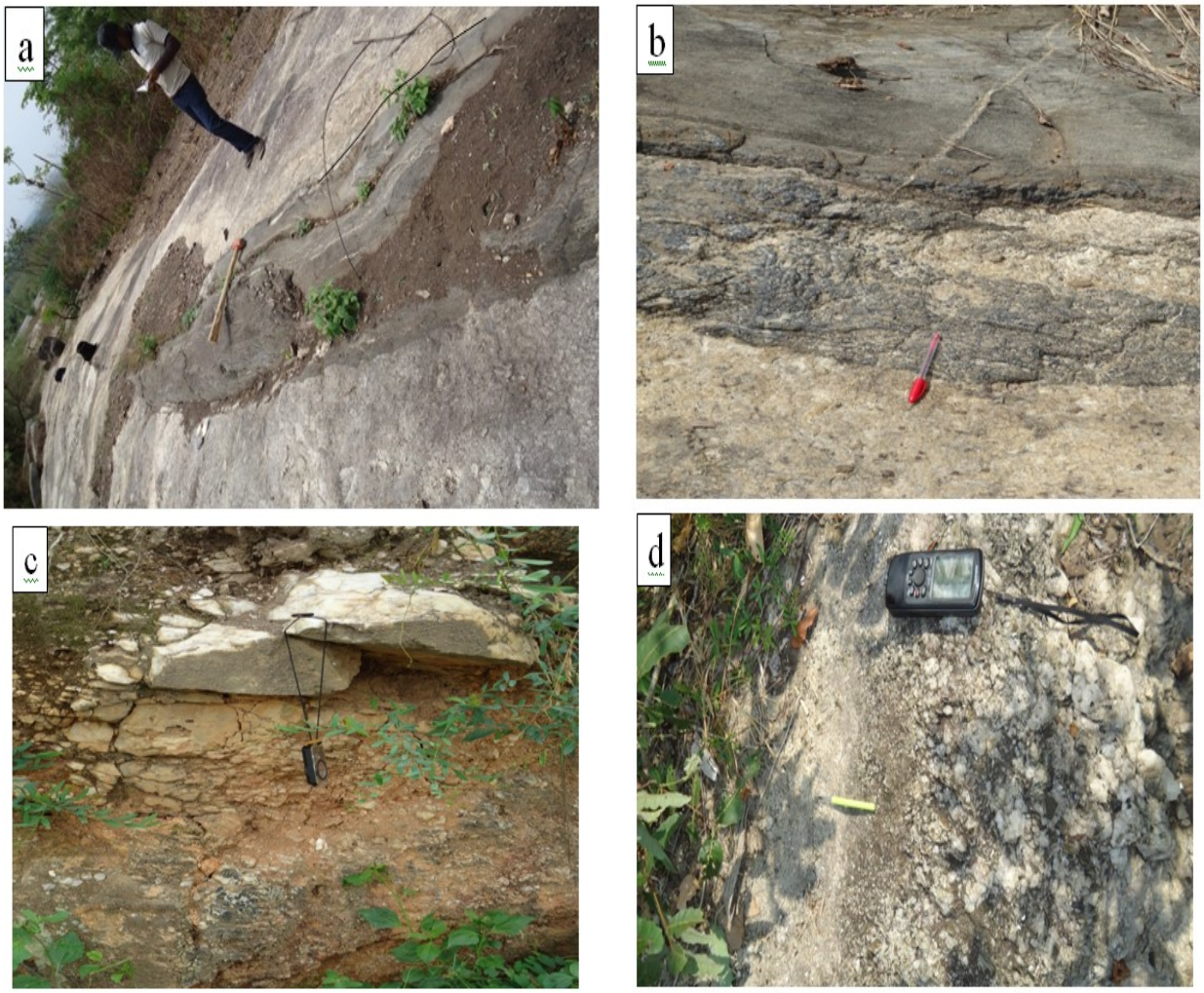

Fig. 4.11: Field photographs of pegmatites of Ijero area showing (a) xenolithic inclusion of the country rock biotite schist in a pegmatite outcrop; (b) sharp contact between the host biotite gneiss and the intruding pegmatite; note the evidence of the impact of late-forming tourmalinising fluid at the intrusive contact (c) unaltered monomineralic quartz core of a compositionally zone pegmatite rimmed by altered muscovite- and K-feldspar-rich intermediate zones; (d) Quartz-rich core (of a pegmatite vein) rimmed by finely crystallised muscovite- and K-feldspar-rich intermediate zone; the latter diffuses into the wall zone.

muscovite and minor amount of tourmalines. The intermediate zone is marked by the occurrences of microcline, quartz, muscovite and albite as the principal minerals, while lepidolite, biotite, garnet, apatite, zircon, beryl and tourmalines occur as accessory minerals. The border zone is dominated by quartz, microcline and tourmaline (schorl) assemblages. Low hill and roughly NNE-SSW trending extensive tabular and steeply dipping pegmatite dykes are found intruding into the biotite schist of the area (Fig. 4.8). Some of these pegmatites show remarkable metallic and gem mineralisations, where cassiterite, tantalo-columbite (Ta>Nb), gem quality beryls and tourmalines, rose and smoky quartz and kaolin have been extracted through small scale mining activities.

Petrographic studies of the pegmatites indicate the abundance of microcline-perthite, quartz, albite and muscovite, with accessory amounts of garnet, tourmaline, zircon and apatite (Fig. 4.12 and Table 4.2).

4.1.3 Komu area

Komu area is underlain by banded gneiss, amphibolites and granitic rocks (Fig. 4.13), which are intruded by pegmatites, dolerite, aplite and quartz veins.

Banded gneiss

The banded gneiss outcrops, though poorly exposed, occur at the western and northern parts of the area. The rock is low-lying, dark grey in colour, and medium to coarse-grained with well-defined foliation. Foliation is marked by intercalations of quartzo-feldspathic and biotite-hornblende-rich bands, which are generally in the north-south direction. Petrographic studies indicate hornblende grains and biotite laths, alternating with felsic bands, comprising plagioclase (oligoclase; An_{30}), quartz, orthoclase and microcline (Fig. 4.14). Accessory minerals include garnet, zircon, sphene, and opaques. Hornblende and biotite grains show alteration to light greenish chlorite, while plagioclase grains are sericitized. These alterations indicate that the rock was initially subjected to retrograde metamorphism.

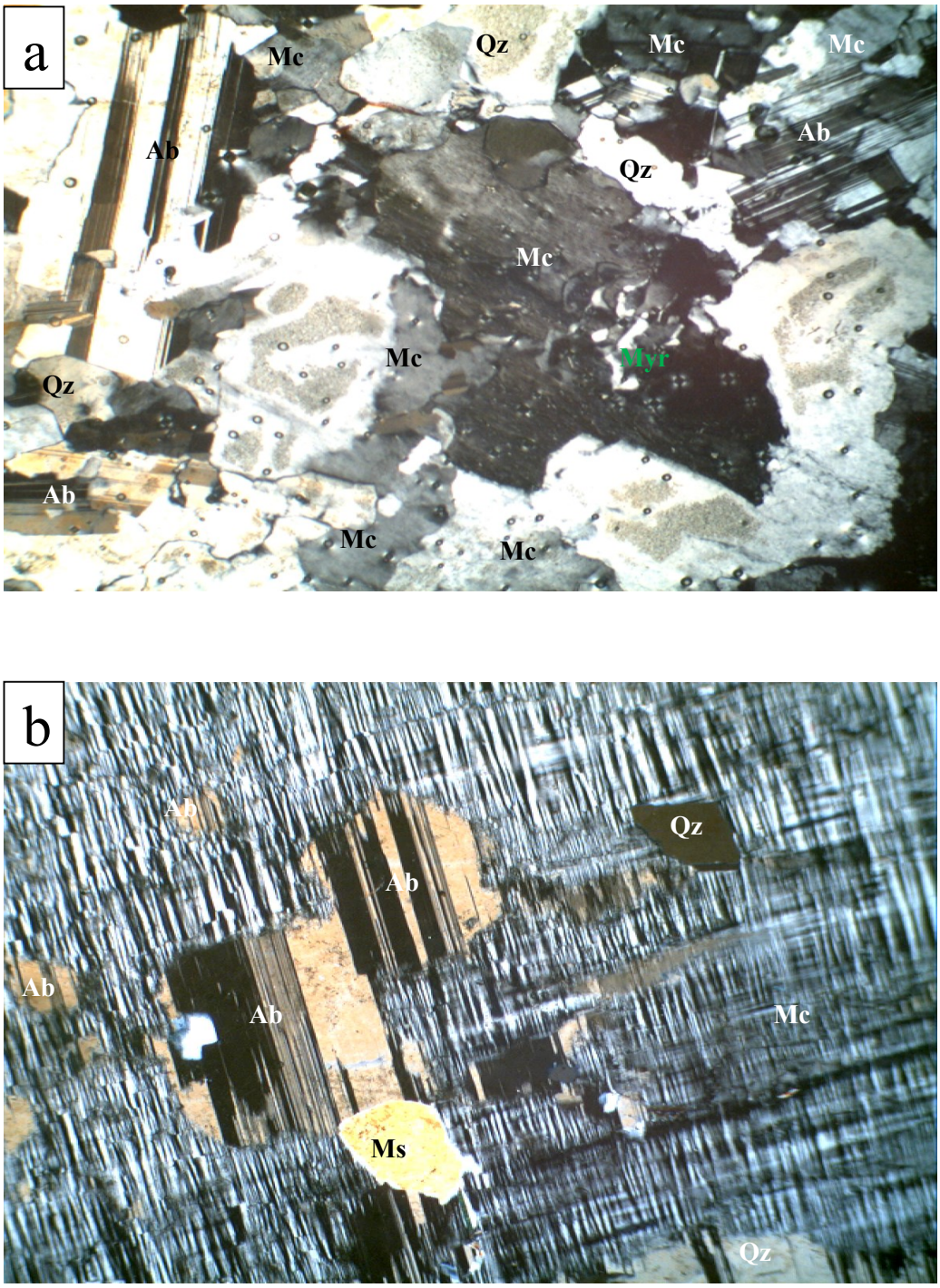

Fig. 4.12: Photomicrograph of pegmatites at Ijero area, showing (a) microcline, albite and quartz; (b) the inclusion of subhedral albite, quartz and muscovite crystals in crossed-hatch twinned microcline grain (Mag. x40). (Mc = microcline; Ab = albite; Qz = quartz; Ms = muscovite and Myr = myrmekite).

Table 4.2: Modal composition of the Ijero mineralised pegmatite

	IJ1	IJ2	IJ3	IJ4	IJ5	IJ6	IJ7	IJ8
Microcline-pertithe	49	53	48	57	50	53	50	42
Albite	16	10	14	8	13	10	13	14
Quartz	23	27	25	22	28	24	22	27
Muscovite	8	6	8	9	5	6	8	8
Biotite	1	1	2	1	-	1	1	1
Schorl	2	1	1	2	1	2	2	1
Garnet	1	1	2	1	1	2	1	2
Total	99.0	98.0	99.0	100.0	98.0	99.0	97.0	98.0

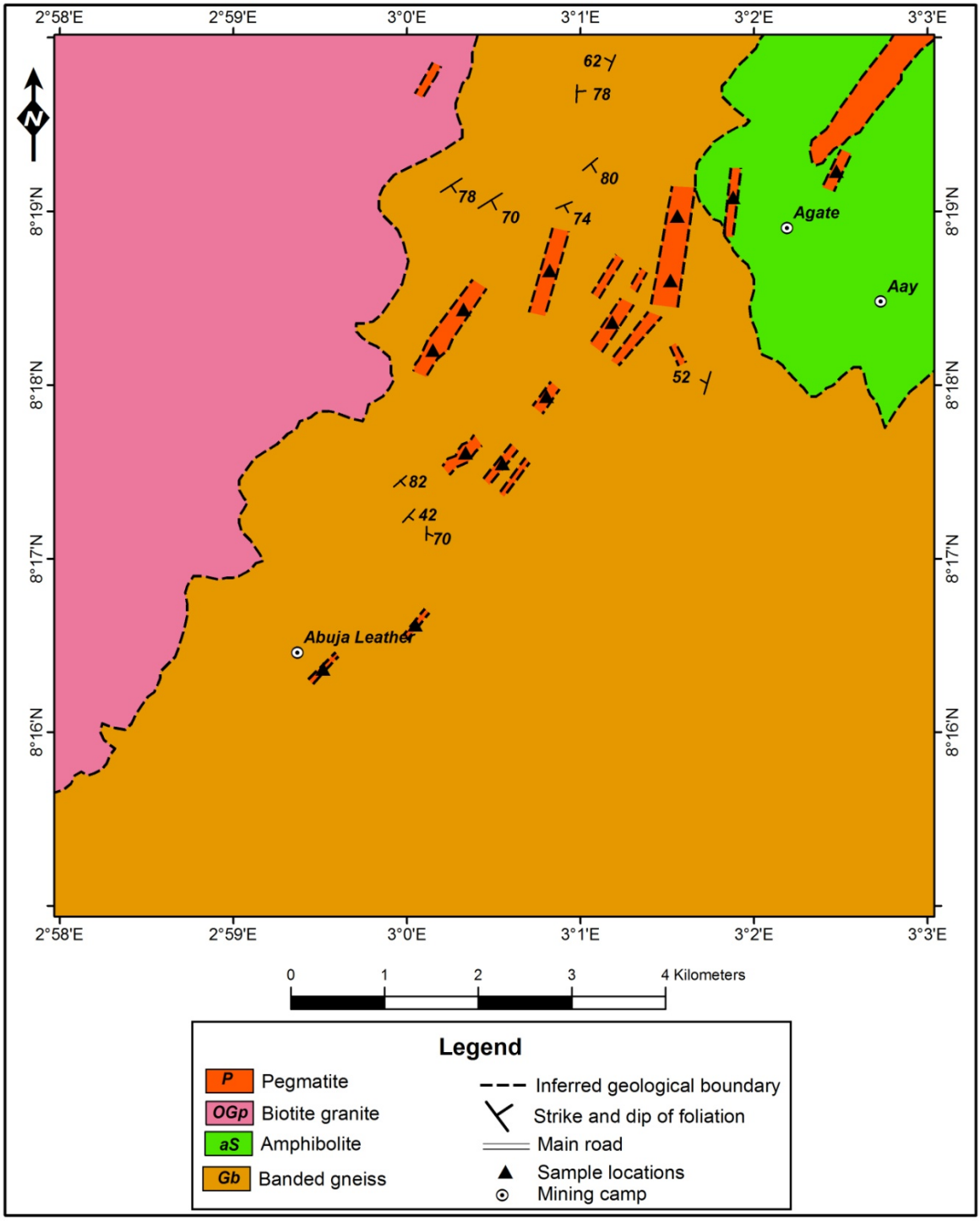

Fig. 4.13: Geological map of Komu area showing sample locations

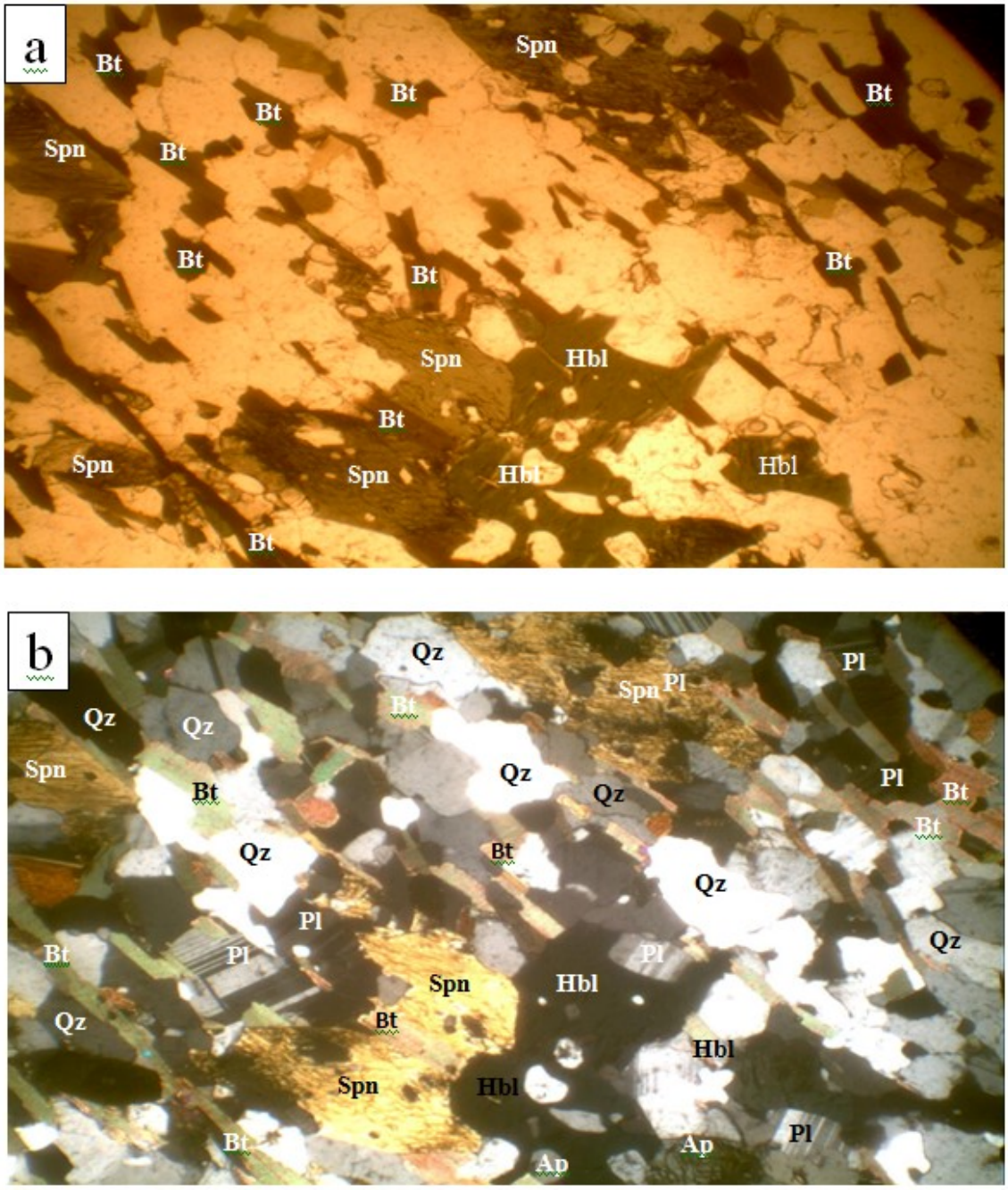

Fig. 4.14: Photomicrograph of banded gneiss in Komu area showingbiotite laths, hornblende, and sphene alternating with plagioclase feldspar and quartz-rich bands (a) under plane-polarised light and (b) under crossed nicols (Mag. x40) (Bt=biotite, Hbl=hornblende, Sph=sphene, Qz=quartz, Pl=plagioclase, Ap=apatite).

Amphibolites

Two petrographic types of amphibolites occur around the northeastern part of the area. The massive amphibolite is dark green in colour due to the preponderance of greenish hornblende and it is medium to coarse-grained. The foliated amphibolite is dark grey in colour, and fine to medium-grained. Thin felsicbands (about 0.5 cm across) of plagioclase feldspars and quartz alternate with the hornblende-rich bands. Under the microscope, massive and foliated amphibolites comprise mainly green hornblende and plagioclase (andesine), with accessory quartz, biotite, augite, sphene, apatite and magnetite (Fig. 4.15).The foliatedamphibolite is particularly marked by dimensional orientation of bladed and acicular amphibole crystals. Alteration of hornblende to epidote, plagioclase to sericite and biotite to greenish chlorite are observed in thin sections.

Granites

Granites occur as low-lying outcrops mainly at the northwestern part of the area. The rocks are porphyritic, weakly foliated and range in composition from true granite to tonalite. Plagioclase, hornblende, augite, orthoclase, and biotite are the major minerals present in the rocks (Fig 4.16). Thin section showed plagioclase and alkali feldspar phenocrysts set in medium to coarse-grained matrix of plagioclase, hornblende, quartz, biotite and microcline. Plagioclase grains are subidiomorphic to xenomorphic in shape and commonly twinned according to albite and pericline laws. Some of the plagioclase crystals are weakly zoned and few display compositional oscillatory zoning in thin sections (Fig. 4.16d). Sericitic alteration of the plagioclase partially obliterated the twinning of the plagioclase in some grains (Fig. 4.16d). Microcline shows characteristic cross-hatched twinning, whilequartz indicates wavy extinction. Hornblende is altered to epidote while biotite showed alteration to greenish chlorite (Fig. 4.16a). Euhedral to subhedral sphene appears as isolated crystals, while augite shows simple twinning (Fig. 4.16b). Accessory constituents include garnet, zircon, apatite, sphene and opaques, while chlorite, sericite, epidote are replacement mineral phases. These replacement mineral assemblages and sphene indicate low temperature deuteric alteration of the tonalite.

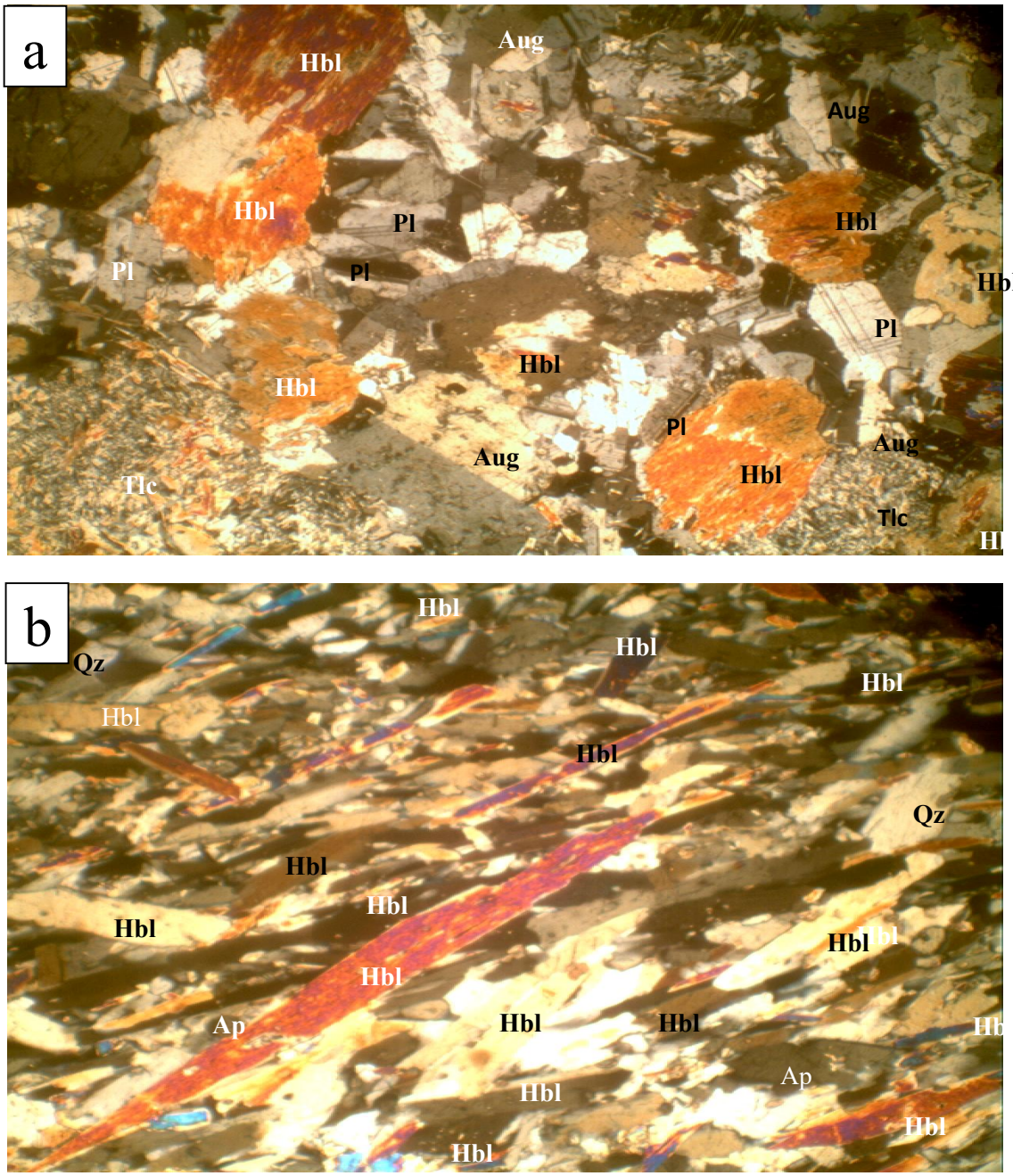

Fig. 4.15: Photomicrographs of Komu:(a) massive amphibolite showing decussate texture of dominantly hornblende grains, plagioclase feldspar and augite (twinned) under crossed polars. Note the secondary alteration of amphibole to talc towards the bottom left of the microphotograph (Mag. x40); and (b) foliated amphibolite showing preferred dimensional orientation of bladed and accicular hornblende crystals under crossed polars (Mag. x40) (Hbl=hornblende; Pl=plagioclase; Aug=augite, tlc= talc; Qz= quartz, Ap=apatite and Spn=sphene).

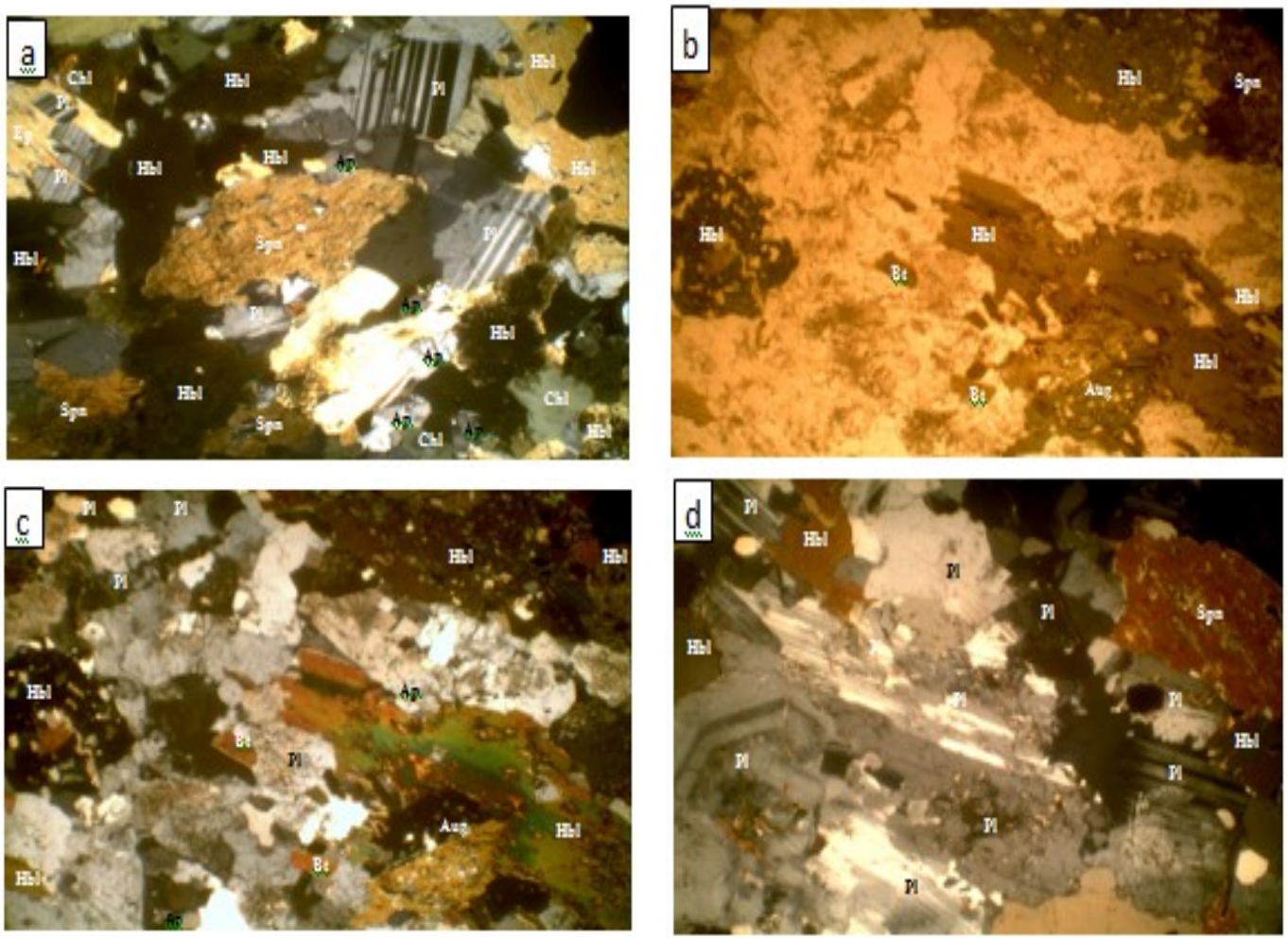

Fig. 4.16: Photomicrograph of tonalite in Komu area showing allotriomorphic texture of: (a) plagioclase, hornblende and sphene under crossed polars. Note the overgrowth of epidote on a plagioclase crystal towards the top left side and chlorite as a replacement mineral towards the bottom right of the microphotograph; (b) partially altered plagioclase feldspar, hornblende crystals, biotite and twinned augite in plane polarised light; (c) under crossed polars; (d) weakly zoned and partially altered plagioclase crystals under crossed nicols (Mag. x40). (Hbl = hornblende; Pl = plagioclase; Bt = biotite; Aug = Augite; Spn = sphene; Qz = quartz; Ap = apatite and Chl = chlorite and Ep = epidote).

Pegmatites

Pegmatites occur as intrusive bodies in the banded gneiss, amphibolites and granitic rocks of the area. They occur as tabular dykes and veins within amphibolites and gneissic outcrops (Fig. 4.17a), showing gradational to sharp contacts with the host rock units. Pegmatite occurrences in miarolitic cavities of banded gneiss in the western part of the area, are particularly noteworthy. These were exposed by the activities of the artisanal miners.

Field relationships of the pegmatites with host rocks revealed some tabular dykes, which extend to about 650 m in length and 50 m in wide; while very few dykes show strike length of approximately 2.5 km. There are some other pegmatite dykes and veins of smaller dimensions, varying in sizes from about 12 m long and 5 m wide and to length of about 150 m and width of 85 m. The pegmatites mostly trend NE-SW direction in the eastern part of the area, while very few dykes indicate trending in NW-SE direction.

Simple (barren) and complex (mineralised) pegmatite bodies were indicated from field relations and mineralogical studies. The former are commonly dykes and veins that lack compositional zoning, and show mineralogical abundances of microcline-perthite, quartz, albite, muscovite and minor to accessory constituents of biotite, garnet and schorl.The latter are commonly compositionally zoned, particularly the smaller dykes that display prominent zoning. The compositional zoning is essentially made up of the quartz-rich core, and the intermediate zone of muscovite-albite-tourmaline-rich rims. This is followed by the wall zone, marked by occurrences of the alkali feldspar and books of muscovite, while the border zone is typified by smaller grains of quartz, microcline, albite and muscovite. In the bigger pegmatite bodies, zoning is not easily discernible. Traces of mineralisation are invariably reflected in the various shades of the constituting minerals. For instance, muscovite commonly indicates pale green, red-pinkish and white varieties. Lepidolite is also found in some mineralised pegmatites. The pegmatites also show secondary emplacements of late-phase muscovite-rich fracture-filling (greissen) veins (Fig. 4.17b), which are often locally associated with metallic and gem mineralisations.

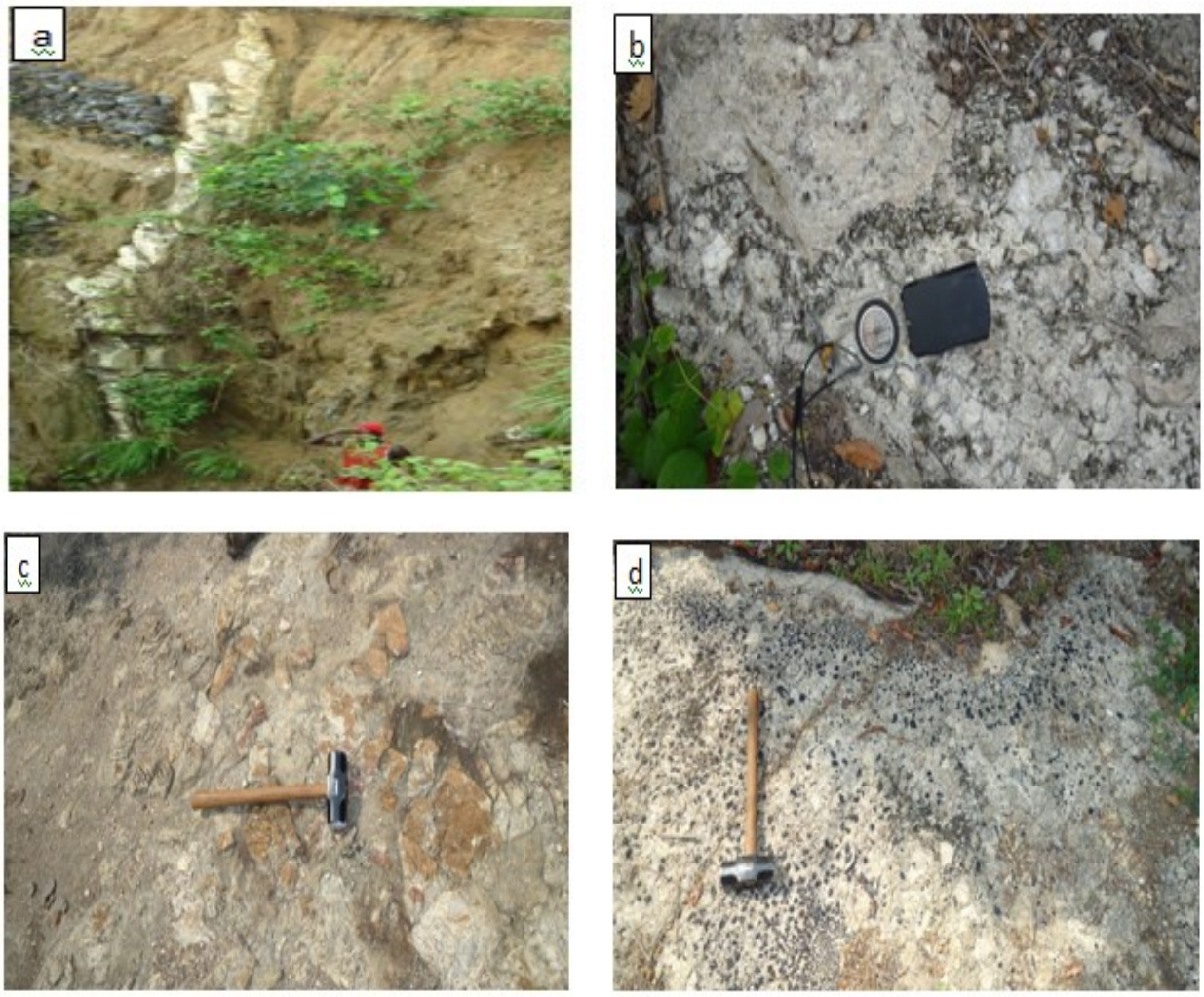

Fig. 4.17: Field photographs of pegmatites of Komu area showing: (a) intrusive pegmatite dyke in the completely altered gneissic rock; (b) Late-phase muscovitised greissen emplaced as fracture-filling vein into a pegmatite outcrop; (c) Light pinkish megacrystic graphic K-feldspar set in groundmass of medium-coarse grained microcline, quartz and muscovite; and (d) ubiquitous schorl (black tourmaline) disseminations within a pegmatite bodies

The microcline is commonly pinkish-whitish in colour. However, visibly perthitic light-green feldspar (amazonite) is localised in some pegmatite bodies in the area. Also, light pinkish megacrystic graphic K-feldspar varieties are locally evident in some pegmatite bodies (Fig. 4.17c). Milky, rose and smoky quartz are also present, while black tourmaline (schorl) show variable abundances in different sub-zones in the pegmatites (Fig 4.17d). The miarolitic cavities are exceptional for some good quality coloured tourmalines, such as elbaite (red), rubelite (red to pinkish) and indicolite (blue) contents. Alteration haloes of the miarolitic pockets are visibly displayed in the host banded gneisses, showing varying thicknesses from 15cm to about 65cm. This is generally referred to as "kankara" by the localminers. Pale green subhedral to euhedral hexagonal beryl crystals are localised in muscovite dominated sub-zones of the pegmatites. Large crystals of almandine garnet areoccasionally found in the pegmatites, while reddish-pink variety of garnet is also being extracted as gemstones from the pegmatites. These pegmatites also show Ta-Nb ores as subhedral crystals. The Ta-Nb ores were extracted from both the surficial eluvial materials and the pegmatite bedrocks.

The thin sections of the pegmatites indicate microcline-perthite, albite, quartz and muscovite as the main minerals (Fig. 4.18), while garnet, schorl, apatite, zircon, topaz, beryl and gem tourmalines are of minor to accessory amounts. The modal compositions of the pegmatites are presented in Table 4.3.

4.1.4 Ofiki area

The rock types in Ofiki area (Fig. 4.19) include banded gneiss, amphibolites and biotite granites. Intruding these rocks are minor rocks, such as pegmatites, microgranites, aplites, dolerite dykes and quartz veins.

Banded gneiss

Banded gneiss accounts for approximately 25% of the basement rocks of the area. It is generally low-lying, dark grey in colour, medium to coarse-grained, and shows a dominant NNW-SSE foliation trends steeply dipping to the east (Fig 4.19). The banded gneiss is marked by alternating bands of mafic (biotite and hornblende) and felsic (quartz and feldspars) components, which are of varying thicknesses. Microcline, quartz, biotite,

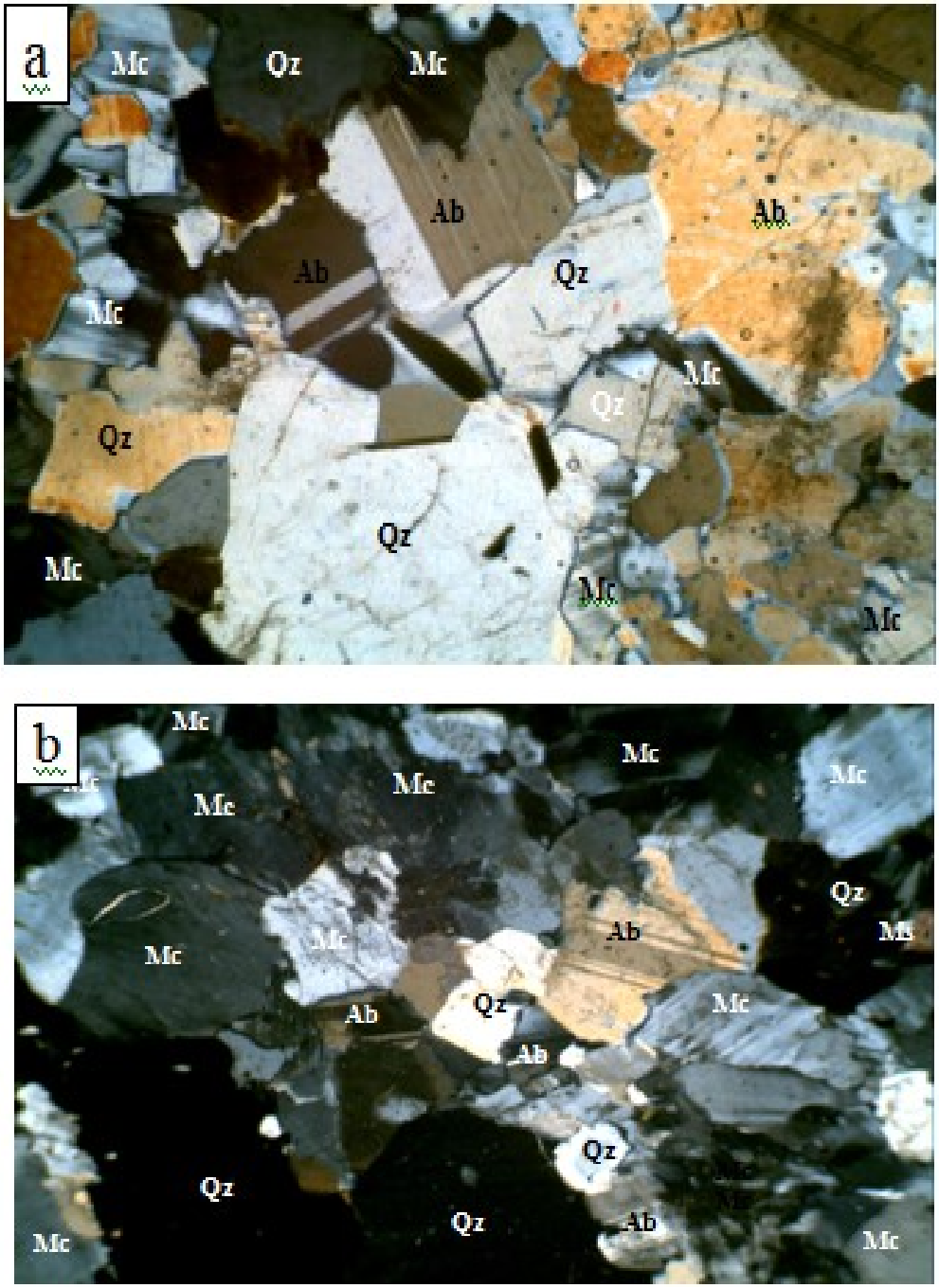

Fig 4.18: Photomicrograph of pegmatites of Komu area, showingintergranular texture of microcline, albite, quartz and muscovite. (b) (Mag. x40). (Mc = microcline; Ab = albite; Qz = quartz; Ms = muscovite).

Table 4.3: Modal composition of the Komu mineralised pegmatite

	KM1	KM2	KM3	KM4	KM5	KM6	KM7	KM8
Microcline-pertithe	36	25	34	28	30	41	31	35
Albite	27	35	25	32	32	23	31	28
Quartz	23	26	25	27	25	24	22	27
Muscovite	8	6	8	9	5	6	8	5
Biotite	1	-	2	-	1	1	-	1
Schorl	4	5	3	2	4	3	6	1
Garnet	1	1	1	1	1	2	1	2
Total	100.0	98.0	98.0	99.0	98.0	100.0	99.0	99.0

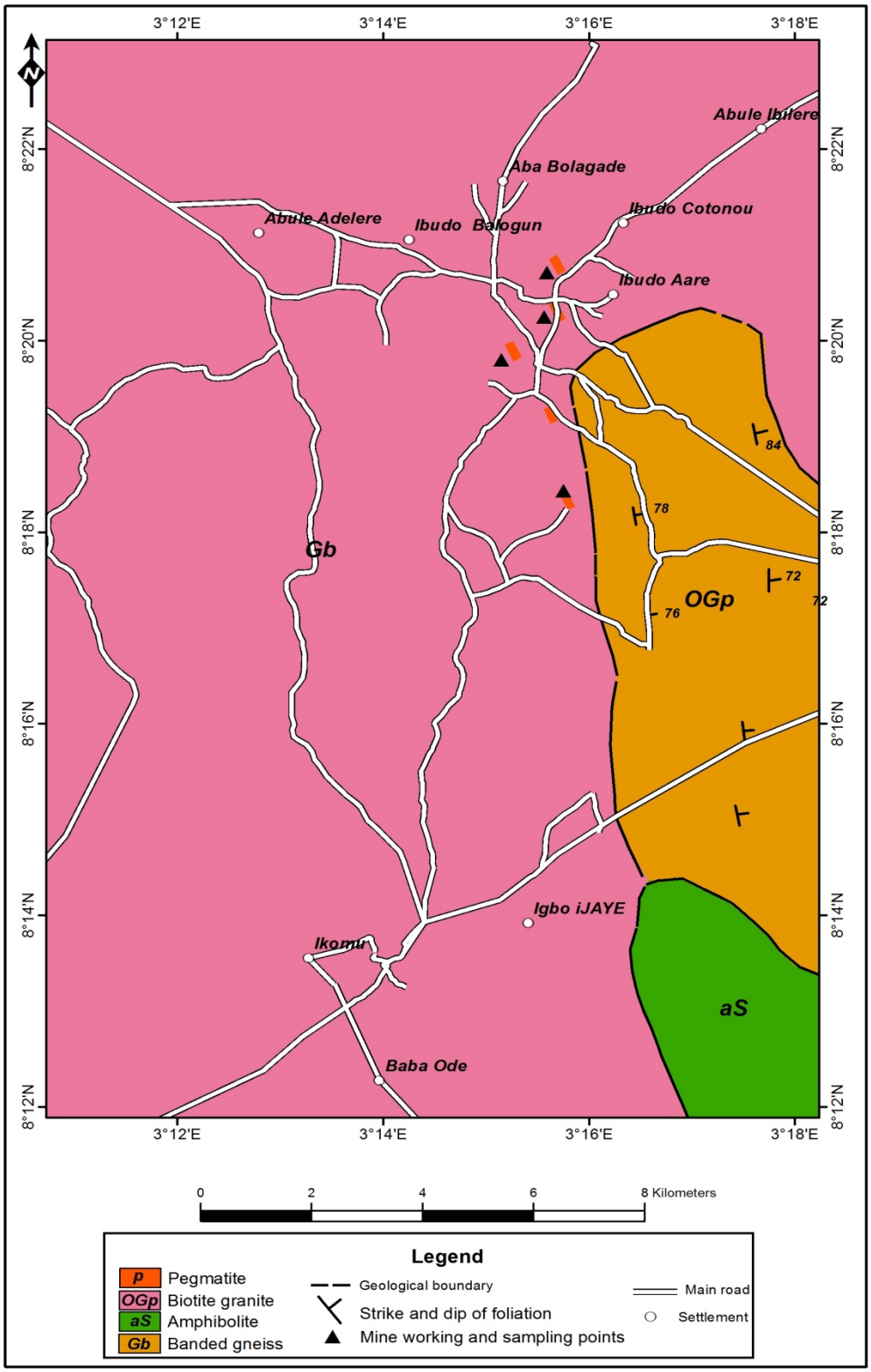

Fig 4.19: Geological map of Ofiki area showing sample locations.

hornblende, plagioclase and orthoclase are the main minerals in the banded gneiss; while accessory minerals include garnet, zircon, apatite and opaques. Biotite laths and hornblende grains alternate with quartz and feldspar grains (Fig. 4.20). Biotite is brown in colour and pleochroic from dark brown to greenish brown. Hornblende is weakly pleochroic from green to greenish brown. Plagioclase is mainly of oligoclase (An_{25-30}) composition, shows albite and pericline twinning, with partial alteration to sericite. Microcline grains show crossed-hatch twinning, while orthoclase shows Carlsbad twinning.

Amphibolites

Amphibolite outcrops are relatively few in Ofiki area. The amphibolites are poorly exposed due to their high susceptibility to weathering, and are mainly observed as boulders withvery few outcrops still preserved *in situ* around Igbojaiye. The soils around these amphibolites are dark and clay-rich, noticeably different from light quartz-rich soils that typify the granitic area. Theamphibolites are dark grey to almost black in colour, which, in hand specimen, are medium to coarse-grained. Two textural varieties were identified, which are the massive and the foliated amphibolite types. The massive amphibolite contains dark greenish hornblende, plagioclase feldspar and quartz grains in hand specimen; while the foliated type contains thin elongated grains of the same minerals which impart foliation in the rock. Petrographic studies show that hornblende and plagioclase are the essential minerals while quartz, biotite, sphene, apatite, magnetite and ilmenite are the accessory minerals (Fig. 4.21). Alteration of the greenish hornblende to chlorite and talc are evident. Plagioclase is oligoclase to andesine in composition, with extensive alteration to sericite.

Biotite granite

Biotite granite is the most widespread crystalline rocks in the Ofiki area. Three textural varieties, a coarse-grained porphyritic, medium to coarse grained, plus fine grained granites, are distinguished. The coarse grained porphyritic biotite granites contain euhedral to subhedral (0.5-5.5 cm) microcline phenocrystsin groundmass of medium tocoarse grained microcline, quartz, biotite, plagioclase, hornblende and opaques

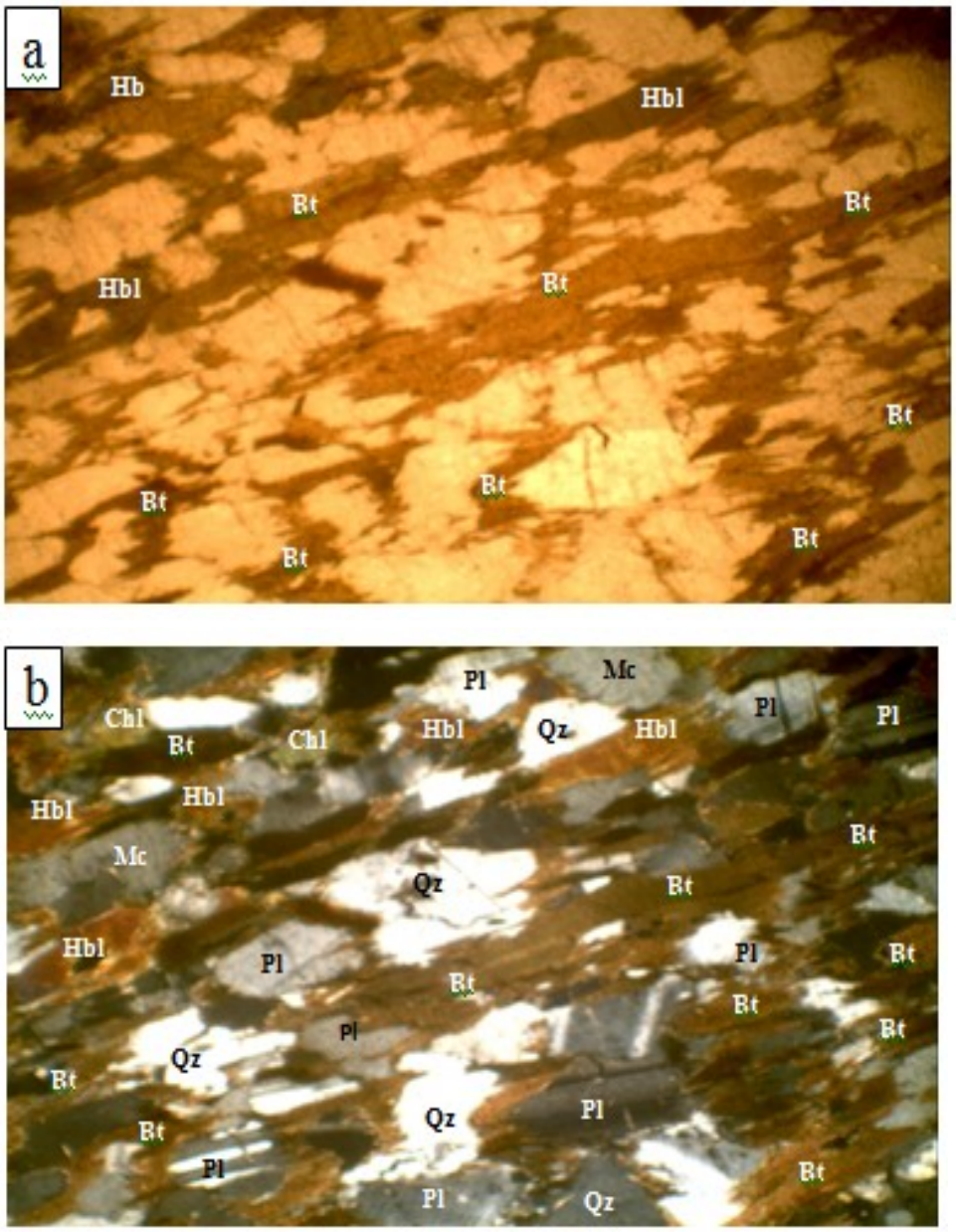

Fig. 4.20: Photomicrographs of banded gneiss in Ofiki area showing preferred alignment of the long axes of biotite laths, alternating with feldspar and quartz-rich bands under (a)plane-polarised light (Mag. x40) and (b) crossed nicols (Mag. x40) (Bt=biotite, Hbl=hornblende, Qz=quartz, Pl=plagioclase, Mc=microcline).

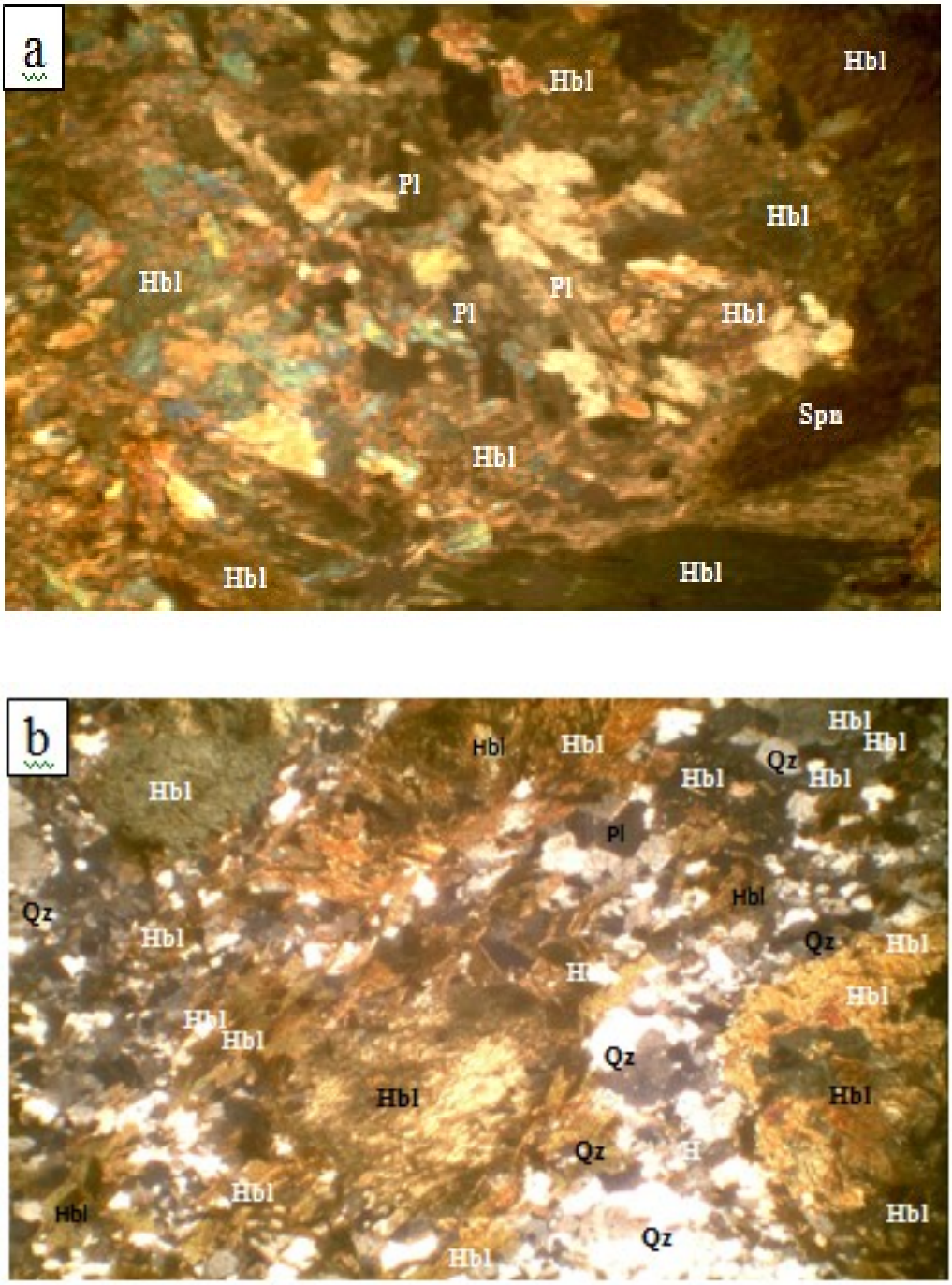

Fig. 4.21: Photomicrographs of massive amphibolite in Ofiki area showing: (a) decussate texture of hornblende grains, plagioclase and sphene under crossed nicols (Mag. x40); (b) foliated amphibolite showing alignment of coarse-grained hornblende crystals, alternating with feldspar and quartz-rich bands (Mag. x40) (Hbl=hornblende; Pl=plagioclase; and Qz = quartz;Sph=sphene).

Fig. 4.22a). In thin sections, the porphyritic variety shows microcline-perthite phenocrysts, set in groundmass of microcline, plagioclase, quartz, biotite and muscovite (Fig. 4.22a). Anhedral microcline shows the characteristic tartan twinning, with some grains showing blebby exsolution lamellae of sodic feldspar. Subhedral to anhedral plagioclase crystals show characteristics albite twinning, while some grains are polysynthetically twinned. Euhedral and oscillatory zoned zircon crystals and apatite grains are common as inclusions in plagioclase and microcline (Fig 4.22b). Biotite crystals show very high relief and are brown in colour. They are pleochroic from deep brown to yellowish brown, while some grains show alteration to chlorite. Anhedral hornblende is pleochroic from pale greenish to brownish. Worm-like myrmekitic intergrowths mark the boundaries between plagioclase and quartz grains (Fig. 4.22a).

The medium to coarse-grained biotite granites are low-lying and show subtle weak foliation of feldspar phenocrysts. Optical studies revealed a granular texture of interlocking mosaic of microcline perthite, quartz, biotite, hornblende, muscovite and plagioclase, withaccessory garnet, zircon, apatite and opaques. The fine-grained granite occurs as dykes within the coarse-grained porphyritic granites. In thin section, fine-grained granite has similar mineralogical composition as other varieties. It, however, shows equigranular texture (Fig. 4.23).

Pegmatites

Pegmatite dykes and veins intrude the peraluminous biotite granites, banded gneiss and amphibolites in the area. The pegmatites are generally low-lying, with occurrences being deeply weathered. Mine workings revealed that some of the pegmatite bodies are poorly zoned. The pegmatites showed graphic intergrowths of microcline and quartz, with books of platy muscovite locally abundant. Muscovite is green to brown while Li-bearing muscovite is pale purple in colour. Schorl (black tourmaline), lepidolite and red garnet crystals (locally up to 2.0 cm in diameter) are present in some of the pegmatites of Ofiki area (Fig. 4.24). Vugs within the pegmatites are hosts to gem quality subhedral to euhedral beryl and tourmaline crystals. Other minerals in minor to accessory amount include biotite, zircon, apatite and tantalo-columbite.

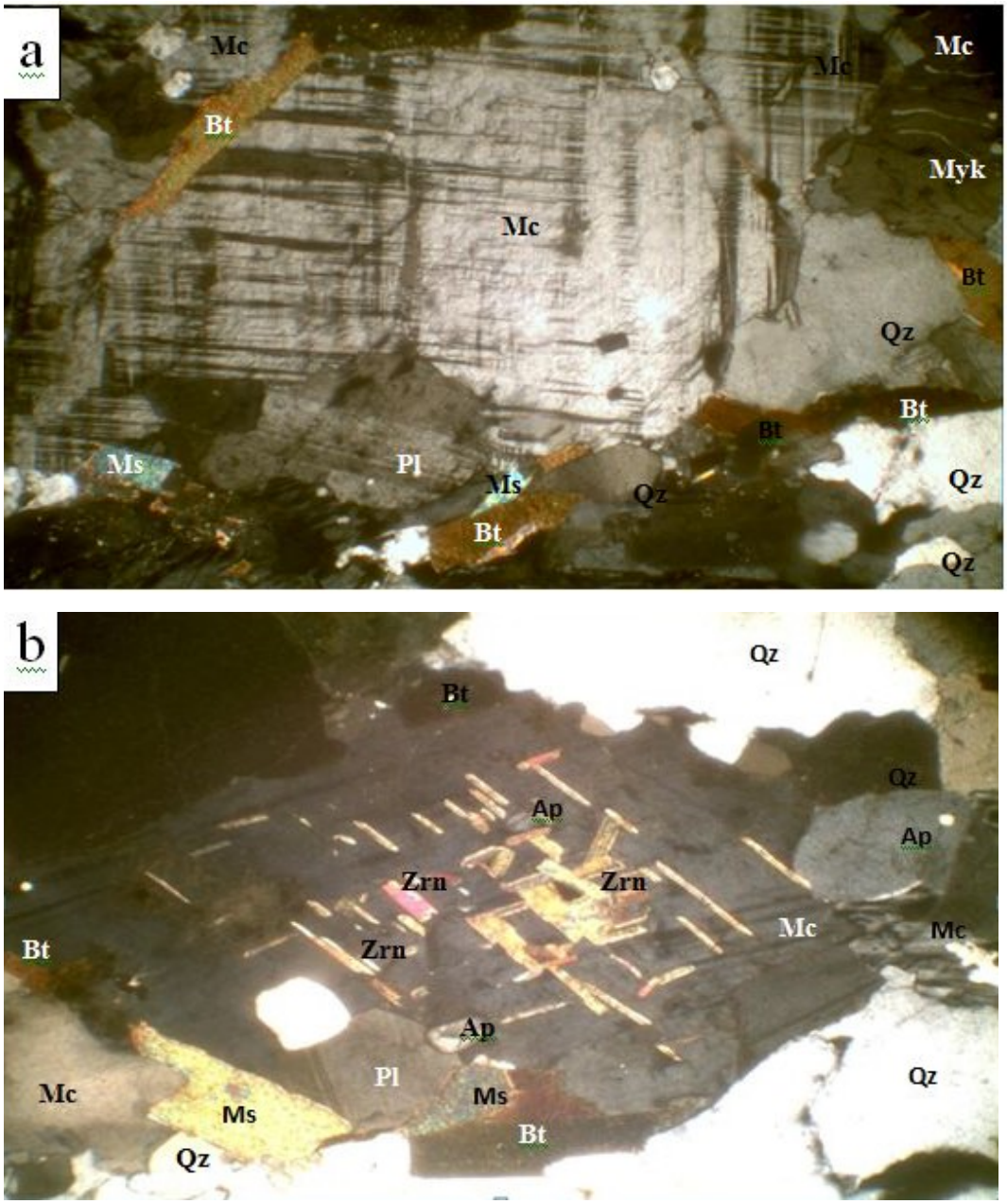

Fig. 4.22: Photomicrographs of the coarse porphyritic biotite granite in Ofiki area, showing: (a) microcline perthite phenocryst set in the finer matrix of microcline, plagioclase, quartz, biotite, muscovite and quartz grains under crossed polars (Mag. x40). Note the blebby myrmekitic feature towards the top right hand side of the photomicrograph, showing contact between microcline and quartz grains; (b)the inclusions of euhedral and oscillatory zoned zircon crystals and apatite grains within the cleavage planes of subhedral microcline grain. (Mc=Microcline Pl= plagioclase, Qz= quartz, Bt= biotite, Ms=muscovite Zrn = zircon and Ap = apatite and Myk=Myrmekite)(Mag. x100).

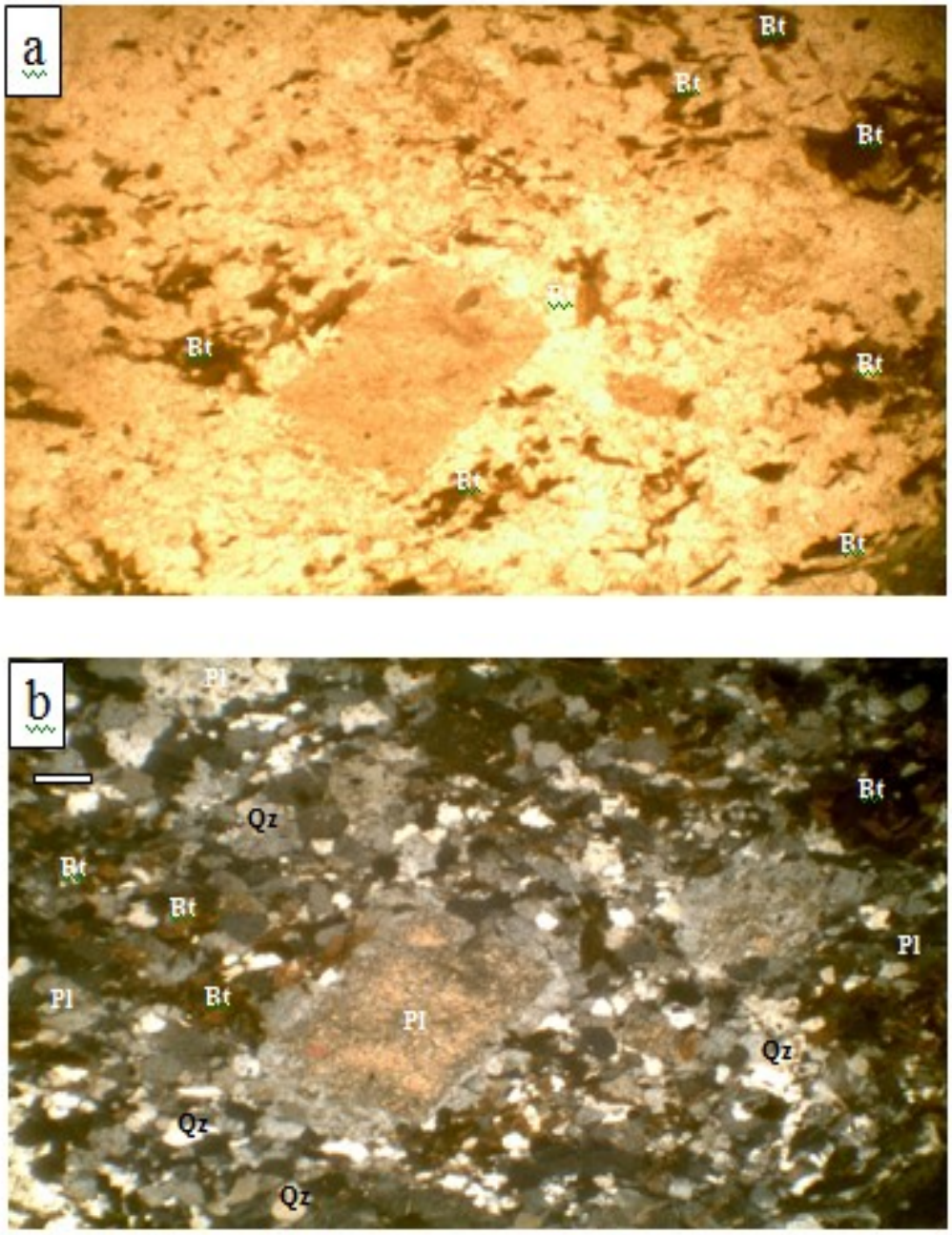

Fig. 4.23: Photomicrograph of the fine-grained granite in Ofiki area, showingeuhedral to subhedral partially altered plagioclase grains in finer-grained matrix of microcline, plagioclase, biotite and quartz. Note the alteration of core segment of the plagioclase crystal to dusty brown sericite (a) under plane-polarised light and (Mag. x40) (b) under crossed polars (Pl=plagioclase; Qz=quartz; and Bt=biotite).

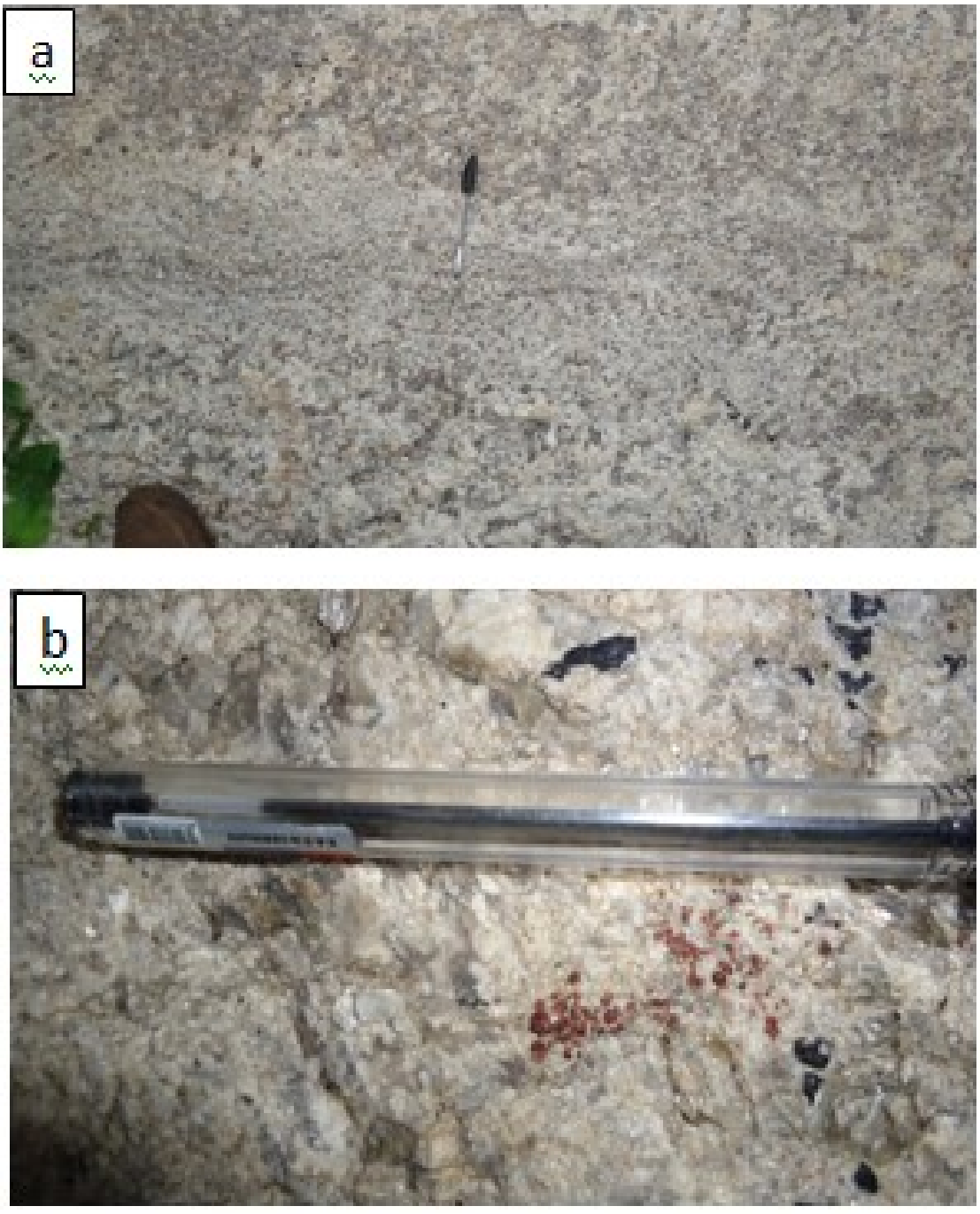

Fig. 4.24: Field photographs of pegmatites of Ofiki area showing: (a) almandine garnet-rich layer within a pegmatite body; (b) subhedral to euhedral garnet and schorl (black tourmaline) in a pegmatite outcrop.

Petrographic studies show intergranular texture of predominantly microcline perthite, albite, quartz and muscovite (Fig. 4.25 and Table 4.4), with minor to accessory amount of garnet, zircon and apatite.

4.1.5 Iwere-Ile area

This area lies between Latitude 7º 55' to 8º 03' N and Longitude 3º 00' to 3º 11' E, covering major towns, such as Iwere-Ile, Ayetoro, Itasa, Ilaji-Ile, Idiko-Ago and Idiko-Ile. The distribution of the principal rock types identified in the areas is shown in (Fig. 4.26), and these are biotite granite gneiss, biotite-hornblende gneiss, biotite granites and pegmatites.

Biotite granite gneiss

Biotite granite gneiss outcrops are low-lying relative to the associated biotite granites of Iwere-Ile area. It is light gray in colour, medium to coarse-grained and granitic to granodioritic in composition. The strike offoliation is generally NW-SE towards the eastern part of the area; while it is NE-SW towards the southwestern part of the study area. The foliation generally shows steep dips to the west. In thin section, the rock shows the alignment of biotite and hornblende-rich bands alternating with bands comprising microcline, plagioclase and quartz. Other accessory minerals include garnet, zircon, apatite and opaques (Fig. 4.27).

Biotite-hornblende gneiss

Biotite-hornblende gneiss is generally low-lying, dark coloured, fine to medium-grained and granitic to dioritic in composition. It shows foliation defined by thicker hornblende-biotite-rich bands, alternating with very thin quartzofeldspathic bands. Petrographic studies revealed alignment of hornblende and biotite grains(and locally with garnet), alternating with plagioclase, microcline and quartz grains (Fig. 4.28). Biotite isstrongly pleochroic from brown to greenish brown. Hornblende crystals are green in colour and pleochroic from greenish to yellowish green. Both biotite and hornblende grains show alteration to light greenish chlorite. Quartz grains are xenoblastic and show undulose extinction. Plagioclase grains are of oligoclase composition, and show intense alteration to sericite. Microcline displays the characteristic crossed hatch twinning. Other accessory minerals include zircon, apatite and opaques.

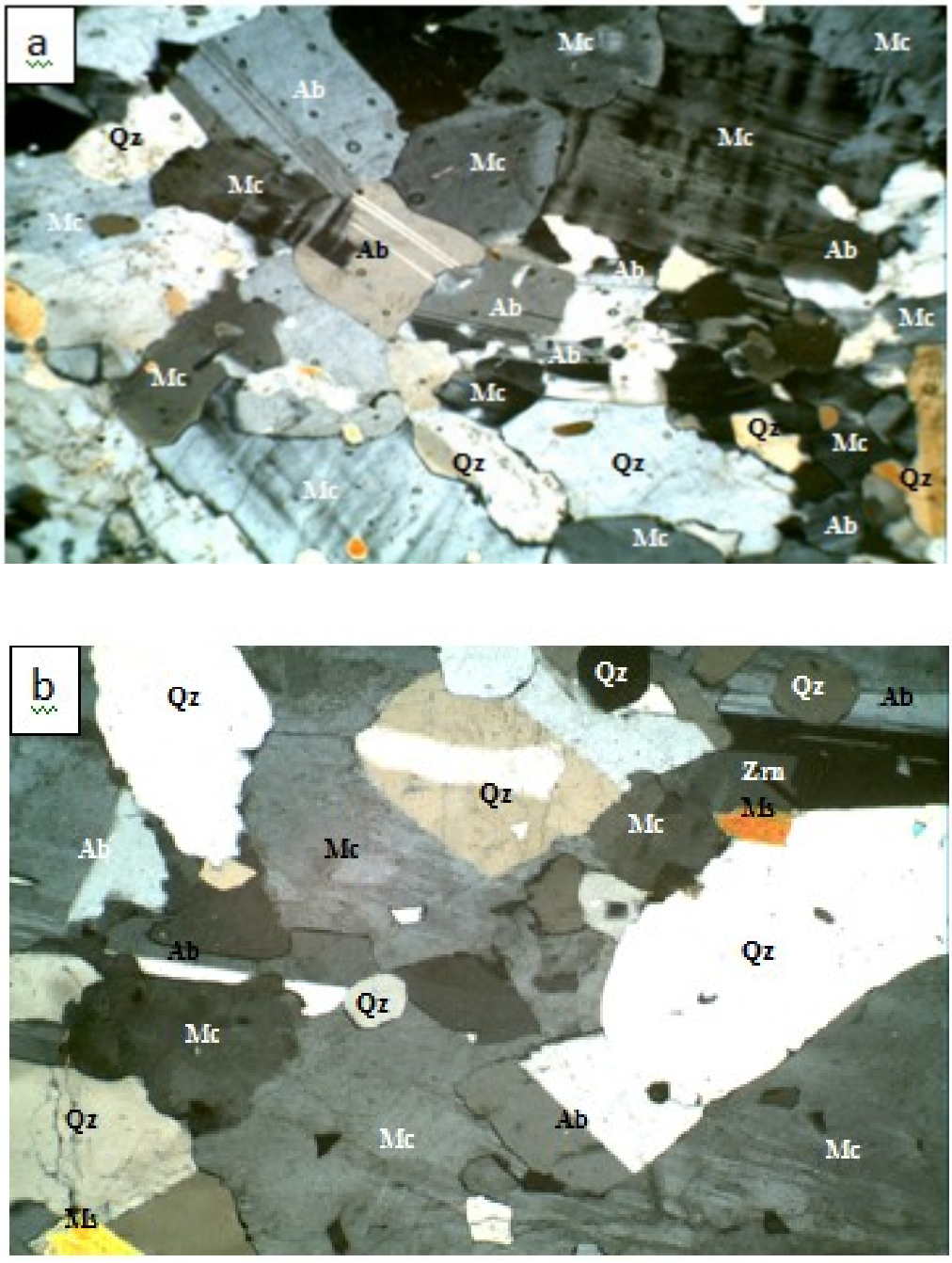

Fig 4.25: Photomicrograph of pegmatites of Komu area, showingintergranular texture of microcline, albite, quartz and muscovite. (b) (Mag. x40). (Mc = microcline; Ab = albite; Qz = quartz; Ms = muscovite; Zrn = zircon).

Table 4.4: Modal composition of the Ofiki mineralised pegmatite

	OF1	OF2	OF3	OF4	OF5	OF6	OF7
Microcline-pertithe	54	56	53	50	55	52	47
Albite	12	7	10	12	10	12	8
Quartz	24	26	25	28	24	24	28
Muscovite	7	6	5	8	6	6	12
Biotite	-	-	1	-	1	1	-
Tourmaline	1	2	3	1	1	2	2
Garnet	1	1	2	1	1	2	2
Total	99.0	98.0	99.0	100.0	98.0	99.0	99.0

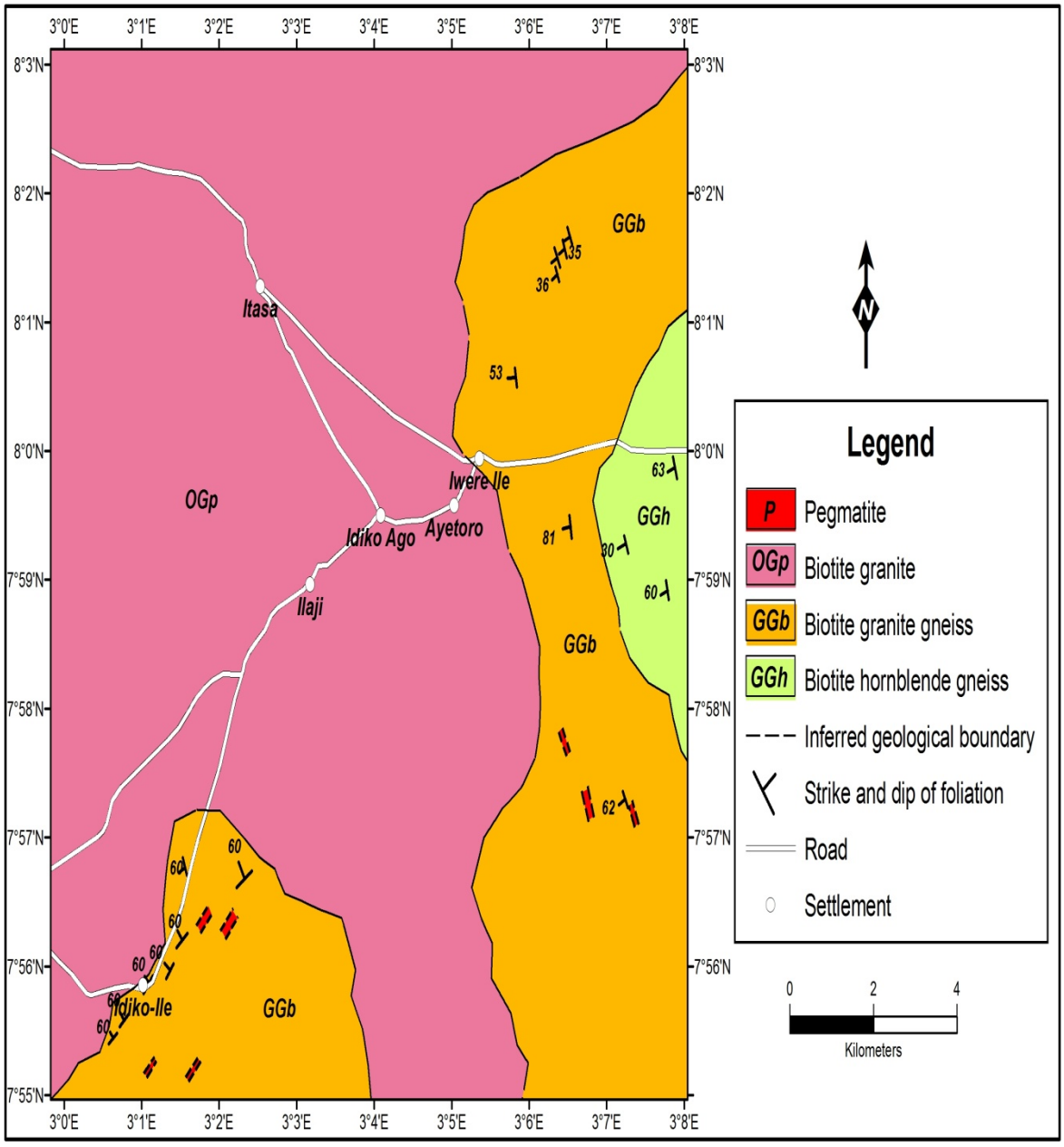

Fig. 4.26: Geological map of Iwere-Ile area showing mining points and sample locations

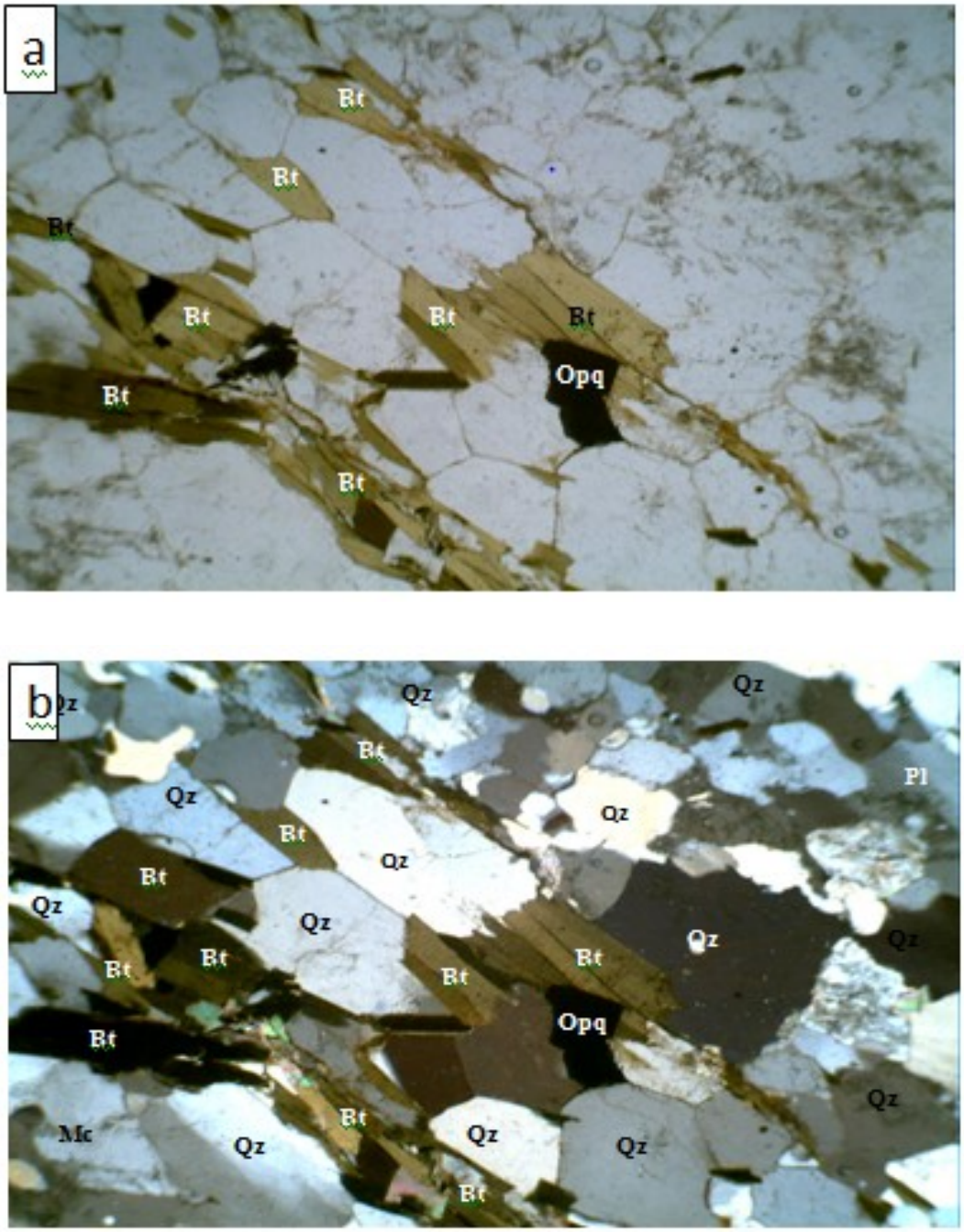

Fig. 4.27: Photomicrographs of biotite granite gneiss in Iwere-Ile area showing alignment of long axes of biotite lathsalternating with quartzofeldspathic bands (a) under plane-polarised light and (b) under crossed nicols (Mag. x40) (Bt= biotite; Qz= quartz; Pl= plagioclase; Mc=microcline) (Mag. x40).

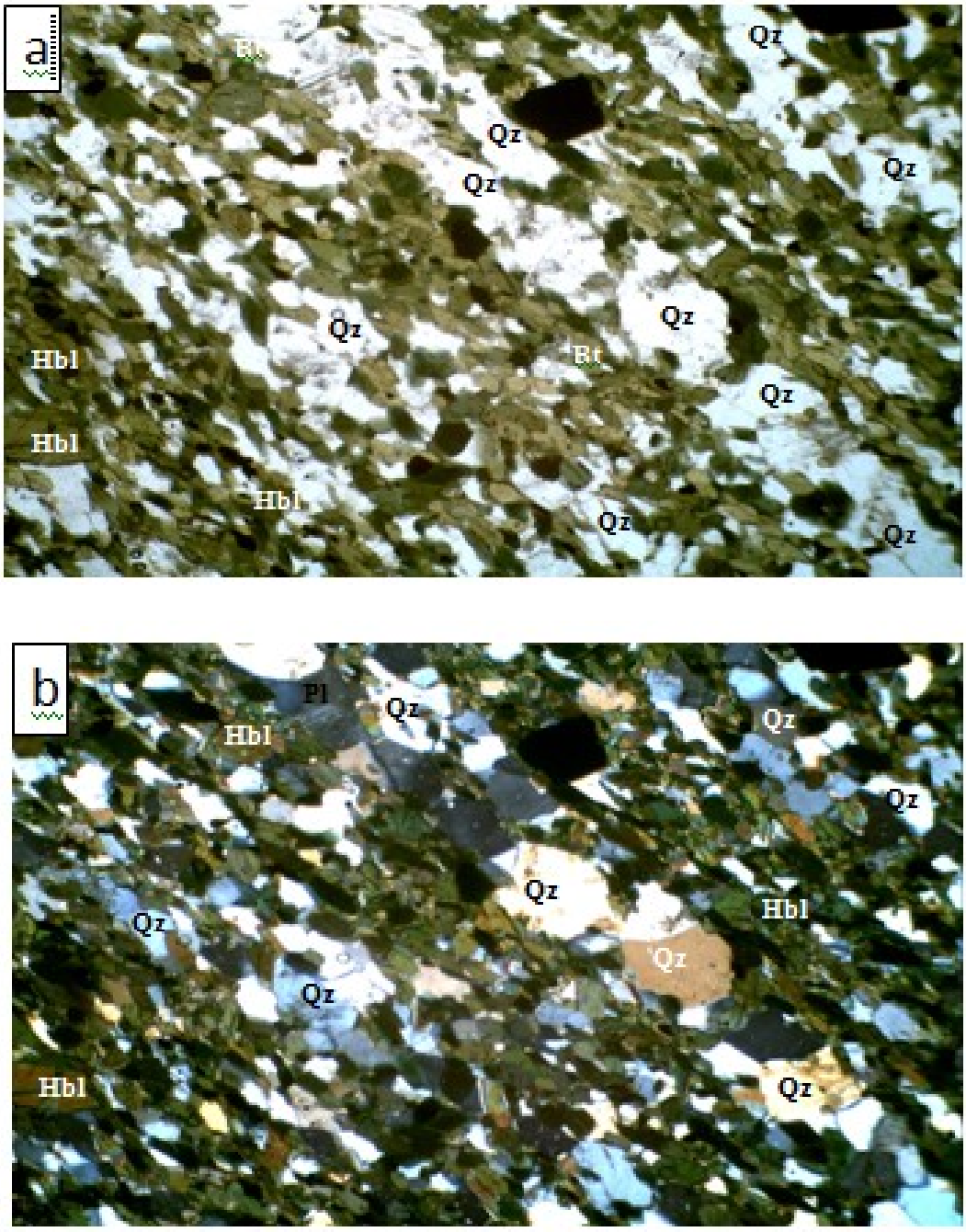

Fig. 4.28: Photomicrographs of biotite-hornblende gneiss in Akoda showing alignment of long axes of hornblende grains and biotite lathsalternating with quartz and feldspar-rich bands (a) under plane-polarised light and (b) under crossed nicols (Mag. x40) (Hbl = hornblende; Bt= biotite; Qz= quartz; Pl= plagioclase) (Mag. x40).

Biotite granites

Biotite granites constitute about 65% of the crystalline rocks of the area. Two textural varieties, a coarse-grained porphyritic and medium-grained granites, are distinguished. The coarse-grained porphyritic biotite granite occurs as prominent inselbergs and extensive ridges, notably around Iwere-Ile, Tijo, Ilaji-Ile, Idiko-Ile and Itasa, while the medium-grained granite are relatively low-lying outcrops and localised around Idiko-Ago. The coarse-grained porphyritic biotite granite is composed of euhedral to subhedral (1.0-5.5 cm) microcline phenocrysts in medium to coarse-grained microcline, quartz, biotite, hornblende, plagioclase and opaques. The microcline phenocrysts are pinkish in colour. The alignments of the K-feldspar phenocrysts and biotite plates, gives the rock a weakly foliated appearance. Partially assimilated xenoliths of mafic rocks are common in the coarse-grained porphyritic biotite granite.

In thin section, phenocrysts of perthitic microcline in a matrix of microcline, quartz, plagioclase, biotite, and occasionally hornblende grains are observed in the porphyritic granite (Fig. 4.29). Muscovite, garnet, zircon, apatite and opaques occur as accessory minerals. Microcline crystals showed the characteristics tartan twinning and worm-like blebbyexsolution intergrowths of sodic feldspar. Biotite is pleochroic from brown to yellowish brown, with inclusions of euhedral zircon. Hornblende is strongly pleochroic from green to yellowish green. Subhedral plagioclase crystals generally show polysynthetic twinning. Myrmekitic intergrowths are evident at the boundary between microcline andplagioclase crystals. Muscovite grains are colourless in thin section, shows perfect cleavage in one direction and bright interference colour under crossed polars.

The medium-grained biotite granite shows equigranular texture of anhedral microcline, quartz, plagioclase, garnet, biotite and muscovite (Fig. 4.29). Few biotite grains show partial alteration to chlorite. Alteration of plagioclase to sericite was also observed in the thin section.

Pegmatites

Pegmatites occur as low-lying, often slightly dipping dykes, intruding the biotite granites and biotite granite gneiss. Other occurrences are in form of small stocks and veins within the host rock. In most places, they have suffered variable degree of weathering, while

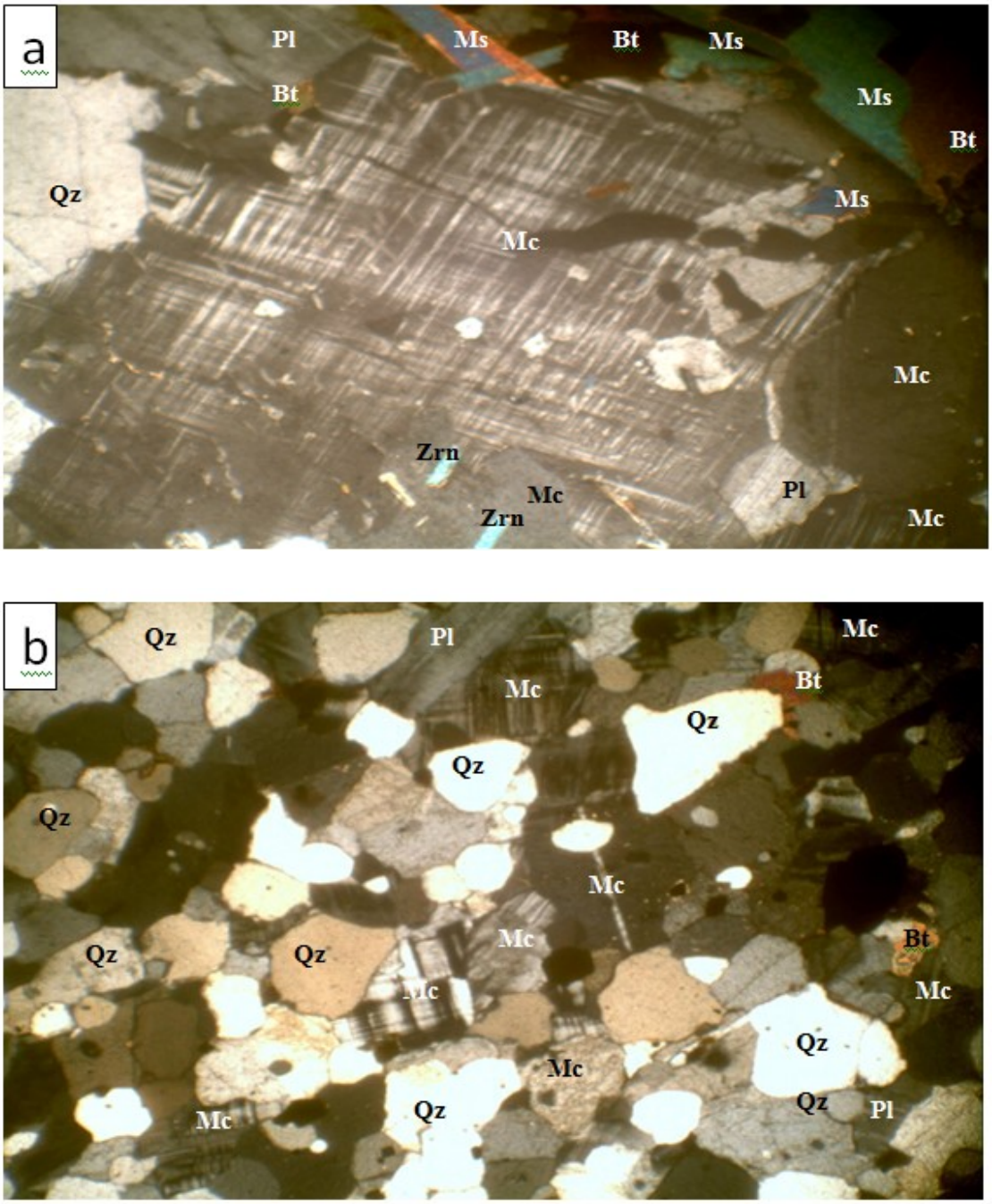

Fig. 4.29: Photomicrographs of (a) coarse porphyritic biotite granite in Iwere-Ile area, showing microcline perthite phenocryst embedded in the finer matrix of microcline, plagioclase, quartz, biotite, and muscovite grains under crossed polars (Mag. x40). (b) medium-grained granite showing equigranular texture of microcline, plagioclase, biotiteand quartz under crossed nicols (Mag. x40). (Mc=Microcline, Pl=plagioclase, Qz=quartz and Bt=biotite; Ms = muscovite; Zrn = zircon).

unaltered pegmatite dykes show macroscopically sharp contacts with their host lithologies (Fig 4.30a). Large dykes of about 180m long and 7m wide occur, while smaller cross-cutting dykes of few centimetres to slightly over one metre in width occur within biotite granites (Fig. 4.30b) and biotite granite gneiss. The general trend of the pegmatite is NW-SE, which is consistent with the regional foliation trend. The pegmatite of the area showed graphic intergrowths of microcline perthite, quartz and muscovite. Microcline crystals are pink to white in colour and visibly pertithic; while albite crystals are usually white to milky-white in colour. Other accessory minerals include tourmaline, lepidolite, beryl, garnet, apatite, zircon and tantalo-columbite.

Zoning of mineralised pegmatites were not clearly observed due to haphazard nature of mining in the area. However, in some of the hang dug pits, the occurrence of monomineralic quartz-rich cores, rimmed by lepidolite-dominated subunit of the intermediate zones, indicate evidence of internal zoning. Few pegmatite dykes indicate weak zoning patterns, which are commonly in form of quartz-rich zone, surrounded by medium to coaser grained microcline- and muscovite-rich intermediate zone (Fig. 4.30c).

The pegmatites at few locations are cross-cut by 30 to 80 cm wide altered vuggy quartz-albite-tourmaline-muscovite-rich veins. They are believed to be product of secondary emplacement by the late albitised and tourmalinised fluids with the characteristics greisen style alteration in veins and fracture-fillings. Some good quality elbaite crystals were found extracted along the margin of the quartz-rich cores; while gem quality blue-green hexagonal beryl crystals and some other coloured tourmalines are locally present in the clay-filled vugs in the late veins. Other minerals won from the pegmatites of the area include gem quality amethyst, rose and smoky quartz crystals. The occurrences of pinkishto reddish (Li-bearing) and greenish books of muscovite, as well as pinkish lepidolite and Ta-Nb ores are associated with the lepidolite-dominated subunit of the intermediate zoneof the pegmatites.

Petrographic studies revealed intergranular texture of microcline-perthite, albite, quartz and muscovite as the essential minerals (Fig. 4.31), while garnet, apatite, zircon, beryl and tourmalines are the accessory amounts. Table 4.5 presents the modal compositions of the minerals in the pegmatites of the area.

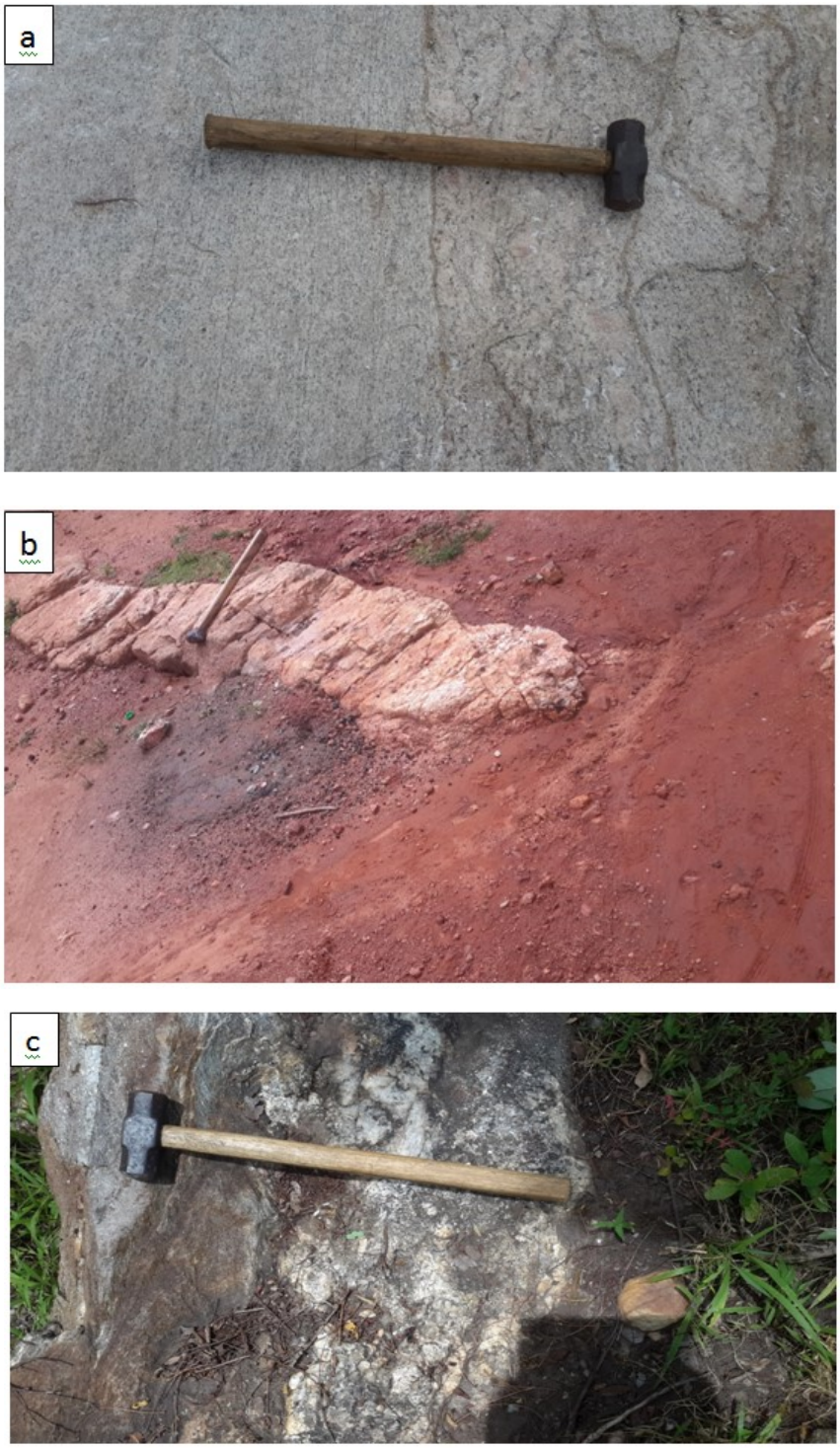

Fig. 4.30: Field photographs of pegmatites of Iwere-Ile area showing: (a) sharp contact with the biotite granites; (b) unaltered pegmatite dyke within completely altered host biotite granite; (c) pegmatite dyke with quartz-dominated core zone rimmed by medium to coarse grained microcline- and muscovite-rich intermediate zone.

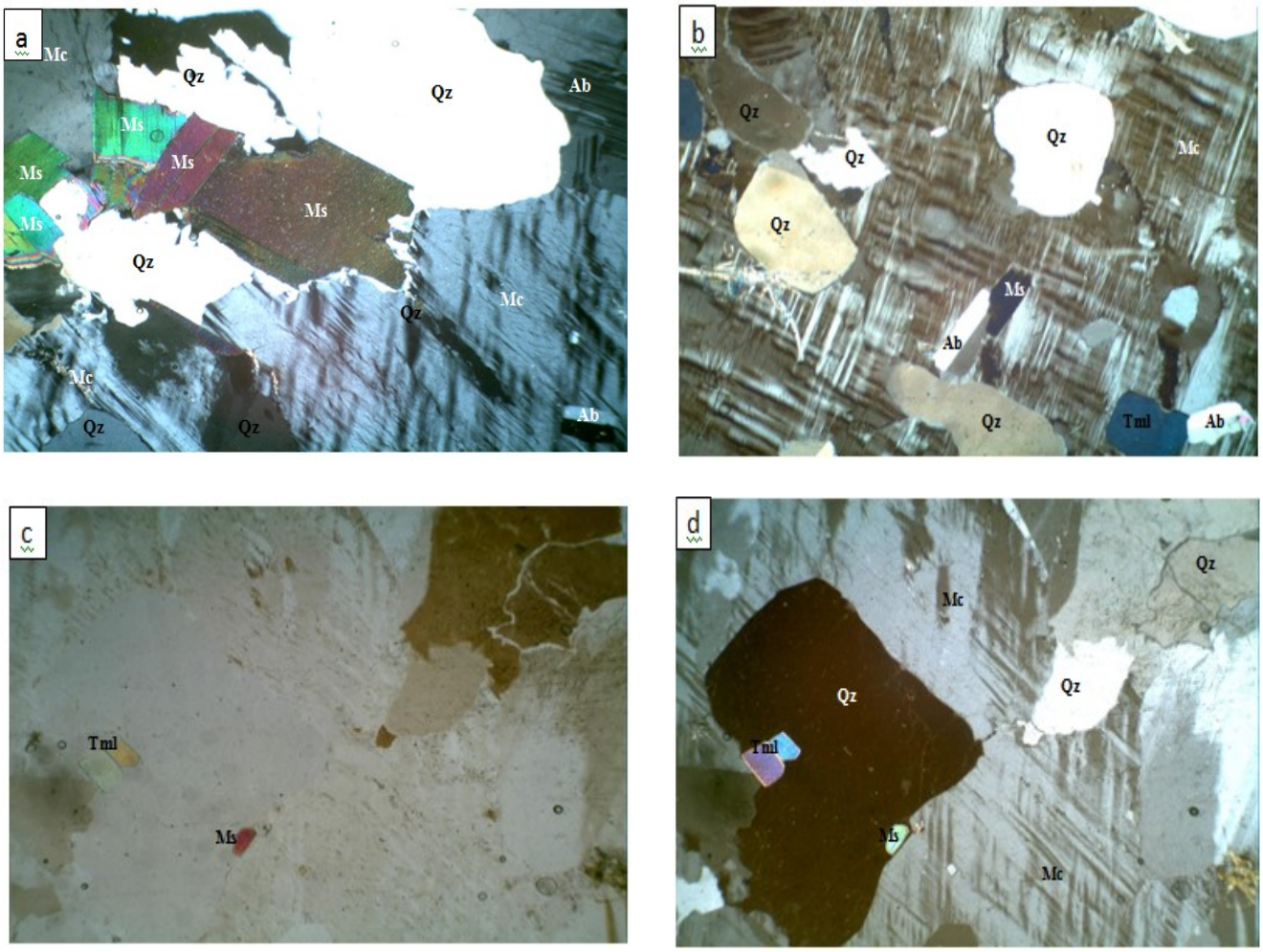

Fig 4.31: Photomicrograph of pegmatites of Iwere-Ile area, showing(a) intergranular texture of microcline, albite, quartz and muscovite. Note the inclusion of albite crystal in the microcline grain toward the bottom right hand side; (b) the inclusions of quartz and albite in microcline grain; (c) inclusion of tourmaline crystals in quartz (not indicated in plane-polarised-light) but (d) well indicated in crossed polars (Mag. x40). (Mc = microcline; Ab = albite; Qz = quartz; Ms = muscovite).

Table 4.5: Modal composition of the Iwere-Ile mineralised pegmatite

	IW1	IW2	IW3	IW4	IW5	IW6	IW7	IW8
Microcline-pertithe	42	56	50	55	44	50	54	45
Albite	7	8	10	12	5	12	8	14
Quartz	32	24	28	25	36	28	23	30
Muscovite	15	8	8	6	10	6	10	8
Biotite	-	-	1	-	1	-	-	-
Tourmaline	2	3	2	1	2	2	2	1
Garnet	1	1	1	1	1	1	1	1
Total	99.0	100.0	100.0	100.0	99.0	99.0	98.0	99.0

4.2 Mineralogical composition of weathering profiles developed over the pegmatites

Pegmatites in the areas of investigation show variations in petrological associations, mineralogical assemblages and geochemical characteristics. Earlier studies have loosely categorised these pegmatites into simple (barren) and complex (mineralised) pegmatites, based on their potential enrichments in rare-metals and gem minerals. Barren and mineralised pegmatites occur together within basement rocks of southwestern Nigeria, and thick residual lateritic profiles developed on some of these pegmatites. The mineralogical characteristics of these residual weathering profiles overlying the pegmatites in the areas of study were investigated, in order to determine the distribution of primary minerals and secondary weathering products that characterised respective horizon of the profiles. These are described in relation to the mineralogical attributes of the parent rocks.

4.2.1Mineralogical composition of weathering profile over Osu barren pegmatites

Thick residual profile, developed over the Osu pegmatite, was sampled at a location about 3.4 km northwest of Oke-Osin Village (07º 40'. 228 / 004º 35' 279). A vertical profile of4.2 m deep, which consists of three horizons were observed in the hand-dug pit. These are the A, B and C-horizons (Fig. 4.32), which are distinguished on the basis of colour, texture, compaction, and the extent of preservation of parent structures. The A-horizon (top soil) is about 1.6 m in thickness and it is dark grey to dark brown in colour. It is principally composed ofquartz pebbles and decomposed organic matter, with lesser amount of unweathered feldspars, clay minerals and muscovite flakes. The B-horizon is about 2.2 m thick and yellowish brown in colour. It is compact and sticky, being clay-rich. The B-horizon subtly grade into the underlying C-horizon.

The C-horizon is composed of saprolite, which about 0.4 m thick and yellowish in colour. It is principally composed of clay minerals, minor amount of muscovite flakes, quartz andpartially altered feldspar materials. It is fairly compacted and shows a lesser degree of thepreserved parental structures. The mineralogical character of the different horizons of the lateritic profile derived from theOsubarren pegmatite, as determined by XRD analysis, shows the predominance of quartz (*ca*. 73.62 wt.%)in the A-horizon, while microcline (*ca*. 10.25 wt.%)and albite (*ca*. 5.84 wt.%) show relatively high contents in this horizon.

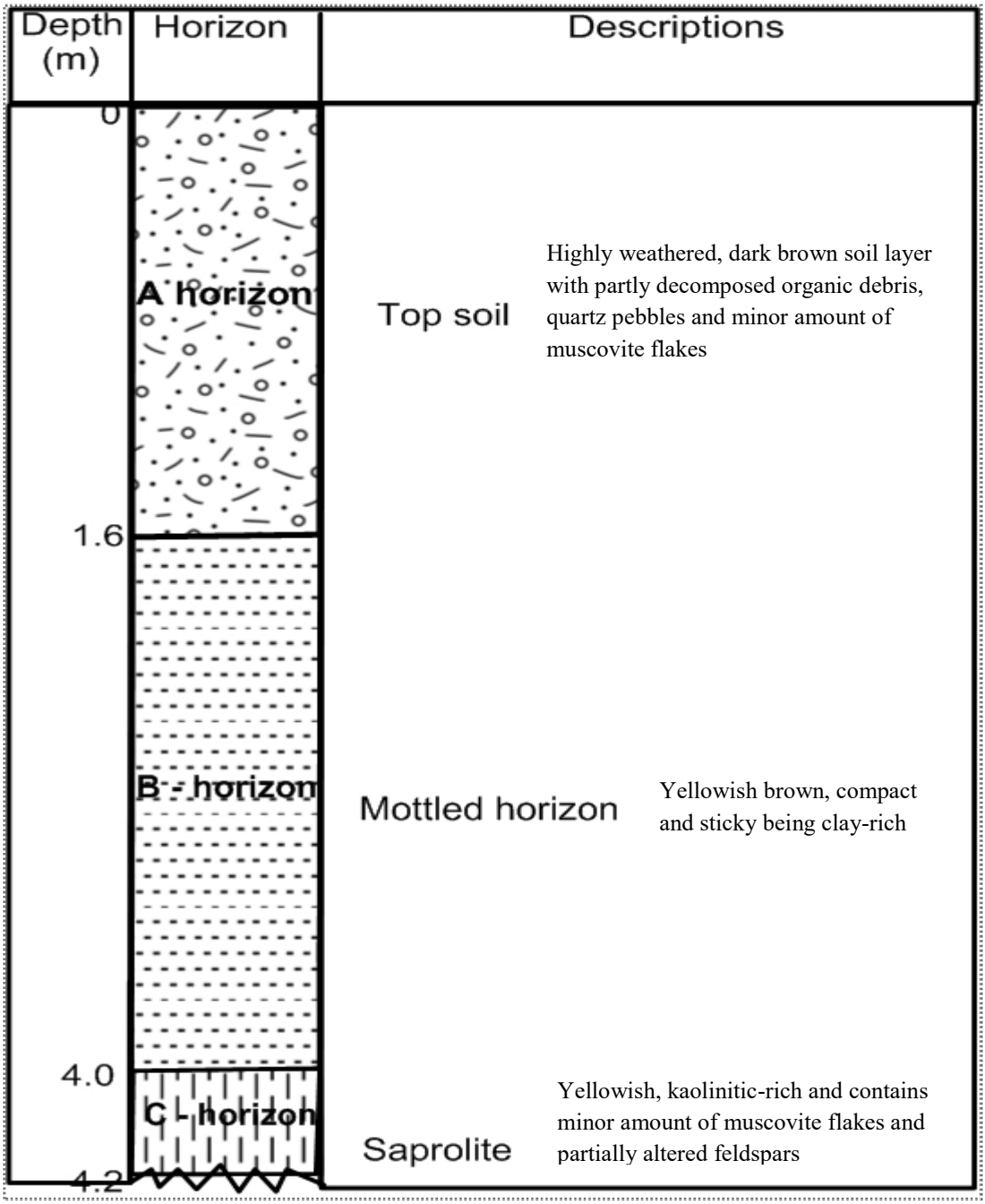

Fig. 4.32: Weathering profile above pegmatite at Osu area

The high contents of these primary minerals may be connected to the possible incipient nature of weathering of the pegmatite. Kaolinite, as a secondary mineral, indicates a low abundance (ca. 10.08 wt.%) in this horizon, while muscovite content of 0.22 wt.% is equally considered relatively low. The low kaolinite abundance in the A-horizon is possibly a reflection of the continuous eluviation of clay materials as suspended particles into the underlying B-horizon, while the low muscovite (0.22 wt.%) contents may possibly be attributed to the low modal abundance of this mineral in the parent pegmatite. Conspicuous peaks of quartz are recorded at 4.26Å, 3.34Å, 2.56Å, 2.45Å, 2.38Å, 2.24Å, 2.12Å, 1.99Å, 1.82Å, 1.67Å, 1.62Å, 1.54Å, 1.45Å and 1.38Å values (Fig. 4.33a).
The B-horizon showsrelatively lower quartz contents (50.37 wt.%), but a slightly enhanced muscovite (3.65 wt.%) abundance and a semblance in microcline and albite contents to the overlying A-horizon. The relatively enhanced muscovite contents may possibly be due to its transport to this zone as solid residue. The B-horizon characteristically indicates a relatively higher kaolinite (35.60 wt.%) contents, being a zone of clay accumulation; while microcline (6.82 wt.%) and albite (3.58 wt.%) indicate depletion in amounts. Distinctive kaolinite peaks are recoded at Å values of 7.12, 4.47 and 3.58, while muscovite indicates few peaks at 9.98Å, 4.49Å, 2.93Å and 2.85Å (Fig 4.33b).

The underlying saprolitic layer (C-horizon) indicatesa reduced kaolinite (ca. 34.56 wt.%)content, as it is evidently composed of partially altered feldspar materials, while slightlyenhanced contents of primary minerals (quartz, 59.2 wt.%; microcline, 9.03 wt.% and albite, 3.94 wt.%) are equally evident in this zone (Fig. 4.33c). The abundances of the primary minerals may be a reflection of the proximal bedrock composition, while the fairly high kaolinite content is consistent with the abundance of incipiently altered feldspars in the saprolitic layer. The mineralogical abundances of the primary mineral phases and the secondary alteration minerals are summarised in Table 4.6 and Fig 4.34; while the X – ray diffraction profiles for the lateritic profile is present in Appendix 4.

On the whole, the *in situ* weathering profile of the Osubarren pegmatite does not show abundance (in minor or accessory amount) of some other accessory minerals, but indicate the presence of the primary minerals and kaolinite as secondary alteration mineral.

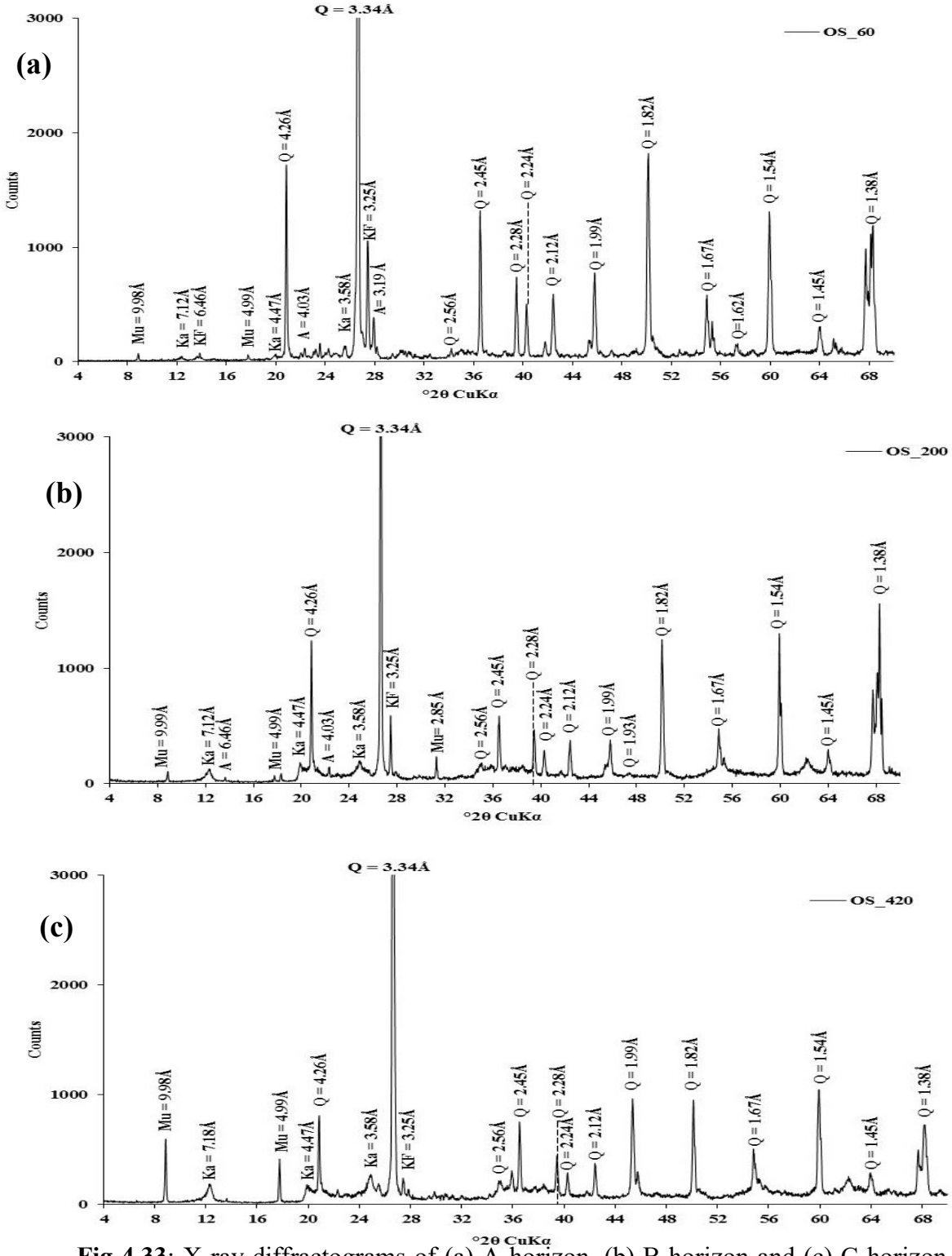

Fig 4.33: X-ray diffractograms of (a) A-horizon, (b) B-horizon and (c) C-horizon samples of the lateritic profile derived from pegmatite of Osu area (Ka = kaolinite; Q = quartz; Mu = muscovite; KF = K-feldspar; and A = albite).

Table 4.6: Quantitative mineralogical composition of the residual weathering profile of the barren pegmatite of Osu area

	Major minerals						
Profile horizon	Depth (m)	Quartz (%)	Muscovite (%)	Kaolinite (%)	Microcline (%)	Albite (%)	Total
A-horizon	0.2	74.39	0.72	8.3	10.05	6.53	99.99
	0.4	75.05	0.27	6.66	12.24	5.77	99.99
	0.6	76.55	0.13	7.82	9.77	5.75	100.0
	0.8	60.86	0.15	13.64	15.68	9.66	99.99
	1.0	71.24	0.12	11.75	10.99	5.9	100.0
	1.2	80.59	0.12	7.58	8.26	3.45	100.0
	1.4	77.89	0.08	8.47	8.82	4.73	99.99
	1.6	72.40	0.15	16.38	6.19	4.88	100.0
B-horizon	1.8	58.26	4.78	28.48	5.39	3.11	100.0
	2.0	54.19	3.15	34.96	5.22	2.48	100.0
	2.2	45.73	4.74	37.09	8.28	4.36	100.0
	2.4	45.14	5.55	40.04	6.23	3.04	100.0
	2.6	52.55	3.63	32.77	7.11	3.94	100.0
	2.8	50.79	4.02	36.09	5.40	3.70	100.0
	3.0	51.28	3.99	34.62	6.05	4.07	100.0
	3.2	47.54	3.17	37.71	6.83	4.75	100.0
	3.4	49.96	3.03	35.58	7.74	3.70	100.0
	3.6	47.92	3.03	37.42	8.93	2.70	100.0
	3.8	50.70	1.04	36.90	7.80	3.57	100.0
C-horizon	4.0	59.63	0.50	24.16	11.2	4.51	100.0
	4.2	58.77	0.32	30.69	6.86	3.36	100.0

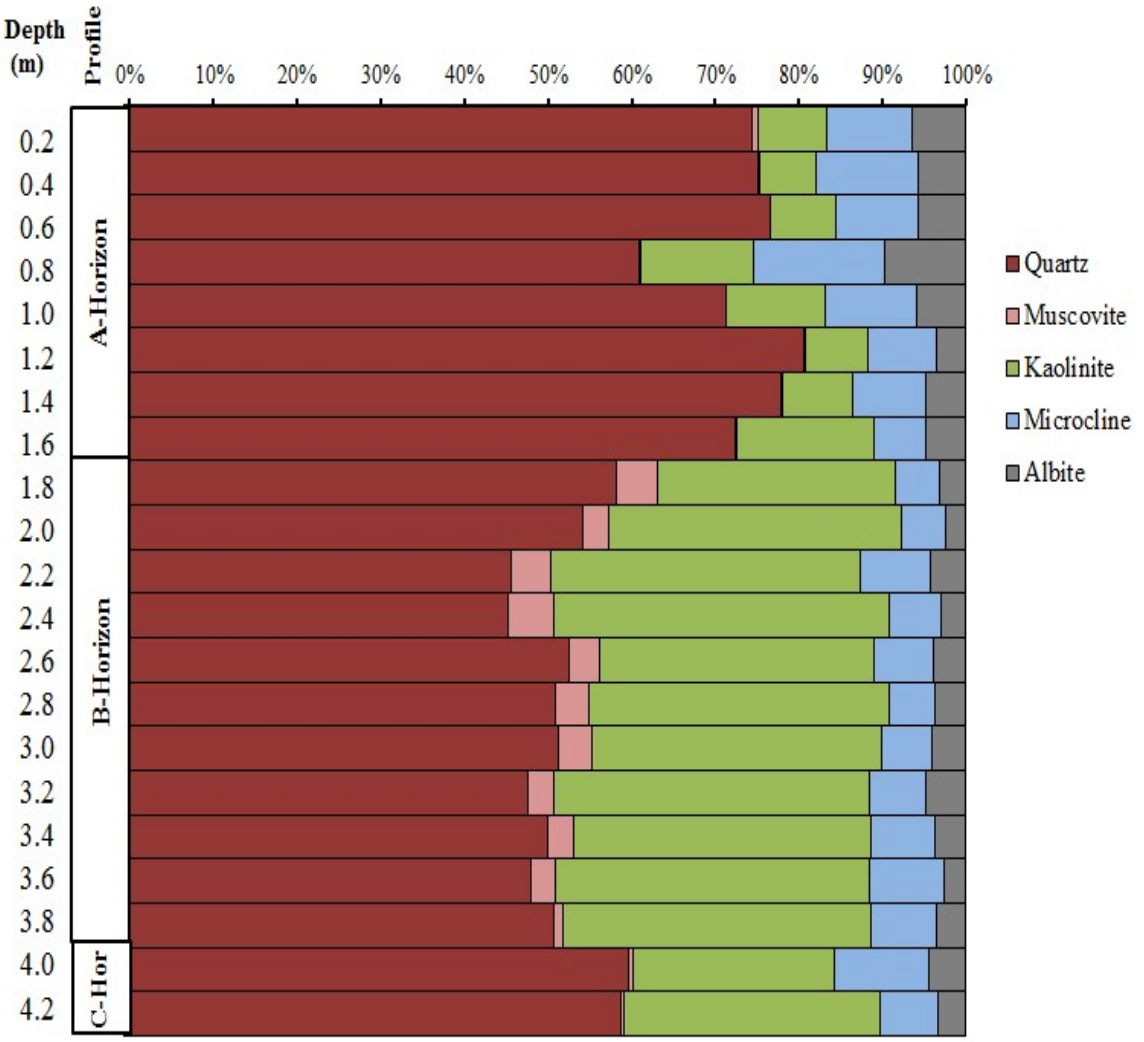

Fig. 4.34: The distribution of mineral phases in different horizons of the weathering profile at Osu area.

4.2.2 Mineralogical composition of weathering profile over Ijero mineralised pegmatites

The investigated weathering profile from Ijero area is located at about 200 m off Ijero-IpotiRoad (07º 49'. 611 / 05º 04'. 281).It is derived from the deep residual weathering of the main complex pegmatite of the area. The profile is about 5.4 metres deep and consists of three physically and chemically distinct layers, which are the A, B and C-horizons (Fig.4.35), respectively. The A-horizon is a relatively thin (0.2 m) loose top soil, which is dark brown in colour. It is composed of organic matter, quartz pebbles, minor muscovite flakes and clay minerals. The B-horizon is 2.8 metres thick: it comprises the 1.2 metres thick lateritic layer, which overlies the 1.6 metres thick mottled zone. The lateritic layer is reddish brown in colour, composed of minor loose quartz pebbles and kaolinite-rich materials. The mottled layer is yellowish red in colour, particularly kaolinite-rich and showing partial retention of the original pegmatite texture. The C-horizon is mainly saprolitic (1.8 m thick), overlying a relatively thinly (0.6 m) exposed and incipiently weathered saprock. The saprolitic layer is light pinkish to yellowish in appearance, and mainly composed of crumbly and partially decomposed feldspar fragments, muscovite flakes and gritty quartz materials. Beneath the C-horizon lies the freshly opened pegmatite bedrock.

The distribution of both the major and minor mineral phases (expressed in wt.%) of the residual profile, as analysed by the XRD, indicatedthat quartz is the main non-weatherable mineral in the parent pegmatite.It shows dominance through all the horizons of the profile. Its abundance varies from 72.67 wt.% in the topsoil (A-horizon) to 62.83 wt.%, 43.6 wt.% and 61.29 wt.% in the lateritic (upper B-horizon), mottled horizon (lower B-horizon) and C-horizon, respectively.

The quartz content in the top soil is partly due to the intense chemical leaching of thelabile components and the downward transportation of clay materials to the underlying B-horizon,thereby making quartz the principal mineralphase of the A-horizon. It is worthy of note that this zone is the most proned to actions of meteoric agents.There is, however, a slight reduction in the quartz contents in the lateritic zone (ca. 62.82 wt.%), while the mottled horizon shows the least quartz abundance (ca. 43.16 wt.%).

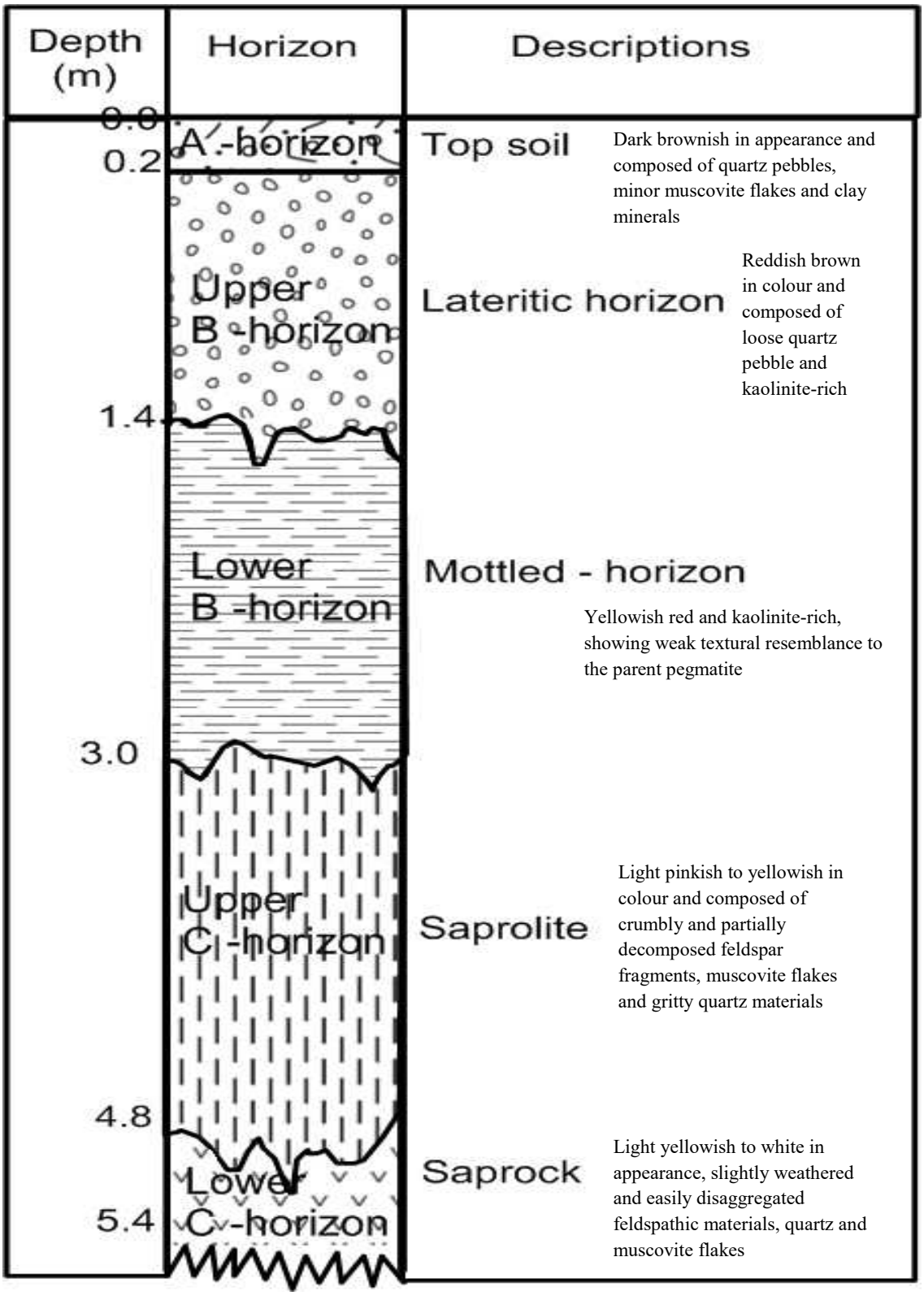

Fig. 4.35: Weathering profile above pegmatite at Ijero area

The relatively reduced quartz contents in the mottled zone essentially results from the secondary accumulation of clay minerals that characterise this zone. This zone is equally noted for much reduced transport of silica components.

Quartz, however, continues its increasing trends below the mottled horizon to the basal bedrock material. Quartz shows peak intensities at 4.26Å, 3.34Å, 2.56Å, 2.45Å, 2.28Å, 2.24Å, 2.12Å, 1.99Å, 1.82Å, 1.67Å, 1.54Å, 1.45Å and 1.38Å values (Fig. 4.36).

The relatively non-weatherable muscovite mineral phase is pervasive in all the horizon of the profile (Table 4.7), but show high contents in the top soil (ca. 4.93 wt.%) and the upper B-horizon (ca. 4.91 wt.%). It however indicates a subtle depletion in abundances down through the profile. Other weatherable primary mineral phases, such as microcline and albite are generally of marginal abundances in the weathering profile, and show occasional appearances in few samples of the horizons (Table 4.7). Muscovite indicates notable peaks at 10.02Å, 4.99Å, 3.10Å, 5.00Å, 3.00Å and 10.00Å values (Fig. 4.36); while albite portrays very few peaks at 6.38Å and 3.19Å values (Fig. 4.36). Potassium feldspar displays very few and small peaks mainly at 3.25Å value (Fig. 4.36). The high susceptibility of the alkaline feldspar to weathering is evident from the few and very small peaks display by this minerals in the diffractograms.

Kaolinite is the principal secondary mineral phase in the profile (Table 4.7), and it indicates the greatest abundance (ca. 47.71 wt.%) in the mottled horizon. This horizon is marked by accumulation of clay minerals. Kaolinite, however, reveal the lowest level in the strongly leached top soil (ca. 14.62 wt.%), but indicate high contents in the basal saprolitic (ca. 31.59 wt.%) and saprock (ca. 35.82 wt.%) zones that are marked by partially decomposed feldspar minerals. Kaolinite shows peak intensities at 7.15Å, 4.47Å, 3.58Å, 7.17Å, 7.14Å and 7.17Å (Fig. 4.36). Rutile (ca. 0.90-1.90 wt.%) and hematite (ca. 0.31 – 1.11 wt.%) show minor abundances in the profile (Fig. 4.36), and are fairly consistent in the B-horizon. Titanium (TiO_2) and Fe (Fe_2O_3) show similar geochemical affinity and are commonly associated in surficial environment. Rutile is indicated by 2.49Å values. Anatase is a hydrated polymorph of rutile, and it is found in the water-dominated (hydrolytic) saprolite zone of the profile. Anatase shows small peaks

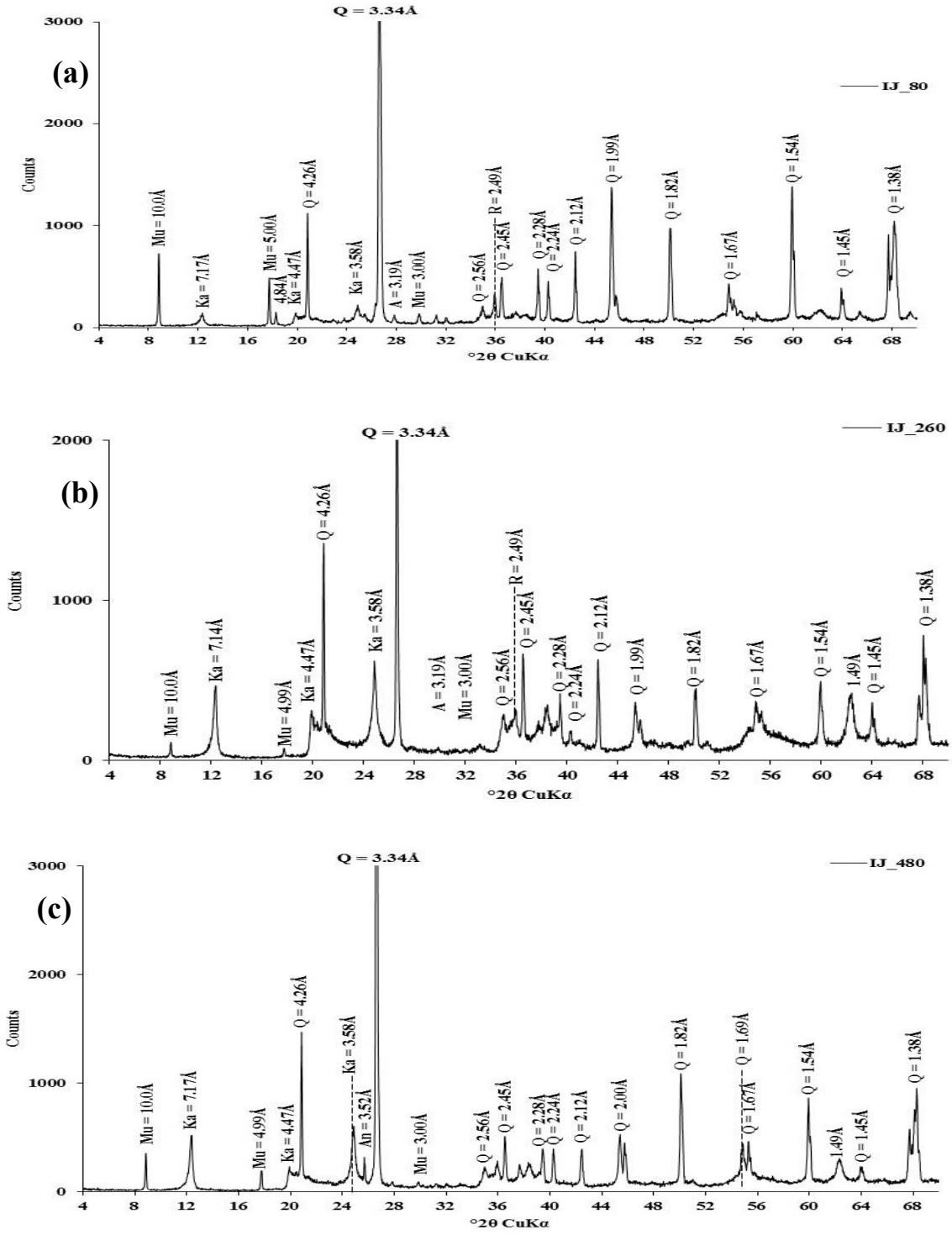

Fig 4.36: X-ray diffractograms of (a) upper B-horizon (0.8 m), (b) lower B-horizon (2.6 m) and (c) lower C-horizon (4.8 m) samples of the lateritic profile derived from mineralised pegmatite of Ijero area (Ka = kaolinite, Q = quartz, Mu = muscovite, A = albite, KF = K-feldspar, R= rutile and An= anatase).

Table 4.7: Quantitative mineralogical composition of the residual weathering profile of the mineralised pegmatite of Ijero area

	Major minerals						Minor minerals		
Profile horizon	Depth (m)	Quartz (%)	Muscovite (%)	Kaolinite (%)	Microcline (%)	Albite (%)	Hematite (%)	Rutile (%)	Total
A-horizon	0.2	72.67	4.93	14.62	6.22	1.56			100.0
Upper B-horizon	0.4	47.78	7.35	44.87					100.0
	0.6	67.47	6.06	16.95	7.82		0.80	0.90	100.0
	0.8	70.4	1.98	25.21			0.95	1.46	100.0
	1.0	59.58	6.12	32.02			0.78	1.52	100.0
	1.2	68.85	4.38	25.09			0.70	0.97	99.99
	1.4	62.78	3.58	31.62			0.71	1.32	100.0
Lower B-horizon	1.6	46.1	2.28	48.80			0.92	1.90	100.0
	1.8	43.27	1.40	53.03			0.94	1.36	100.0
	2.0	40.15	2.30	55.52			0.65	1.38	100.0
	2.2	54.3	1.92	41.86			0.58	1.34	100.0
	2.4	54.64	2.06	41.08			0.86	1.36	100.0
	2.6	29.99	1.57	66.45			1.11	0.90	100.0
	2.8	32.39	12.18	37.29	11.49	5.70	0.95		100.0
	3.0	44.42	6.80	48.78					100.0
Upper C-horizon	3.2	61.65	17.39	20.96					100.0
	3.4	69.63	2.89	27.47					99.99
	3.6	64.3	3.18	31.20			0.69	0.62	99.99
	3.8	62.58	4.18	33.25					100.0
	4.0	57.56	3.06	39.38					100.0
	4.2	59.35	2.39	38.26					100.0
	4.4	73.53	1.13	25.34					100.0
	4.6	54.15	0.56	36.15	2.77	5.15	1.24		100.0
	4.8	51.52	0.61	44.94				2.93	100.0
	5.0	71.94	5.03	23.04					100.0
	5.2	57.13	2.03	38.83		0.97	1.04		100.0
Lower C-horizon	5.4	53.86	0.55	45.58					99.99

commonly at 3.52Å (Fig 4.36). The distribution of the primary and seconadray alteration minerals in the horizons of the weathering profile is summarised in Table 4.7 and Fig 4.37; while the X– ray diffraction profiles for the lateritic profile is present in Appendix 4.

4.2.3 Mineralogical composition of weathering profile over Komu mineralised pegmatite

The studied profile in the Komu area is located at about 1.5 km northeast (08º 17.692' / 03º 14. 962') of the Abuja Mining Camp, off the road to Agate Camp (Fig. 4.13). The vertical residual profile is about 4.6 m deep, and it is directly overlying mineralised pegmatite bedrock. It can be distinguished into A, B and C-horizons based on physical characteristics, such as colour, texture, compaction and the degree of preservation of the protolith features. The A-horizon is a fairly thick (0.6 m) dark brownish layer that is gravelly and organic matter-rich. The brownish yellow B-horizon is about 1.8 m thick and relatively clay-rich. The C-horizon is about 2.2 m thick, yellowish in colour and comprises the partially decomposed saprolite and saprock layers. Summary of the descriptions and thicknesses of the constituting horizons are provided in Fig.4.38.

The mineralogical data of the lateritic profile, derived from XRD analysis, show thepredominance of quartz (ca. 80.72 wt.%) butlesser amounts of microcline (ca. 8.52 wt.%), albite (ca. 3.06 wt.%) and muscovite (ca. 1.46 wt.%) in the A-horizon. All these primary mineral phases show fairly high contents in the A-horizon (top soil). Kaolinite content (ca. 5.44 wt.%) is relatively lower in the A-horizon, as compared to B (ca. 14.27 wt.%) and C-horizons (ca. 8.58 wt.%), respectively. This trend can be attributed to the intense eluviation processes that mark the A-horizon, which make it depleted in clay minerals. Quartz indicates peak intensities at 4.25Å, 3.34Å, 2.45Å, 2.28Å, 2.24Å, 2.12Å, 1.99Å, 1.82Å, 1.67Å, 1.66Å, 1.61Å, 1.54Å, 1.45Å, 1.42Å and 1.38Å values (Fig. 4.39). Schorl (black tourmaline) show minor amount (ca. 2.38 %) in the A-horizon. It displays very few peaks commonly at 4.00Å and 2.59Å (Fig. 4.39).

Quartz, the main chemically resistant primary mineral in pegmatites, indicates a relatively reduced content (ca. 55.4 wt.%) in the lateritic upper B-horizon. It, however, shows narrow variations within the horizons, and indicates reducing trends towards the base of the profile.

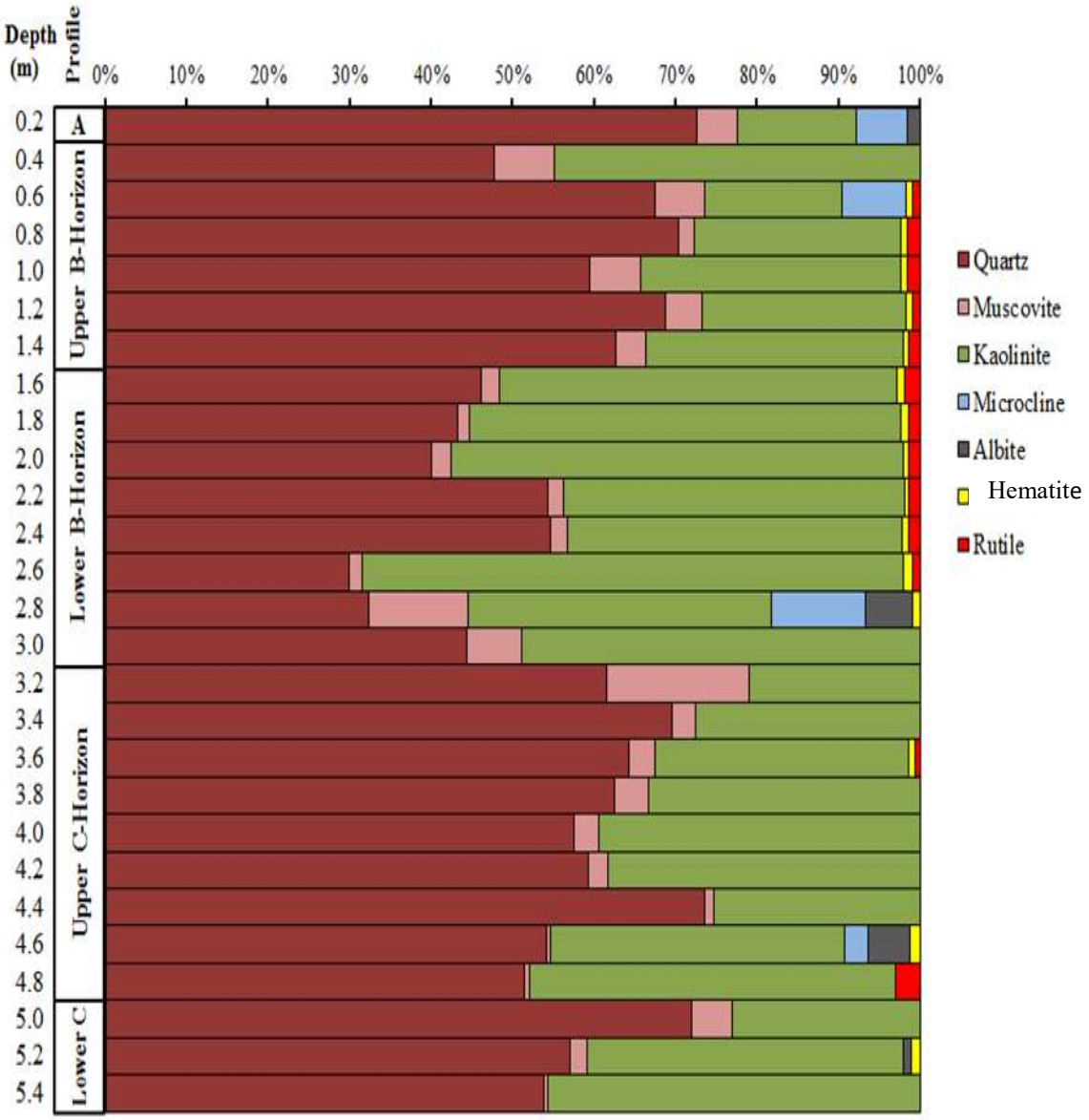

Fig. 4.37: The distribution of mineral phases in different horizons of the mineralised pegmatite weathering profile at Ijero area.

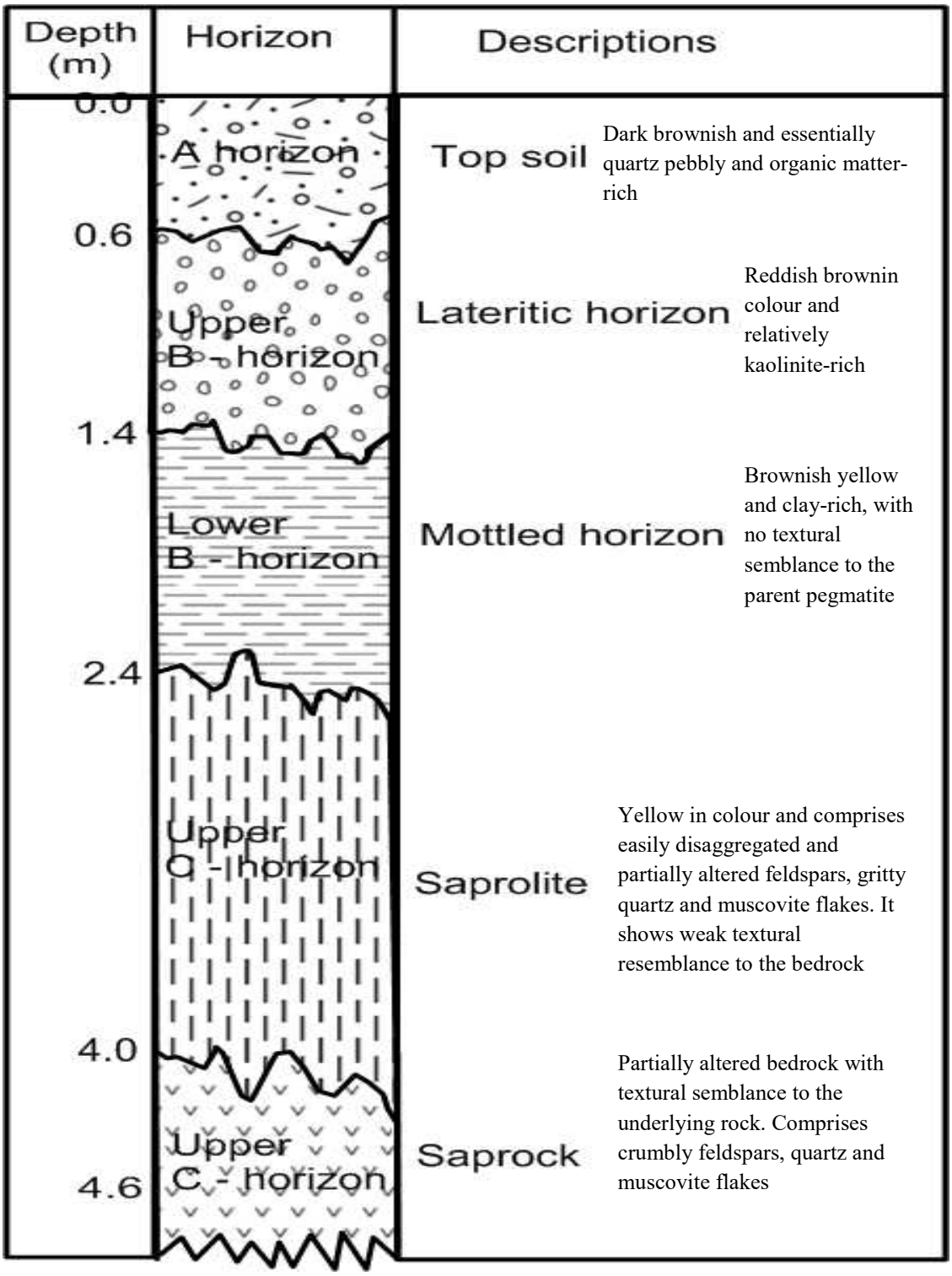

Fig. 4.38: Weathering profile above mineralised pegmatite at Komu area.

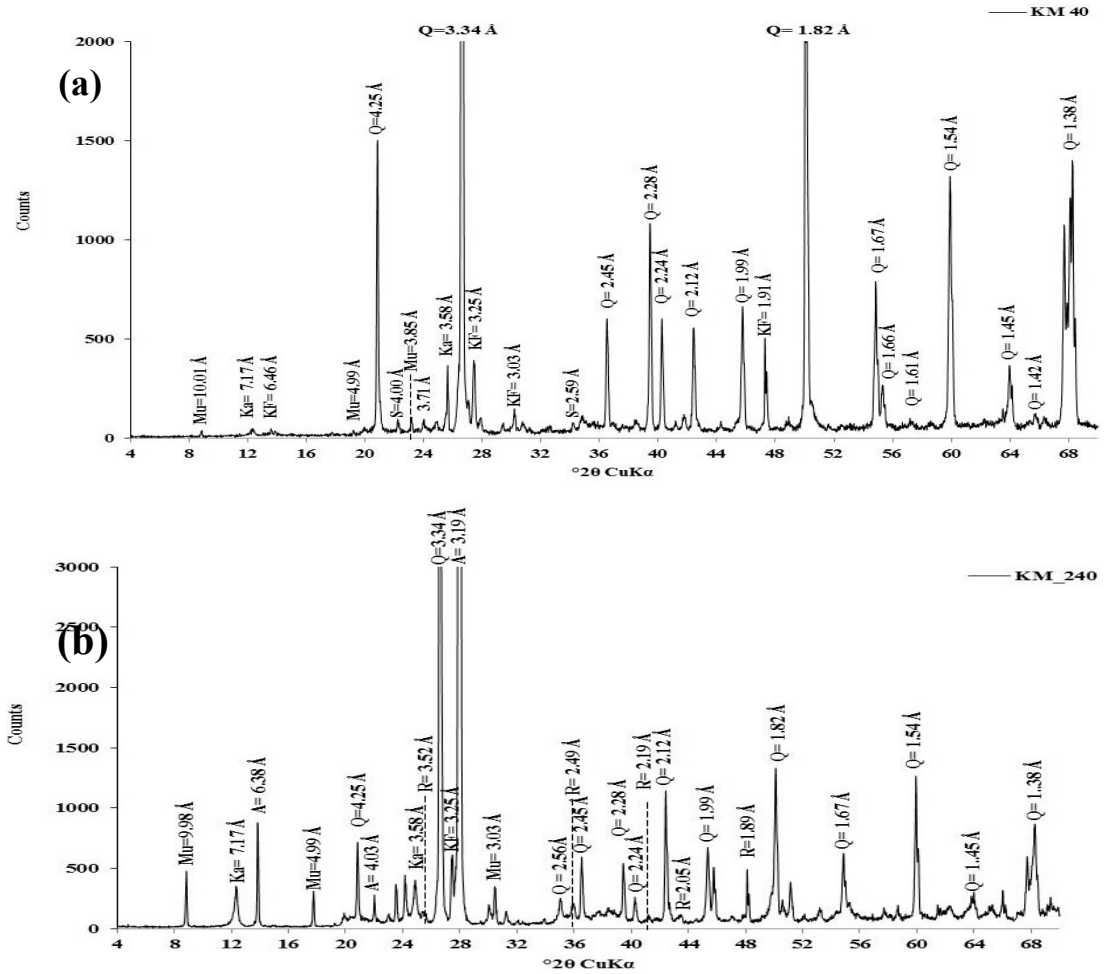

Fig 4.39: X-ray diffractograms of (a) A-horizon (0.4 m) (b) lower B-horizon (2.4 m)

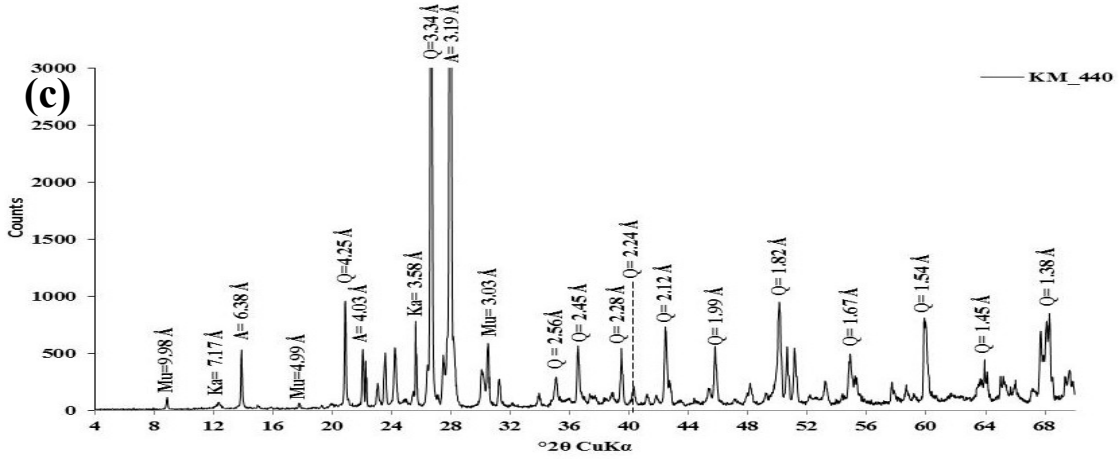

and (c) lower C-horizon (4.4 m) samples of the lateritic profile derived from mineralised pegmatite of Komu area (Ka = kaolinite; Q = quartz; Mu = muscovite; A = albite; KF = K-feldspar; S = schorl; and R = rutile).

Muscovite exhibits a small range (ca. 1.36-1.53 wt.%) in the A-horizon, but shows a much reduced contents in the B- and upper C-horizon. It, however, shows increasing abundance (ca. 3.18 wt.%) in the lower C-horizon, invariably reflecting its proximity to the bedrock. Other primary minerals, such as microcline (ca. 4.08-44.91 wt.%) and albite (ca. 2.16 - 56.42 wt.%) indicate high contents all through the profile. This possibly shows that thepegmatite is incipiently weathered and the extent of alteration of these highly weathering susceptible minerals is still relatively low. The feldspars, quartz and muscovite indicate enhanced contents in the upper and lower C-horizons, which is consistent with their closeness to the underlying bedrock pegmatite. X-ray diffractogram of Fig 4.39 indicates peaks intensities of albite at 6.38Å, 4.03Å, 3.19Å, 2.95Å and 1.89Å, respectively; while K-feldspar only shows few peaks at 6.46Å, 3.25Å, 3.03Å and 1.91Å values.

Kaolinite is the main product of alteration of feldspars. It shows relatively enhanced value (ca. 10.59 - 19.6 wt.%) in the clay-rich B-horizon, but display generally reduced trends in the A-horizon (ca. 5.44 wt.%) and C-horizon (ca. 5.95 wt.%), respectively. If the kaolinite content of this residual profile is compared to that of other pegmatite weathering profiles investigated elsewhere, the weathering profile of Komu pegmatite indicates relatively lower kaolinite contents. This compositional attribute can be mainly ascribed to the incipient weathering of the pegmatites and possibly the fairly high elevation of the residual profile. Kaolinite displays few peaks mainly at 7.12Å and 3.58Å (Fig. 4.39).

Rutile show minor amount (ca. 0.16 – 1.53 wt.%) towards the base of the residual profile, particularly the C-horizon. Rutile indicates few peaks at 3.52Å, 2.49Å, 2.19Å, 2.05Å and 1.89Å, respectively (Fig. 4.39). The mineralogical abundances of primary mineral phases and the secondary alteration minerals of the weathering profile are presented in Table 4.8 and Fig. 4.40; while the X – ray diffraction profiles for the lateritic profile is present in Appendix 4.

Table 4.8: Quantitative mineralogical composition of the residual weathering profile of the mineralised pegmatite of Komu area

	Major minerals						Minor minerals		
Profile horizon	Depth (m)	Quartz (%)	Muscovite (%)	Kaolinite (%)	Microcline (%)	Albite (%)	Schorl (%)	Rutile (%)	Total
A-horizon	0.2	86.80	1.53	3.83	5.46	2.37			99.99
	0.4	79.50	1.48	3.11	11.35	2.16	2.38		99.98
	0.6	75.85	1.36	9.38	8.75	4.66			100.0
Upper B-horizon	0.8	62.38	0.22	13.09	9.54	14.76			99.99
	1.0	55.08	0.27	13.07	11.78	19.8			100.0
	1.2	50.71	0.24	17.94	10.21	20.91			100.0
	1.4	53.43	0.19	13.97	9.97	22.44			100.0
Lower B-horizon	1.6	36.37	0.22	15.61	21.64	26.18			100.0
	1.8	35.24	0.15	10.59	31.98	22.03			99.99
	2.0	36.38	0.03	10.75	12.57	40.26			99.99
	2.2	29.99	0.08	19.6	4.08	45.95		0.32	100.0
	2.4	42.01	0.16	13.51	7.58	35.46		1.28	100.0
Upper C-horizon	2.6	27.31	0.04	5.05	44.91	22.68			99.99
	2.8	33.35	0.05	4.47	38.96	23.17			100.0
	3.0	34.17	0.12	13.88	20.32	30.75		0.78	100.0
	3.2	43.6	0.06	12.05	7.44	36.67		0.16	99.98
	3.4	34.16	0.03	8.61	10.49	46.71			100.0
	3.6	27.58	0.06	11.41	11.96	48.65		0.33	99.99
	3.8	25.47	2.22	8.89	12.1	50.37		0.94	99.99
	4.0	27.61	3.16	10.43	11.89	46.42		0.49	100.0
Lower C-horizon	4.2	32.67	1.99	8.88	11.01	44.92		0.52	99.99
	4.4	32.22	5.25	7.72	13.47	40.04		1.32	100.0
	4.6	33.04	2.29	6.79	12.85	43.50		1.53	100.0

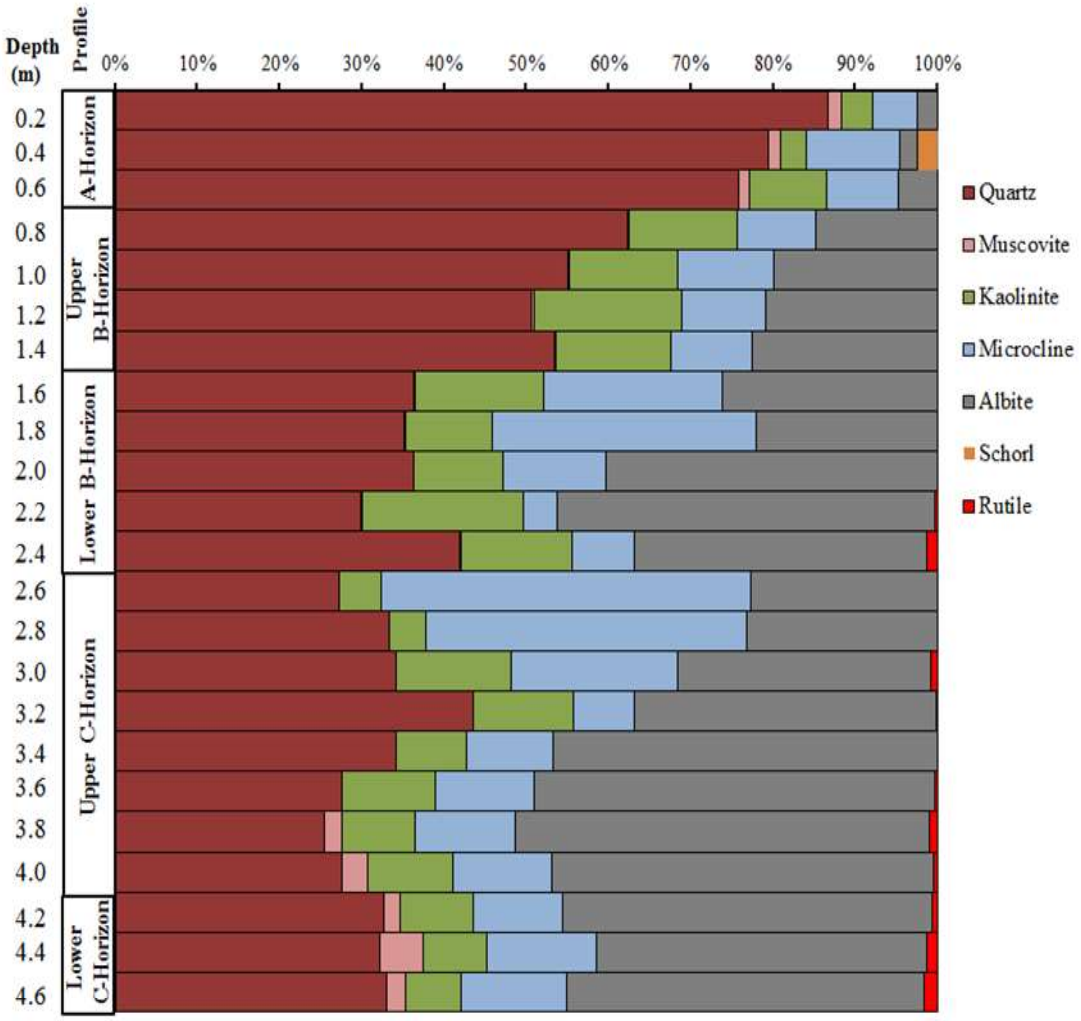

Fig. 4.40: The distribution of mineral phases in different horizons of the mineralised pegmatite weathering profile at Komu area.

4.2.4 Mineralogical composition of weathering profile over Ofiki mineralised pegmatite

The studied *in situ* weathering profile (N 08°21′.133″ / E 003°14′.692″) in Ofiki area is derived from a mineralised pegmatite dyke. The vertical profile is located about 1.2 km northwest of Ibudo Are Mining Camp (Fig. 4.19), which has been exposed by informal mining activities of artisanal miners for tourmalines and beryls. The profile is about 6.6 m deep, and can be divided into three distinctive horizons, using colour, texture, extent of compaction and relict parent features. These are essentially the A, B, and C-horizons (Fig. 4.41 and Fig. 4.42).

The A-horizon is about 1.0 m thick, brownish gray to brownish in colour, with humic contents ofpartially decomposed organic materials. It is composed of quartz pebbles andminor amount of clay materials. The B-horizon is about 3.6 m thick and brownish to light pinkish in colour. It is clay-rich and shows minor content of muscovite plates. This zone gradually grades into the C-horizon, which is about 2 m thick, light pinkish to yellowish in appearance and composed of crumbly and partially altered pegmatite rock material. The C-horizon grades into the underlying pegmatite parent rock.

The mineralogical character of the different horizons of the weathering profile derived from Ofiki mineralised pegmatite, as determined by XRD analysis, shows that the A-horizon (top soil) of the residual profile is dominated by quartz (ca. 68.51 wt.%) with fairly high abundance of muscovite (ca. 5.30 wt.%) and enhanced content of kaolinite (ca. 19.55 wt.%). The relatively high abundances of quartz and muscovite reveal the non-susceptibility of these primary minerals to weathering processes;while high kaolinite contents in the A-horizon could perhaps reflect a less rigorous transportation of kaolinite as suspended material to the B-horizon and high degree of weathering witnessed by the parent pegmatite bedrocks. The abundance of quartz in the A-horizon is revealed by its intensities at 4.25Å, 3.34Å, 2.56Å, 2.45Å, 2.28Å, 2.24Å, 2.12Å, 1.99Å, 1.82Å, 1.67Å, 1.54Å, 1.45Å and 1.38Å values; while the abundance of muscoviteis indicated by peak intensities at 9.88Å and 4.99Å, (Fig. 4.43a).

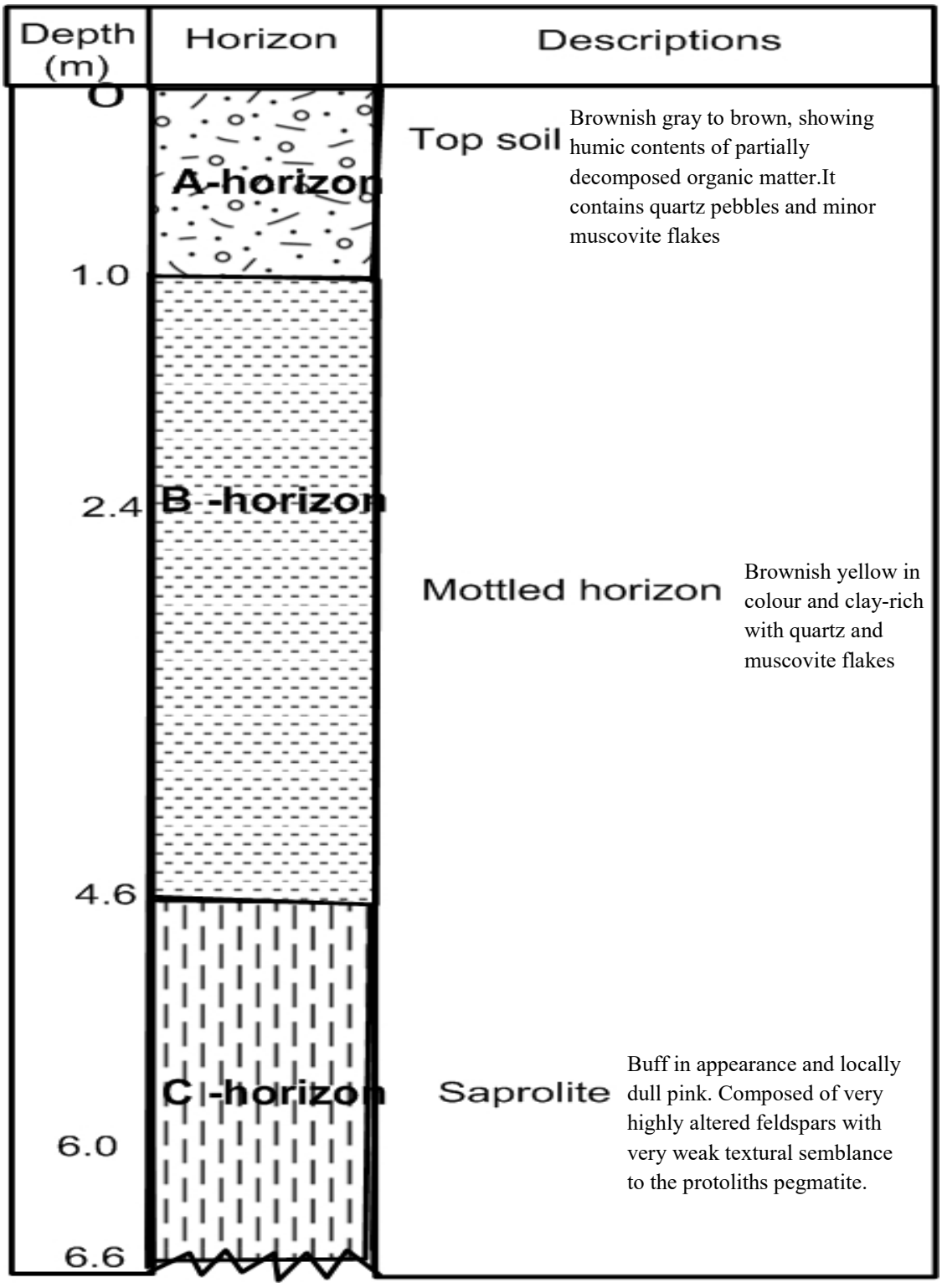

Fig. 4.41: Weathering profile above the mineralised pegmatite at Ofiki area

Fig. 4.42: Field photograph showing the sampled pegmatite lateritic profile at Ofiki area

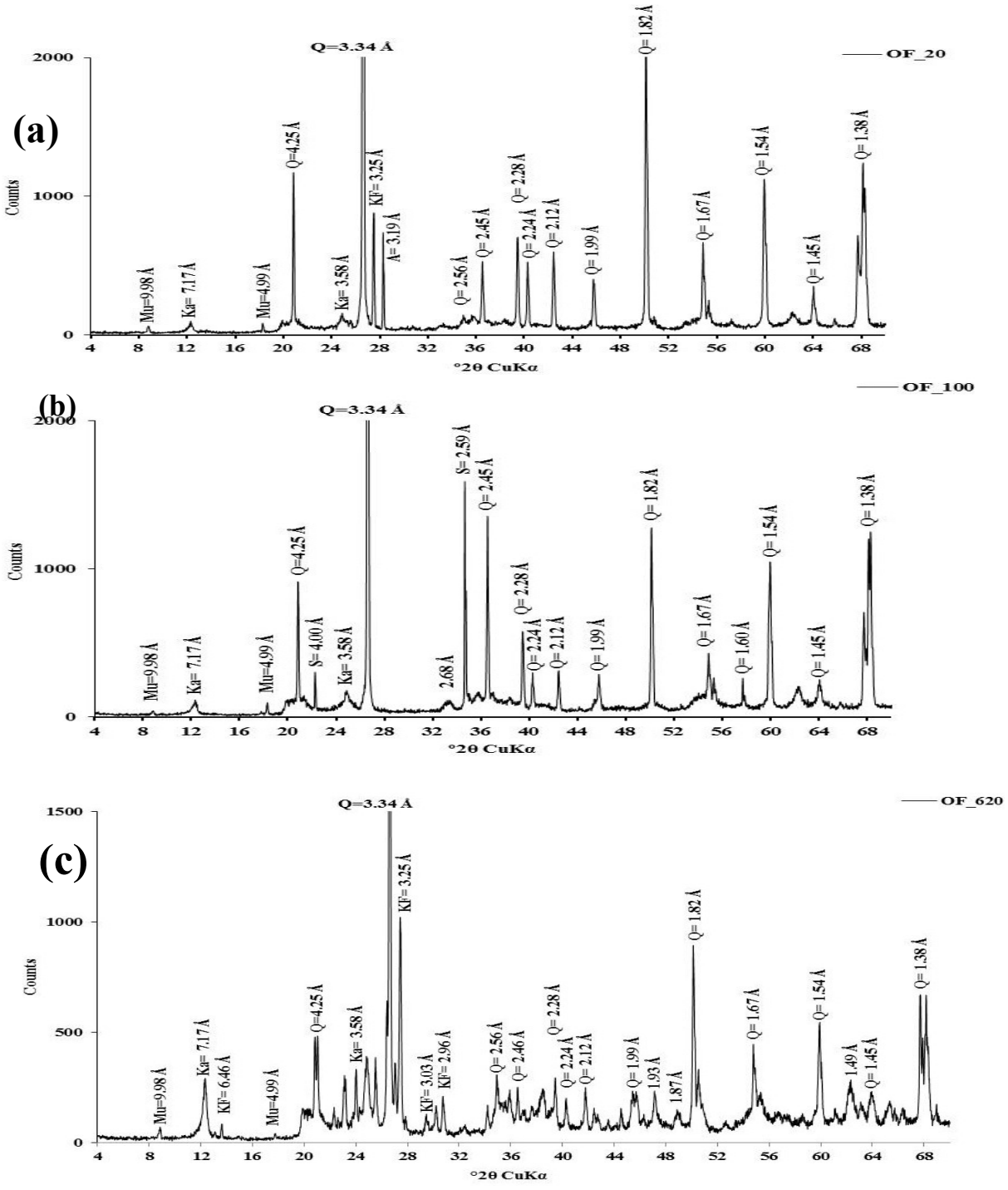

Fig 4.43: X-ray diffractograms of (a) A-horizon (0.2 m), (b) A-horizon (1.0 m) and C-horizon samples of the lateritic profile derived from mineralised pegmatite of Ofiki area (Ka = kaolinite; Q = quartz; Mu = muscovite; A = albite; KF = K-feldspar; S = schorl).

The B-horizon shows reduced contents of quartz (ca. 54.02 wt.%) but enhanced muscovite (ca. 13.49 wt.%) and kaolinite (ca. 26.62 wt.%) contents. Kaolinite, as a secondary mineral,is understandably derived from the chemical weathering of feldspars; while the enhancement in muscovite in the B-horizon can be primarily ascribed to its relative non-weatherability in the supergene environment and possibly due to its transport as solid suspended material into this horizon. Kaolinite indicates peaks at 7.17Å and 3.58Å; while muscovite displays peaks at 9.98Å and 4.99Å (Fig. 4.43b). The C-horizon indicates the least contents of quartz (ca. 47.20 wt.%) amongst the profile horizons, but with increase abundances of muscovite (ca. 10.93 wt.%) and kaolinite (ca. 36.88 wt.%). These enhanced contents of the primary minerals (quartz and muscovite) and kaolinite (secondary mineral) in pegmatite saprolite zone could possibly be a gradually conformity of the partially decomposed C-horizon to modal abundances of quartz and muscovite in the underlying pegmatite bedrock. The XRD data show the moderate amount of albite (ca. 3.04 wt.%) and microcline (ca. 4.19 wt.%) in the upper A-horizon, while their absence in the intermediate B-horizon can be attributed to their high degree of weathering among pegmatite primary minerals. The presence of microcline in the C-horizon can be linked to its proximity to the basal pegmatite rock materials. Microcline displays peak intensities at 3.25, 6.46, 3.03 and 2.96Å in the C-horizon (Fig. 4.43c). The quantitative mineralogical composition (expressed in wt.%) of the different horizons of the profileis presented in Table 4.9 and Figure 4.44.

Schorl and hematite, as minor minerals, are sparse and only show sporadic appearances in few horizons of the residual profile. Goethite (ca. 3.65–17.60 wt.%)andhematite (ca. 5.34 – 7.81 wt.%), however, show fairly high variability amongst samples of the same horizon, and are found in the lower B-horizon. Goethite could possibly be product of hydrolytic and oxidative alteration of magnetite in the relatively water-rich B-horizon. Schorl indicates very few peaks at 4.00Å and 2.59Å values (Fig. 4.43), while hematite could be identified with a peak value of 2.69Å (Fig. 4.43). Goethite could not be reflected in the diffractograms because of its amorphous nature in pedogenic condition; however, it was part of the mineral phases evaluated during the XRD quantitative determination of various mineral phases of the lateritic profile.

Table 4.9: Quantitative mineralogical composition of the weathering profile of the mineralised pegmatite of Ofiki area

		Major minerals					Minor minerals			
Profile horizon	Depth (m)	Quartz (%)	Muscovite (%)	Kaolinite (%)	Microcline (%)	Albite (%)	Schorl (%)	Hematite (%)	Goitite (%)	Total
A-horizon	0.2	74.08	1.78	16.03	3.50	4.52				100.0
	0.4	70.02	3.30	18.82	4.22	3.04		0.62		100.0
	0.6	69.63	5.68	15.16	6.21	3.32				100.0
	0.8	67.25	7.65	20.98	2.84	1.28				100.0
	1.0	61.58	8.10	26.77			3.55			100.0
B-horizon	1.2	56.85	11.12	32.03						100.0
	1.4	60.59	12.76	26.65						100.0
	1.6	66.66	12.57	20.77						100.0
	1.8	55.34	12.22	27.10				5.34		100.0
	2.0	44.54	13.68	33.97				7.81		100.0
	2.2	46.66	14.45	33.32				5.57		100.0
	2.4	46.12	20.30	21.30					12.28	100.0
	2.6	50.35	16.73	23.14					9.78	100.0
	2.8	51.02	13.75	23.69					11.56	100.0
	3.0	60.77	13.57	25.66						100.0
	3.2	43.64	12.57	26.19					17.6	100.0
	3.4	49.40	17.54	19.83					13.23	100.0
	3.6	63.37	11.38	20.75					4.50	100.0
	3.8	53.77	12.02	29.81					4.39	99.99
	4.0	54.38	14.58	25.70					5.34	100.0
	4.2	60.70	12.21	27.08						99.99
	4.4	51.75	10.50	33.04					4.70	99.99
	4.6	56.37	10.84	29.14					3.65	100.0
C-horizon	4.8	45.00	15.20	39.81						100.0
	5.0	49.73	11.66	34.90	3.72					100.0
	5.2	46.12	13.82	35.46						100.0
	5.4	56.09	9.84	34.07	4.60					100.0
	5.6	39.98	10.70	45.46	3.86					100.0
	5.8	48.25	8.42	41.01	2.33					100.0
	6.0	51.83	7.34	32.98	7.85					100.0
	6.2	32.42	10.41	43.07	14.10					100.0
	6.4	43.54	13.00	33.68	9.78					100.0
	6.6	59.06	8.94	28.38	3.62					100.0

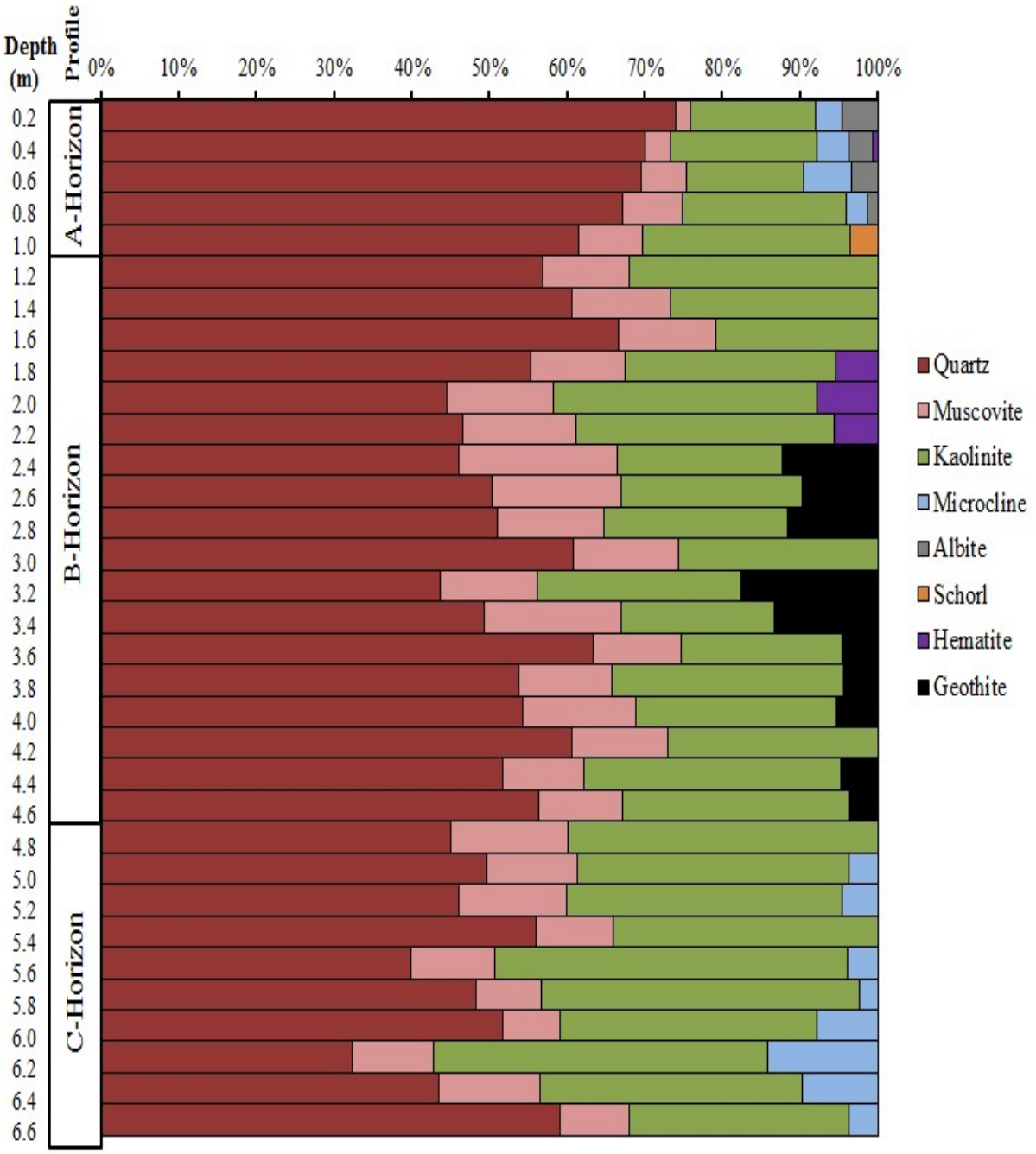

Fig. 4.44: The distribution of mineral phases in different horizons of the mineralised pegmatite weathering profile at Ofiki area.

4.2.5 Mineralogical composition of weathering profile over Iwere mineralised pegmatite

The residual weathering profile investigated in Iwere-Ile area is located at about 1.3 km off Iwere-Ile –Idiko- Ile Road (N 07º 58. 572', E 03º 28. 853'), which is equally 1.6 km northeast of the Oyan River bridge. The lateritic profile is about 4.0 m deep and developed from a mineralised pegmatite dyke, excavated for tourmaline and emerald extraction by local miners. On the basis of colour, texture, compaction and the degree of preservation of parental structure, the profile can be divided into three zones from surface to the bottom. These are the A, B and C-horizons (Fig. 4.45).

The A-horizon is composed of two fairly distinguishable layers, the A_0 and A_1 layers. The topmost A_0 layer is dark grey in colour and composed of partially decomposed organic matter, quartz pebbles and small amount of other rock-forming minerals. This layer is 0.2 m thick and overlies the A_1 layer of the A-horizon. The A_1 top soil layer is brown in colour, extensively leached and consisting of quartz pebbles and less amount of organic matter accumulation (mainly undecomposed plant roots and rootlets). The B-horizon comprises the lateritic and mottled layers. The lateritic horizon is brownish yellow, concretionary and relatively clay-rich. The layer is about 0.8 m thick and rest on the mottled horizon. The mottled horizon is about 0.8 m thick, showing yellowish red to reddish brown colour, and characteristically clay mineral-rich. The mottled horizon subtly grade into the C-horizon. The C-horizon is composed of the saprolite and saprock layers. The saprolite is about 1.0 m thick, yellowish brown in colour, showing small amount of muscovite flakes, partially decomposed feldspar fragments and quartz grains. The saprockoverlies the basal pegmatite parent rock, and it is about 0.6 m thick. It composed of crumbly but still largely coherent yellowish weathered parent material.

The mineralogical composition of the constituting horizons of the profile, as analysed by XRD, reveals that the A-horizon showing enrichments in primary minerals, such asquartz (ca. 84.28 wt.%) and microcline (ca. 11.50 wt.%), but minor abundance of muscovite (ca.

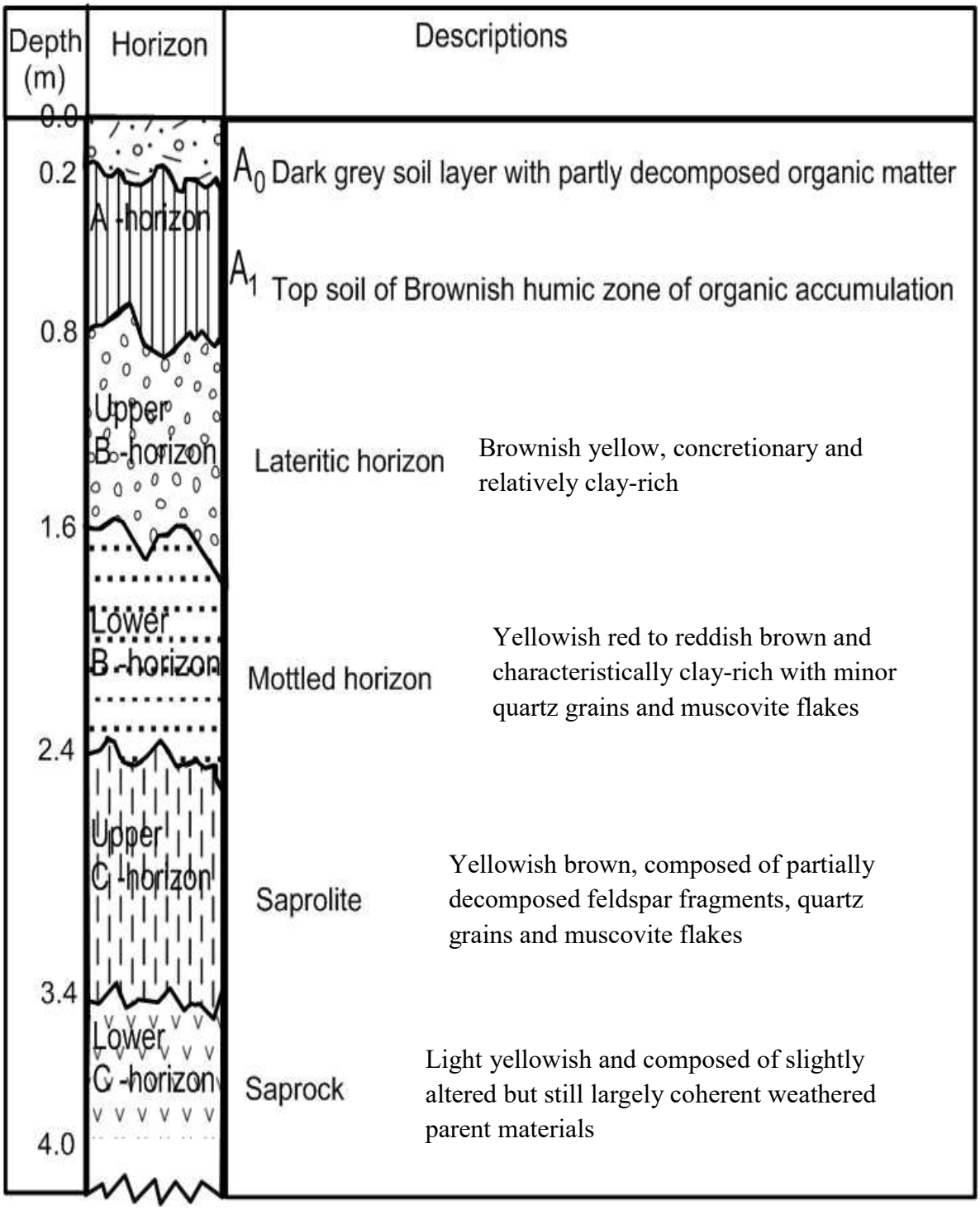

Fig. 4.45: Weathering profile above the mineralised pegmatite at Iwere area

1.31 wt.%). The high abundance of quartz can be mainly ascribed to its high modal abundance in the parent pegmatite rock and it's chemical resistant to weathering processes. The relatively high amount of microcline (a weathering susceptible mineral) invariably indicates the incipient weathering of the pegmatite. The low kaolinite (ca. 2.93 wt.%) contents in the A-horizon can be attributed to the intensive leaching processes that marked this horizon and possibly relatively lower extent of chemical weathering of the feldspars. The X-ray diffractogram of the A-horizon lateritic sample reveals prominent peaks of quartz at 4.25Å, 3.34Å, 2.56Å, 2.45Å, 2.28Å, 2.24Å, 2.12Å, 1.99Å, 1.82Å, 1.67Å, 1.54Å, 1.45Å and 1.38Å values (Fig. 4.46), thereby confirming the high abundance of quartz. The fairly high amount of microcline is indicated by few peaks at 6.48Å, 3.25Å and 3.03Å values, while muscovite shows small peaks at 9.98Å and 4.99Å values (Fig. 4.46).

Quartz shows reduction in abundances in the lateritic horizon (upper B-horizon) to the basal pegmatite rock. The average quartz contents is ca. 59.85 wt.% in the lateritic layer, ca. 47.74 wt.% in the mottled zone, ca. 35.27 wt.% in the partially altered saprolitic layer and ca. 34.30 wt.% in the basal saprock. These distribution trends of quartz (primary mineral in pegmatites) are consistent with the systematic reduction in the eluviation processes that typifies the upper layers of the profile and the contemporaneous illuviation processes down the weathering profile that tend to facilitate the enhancement of other components at the expense of quartz. The least content indicated by the saprock zone is more or less in conformity to the modal quartz abundances in the pegmatite bedrock. Muscovite shows increasing contents from the top soil to the saprock zone, with its peak abundance in the saprock reflecting the modal composition of the mineral proximal to the basal pegmatite rock material.

Kaolinite (ca. 14.76 wt.%) is generally concentrated in the B-horizon, but shows depletion in abundances in the overlying A-horizon (ca. 2.93 wt.%) and the underlying C-horizon (ca. 7.87 wt.%), respectively. These abundances of kaolinite are consistent with the characteristics of the B-horizon as the zone of clay mineral accumulation. Kaolinite shows

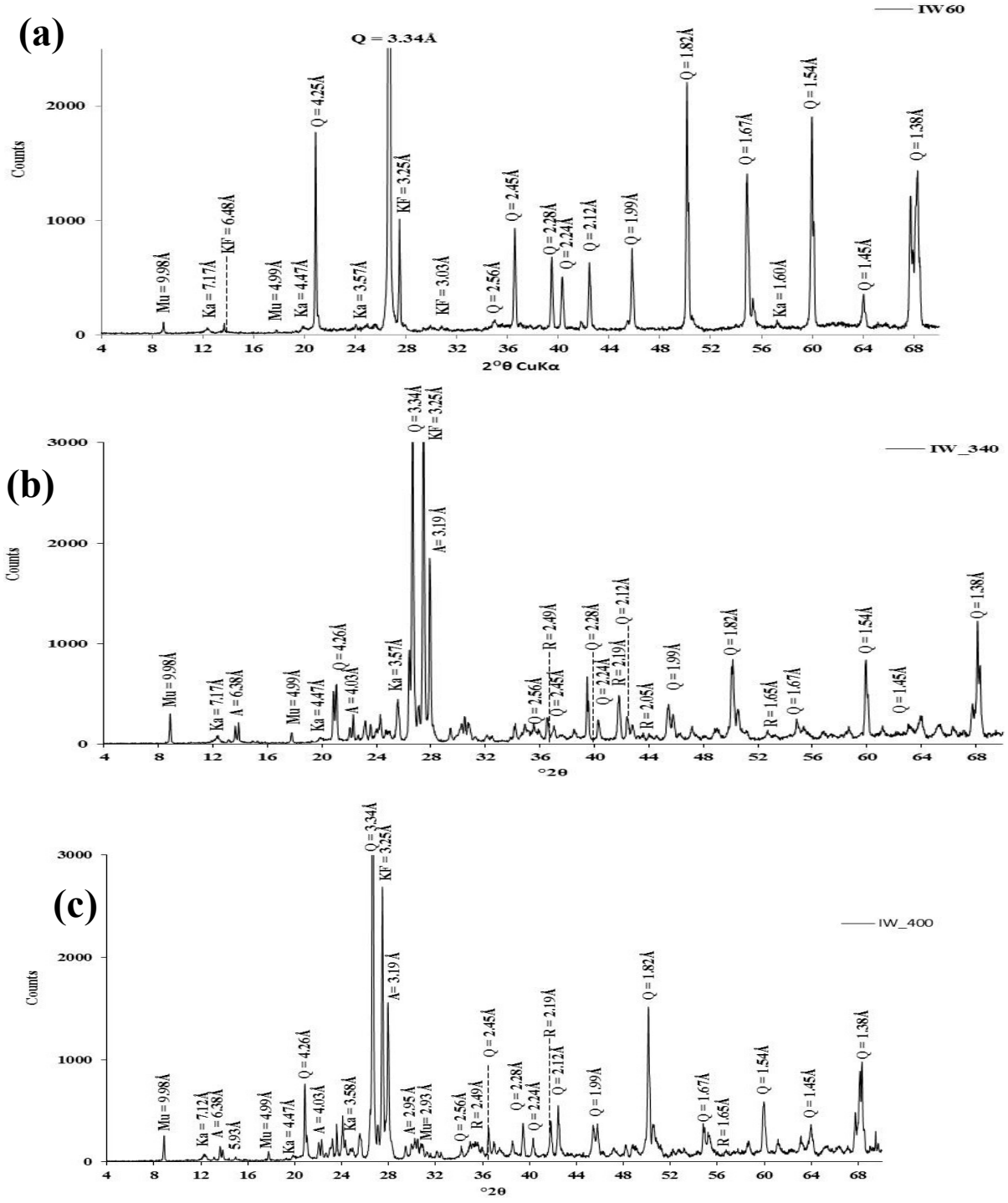

Fig 4.46: X-ray diffractograms of (a) A-horizon (0.6 m), (b) upper C-horizon and lower C-horizon samples of the lateritic profile derived from mineralised pegmatite of Iwere area (Ka = kaolinite; Q = quartz; Mu = muscovite; KF = K-feldspar; A= albite; R =rutile).

peak intensities at 7.17Å, 4.47Å, 3.57Å and 1.60Å values (Fig 4.46). There is a significant increase in the microcline and albite contents from the top soil to the basal saprock zone. The absolute values of the abundances of these feldspars invariably indicate that the pegmatite is incipiently weathered. This is amply reflected in the relatively high contents of the unweathered feldspar components from the top soil to thebasal saprock zone, as well as the relatively low abundances of kaolinite in the constituting horizons. Microcline indicates high peaks commonly at 3.25Å value,while albite peaks are revealed at 6.38Å, 4.03Å, 3.19Å and 2.95Å values (Fig. 4.46). The quantitative mineralogical composition (expressed in wt.%) of the constituting horizons of the profile is summarised in Table 4.10 and Fig. 4.47; while the X – ray diffraction profiles for the weathering profile is present in Appendix 4.

Rutile (ca. 1.00 - 3.38 wt.%) is not pervasive throughout the horizons of the profile, as it only show appearances in some samples of the residual profile. It is found in the B- and upper C-horizon, and as a minor component, it shows few peaks at 2.49Å, 2.19Å, 2.05Å and 1.65Å values (Fig. 4.46).

4.2.6 Indicator minerals of the rare-element pegmatites derived from their *in situ* weathering profiles

Indicator mineralogy involves the determination and application of some key index (pathfinder) minerals genetically related to a mineral deposit in backtracking to the source of the deposit through the use of geological media including soils, stream sediments and glacial tills. It is a very potent tool in mineral exploration, as it provides vectors towards important mineralisations (Grigsby, 1990; Rupasinghe *et al*., 1994; McQueen and Cross, 1998; Averill, 2001; Yang *et al.*, 2009; Kelley *et al*., 2011; Mackay and Simandl, 2015; McMartin *et al.*, 2011; Pisiak *et al*., 2017; Bedard *et al.,* 2017; Taylor, *et al.,* 2017; Uribe-Mogollon, 2017). Indicator minerals engaged in mineral deposit targeting are commonly weathering-resistant, and, as such, carry the geochemical signatures of the deposit being explored (Sack and Ghiorso, 1991; Griffin *et al.,* 1994; Zhou *et al*., 1994; Griffin and Ryan, 1995; Belousova *et al.*, 2001; 2002; Bouzari et al., 2011; Dupuis and Beaudoin,

Table 4.10: Quantitative mineralogical composition of the residual weathering profile of the mineralised pegmatite of Iwere area

		Major mineral					Minor mineral	
Profile horizon	Depth (m)	Quartz (%)	Muscovite (%)	Kaolinite (%)	Microcline (%)	Albite (%)	Rutile (%)	Total
A-Horizon	0.2	87.63	0.67	1.21	10.49			100.00
	0.4	84.50	1.34	2.79	11.36			99.99
	0.6	84.13	1.47	2.94	11.48			100.02
	0.8	80.86	1.74	4.76	12.66			100.02
Upper B-horizon	1.0	61.37	4.36	13.78	10.05	10.46		100.02
	1.2	62.42	3.35	15.86	10.61	7.75		100.02
	1.4	59.49	3.75	15.31	12.71	6.69	2.05	100.00
	1.6	56.14	4.37	18.24	14.70	6.55		100.00
Lower B-horizon	1.8	51.48	3.52	20.32	16.76	7.94		100.02
	2.0	46.58	5.63	13.43	20.18	14.18		100.00
	2.2	43.54	6.43	12.52	18.28	17.00	2.24	100.01
	2.4	49.34	5.89	8.63	16.11	18.81	1.22	100.00
Upper C-horizon	2.6	40.22	4.60	9.50	22.91	22.77		100.00
	2.8	39.54	3.56	11.88	21.38	23.64		100.00
	3.0	33.50	2.09	13.29	20.16	27.58	3.38	100.00
	3.2	30.83	2.27	8.46	27.77	29.66	1.00	99.99
	3.4	32.26	3.10	5.04	41.48	18.00	0.14	100.02
Lower C-horizon	3.6	31.25	5.10	4.90	33.55	24.96	0.45	100.01
	3.8	35.23	6.14	5.62	25.34	27.66		99.99
	4.0	36.23	4.13	4.25	32.79	22.59		99.99

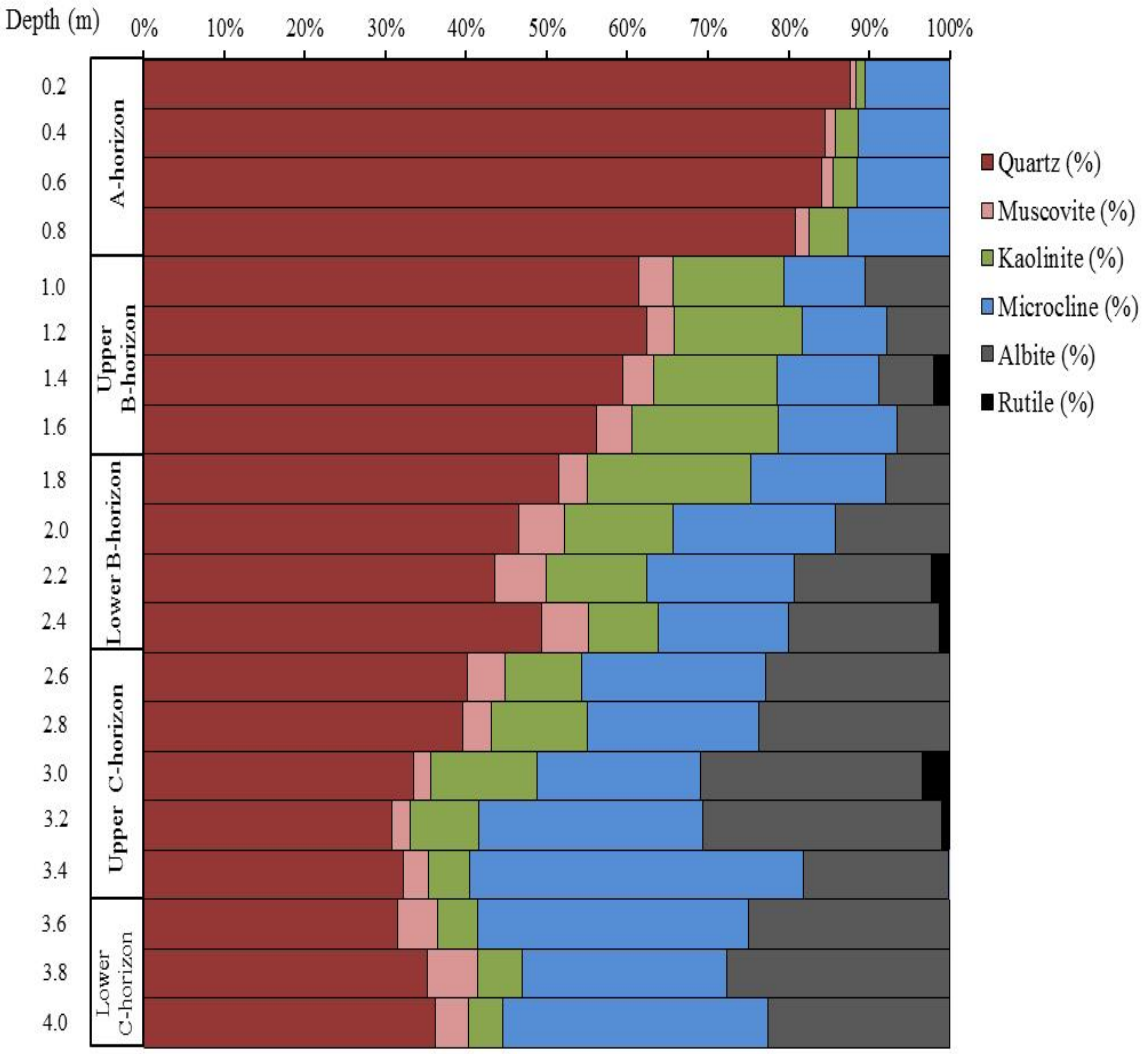

Fig. 4.47: The distribution of mineral phases in different horizons of the mineralised pegmatite weathering profile at Iwere area.

2011; McClenaghan, 2011; Dare *et al.*, 2012; Acosta-Gongora, 2014; Boutroy *et al*., 2014; Doucet, 2014; Mao, 2016). The mineralogical indicators can be ore and/or accessory minerals and their possible alteration-related minerals (McClenaghan, 2011).

The compositional differences between the barren pegmatite of Osu area and the ore-related pegmatites of Ijero, Komu, Ofiki and Iwere areas, explored through the XRD data of their residual weathering profiles, are correlated with their charcteristics indicator minerals. The *in situ*-derived weathering profile of the Osu barren pegmatite indicates varying abundances of quartz, muscovite, microcline and albite as primary minerals and kaolinite as secondary alteration mineral; but it does not show any presence of pegmatite ore-related mineral either in minor or accessory amounts. The residual pegmatite weathering profiles of Ijero, Komu, Ofiki and Iwere areas show minor to accessory constituents of rutile, magnetite and schorl, as well as hematite and goethite (oxidative and hydrolytic alteration minerals of magnetite) and anatase (hydrated polymorph of rutile) in the various horizons of these weathering profiles. These highlighted ore-related indicator minerals in the rare-element pegmatite weathering profiles offer important clues (guides) towards exploring for these pegmatites underneath lateritic covers.

4.3 Geochemical characteristics of the pegmatites and the weathering profiles

The chemical character of the pegmatites and their respective *in situ*-derived lateritic profiles, were established through a combination of determinative techniques. These were undertaken with the principal objectives of comparing the geochemical dispersion trends within the constituting horizons of the lateritic profiles with the bulk chemical composition of the parent bedrock samples. Mineral chemistry of some of selected discrete mineral phases in the pegmatites was also investigated, in order to determine their mineralisationpotential for possible distinction between mineralised and barren pegmatites.

4.3.1 Whole-rock pegmatite geochemistry

The mean and ranges of major and trace element geochemical data of pegmatites from the study localities are presented in Table 4.11. The pegmatites are highly siliceous, with averageSiO_2 contents greater than 72 wt.%. Average alumina abundances of the pegmatites range between 14.29 wt.% and 15.59 wt.%, while the mean Fe_2O_3 (0.45-0.64 wt.%) concentrations are lower in Ijero, Komuand Ofiki and but higher in Iwere (1.15 wt.%) and Osu (1.13 wt.%) pegmatites. Mean MnO abundances are generally lower than 0.32 wt.% in the pegmatites, with the lowest value (0.09 wt.%) in the Osu pegmatite. Average TiO_2 levels in all the pegmatites are generally below 0.63 wt.%.

CaO contents vary widely among samples (Table 4.11), while MgO concentrations are generally below 0.13 wt.%. The variations in K_2O and Na_2O values (Table 4.11) can be attributed to the very coarse-grained size of the pegmatite samples. The mean P_2O_5 (0.27 wt.%) contentsof the Osu pegmatite is higher, when compared to those of other pegmatites which is less than 0.11 wt.%.The average LOI values of 0.44–0.89 indicated that the pegmatite samples have not been exposed to chemical weathering.

The trace element compositions of the whole-rock pegmatites (Table 4.11) revealed mean rare-alkali contents of Rb (293, 625, 456, 188 and 97 ppm), Cs (71, 102, 220, 42 and 17 ppm), Ba (117, 19, 34, 76 and 85 ppm) and Sr (23, 20, 39, 24 and 66 ppm) for the Ijero, Komu, Ofiki, Iwere and Osu pegmatites, respectively. Average Sn contents of 13, 18, 18, 14 and 6; ppm; Nb of 45, 70, 36, 31 and 16 ppm; Ta of 17, 46, 32, 23 and 4 ppm, were correspondingly obtained from Ijero, Komu, Ofiki, Iwere-Ile and Osu pegmatites.

The bulk chemical data of the pegmatites (Table 4.11) showed that the Ijero, Komu, Ofiki and Iwere pegmatites are enriched in lithophile trace elements Rb, Cs, Ga, Sn, Nb and Ta; whereas the Osu pegmatite is deficient in these elements. On the contrary, Ba and Sr contents in the Osu pegmatite are generally higher than those of other pegmatites.The above geochemical patterns revealed that the pegmatites of Ijero, Komu, Ofiki and Iwere are rare-metal-bearing (mineralised) (Selway *et al*., 2005; Wise and Brown, 2010);while that of Osu is observed to be deficient in rare-element, and consequently non-mineralised.

Table 4.11: Mean and range major, trace and rare-earth element compositions of the pegmatites

	OSP		IJP		KMP		OFP		IWP	
Major Oxide	Mean (n=7)	Range (n=7)	Mean (n=5)	Range (n=5)	Mean (n=5)	Range (n=5)	Mean (n=10)	Range (n=10)	Mean (n=10)	Range (n=10)
SiO_2	72.47	70.43-73.90	73.39	71.03-76.12	78.86	70.75-78.15	73.23	69.95-77.20	73.53	68.26-78.16
Al_2O_3	15.59	14.56-18.21	14.69	13.84-16.04	15.5	13.29-17.93	15.2	12.90-17.24	14.29	10.52-17.51
Fe_2O_3	1.13	0.37-1.85	0.63	0.34-1.16	0.45	0.22-0.69	0.64	0.38-1.12	1.15	0.55-2.33
MnO	0.09	0.02-0.17	0.32	0.03-0.77	0.08	0.01-0.2	0.14	0.03-0.29	0.21	0.01-0.96
MgO	0.13	0.05-0.25	0.08	0.03-0.21	0.05	0.02-0.08	0.03	0.0-0.08	0.22	0.04-0.90
CaO	0.61	0.36-0.84	0.5	0.06-0.74	0.52	0.24-0.75	0.33	0.24-0.44	0.79	0.07-1.21
Na_2O	2.18	1.38-3.42	2.52	2.13-2.90	4.07	3.05-5.39	3.48	2.62-4.80	3.16	2.02-4.91
K_2O	6.6	5.91-7.92	6.07	4.94-7.36	3.35	2.21-4.68	6.26	4.13-7.56	5.53	3.16-7.74
TiO_2	0.16	0.01-0.42	0.02	0.01-0.03	0.13	0.05-0.22	0.03	0.02-0.04	0.63	0.32-0.93
P_2O_5	0.27	0.05-0.90	0.1	0.05-0.17	0.02	0.01-0.03	0.08	0.01-0.14	0.14	0.03-0.30
LOI	0.73	0.06-1.30	0.65	0.51-1.06	0.89	0.28-1.23	0.44	0.10-0.78	0.7	0.06-1.10
Total	99.78	99.52-100.14	99.92	99.69-100.3	99.82	99.54	99.86	99.72-99.95	100.35	
Trace element										
Rb	97	27-226	293	167-565	625	497-885	456	145-774	188	30-476
Cs	17	2-24	71	14-252	102	29-250	220	26-440	22	12-35
Ba	85	16-202	117	9-329	51	23-88	51	24-92	78	4-194
Sr	66	27-141	23	8-70	20	2-43	39	9-51	24	4-43
Ga	17	14-24	23	13-38	30	19-47	15	9-26	22	13-27
Be	9	3-13	6	4-8	20	7-37	17	8-27	13	5-25
Sn	6	3-11	13	4-18	18	7-28	18	11-28	14	2-28
Nb	16	23-11	45	4-94	70	52-93	36	19-53	31	10-54
Ta	4	2-6	17	13-25	46	18-134	32	16-62	23	13-75
Y	8	3-17	25	12-63	9	3-15	11	6-16	16	6-33
Zn	14	6-25	23	8-49	48	22-71	22	16-30	47	5-150
Zr	67	35-96	36	12-42	18	15-25	26	11-47	59	12-75
Hf	3	1-7	5	4-6	5	2-6	6	2-12	6	3-10
Th	4	1-9	6	5-7	6	4-7	6	3-9	7	3-12
U	11	4-20	6	4-7	7	3-13	10	2-19	7	2-13
K/Rb	564.6	484.2-2056.1	171.9	105.5-365.7	44.5	20.7-67.9	114	49.5-437.8	2440.08	110.4-874.1
K/Cs	2240.5	2171-32860	709.4	236.4-2562	272.5	155.3-861.3	236.1	77.9-1825.6	1045	640.1-1344.7
Nb/Ta	4.01	2.33-11.0	2.65	0.27-2.94	1.52	0.69-3.31	1.13	0.49-1.91	1.35	0.51-2.67

Table 4.11 (Continued)

	IJP		KMP		OFP		IWP		OSP	
REE	Mean	Range n=5	Mean	Range n=5	Mean	Range n=10	Mean	Range n=10	Mean	Range n=7
La	2.94	1.5-6.2	1.86	1.3-2	4.00	2.5-5	7.20	1.2-15.7	4.90	1.0-10
Ce	6.40	1.0- 17	3.60	2.0-7.0	5.30	2.0-9.0	15.70	2.1-36.8	11.80	6.4-24
Pr	2.70	1.5-5.0	0.36	0.3-0.4	0.90	0.6-1.2	1.80	0.2-4.5	0.50	0.3-0.8
Nd	4.96	2.0-10	2.64	2.0-4.0	2.70	2.0-4.0	7.50	0.7-21.1	4.90	2.0-10
Sm	2.70	1.0-6.0	2.26	1.3-4.0	2.10	1.0-4.0	2.20	0.2-5.6	3.70	2.0-8
Eu	0.26	0.1-0.4	0.12	0.1-0.2	0.10	0.1-0.2	0.30	0.1-0.9	0.50	0.3-0.6
Gd	1.86	1.1-2.6	0.72	0.2-1.4	0.30	0.2-0.5	2.10	0.2-5.1	0.50	0.5-0.6
Tb	0.56	0.3-0.7	0.14	0.1-0.2	1.60	1.2-2.6	0.40	0.1-1.1	0.30	0.1-0.9
Dy	3.34	1.8-7.8	0.46	0.2-0.9	1.80	1.4-2.7	2.40	0.2-6.5	0.50	0.4-0.8
Ho	1.40	0.4-2.2	0.16	0.1-0.3	0.30	0.2-0.4	0.40	0.1-0.9	0.20	0.1-0.3
Er	1.88	0.5-6.5	0.22	0.1-0.3	0.70	0.5-1.1	1.10	0.1-2.4	0.30	0.2-0.4
Tm	0.96	0.1-1.6	0.12	0.1-0.2	0.20	0.1-0.2	0.20	0.1-0.5	0.20	0.1-0.4
Yb	3.64	1.2-8.4	0.22	0.1-0.3	1.10	0.6-2.2	1.50	0.2-3.8	0.20	0.1-0.3
Lu	0.72	0.2-1.2	0.12	0.1-0.2	0.20	0.1-0.3	0.20	0.0-0.7	0.20	0.1-0.3

Fractionation indices, such as, K/Rb, K/Cs, Nb/Ta and Na/K ratios are routinely applied as rare-metal discriminators in whole-rock pegmatites (Selway *et al*., 2005, Kuster *et al*., 2009).Lower average K/Rb ratios (44.48 to 244.08) were recorded in the pegmatites of Ijero, Komu, Ofiki and Iwere compared to the Osu pegmatite (306.67) (Table 4.11). Similarly, lower average K/Cs (236.12 – 1042.42) and Nb/Ta (1.13 – 2.65) ratios were obtained from Ijero, Komu, Ofiki and Iwere pegmatites as against higher K/Cs (3221.58) and Nb/Ta (4.) ratios in the Osu pegmatite.

Lower K/Rb, K/Cs and Nb/Ta in pegmatites' whole-rock chemical data have been interpreted to indicate higher degree of fractionation and higher rare-metal-bearing potential of the pegmatites (Selway *et al*., 2005; Kuster *et al*., 2009; Akoh *et al*., 2015). The mineralised pegmatites of Ijero, Komu, Ofiki and Iwere displayed these geochemical signatures, whereas the Osu barren pegmatite is devoid of these geochemical patterns.

4.3.2 Pegmatite mineral chemistry

4.3.2.1 K-feldspar chemistry

The K-feldspar samples analysed were collected from fairly large crystals (up 0.3 m in diameter), and are commonly whitish to pinkish in colour, with the characteristic cross-hatched twinning. Exsolution lamellae were avoided during EMPA analyses, therefore the microprobe-derived bulk composition of the microcline samples ranged between Or_{83} and Or_{95}.

Representative chemical analyses of K-feldspar samples from the investigated pegmatites are given in Table 4.12; while the overall bulk chemical data and the EMPA calculated cation formulae are presented in Appendix 5 and Appendix 6. The chemical data show very restricted variations in SiO_2 (63.25–64.96 wt.%), Al_2O_3 (18.12– 19.84 wt.%), FeO (0.001–0.112 wt.%) and MnO (0.007–0.047 wt.%). K_2O also indicates narrow ranges among pegmatites (14.36-16.68 wt.%), while other alkali oxides, such as,MgO (0.003–0.050 wt.%) and CaO (0.001–0.070 wt.%) equally portray minor variations in the K-feldspar samples. However, Na_2O (0.55–2.06 wt.%) varied widely among samples, with Osu K-feldspar indicating lower Na_2O values.

The averages and ranges of rare-alkalis and ore elements of the K-feldspar are presented in Table 4.12. Moderate rare-alkali abundances in the K-feldspar, mainly typified by Li (1102-1699 ppm) contents, Rb concentrations (1037-2984 ppm) and Cs (353-1165 ppm) are generally recorded in Ijero, Komu, Ofiki and Iwere pegmatites; while low values of Li (104 ppm), Rb (257 ppm), and Cs (33 ppm) are indicated in the K-feldspar samples of Osu pegmatite. The Ofiki K-feldspar samples are enriched in Rb (up to 3955 ppm) and Cs (1823 ppm), indicating the highest concentrations among the investigated rare-element pegmatites. Rare-metal concentrations of Sn (2-4 ppm), Nb (30-33 ppm), Ta (21-24 ppm)and Ga (33-70 ppm) are of modest levels in the K-feldspar of Ijero, Komu, Ofiki and Iwere; whereas lower contents of Sn (2 ppm), Nb (4 ppm), Ta (5 ppm) and Ga (20 ppm) are indicated in the K-feldspar samples of Osu pegmatites.

K/Rb ratio, as a rare-alkali fractionation indicator, is generally low in the K-feldspar samples of Ijero (129.44), Komu (80.83), Ofiki (43.62) and Iwere (96.24) pegmatites, while higher K/Rb (527.31) ratio is indicated in Osu K-feldspar samples. Values of other geochemical fractionation indices, including K/Cs (111.75-380.61), K/Ba (148.77-335.54) and Nb/Ta (1.3-1.5) arelower in the K-feldspar samples of Ijero, Komu, Ofiki and Iwere pegmatites, indicating that the pegmatites are moderately evolved. On the other hand, conspicuously high K/Cs (4125.22), K/Ba (1339.68) and Nb/Ta (3.7) ratios reflected in the K-feldspar samples of Osu pegmatites, signify that the pegmatite is poorly evolved and non-mineralised. Elevated Ta contents, revealed in Ta/W (13.8-25.3) ratio inthe K-feldspar samples of Ijero, Komu, Ofiki and Iwere pegmatites, also substantiate the rare metal-bearing potential of these pegmatites; while Ta/W (6.0) ratio of the Osu K-feldspar samples reinforced its non-mineralised geochemical signature.

Rare-alkali fractionation diagram, such as K/Rb against Cs (Fig. 4.48a), amply demonstrates the degree of substitution of potassium by rubidium in the K-feldspar crystal structure (Trueman and Cerny, 1982; Shearer *et al*., 1985; Moller and Morteani, 1987; Smeds, 1992; Morteani *et al.*, 1995; Trumbull, 1995; Morteani *et al*., 2000; Alfonso *et al., 2003*; Selway *et al*., 2005; Wise and Brown, 2010; Neiva, 2013) and also indicates the Li,Cs, Be and Ta fractionation trends in pegmatites. The K/Rb versus Cs discrimination plot (Fig. 4.48a) indicates a negative correlation trend between K/Rb and Cs.

Table 4.12: Mean and average major and trace element compositions of the K-feldspar samples

	OSK		IJK		KMK		OFK		IWK	
	Mean n=5	Range n=5	Mean n=5	Range n=5	Mean n=5	Range n=5	Mean n=5	Range n=5	Mean n=5	Range n=5
SiO_2	64.30	63.73-64.96	63.66	63.26-64.24	63.49	63.25-64.62	63.95	63.62-64.36	63.94	63.44-64.36
TiO_2	0.004	0.002-0.008	0.00	0.00-0.01	0.02	0.009-0.05	0.01	0.005-0.009	0.02	0.02-0.05
Al_2O_3	18.58	18.27-19.01	18.51	18.27-18.73	18.80	18.2-19.84	18.60	18.24-19.08	18.52	18.12-18.86
FeO	0.03	0.015-0.05	0.02	0.01-0.04	0.01	0.001-0.029	0.03	0.009-0.112	0.05	0.01-0.09
MnO	0.02	0.008-0.034	0.01	0.00-0.01	0.02	0.008-0.03	0.01	0.007-0.012	0.02	0.01-0.047
MgO	0.02	0.004-0.05	0.00	0.00-0.00	0.00	0.003-0.006	0.00	0.003-0.006	0.01	0.003-0.03
CaO	0.01	0.003-0.02	0.00	0.00-0.00	0.02	0.02-0.03	0.02	0.01-0.03	0.04	0.016-0.07
Na_2O	0.73	0.55-0.86	1.88	1.75-2.06	1.86	1.78-1.92	1.72	1.47-1.96	1.69	1.43-1.92
K_2O	16.31	16.05-16.68	16.18	15.82-16.66	15.84	15.8-16.02	15.69	14.36-16.43	15.96	15.65-16.2
P_2O_5	0.02	0.002-0.035	0.03	0.01-0.07	0.02	0.02-.03	0.06	0..05-0.19	0.03	0.008-0.04
Total	100.02	99.56-100.23	100.31	100.1-100.55	100.10		100.09	99.815-100.218	100.27	99.6-100.96
Trace elements										
Li	104	45-245	1102	756-1440	1376	1118-1682	1656.00	1018-2871	1699	991-2611
Rb	257	72-452	1037	671-1326	1626	1089-1986	2984.00	2336-3955	1376	963-1722
Cs	33	26-41	353	214-428	497	213-830	1164.80	695-1823	433	183-1000
Ba	101	52-141	448	189-824	883	546-1341	732.20	175-1175	395	230-810
Sr	87	58-131	160	56-249	190	68-319	212.40	58-452	161	109-226
Ga	20	13-32	33	28-47	43	27-67	50.80	45-57	70	27-193
Be	16	11-22	17	28-47	16	9-28	14.00	8.0-27	32	16-58
B	24	17-33	18	7-28	18	11-27	25.60	16-38	19	12-31
Sn	2	1-3	3	2-6	3	1-5	2.40	2-4	4	2-8
Nb	11	9-22	30	21-39	32	23-41	31.20	27-36	33	17-54
Ta	3	2-7	23	19-28	23	19-28	20.60	16-26	24	13-39
W	0.5	0.2-1	1.4	1-2	2	1-2	1.20	0.5-2.0	2	1-3
Y	1.4	1-2	1.6	1-23	2	1-2	1.66	0.5-3	3	1-6
Zn	1.6	1-3	1.2	1-3	1.4	1-2	1.20	1-2	18	13-25
Zr	1.4	1-2	1.4	1-2	2	1-2	1.48	0.4-3.0	2	1-3
Hf	0.2	0.1-0.2	0.14	0.1-.02	0.22	0.1-0.2	0.22	0.2-0.03	0	0.1-0.4
Th	0.2	0.1-0.2	0.38	0.2-.08	0.22	0.1-0.2	0.86	0.2-2.0	2	1-3
U	0.2	0.1-0.2	0.50	0.2-1.0	0.26	0.1-0.2	1.36	0.4-3.0	2	1-3
K/Ba	1340	949.86-2591.53	299.7	159.3-695.9	148.8	99.1-240.4	177.8	101.4-752.0	336	163.1-577.6
Rb/Sr	2.75	1.24-4.05	8.86	4.25-20	12.6	3.4-29.2	20.11	8.8-43.4	9.63	4.3-15.8
K/Rb	527	3015-1366.7	129.4	99.0-129.44	80.8	66.4-120.6	43.62	30.1-54.9	96.24	75.4-138.0
K/Cs	4125.33	3323.3-5122.4	380.6	323.01-613.43	264.5	156.8-616.3	111.8	72.2-194.9	305.79	129.9-721.9
Nb/Ta	3.67	2.88-4.5	1.28	0.91-1.71	1.4	0.82-1.71	1.55	1.3-2.1	1.394	1.31-1.52
Ta/W	11.17	3-17.5	18.3	11.5-26	16.3	11.0-28	25.3	8-52	13.8	10.5-19
Al/Ga	5388.8	3145.0-7444.2	3099.2	2095.1-3645	2548	1498-3890	1949.57	1742.4-2183.5	2263	517.3-3672.5
Zr/Hf	9	5.0-10	11	5.0-20.0	7	3.33-10.0	6.734	2-15	12.5	7.5-20
Na/K	0.04	0.03-0.05	0.1	0.1-0.12	0.11	0.1-0.11	0.1	0.08-0.12	0.08	0.09

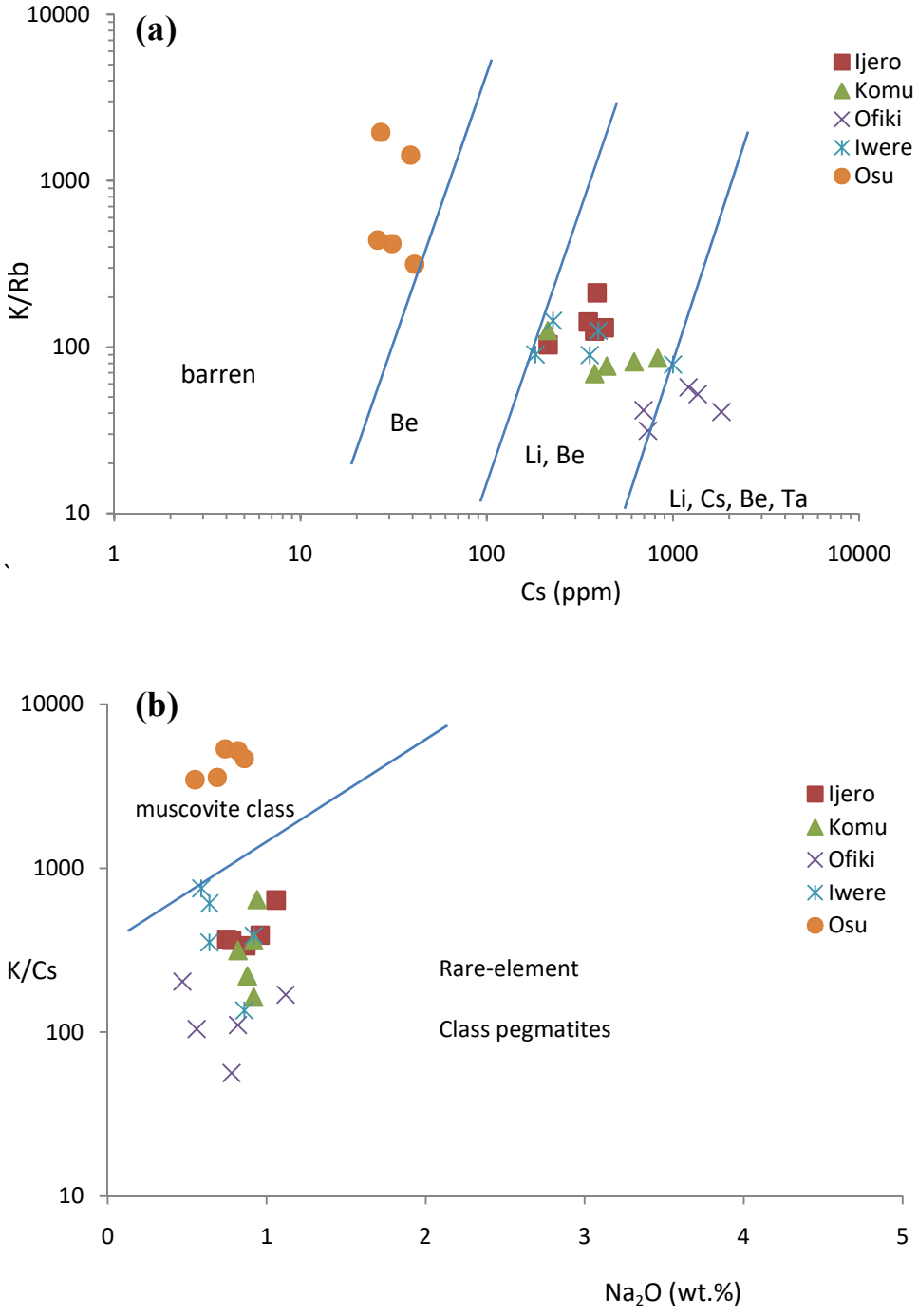

Fig.4.48: Plot of (a) K/Rb vs. Cs and (b) K/Cs vs. Na_2O (wt %)for the K-feldspar samples of the pegmatites (modified after Trueman and Cerny, 1982).

The K-feldspar samples of Ijero, Komu, Ofiki and Iwere pegmatites plot mainly in the Li, Be field on the K/Rb/Cs discrimination plot (Fig. 4.48a) of Trueman and Cerny (1982), with discrimination lines patterned after the investigated LCT-pegmatites of Winnipeg River district, Canada. On the contrary, the K-feldspar samples of Osu pegmatite plot in the barren field of the discrimination diagram (Fig. 4.48a).

The K/Cs versus Na_2O discrimination plot (Fig. 4.48b) for the K-feldspar samples signifies that Ijero, Komu, Ofiki and Iwere pegmatites are rare element-bearing; while those of Osu cluster in the less fractionated muscovite class pegmatite field (Trueman and Cerny, 1982). In Fig. 4.49a, K/Rb and Ga exhibits an overall negative correlation trend, with the mineralised pegmatites of Ijero, Komu, Ofiki and Iwere plotting in the lower half of the data field, signifying enhanced Ga contents during the geochemical evolution of these rare-element pegmatites. The Osu pegmatite indicates chemical evolution towards less fractionation end that points to reducedGa levels. Similarly, Ta and K/Rb (Fig. 4.49b) portrays inverse relationship, with K-feldspar samples of Osu pegmatites conspicuously plotting towards the lower half of the variation plot, invariably showing low Ta concentration levels. The above geochemical trends revealed the enhancement of Ga and Rb contents, in the late residual pegmatite melts, as fractionation progresses (Moller and Morteani, 1987; Morteani and Gaupp, 1989; Morteani *et al*., 2000).

The enhancement in the LILEs (Rb, Cs, Li) and HFSEs (Ta, Nb, Sn, Ga) contents in the K-feldspar samples of Ijero, Komu, Ofiki and Iwere pegmatites, as well as, low K/Rb,K/Cs, K/Ba and Nb/Ta ratios indicates that these pegmatites are moderately geochemically evolved, rare element-bearing, and therefore mineralised (Moller and Morteani, 1987; Morteani *et al.,* 2000; Alfonso *et al*., 2003; Selway *et al.*, 2005); whereas those of Osu pegmatite has high values of K/Rb, K/Cs, K/Ba and Nb/Ta ratios indicating that the pegmatite is non-evolved to very poorly evolved, rare-element deficient and non-mineralised.

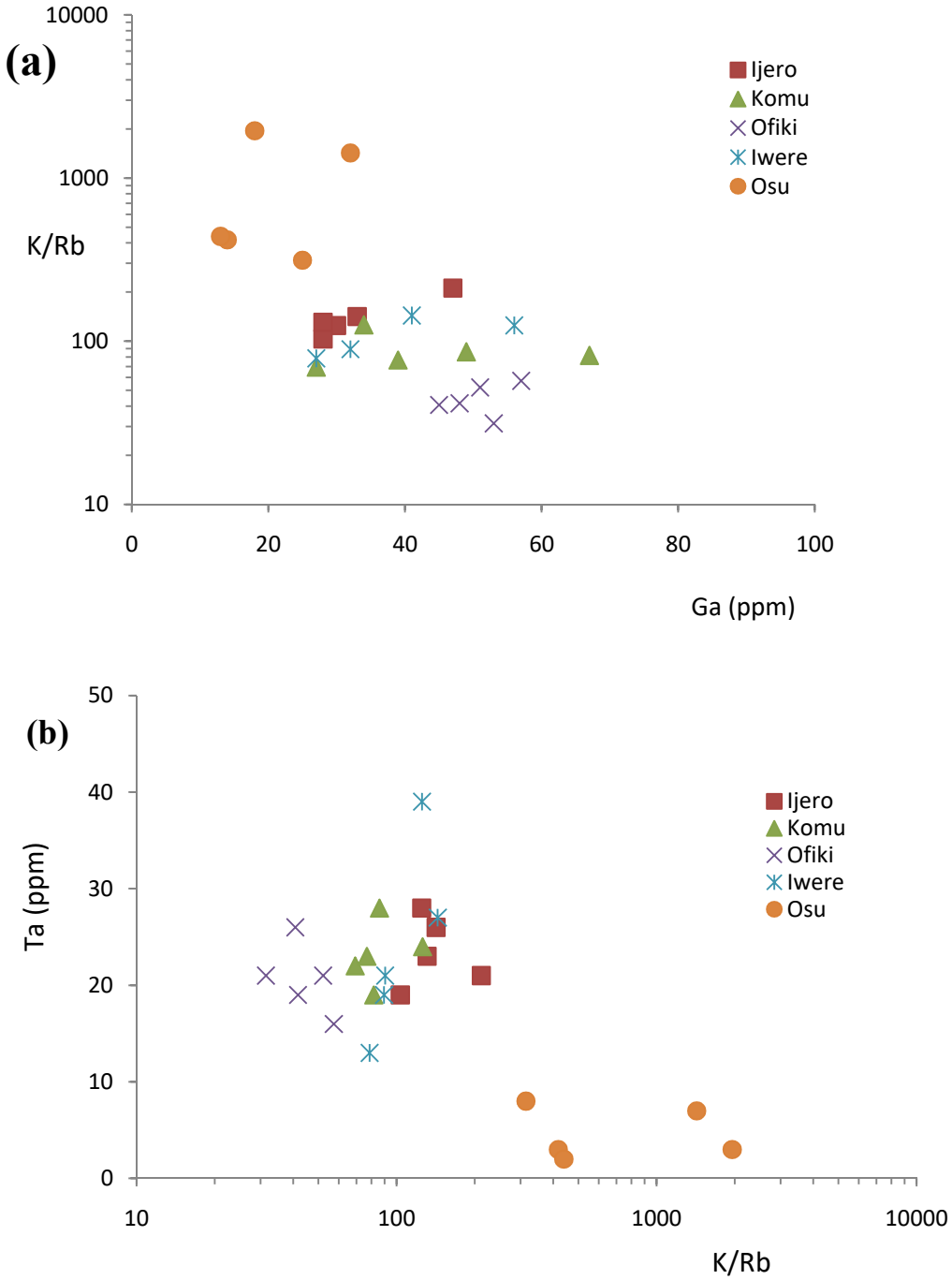

Fig. 4.49: Plot of (a) K/Rb vs. Ga and Ta vs K/Rb for the K-feldspar samples of the pegmatites (modified after Cerny, *et al*., 1985).

4.3.2.2 Muscovite chemistry

The bulk composition of the muscovite samples, presented in Table 4.13, show the averages and ranges of the major and trace element abundances; while the overall bulk chemical data and calculated EMPA cation formulae of the representative muscovite samples from the pegmatites are displayed in Appendix 7 and Appendix 8. The Table generally shows restricted ranges in SiO_2 (45.50–46.38 wt.%) Al_2O_3 (32.06–36.54 wt.%), MnO (0.01-0.27 wt.%) and TiO_2 (0.01–0.03 wt.%). FeO contents are slightly variable in the representative muscovite samples, with high mean abundances recorded in Ofiki (3.57 wt.%) and Iwere (2.88 wt.%) samples. Narrow ranges are also indicated in the K_2O (10.07-10.90 wt.%) concentrations, while other major alkali oxides, such as, Na_2O (0.53–0.99 wt.%), MgO (0.01-0.79 wt.%) and CaO (0.01-0.06 wt.%) are generally low and show slight variability in compositions.

The muscovite samples of Ijero, Komu, Ofiki and Iwere record elevated levels of rare-alkali abundances, with Li generally ranging from 1363 to 27,323 ppm; Rb varying between 3441 and 6117 ppm; and Cs abundances between 1301 and 4693 ppm (Table 4.13). On the contrary, the muscovite samples of the Osu pegmatites correspondingly portray low average concentration levels of Li (452 ppm), Rb (296 ppm) and Cs (46 ppm).

The muscovite samples of Ijero, Komu, Ofiki and Iwere pegmatites also indicate high concentration of oreelements, such as, Ta, Nb and Sn when compared to the Osu muscovite samples. For example, the mean Ta contents in these muscovite samples ranged between 172 and 249 ppm; Nb varies from 208 to 296 ppm and Sn contents between 65 and 518 ppm (Table 4.13). Komu muscovite samples indicate the highest mean Ta value (249 ppm), while the cassiterite-bearing Ijero pegmatite shows the highest mean Sn (518 ppm) concentration. Other ore elements, including Ga, W and Zn are observed to be more abundant in these pegmatites (Table 4.13). On the other hand, the Osu muscovite samples respectively show very low contents of Ta (14 ppm), Nb (23 ppm) and Sn (26 ppm).

The rare-alkalis (Li, Rb and Cs) and other ore elements (Sn, Nb and Ta) in the muscovite samples of the mineralised pegmatites of Ijero, Komu, Ofiki and Iwere showing their

Table 4.13: Mean and average major and trace element compositions of the muscovite samples

	IJM		KMM		OFM		IWM		OSM	
Major Oxide	Mean	Range	Mean	Range	Mean	Range	Mean	Range	Mean	Range
SiO_2	45.83	45.5-46.15	45.70	45.54-45.92	45.80	45.67-45.97	46.05	45.59-46.38	46.13	45.84-46.33
TiO_2	0.026	0.01-0.070	0.170	0.06-0.30	0.088	0.02-0.21	0.194	0.07-0.24	0.086	0.02-0.23
Al_2O_3	34.60	34.42-34.92	35.21	33.74-36.54	33.83	33.24-34.74	33.15	32.06-36.29	34.88	33.19-35.62
FeO	1.71	1.63-1.77	1.42	0.09-3.03	3.57	3.49-3.67	2.88	0.05-3.78	1.73	1.15-3.33
MnO	0.09	0.03-0.14	0.15	0.05-0.27	0.06	0.04-0.08	0.09	0.04-0.20	0.04	0.01-0.11
MgO	0.11	0.01-0.47	0.06	0.01-0.13	0.19	0.02-0.41	0.58	0.01-0.79	0.46	0.33-0.52
CaO	0.01	0.01-0.02	0.01	0.010.02	0.01	0.01-0.02	0.01	0.01-0.02	0.02	0.01-0.06
Na_2O	0.65	0.56-0.77	0.682-0.61	0.61	0.63	0.61-0.65	0.59	0.53-0.67	0.86	0.7-0.99
K_2O	10.66	10.59-10.83	10.566-10.45	10.45	10.67	10.47-10.76	10.75	10.56-10.90	10.42	10.07-10.61
Li_2O*	3.58	3.49-3.68	3.538-3.50	3.50	3.58	3.54-3.63	3.65	3.523.75	3.67	3.59-3.73
H_2O*	4.61	4.59-4.64	4.626-4.59	4.59	4.62	4.6-4.65	4.61	4.59-4.64	4.66	4.62-4.69
Total	101.88	101.20	102.1-101.7	101.69	103.04	102.74	102.86	102.4-103.29	102.94	102.28-103.50
ppm										
Li	2185	1173-3511	1363	697-1742	21135	19596-23388	8118	2036-27323	453	316-905
Rb	4292	2761-5267	4210	2848-5632	6117	5709-6543	3441	2120-4895	296	129-462
Cs	1301	959-1912	2027	998-3127	4693	3672-5638	1622	968-2625	46	37-65
Ba	81	27-158	40	24-56	23	12-36	22	15-30	83	27-196
Sr	105	60-178	29	23-37	22	13485	16	11-18	14	6-25
Ga	279	158-383	213	138-262	83	58-118	168	112-236	61	49-97
Be	31	21-37	26	22-33	30	18-48	29	17-56	19	10-28
B	274	77-424	216	163-269	122	68-148	111	75-160	105	93-122
Sn	518	143-742	277	183-377	65	31-114	115	61-193	26	18-36
Nb	270	144-406	296	158-406	208	107-312	242	128-334	23	10-33
Ta	177	94-286	249	168-332	192	103-294	172	98-224	14	11-19
W	33	20-44	31	22-42	293	205-559	39	31-44	12	10-16
Y	6	3-8	13	8-19	3	2-4	3	2-4	5	2-8
Zn	517	317-789	223	183-267	200	82-427	139	113-207	48	18-79
Zr	33	26-45	13	8-16	5	3-8	3	1-3	3	2-4
Hf	3.6	2.0-6.0	1.7	1.2-2.2	0.4	0.2-0.6	0.3	0.2-0.4	0.6	0.3-1.0
Th	1.8	1.0-3.0	1.8	1-2	0.3	0.2-0.6	1.6	1.0-2.0	0.4	0.2-0.8
U	1.6	1.0-2.0	1.8	1-3	0.2	0.1-0.4	2.0	1.0-2.0	0.5	0.3-0.8
K/Ba	1570	582-3428	2493	1648-3871	4264	2743-5337	4417	3071-6297	1836	466-3309
Rb/Sr	49.5	15.7-71.7	147.5	103.5-204.7	319.8	182-514	215.5	118-306	23.0	15646.0
K/Rb	22.7	17.8-33.3	23.1	16.2-31.8	15.2	14-16	29.8	19-47	367.7	198-709
K/Cs	77.42	48.09-96.51	54.16	28.96-93.09	20.12	16-25	65.17	35-97	2373.67	2182-2736
Nb/Ta	1.56	1.15-2.01	1.20	0.94-1.88	1.10	0.94-1.43	1.41	0.96-1.77	1.64	0.77-2.54
Ta/W	5.73	2.149.45	8.29	5.09-12.77	0.69	0.5-1.31	4.33	2.51-5.09	1.21	1.0-1.60
Al/Ga	723	482-1156	933	730-1301	2378	1559-3050	1149	722.54-1554	3198	1931-3773
Zr/Hf	10.37	5.33-15.0	7.73	5.33-12.5	17.23	6.7-40	9.00	2.5-15.0	5.18	3.75-7.50
Na/K	0.05	0.05-0.06	0.06	0.05-0.06	0.05	0.049-0.05	0.05	0.04-0.05	0.07	0.06-0.08

moderate to high rare element-bearing potential, compare favourably with other notable rare-metal-bearing pegmatites elsewhere in Nigeria (Adekeye and Akintola, 2007; Akoh *et al*., 2015) (Table 4.14). The generally low abundances of the rare-alkalis and ore elements in the Osu pegmatite muscovite samples indicated low rare metal-bearing geochemical signature.

Fractionation indicators in muscovite samples, such as K/Rb, K/Cs, Nb/Ta and Ta/W, have been used to determine the degree of chemical fractionation of pegmatites and their prospects for rare-metal mineralisation (Gordiyenko, 1971; Cerny and Burt, 1984, Cerny *et al.*, 1985; Moller and Morteani, 1987; Cerny, 1989; Smeds,1992; Morteani *et al*.,1995; Wise, 1995; Morteani and Gaupp, 1989; Morteani *et al*., 2000; Alfonso *et al*., 2003; Selway *et al*., 2005; Roda Robles *et al*., 2006; 2007; Kuster *et al*., 2009). The mean K/Rb (15.2-29.8) and K/Cs (20.12-77.42) ratios (Table 4.13) are generally low in the muscovite samples of Ijero, Komu, Ofiki and Iwere pegmatites; these values are consistent with values expected for rare metal-bearing and geochemically evolved pegmatites (Selway *et al*., 2005; Adekeye and Akintola, 2007; Kuster, 2009; Akoh *et al.*, 2015) (Table 4.14). The Osu muscovite samples showed high values of K/Rb (367.7) and K/Cs (2373.7) ratios (Table 4.13), suggesting the very low rare metal-bearing potential and possibly poorly evolved status of the Osu pegmatite. Nb/Ta ratio, as a rare-metal mineralisation enrichment parameter, varies between 1.10 and 1.56 (Table 4.13) in the muscovite samples of Ijero, Komu, Ofiki andIwere pegmatites,indicating their moderate endowment in Ta-Nb ores; while Ta/W ratio varying between 0.69 and 8.29 possibly shows the late enhancement of tantalum relative to tungsten in the residual melts of these pegmatites with progressing fractionation (Moller and Morteani, 1987). The Osu muscovite samples, however, indicate higher Nb/Ta (1.64) and lower Ta/W (1.21) ratios, and these possibly account for the Osupegmatite's lack of Ta-Nb oxide minerals.

The K/Rb ratio is generally taken as the best fractionation index in muscovite, as it measures the degree of substitution of rubidium for potassium in the muscovite crystal structure (Alfonso *et al*., 2003; Selway *et al*., 2005; Neiva, 2013). The values of K/Rb inmuscovite have been diversely graphically correlated with common rare alkalis (Li, Rb, Cs, Ba) and other ore elements to qualitatively evaluate the rare-element potentials of

Table 4.14: Average trace element compositions of the analysed muscovite samples compared with other published muscovite analytical data.

Trace element	IJM n=5	KMM n=5	OFM n=5	IWM n=5	NSM n=9	ADM n=6
F	Nd	Nd	Nd	Nd	2108	14583
Rb	4292	4210	6117	3441	5302	6004
Cs	1301	2027	4693	1622	548	701
Ga	279	213	83	168	159	160
Sn	518	277	65	115	352	523
Nb	270	296	208	242	158	184
Ta	177	249	192	172	97	107
W	33	31	293	39	Nd	139
K/Rb	22.7	23.1	15.2	29.8	15.28	10.76
K/Cs	77.42	54.16	20.12	65.17	147.85	179.53
Nb/Ta	1.56	1.2	1.1	1.41	1.72	1.56
Ta/W	5.73	8.29	0.69	4.33	-	0.77

1. Mean Ijero muscovite sample (this study)
2. Mean Komu muscovite sample (this study)
3. Mean Ofiki muscovite sample (this study)
4. Mean Iwere muscovite sample (this study)
5. Mean Nassarawa muscovite sample (Adekeye and Akintola, 2007)
6. Mean Angwan Doka muscovite sample (Akoh *et al.,* 2015)

Nd- Not determined

pegmatites (Trueman and Cerny, 1982; Cerny and Burt, 1984; Moller and Morteani, 1987; Morteani *et al*., 2000; Alfonso *et al*., 2003; Okunlola, 2005; Adekeye and Akintola, 2007; Kuster, 2009; Okunlola and Oyedokun, 2009; Wise and Brown, 2010; Elueze and Aromolaran, 2014, Akoh *et al*., 2015).

The K/Rb against Rb (Fig. 4.50) discrimination plot (Stavrov*et al*., 1969) indicates the muscovite samples of Ijero, Komu, Ofiki and Iwere pegmatites plotting in the mineralised field of the fractionation diagram; while the muscovite samples of the Osu pegmatite plot in barren field of the diagram. An inverse correlation is indicated between K/Rb ratios and Rb contents of the plotted muscovite samples, possibly indicating enhancement in Rb contents with protracted fractionation. The K/Rb versus Cs (Fig. 4.51a) and K/Rb against Zn (Fig 4.51b) of the pegmatites reveal the rare-element geochemical signature of Ijero, Komu, Ofiki and Iwere pegmatites, with the Osu pegmatite falling within the poorly fractionated muscovite class pegmatites field. The moderate degree of fractionation of the Ijero, Komu, Ofiki and Iwere mineralised pegmatites can be clearly observed in the muscovite samples plotting in the middle component of the fractionation trend (Fig. 4.51b), while the Osu muscovite samples cluster towards the least fractionation end of the diagram.

The muscovite samples of the Osu pegmatite showed low contents of Rb, Cs, Ta, Ga and W (Table 4.13), as opposed to those Ijero, Komu, Ofiki and Iwere that are marked by moderate to high abundances of these rare-alkalis and rare-metals. The Rb/Ta rare-metal discrimination plot (Fig. 4.52) showedthat only the Ijero, Komu, Ofiki and Iwere muscovite plot in the Ta-mineralised field, following the minimum Ta (20 ppm) contents for Ta-prospective (Beus, 1966) and minimum Ta (>65 ppm) content for Ta-mineralised (Gordiyenko, 1971) pegmatites.Other rare-metal mineralisation plots, including Ta/Ga (Fig. 4.53a), Ta/Cs+Rb (Fig. 4.53b), Ta/Cs (Fig. 4.54a) and Ta/K/Cs (Fig. 4.54b)essentially portray the pegmatites of Ijero, Komu, Ofiki and Iwere areas to plot above Beus (1966) and Gordiyenko (1971) Ta-mineralisation discrimination lines, whereas the Osu pegmatite falls below these aforementioned defining lines.The Ta/W versus Cs (Fig. 4.55) plot for the pegmatites indicates overall positive correlation between the Ta/W and the Cs contents of the muscovite samples.

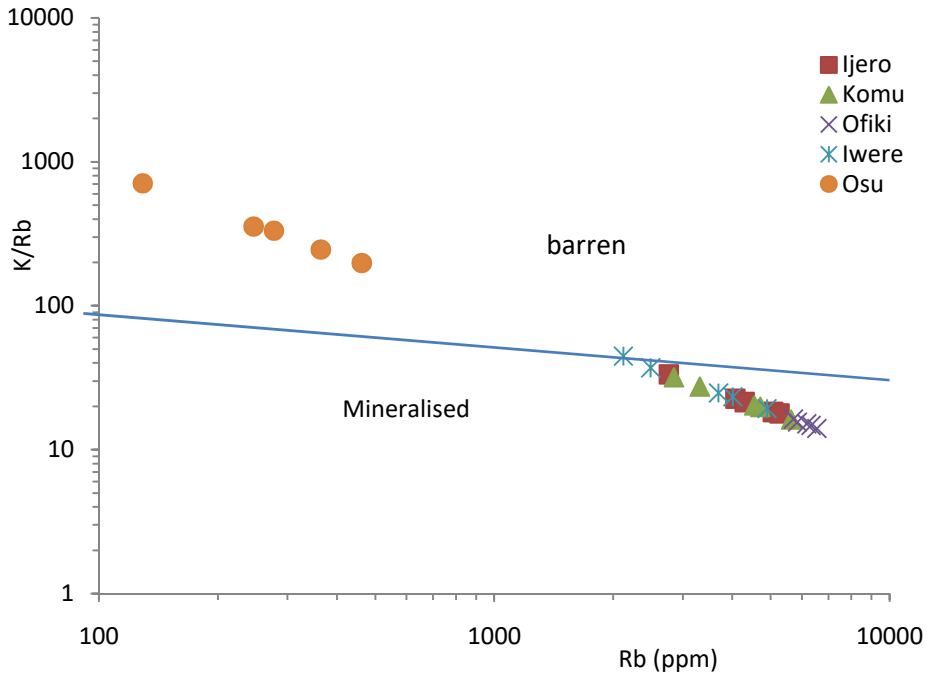

Fig. 4.50: Plot of K/Rb vs. Rb for the muscovite samples (modified after Stavrov *et al.*, 1969).

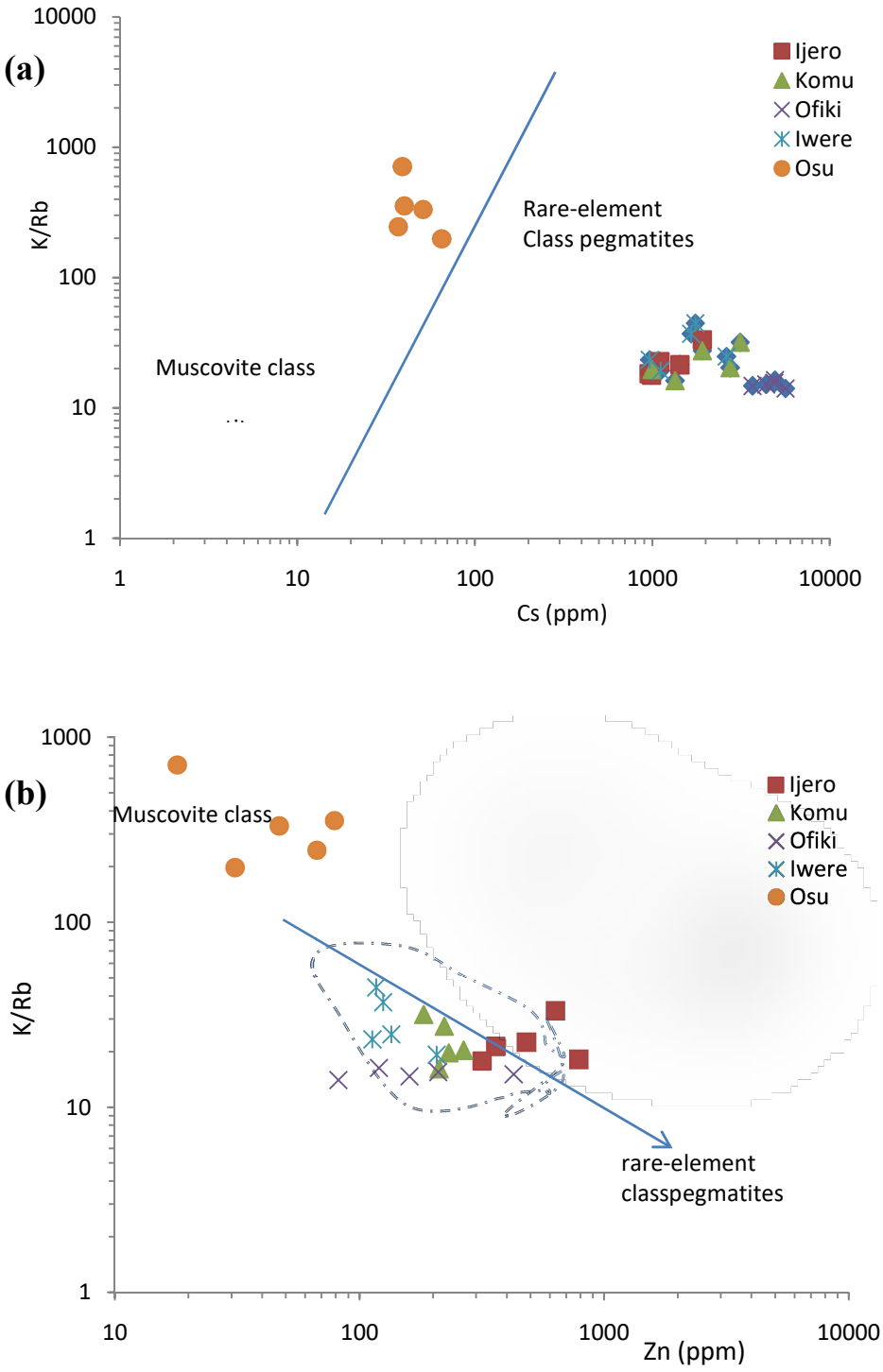

Fig. 4.51a: Plot of (a) K/Rb vs. Cs and (b) K/Rb vs. Zn for the muscovite samples (modified after Cerny and Burt, 1984).

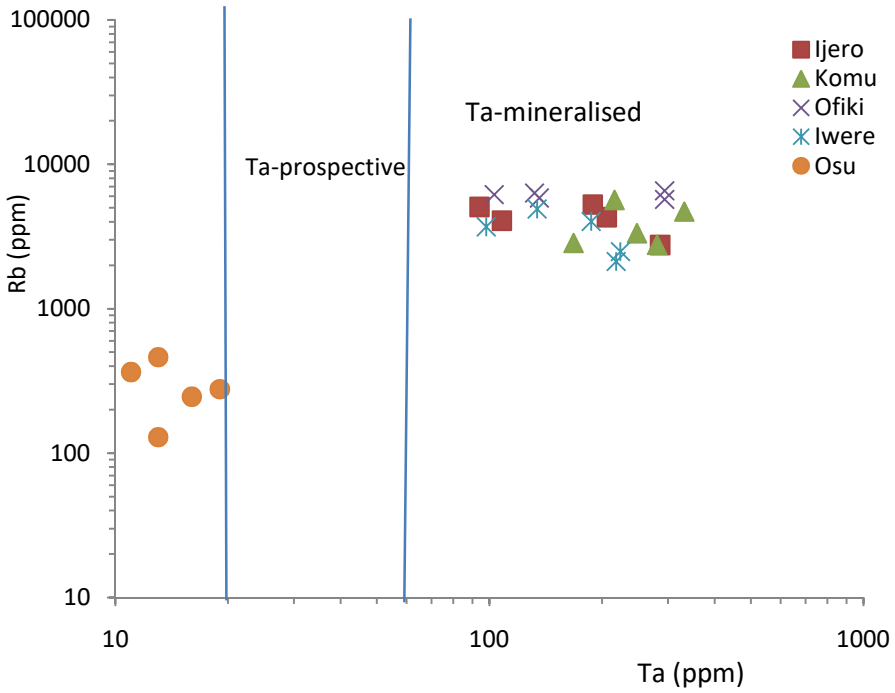

Fig. 4.52: Plot of Rb vs. Ta for the muscovite samples (modified after Kuster *et al*., 2009). Note that minimum Ta contents for Ta-prospective and Ta-mineralised are respectively from Beus (1966) and Gordiyenko (1971).

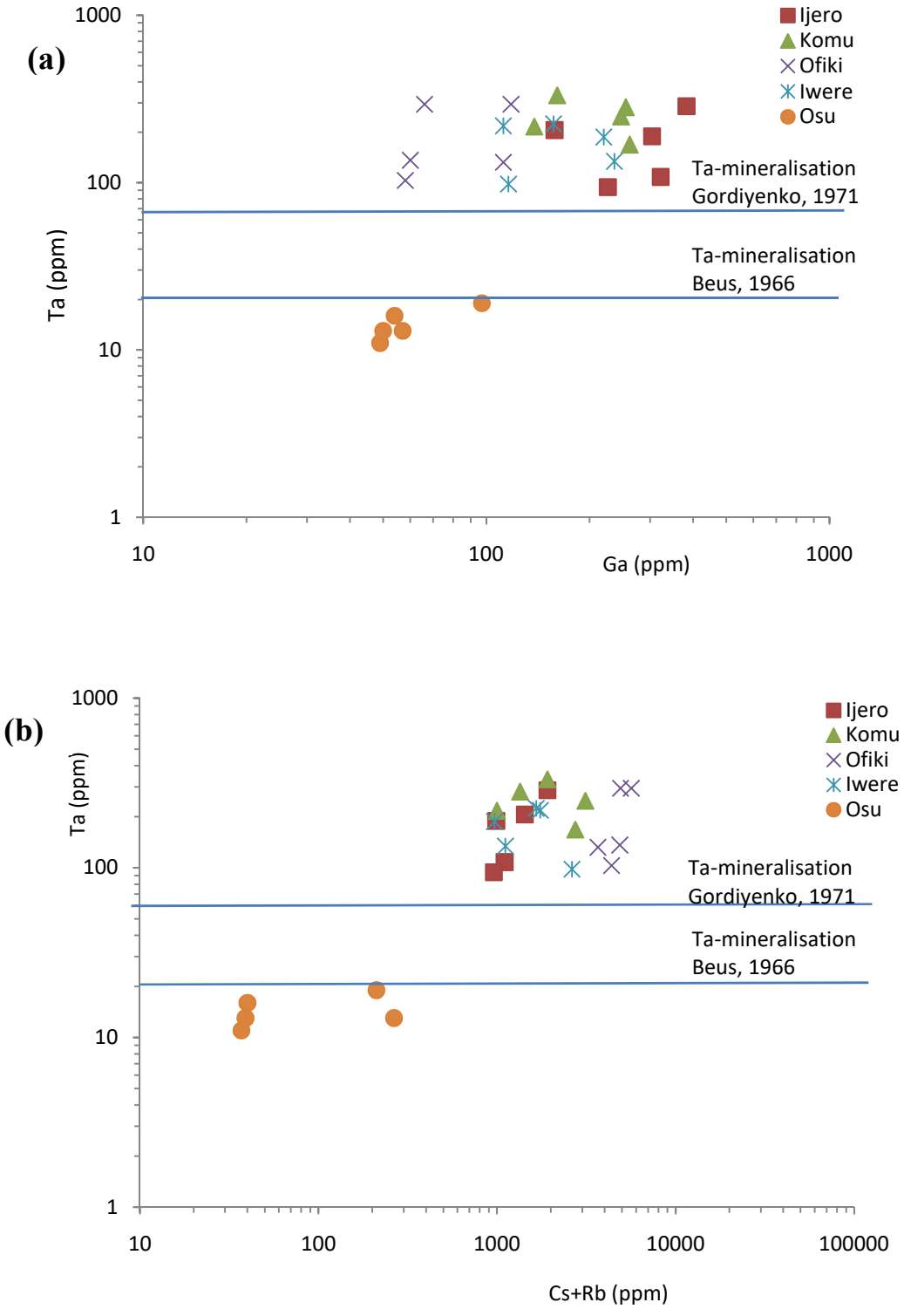

Fig. 4.53a: Plot of (a) Ta vs. Ga and (b) Ta vs. Cs+Rb for the muscovite samples (modified after Moller and Morteani, 1987).

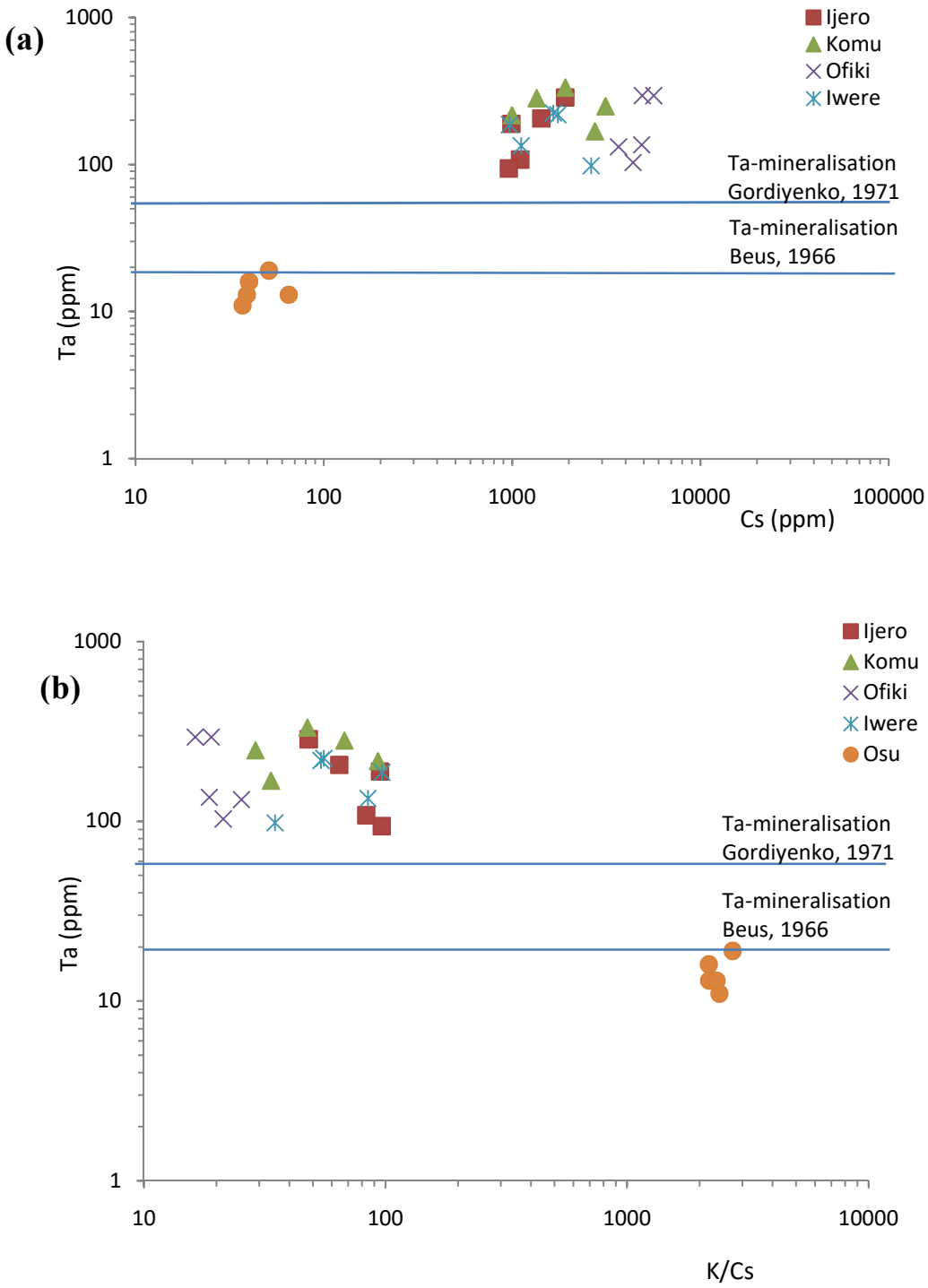

Fig. 4.54: Plot of (a) Ta vs. Cs and (b) Ta vs. K/Csfor the muscovite samples (modified after Moller and Morteani, 1987).

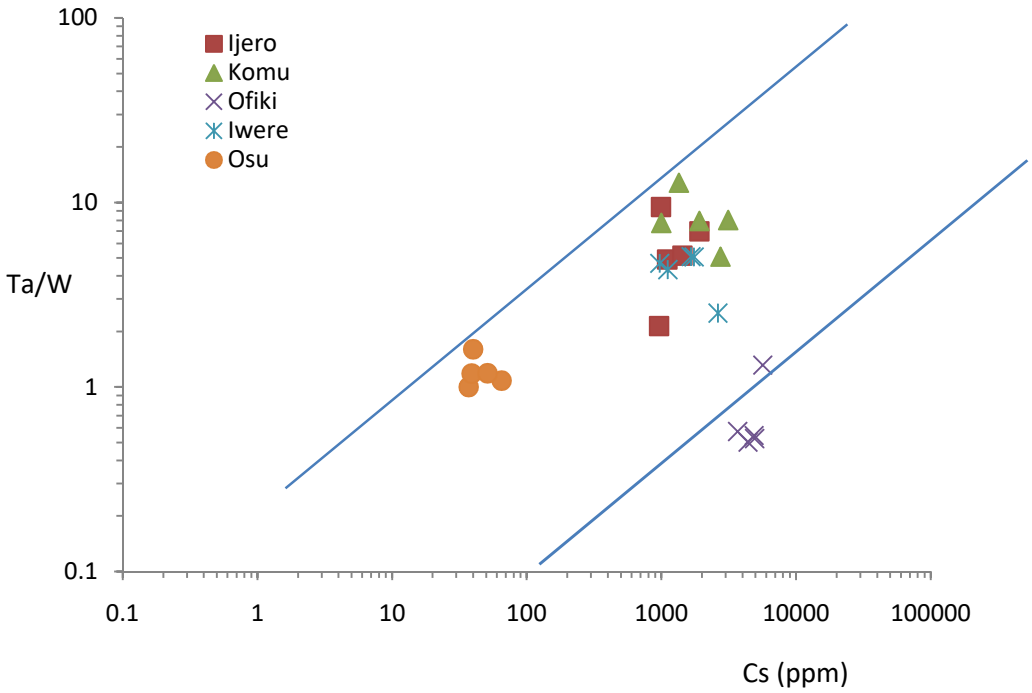

Fig. 4.55: Plot of Ta/W vs. Cs for the muscovite samples (modified after Moller and Morteani, 1987)

The data points representing Osu pegmatite are found at the lower Ta/W and Cs data field, while the mineralised pegmatites of Ijero, Komu, Ofiki and Iwere areas reflect higher abundances in tantalum, tungsten and cesium by plotting in the upper half of the data field.

On the whole, the lithophile trace elements Rb, Li, Cs, Ga, Sn, Nb, Ta, W and Be are more enhanced in the mineralised pegmatites of Ijero, Komu, Ofiki and Iwere, whereas these elements are remarkably of low concentration levels in the non-mineralised pegmatite of Osu area (Table 4.13). The low values of K/Rb, K/Cs and Nb/Ta plus higher Ta/W in the muscovite samples of Ijero, Komu, Ofiki and Iwere pegmatites, as well as applicable fractionation and rare-metal discrimination plots establish the rare metal-bearing potential of these pegmatites. Conversely, the Osu non-mineralised pegmatite signifies higher K/Rb, K/Cs and Nb/Ta as well as lower Ta/W ratios (Table 4.13), while relevant discrimination diagrams confirm its poorly evolved status and its very low rare-metal bearing potential. The mineralogical assemblages, earlier established(including lepidolite, lithian muscovite, beryl, elbaite, tantalo-columbite, cassisterite and rutile) in the Ijero, Komu, Ofiki and Iwere mineralised pegmatites, are consistent with their moderately geochemically evolved status. These pegmatites compare favourably with other rare-metal bearing pegmatites elsewhere in Nigeria (Nassarawa: Adekeye and Akintola, 2007;Angwan Doka pegmatites:Akoh *et al.*, 2015) (Table 4.14), and petrochemically belong to the lithium-cesium-tantalum (LCT) petrogenetic family of Cerny (1991) and Cerny and Ercit (2005).

4.3.2.3 Columbo-tantalite ore composition

Columbite ($[Fe,Mn]Nb_2O_6$) and tantalite ($[Fe,Mn]Ta_2O_6$) occur as solid solution series of orthorhombic minerals in rare-element pegmatites (Cerny and Ercit, 1989; Cerny *et al*., 1992; Ercit *et al*., 1995). The presence of these oxides in pegmatites are convincing evidence of extended geochemical fractionation of pegmatitic melts and occurrenes of rare-element (mineralised) pegmatites (Cerny and Ercit, 1989; Ercit *et al.*, 1992; Anthony *et al.*, 2004; Selway *et al*., 2005).

In the study areas, columbo-tantalite ore samples are found as black, subhedral to euhedral crystals, ranging in size from 1.2 to 4.0 cm in thickness. They are marked by submetallic

lustre and show uneven fracture when broken. They are commonly recovered from the elluvial segment, pegmatite weathering crust and unaltered rock components of the mineralised pegmatite bodies of the areas of investigation.

Representative electron microprobe analyses of the columbo-tantalite samples in the mineralised pegmatite of Ijero, Komu, Ofiki and Iwere areas are presented in Table 4.15. It indicates fairly variable Ta_2O_5 and Nb_2O_5 contents among samples within each locality. Ta_2O_5 range of 49.82-62.01, 16.97-54.12, 31.26-42.42 and 43.83-51.08 wt.% were correspondingly obtained for columbo-tantalite samples from Ijero, Komu, Ofiki and Iwere areas, while Nb_2O_5 variations recorded for the same samples are respectively 18.70-30.31, 29.18–63.75, 31.62–42.83 and 31.11–38.32 wt.%. Columbo-tantalite samples of Ijero pegmatites are marked by high concentrations of SnO_2 up to 5.5 wt.%, as the pegmatite is cassiterite-bearing; while SnO_2 contents of columbo-tantalite samples from other pegmatites are generally below1.5 wt.%. The analysed columbo-tantalite minerals generally show low WO_3, TiO_2 but fairly high FeO and MnO contents (Table 4.15). The coltan samples are generally marked by low contents of radioactive elements (UO_2 and ThO_2), but the Ofiki columbo-tantalite samples are uranium-bearing showing UO_2abundances ranging from 4.39 to 10.12 wt.% and ThO_2 varying from 0.36 to 0.86 wt.%.

The computed Ta/(Ta+Nb) and Mn/(Mn+Fe) (Table 4.15) molar ratios from the EMPA data of the columbite-tantalite samples were plotted in the columbite-tantalite series discrimination quadrilateral (Fig. 4.56), which is marked by ferrocolumbite ($FeNb_2O_6$), manganocolumbite ($MnNb_2O_6$), ferrotantalite ($FeTa_2O_6$) and manganotantalite ($MnTa_2O_6$) end members (Cerny and Ercit, 1985; 1989). The mineralogical classification and compositional fields are columbite-(Fe), columbite-(Mn), tantalite-(Fe) and tantalite-(Mn) with an empirically-derived tantalite-tapiolite miscibility gap (Cerny and Ercit, 1985; 1989; Cerny *et al*., 1992).

The columbite-tantalite samples from Ijero pegmatite plot in the tantalite-(Fe) and tantalite-(Mn) compositional fields, having average Mn/(Mn+Fe) and Ta/(Ta+Nb) molar

ratios of 0.44 and 0.58, respectively; whereas those of Komu pegmatite plot within the columbite-(Fe) and columbite-(Mn) discrimination fields, correspondingly indicating

Table 4.15: Representative electron microprobe compositions of columbite-tantalite of thepegmatite

Wt %	IJT1	IJT2	IJT3	IJT4	IJT5	KMT1	KMT2	KMT3	KMT4	KMT5	OFT1	OFT2	OFT3	OFT4	IWT1	IWT2	IWT3	IWT4
WO_3	0.39	0.28	0.28	0.48	0.62	0.95	0.32	0.16	0.47	0.32	0.52	0.38	0.72	0.98	0.22	0.16	0.12	0.32
Ta_2O_5	49.82	58.35	53.43	62.01	55.35	16.97	46.23	21.02	44.72	54.12	31.26	40.32	41.52	42.42	45.12	51.08	45.81	43.83
Nb_2O_5	30.31	23.58	27.47	18.70	22.39	62.75	36.25	62.02	36.78	29.18	42.83	33.02	34.23	31.62	38.32	31.11	36.39	36.93
SnO_2	4.03	3.14	3.18	5.50	4.52	0.01	0.15	0.04	0.08	0.04	0.03	1.15	1.09	1.24	0.43	0.28	0.64	1.22
TiO_2	0.67	0.68	0.26	0.19	1.68	2.08	1.22	1.08	1.93	1.01	0.85	1.02	1.54	2.62	0.31	0.47	1.53	0.81
FeO	9.54	7.98	6.98	8.91	6.99	9.12	6.98	4.58	6.93	6.16	9.52	8.13	9.89	7.98	6.73	6.92	6.69	7.31
MnO	5.02	5.78	8.56	4.10	8.32	7.92	8.60	5.16	8.98	9.12	5.24	5.18	6.38	6.37	8.96	9.81	8.73	9.79
UO_2	0.09	0.18	0.10	0.03	0.07	0.32	0.34	0.16	0.29	0.12	9.12	10.12	4.39	5.96	0.03	0.08	0.05	0.06
ThO_2	0.04	0.02	0.02	0.06	0.02	0.05	0.05	0.04	0.04	0.06	0.61	0.86	0.36	0.76	0.01	0.02	0.03	0.02
Total	99.91	99.99	100.28	99.97	99.96	100.17	100.14	100.26	100.22	101.13	99.98	100.18	100.12	99.95	100.13	99.93	99.99	100.29
Number of cations on the basis of 6 oxygen atoms																		
W	0.007	0.005	0.005	0.009	0.012	0.015	0.006	0.003	0.008	0.06	0.009	0.007	0.013	0.018	0.004	0.003	0.002	0.006
Ta	0.957	1.165	1.042	1.276	1.095	0.275	0.858	0.346	0.821	1.045	0.579	0.787	0.784	0.811	0.835	0.980	0.847	0.809
Nb	0.968	0.783	0.891	0.640	0.736	1.688	1.119	1.669	1.123	0.936	1.319	1.072	1.074	1.005	1.178	0.992	1.119	1.133
Sn	0.114	0.092	0.091	0.166	0.131	—	0.004	0.001	0.002	0.001	0.001	0.033	0.030	0.035	0.012	0.008	0.017	0.033
Ti	0.036	0.038	0.014	0.011	0.092	0.093	0.063	0.049	0.098	0.054	0.044	0.055	0.080	0.139	0.016	0.025	0.078	0.041
Fe	0.564	0.490	0.419	0.564	0.425	0.454	0.398	0.586	0.391	0.366	0.542	0.488	0.574	0.469	0.383	0.408	0.381	0.415
Mn	0.300	0.359	0.520	0.263	0.513	0.399	0.497	0.264	0.541	0.548	0.302	0.315	0.375	0.379	0.516	0.586	0.503	0.563
U	0.001	0.003	0.002	0.001	0.001	0.004	0.005	0.002	0.004	0.002	0.138	0.162	0.068	0.093	0.000	0.001	0.001	0.001
Th	0.001	0.000	0.000	0.001	0.000	0.001	0.001	0.001	0.001	0.001	0.009	0.014	0.006	0.012	0.000	0.000	0.000	0.000
∑	2.947	2.935	2.984	2.931	3.005	2.928	2.951	2.920	2.962	2.959	2.943	2.933	3.004	2.961	2.944	3.003	2.949	3.001
Mn/Mn+Fe	0.35	0.42	0.55	0.32	0.55	0.47	0.56	0.31	0.58	0.60	0.36	0.39	0.40	0.45	0.57	0.59	0.57	0.58
Ta/Ta+Nb	0.50	0.60	0.54	0.67	0.60	0.14	0.43	0.17	0.42	0.53	0.31	0.42	0.42	0.45	0.41	0.50	0.43	0.42
Class	tan-(Fe)	tan-(Fe)	tan-(Mn)	tan-(Fe)	tan-(Mn)	col-(Fe)	tan-(Mn)	col-(Fe)	tan-(Mn)	tan-(Mn)	col-(Fe)	tan-(Fe)	tan-(Fe)	tan-(Fe)	tan-(Mn)	an-Mn)	tan-(Mn)	tan-(Mn)

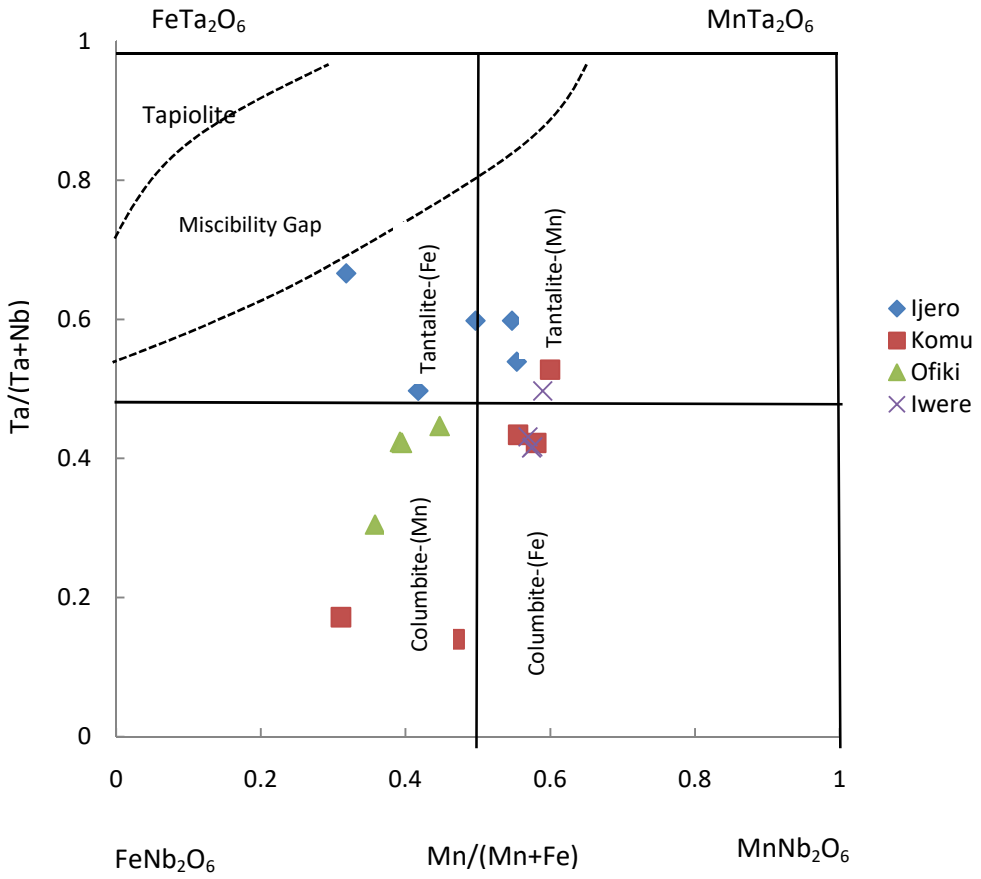

Fig. 4.56: Chemical compositions of the columbo-tantalite samples from the pegmatites plotted in Ta/(Ta+Nb) vs. Mn/(Mn+Fe) columbite quadrilateral (modified after Cerny and Ercit, 1985; 1989).

mean Mn/(Mn+Fe) and Ta/(Ta+Nb) molar ratios of 0.50 and 0.34. The Ofiki columbite-tantalite mineral samples discretely cluster into the columbite-Fe compositional field, showing average Mn/(Mn+Fe) and Ta/(Ta+Nb) molar ratios of 0.4; while those of Iwere pegmatite plot within the columbite-(Mn) compositional field, having mean Mn/(Mn+Fe) and Ta/(Ta+Nb) molar ratios of 0.58 and 0.44, respectively. There are few compositional overlaps of the columbo-tantalites among study localities. These are essentially reflections of the differences in the degree of geochemical evolution of the respective pegmatite bodies and possible differences in the chemistry of pegmatite melts.

4.3.3 Geochemical compositions ofthe weathering profiles over the pegmatites

The chemical compositions of the bedrock pegmatite types and their respective in situ-derived lateritic profiles are discussed in this section. The geochemical variation trends in the horizons of the respective weathering profile are appraised and correlated among weathering profiles of the pegmatite types, so as to derive geochemical criteria that can be employed to discriminate between barren and mineralised pegmatites underneath lateritic profiles.

4.3.3.1 Geochemical composition of the weathering profile over the Osu barren pegmatite

The whole-rock chemical data of the Osu barren pegmatite are presented in Table 4.16. The silica content of the pegmatite ranged between 70.43 and 73.93 wt.%, showing a mean concentration of 72.47 wt.%. The alumina content varies between 14.56 and 18.21 wt.%; while Fe_2O_3 indicates a low content ranging from 0.37 to 1.83 wt.%. The MgO and CaO are generally low, indicating mean concentrations of 0.13 and 0.61 wt.%, respectively. K_2O and Na_2O, on the other hand, show moderate levels with mean concentrations of 6.60 and 2.18 wt.%, respectively. The abundances of the above oxides are consistent with the chemistry of typical granitic pegmatites.P_2O_5 content of the pegmatite varies between 0.05 and 0.9 wt.%, showing a mean concentration of 0.27 wt.%. The low P_2O_5 in the Osu non-mineralised pegmatite can be ascribed to the relatively low modal abundance of apatite in the rock.

Barium (16 – 202 ppm) and Sr (27-141 ppm) contents with the corresponding mean values of 85 and 66 ppm show wide variations among samples and are generally low. The low Ba and Sr concentrations in the pegmatite could possibly reflect very low modal abundances of plagioclase in the rock, as these elements can substitute for Ca and are commonly incorporated into the Ca sites of the plagioclase crystal structure.

Rubidium and Cs respectively show mean concentrations of 97 and 17 ppm in the pegmatite. Rubidium and Cs, as rare alkalis in the barrenOsu pegmatite, are of low values when compared to the mineralised pegmatites. Tin, Nb, Ta respectively indicate average contents of 6, 16 and 4 ppm in the Osu non-mineralised pegmatites, while 9 and 14 ppm are correspondingly obtained for Be and Ga in the pegmatite. Other relatively immobile trace elements, such as Zr, Th, Hf, Y and U are generally low in the pegmatite, indicating mean concentration of 23, 4, 3, 8 and 11ppm, respectively (Table 4.16).

The REEs contents of the Osu non-mineralised pegmatite indicate wide variations (6-49 ppm) among samples, showing mean concentration value of 29 ppm. The pegmatite is, however, preferentially more enhanced in LREEs (26 ppm) relative to the HREEs (3 ppm). The relative LREEs/HREEs geochemical distribution in the pegmatite is closelyconnected to the relative abundances of accessory mineral phases that host different REEs. The whole-rock pegmatite shows negative Ce (Ce/Ce*=0.69) anomaly, indicating low abundance of Ce-bearing accessory minerals; while the negative Eu (Eu/Eu*= 0.55) anomaly could be a reflection low abundance of plagioclase (albite) feldspar in the pegmatite.

The bulk chemical composition of the non-mineralised Osu pegmatite residual profile is given Table 4.17, while the chemical variation trends with depths are displayed in Fig. 4.62. The A-horizon of the residual profile is highly siliceous, showing SiO_2 concentration of 78.90 wt.%, relative to 62.41 and 63.67 wt.% in B and C-horizons, respectively. The abundance of silica in the constituting horizons of the lateritic profile is confirmed by the prominent peaks of quartz in the X-ray diffractograms (Fig. 4.33).Alumina shows enrichment in the C-horizon (21.05 wt.%) and B-horizon (22.10 wt.%)of the residual profile, while the A-horizon (9.03 wt.%) has undergone profound depletion in Al_2O_3.

Table 4.16: Whole-rock major, trace and rare-earth element compositions of the Osubarren pegmatite

Major oxides	OSP1	OSP2	OSP3	OSP4	OSP5	OSP6	OSP7	Mean	Range
(wt.%)									
SiO_2	72.92	72.15	72.85	70.43	72.77	72.29	73.90	72.47	70.43-73.90
Al_2O_3	14.98	15.70	15.01	18.21	14.86	15.78	14.56	15.59	14.56-18.21
Fe_2O_3	0.37	0.99	0.99	0.98	1.04	1.85	1.67	1.13	0.37-1.85
MnO	0.02	0.02	0.02	0.17	0.15	0.16	0.09	0.09	0.02-0.17
MgO	0.08	0.15	0.15	0.05	0.07	0.25	0.19	0.13	0.05-0.25
CaO	0.67	0.84	0.78	0.37	0.78	0.44	0.36	0.61	0.36-0.84
Na_2O	2.35	1.78	3.42	2.15	2.71	1.38	1.49	2.18	1.38-3.42
K_2O	7.92	6.69	6.50	6.56	6.28	5.91	6.36	6.60	5.91-7.92
TiO_2	0.01	0.12	0.11	0.03	0.03	0.42	0.40	0.16	0.01-0.42
P_2O_5	0.12	0.05	0.90	0.13	0.36	0.18	0.15	0.27	0.05-0.90
LOI	0.14	1.03	0.95	0.06	0.74	1.30	0.89	0.73	0.06-1.30
Total	99.58	99.52	99.68	100.14	99.79	99.96	100.06	99.78	99.52-100.14
CIA	49.40	55.05	55.75	56.39	50.85	61.14	57.98	55.04	64.20-52.13
Trace element									
Rb	126	27	45	87	226	62	109	97	27-226
Cs	2	4	10	8	24	4	4	17	2-24
Ba	22	23	107	202	16	130	94	85	16-202
Sr	76	74	83	141	31	31	27	66	27-141
Ga	15	6	8	14	31	10	16	14	6-31
Be	13	12	8	12	28	4	3	11	3-28
Sn	5	4	3	3	6	10	11	6	3-11
Nb	14	11	21	23	12	12	22	16	11-23
Ta	6	4	6	5	5	2	2	4	2-6
Y	5	4	6	7	3	17	17	8	3-17
Zn	8	6	25	16	8	22	14	14	6-25
Zr	35	75	96	65	87	60	52	67	35-96
Hf	1	1	1	1	1	7	6	3	1-7
Th	2	1	2	5	5	6	7	4	1-9
U	9	19	6	20	4	12	10	11	4-20

Table 4.16 (Continued)

Rare-earth element	OSP1	OSP2	OSP3	OSP4	OSP5	OSP6	OSP7	Mean	Range
La	4.20	2.40	1.00	10.00	6.00	4.93	5.50	4.86	1.00-10.0
Ce	8.70	6.40	16.00	24.00	8.00	11.20	8.30	11.8	6.40-24.0
Pr	0.80	0.50	0.60	0.40	0.50	3.30	3.40	1.36	0.40-3.40
Nd	5.00	2.00	4.00	10.00	4.00	3.80	5.70	4.93	2.00-10.0
Sm	4.00	4.00	8.00	2.00	3.00	2.50	2.40	3.70	2.00-8.00
Eu	0.40	0.50	0.50	0.60	0.60	0.30	0.30	0.46	0.30-0.60
Gd	0.50	0.60	0.60	0.50	0.50	0.80	0.30	0.54	0.50-3.30
Tb	0.10	0.10	0.20	0.20	0.10	0.90	0.50	0.30	0.10-0.90
Dy	0.80	0.40	0.60	0.60	0.40	0.40	0.50	0.53	0.40-0.80
Ho	0.10	0.10	0.10	0.20	0.20	1.00	0.60	0.33	0.10-1.00
Er	0.20	0.4	0.20	0.20	0.30	0.20	0.30	0.26	0.20-0.40
Tm	0.10	0.10	0.20	0.10	0.10	0.40	0.30	0.19	0.10-0.40
Yb	0.20	0.10	0.20	0.20	0.10	0.20	0.30	0.19	0.10-0.30
Lu	0.10	0.10	0.10	0.20	0.20	0.30	0.30	0.20	0.10-0.30
LREE	23.10	15.80	30.10	47.00	22.10	26.03	25.60	26.11	15.80-47.00
HREE	2.10	1.90	2.20	2.20	1.90	4.20	3.10	2.51	1.90-4.20
∑REE	25.20	17.70	32.30	49.20	24.00	6.20	28.70	28.62	6.20-49.20
LREE/HREE	11.00	8.32	13.68	21.36	11.63	5.50	8.26	9.80	8.30-11.19
Ce/Ce*	0.53	0.76	1.69	0.80	0.54	0.26	0.27	0.69	0.26-1.69
Eu/Eu*	0.56	0.57	0.40	0.97	0.79	0.26	0.27	0.55	0.26-0.97
La/Yb	21.00	24.00	5.00	50.00	60.00	24.65	18.33	25.58	10.00-33.33

T**able 4.17:** Major, trace and rare-earth element composition of the lateritic profile derived from the Osu barren pegmatite

Sample #	A1	A2	A3	A4	A5	A6	A7	A8	B1	B2	B3	B4	B5	B6	B7	B8	B9	B10	B11	C1	C2
Depth (m)	0.2	0.4	0.6	0.8	1.0	1.2	1.4	1.6	1.8	2.0	2.2	2.4	2.6	2.8	3.0	3.2	3.4	3.6	3.8	4.0	4.2
wt. %																					
SiO_2	79.95	82.64	81.3	76.31	76.66	78.18	81.01	75.19	67.44	66.24	63.88	58.4	63.02	60.23	65.86	60.13	59.19	61.95	60.22	64.56	63.12
Al_2O_3	9.24	8.54	9.23	12.46	12.53	10.67	9.51	13.66	19.07	19.34	21.53	24.49	21.66	22.63	18.68	23.66	25.62	22.18	24.29	19.45	22.65
Fe_2O_3	2.57	1.85	1.73	2.45	2.48	3.45	2.42	3.20	4.37	5.45	4.97	6.09	5.38	6.14	4.69	4.96	3.72	4.20	4.47	4.56	4.52
MnO	0.14	0.10	0.15	0.11	0.10	0.10	0.07	0.07	0.03	0.04	0.03	0.04	0.03	0.03	0.02	0.01	0.01	0.03	0.04	0.02	0.01
MgO	0.22	0.18	0.03	0.09	0.09	0.13	0.07	0.08	0.09	0.09	0.09	0.13	0.10	0.16	0.15	0.08	0.07	0.06	0.08	0.08	0.08
CaO	0.29	0.21	0.25	0.24	0.27	0.28	0.25	0.22	0.17	0.17	0.18	0.19	0.17	0.18	0.16	0.17	0.16	0.13	0.12	0.12	0.15
Na_2O	0.88	0.90	1.11	1.92	1.17	1.06	1.16	0.96	0.71	0.41	0.69	0.62	0.63	0.61	0.69	0.61	0.59	1.13	1.10	1.19	1.11
K_2O	2.40	2.68	2.93	2.38	2.49	1.57	1.62	1.71	1.51	1.45	1.33	1.73	1.29	1.49	1.60	1.85	1.76	2.63	1.58	2.58	1.37
TiO_2	0.30	0.21	0.28	0.27	0.28	0.38	0.29	0.27	0.28	0.34	0.38	0.39	0.37	0.43	0.29	0.32	0.20	0.21	0.28	0.17	0.22
P_2O_5	0.04	0.11	0.13	0.13	0.15	0.15	0.14	0.12	0.11	0.11	0.16	0.15	0.09	0.08	0.12	0.09	0.08	0.08	0.05	0.10	0.05
LOI	3.33	2.09	2.50	3.26	3.42	3.62	3.00	4.15	5.97	6.33	6.62	7.64	6.96	7.68	7.48	7.83	8.31	7.07	7.7	6.95	6.71
Total	99.36	99.52	99.52	99.65	99.64	99.59	99.57	99.65	99.75	99.69	99.86	99.87	99.72	99.69	99.74	99.74	99.73	99.67	99.73	99.58	99.84
CIA (%)	66.90	64.20	62.87	68.96	72.18	74.40	71.26	79.38	87.08	90.38	89.15	89.23	89.80	89.47	86.66	88.64	89.88	83.51	89.14	82.28	88.80
ppm																					
Li	18	17	15	29	24	22	23	27	50	34	39	36	36	36	35	38	32	38	33	43	30
Rb	19	31	34	27	33	27	42	22	32	40	27	31	48	73	37	54	45	71	53	64	61
Cs	2	1	2	3	3	3	2	2	4	3	3	3	4	3	3	2	3	3	3	3	3
Ba	65	55	64	71	67	104	64	59	60	54	56	46	65	45	47	56	47	50	56	52	50
Sr	16	15	16	18	16	23	17	15	15	15	19	16	18	17	19	22	19	18	21	16	13
Ga	10	9	10	13	12	12	10	14	19	22	22	21	25	23	22	24	22	24	25	25	19
Be	2	2	2	1	2	2	2	2	2	2	2	2	3	2	2	2	2	1	2	3	2
Sn	3	4	4	4	4	4	3	4	6	7	7	7	8	8	7	8	7	9	8	9	7
Nb	6	5	7	8	9	9	7	10	13	14	14	14	17	16	14	13	11	18	12	19	13
Ta	1	1	1	2	2	2	1	2	2	2	1	2	2	2	2	2	2	2	2	2	2
Y	6	5	6	6	4	6	5	5	7	6	6	7	10	9	7	5	5	6	5	5	7
Zn	26	14	15	23	26	31	25	23	24	24	27	24	34	24	26	20	19	23	18	22	27
Zr	106	91	98	80	78	116	91	67	68	68	72	76	77	90	71	63	35	38	44	62	57
Hf	1	1	1	1	1	1	1	1	1	1	1	1	2	2	1	1	1	1	1	1	1
Th	3	3	3	3	3	5	3	3	4	4	4	4	5	4	3	3	3	3	4	3	4
U	4	5	4	4	4	4	3	5	9	11	14	12	14	13	14	11	11	13	15	14	12

Table 4.17 (Continued)

Sample #	A1	A2	A3	A4	A5	A6	A7	A8	B1	B2	B3	B4	B5	B6	B7	B8	B9	B10	B11	C1	C2
Depth (m)	0.2	0.4	0.6	0.8	1.0	1.2	1.4	1.6	1.8	2.0	2.2	2.4	2.6	2.8	3.0	3.2	3.4	3.6	3.8	4.0	4.2
La	9.7	7.5	8.9	7.6	6.9	12.3	8.5	7.1	8.3	8.1	6.6	9.2	13	9.8	8.3	5.2	6.8	7.3	7.5	6.9	8.3
Ce	23.57	18.77	21.14	17.71	18.74	29.76	20.01	17.9	19.85	18.35	14.16	18.24	24.32	16.82	13.65	8.92	11.57	11.42	12.76	12.5	18.42
Pr	2.1	1.6	1.8	1.5	1.3	2.5	1.7	1.4	1.6	1.5	1.5	1.9	3.1	2.3	2.2	1.3	1.5	1.6	1.8	1.6	1.6
Nd	8.4	7	6.3	7.2	5.4	9.9	6.1	5.3	6.5	6	5	7.4	11.9	8.6	8	6.2	6.1	7.1	7	5.4	6.4
Sm	1.7	1	1.1	1.4	1.1	1.8	1.5	0.8	1.2	1.3	0.9	1.1	1.9	1.8	2	1.4	1.1	1.1	1.3	1.1	0.8
Eu	0.3	0.2	0.2	0.1	0.2	0.3	0.2	0.2	0.2	0.3	0.2	0.3	0.5	0.3	0.3	0.2	0.2	0.3	0.2	0.2	0.2
Gd	1.6	0.9	0.9	1.2	0.6	1.6	1	1.2	1.2	1.5	1.2	1.1	1.9	1.6	1.4	1.1	0.8	1.6	1.2	0.9	0.9
Tb	0.1	0.1	0.1	0.1	0.1	0.1	0.1	0.1	0.1	0.1	0.1	0.1	0.2	0.2	0.2	0.1	0.1	0.1	0.1	0.1	0.1
Dy	1.2	0.7	1.1	0.8	0.8	1.1	1	0.7	1.1	0.9	1.1	1.3	2.4	1.7	1.7	0.9	0.8	0.9	1.2	0.8	1.2
Ho	0.2	0.2	0.2	0.2	0.1	0.2	0.2	0.1	0.2	0.2	0.2	0.3	0.3	0.3	0.3	0.2	0.1	0.2	0.2	0.2	0.2
Er	0.6	0.5	0.5	0.5	0.4	0.5	0.6	0.6	0.7	0.7	0.7	0.8	1.2	0.9	1	0.6	0.8	0.8	0.5	0.4	0.7
Tm	0.1	0.1	0.1	0.1	0.1	0.1	0.1	0.1	0.1	0.1	0.2	0.1	0.2	0.2	0.1	0.1	0.1	0.1	0.1	0.1	0.1
Yb	0.6	0.5	0.7	0.6	0.5	0.8	0.5	0.8	1.1	0.9	0.9	0.8	1.5	1.2	1.1	0.6	0.7	0.6	0.7	0.7	1
Lu	0.1	0.1	0.1	0.1	0.1	0.1	0.1	0.1	0.1	0.1	0.1	0.2	0.2	0.2	0.1	0.2	0.1	0.1	0.1	0.1	0.1
LREE	47.4	37.0	40.3	36.7	34.2	58.2	39.0	33.9	38.9	37.1	29.6	39.2	56.6	41.2	35.9	24.3	28.1	30.4	31.8	28.6	36.6
HREE	2.9	2.2	2.8	2.4	2.1	2.9	2.6	2.5	3.4	3	3.3	3.6	6.0	4.7	4.5	2.7	2.7	2.8	2.9	2.4	3.4
∑REE	50.3	39.2	43.1	39.1	36.3	61.1	41.6	36.4	42.3	40.1	32.9	42.8	62.6	45.9	40.4	27.0	30.8	33.2	34.7	31.0	40.0
LREE/HREE	16.3	16.8	14.4	15.3	16.3	20.1	15.0	13.6	11.4	12.4	9.0	10.9	9.4	8.8	8.0	9.0	10.4	10.9	11.0	11.9	10.8
Ce/Ce*	0.35	0.41	0.38	0.41	0.47	0.32	0.39	0.44	0.40	0.40	0.39	0.33	0.25	0.28	0.28	0.38	0.35	0.32	0.32	0.35	0.39
Eu/Eu*	0.42	0.59	0.56	0.31	0.69	0.40	0.46	0.57	0.47	0.49	0.54	0.62	0.47	0.40	0.41	0.45	0.60	0.52	0.45	0.56	0.66
La/Yb	16.17	15.00	12.71	12.67	13.80	15.38	17.00	8.88	7.55	9.00	7.33	11.50	8.67	8.17	7.55	8.67	9.71	12.17	10.71	9.86	8.30

$Ce/Ce^* \rightarrow Ce_N/(La_N \times Pr_N)^{½}$, $Eu/Eu^* \rightarrow Eu_N/(Sm_N \times Gd_N)^{½}$ (where N is normalised by Cl-chondrite (Sun and McDonough, 1989))

The Al_2O_3impoverishment in the A-horizon can be ascribed to the intense eluviation of materials from this zone to lower horizons, thereby making free quartz to be more dominant in the A-horizon. Enrichment in alumina in the C- and B-horizons is indicated by the prominent peaks of kaolinite in the X-ray diffractogram (Fig. 4.33).

Fe_2O_3 has mean concentrations of 1.13,4.54, 4.95 and 2.52wt.% in the parent pegmatite, C, B and A-horizons, respectively. It, therefore, shows significant enhancement down the residual profile. The high abundance of Fe_2O_3 in the underlying C-horizons is a slight deviation from what is commonly obtainable in lateritic profiles from humid tropical cli-mates. The possibility of the vertical solution transport of the leached Fe_2O_3 within the profile and its eventual concentration into the saprolite at low pH, can be suggested for this occurrence.

MgO and CaO, as expected, indicate strong depletion in the weathering profile relative to the parent rocks. The concentrations of MgO are respectively 0.11, 0.08, 0.1 and 0.10 wt.% in the rock, C, B and A-horizon; while those of CaO are 0.61, 0.14, 0.16 and 0.25 wt.% in the same horizon. Na_2O and K_2O have both indicated moderate depletion in the lateritic profile relative to the pegmatite bedrock. Average K_2O concentrations are correspondingly 6.60, 1.98, 1.66 and 2.22 wt.% in the rock, C, B and A-horizon, while those of Na_2O are 2.18, 1.15, 0.80 and 1.15 wt.% in the rock, A, B and C-horizon, respectively.The abundances of these two oxides in the residual profile can be confirmed by the presence of K-feldspar, albite and muscovite peaks in their related diffractograms (Fig. 4.33), indicating incipient weathering of the parent pegmatite..

TiO_2(0.16 wt.%) is of low abundance in the non-mineralised Osu pegmatite, but shows slight enrichment in the C- (0.28 wt.%), B- (0.32 wt.%) andA-horizon (0.26 wt.%), respectively. P_2O_5 (0.27 wt.%) is also of low value in the parent rock but indicates strong depletion in all the horizons of the weathering profile.

The fresh whole-rock pegmatite has a mean LOI value of 0.73 wt.%, while the weathering profile indicate LOI levels varying from 2.64 to 7.41 wt.%. The saprolite-dominating C-horizon indicates the highest (6.71-8.31 wt.%) LOI values among the horizons of the profile (Table 4.17 and Fig. 4.57), which reflects the abundance of clay minerals that characterise this zone.

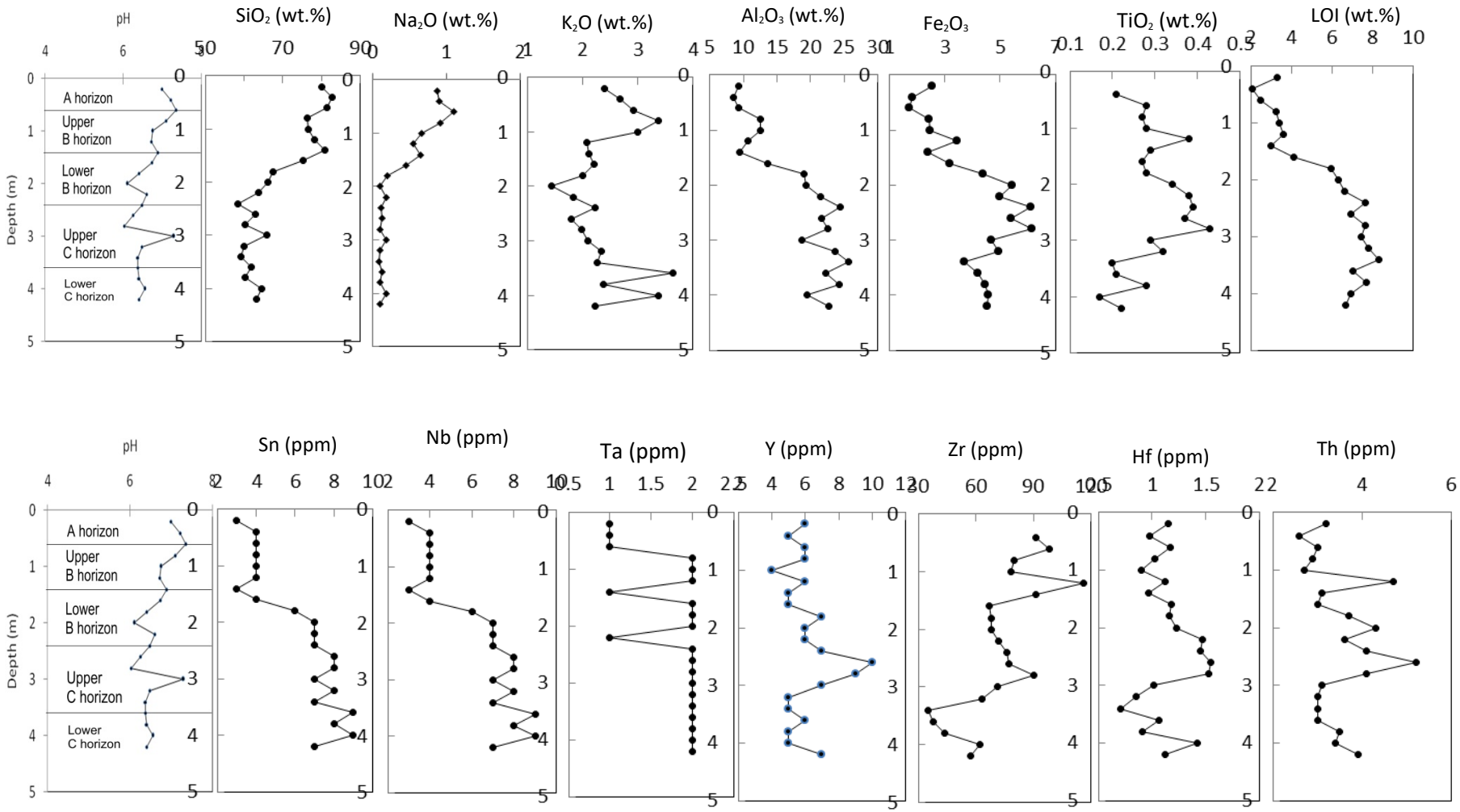

Fig. 4.57: Chemical elements distribution with depth in the Osu barren pegmatite profile

Using the Al_2O_3-SiO_2-Fe_2O_3 ternary diagram (Schellmann, 1983), most of the lateritic profile samples of the Osu non-mineralised pegmatite cluster within the weak lateritisation field, particularly those of the C-horizon and some from the B-horizon (Fig.4.58). The samples from A-horizon and some of the B-horizon plot in the kaolinisation field, towards the SiO_2 enhanced axis of the ternary diagram.

The CIA value of 55.04 % of the bedrock pegmatite sample indicates more or less negligible alteration of the parent rock (Nesbitt and Young, 1982). The CIA values slightly less 70 % for the A-horizon reflect the moderate extent of weathering alteration that marks the horizon, while CIA value ranging from 71 % to approximately 90 % indicates a moderate to high degree weathering alteration of the rock. The degree of weathering alteration increases down the lateritic profile (Fig. 4.59).

The trace element compositions of the *in situ* derived lateritic profile from the barren pegmatite of Osu area are similarly presented in Table 4.17. It shows that the Ba content in the C-horizon decreases from 52 ppm to 65 ppm in the B-horizon and latter increases to 61 ppm in the A-horizon; while Sr indicates marginal decrease from 18 to 17 and 16 ppm in the same horizons. The chemical data shows that Ba and Sr have suffered strong depletionin the weathering profile when compared with the mean bedrock pegmatite concentrations of 85 and 66 ppm, respectively for Ba and Sr.

The rare alkalis, Rb and Cs, likewise indicate similar geochemical patterns to labile major oxides, having their concentrations strongly decreasing upward. For instance, Rb shows reduction from 97 ppm in the bedrock to 63, 46 and 29 ppm respectively in the C, B and A-horizons, while Cs contents display strong depletion from 17 ppm in the parent rock to 3, 3 and 2 ppm respectively in the C, B and A-horizons.

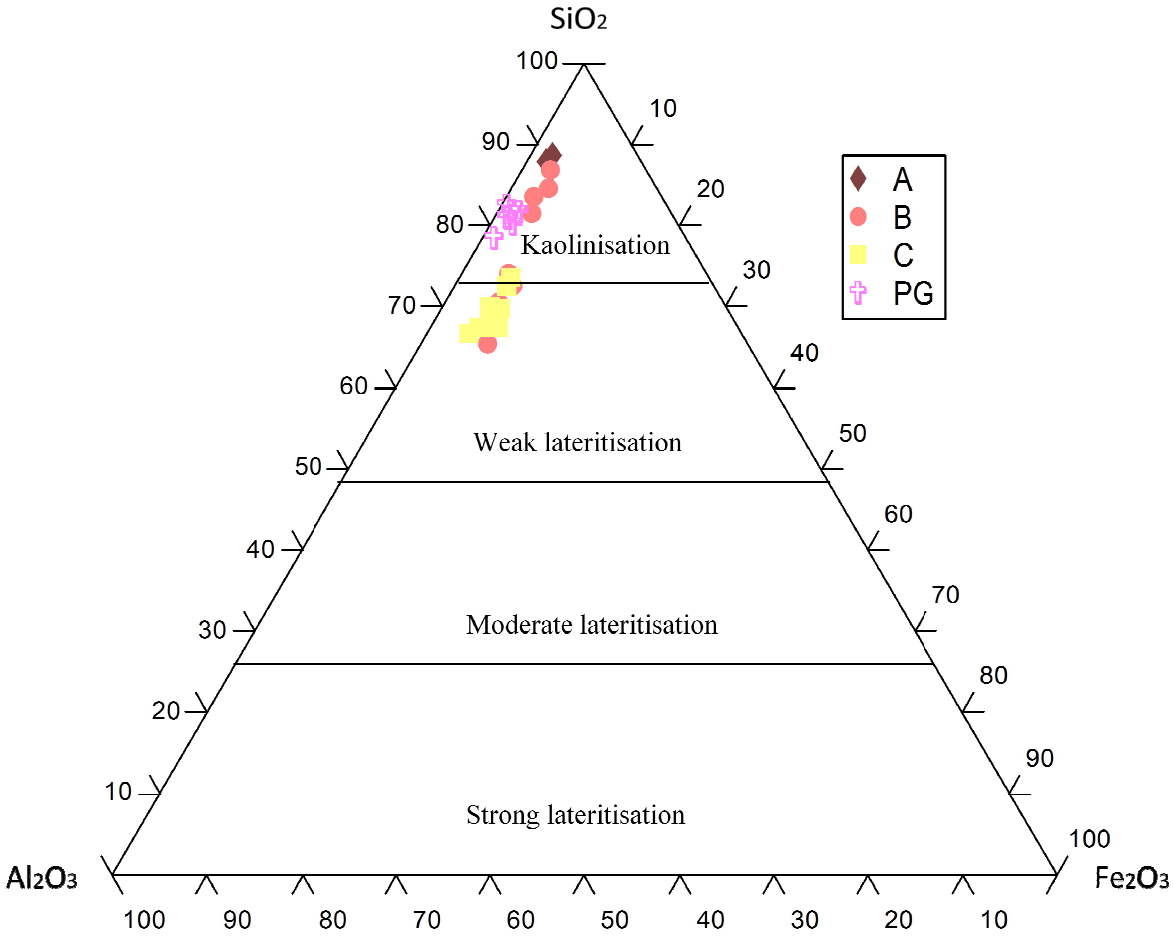

Fig. 4.58: Al_2O_3-SiO_2-Fe_2O_3 ternary plot for the lateritic profile derived from the barren pegmatite of Osu area (after Schellmann, 1983),

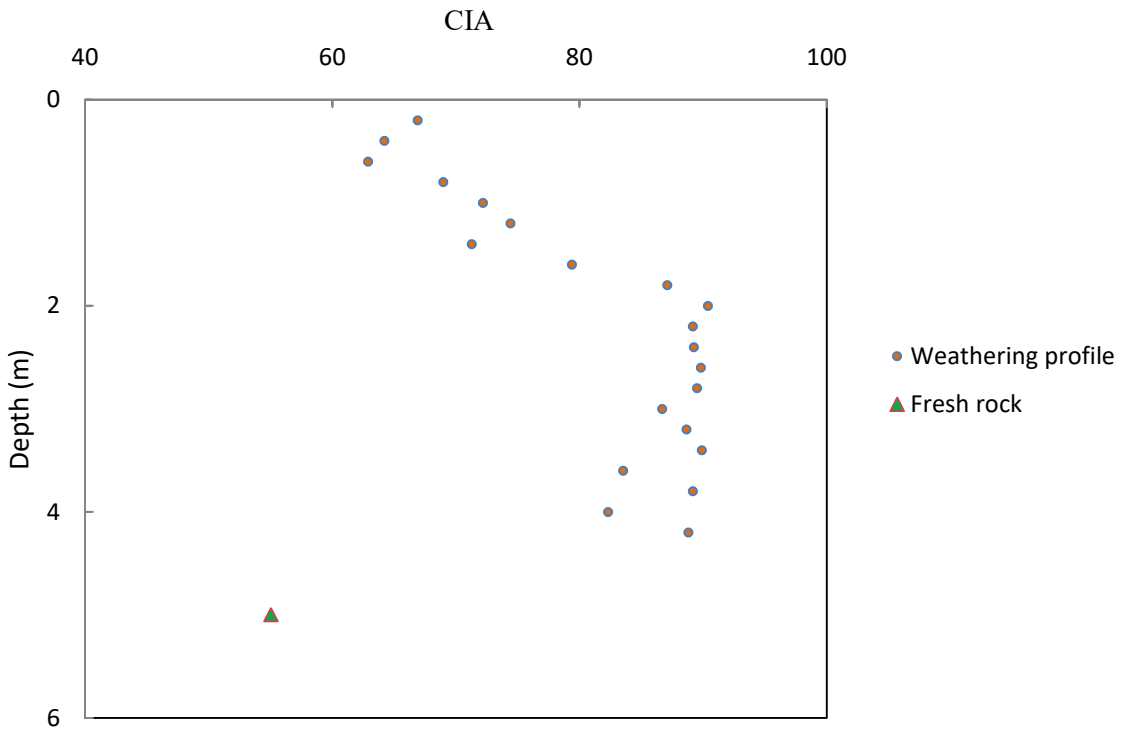

Fig. 4.59: Variation of chemical index of alteration (CIA) with depth in the *in situ*-derived lateritic profile from the barren pegmatite of Osu area (after Nesbitt and Young, 1982).

The total REEs contents of the weathered non-mineralised pegmatite of Osu ranged from 27 to 63 ppm (Table 4.17). The upper A-horizon has total REEs contents that vary between 36 and 61 ppm, with the mean concentration of 43 ppm. The LREEs in the A-horizon show moderate abundances ranging from 34 to 58 ppm, while the HREEs display relatively low levels varying from 2 to 3 ppm.

The B-horizon, on the other hand, portrays a total REEsabundance varying from 27 to 63 ppm, with the LREEs ranging between 24 and 57 ppm and low HREEs between 2 and 4 ppm. The C-horizon indicates similar trends in the total REE abundances, ranging between 27 and 63 ppm, with the LREE quantitatively dominating the REE contents in the horizon. The weathering profile derived from the Osu non-mineralised pegmatite portrays negative cerium (Ce/Ce* = 0.32 –0.47) and europium (Eu/Eu*=0.31-0.69) anomalies. The total REEs (41 ppm) contents of the weathering profile indicateenhancement when compared to total REEs content of 29 ppm in the unaltered bedrock.

The REE data of the parent pegmatite bedrock and the residual weathering profiles were normalised, using the upper continental crust values (Sun and McDonough, 1989). The resulting chondrite-normalised REE patterns are presented in Figure 4.60, which display enrichement of the LREEs relative to the HREEs, and showing no significant cerium and europium anomalies for the parent bedrock. The *in situ*-derived weathering profile displays strong and similar LREEs enrichment relative to the strong depletion of the HREEs in all the horizons of the profile.

The relatively low REEs contents in both the parentbedrock pegmatite and its *in situ*-derived residual profile are possibly a reflection of relatively low modal abundance of the REE-bearing accessory mineral phases in the parent pegmatite bedrock.

On the whole, the rare alkalis and the rare-metal concentrations in the Osu barren pegmatite bedrock samples and its *in situ*-derived weathering profile show very low values.

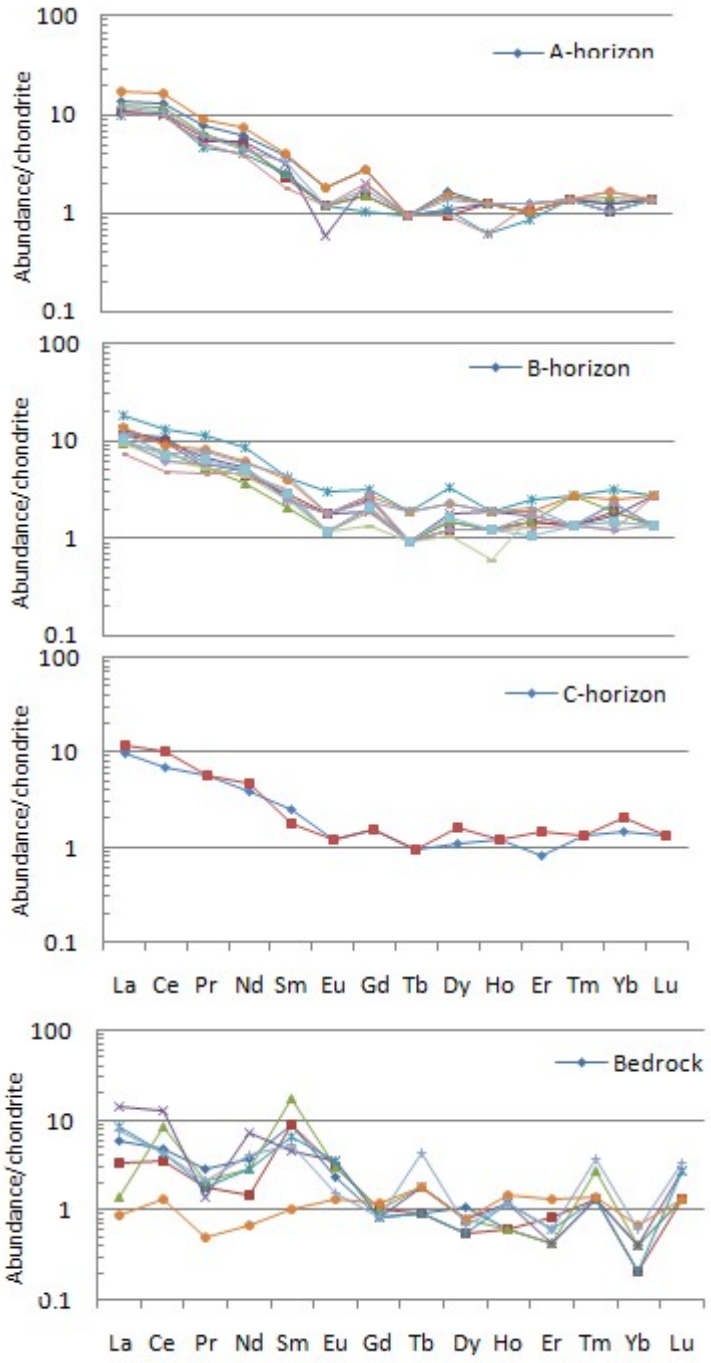

Fig. 4.60: Chondrite-normalised REE patterns for the bedrock and the *in situ*-derived weathering profile of the Osu barren pegmatite

4.3.3.2 Geochemical composition of the weathering profile above the mineralisedpegmatite of Ijero area

Geochemical data of the whole-rock mineralised pegmatite of Ijero area are presented in Table 4.18. The pegmatite is highly siliceous, showing SiO_2 concentrations varying from 71.03 to 76.12 wt.%, with mean value of 74.39 wt.%. Al_2O_3 contents in the pegmatite ranged between 13.84 and 16.04 wt.%, indicating average concentration of 14.69 wt.%; while Fe_2O_3 displayed a reduced content varying between 0.34 and 1.16 wt.%, with mean concentration of 0.63 wt.%.

Mean Ba (117 ppm) and Sr (23 ppm) contents in the whole-rock pegmatite show similar abundances to the Osu non-mineralised pegmatite. Rare alkalis, such as Rb and Cs, indicate mean contents of 293 and 72 ppm, respectively in the pegmatite. These alkali elements are comparatively high in the pegmatite when compared to the non-mineralised pegmatite of the Osu area.

The main pegmatite petrogenetic elements, such as Ga, Be, Sn, Nb, Ta and Y show moderate enrichments in the Ijero mineralised pegmatite when compared with the Osu non-mineralised pegmatite. These elements correspondingly indicate mean concentrations of 23, 6, 13, 45, 17 and 25 ppm in the whole-rock pegmatite. Moreover, other HFSE, such as Zr, Hf, Th and U also show moderate enhancements in the mineralised pegmatite relative to the Osu barren pegmatite (Table 4.16 and Table 4.18)

The total REEs concentration of the Ijero mineralised pegmatite is about 34 ppm (Table 4.18). The LREEs (22 ppm) contents display more enhancement relative to the HREE (13 ppm), with the mean LREEs/HREEs ratio slightly higher than 1.75. The pegmatite show negative Ce ($Ce/Ce^* = 0.13 – 0.58$) and Eu ($Eu/Eu^* = 0.17- 0.47$) anomalies. The total REE content of the Ijero whole-rock pegmatite (34 ppm) is relatively higher than those of the non-mineralisedpegmatite (27 ppm) of Osu area.

The major and trace element compositions in the *in-situ*-derived weathering profile from the mineralised pegmatite of Ijero area are presented in Table 4.19; while the chemical variations and dispersion trends within the lateritic profile are illustrated in Fig. 4.61. The

Table 4.18: Whole–rock major, trace and rare-earth element composition of the mineralised pegmatite of Ijero area

Major oxides	IJP1	IJP2	IJP3	IJP4	IJP5	Mean	Range
(wt.%)							
SiO_2	71.03	75.73	72.95	76.12	76.1	74.39	71.03-76.12
Al_2O_3	15.3	13.84	16.04	14.15	14.13	14.69	13.84-16.04
Fe_2O_3	1.16	0.52	0.34	0.35	0.8	0.63	0.34-1.16
MnO	0.77	0.69	0.05	0.05	0.03	0.32	0.03-0.77
MgO	0.21	0.05	0.05	0.03	0.06	0.08	0.03-0.21
CaO	0.74	0.67	0.06	0.51	0.52	0.50	0.06-0.74
Na_2O	2.67	2.90	2.23	2.66	2.13	2.52	2.13-2.90
K_2O	7.18	5.14	7.36	5.72	4.94	6.07	4.94-7.36
TiO_2	0.22	0.2	0.11	0.14	0.12	0.16	0.11-0.22
P_2O_5	0.05	0.17	0.14	0.11	0.05	0.10	0.05-0.17
LOI	0.55	0.55	0.59	0.51	1.06	0.65	0.51-1.06
Total	99.88	100.46	99.92	100.35	99.94	100.65	99.69-100.3
CIA	52.09	51.11	52.42	51.77	56.40	52.68	62.06-44.59
Trace element							
Rb	565	189	167	168	375	293	167-565
Cs	252	33	39	14	16	71	14-252
Ba	222	329	11	9	13	117	9-329
Sr	70	17	11	8	10	23	8-70
Ga	38	20	23	23	138	23	13-38
Be	5	6	4	8	6	6	4-8
Sn	18	16	4	11	16	13	4-18
Nb	54	4	42	33	94	45	4-94
Ta	25	15	18	13	12	17	13-25
Y	63	18	17	13	12	25	12-63
Zn	8	22	18	17	49	23	8-49
Zr	42	32	52	33	23	36	12-42
Hf	5	4	4	6	5	5	4-6
Th	7	5	7	5	6	6	5-7
U	5	6	4	6	7	6	4-7

Table 4.18: (Continued)

	IJP1	IJP2	IJP3	IJP4	IJP5	Mean	Range
Rare earth element							
La	6.2	1.5	3	2	2	2.94	1.5-6.2
Ce	17	7	3	4	1	6.4	1-17
Pr	2	1.5	2	5	3	2.7	1.5-5
Nd	10	5.8	5	2	2	4.96	2-10
Sm	3	1.5	1	6	2	2.7	1-6
Eu	0.4	0.1	0.2	0.2	0.4	0.26	0.1-0.4
Gd	2.4	1.1	2.6	1.8	1.4	1.86	1.1-2.6
Tb	0.7	0.7	0.3	0.5	0.6	0.56	0.3-0.7
Dy	7.8	2.3	2.6	2.2	1.8	3.34	1.8-7.8
Ho	2	0.4	2.2	1.8	0.6	1.4	0.4-2.2
Er	6.5	0.6	0.5	0.5	1.3	1.88	0.5-6.5
Tm	1.1	0.1	1.6	1.2	0.8	0.96	0.1-1.6
Yb	8.4	1.2	3.6	2.8	2.2	3.64	1.2-8.4
Lu	1.2	0.2	0.8	0.8	0.6	0.72	0.2-1.2
LREE	41	18.5	16.8	21	11.8	21.82	8.2-47.2
HREE	27.7	5.5	11.6	9.8	7.9	12.5	4.5-28.4
∑REE	68.7	24	28.4	30.8	19.7	34.32	12.7-75.6
LREE/HREE	1.48	3.36	1.45	2.14	1.49	1.75	1.82-1.66
Ce/Ce*	0.38	0.58	0.23	0.21	0.13	0.29	0.22-0.24
Eu/Eu*	0.30	0.31	0.35	0.17	0.47	0.29	0.38-0.20
La/Yb	0.74	1.25	0.83	0.71	0.91	0.81	1.25-0.74

Table 4.19: Major, trace and rare-earth element composition of the lateritic profile derived from mineralised pegmatite of Ijero area

Sample #	A1	B1	B2	B3	B4	B5	B6	B7	B8	B9	B10	B11	B12	B13	B14
Depth (m)	0.2	0.4	0.6	0.8	1.0	1.2	1.4	1.6	1.8	2.0	2.2	2.4	2.6	2.8	3.0
wt. %															
SiO_2	60.44	76.72	66.44	60.6	69.2	65.79	57.85	60.13	58.82	60.11	64.51	64.17	54.35	64.17	60.69
Al_2O_3	24.29	12.73	19.59	21.94	17.8	20.56	25.98	10.9	25.09	24.91	22.52	22.46	29.2	22.84	25.05
Fe_2O_3	4.55	3.35	4.08	6.08	4.04	3.90	5.20	2.40	5.46	5.03	3.46	3.75	4.79	3.69	3.95
MnO	0.03	0.03	0.03	0.03	0.02	0.02	0.02	0.05	0.05	0.02	0.02	0.01	0.02	0.02	0.02
MgO	0.09	0.07	0.09	0.13	0.09	0.04	0.04	0.22	0.1	0.06	0.1	0.05	0.06	0.04	0.04
CaO	0.03	0.05	0.02	0.04	0.02	0.03	0.02	0.05	0.03	0.01	0.03	0.03	0.02	0.02	0.01
Na_2O	0.04	0.04	0.11	0.04	0.06	0.07	0.05	0.13	0.03	0.02	0.07	0.13	0.03	0.02	0.03
K_2O	1.20	0.55	1.91	1.08	1.23	1.2	1.31	0.82	0.98	0.89	1.63	1.38	0.76	0.94	0.97
TiO_2	0.48	0.35	0.36	0.55	0.33	0.32	0.42	0.36	0.48	0.44	0.32	0.4	0.47	0.41	0.43
P_2O_5	0.06	0.06	0.06	0.08	0.03	0.05	0.04	0.06	0.06	0.04	0.05	0.04	0.05	0.05	0.05
LOI	8.33	5.63	6.83	9.02	6.68	7.58	8.73	5.07	8.52	8.11	6.85	7.2	9.92	7.41	8.34
Total	99.58	99.59	99.56	99.62	99.6	99.59	99.71	99.4	99.65	99.68	99.56	99.66	99.67	99.59	99.64
CIA (%)	94.48	94.42	89.56	94.38	92.40	93.33	94.42	90.14	95.56	96.09	92.09	92.73	96.98	95.46	95.73
Trace elemen															
Li	543	529	318	437	446	320	418	421	374	372	364	427	403	381	436
Rb	27	87	84	118	124	103	133	111	128	109	93	130	102	96	109
Cs	17	27	21	27	31	18	24	22	26	27	16	26	28	24	30
Ba	57	56	53	32	60	67	32	47	74	53	62	38	37	37	51
Sr	11	11	11	9	15	9	9	11	12	11	9	10	10	10	12
Ga	18	38	22	42	37	32	36	42	37	34	38	36	39	34	38
Be	71	61	289	66	36	12	41	49	52	20	21	24	15	21	35
Sn	33	49	27	54	37	36	45	36	32	31	38	40	33	32	35
Nb	46	58	94	83	193	50	72	105	87	53	92	48	37	62	81
Ta	39	40	42	30	94	20	34	62	46	48	32	22	26	30	58
Y	10	5	6	9	7	9	7	6	9	9	6	8	10	9	9
Zn	38	46	32	50	49	72	37	36	36	34	36	33	35	31	36
Zr	110	83	77	129	64	71	89	122	93	118	56	76	91	76	83
Hf	3	5	9	11	13	17	12	12	18	13	11	11	12	21	12
Th	4	6	8	8	10	14	15	19	16	15	13	15	14	14	14
U	3	4	2	2	4	2	3	4	3	4	2	3	4	3	5

Table 4.19 (Continued)

Sample #	A1	B1	B2	B3	B4	B5	B6	B7	B8	B9	B10	B11	B12	B13	B14
Depth (m)	0.2	0.4	0.6	0.8	1.0	1.2	1.4	1.6	1.8	2.0	2.2	2.4	2.6	2.8	3.0
La	9.2	12.4	9.7	7.3	11.4	7.3	7.2	7.2	10.6	10.7	7.5	12.0	7.3	11.2	10.6
Ce	19.4	21.9	30.7	24.4	37.0	15.8	14.5	15.4	20.5	19.4	12.4	19.8	12.6	20.4	19.1
Pr	2.1	3.1	1.9	1.6	2.7	1.6	1.5	1.7	2.3	2.3	1.8	2.7	1.9	2.6	2.8
Nd	6.8	10.9	7.7	5.2	9.2	5.3	5.5	6.0	7.4	8.8	6.4	9.2	7.6	9.0	10.3
Sm	1.7	1.8	1.0	1.2	2.5	1.3	1.2	1.0	1.6	1.6	1.3	2.0	1.4	1.7	1.6
Eu	0.2	0.3	0.2	0.3	0.4	0.2	0.2	0.2	0.3	0.3	0.2	0.3	0.3	0.3	0.3
Gd	1.3	1.5	1.3	1.0	1.4	0.9	1.1	1.3	1.4	1.5	1.1	1.3	1.2	1.5	1.4
Tb	0.1	0.1	0.1	0.1	0.1	0.1	0.1	0.1	0.1	0.1	0.1	0.1	0.1	0.1	0.1
Dy	0.8	1.6	0.8	0.9	1.3	0.8	1.0	0.9	1.2	1.1	0.8	1.0	1.0	1.0	1.2
Ho	0.1	0.2	0.2	0.1	0.2	0.1	0.1	0.2	0.2	0.2	0.2	0.2	0.2	0.2	0.2
Er	0.4	0.7	0.1	0.4	0.7	0.3	0.4	0.4	0.5	0.5	0.4	0.6	0.6	0.6	0.6
Tm	0.1	0.1	0.1	0.1	0.1	0.1	0.1	0.1	0.1	0.1	0.1	0.1	0.1	0.1	0.1
Yb	0.5	0.6	0.3	0.3	0.7	0.3	0.5	0.4	0.7	0.6	0.4	0.5	0.6	0.6	0.6
Lu	0.1	0.1	0.1	0.1	0.1	0.1	0.1	0.1	0.1	0.1	0.1	0.1	0.1	0.1	0.1
LREE	40.7	51.9	52.5	41.0	64.6	32.4	31.2	32.8	44.1	44.6	30.7	47.3	32.3	46.7	46.1
HREE	2.1	3.4	1.7	2.0	3.2	1.8	2.3	2.2	2.9	2.7	2.1	2.6	2.7	2.7	2.9
∑REE	42.8	55.3	54.2	43.0	67.8	34.2	33.5	35.0	47.0	47.3	32.8	49.9	35.0	49.4	49.0
LREE/HREE	19.4	15.3	30.9	20.5	20.2	18.0	13.6	14.9	15.2	16.5	14.6	18.2	11.9	17.3	15.9
Ce/Ce*	0.33	0.25	0.42	0.47	0.36	0.38	0.38	0.37	0.30	0.29	0.31	0.26	0.31	0.27	0.26
Eu/Eu*	0.38	0.42	0.49	0.63	0.42	0.52	0.49	0.49	0.46	0.44	0.47	0.43	0.53	0.43	0.46
La/Yb	18.40	20.67	32.33	24.33	16.29	24.33	14.40	18.00	15.14	17.83	18.75	24.00	12.17	18.67	17.67

Table 4.19 (Continued)

Sample #	C1	C2	C3	C4	C5	C6	C7	C8	C9	C10	C11	C12
Depth(m)	3.2	3.4	3.6	3.8	4.0	4.2	4.4	4.6	4.8	5.0	5.2	5.4
wt. %												
SiO_2	71.02	72.92	70.29	65.5	66.91	71.92	77.34	68	64.85	75.6	69.59	62.2
Al_2O_3	17.66	17.57	19.2	22.7	21.41	17.63	13.64	21.2	23.47	16.81	21	26.1
Fe_2O_3	2.53	1.86	2.2	2.48	2.59	2.15	2.09	2.2	2.81	1.3	2.01	2.26
MnO	0.03	0.02	0.01	0.02	0.02	0.01	0.03	0.02	0.04	0.02	0.04	0.05
MgO	0.07	0.02	0.04	0.04	0.04	0.04	0.07	0.02	0.03	0.01	0.03	0.02
CaO	0.02	0.01	0.01	0.01	0.01	0.01	0.04	0.01	0.02	0.01	0.02	0.02
Na_2O	0.15	0.08	0.08	0.1	0.11	0.07	0.08	0.05	0.03	0.05	0.06	0.06
K_2O	2.16	1.44	1.37	2.11	2.01	1.29	1.41	1.37	0.87	0.33	0.32	0.43
TiO_2	0.22	0.16	0.2	0.24	0.23	0.22	0.16	0.23	0.22	0.11	0.06	0.08
P_2O_5	0.02	0.02	0.02	0.03	0.03	0.03	0.02	0.03	0.04	0.02	0.04	0.03
LOI	5.61	5.49	6.09	6.42	6.1	6.24	4.61	6.5	7.32	5.38	6.53	8.27
Total	99.51	99.61	99.59	99.6	99.46	99.61	99.5	99.6	99.7	99.65	99.7	99.5
CIA (%)	87.08	91.14	92.16	90.19	90.02	92.02	88.74	93.05	95.81	97.35	97.76	97.75
ppm												
Li	379	297	362	439	437	348	337	424	327	185	180	219
Rb	189	176	199	183	199	189	197	126	168	173	164	173
Cs	13	12	17	18	18	17	12	21	20	11	9	11
Ba	24	24	22	24	25	21	36	22	42	13	14	15
Sr	5	5	6	6	6	6	4	7	6	4	4	4
Ga	41	31	35	46	46	33	32	39	34	20	28	33
Be	8	11	10	13	7	12	30	17	16	10	34	46
Sn	47	35	36	52	55	33	37	42	29	13	13	16
Nb	110	48	49	83	207	48	98	86	119	86	416	936
Ta	32	16	18	30	48	18	22	36	42	32	118	220
Y	10	26	37	25	37	27	26	25	27	28	39	33
Zn	46	26	30	40	40	28	42	41	38	32	88	101
Zr	43	35	44	45	54	46	25	50	63	51	44	55
Hf	11	14	11	13	11	11	15	12	13	12	17	12
Th	13	13	16	11	12	13	12	10	11	13	12	16
U	2	2	2	2	3	2	2	3	3	3	3	4

Table 4.19 (Continued)

Sample #	C1	C2	C3	C4	C5	C6	C7	C8	C9	C10	C11	C12
Depth (m)	3.2	3.4	3.6	3.8	4.0	4.2	4.4	4.6	4.8	5.0	5.2	5.4
La	9.1	7.0	8.1	5.2	5.5	6.9	5.7	6.2	8.1	7.1	6.0	5.0
Ce	14.2	10.9	14.5	10.0	10.2	11.9	10.7	11.1	18.7	10.9	9.8	8.8
Pr	2.1	1.6	1.8	1.4	1.5	1.5	1.5	1.5	2.2	1.5	1.4	1.2
Nd	6.6	5.3	6.7	5.0	5.9	5.5	4.9	5.7	6.4	5.1	5.6	5.2
Sm	1.3	1.0	1.3	1.0	1.1	1.2	1.2	1.2	1.7	1.0	1.4	1.6
Eu	0.2	0.2	0.2	0.2	0.2	0.2	0.2	0.3	0.1	0.1	0.1	0.1
Gd	1.2	0.8	0.9	0.7	0.9	1.1	1.1	0.9	1.1	1.0	0.9	1.3
Tb	0.1	0.1	0.1	0.1	0.1	0.1	0.1	0.1	0.1	0.1	0.2	0.2
Dy	1.1	0.8	0.8	0.7	0.7	0.9	1.2	0.9	0.8	0.8	1.2	1.3
Ho	0.2	0.2	0.1	0.1	0.1	0.1	0.2	0.1	0.2	0.1	0.1	0.1
Er	0.3	0.3	0.4	0.3	0.3	0.4	0.3	0.3	0.4	0.3	0.2	0.2
Tm	0.1	0.1	0.1	0.1	0.1	0.1	0.1	0.1	0.1	0.1	0.1	0.1
Yb	0.4	0.3	0.4	0.3	0.3	0.5	0.5	0.3	0.4	0.3	0.3	0.4
Lu	0.1	0.1	0.1	0.1	0.1	0.1	0.1	0.1	0.1	0.1	0.1	0.1
LREE	34.7	26.8	33.5	23.5	25.3	28.3	25.3	26.9	38.3	26.7	25.2	23.2
HREE	2.3	1.9	2.0	1.7	1.7	2.2	2.5	1.9	2.1	1.8	2.2	2.4
∑REE	37.0	28.7	35.5	25.2	27.0	30.5	27.8	28.8	40.4	28.5	27.4	25.6
LREE/HREE	15.1	14.1	16.8	13.8	14.9	12.9	10.1	14.2	18.3	14.8	11.4	9.7
Ce/Ce*	0.28	0.32	0.33	0.38	0.37	0.35	0.37	0.36	0.34	0.33	0.35	0.40
Eu/Eu*	0.45	0.63	0.52	0.67	0.56	0.49	0.49	0.66	0.29	0.40	0.35	0.27
La/Yb	22.75	23.33	20.25	17.33	18.33	13.80	11.40	20.67	20.25	23.67	20.00	12.50

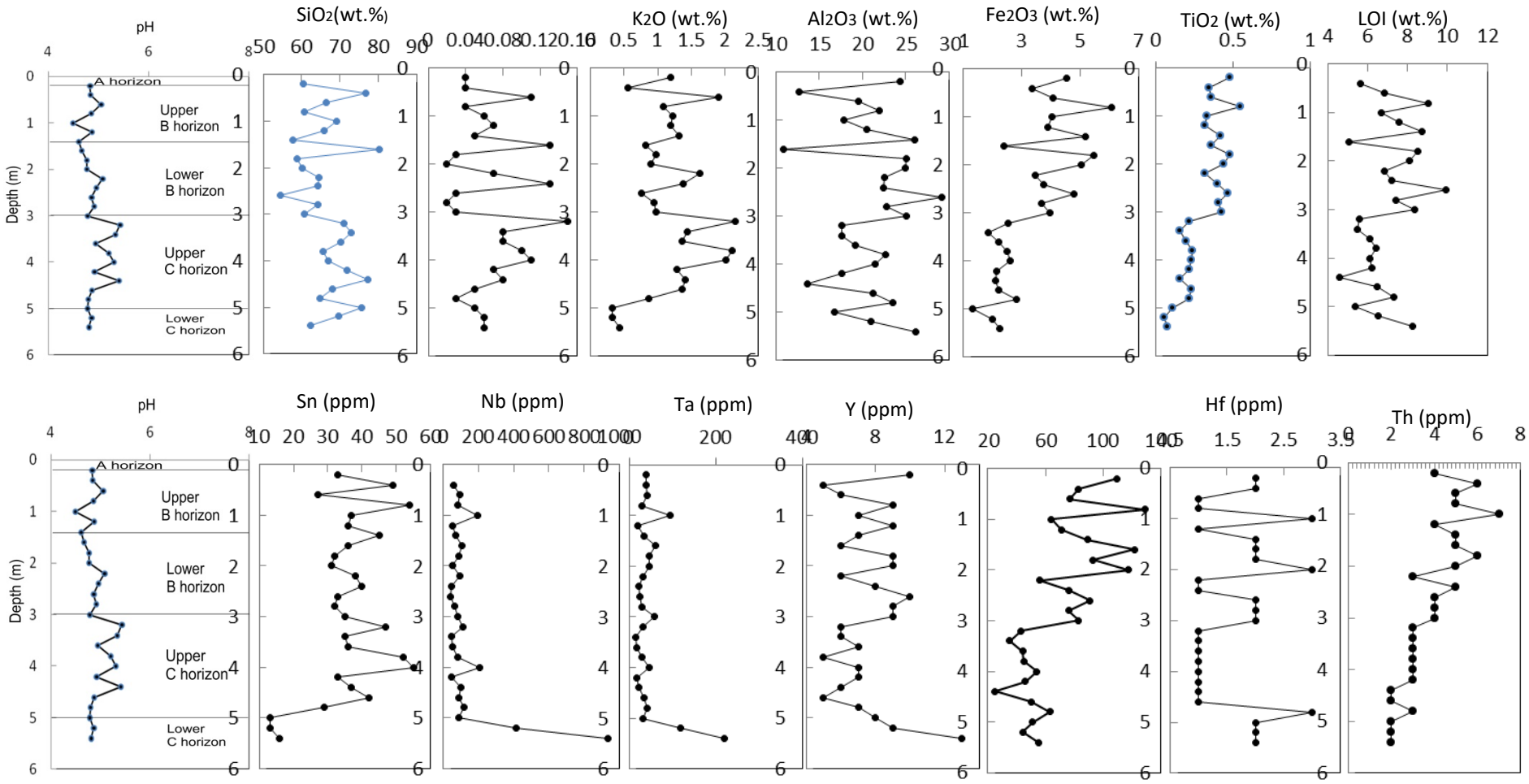

Fig. 4.61: Chemical elements distribution with depth in the Ijero mineralised pegmatite profile

mean silica contents in the A, B and C-horizons are 60.44, 64.54 and 69.67 wt.%,respectively. This indicates silica depletion in the horizons of the lateritic profile relative to the parent rock (74.39 wt. %). The silica contents in the residual profile are largely reflected as prominent quartz peaks on the X-ray charts (Figs. 4.36). Alumina contents in the weathering profile correspondingly showed mean values of 19.86, 21.54 and 24.29 wt.% in the C, B and A-horizons, indicatingan enhancement when compared to the mean contents of 14.69 wt.% recorded in the whole-rock pegmatite. The enhanced alumina contents in the residual profile can be attributed to weathering of feldspars to kaolinite (Fig 4.36). Fe_2O_3 is enriched in the weathering profile relative to the pegmatite bedrock. It has concentrations of 0.63, 2.21, 4.23 and 4.55 wt.% respectively in the rock, C, B and A-horizons, which may be due to the presence of hematite and/or goethite.

CaO show strong depletions in the weathering profile relative to the parent rock. The concentrations of CaO are respectively 0.05, 0.02, 0.03 and 0.03 wt.% in the rock, C-, B- and A-horizons. Na_2O contents are correspondingly 2.52, 0.08, 0.06 and 0.04 wt.% in the parent rock, C, B and A-horizons; while those of K_2O are 6.07, 1.26, 1.12 and 1.20 wt.% in the same horizons. The generally decrease in CaO, Na_2O and K_2O contents in the weathering profile relative to the parent rock is due to intensive leachings of these labile oxides in the weathering environment.

TiO_2, due to the relative stability of rutile and anatase minerals, has been enhanced in the lateritic profile with concentrations of 0.16, 0.18, 0.40 and 0.48 wt.% respectively in the whole-rock pegmatite, C, B and A-horizons. P_2O_5 indicates depletion in the weathering horizons relative to the parent rock, as it shows mean concentration values of 0.1, 0.03, 0.05 and 0.06 wt. % in the whole-rock samples, C, B and A-horizons, respectively.

The mean LOI value of the whole-rock pegmatite of Ijero area is 0.51 wt.%, while average LOI values of 6.21, 7.56 and 8.33 wt.% were correspondingly recorded for C, B and A-horizons of the residual lateritic profile (Table 4.18 and Fig.4.61). The Al_2O_3-SiO_2-Fe_2O_3(Schellman, 1983) ternary diagramwas employed to characterise the maturity of the laterite. The diagram indicates the pegmatite to be weakly lateritised, as most of

thelateritic samples plot within the weak lateritisation field (Fig. 4.62). While few samples of

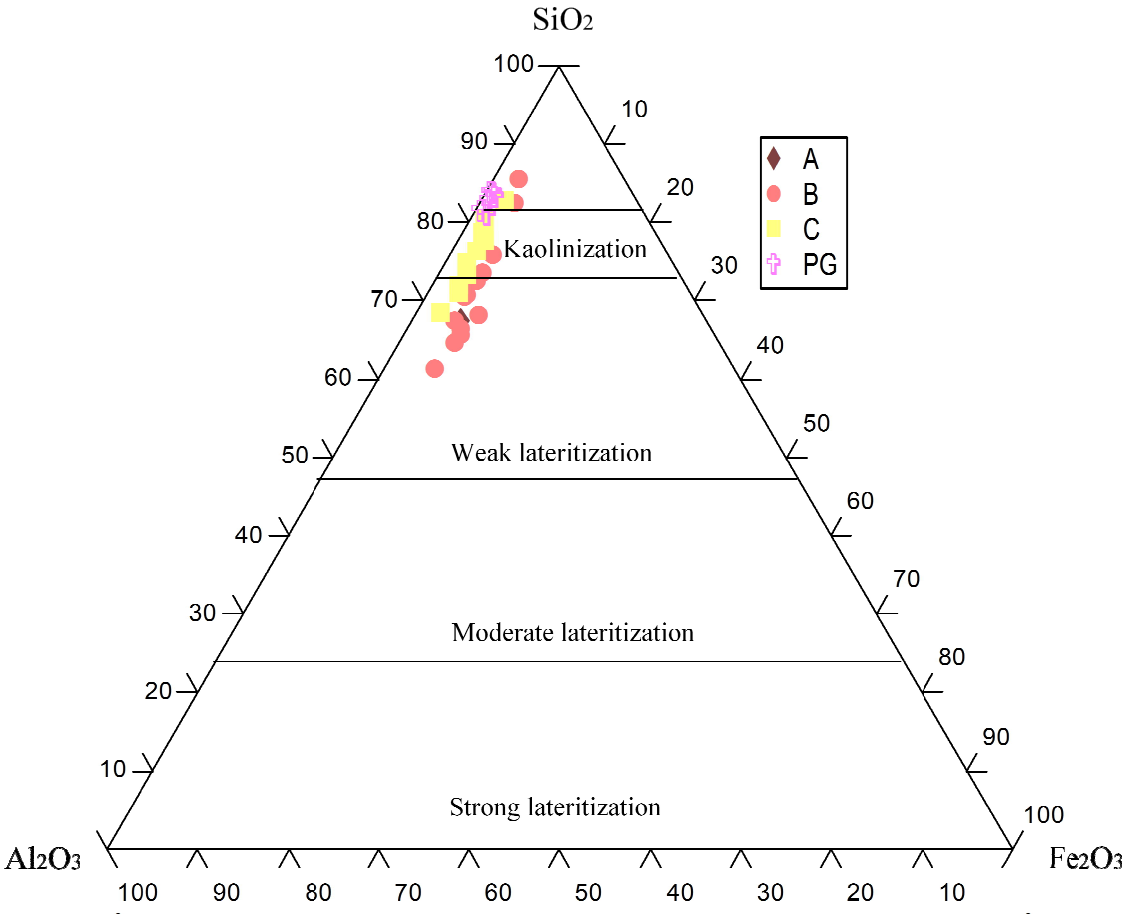

Fig. 4.62: Al_2O_3-SiO_2-Fe_2O_3 ternary plot for the lateritic profile derived from the mineralised pegmatite of Ijero area (after Schellmann, 1983).

the C-horizon cluster within the kaolinisation field, the whole-rock samples indicate trends towards SiO_2 enhanced axis of the ternary plot. The mean CIA value of 52.68 of the whole-rock samples signifies relatively unaltered bedrock; while CIA values of 94.48, 93.81 and 92.75 respectively in the A, B and C-horizons indicate high degree of chemical weathering of the regolith profile. These trends are also amplified in Fig. 4.63, which shows the alteration intensity increasing from low value in the fresh rock to higher values in the more intensely altered lateritic profile (Nesbitt and Young, 1982).

Table 4.19 shows the trace element data of the residual profile developed over the mineralised pegmatite of Ijero area. Barium and Sr were found to show strong depletions in the residual profile relative to the parent whole-rock samples. For instance, Ba has mean concentrations of 117, 26, 50 and 57 ppm in the parent rock, C, B and A-horizons, respectively; while Sr values are 23, 5, 11 and 11 ppm in the same horizons. The rare-alkalis, Rb and Cs, showed enhancements in the whole-rock samples of the mineralised pegmatite relative to its regolith profile. Mean Rb contents of 293, 184, 109 and 27 ppm were respectively recorded in the parent rock, C, B and A-horizons and Cs shows 71, 15, 26 and 17 ppm in the same horizons.

Other pegmatophile elements, such as, Sn, Nb and Ta are more enhanced in the residual profile relative to the whole-rock samples. For example, mean Sn contents in the rock, C, B and A-horizons are 13, 34, 38 and 33 ppm; while Nb concentrations are 45, 191, 80 and 46 ppm in the same horizons. Tantalum levels inreases from 17 ppm in the parent rock to 53, 42 and 39 ppm, respsectively in the C, B and A-horizons. Zinc and Zr indicate remarkable enrichments in the residual lateritic profile when compared to the fresh pegmatite samples. The mean Zn concentrations are 23, 46, 40 and 38 ppm in the parent rock, C, B and A-horizons, respectively; while Zr contents are 36, 46, 88 and 110 ppm in the same horizons.

Yttrium shows mild enhancement in the residual profile relative to the bedrock, as it ranges from 29 to 28 and 10 ppm in the C, B and A-horizons, respectively when compared

to 25 ppm recorded in the parent rock. Hafnium and Th have been examined to be moderately enhanced in the residual lateritic profile relative to the whole-rock pegmatite

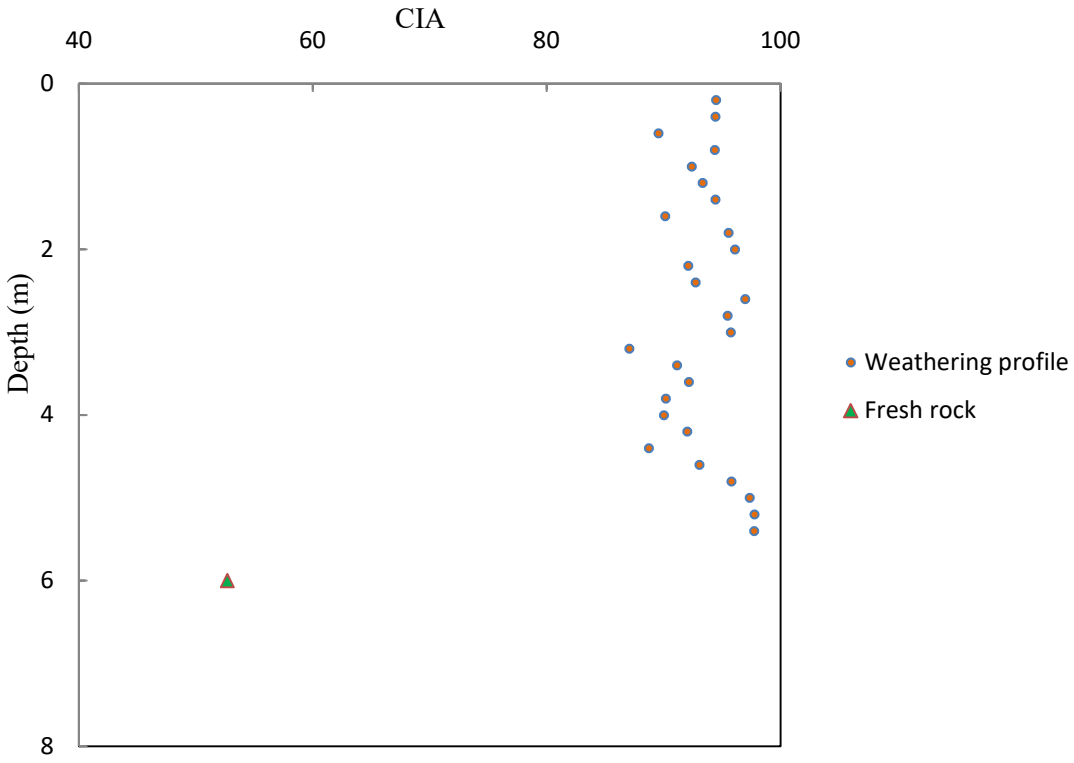

Fig. 4.63: Variation of chemical index of alteration (CIA) with depth in the *in situ*-derived lateritic profile from the mineralised pegmatite of Ijero area (after Nesbitt and Young, 1982).

samples,while U shows marginal depletion. These are revealed in the mean concentrations of these elements in the rock, A, B and C-horizons, which are respectively as follows: Hf (5, 11, 13 and 3); Th (6, 13, 15 and 4) and U (6, 3, 3 and 3) ppm.

The total REEs contents of residual weathering profile of the mineralised pegmatite of Ijero area range from 43 to 45 and 30 ppm respectively in the A, B and C-horizons, relative to 34 ppm recorded in the parent pegmatite. This trend revealed the marginal enrichment of the REEs contents in the residual profile as compared to the parent rock. The mean LREEs contents in the B-horizon (43 ppm) are much more enhanced than in A and C-horizons that correspondingly indicate 41 and 28 ppm. HREEs display very low levels (2 - 3 ppm) in the constituting horizons, relative to LREEs. The weathering profile derived from the mineralised pegmatite of Ijero area portrays negative cerium (Ce/Ce* = 0.25 – 0.47) and europium (Eu/Eu* = 0.271 - 0.67) anomalies. The relatively low REE contents in the whole-rock pegmatite and its *in situ*-derived residual profile are possibly due to the moderate modal abundances of the REE-bearing accessory mineral phases in the parent rock.

The chrondrite-normalised REE diagram of the Ijero mineralised whole-rock pegmatite samples indicates similar LREE and HREE distribution patterns, but the *in situ*-derived weathering profile show right steep-sided REE pattern and appreciable depletion of the HREE relative to strong enhancement of the LREE (Fig. 4. 64).

On the whole, the mineralised pegmatite of Ijero area and its *in situ*-derived lateritic profile indicate enrichments of rare alkalis and other immobile HFSEs, as compared to the Osu barren pegmatite and its residual profile of Osu area.

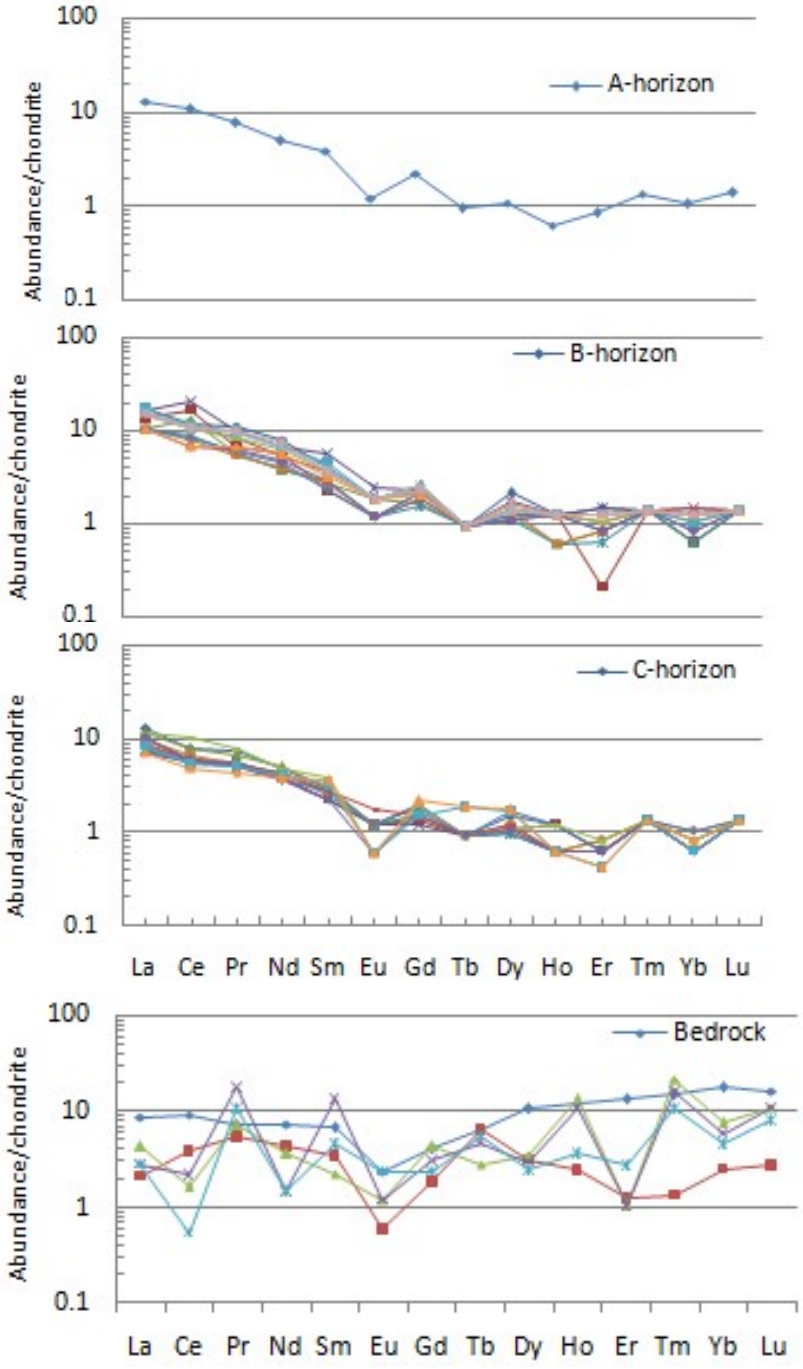

Fig. 4.64: Chondrite-normalised REE patterns for the bedrock and the *in situ*-derived weathering profile of the Ijero mineralised pegmatite

4.3.3.3 Geochemical composition of the weathering profile above the mineralisedpegmatite of Komu area

The major and trace element abundances of the whole-rock mineralised pegmatite of Komu area are given in Table 4.20. The concentration of silica in the pegmatite is very high, and it varies between 70.75 and 78.15 wt.%, with mean concentration of 74.86 wt.%. Alumina levels in the whole-rock samples ranged between 13.29 and 17.93 wt.%, showing mean contents of 15.50 wt.%. Fe_2O_3 and MnO contents are low, displaying average concentration of 0.45 and 0.08 wt.%, respectively.

CaO concentrations are very low in the pegmatite, ranging between 0.24 and 0.75 wt.%, and showing mean concentration of 0.52 wt.%. On the contrary, K_2O (2.21 - 4.68 wt.%) and Na_2O (3.05 –5.39 wt.%) range widely in the pegmatite, indicating corresponding mean concentrations of 3.35 and 4.07 wt.%. TiO_2 content is moderately low in the pegmatite, with mean concentrations of 0.13 wt.%.

Barium(19 ppm) and Sr (20 ppm) contents of the whole-rock pegmatite samples are low contrary to the expectation of elevated concentrations in pegmatites. These elements are known to be commonly incorporated into feldspar and muscovite structures in pegmatites.

Important pegmatite petrogenetic elements, such as Rb, Cs, Ga and Be are moderately high in the pegmatite, with corresponding values of 625, 102, 30 and 20 ppm (Table 4.20). Other pegmatophile elements including Sn (18 ppm), Nb (70 ppm), Ta (46 ppm) equally show moderately high contents in the pegmatite. Yttrium, Zr, Hf, Th and U contents in the pegmatite are moderately low, indicating mean concentrations of 9, 18, 5, 6 and 7 ppm, respectively.

The total rare-earth element (REEs) contents of the Komu mineralised pegmatite is 13 ppm (Table 4.20). Light rare-earth elements (LREEs) show greater average concentration of 12 ppm, relative to the heavy rare-earth elements (HREEs) that indicate mean contents

Table 4.20: Whole–rock major, trace and rare-earth element composition of the mineralised pegmatite of Komu area

Major oxides	KMP1	KMP2	KMP3	KMP4	KMP5	Mean	Range
(wt.%)							
SiO_2	75.24	70.75	74.45	75.71	78.15	74.86	70.75-78.15
Al_2O_3	15.65	17.93	15.37	15.26	13.29	15.50	13.29-17.93
Fe_2O_3	0.46	0.22	0.46	0.41	0.69	0.45	0.22-0.69
MnO	0.09	0.03	0.07	0.20	0.01	0.08	0.01-0.20
MgO	0.06	0.04	0.04	0.02	0.08	0.05	0.02-0.08
CaO	0.28	0.75	0.72	0.24	0.60	0.52	0.24-0.75
Na_2O	4.57	5.39	3.44	3.92	3.05	4.07	3.05-5.39
K_2O	2.21	4.68	4.10	3.01	2.76	3.35	2.21-4.68
TiO_2	0.10	0.14	0.22	0.12	0.05	0.13	0.05-0.22
P_2O_5	0.03	0.03	0.02	0.03	0.01	0.02	0.01-0.03
LOI	1.18	0.28	0.85	1.23	0.92	0.89	0.28-1.23
Total	99.88	100.14	99.74	100.12	99.61	99.818	99.54-100.11
CIA	60.03	50.31	54.00	58.77	57.91	55.72	63.86-47.67
Trace element							
Rb	885	497	501	669	573	625	497-885
Cs	46	250	63	29	124	102	29-250
Ba	88	63	24	56	23	51	23-88
Sr	3	2	42	43	9	20	2-43
Ga	33	19	47	31	24	30	19-47
Be	21	7	37	11	26	20	7-37
Sn	22	7	15	28	18	18	7-28
Nb	93	88	52	53	65	70	52-93
Ta	134	26	33	18	21	46	18-134
Y	10	3	15	6	12	9	3-15
Zn	71	30	59	57	22	48	22-71
Zr	19	12	25	15	17	18	15-25
Hf	2	6	6	5	5	5	2-6
Th	7	4	6	5	6	6	4-7
U	8	3	5	7	13	7	3-13

Table 4.20 (Continued)

	KMP1	KMP2	KMP3	KMP4	KMP5	Mean	Range
La	2	1.3	2	2	2	1.86	1.3-2
Ce	4	2	2	3	7	3.6	2-7
Pr	0.4	0.3	0.4	0.3	0.4	0.36	0.3-0.4
Nd	4	2.2	3	2	2	2.64	2-4
Sm	4	1.3	2	2	2	2.26	1.3-4
Eu	0.1	0.1	0.1	0.2	0.1	0.12	0.1-0.2
Gd	1.4	0.2	0.2	1.2	0.6	0.72	0.2-1.4
Tb	0.1	0.1	0.1	0.2	0.2	0.14	0.1-0.2
Dy	0.9	0.2	0.6	0.4	0.2	0.46	0.2-0.9
Ho	0.1	0.1	0.1	0.3	0.2	0.16	0.1-0.3
Er	0.3	0.1	0.3	0.3	0.1	0.22	0.1-0.3
Tm	0.1	0.1	0.1	0.1	0.2	0.12	0.1-0.2
Yb	0.3	0.1	0.3	0.3	0.1	0.22	0.1-0.3
Lu	0.1	0.1	0.1	0.2	0.1	0.12	0.1-0.2
LREE	15.9	7.4	9.7	10.7	14.1	11.6	7.4-15.9
HREE	1.9	0.8	1.6	1.8	1.1	1.4	0.8-1.9
∑REE	17.8	8.2	11.3	12.5	15.2	13.0	8.0-17.8
LREE/HREE	8.4	9.3	6.1	5.9	12.8	8.0	5.9-12.8
Ce/Ce*	0.73	0.74	0.52	0.73	0.97	0.76	0.74-0.97
Eu/Eu*	2.02	1.41	2.02	1.75	2.02	1.84	1.41-2.02
La/Yb	6.67	13.00	6.67	6.67	20.00	8.45	13.00-6.67

of 1 ppm. The pegmatite shows positive Eu anomaly (Eu/Eu* = 1.84), possibly showing the higher abundance of albite (plagioclase) in the rock; whereas a negative Ce anomaly (Ce/Ce* = 0.74) is recorded in the rock (Table 4.20). The geochemical abundances of the LREEs and HREEs in the pegmatites are possible reflection of themodal abundances of accessory mineral phases that host the REEs in the pegmatite. These minerals include albite, zircon, garnet, apatite, rutile, ilmenite and magnetite. The pegmatite petrogenetic elements,such as Sn, Nb, Ta, Be, Ga, Rb and Cs in the Komu mineralised pegmatite display higher concentrations when compared to the Osu barren pegmatite (Table 4.16 and Table 4.20).

The chemical data for the residual weathering profile of the Komu mineralised pegmatite are presented in Table 4.21, while chemical variations and dispersion trends within the profile are illustrated in Fig. 4.65. The mean silica contents are 74.86, 71.60, 69.71 and86.5wt.%, respectively in the parent rock, C, B and A-horizons. These indicate that, relative to the parent rock, there has been an enrichment of silica in the A-horizon. The high silica contents of the weathering profile are supported by the prominent quartz peaks in the X-ray charts of the lateritic profile (Figs. 4.39a). Alumina indicates marginal enrichments relative to the bedrock composition, particularly in the B and C-horizons. The corresponding mean concentrations of Al_2O_3 are 15.5, 16.33, 18.65 and6.5 wt.% in the whole-rock samples, C, B and A-horizons. The low alumina abundances in the residual profile are evident in the low contents of kaolinite in the weathering horizons (Fig. 4.39 and Fig. 4.40).

Fe_2O_3 expectedly displays a strong enhancement in the residual profile relative to the parent rock. The mean concentrations of Fe_2O_3 are respectively 0.45, 1.37, 2.24 and 2.32 wt.% in the parent rock, C, B and A-horizons. TiO_2 show slight enrichments in the weathering profile, relative to the bedrock pegmatite, with the correspondingly values of 0.13, 0.27, 0.20 and 0.19 wt.% in the parent rock, C, B and A-horizons. These moderate abundances of TiO_2 in the profile horizons could be due relative stability of rutile in weathering profiles.

Table 4.21: Major, trace and rare-earth element composition of the lateritic profile derived from mineralised pegmatite of Komu area

Sample #	A1	A2	A3	B1	B2	B3	B4	B5	B6	B7	B8	B9
Depth(m)	0.2	0.4	0.6	0.8	1.0	1.2	1.4	1.6	1.8	2.0	2.2	2.4
wt. %												
SiO_2	88.3	84.99	86.22	67.91	67.63	74.38	68.6	68.3	70.25	71.1	69.00	70.22
Al_2O_3	4.94	6.98	7.57	20.16	21.73	15.07	18.34	19.93	17.71	17.3	19.53	18.12
Fe_2O_3	2.70	2.37	1.89	2.53	2.61	3.13	3.29	1.94	1.76	1.51	1.58	1.87
MnO	0.23	0.14	0.04	0.04	0.03	0.05	0.05	0.06	0.05	0.03	0.03	0.14
MgO	0.13	0.12	0.05	0.06	0.07	0.08	0.1	0.09	0.05	0.04	0.04	0.09
CaO	0.09	0.12	0.06	0.35	0.28	0.17	0.4	0.44	0.35	0.57	0.66	0.55
Na_2O	0.25	0.38	0.25	1.33	1.11	0.78	1.85	1.96	1.81	3.67	3.7	3.4
K_2O	0.65	1.87	0.75	1.05	1.33	0.98	1.03	1.8	3.34	0.96	0.93	0.91
TiO_2	0.19	0.23	0.15	0.19	0.23	0.29	0.21	0.16	0.13	0.08	0.21	0.32
P_2O_5	0.01	0.66	0.02	0.03	0.03	0.03	0.04	0.03	0.03	0.03	0.03	0.04
LOI	1.72	2.16	2.52	6.09	4.76	4.71	5.74	5.05	4.19	4.42	4.22	4.16
Total	99.2	99.42	99.52	99.74	99.8	99.68	99.68	99.66	99.69	99.7	99.89	99.81
CIA (%)	79.4	70.88	85.04	83.58	85.2	85.03	78.97	76.94	71.01	68.1	70.19	70.51
µg/g												
Li	28	33	35	68	45	68	81	72	58	71	63	62
Rb	32	96	44	58	56	57	65	96	162	43	46	47
Cs	1	4	2	6	5	7	8	6	7	5	5	5
Ba	16	22	35	37	43	40	57	30	51	27	43	11
Sr	5	8	4	9	8	7	13	12	11	10	9	8
Ga	10	12	12	30	27	51	28	37	26	33	28	48
Be	3	13	9	26	16	27	32	21	29	19	42	25
Sn	2	2	4	8	8	14	18	24	22	32	44	52
Nb	110	116	227	42	212	178	82	36	39	33	38	455
Ta	13	23	16	27	36	18	20	20	14	15	18	40
Y	34	22	21	23	25	18	18	24	31	25	16	9
Zn	28	24	13	17	19	14	18	18	14	13	10	19
Zr	79	69	41	35	42	30	46	31	20	22	14	19
Hf	4	3	6	4	2	6	6	4	7	5	5	8
Th	26	21	10	12	14	10	13	11	9	4	3	22
U	6	6	4	4	4	4	4	4	3	2	2	6

Table 4.21 (Continued)

Sample #	A1	A2	A3	B1	B2	B3	B4	B5	B6	B7	B8	B9
Depth (m)	0.2	0.4	0.6	0.8	1.0	1.2	1.4	1.6	1.8	2.0	2.2	2.4
La	14.5	11.2	5.3	7.2	7.6	6.7	7.9	4.9	4.1	3.3	3.2	12.5
Ce	45.17	34.34	16.59	22	22.69	19.76	19.53	16.26	11.91	11.6	12.26	30.63
Pr	4.5	3.4	1.4	1.8	1.6	1.5	2	0.9	1.1	0.6	0.9	3.7
Nd	18.3	13.9	5.1	6.7	6.9	5.7	7.9	4.2	3.8	2.7	2	14.3
Sm	6.4	4.1	1.7	2	2.2	1.8	2	1.3	1	0.9	0.5	4.4
Eu	0.1	0.1	0.1	0.1	0.1	0.1	0.1	0.1	0.1	0.1	0.1	0.1
Gd	4.1	3.1	1.4	2	2.4	1.2	2.1	1.5	1.3	1	0.4	3.8
Tb	0.6	0.4	0.2	0.2	0.2	0.2	0.3	0.2	0.2	0.2	0.2	0.5
Dy	3.3	2.1	1.4	1.6	1.5	1.5	2.1	1.5	1.6	1.4	0.9	2.6
Ho	0.6	0.3	0.2	0.3	0.3	0.2	0.4	0.3	0.3	0.3	0.2	0.4
Er	1.7	1.1	0.7	1	1.2	0.7	1.1	0.9	1.1	1	0.5	1.2
Tm	0.5	0.2	0.2	0.2	0.2	0.2	0.2	0.2	0.2	0.2	0.2	0.3
Yb	4	1.8	1.4	1.2	1.2	1.2	1.5	1.5	1.7	1.5	0.9	2.6
Lu	0.8	0.3	0.2	0.3	0.2	0.1	0.2	0.3	0.3	0.2	0.2	0.4
LREE	93.1	70.1	31.6	41.8	43.5	36.8	41.5	29.2	23.3	20.2	19.4	69.4
HREE	11.5	6.2	4.3	4.8	4.8	4.1	5.8	4.9	5.4	4.8	3.1	8
∑REE	104.6	76.3	35.9	46.6	48.3	40.9	47.3	34.1	28.7	25.0	22.5	77.4
LREE/HREE	8.1	11.3	7.3	8.7	9.1	9.0	7.2	6.0	4.3	4.2	6.2	8.7
Ce/Ce*	0.27	0.31	0.49	0.43	0.45	0.46	0.36	0.63	0.53	0.79	0.68	0.27
Eu/Eu*	0.12	0.17	0.39	0.30	0.26	0.40	0.29	0.43	0.52	0.63	1.33	0.15
La/Yb	3.63	6.22	3.79	6.00	6.33	5.58	5.27	3.27	2.41	2.20	3.56	4.81

Table 4.21 (Continued)

Sample #	C1	C2	C3	C4	C5	C6	C7	C8	C9	C10	C11
Depth (m)	2.6	2.8	3.0	3.2	3.4	3.6	3.8	4.0	4.2	4.4	4.6
wt. %											
SiO_2	70.75	70.5	68.5	74.46	71.84	68.27	70.37	72.91	74.6	74.26	71.13
Al_2O_3	16.3	18.2	17.7	14.67	16.83	18.14	16.91	15.8	15.12	15.15	14.83
Fe_2O_3	1.19	2.21	1.98	1.24	1.74	2.58	0.85	0.66	0.57	0.86	1.21
MnO	0.03	0.04	0.13	0.07	0.11	0.29	0.21	0.04	0.07	0.1	0.07
MgO	0.07	0.06	0.17	0.07	0.12	0.17	0.02	0.01	0.06	0.06	0.07
CaO	0.22	0.3	0.45	0.67	0.69	0.8	0.89	0.87	0.79	0.75	0.69
Na_2O	2.21	1.48	3.16	4.88	4.99	5.82	7.11	6.73	6.13	5.85	5.07
K_2O	6.63	1.23	3.63	0.57	0.57	0.59	0.7	0.62	0.77	0.81	1.37
TiO_2	0.09	0.25	0.36	0.30	0.11	0.28	0.35	0.25	0.23	0.42	0.32
P_2O_5	0.04	0.03	0.04	0.04	0.04	0.05	0.04	0.04	0.04	0.04	0.04
LOI	2.11	5.36	3.75	2.9	2.63	2.84	2.54	2.00	1.58	1.68	5.07
Total	99.65	99.7	99.80	99.87	99.67	99.79	99.93	99.92	99.85	99.95	99.87
CIA (%)	59.25	80.9	64	59.8	62.54	60.86	54.58	54.25	55.03	56.08	57.24
µg/g											
Li	64	84	55	68	63	61	58	59	55	58	2
Rb	375	73	202	38	30	32	33	33	43	46	72
Cs	19	8	16	11	12	13	15	13	15	14	15
Ba	42	27	23	45	33	26	13	30	19	28	36
Sr	12	8	14	10	9	9	10	11	10	10	10
Ga	20	27	47	20	36	28	24	24	31	24	42
Be	15	12	12	15	30	15	18	15	18	21	15
Sn	32	26	18	34	24	34	49	28	18	16	14
Nb	33	192	35	45	116	148	72	52	62	137	66
Ta	28	52	20	18	40	48	24	20	20	40	15
Y	24	11	19	40	19	22	22	12	14	17	18
Zn	12	15	26	12	28	43	6	6	7	17	19
Zr	32	14	30	29	19	20	23	11	15	15	12
Hf	8	6	9	5	3	7	6	5	8	5	5
Th	5	14	16	7	8	9	6	5	6	10	8
U	2	5	6	3	3	4	3	3	3	4	3

Table 4.21 (Continued)

Sample #	C1	C2	C3	C4	C5	C6	C7	C8	C9	C10	C11
Depth (m)	2.6	2.8	3.0	3.2	3.4	3.6	3.8	4.0	4.2	4.4	4.6
La	3.5	7.3	7.8	5.7	5.9	8.2	4.3	4.1	3.7	5.4	5.1
Ce	7.4	23.8	18.2	13.4	13.3	18.3	10.1	9.4	8.3	12.5	10.0
Pr	0.9	1.9	2.3	1.4	1.6	2.4	1.1	1.1	0.9	1.6	1.3
Nd	3.5	6.8	10	5.2	5.5	9.6	4.5	3.9	3.9	5.7	5.5
Sm	1	2.2	3.4	1.7	1.9	3.2	1.6	1.1	1.3	2	2
Eu	0.1	0.1	0.3	0.1	0.1	0.4	0.1	0.1	0.1	0.1	0.2
Gd	1.2	2.2	3.7	1.9	2.1	2.7	1.4	1.2	1.2	1.7	1.8
Tb	0.1	0.3	0.6	0.3	0.3	0.3	0.2	0.2	0.1	0.2	0.2
Dy	1	1.7	4	2.1	2.2	2.9	1.7	1.4	1.7	2.1	2.2
Ho	0.2	0.3	0.8	0.4	0.4	0.6	0.3	0.3	0.2	0.4	0.4
Er	0.6	0.7	2.6	1.4	1.3	2	1.2	1.2	0.8	1.3	1.2
Tm	0.2	0.2	0.5	0.3	0.3	0.3	0.2	0.2	0.2	0.3	0.2
Yb	1.2	1.2	4.2	2.2	2.2	2.8	2.1	1.7	1.6	1.8	1.7
Lu	0.2	0.2	0.6	0.3	0.4	0.5	0.3	0.3	0.3	0.3	0.3
LREE	17.6	44.3	45.7	29.4	30.4	44.8	23.1	20.9	19.4	29.0	25.9
HREE	3.5	4.6	13.3	7	7.1	9.4	6	5.3	4.9	6.4	6.2
∑REE	21.1	48.9	59.0	36.4	37.5	54.2	29.1	26.2	24.3	35.4	32.1
LREE/HREE	5.0	9.6	3.4	4.2	4.3	4.8	3.8	3.9	4.0	4.5	4.2
Ce/Ce*	0.50	0.43	0.33	0.43	0.39	0.32	0.48	0.47	0.52	0.39	0.40
Eu/Eu*	0.54	0.27	0.29	0.33	0.30	0.40	0.40	0.52	0.48	0.32	0.44
La/Yb	2.92	6.08	1.86	2.59	2.68	2.93	2.05	2.41	2.31	3.00	3.00

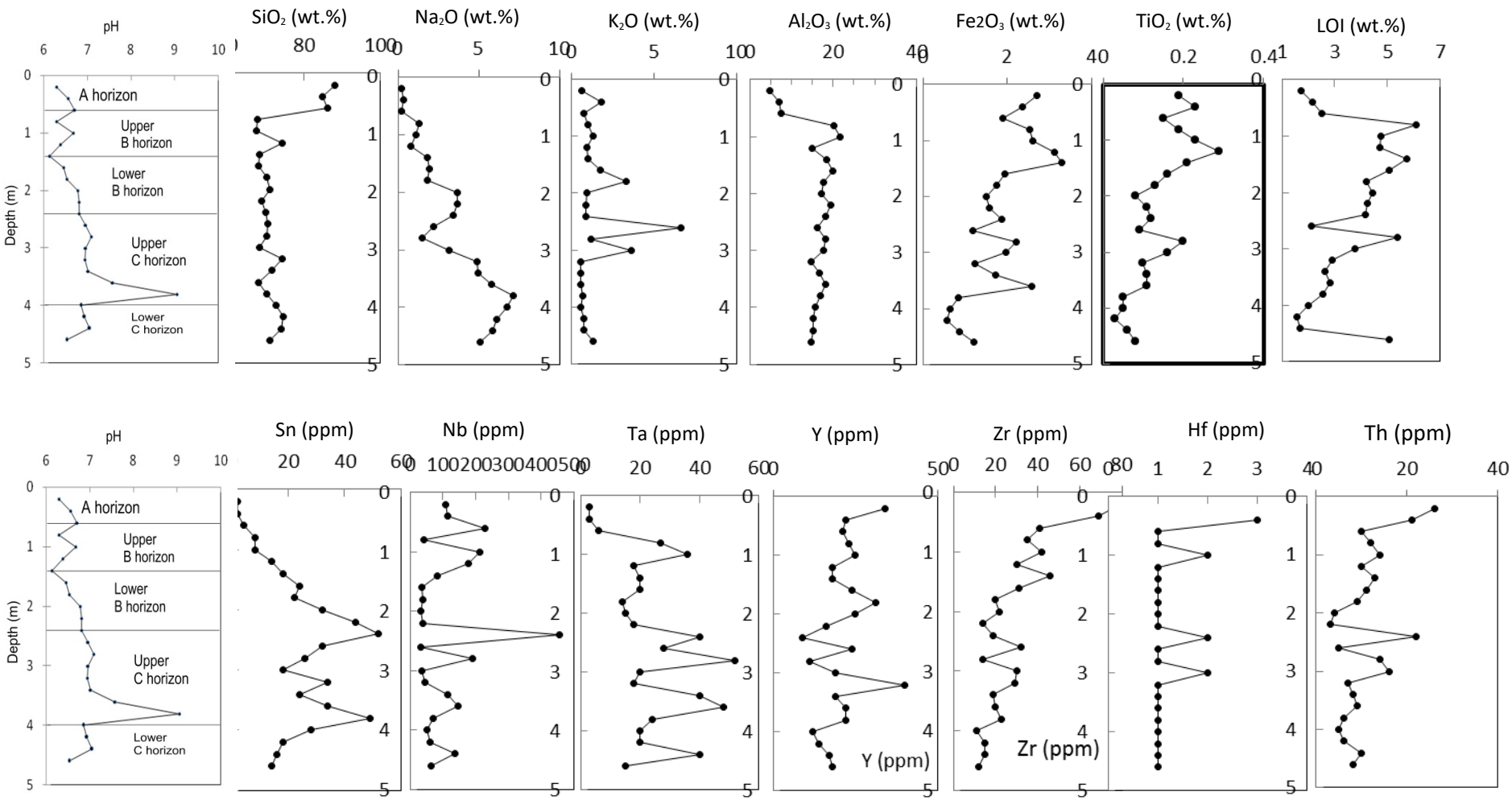

Fig. 4.65: Chemical elements distribution with depth in the mineralised pegmatite of Komu area

CaO content is of very low levels in both parent rock and its residual lateritic profile. The concentrations of this labile oxide decrease upwards from the bedrock to A-horizon of the profile. Concentrations of CaO are 0.52, 0.65, 0.42 and 0.09 wt.% in the parent rock, C, B and A-horizons, respectively. The corresponding contents of Na_2O and K_2O also show similar geochemical patterns to CaO, with their concentrations decreasing upward fromthe bedrock to A-horizon. The mean concentrations of Na_2O in the parent rock, C, B and A-horizons are 4.07, 4.86, 2.18 and 0.29 wt.%, respectively; while those of K_2O are 3.35, 1.6, 1.37 and 1.09 wt.% in the same horizons. The high values of K_2O and Na_2O in the profile horizons reveal the mild alteration of feldspars in the parent rock. On the contrary,P_2O_5 shows marginal enrichments in the weathering profile relative to the bedrock. The mean concentration of P_2O_5 in the parent rock, C, B and A-horizons are 0.02, 0.04, 0.03 and 0.23 wt.%, respectively. These geochemical trends are possibly connected with moderately enhanced modal composition of apatite in the protolith pegmatite.

The mean LOI value for the whole-rock pegmatite of Komu area is 0.89 wt.%; while the average LOI values of 2.95, 4.82 and 2.13 wt.% were respectively obtained from the C, B and A-horizons of the weathering profile (Table 4.21 and Fig. 4.65). The clay-rich B-horizon of the weathering profile exhibits the highest LOI values, and this may be due to the presence of kaolinites, hydroxides and oxyhydroxides of irons and other cation complexes associated with clay components that typify this zone. The discrimination of the lateritic profile using Al_2O_3-SiO_2-Fe_2O_3 (Schellman, 1983) ternary plot (Fig. 4.66)revealed kaolinisation of the laterite.

The mean CIA value of 55.72 of the whole-rock pegmatite samples signifies a mild alteration of the rock, while corresponding CIA values of 60.40, 76.61 and 78.5 in the C, B and A-horizons indicate moderate chemical weathering of the lateritic profile. The CIA trends of the parent rock and its *in situ*-derived residual profile are illustrated in Fig. 4.67 (Nesbitt and Young, 1982), which indicates a low value in the whole-rock pegmatite and a progressively higher alteration in the lateritic profile.

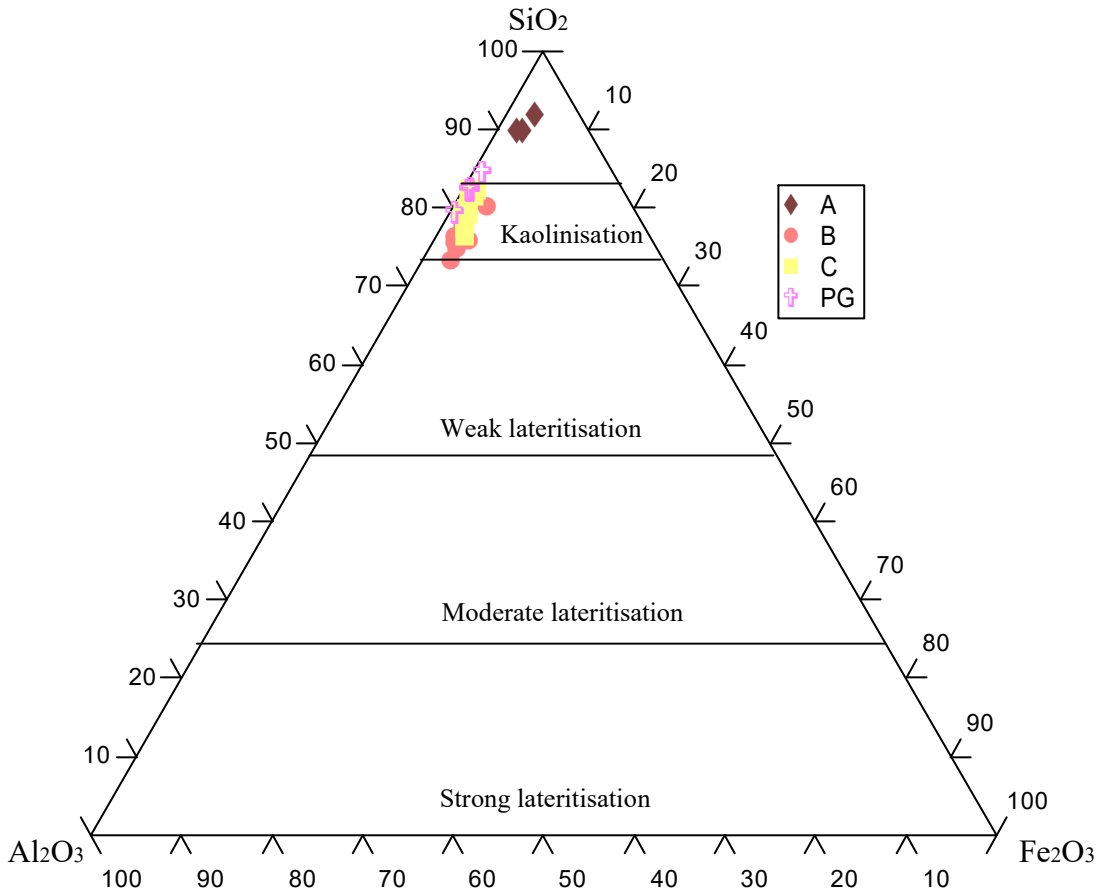

Fig. 4.66: Al_2O_3-SiO_2-Fe_2O_3 ternary plot for the lateritic profile derived from the mineralised pegmatite of Komu area (after Schellmann, 1983),

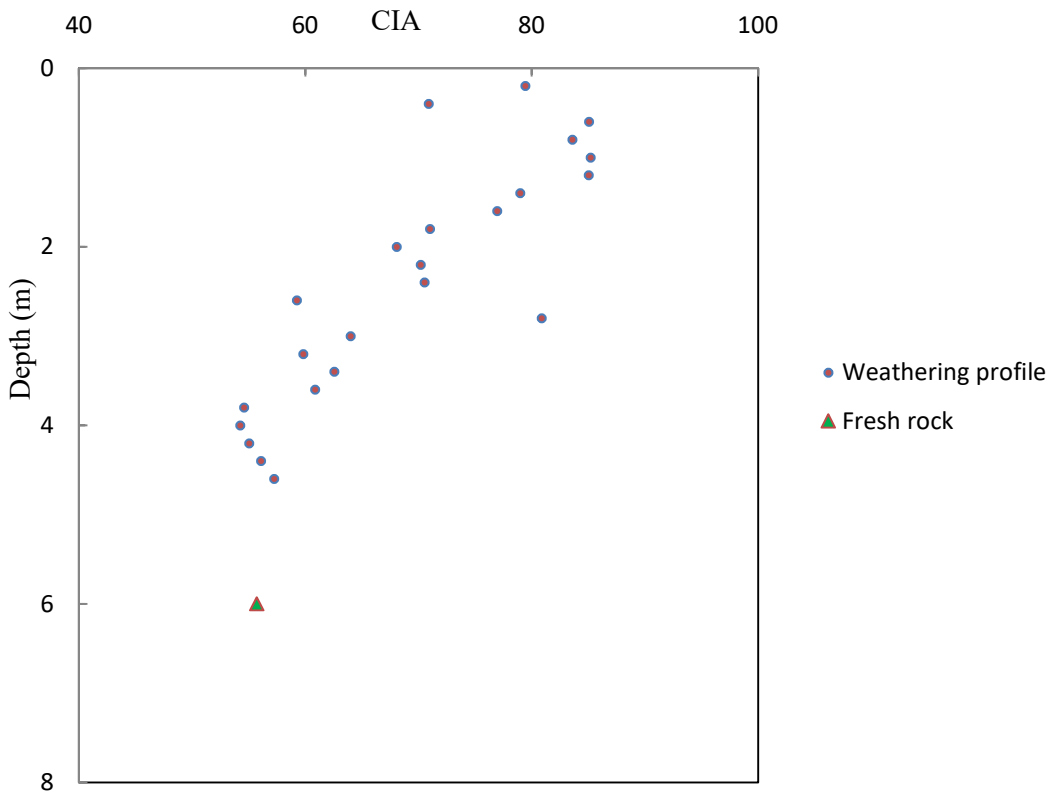

Fig. 4.67: Variation of chemical index of alteration (CIA) with depth in the *in situ*-derived lateritic profile from the mineralised pegmatite of Komu area (after Nesbitt and Young, 1982)

Trace element composition of the residual profile of the mineralised pegmatite of the Komu area are also presented in the Table 4.21; while the chemical variation and dispersion trends within the profile are illustrated in Fig. 4.65. Barium and Sr showed slightdepletion in the weathering profile compared to the parent rock. The mean concentrations of Ba are respectively 51, 29, 37 and 24 in the parent rock, C, B and A-horizons;while Sr showed mean values of 20, 10, 10 and 6 ppm in the same horizons.

The rare alkalis, Rb and Cs, showed enrichment in the whole-rock pegmatite samples relative to the weathering profile. Mean Rb contents of 625, 89, 70 and 57 ppm were correspondingly obtained in the parent rock, C, B and A-horizons, while Cs displays 102, 14, 6 and 2 ppm in the same horizons. Beryllium and Ga are mildly enhanced in the residual profile relative to the parent pegmatite. The average Be contents are respectively 20, 17, 26 and 8 ppm in the parent rock, C-, B- and A-horizons, and those of Ga are 31, 29, 34 and 11 ppm in the same horizons. These geochemical patterns show that the weathering is at incipient stage and there has been low degree of redistribution and remobilisation of chemical elements within the residual profile.

Pegmatite petrogenetic elements, such as Sn, Nb and Ta indicate significant enrichments in the lateritic profiles as compared to the bedrock pegmatite samples. For instance, the average Sn concentrations in the parent rock, C, B and A-horizons are 18, 27, 25 and 3 ppm while Nb contents are 70, 87, 124 and 151 ppm in the same horizons. Tantalum levels increase from 46 ppm in the parent rock to 50, 63 and 84 ppm, respectively in the C, B and A-horizons. Other immobile pegmatophile elements, such as Y, Zr, Hf, Th and U generally show moderate abundances in both the parent and the residual profile. They, however, show enhancement in the overlying residual profile. The mean concentrations of these elements in the parent rock, C, B and A-horizons respectively are as follow: Y (9, 20, 21 and 63 ppm); Zr (18, 20, 29 and 63 ppm); Hf (5, 6, 5 and 4 ppm); Th (6, 9, 11 and19 ppm) and U (7, 4, 4 and 5ppm).

The total REEs contents of residual weathering profile of the mineralised pegmatite of Komu area ranged from 37 to 41 and 72 ppm, respectively in the C, B and A-horizons, relative to 13 ppm recorded in the parent pegmatite. This trend revealed the strong enrichment of the REEs contents in the residual profile as compared to the parent rock Table 4.20 and Table 4.21).

The light rare-earth element (LREEs) (65 ppm) contents in the A-horizon are much moreenhanced than in B (36 ppm) and C (30 ppm)-horizons. Heavy rare-earth elements are low (5 - 7 ppm) relative to LREEs (65 ppm) in the constituting horizons. The weathering profile derived from the mineralised pegmatite of the Komu area portrays negative to moderate cerium (Ce/Ce* = 0.22 – 1.11) and weak negative europium (Eu/Eu* = 0.21 - 0.53) anomalies.

The whole-rock pegmatite chondrite-normalised REE pattern shows a slight LREE enhancement relative to HREE without any any significant cerium and europium anomaly. The horizons of the residual weathering profile, however, display flattened LREE and HREE profile, marked by the occurrence of negative europium anomaly (Fig 4.68). The REE patterns of the weathering profile also show slight enhancement in LREE relative to HREE.

On the whole, the mineralised pegmatite of the Komu area and its residual lateritic profile showed relative enrichments of rare alkalis and other immobile high field strength elements (HFSEs), compared to the Osu non-mineralised pegmatite and its residual profile.

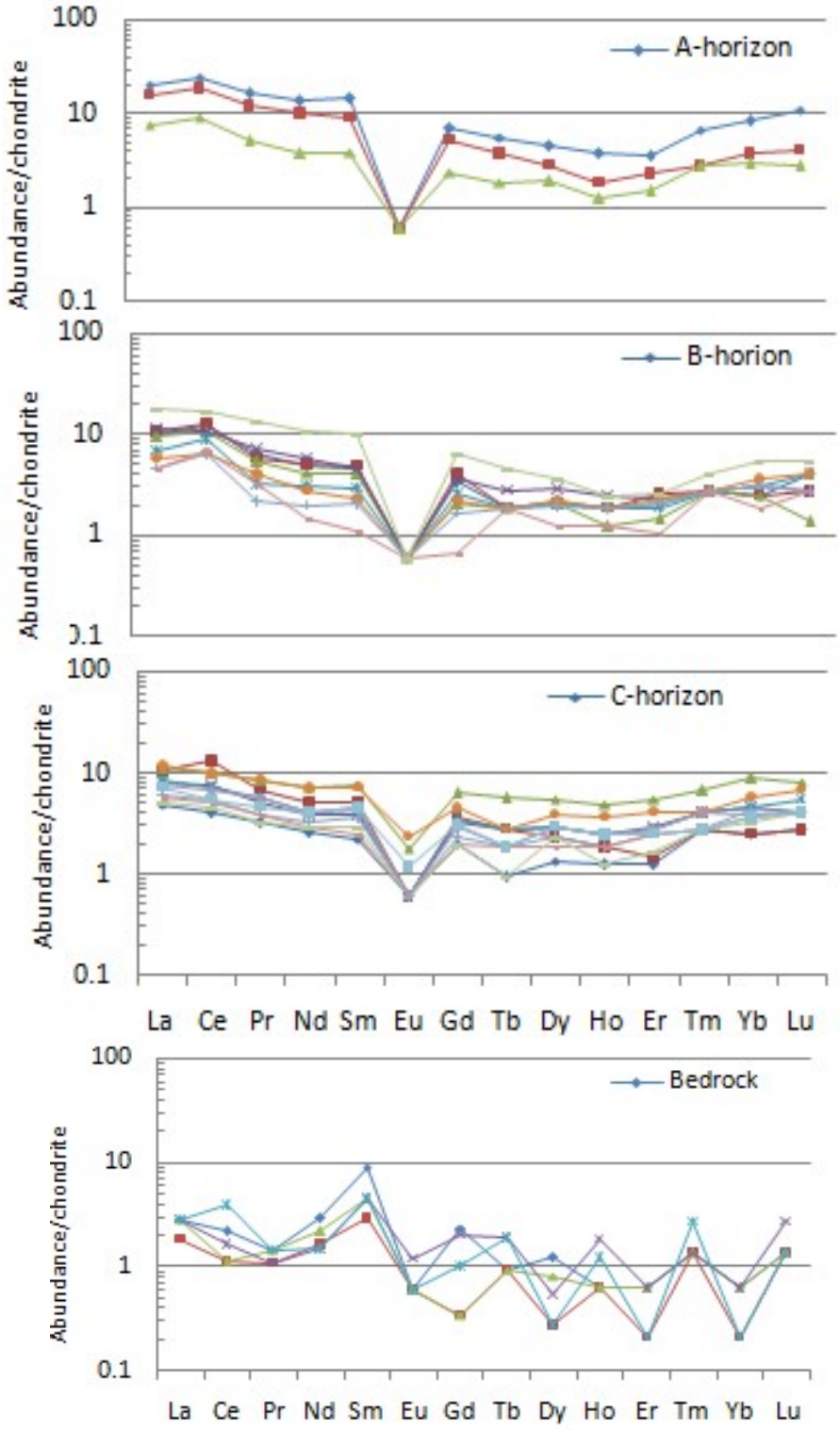

Fig. 4.68: Chondrite-normalised REE patterns for the bedrock and the *in situ*-derived weathering profile of the Komu mineralised pegmatite

4.3.3.4 Geochemical composition of the weathering profile above the mineralised pegmatite of Ofiki area

Whole-rock major and trace element abundances of the mineralised pegmatite of Ofiki area are presented in Table 4.22. The pegmatite shows silica concentration ranging from 69.95 to 77.20 wt.%, with mean silica value of 73.25 wt.%. Alumina abundances in the whole-rock pegmatite vary between 12.90 and 17.24 wt.%, showing average concentration of 15.20 wt.%. Fe_2O_3 indicates low contents, varying between 0.38 and 1.12wt. % with average concentration of 0.64 wt.%.

K_2O (4.13 -7.65 wt.%) and Na_2O (2.62 – 4.80 wt.%) vary widely among samples, showing corresponding mean concentrations of 6.26 and 3.48 wt.%. P_2O_5 shows wide variation among samples, indicating a low content of apatite in the whole-rock pegmatite samples.

Mean concentrations of Ba and Sr in the Ofiki pegmatite are 53 and 39 ppm, respectively; while Ga (15 ppm), Be (17 ppm), Sn (18 ppm), Nb (36 ppm) and Ta (32 ppm), as petrogenetic elements in pegmatite, expectedly show high levels in the whole rock pegmatite when compared to the Osu non-mineralised pegmatite. Other HFSE, such as Y (11 ppm), Zr (26 ppm), Hf (6 ppm), Th (6 ppm) and U (10 ppm) in the pegmatite, however, signify moderate abundances similar to Ijero and Komu mineralised pegmatite.

The total REEs contents of the Ofiki mineralised pegmatite is 21 ppm (Table 4.22). The LREEs (15 ppm) contents indicate more enhancement relative to the HREE (6 ppm), with the mean LREEs/HREEs ratio slightly higher than 2.7. The pegmatite shows negative Ce (Ce/Ce^*= 0.23 – 0.60) and Eu (Eu/Eu^* = 0.13- 0.52) anomalies.

Major and trace element geochemical data of the residual lateritic profile derived from the mineralised pegmatite of Ofiki area are presented in Table 4.23; while variation diagrams indicating element dispersion trends within profile are exemplified in Fig. 4.69. The A-horizon of the residual profile shows high silica contents, ranging from 72.11 to 78.86 wt.%, with mean SiO_2 concentration of 75.61 wt.%. The B- and C-horizons are less siliceous, indicating mean silica contents of 60.58 and 57.52 wt.%, respectively.

Table 4.22: Whole–rock major, trace and rare-earth element composition of the mineralised pegmatite of Ofiki area

Major oxides	OFP1	OFP2	OFP3	OFP4	OFP5	OFP6	OFP7	OFP8	OFP9	OFP10	Mean	Range
(wt.%)												
SiO_2	77.20	72.98	74.72	72.32	73.66	72.60	69.95	70.27	77.17	71.43	73.23	69.95-77.20
Al_2O_3	12.90	15.25	14.31	15.90	14.66	15.76	17.24	16.67	13.24	16.03	15.20	12.90-17.24
Fe_2O_3	0.40	0.38	0.42	0.67	0.45	0.80	0.83	0.62	1.12	0.73	0.64	0.38-1.12
MnO	0.03	0.29	0.18	0.09	0.03	0.14	0.24	0.11	0.17	0.08	0.14	0.03-0.29
MgO	0.01	0.02	0.02	0.02	0.00	0.02	0.07	0.01	0.08	0.02	0.03	0.00-0.08
CaO	0.36	0.37	0.39	0.36	0.24	0.31	0.33	0.25	0.44	0.28	0.33	0.24-0.44
Na_2O	2.95	3.01	3.57	2.95	2.62	3.69	4.48	3.67	3.06	4.80	3.48	2.62-4.80
K_2O	5.30	6.93	5.72	6.72	7.30	6.29	6.46	7.65	4.13	6.11	6.26	4.13-7.65
TiO_2	0.02	0.02	0.02	0.03	0.02	0.03	0.02	0.03	0.04	0.02	0.03	0.02-0.04
P_2O_5	0.06	0.14	0.11	0.11	0.11	0.01	0.04	0.04	0.09	0.05	0.08	0.01-0.14
LOI	0.51	0.50	0.48	0.78	0.63	0.10	0.20	0.60	0.30	0.30	0.44	0.10-0.78
Total	99.74	99.89	99.94	99.95	99.72	99.75	99.86	99.92	99.84	99.85	99.83	99.72-99.95
CIA	52.21	50.73	50.73	53.34	52.60	51.02	51.73	51.19	52.47	50.71	51.64	62.88-48.07
(ppm)												
Rb	579	493	342	256	413	634	774	145	693	231	456	145-774
Cs	259	128	26	47	258	350	433	110	440	146	220	26-440
Ba	47	92	30	53	40	67	54	24	48	68	51	24-92
Sr	41	41	9	40	42	47	49	51	41	32	39	9-51
Ga	18	15	13	10	23	17	26	18	9	22	15	9-26
Be	12	16	26	8	11	14	23	14	27	18	17	8-27
Sn	22	18	28	14	20	12	16	22	11	16	18	11-28
Nb	42	19	20	38	53	48	27	31	43	38	36	19-53
Ta	22	34	41	28	38	19	62	37	24	16	32	16-62
Y	6	15	5	12	10	14	8	16	8	12	11	6-16
Zn	30	20	27	18	26	18	22	16	26	18	22	16-30
Zr	37	26	47	11	29	34	20	17	24	16	26	11-47
Hf	6	4	4	9	5	8	12	6	4	2	6	2-12
Th	3	4	4	6	9	7	6	9	8	4	6	3-9
U	10	2	8	5	18	8	15	19	9	5	10	2-19

Table 4.22 (Continued)

	OFP1	OFP2	OFP3	OFP4	OFP5	OFP6	OFP7	OFP8	OFP9	OFP10	Mean	Range
La	5.0	4.0	5.0	5.0	5.0	3.2	2.5	2.6	4.3	3.8	4.0	2.5-5.0
Ce	3.0	3.0	5.0	5.0	2.0	5.6	5.5	5.8	9.0	8.6	5.3	2.0-9.0
Pr	0.8	1.2	0.6	0.9	0.8	0.8	0.7	0.7	1.2	1.1	0.9	0.6-1.2
Nd	3.0	2.0	3.0	2.0	2.0	2.1	2.9	3.0	4.0	3.2	2.7	2.0-4.0
Sm	4.0	2.0	2.0	3.0	2.0	1.2	1.0	1.1	2.2	2.2	2.1	1.0-4.0
Eu	0.1	0.1	0.2	0.1	0.2	0.1	0.1	0.1	0.1	0.1	0.1	0.1-0.2
Gd	0.2	0.3	0.3	0.2	0.3	0.3	0.3	0.3	0.5	0.3	0.3	0.2-0.5
Tb	1.4	1.3	1.2	2.1	1.4	1.4	1.2	1.3	2.6	2.0	1.6	1.2-2.6
Dy	1.5	1.9	1.5	1.4	1.6	1.8	1.9	1.5	2.7	1.8	1.8	1.4-2.7
Ho	0.2	0.3	0.2	0.3	0.2	0.2	0.4	0.2	0.4	0.2	0.3	0.2-0.4
Er	0.6	0.6	0.9	0.8	0.7	0.5	1.1	0.6	1.1	0.5	0.7	0.5-1.1
Tm	0.1	0.2	0.2	0.2	0.1	0.1	0.2	0.1	0.2	0.1	0.2	0.1-0.2
Yb	0.8	1.3	0.9	0.6	1.4	0.9	2.2	0.8	1.5	0.6	1.1	0.6-2.2
Lu	0.1	0.2	0.2	0.1	0.2	0.1	0.3	0.1	0.2	0.1	0.2	0.1-0.3
LREE	16.1	12.6	16.1	16.2	12.4	13.3	12.9	13.5	21.3	19.3	15.4	8.4-23.9
HREE	4.70	5.70	5.20	5.50	5.50	5.20	7.20	4.70	8.60	5.30	5.80	4.00-9.40
∑REE	20.9	18.3	21.3	21.7	17.9	18.5	20.2	18.2	29.8	24.6	21.1	12.4-33.2
LREE/HREE	3.40	2.20	3.10	3.00	2.20	2.60	1.80	2.90	2.50	3.60	2.70	2.10-2.50
Ce/Ce*	0.28	0.26	0.42	0.34	0.23	0.49	0.60	0.59	0.44	0.46	0.40	0.38-0.40
Eu/Eu*	0.16	0.29	0.52	0.26	0.46	0.30	0.40	0.40	0.17	0.13	0.27	0.46-0.17
La/Yb	6.17	3.03	5.62	7.81	3.62	3.40	1.16	3.21	2.79	6.13	3.64	4.03-2.33

Table 4.23 Major, trace and rare-earth element composition of the lateritic profile derived from mineralised pegmatite of Ofiki area

Sample #	A1	A2	A3	A4	A5	B1	B2	B3	B4	B5	B6	B7	B8	B9	B10	B11
Depth(m)	0.2	0.4	0.6	0.8	1.0	1.2	1.4	1.6	1.8	2.0	2.2	2.4	2.6	2.8	3.0	3.2
wt. %																
SiO_2	78.86	77.47	75.48	74.14	72.11	68.19	66.9	65.96	61.64	62.25	58.82	58.54	56.26	57.39	60.44	56.59
Al_2O_3	7.05	8.93	10.21	9.23	11.25	15.67	17.70	19.25	21.16	19.72	22.43	21.85	20.05	19.24	24.65	18.55
Fe_2O_3	2.56	4.05	4.61	4.89	3.77	6.84	5.96	5.55	7.12	6.66	7.51	9.41	12.26	14.98	5.47	13.18
MnO	0.15	0.09	0.06	0.1	0.06	0.08	0.11	0.07	0.38	0.42	0.54	0.37	0.62	0.07	0.10	0.73
MgO	0.12	0.16	0.04	0.06	0.11	0.07	0.10	0.12	0.10	0.06	0.07	0.15	0.10	0.07	0.06	0.10
CaO	0.20	0.06	0.11	0.04	0.05	0.04	0.05	0.05	0.05	0.04	0.03	0.02	0.03	0.02	0.02	0.02
Na_2O	2.47	2.85	2.01	2.02	1.82	0.62	0.45	0.86	0.36	0.32	0.64	0.43	0.85	0.37	0.54	0.53
K_2O	1.77	1.92	1.62	2.26	2.91	1.21	1.05	1.32	0.98	0.82	0.99	1.61	1.27	1.04	1.00	0.79
TiO_2	0.73	0.33	0.41	0.41	0.55	0.48	0.63	0.47	0.51	0.54	0.55	0.46	0.53	0.55	0.58	0.61
P_2O_5	0.07	0.05	0.05	0.07	0.07	0.06	0.06	0.04	0.04	0.05	0.04	0.04	0.04	0.03	0.02	0.06
LOI	5.48	3.91	5.18	6.37	6.89	6.33	6.59	5.90	6.96	9.27	8.06	6.81	7.67	5.92	6.68	8.25
Total	99.46	99.84	99.74	99.57	99.65	99.59	99.6	99.39	99.66	99.45	99.68	99.71	99.68	99.68	99.56	99.41
CIA (%)	87.34	93.39	94.45	97.16	96.81	95.97	93.77	89.12	92.65	96.76	94.22	86.59	92.47	93.10	92.90	95.20
µg/g																
Li	18	27	29	18	22	44	29	40	29	44	122	50	40	62	33	83
Rb	49	33	45	32	43	56	66	89	59	85	191	160	87	101	87	182
Cs	4	3	4	4	5	6	6	5	7	6	11	13	7	9	8	12
Ba	37	16	22	44	31	39	58	84	32	52	81	42	28	34	59	87
Sr	33	14	12	9	10	9	13	8	10	8	6	9	7	8	11	7
Ga	14	12	16	18	22	21	22	26	28	33	49	36	27	31	31	46
Be	9	9	6	6	9	19	29	9	36	26	15	15	26	19	29	24
Sn	8	6	8	6	8	12	14	24	18	28	62	56	24	30	28	70
Nb	34	25	27	30	26	34	39	44	37	65	131	64	65	68	47	101
Ta	18	15	12	21	15	18	27	12	18	27	33	33	24	27	21	30
Y	27	14	13	11	13	15	26	21	15	18	30	17	21	25	22	17
Zn	19	14	16	16	23	20	25	26	25	27	46	35	27	29	33	48
Zr	53	32	96	70	18	174	246	151	245	221	173	210	208	236	254	165
Hf	5	7	4	9	7	7	12	10	6	14	4	12	17	13	6	13
Th	8	6	8	9	9	18	9	9	10	10	10	19	17	8	11	19
U	5	3	4	5	6	5	5	4	7	6	6	5	3	4	6	6

Table 4.23 (Continued)

Sample #	A1	A2	A3	A4	A5	B1	B2	B3	B4	B5	B6	B7	B8	B9	B10	B11
Depth (m)	0.2	0.4	0.6	0.8	1.0	1.2	1.4	1.6	1.8	2.0	2.2	2.4	2.6	2.8	3.0	3.2
La	17.5	8.7	8.6	8.4	11.0	10.8	12.0	10.0	12.4	12.3	9.0	17.2	13.1	16.6	21.8	16.9
Ce	75.1	56.5	56.2	84.9	110.3	97.1	114.2	81.1	366.2	354.3	169.0	245.5	37.5	61.2	316.6	275.3
Pr	4.3	1.9	2.0	1.8	2.2	2.2	2.5	2.2	2.7	2.5	2.3	4.2	3.4	4.0	5.3	4.5
Nd	14.8	7.4	7.5	6.4	8.2	7.6	9.8	8.8	10.0	8.9	7.6	15.6	13.2	14.8	19.1	15.0
Sm	2.9	1.8	2.0	1.4	1.5	1.6	1.9	2.1	2.0	2.2	1.9	3.0	2.7	3.1	3.3	3.1
Eu	0.4	0.3	0.2	0.3	0.3	0.3	0.3	0.3	0.3	0.4	0.3	0.4	0.4	0.5	0.6	0.5
Gd	2.8	2.2	1.2	1.2	1.1	1.4	1.2	1.9	1.3	1.5	1.5	2.2	1.9	2.9	2.9	2.0
Tb	0.5	0.2	0.1	0.1	0.2	0.1	0.2	0.3	0.2	0.2	0.2	0.3	0.2	0.5	0.3	0.3
Dy	2.5	1.9	1.2	1.2	1.5	1.0	1.5	2.5	1.9	1.3	1.5	2.3	1.8	2.9	2.4	2.4
Ho	0.4	0.3	0.2	0.2	0.2	0.2	0.3	0.4	0.4	0.3	0.2	0.5	0.3	0.5	0.5	0.5
Er	1.4	1.2	0.5	0.7	0.5	0.7	1.0	1.2	0.9	0.7	1.0	1.3	0.9	1.6	1.5	1.2
Tm	0.2	0.2	0.1	0.1	0.1	0.1	0.1	0.2	0.2	0.1	0.2	0.2	0.1	0.2	0.3	0.2
Yb	1.2	1.5	0.7	0.7	0.8	0.8	1.0	1.6	1.3	0.8	1.2	1.2	1.2	1.7	1.5	1.6
Lu	0.2	0.2	0.1	0.1	0.1	0.1	0.1	0.2	0.2	0.1	0.2	0.2	0.2	0.3	0.2	0.2
LREE	117.8	78.8	77.7	104.4	134.6	121.0	141.9	106.4	394.9	382.1	191.6	288.1	72.2	103.1	369.6	317.3
HREE	6.4	5.5	2.9	3.1	3.4	3.0	4.2	6.4	5.1	3.5	4.5	6.0	4.7	7.7	6.7	6.4
∑REE	124.2	84.3	80.6	107.5	138.0	124.0	146.1	112.8	400.0	385.6	196.1	294.1	76.9	110.8	376.3	323.7
LREE/HREE	18.4	14.3	26.8	33.7	39.6	40.3	33.8	16.6	77.4	109.2	42.6	48.0	15.4	13.4	55.2	49.6
Ce/Ce*	0.33	0.61	0.59	0.78	0.70	0.66	0.64	0.63	1.08	1.11	0.94	0.60	0.30	0.31	0.54	0.62
Eu/Eu*	0.28	0.35	0.36	0.53	0.53	0.46	0.45	0.34	0.43	0.44	0.41	0.31	0.35	0.30	0.31	0.36
La/Yb	14.58	5.80	12.29	12.00	13.75	13.50	12.00	6.25	9.54	15.38	7.50	14.33	10.92	9.76	14.53	10.56

Table 4.23 (Continued)

Sample #	B12	B13	B14	B15	B16	B17	B18	C1	C2	C3	C4	C5	C6	C7	C8	C9
Depth (m)	3.4	3.6	3.8	4.0	4.2	4.4	4.6	4.8	5.0	5.2	5.4	5.6	5.8	6.0	6.2	6.4
wt. %																
SiO_2	56.73	61.02	59.36	62.66	60..29	59.05	58.39	56.92	55.87	56.86	60.71	55.45	57.19	59.36	52.77	62.56
Al_2O_3	19.11	21.36	24.09	20.26	24.82	25.12	23.25	26.75	25.94	26.42	24.75	28.28	26.45	25.44	29.39	21.85
Fe_2O_3	12.32	7.48	5.26	7.53	5.34	7.06	8.23	5.94	3.42	3.97	3.11	4.14	3.83	2.50	3.16	2.87
MnO	0.74	0.31	0.81	0.04	0.02	0.02	0.02	0.02	0.01	0.02	0.03	0.04	0.05	0.06	0.07	0.09
MgO	0.11	0.16	0.10	0.10	0.04	0.08	0.07	0.1	0.06	0.06	0.05	0.02	0.04	0.03	0.05	0.04
CaO	0.01	0.03	0.02	0.01	0.01	0.01	0.01	0.01	0.02	0.02	0.01	0.01	0.01	0.01	0.02	0.01
Na_2O	0.71	0.11	0.09	0.09	0.83	0.23	1.05	0.85	1.75	1.05	1.04	1.02	1.23	1.08	1.66	1.14
K_2O	1.99	2.10	1.50	1.81	1.62	0.79	1.53	1.65	4.79	3.50	1.93	3.08	2.69	3.54	5.84	4.15
TiO_2	0.46	0.74	0.52	0.51	0.44	0.48	0.44	0.44	0.39	0.37	0.43	0.42	0.52	0.55	0.3	0.24
P_2O_5	0.04	0.03	0.04	0.03	0.02	0.02	0.02	0.02	0.01	0.03	0.02	0.02	0.03	0.02	0.04	0.03
LOI	7.11	6.3	7.51	6.5	6.21	6.99	6.52	6.96	7.43	7.35	7.62	8.21	7.65	7.06	6.3	6.59
Total	99.33	99.64	99.30	99.55	99.64	99.84	99.53	99.66	99.69	99.65	99.70	99.69	99.63	99.65	99.69	99.57
CIA (%)	88.13	87.37	89.90	89.18	95.19	94.83	94.20	92.81	90.77	93.02	94.98	95.02	96.26	87.99	80.73	83.09
µg/g																
Li	54	65	69	32	36	42	52	47	38	36	28	18	55	30	37	38
Rb	156	163	149	51	57	81	95	100	86	67	58	37	140	246	182	97
Cs	10	11	9	5	6	6	8	8	7	9	8	6	16	17	14	14
Ba	81	47	62	37	50	33	44	44	39	52	55	88	122	112	168	121
Sr	7	10	6	6	7	6	6	7	6	7	6	7	10	14	13	13
Ga	39	40	40	24	26	29	34	30	32	30	30	26	31	34	39	39
Be	26	30	29	33	19	13	26	9	33	23	16	6	19	42	148	378
Sn	58	64	44	14	16	22	28	18	22	22	10	8	20	12	36	40
Nb	75	100	108	41	58	119	116	91	134	76	118	124	138	105	133	209
Ta	27	51	33	15	21	42	42	33	48	39	57	72	117	105	138	204
Y	17	22	36	38	32	29	19	16	21	18	15	18	12	11	29	11
Zn	30	45	37	21	25	26	30	22	23	31	20	20	19	18	27	41
Zr	208	207	185	178	167	130	94	92	97	162	141	193	108	88	82	108
Hf	4	13	7	9	5	7	14	8	12	7	9	16	12	6	9	6
Th	9	11	11	11	10	11	19	6	13	18	9	12	19	8	10	10
U	3	6	4	5	6	6	4	3	4	4	4	6	3	4	6	5

Table 4.23 (Continued)

Sample #	B12	B13	B14	B15	B16	B17	B18	C1	C2	C3	C4	C5	C6	C7	C8	C9
Depth (m)	3.4	3.6	3.8	4.0	4.2	4.4	4.6	4.8	5.0	5.2	5.4	5.6	5.8	6.0	6.2	6.4
La	16.0	20.2	14.2	14.8	14.5	12.6	11.0	9.1	8.7	9.2	7.2	9.0	9.7	9.5	10.0	9.1
Ce	112.0	304.5	35.1	31.2	24.9	22.6	16.9	13.9	13.1	15.4	12.7	17.7	17.4	15.9	22.0	15.9
Pr	4.0	5.0	3.9	3.7	3.7	3.2	3.0	2.3	2.5	2.4	2.0	2.6	2.8	2.7	2.9	2.5
Nd	14.6	18.5	16.4	13.9	14.5	12.9	11.6	10.2	8.7	9.6	8.4	10.3	10.3	11.0	11.0	9.5
Sm	2.9	3.9	3.8	3.8	3.2	2.9	3.0	1.9	2.0	2.4	2.2	2.7	2.5	2.6	3.4	3.0
Eu	0.6	0.6	0.5	0.4	0.5	0.4	0.3	0.3	0.3	0.3	0.2	0.3	0.3	0.4	0.3	0.3
Gd	2.5	3.7	3.7	3.9	3.1	2.5	2.0	1.9	1.5	2.1	1.9	2.2	2.5	2.3	3.2	2.1
Tb	0.3	0.4	0.5	0.6	0.4	0.3	0.2	0.2	0.2	0.2	0.2	0.2	0.3	0.2	0.3	0.3
Dy	2.0	3.0	3.5	4.1	3.4	1.8	1.6	1.8	1.5	1.6	1.4	1.2	1.6	1.4	1.7	1.6
Ho	0.5	0.6	0.6	0.6	0.6	0.4	0.3	0.3	0.3	0.3	0.2	0.3	0.3	0.2	0.3	0.3
Er	1.1	1.6	1.5	2.0	1.8	0.8	0.8	0.9	0.7	0.8	0.8	0.8	0.7	0.6	0.6	0.6
Tm	0.2	0.2	0.2	0.3	0.3	0.2	0.2	0.1	0.1	0.1	0.1	0.1	0.1	0.1	0.1	0.1
Yb	1.0	2.0	1.9	2.4	1.7	1.0	0.9	0.9	0.8	0.9	0.7	0.9	0.7	0.8	0.8	0.7
Lu	0.2	0.3	0.3	0.3	0.3	0.1	0.1	0.1	0.1	0.1	0.1	0.2	0.1	0.1	0.1	0.1
LREE	152.6	356.4	77.6	71.7	64.4	57.1	47.8	39.6	36.8	41.4	34.6	44.8	45.5	44.4	52.8	42.4
HREE	5.3	8.1	8.5	10.3	8.5	4.6	4.1	4.3	3.7	4.0	3.5	3.7	3.8	3.4	3.9	3.7
∑REE	157.9	364.5	86.1	82.0	72.9	61.7	51.9	43.9	40.5	45.4	38.1	48.5	49.3	47.8	56.7	46.1
LREE/HREE	28.8	44.0	9.1	7.0	7.6	12.4	11.7	9.2	9.9	10.3	9.9	12.1	12.0	13.1	13.5	11.4
Ce/Ce*	0.43	0.57	0.26	0.25	0.22	0.25	0.23	0.27	0.25	0.27	0.31	0.29	0.26	0.26	0.29	0.27
Eu/Eu*	0.36	0.26	0.24	0.21	0.28	0.29	0.28	0.36	0.40	0.31	0.27	0.28	0.27	0.32	0.21	0.27
La/Yb	16.00	10.10	7.47	6.17	8.53	12.60	12.22	10.11	10.88	10.22	10.29	10.00	13.86	11.88	12.50	13.00

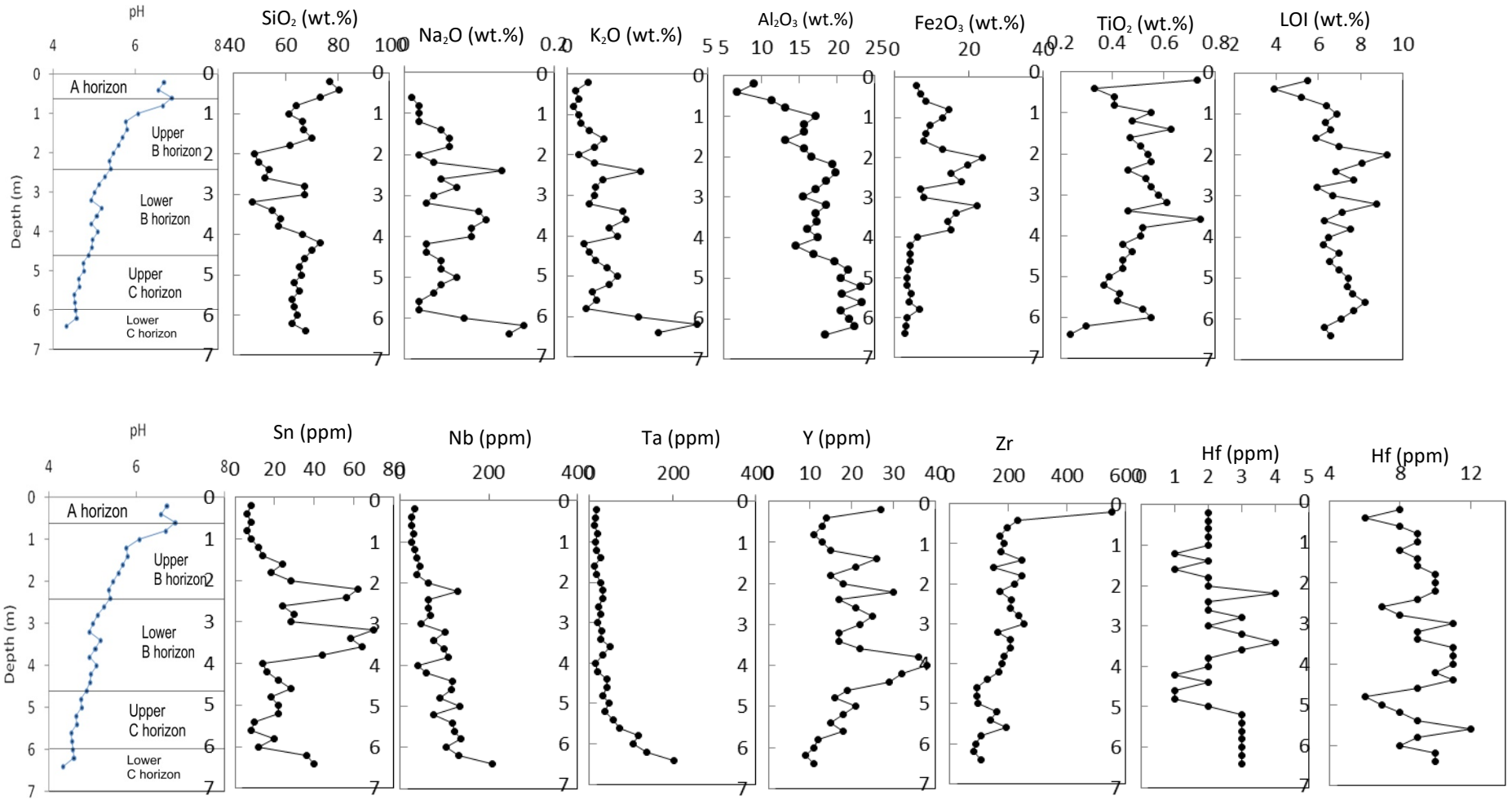

Fig. 4.69: Chemical elements distribution with depth in the mineralised pegmatite of Ofiki area

The high silica abundances in these horizons are further buttressed by high peaks of quartz in the X-ray diffractograms of the residual profile (Figs. 4.43). Al_2O_3 indicatesenrichments in the C- (26.14 wt.%)and B- (21.02 wt.%) horizons but depletion in the A-horizon (9.33 wt.%), when compared to the whole-rock pegmatite mean concentration of 15.20 wt.%.The lower alumina contents of the A-horizon could possibly be connected with the intense eluviation of alumina-bearing (kaolinite) components in this zone.

There is significant upgrading of Fe_2O_3 in the weathering profile relative to the pegmatite bedrock. Fe_2O_3 is particularly enhanced in the B-horizon, showing 8.23 wt.%; while the parent rock, C and A-horizons correspondingly indicate mean concentrations of 0.64, 3.66 and 3.98 wt.%. The relative enhancements of Fe_2O_3 concentrations in the residual profile can be attributed to the relative immobility of iron in the weathering profile.

CaO witnessed intense leaching in the weathering horizon, showing low concentrations when compared to the parent rock. Average CaO contents are 0.33, 0.01, 0.03 and 0.12 wt.% in the parent rock, C, B and A-horizon, respectively. Na_2O and K_2O show strong depletion in the lateritic profile relative to the parent rock. Na_2O concentrations are 3.48, 1.20, 0.50 and 2.23 wt.%, while those of K_2O are 6.26, 3.46, 1.30 and 2.10 in the parent rock, C, B and A-horizons, respectively. P_2O_5 is slightly depleted in the lateritic profile, probably due to its mobility.

The LOI data for the fresh whole-rock samples indicate a mean value of 0.44 wt.%, while the computed LOI value for the residual profile ranged from 7.24, 6.97 and 4.86 wt.% in the C, B and A-horizon, respectively. The lower LOI value in the A-horizon is largely due to the high intensity of evaporation that marks this zone, while higher LOI values in the B and C-horizon are closely associated with the abundance of hydrous minerals that typify these zones (Table 4.23 and Fig. 4.69). Based on the laterite maturity parameters established, using Al_2O_3-SiO_2-Fe_2O_3 (Schellmann, 1983) ternary diagram, the residual lateritic profile from the Ofiki mineralised pegmatite can be considered to be weakly lateritised. Most of the lateritic samples plot in the weak lateritisation field, while few lateritic samples from the C and B-horizon cluster in the kaolinisation field of the ternary plot (Fig.4.70). The CIA value of 51.64 signifies negligible alteration of the whole-rock

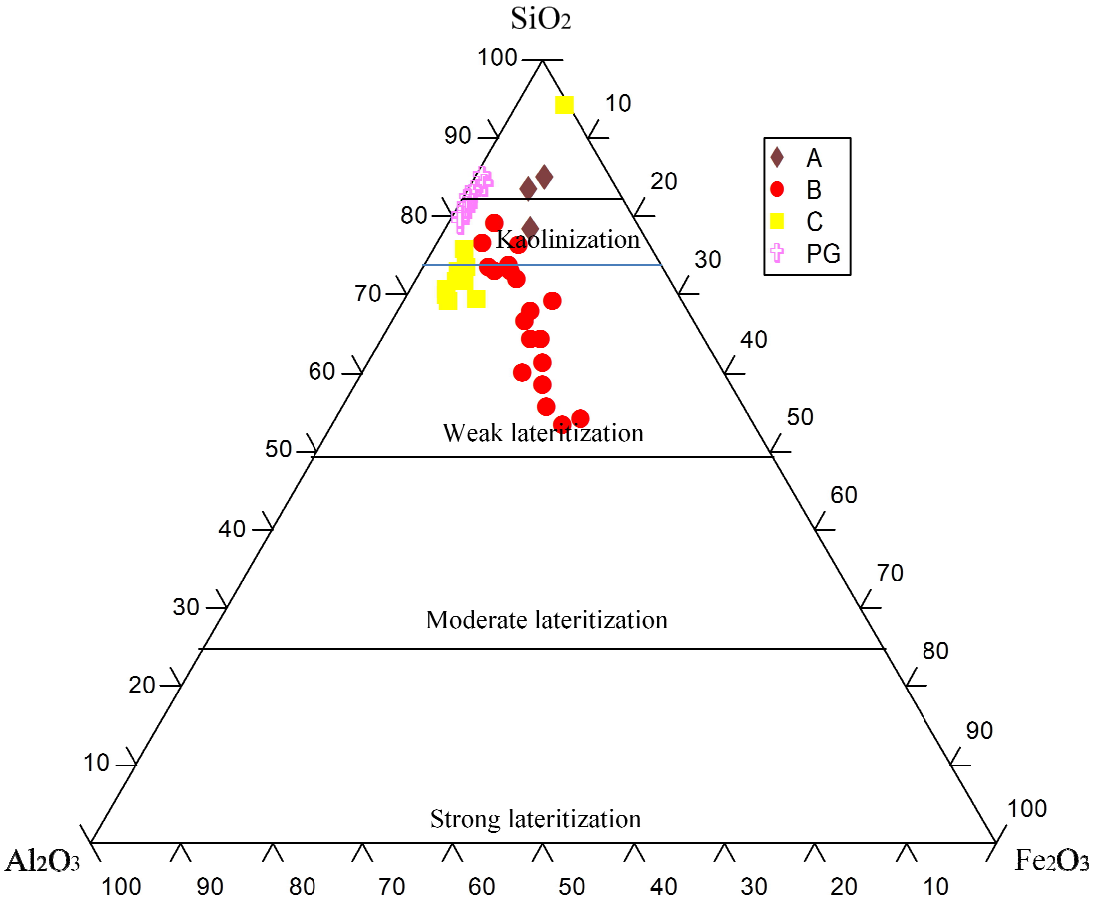

Fig. 4.70: Al_2O_3-SiO_2-Fe_2O_3 ternary plot for the lateritic profile derived from the mineralised pegmatite of Ofiki area (after Schellmann, 1983),

pegmatite (Nesbitt and Young, 1982), while the corresponding CIA values of 90.52, 92.78 and 93.83 for the C, B and A-horizons indicate a high degree of chemical weathering of the rock. There is an obvious trend from the low value in the unaltered pegmatite bedrock toprogressively increasing values in the more intensely altered residual profile (Fig. 4.71).

The trace element chemical data of the pegmatite residual weathering profile of Ofiki area are given in Table 4.23. Barium showedslightdepletion in the residual lateritic profile relative to the parent rock. The mean contents of Ba in the rock, C, B and A-horizons are respectively 52, 89, 51 and 30 ppm. Rubidium and Cs are expectedly high in the parent rock compared to the weathering profile. The average Rb concentrations of 456, 113, 106 and 40 ppm were recorded for the parent rock, C, B and A-horizon, respectively; while those of Cs are 220, 11, 8 and 4 ppm in the same horizons.

Tin, Nb and Ta contentsin the residual profile show enrichments compared to the bedrock. For example, the mean Sn contents in the parent rock, C, B and A horizons are 18, 21, 34 and 7 ppm; Nb concentrations are 36, 125, 73 and 28 ppm; while Ta contents are 32, 90, 28 and 36 ppm in the same horizons. Zirconium, Y and Th are enhanced in the regolith profile as compared to the parent rock. The mean Zr contents in the parent rock, C, B and A-horizons respectively are 26, 119, 192 and 54 ppm; while those of Y are 11 17, 23 and 16 ppm in the same horizons. Thorium has average concentrations of 6, 12, 12and 9 ppm in the parent rock, C, B and A-horizons, respectively. Hafnium shows similar residual character to thorium in the residual profile; while U suffers depletion in the residual profile relative to the parent rock (Table 4.23).

The total REEs contents of the residual weathering profile of the mineralised pegmatite of Ofiki area range from 46 to 183 and 81 ppm respectively in the C, B and A-horizons,relative to 21 ppm recorded in the parent pegmatite. These trends reveal the significant enrichment of the REEs contents in the residual profile as compared to the parent rock. The LREEs contents in the B-horizon (177.80 ppm) are much more enhanced than in A and C-horizons that are correspondingly 91.43 and 42.48 ppm. HREEs contents are very low (3 - 6 ppm) in the horizons, relative to LREEs.The weathering profile derived

from the mineralised pegmatite of Ijero area showed negative cerium (Ce/Ce* = 0.27 – 0.56)

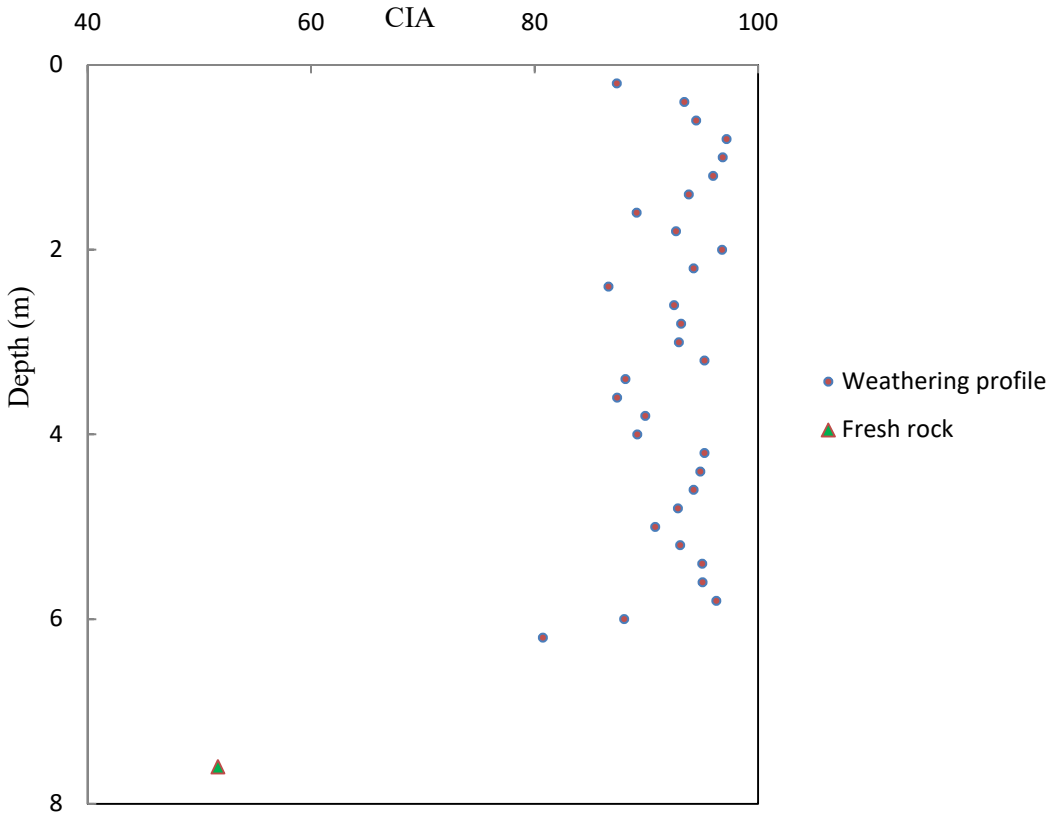

Fig. 4.71: Variation of chemical index of alteration (CIA) with depth in the *in situ*-derived lateritic profile from the mineralised pegmatite of Ofiki area (after Nesbitt and Young, 1982).

anomalies. The relatively enhanced REE contents in the *in situ*-derived residual profile of Ofiki area are possibly due to high degree of chemical weathering in the profile and the relatively higher modal abundance of the REE-bearing accessory mineral phases in the parent rock.

The chondrite-normalised REE patterns for the parent pegmatite bedrock and its *in situ*-derived lateritic profile are presented in Fig. 4.72. The bedrock pegmatite exhibits a slight LREEs enhancement, relative to HREEs showing weak cerium anomaly. The steep-sided HREE patterns aptly demonstrate the strong enrichment in LREEs relative to HREEs in the residual profile and the high degree of weathering of the parent rock.

On the whole, the mineralised pegmatite of Ofiki area and its *in situ*-derived lateritic profile indicate enrichments of rare alkalis and other immobile HFSEs, compared to the non-mineralised pegmatite of the Osu area.

4.3.3.5 Geochemical composition of the weathering profile above the mineralised pegmatite of Iwere area

Major and trace element concentrations of the whole-rock mineralised pegmatite of Iwere area are presented in Table 4.24. The pegmatite is highly siliceous, indicating silica concentrations ranging from 69.26 to 79.36 wt.% with mean concentration of 74.13 wt.%. Alumina contents in the whole-rock pegmatite samples varies between 10.52 and 17.51 wt.%, with a mean concentration of 14.29 wt.%. Fe_2O_3 varies between 0.55 and 2.33 wt.% with mean concentration of 1.15 wt.%.

Na_2O (2.02 – 4.91 wt.%) and K_2O (2.16 – 7.74 wt.%) also range widely in the pegmatite, indicating mean concentrations of 3.08 and 5.53 wt.%, respectively. TiO_2 in the pegmatite ranges between 0.32 and 0.93 wt. %, showing mean concentration of 0.63 wt.%. P_2O_5 concentration in the pegmatite is below 0.30 wt.%.

Barium and strontium respectively show mean concentration of 78 and 24 ppm in the whole-rock pegmatite. Pegmatophile elements, such as Rb, Cs, Sn, Nb and Ta, indicate

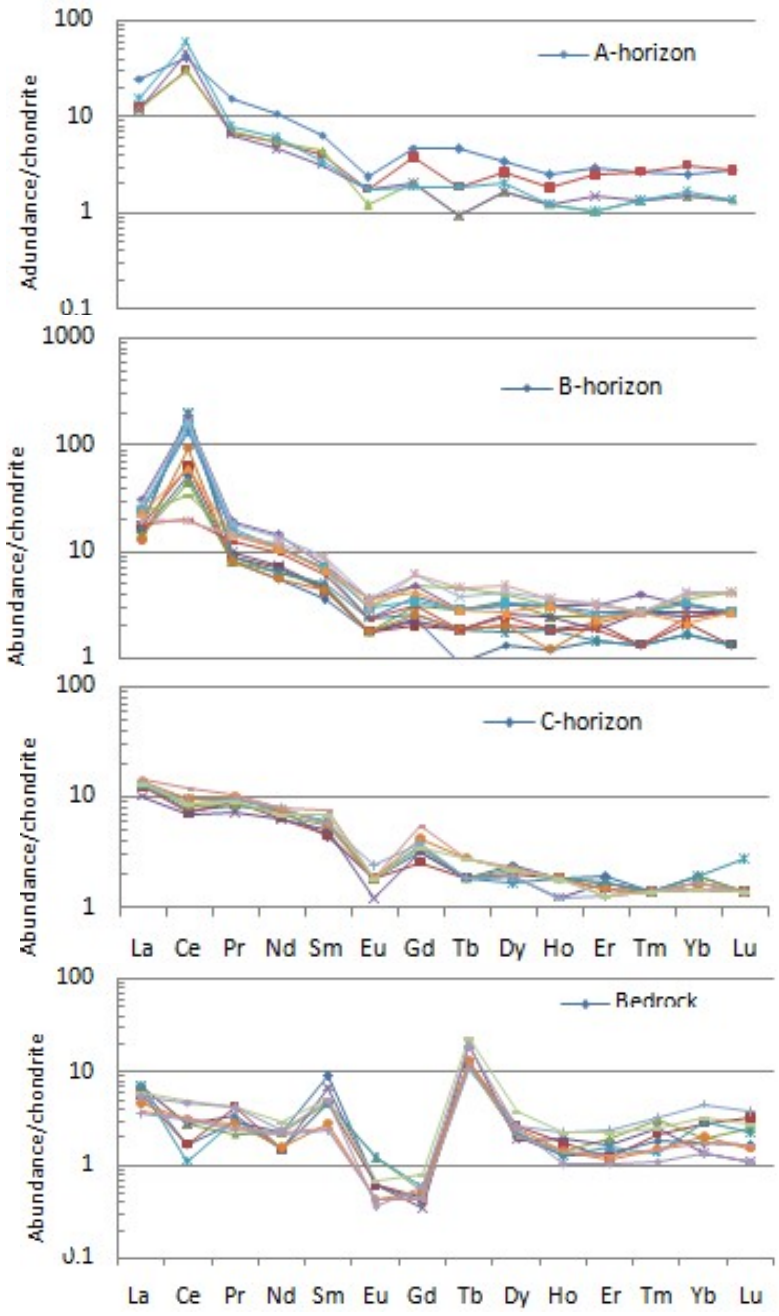

Fig. 4.72. Chondrite-normalised REE patterns for the bedrock and the *in situ*-derived weathering profile of the Ofiki mineralised pegmatite

Table 4.24: Whole–rock major, trace and rare-earth element composition of the mineralised pegmatite of Iwere area

Major oxides	IWP1	IWP2	IWP3	IWP4	IWP5	IWP6	IWP7	IWP8	IWP9	IWP10	Mean	Range
(wt.%)												
SiO_2	77.33	74.44	69.26	68.64	78.16	75.12	74.16	71.05	72.02	75.12	73.53	68.26-78.16
Al_2O_3	10.52	13.86	17.51	17.28	10.56	14.26	14.61	16.12	14.04	14.18	14.29	10.52-17.51
Fe_2O_3	2.33	1.51	0.90	1.92	1.61	0.68	0.55	0.59	0.65	0.74	1.15	0.55-2.33
MnO	0.06	0.08	0.10	0.96	0.05	0.47	0.20	0.01	0.09	0.03	0.21	0.01-0.96
MgO	0.40	0.20	0.14	0.90	0.22	0.09	0.04	0.08	0.70	0.09	0.22	0.04-0.90
CaO	1.10	0.73	0.38	0.97	0.07	1.07	1.21	1.18	0.54	0.69	0.79	0.07-1.21
Na_2O	2.02	2.49	4.40	2.56	3.24	2.18	3.36	4.18	2.22	4.91	3.16	2.02-4.91
K_2O	4.86	5.74	6.33	5.45	4.54	6.27	4.68	6.56	7.74	3.16	5.53	3.16-7.74
TiO_2	0.89	0.58	0.41	0.93	0.48	0.62	0.51	0.32	0.71	0.83	0.63	0.32-0.93
P_2O_5	0.19	0.10	0.20	0.22	0.12	0.03	0.30	0.04	0.06	0.13	0.14	0.03-0.30
LOI	0.76	0.78	0.82	0.82	1.10	0.06	0.78	0.66	0.63	0.57	0.70	0.06-1.10
Total	100.5	100.5	100.5	100.7	100.2	100.9	100.4	100.8	99.4	100.5	100.4	
CIA	49.57	50.99	54.51	59.32	52.75	52.46	55.13	47.53	47.01	53.35	52.23	
µg/g												
Rb	280	108	476	186	171	104	130	261	142	30	188	30-476
Cs	23	26	35	12	16	22	15	19	29	19	22	12-35
Ba	116	97	194	88	138	24	4	86	20	8	78	4-194
Sr	43	32	30	27	35	14	16	22	4	14	24	4-43
Ga	13	27	18	26	23	25	18	25	22	26	22	13-27
Be	14	7	24	15	5	6	15	7	16	25	13	5-25
Sn	12	19	25	13	6	7	12	28	2	11	14	2-28
Nb	17	48	20	19	32	54	10	36	30	44	31	10-54
Ta	13	18	15	37	23	23	13	32	21	39	23	13-75
Y	19	6	12	33	26	15	13	16	8	12	16	6-33
Zn	90	30	50	150	40	5	14	30	30	30	47	5-150
Zr	32	75	49	21	33	12	59	24	29	56	59	12-75
Hf	7	5	3	5	8	10	5	4	8	5	6	3-10

Th	9	8	4	12	5	3	7	10	10	6	7	3-12
U	18	4	10	13	5	2	6	4	9	3	7	2-13

Table 4.24 (Continued)

	IWP1	IWP2	IWP3	IWP4	IWP5	IWP6	IWP7	IWP8	IWP9	IWP10	Mean	Range
La	15.70	9.40	6.90	15.5	9.10	1.20	6.30	3.00	4.00	1.20	7.20	1.20-15.70
Ce	33.60	19.70	14.30	36.8	18.70	2.50	13.50	6.30	9.40	2.10	15.70	2.10-36.80
Pr	3.70	2.20	1.60	4.5	2.30	0.30	1.70	0.80	1.20	0.20	1.80	0.20-4.50
Nd	15.50	8.10	6.40	21.1	9.70	0.80	5.50	2.90	4.10	0.70	7.50	0.70-21.10
Sm	4.00	1.80	1.50	5.6	2.30	0.40	2.40	1.80	2.40	0.20	2.20	0.20-5.60
Eu	0.80	0.30	0.20	0.9	0.50	0.10	0.10	0.10	0.10	0.10	0.30	0.10-0.90
Gd	3.80	1.70	1.20	5.1	3.20	0.50	1.80	2.00	1.90	0.20	2.10	0.20-5.10
Tb	0.80	0.30	0.20	1.1	0.60	0.10	0.40	0.40	0.30	0.10	0.40	0.10-1.10
Dy	4.60	1.60	1.10	6.5	3.70	0.60	1.90	2.10	1.30	0.20	2.40	0.20-6.50
Ho	0.60	0.30	0.20	0.9	0.70	0.10	0.40	0.30	0.20	0.10	0.40	0.10-0.90
Er	1.50	0.80	0.50	2.4	2.30	0.30	1.50	1.00	0.50	0.10	1.10	0.10-2.40
Tm	0.20	0.10	0.10	0.5	0.30	0.10	0.40	0.20	0.10	0.10	0.20	0.10-0.50
Yb	1.40	0.80	0.50	3.5	2.10	0.40	3.80	1.30	0.80	0.20	1.50	0.20-3.80
Lu	0.20	0.10	0.10	0.4	0.30	0.10	0.70	0.20	0.10	0.00	0.20	0.00-0.70
LREE	77.10	43.20	32.20	89.5	45.80	5.70	31.30	16.90	23.10	4.70	36.90	4.70-89.70
HREE	9.30	4.10	2.60	15.3	10.10	1.70	9.10	5.50	3.30	0.80	6.20	0.80-15.90
∑REE	86.40	47.20	34.80	104.8	55.80	7.40	40.40	22.40	26.40	5.50	43.10	5.50-105.5
LREE/HREE	8.30	10.70	12.20	5.8	4.50	3.30	3.50	3.10	7.00	5.90	6.00	5.90-5.70
Ce/Ce*	0.25	0.32	0.37	0.24	0.31	0.93	0.37	0.54	0.46	0.95	0.36	0.95-0.24
Eu/Eu*	0.28	0.40	0.46	0.22	0.32	0.87	0.21	0.24	0.14	1.77	0.32	1.54-0.22
La/Yb	11.21	11.75	13.80	4.43	4.33	3.00	1.68	2.31	5.00	6.00	4.90	6.00-4.19

moderately high levels in the pegmatite, with corresponding mean contents of 188, 22, 14, 31 and 23 ppm. The mean Y, Zr, Hf, Th and U concentrations in the pegmatite are respectively 16, 39, 6, 7 and 7 ppm. The Iwere mineralised pegmatite is moderately enhanced in pegmatophile and other high field strength elements (HFSEs) when compared to the barren Osu pegmatite.

The total REE of the Iwere mineralised pegmatite is 43 ppm. Light rare-earth elements (LREEs) show enhanced mean concentration of 37 ppm, relative to the HREEs that indicate mean contents of 6 ppm. The pegmatite shows negative Eu anomaly (Eu/Eu* = 0.32) and Ce (Ce/Ce* = 0.36) anomalies (Table 4.24). The geochemical abundances of the LREEs and HREEs in the pegmatites are possible reflection of the modal abundances of accessory mineral phases that host the REEs in the pegmatite. These minerals include zircon, garnet, apatite, rutile, ilmenite and magnetite.

Geochemical data of the weathering profile derived from the mineralised pegmatite of Iwere area are presented in Table 4.25, while chemical variations and dispersion trends within the profile are exemplified in Fig. 4.73. The Table shows the A-horizon to be more siliceous than the B and C-horizons. The silica concentrations in the A-horizon vary between 77.45 and 87.20 wt.%, with mean contents of 81.29 wt.%. The B and C-horizon respectively show mean concentrations of 67.45 and 68.50 wt.%. The silica abundances in the residual profile are reflected as prominent quartz peaks in the X-ray charts (Figs. 4.46) of the constituting horizons of the residual profile. Alumina is slightly enhanced in the weathering profile relative to the parent rock. The mean concentration of Al_2O_3 in the parent rock, C, B and A-horizons are correspondingly 14.29, 16.86, 17.25 and 7.98 wt.%.

The minor enhancement of alumina in the residual profile is due to loss of alkalis and alkaline earth elements.

Fe_2O_3 is enriched in the weathering profile when compared to the pegmatite parent rock. It has concentrations of 1.15, 1.18, 3.15 and 2.46 wt.% in the rock, C, B and A-horizons. CaO showed depletion in the residual profile relative to the parent rock.The concentrations of CaO are respectively 0.80, 0.75, 0.30 and 0.06 wt.% in the rock, C, B and A-horizons. Na_2O and K_2O are mildly leached in the weathering profile relative to the

Table 4.25: Major, trace and rare-earth element composition of the lateritic profile derived from mineralised pegmatite of Iwere

Sample #	A1	A2	A3	A4	B1	B2	B3	B4	B5	B6	B7	B8	C1	C2	C3	C4	C5	C6	C7	C8
Depth (m)	0.2	0.4	0.6	0.8	1.0	1.2	1.4	1.6	1.8	2.0	2.2	2.4	2.6	2.8	3.0	3.2	3.4	3.6	3.8	4.0
wt. %																				
SiO_2	87.20	81.65	78.91	77.45	69.73	68.90	67.90	65.90	63.82	66.64	67.90	68.80	68.94	67.50	65.61	67.30	70.55	69.77	68.95	69.34
Al_2O_3	4.45	8.12	9.76	10.60	15.80	15.65	16.70	18.36	19.80	17.00	16.90	17.80	16.76	17.60	18.0	16.50	16.27	16.20	16.21	17.36
Fe_2O_3	1.58	2.20	2.57	3.49	3.34	3.86	3.61	3.41	3.65	3.18	2.20	1.95	1.87	1.69	1.14	0.95	1.00	0.75	1.39	0.68
MnO	0.05	0.04	0.04	0.07	0.03	0.02	0.03	0.03	0.02	0.03	0.03	0.02	0.02	0.01	0.02	0.03	0.02	0.03	0.06	0.02
MgO	0.15	0.25	0.08	0.11	0.14	0.16	0.15	0.13	0.17	0.15	0.15	0.14	0.12	0.09	0.08	0.08	0.06	0.03	0.13	0.08
CaO	0.03	0.06	0.07	0.07	0.08	0.13	0.18	0.18	0.28	0.38	0.49	0.64	0.60	0.94	0.86	0.80	0.39	0.67	1.07	0.66
Na_2O	0.19	0.29	0.16	0.18	1.63	2.07	2.13	2.63	2.21	2.38	2.13	2.46	2.89	3.15	3.62	3.61	2.07	2.43	3.13	3.06
K_2O	3.27	3.41	3.88	3.91	3.23	3.85	3.84	4.43	4.32	4.69	4.41	2.80	4.39	4.22	4.93	3.68	5.84	5.63	4.76	5.24
TiO_2	0.47	0.26	0.47	0.37	0.83	0.46	1.41	0.74	0.49	0.52	1.68	1.07	0.47	0.33	2.19	0.87	0.21	0.45	0.43	0.15
P_2O_5	0.04	0.04	0.04	0.04	0.04	0.04	0.04	0.04	0.08	0.03	0.03	0.03	0.13	0.04	0.04	0.03	0.04	0.03	0.03	0.03
LOI	2.16	2.99	3.89	3.61	4.65	4.34	3.97	3.81	4.80	4.60	3.77	3.75	3.41	4.89	3.29	2.66	3.30	3.71	3.45	3.35
Total	99.59	99.60	99.47	99.90	99.50	99.48	99.96	99.66	99.64	99.60	99.69	99.46	99.62	99.61	99.78	99.51	99.75	99.70	99.61	99.97
CIA (%)	66.09	78.39	79.30	82.17	83.76	80.34	79.34	74.17	73.87	71.49	70.21	68.50	65.05	66.15	66.59	62.76	58.33	58.74	61.46	60.48
Trace element																				
Li	24	37	37	44	55	73	71	74	99	97	107	93	97	102	80	80	75	78	110	133
Rb	44	59	59	72	87	103	100	114	132	127	116	98	112	86	89	93	172	125	79	86
Cs	1	2	3	5	5	6	6	6	7	8	7	5	6	6	5	6	8	6	6	8
Ba	29	24	15	38	28	30	45	26	52	37	59	27	50	77	80	109	164	116	105	123
Sr	12	12	14	15	18	21	23	24	26	23	28	28	29	32	32	33	36	35	31	38
Ga	15	39	19	42	26	39	17	77	23	27	20	39	18	30	19	47	25	36	18	23
Be	4	3	8	13	2	22	17	32	12	22	38	22	16	32	23	13	31	33	23	22
Sn	5	3	7	5	13	8	24	31	22	17	38	12	21	33	12	19	31	23	17	32
Nb	3	4	12	19	29	24	35	22	32	45	58	24	23	31	19	54	23	36	24	27
Ta	2	5	7	13	22	18	13	17	23	29	43	16	12	25	12	42	12	23	18	14
Y	14	13	16	16	19	25	33	20	23	13	30	10	28	21	39	18	25	17	28	12
Zn	7	12	12	25	17	38	17	17	27	25	18	33	13	24	12	33	19	26	13	15
Zr	90	75	82	95	89	90	92	82	45	34	54	24	34	15	32	67	33	56	33	28
Hf	7	13	13	9	11	17	13	15	13	26	15	6	18	22	36	13	33	12	4	10
Th	4	8	6	7	9	7	7	13	26	23	9	13	9	17	15	8	13	10	6	10
U	2	2	3	7	6	4	4	3	3	3	4	3	4	2	2	4	2	3	3	3

Table 4.25: (Continued)

Sample #	A1	A2	A3	A4	B1	B2	B3	B4	B5	B6	B7	B8	C1	C2	C3	C4	C5	C6	C7	C8
Depth (m)	0.2	0.4	0.6	0.8	1.0	1.2	1.4	1.6	1.8	2.0	2.2	2.4	2.6	2.8	3.0	3.2	3.4	3.6	3.8	4.0
La	10.6	8.9	10.4	11.2	11.6	12	13.4	11.7	8.1	7.5	6.7	5.9	5.6	6.3	4.5	4.5	3.5	4.2	4.3	4.2
Ce	27.38	22.3	29.27	41.2	39	37.7	29	24.9	14	12.4	10.6	8.13	7.7	6.9	5.88	8.29	6.63	5.83	8.08	8.36
Pr	2.4	1.8	2.2	2.3	2.8	2.4	2.8	2.5	1.8	1.6	1.5	1.3	1.1	1.5	0.9	0.9	0.8	1.1	1	1.3
Nd	9.1	7.3	9.1	8.9	9.2	9.4	11.5	9.4	7.1	6.9	5.7	5.5	4.7	5.2	3.9	4.1	4.5	3.9	4.5	4.8
Sm	2.1	1.4	1.6	1.6	1.8	1.8	2	2.1	1.6	1.6	1.4	1.1	1.1	1.4	1.1	1.2	1.1	1.1	1.3	1.2
Eu	0.2	0.2	0.2	0.3	0.3	0.4	0.3	0.3	0.4	0.3	0.2	0.3	0.2	0.3	0.3	0.3	0.3	0.2	0.3	0.3
Gd	1.2	1	1.3	1.6	1.4	1.4	1.4	1.4	0.9	0.12	1.3	0.9	1	1	1	0.9	1	1.1	1.2	1.3
Tb	0.1	0.1	0.1	0.1	0.01	0.1	0.1	0.1	0.1	0.2	0.1	0.1	0.1	0.1	0.2	0.1	0.1	0.1	0.2	0.02
Dy	0.7	1	1.2	0.7	0.9	1.2	1	0.9	1	1.2	0.9	1.1	1	1	0.9	0.9	1	1.8	1.9	1.7
Ho	0.2	0.2	0.2	0.1	0.2	0.2	0.1	0.2	0.2	0.2	0.2	0.2	0.2	0.2	0.1	0.2	0.2	0.3	0.4	0.3
Er	0.4	0.5	0.5	0.2	0.3	0.4	0.5	0.5	0.4	0.3	0.6	0.4	0.5	0.6	0.4	0.6	0.3	1	1.2	1
Tm	0.1	0.1	0.1	0.1	0.1	0.1	0.1	0.1	0.1	0.1	0.1	0.1	0.1	0.1	0.1	0.1	0.1	0.1	0.2	0.2
Yb	0.5	0.4	0.5	0.7	0.7	0.5	0.6	0.6	0.6	0.4	0.5	0.7	0.8	0.9	0.6	0.6	0.7	1.3	1.5	1.2
Lu	0.1	0.1	0.1	0.1	0.1	0.1	0.1	0.1	0.1	0.1	0.1	0.1	0.1	0.1	0.1	0.1	0.2	0.3	0.3	0.3
LREE	53.0	42.9	54.1	67.1	66.1	65.1	60.4	52.3	33.8	30.4	27.4	23.1	21.4	22.6	17.6	20.2	17.8	17.4	20.7	22.1
HREE	2.1	2.4	2.7	2.0	2.3	2.6	2.5	2.5	2.5	2.5	2.5	2.7	2.8	3.0	2.4	2.6	2.6	4.9	5.7	4.7
∑REE	55.1	45.3	56.8	69.1	68.4	67.7	62.9	54.8	36.3	32.9	29.9	25.8	24.2	25.6	20.0	22.8	20.4	22.3	26.4	26.8
LREE/HREE	26.2	18.9	21.0	34.6	29.6	26.0	25.1	21.9	14.5	13.2	11.9	9.6	8.6	8.5	8.3	8.8	7.9	4.6	4.6	5.7
Ce/Ce*	0.34	0.39	0.37	0.41	0.36	0.37	0.29	0.30	0.32	0.33	0.34	0.34	0.37	0.28	0.39	0.47	0.50	0.37	0.45	0.38
Eu/Eu*	0.35	0.47	0.39	0.43	0.43	0.50	0.41	0.40	0.66	1.57	0.42	0.69	0.53	0.58	0.65	0.66	0.65	0.51	0.55	0.55
La/Yb	21.20	22.25	20.80	16.00	16.57	24.00	22.33	19.50	13.33	18.75	13.40	8.43	7.00	7.00	7.50	7.50	5.00	3.23	2.87	4.00

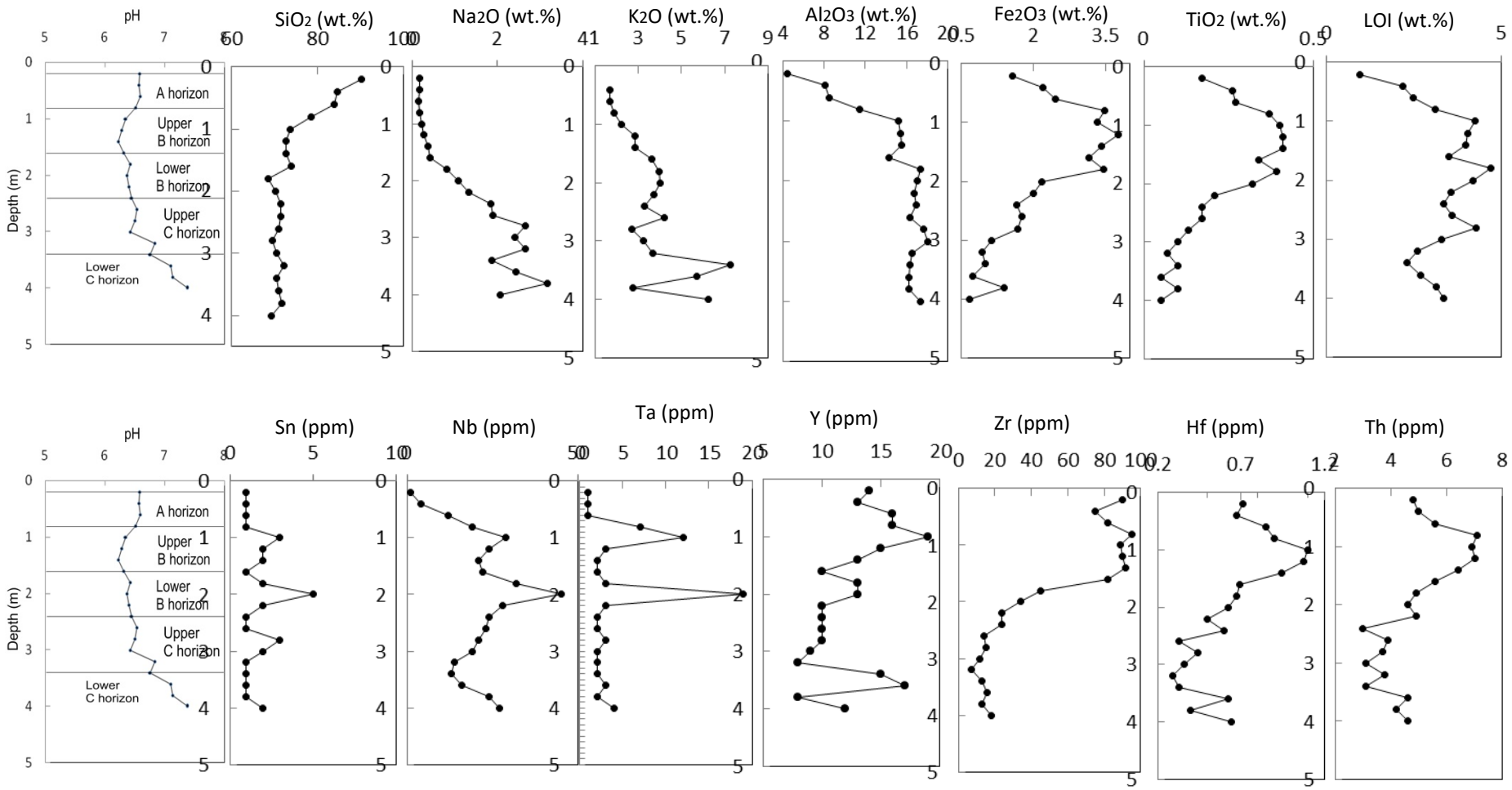

Fig. 4.73: Chemical elements distribution with depth in the weathering profile of the mineralised pegmatite of Iwere area

parent rock.The mean concentrations of Na_2O are 3.16, 2.99, 2.21 and 0.72 wt.% in the parent rock, C, B, and A-horizons, respectively; while those of K_2O are 5.53, 4.84, 3.95, and 3.44 wt.%. The Na_2O and K_2O values show incipient weathering of the parent rock.

TiO_2 is enhanced in the weathering profile relative to the parent rock, with concentrations of 0.63, 0.64, 0.90 and 0.39 wt.%, respectively in the whole-rock pegmatite, C, B and A-horizons. The slightly enhanced concentration of TiO_2 in the weathering profile can be attributed to the relative stability of rutile in the profile (Fig. 4.46 and Fig. 4.47). P_2O_5 is strongly depleted in the lateritic profile relative to the bedrock, as it shows mean concentrations below 0.04 wt. % in all the constituting horizons of the residual profile.

The mean LOI value of the whole-rock pegmatite of Iwere area is 0.73 wt.% (Table 4.24); while average LOI values of 3.17, 3.95 and 2.19 wt.% were correspondingly recorded for C, B and A-horizon of the lateritic profile (Table 4.25 and Fig. 4.73). The Al_2O_3 –SiO_2-Fe_2O_3 (Schellmann, 1983) ternary plot indicated that most of the laterite samples are kaolinised (Fig. 4.74). The clustering of the A-horizon samples in the SiO_2-axis (Fig. 4.74) showed the samples to be highly siliceous. The mean CIA value of 52.23 of the whole-rock samples indicates relatively unaltered bedrock, while CIA values of 62.45, 75.21 and 76.49 respectively in the C, B and A-horizons portray moderate extents of chemical weathering of the residual profile. These trends are also illustrated in Fig. 4.75, which shows alteration intensity increasing from low value in the whole-rock sample to higher value in the more intensely altered lateritic profile (Nesbitt and Young, 1982).

The trace element concentrations of the residual profile developed over the mineralised pegmatite of Iwere area are given in Table 4.25. Due to the incipient weathering, Ba and Sr contents in the bedrock and weathering profile are more or less constant. For instance,Ba contents in the parent rock, C, B and A-horizon are correspondingly 78, 103, 48 and 27 ppm; while those of Sr are 24, 33, 48 and 13 ppm in the same horizons.

Rubidium indicates low extent of depletion in the lateritic profile relative to the bedrock pegmatite. This could possibly results from the incipient weathering of the rock. Rubidiumhas mean concentrations of 188, 105, 109 and 59 ppm in the parent rock, C, B and A-horizons, respectively.

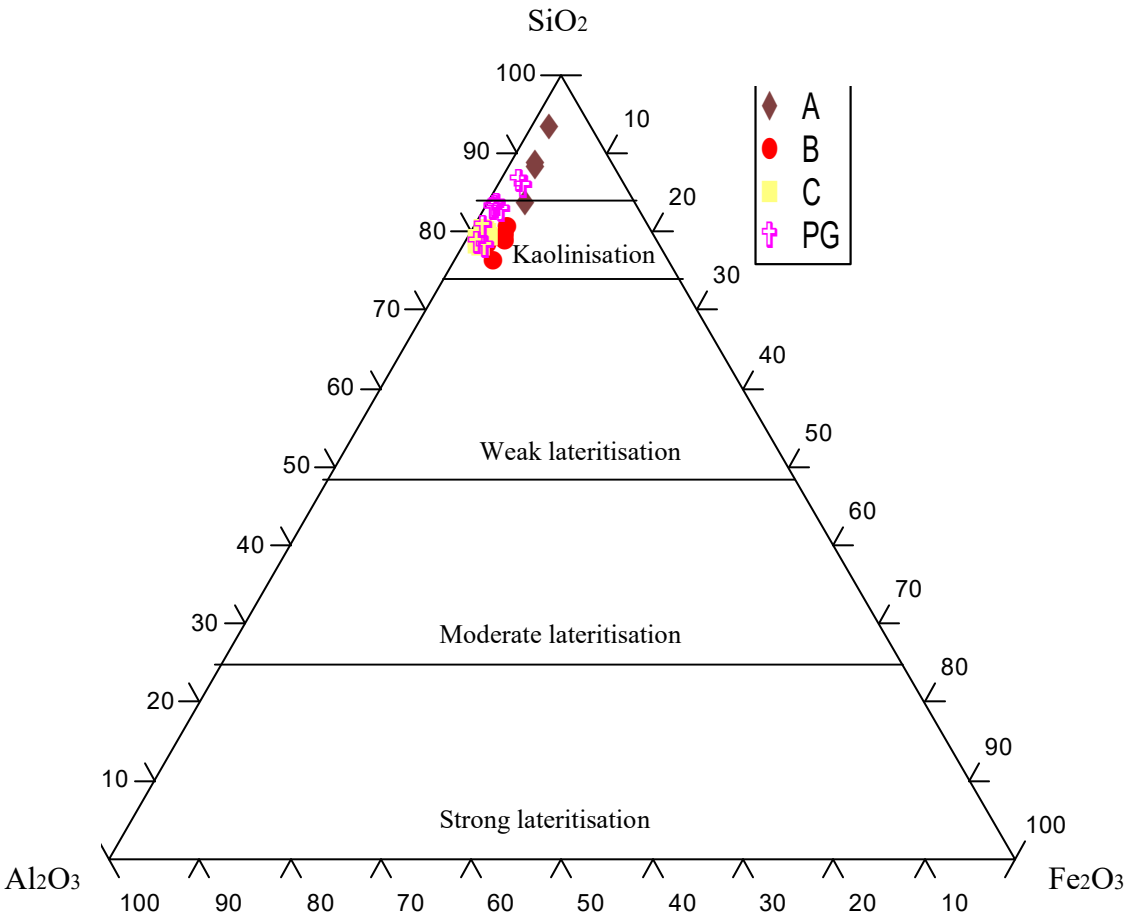

Fig. 4.74: Al_2O_3-SiO_2-Fe_2O_3 ternary plot for the lateritic profile derived from the mineralised pegmatite of Iwere area (after Schellmann, 1983)

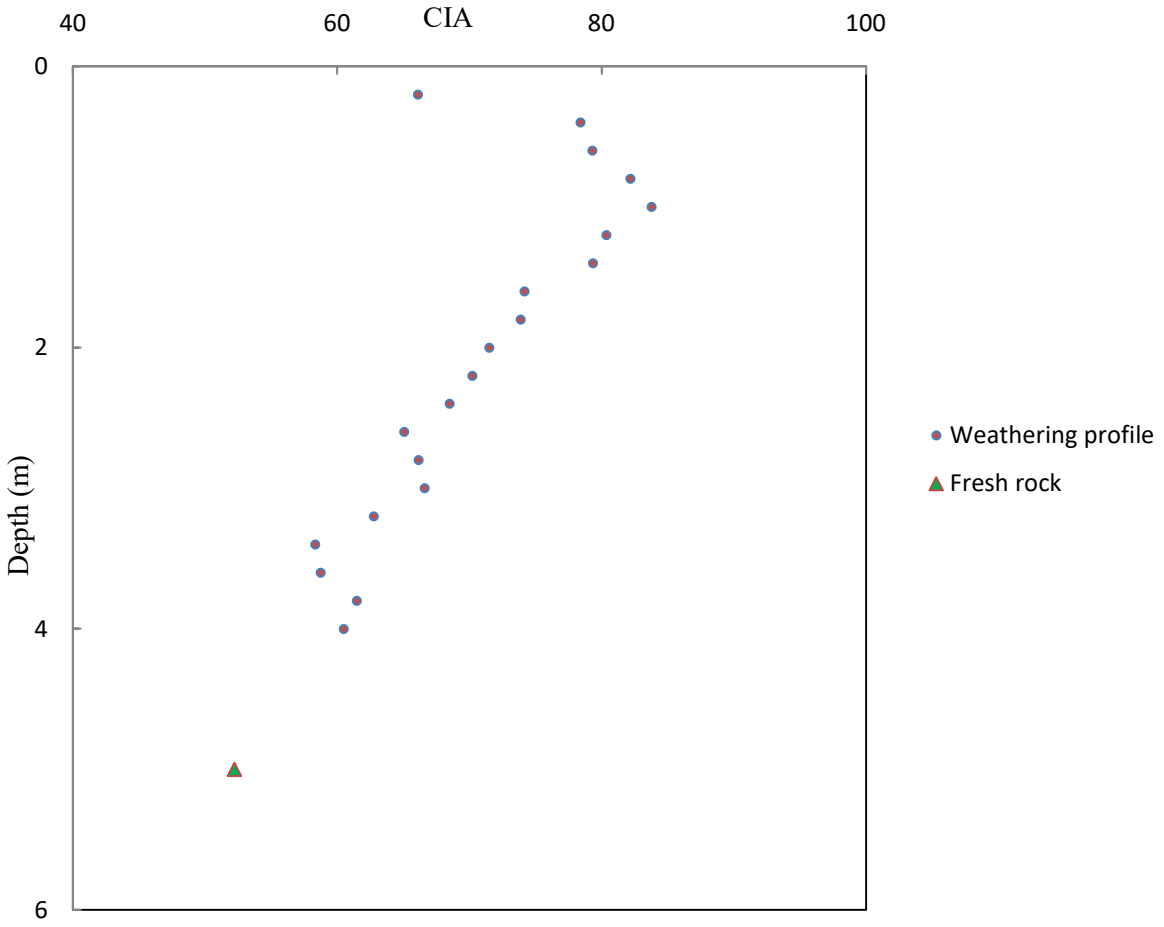

Fig. 4.75: Variation of chemical index of alteration (CIA) with depth in the *in situ*-derived lateritic profile from the mineralised pegmatite of Iwere area (after Nesbitt and Young, 1982).

On the contrary, Cs show strong depletions in the weathering profile when compared with the bedrock composition. Cesium indicates average contents of 22, 6, 6 and 3 ppm in the parent rock, C, Band A-horizons, respectively. Beryllium and Ga also indicate low enrichements in the weathering profile relative to the parent rock due to incipient weathering. The mean concentrations of Be in the parent, C, B and A-horizons are correspondingly 13, 24, 21 and 7 ppm,while those of Ga are 22, 27, 34 and 29 ppm in the same horizons.

Contrary to expectations, pegmatite petrogenetic immobile elements, including Sn, Nb and Ta, show low extent of enrichments in the weathering horizons relative to the whole-rock samples. The mean Sn contents in the parent rock, C-, B- and A-horizons are 14, 24, 29 and 4 ppm; while Nb concentrations are 31, 38, 46 and 10 ppm in the same horizons. Tantalum contents are respectively 23, 29, 31 and 7 ppm in the bedrock, C-, B- and A-horizons. These geochemical trends may perhaps be connected to the fact that the rock is incipiently weathered, and there have been low extents of redistributions/ remobilisation of some elements within the horizons of the weathering profile. Yttrium, Zr, Hf and Th more or less retain their bedrock concentrations in the weathering profile (Table 4.25); while U suffers strong depletion in the weathering profile due to the prevailing oxic and acidic conditions of the weathering environment.

The total REEs contents of the residual weathering profile of the mineralised pegmatite of Iwere area ranged from 24 to 48 and 56 ppm respectively in the C, B and A-horizons, relative to 43 ppm recorded in the parent pegmatite. These trends reveal the marginal enrichment of the REEs contents in the residual profile as compared to the parent rock. The LREEs contents in the A-horizon (54 ppm) are more enhanced than in B and C-horizons that correspondingly indicate 45 and 20 ppm. HREEs values (2 - 4 ppm) are low in the constituting horizons, relative to LREEs. The weathering profile derived from the mineralised pegmatite of Iwere area portrays negative cerium ($Ce/Ce^*=0.33 – 0.40$) and europium ($Eu/Eu^*=0.41-0.63$) anomalies. The relatively low REE content in both fresh pegmatite and its *in situ*-derived residual is possibly a reflection of the moderate modal abundances of the REE-bearing accessory mineral phases in the parent rock.

The chrondrite-normalised REE patterns (Fig. 7.76) show low enrichment in LREEs relative to the HREEs in whole-rock pegmatite, displaying generally flat REE patterns with respect to the normalised upper continental crust value (Sun and McDonough, 1989). On the contrary, the horizons of the *in situ*-derived weathering profile show similar trends but strong depletions in LREEs relative to HREEs.

On the whole, the mineralised pegmatite of Iwere area and its *insitu*-derived lateritic profile indicate moderate enrichments of rare alkalis and other immobile HFSEs, as compared to the Osu non-mineralised pegmatite and its residual profile.

4.4. The laterite-forming environment

The evolution and composition of lateritic profiles largely depend on bedrock character, climate and the chemical character of the aqueous media (Tardy, 1997; Butt *et al.*, 2000; Giorgis *et al.*, 2014). In the study areas the climatic condition, exemplified by high annual mean temperature (29.9°C) and high humidity, are consistent with those suggested by Tardy *et al.* (1993) as typical laterite-forming conditions. The chemistry of the aqueous media appears to have greater control during laterite formation, as it facilitates selective leaching of the alkalis and silicon with the eventual enrichment of iron and other immobile (residual) elements. The processes of leaching and residual concentration of elements were accomplished through precise combination of pH and Eh (Giorgis *et al.*, 2014).

The prevailing pH and Eh conditions for the formation of the investigated pegmatiteprofiles are presented in Appendix 9 and represented on the Eh-pH plot (Fig. 4.77), following Garrels and Christ (1965) and Norton (1973). Despite the low Fe_2O_3/Al_2O_3 ratios of the bedrock pegmatites, the formation of the pegmatite profiles occurred at low pH (4.49-6.45) and high Eh (0.2–0.36) values,*i.e*, under acidic and oxidising conditions. This assertion is also indicated on the Eh-pH plot (Fig. 4.77),where the pegmatite profiles plot in the acidic-oxidant field showing the combined influence of acidic rainwater and groundwater in the formation of the residual lateritic profiles. The neutral to very slightly alkaline pH conditions encountered in few lower C-horizons were mainly due to the presence partially altered feldspar (alkali-rich) materials (Appendix

9).The Eh and pH conditions, more than bedrock character, possibly resulted in pegmatite laterite profiles.

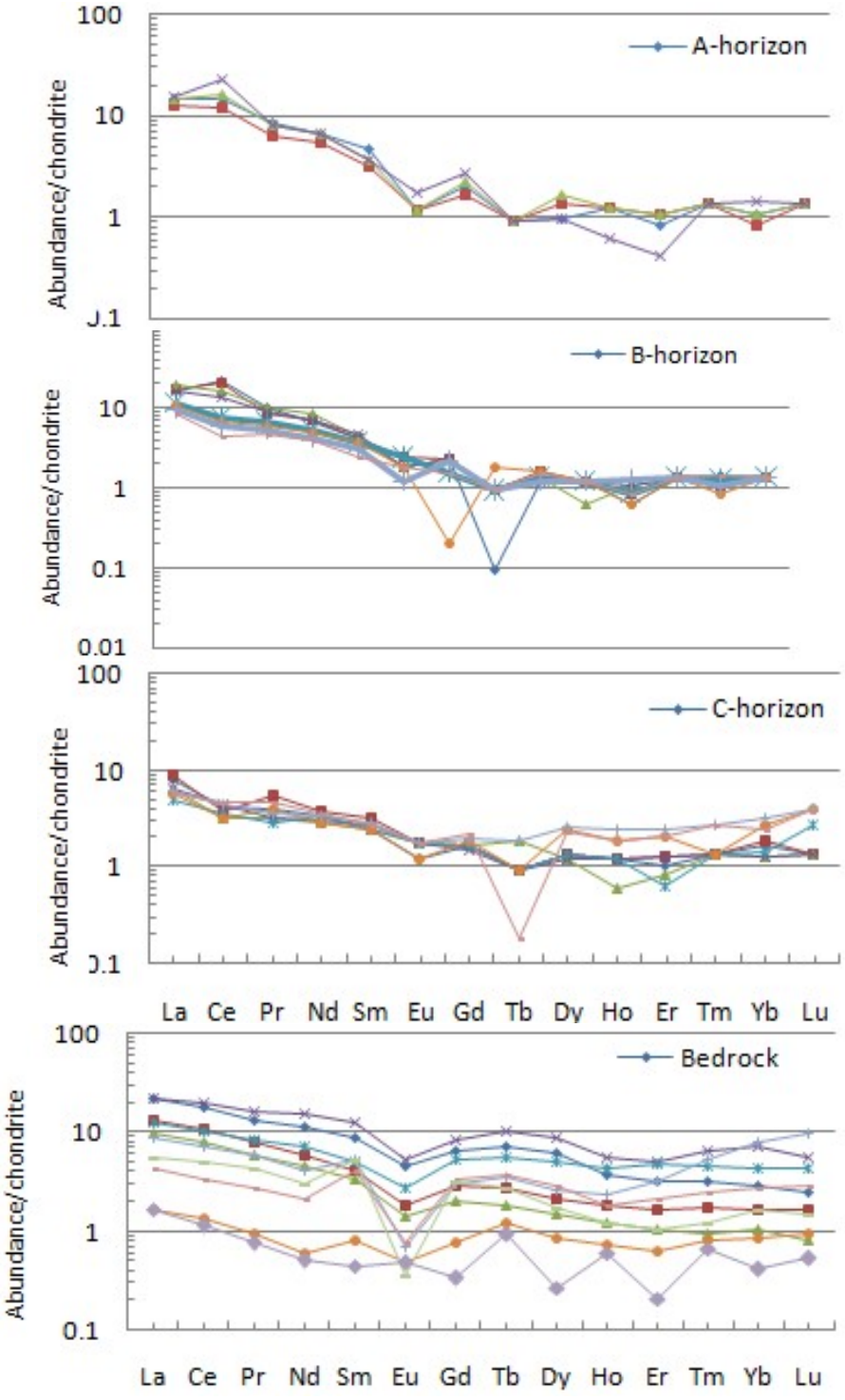

Fig. 4.76.

Chondrite-normalised REE patterns for the bedrock and the *in situ*-derived weathering profile of the Iwere mineralised pegmatite.

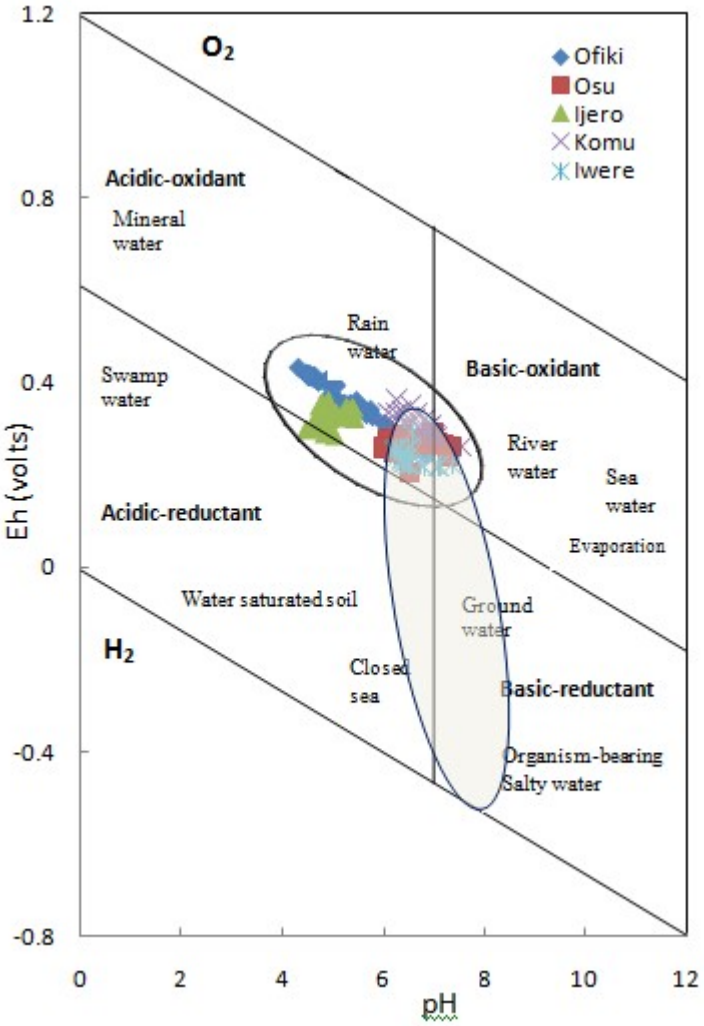

Fig. 4.77: Eh-pH plot showing conditions and environments for the formation of laterites (modified after Garrels and Christ, 1965 and Norton, 1973)

4.5. Geochemical criteria for discriminating between rare metal-bearing and barren pegmatites under lateritic covers

4.5.1 Correlation analysis of the bulk geochemical data of the weathering profiles

Pearson's product-moment coefficients of linear correlation were computed for relevant pegmatite petrogenetic elementsat 0.05 significance level, so as to isolate valuable element pairs with useful geochemical patterns within the investigated residual profiles. The element pairs that portray consistently high correlations were employed in deciphering the relative enhancements/depletions in the weathering profiles and also in identifying suitable geochemical ratios, as well as, in plotting relevant discrimination diagrams to distinguish between rare metal-bearing and barren pegmatites underneath lateritic profiles.

The correlation matrices for the bulk geochemical data for the barren pegmatite profile at Osu and the respective mineralised pegmatite residual profiles at Ijero, Komu, Ofiki and Iwere areas are correspondingly displayed in Table 4.26 through Table 4.30. Correlation matrices are very informative, as they may indicate the discriminating variables (i.e. geochemical element pairs) that are directly or indirectly linked to the underlying causative geological processes (Rupasinghe *et al*., 1994; Swan and Sandilands, 1995; Fernando *et al*., 1996; Ranasinghe*et al*., 2005; Broster *et al*., 2009).

A number of significant interelement correlations were deciphered in the bulk chemical data of the residual profile of the Osubarren and other mineralised pegmatites of the study areas. For instance, SiO_2 in the residual profiles of the Osubarren pegmatite is positivelycorrelated with CaO (0.82), Na_2O (0.93) and Ba (0.60) (Table 4.26).These correlations possibly indicate the alkaline characters of the protolith pegmatite and the similar behavior of these elements during incipient stage of weathering.

The residual character of Al_2O_3 with Fe_2O_3 (0.82), Ga (0.92), Sn (0.89), Nb (0.76), Ta (0.52) and U (0.90) (Table 4.26) in the Osunon-mineralised pegmatite residual profile are all indicated by the high positive correlations amongst these element pairs. Fe_2O_3, likewise, demonstrates geochemical enrichment with other elements in the Osu weatheringprofile by indicating moderate to high positive correlations with TiO_2 (0.50), Ta (0.46), Sn

Table 4.26: Correlation matrix for the major and trace elements of the lateritic profile derived from the barren pegmatite of Osu area

	SiO_2	Al_2O_3	Fe_2O_3	MnO	MgO	CaO	Na_2O	K_2O	TiO_2	P_2O_5	Li	Rb	Cs	Ba	Sr	Ga	Be	Sn	Nb	Ta	Y	Zn	Zr	Hf	Th	U
SiO_2	1.00																									
Al_2O_3	-0.99	1.00																								
Fe_2O_3	-0.86	**0.82**	1.00																							
MnO	0.**87**	-0.88	-0.75	1.00																						
MgO	0.36	-0.41	-0.13	**0.51**	1.00																					
CaO	**0.82**	-0.82	-0.63	**0.87**	0.44	1.00																				
Na_2O	**0.93**	-0.93	-0.88	**0.93**	0.43	**0.82**	1.000																			
K_2O	0.15	-0.17	-0.42	0.23	-0.16	-0.04	.033	1.00																		
TiO_2	-0.14	0.10	**0.50**	0.04	0.30	0.27	-0.15	-0.62	1.000																	
P_2O_5	0.30	-0.31	-0.11	0.19	-0.14	0.38	0.23	-0.07	0.32	1.00																
Li	-0.76	**0.74**	**0.72**	-0.77	-0.45	-0.73	-0.76	-0.06	0.07	-0.02	1.00															
Rb	-0.29	0.31	-0.07	-0.10	-0.32	-0.30	-0.09	0.40	-0.28	-0.14	0.22	1.00														
Cs	-0.53	**0.52**	**0.55**	-0.44	-0.35	-0.36	-0.55	-0.15	0.24	0.03	**0.67**	0.31	1.00													
Ba	**0.60**	-0.60	-0.44	**0.61**	0.08	**0.67**	**0.52**	-0.01	0.23	0.34	-0.43	-0.14	0.03	1.00												
Sr	-0.18	0.16	0.09	-0.07	-0.10	0.00	-0.13	-0.03	0.29	0.11	0.04	0.31	0.08	0.41	1.00											
Ga	-0.94	**0.92**	**0.85**	-0.87	-0.39	-0.87	-0.92	-0.11	0.10	-0.29	**0.81**	0.30	**0.56**	-0.54	0.23	1.00										
Be	-0.15	0.13	0.30	-0.27	0.08	-0.18	-0.27	-0.37	0.10	-0.06	0.16	-0.25	0.17	-0.04	-0.09	0.26	1.00									
Sn	-0.92	**0.89**	**0.81**	-0.86	-0.35	-0.91	-0.89	0.02	-0.00	-0.33	**0.77**	0.25	**0.48**	-0.56	0.17	**0.97**	0.23	1.00								
Nb	-0.81	**0.76**	**0.82**	-0.78	-0.37	-0.77	-0.84	0.01	0.10	-0.14	**0.82**	0.10	**0.62**	-0.44	0.04	**0.90**	0.29	**0.91**	1.00							
Ta	-0.54	**0.52**	**0**.46	-0.44	-0.41	-0.41	-0.53	0.10	-0.01	-0.10	**0.48**	0.35	**0.59**	-0.06	0.13	**0.53**	0.00	**0.50**	**0.54**	1.00						
Y	-0.37	0.34	**0.61**	-0.29	0.26	-0.20	-0.36	-0.41	**0.54**	-0.18	0.34	-0.15	**0.54**	-0.12	-0.08	0.38	0.24	0.35	**0.47**	0.21	1.00					
Zn	0.03	-0.06	0.24	0.04	0.02	0.28	-0.08	-0.34	**0.51**	0.22	0.06	-0.34	**0.55**	0.45	0.07	0.02	0.26	-0.05	0.23	0.12	**0.57**	1.00				
Zr	**0.68**	-0.72	-0.30	**0.70**	**0.68**	**0.80**	**0.64**	-0.23	**0.51**	0.35	-0.54	-0.54	-0.27	**0.62**	0.02	-0.66	0.12	-0.66	-0.50	-0.44	0.17	0.39	1.00			
Hf	-0.25	0.19	**0.59**	-0.16	0.20	-0.13	-0.27	-0.27	**0.54**	0.14	0.36	-0.32	0.37	-0.10	-0.26	0.31	0.42	0.30	**0.53**	-0.00	**0.68**	**0.50**	0.28	1.00		
Th	-0.33	.030	**0.63**	-0.24	0.05	-0.11	-0.43	-0.58	**0.63**	-0.00	0.26	-0.28	**0.59**	0.26	0.10	0.35	0.45	0.34	0.43	0.03	**0.73**	**0.67**	0.24	**0.66**	1.00	
U	-0.92	**0.90**	**0.84**	-0.85	-0.24	-0.89	-0.89	-0.17	0.11	0-.31	**0.74**	0.22	**0.51**	-0.60	0.15	**0.95**	0.27	**0.94**	**0.85**	0.37	0.43	0.01	-0.60	0.37	0.37	1.00

Table 4.27: Correlation matrix for the major and trace elements of the lateritic profile derived from the mineralised pegmatite of Ijero area

	SiO_2	Al_2O_3	Fe_2O_3	MnO	MgO	CaO	Na_2O	K_2O	TiO_2	P_2O_5	Li	Rb	Cs	Ba	Sr	Ga	Be	Sn	Nb	Ta	Y	Zn	Zr	Hf	Th	U
SiO_2	1.00																									
Al_2O_3	-0.96	1.00																								
Fe_2O_3	-0.74	**0.53**	1.00																							
MnO	0.05	-0.06	0.04	1.00																						
MgO	0.14	-0.33	0.36	0.42	1.00																					
CaO	0.23	-0.4	0.27	**0.48**	**0.71**	1.00																				
Na_2O	0.46	-0.46	-0.41	-0.07	0.23	0.08	1.00																			
K_2O	-.009	-0.05	-0.01	-0.39	0.04	-0.22	**0.61**	1.00																		
TiO_2	-0.57	0.35	**0.91**	-0.05	**0.52**	0.35	-0.28	0.06	1.00																	
P_2O_5	-0.37	0.18	**0.72**	0.35	**0.62**	**0.61**	-0.28	-0.22	**0.76**	1.00																
Li	-0.19	0.02	**0.48**	-0.21	0.40	0.32	-0.02	0.34	**0.69**	0.40	1.00															
Rb	-0.09	-0.09	0.40	-0.25	0.38	0.29	0.17	**0.55**	**0.57**	0.33	**0.91**	1.00														
Cs	-0.28	0.11	**0.60**	0.02	0.43	0.32	-0.26	-0.03	**0.73**	**0.59**	**0.74**	**0.58**	1.00													
Ba	-0.25	0.07	**0.62**	0.16	**0.49**	**0.46**	-0.24	0.02	**0.66**	**0.60**	0.44	0.31	**0.61**	1.00												
Sr	-0.34	0.14	**0.73**	-0.01	**0.53**	0.32	-0.23	-0.04	**0.82**	**0.63**	**0.62**	0.42	**0.82**	**0.81**	1.00											
Ga	-0.08	0.03	0.10	-0.05	0.22	0.08	0.22	0.33	0.17	0.03	0.41	0.42	-0.16	-0.03	0.09	1.00										
Be	-0.06	-0.05	0.29	0.25	0.31	0.20	0.12	0.13	0.26	**0.47**	0.02	0.04	0.39	0.29	0.34	-0.40	1.00									
Sn	-0.05	-0.10	0.28	-0.31	0.24	0.20	0.27	**0.63**	0.41	0.16	**0.76**	0.88	0.21	0.13	0.21	**0.71**	-0.14	1.00								
Nb	-0.06	0.19	-0.26	**0.51**	-0.20	-0.06	-0.00	-0.35	-0.48	-0.17	-0.48	-0.49	-0.31	-0.35	-0.34	-0.05	0.02	-0.45	1.00							
Ta	-0.09	0.19	-0.13	**0.57**	-0.07	-0.01	-0.11	-0.45	-0.33	-0.04	-0.36	-0.45	-0.10	-0.18	-0.10	-0.06	0.09	-0.48	**0.95**	1.00						
Y	-0.57	**0.61**	0.33	0.28	-0.13	-0.06	-0.42	-0.54	0.15	0.22	-0.27	-0.36	0.09	0.02	0.05	-0.28	-0.05	-0.50	**0.55**	**0.57**	1.00					
Zn	-0.06	0.13	-0.11	**0.47**	-0.16	0.14	-0.07	-0.39	-0.37	0.03	-0.41	-0.37	-0.26	-0.17	-0.26	-0.05	-0.04	-0.34	**0.82**	**0.79**	**0.53**	1.00				
Zr	-0.43	0.24	**0.77**	0.25	**0.62**	0.44	-0.31	-0.28	**0.85**	**0.82**	0.47	0.34	**0.66**	**0.51**	**0.70**	0.05	0.27	0.15	-0.21	-0.03	0.33	-0.12	1.00			
Hf	-0.21	0.21	0.26	0.35	0.06	0.01	-0.57	-0.61	0.17	0.13	0.00	-0.23	0.37	0.29	0.39	-0.16	-0.06	-0.40	0.18	0.39	0.34	0.12	0.39	1.00		
Th	-0.22	-0.00	**0.72**	0.05	**0.53**	0.41	-0.12	-0.03	**0.76**	**0.58**	**0.56**	0.45	**0.70**	**0.70**	**0.89**	0.16	0.33	0.31	-0.32	-0.11	-0.02	-0.23	**0.67**	0.37	1.00	
U	-0.20	0.21	0.19	0.24	.009	0.05	-0.40	-0.58	0.25	0.20	0.21	-0.12	0.39	0.21	0.47	0.11	-0.08	-0.21	0.26	**0.47**	0.38	0.15	0.43	**0.72**	0.34	1.00

Table 4.28: Correlation matrix for the major and trace elements of the lateritic profile derived from the mineralised pegmatite of Komu area

	SiO_2	Al_2O_3	Fe_2O_3	MnO	MgO	CaO	Na_2O	K_2O	TiO_2	P_2O_5	Li	Rb	Cs	Ba	Sr	Ga	Be	Sn	Nb	Ta	Y	Zn	Zr	Hf	Th	U
SiO_2	1.00																									
Al_2O_3	-0.96	1.00																								
Fe_2O_3	-0.74	**0.53**	1.00																							
MnO	0.05	-0.06	.04	1.00																						
MgO	0.14	-0.33	0.36	0.42	1.00																					
CaO	0.23	-0.40	0.27	**0.48**	**0.71**	1.00																				
Na_2O	0.46	-0.46	-0.41	-0.07	0.23	0.08	1.00																			
K_2O	-1.01	-0.05	-0.01	-0.38	0.04	-0.22	**0.61**	1.00																		
TiO_2	-0.57	0.35	**0.91**	-0.05	**0.52**	0.35	-0.28	0.06	1.00																	
P_2O_5	-0.37	0.18	**0.72**	0.35	**0.62**	**0.61**	-0.28	-0.22	**0.76**	1.00																
Li	-.019	0.02	**0.48**	-0.21	0.40	0.32	-0.02	0.34	**0.69**	0.40	1.00															
Rb	-0.09	-0.09	0.40	-0.25	0.38	0.29	0.17	**0.55**	**0.57**	0.33	**0.91**	1.00														
Cs	-0.28	0.11	**0.60**	0.02	0.43	0.32	-0.26	-0.03	**0.73**	**0.59**	**0.74**	**0.58**	1.00													
Ba	-0.25	0.07	**0.62**	0.16	**0.49**	**0.46**	-0.24	0.02	**0.66**	**0.60**	0.44	0.31	**0.61**	1.00												
Sr	-0.34	0.14	**0.73**	-0.01	**0.53**	0.32	-0.23	-0.04	**0.82**	**0.63**	**0.62**	0.42	**0.82**	**0.81**	1.00											
Ga	-0.08	0.03	0.10	-0.05	0.22	0.08	0.22	0.33	0.17	0.03	0.41	0.42	-0.16	-0.03	0.09	1.00										
Be	-0.06	-0.05	0.29	0.25	0.31	0.20	0.12	0.13	0.26	**0.47**	0.02	0.04	0.39	0.29	0.34	-0.40	1.00									
Sn	-0.05	-0.10	0.28	-0.31	0.24	0.20	0.27	**0.63**	0.41	0.16	**0.76**	0.88	0.21	0.13	0.21	**0.71**	-0.14	1.00								
Nb	-0.06	0.19	0.26	**0.51**	-0.20	-0.06	-0.04	-0.35	-0.48	-0.17	-0.48	-0.49	-0.31	-0.35	-0.34	-0.05	0.02	-0.45	1.00							
Ta	-0.09	0.19	-0.13	**0.57**	-0.07	-0.01	-0.11	-0.45	-0.33	-0.04	-0.36	-0.45	-0.10	-0.18	-0.10	-0.06	0.09	-0.48	**0.95**	1.00						
Y	-0.57	**0.61**	0.33	0.28	-0.13	-0.06	-0.42	-0.54	0.15	0.22	-0.27	-0.36	0.09	0.02	0.05	-0.28	-0.08	-0.50	**0.55**	**0.57**	1.00					
Zn	-0.06	0.13	-0.11	**0.47**	-0.16	0.14	-0.07	-0.39	-0.37	0.03	-0.41	-0.37	-0.26	-0.17	-0.26	-0.05	-0.04	-0.34	**0.82**	**0.79**	**0.53**	1.00				
Zr	-0.43	0.24	**0.77**	0.25	**0.62**	0.44	-0.31	-0.28	**0.85**	**0.82**	0.47	0.34	**0.66**	**0.51**	**0.70**	0.05	0.27	0.15	-0.21	-0.03	0.33	-0.12	1.00			
Hf	-0.21	0.21	0.26	0.35	0.06	0.01	-0.57	-0.61	0.17	0.13	0.00	-0.23	0.37	0.29	0.39	-0.16	-.006	-0.40	0.18	0.39	0.34	0.119	0.39	1.00		
Th	-0.22	-0.00	**0.72**	0.05	**0.53**	0.41	-0.12	-0.03	**0.76**	**0.58**	**0.56**	0.45	**0.70**	**0.70**	**0.89**	0.16	0.33	0.31	-0.32	-0.11	-0.02	-0.23	**0.67**	0.37	1.00	
U	-0.20	0.21	0.19	0.24	0.09	0.05	-0.40	-0.58	0.25	0.20	0.21	-0.12	0.39	0.21	0.47	0.11	-0.08	-0.21	0.26	**0.47**	0.38	0.15	0.43	**0.72**	0.34	1.00

Table 4.29: Correlation matrix for the major and trace elements of the lateritic profile derived from the mineralised pegmatite of Ofiki area

	SiO_2	Al_2O_3	Fe_2O_3	MnO	MgO	CaO	Na_2O	K_2O	TiO_2	P_2O_5	Li	Rb	Cs	Ba	Sr	Be	Sn	Nb	Ta	Y	Zn	Zr	Th	U
SiO_2	1.000																							
Al_2O_3	-0.42	1.00																						
Fe_2O_3	-0.78	0.04	1.00																					
MnO	-0.74	0.07	**0.83**	1.00																				
MgO	-0.05	-0.13	0.35	0.35	1.00																			
CaO	0.39	-0.45	0.02	-0.07	0.25	1.00																		
Na_2O	-0.10	0.02	-0.07	0.20	0.43	-0.10	1.00																	
K_2O	-0.21	0.19	-0.19	0.07	0.04	-0.29	**0.87**	1.00																
TiO_2	-0.23	-0.22	0.38	0.31	0.33	0.34	-0.04	-0.19	1.00															
P_2O_5	-0.09	-0.28	**0.51**	0.27	0.35	0.**61**	-0.14	-0.32	0.26	1.00														
Li	-0.58	0.28	**0.50**	**0.57**	0.13	-0.29	0.11	0.09	0.25	-0.09	1.00													
Rb	-0.54	-0.03	0.26	0.46	0.02	-0.35	**0.50**	**0.62**	0.21	-0.20	0.**64**	1.00												
Cs	-0.47	0.14	0.05	0.23	-0.17	-0.45	0.42	0.**61**	0.10	-0.31	**0.47**	**0.89**	1.00											
Ba	-0.47	0.06	**0.52**	0.43	0.37	-0.02	0.22	0.14	**0.51**	0.09	0.38	0.42	0.34	1.00										
Sr	0.42	-0.53	-0.17	-0.15	0.20	**0.85**	0.15	-0.01	0.39	0.46	-0.36	-0.09	-0.11	0.06	1.00									
Be	-0.09	0.06	-0.14	-0.04	-0.12	-0.09	**0.60**	**0.77**	-0.21	0.02	0.04	**0.49**	0.**49**	0.11	0.18	1.00								
Sn	-0.70	0.32	**0.58**	**0.71**	0.35	-0.30	0.43	0.38	0.29	-0.05	0.**81**	**0.72**	0.**54**	0.**69**	-0.28	0.21	1.00							
Nb	-0.34	0.47	-0.16	0.09	-0.37	-0.52	0.18	0.42	-0.13	-0.61	0.46	**0.57**	0.**63**	0.01	-0.35	0.32	0.39	1.00						
Ta	-0.11	0.17	-0.35	-0.19	-0.45	-0.34	0.32	**0.61**	-0.20	-0.37	0.03	0.**54**	0.**74**	-0.06	0.02	**0.68**	0.06	0.72	1.00					
Y	0.05	0.05	0.03	0.19	0.17	0.04	0.07	-0.11	0.36	-0.18	0.30	-0.07	-0.25	-0.03	-0.10	-0.32	0.18	0.01	-0.38	1.00				
Zn	-0.66	0.36	**0.55**	**0.63**	0.29	-0.27	0.26	0.23	0.40	-0.06	**0.80**	0.**58**	0.41	0.**69**	-0.30	0.11	**0.92**	0.34	-0.06	0.33	1.00			
Zr	0.19	-0.31	0.19	0.17	0.38	**0.80**	0.01	-0.30	**0.55**	**0.50**	-0.20	-0.32	-.040	0.23	**0.75**	-0.25	-0.09	-0.53	-0.46	0.27	-0.04	1.00		
Th	-0.26	0.24	0.15	0.15	-0.17	-0.25	0.05	0.12	0.23	-0.15	0.13	0.10	0.09	0.31	-0.21	0.11	0.27	0.22	0.14	0.39	0.37	0.03	1.00	
U	-0.21	0.11	0.22	0.03	-0.07	0.06	-0.07	-0.01	0.29	0.16	0.04	-0.03	-0.07	0.43	0.05	0.22	0.16	-0.05	-0.05	0.16	0.34	0.17	**0.68**	1.00

Table 4.30: Correlation matrix for the major and trace elements of the lateritic profile derived from the mineralised pegmatite of Iwere area

	SiO_2	Al_2O_3	Fe_2O_3	MnO	MgO	CaO	Na_2O	K_2O	TiO_2	P_2O_5	Li	Rb	Cs	Ba	Sr	Ga	Be	Sn	Nb	Ta	Y	Zn	Zr	Hf	Th	U
SiO_2	1.00																									
Al_2O_3	-0.99	1.00																								
Fe_2O_3	0.15	-0.18	1.00																							
MnO	**0.53**	-0.54	0.17	1.00																						
MgO	0.30	-0.30	**0.58**	0.08	1.00																					
CaO	-0.62	**0.66**	-0.69	-0.24	-0.48	1.00																				
Na_2O	-0.60	**0.63**	-0.78	-0.24	-0.56	**0.98**	1.00																			
K_2O	-0.62	**0.57**	-0.52	-0.45	-0.54	0.36	**0.49**	1.00																		
TiO_2	0.16	-0.19	**0.98**	0.14	**0.62**	-0.75	-0.83	-0.48	1.00																	
P_2O_5	0.45	-0.46	0.39	0.03	0.09	-0.49	-0.50	-0.39	0.35	1.00																
LOI	-0.72	**0.71**	0.48	-0.41	0.18	0.15	0.04	0.05	0.46	-0.16	1.00															
Li	-0.85	**0.84**	-0.35	-0.44	-0.19	**0.72**	**0.68**	**0.58**	-0.36	-0.64	1.00															
Rb	-0.72	**0.66**	-0.07	-0.47	-0.24	0.17	0.26	**0.78**	-0.03	-0.27	**0.47**	1.00														
Cs	-0.90	**0.86**	-0.01	-0.38	-0.30	0.42	0.44	**0.74**	-0.09	-0.47	**0.81**	**0.79**	1.00													
Ba	0.05	-0.10	**0.92**	0.07	0.44	-0.74	-0.78	0-.25	**0.93**	0.35	-0.31	0.13	0.06	1.00												
Sr	-0.81	**0.81**	-0.64	-0.48	-0.61	**0.82**	**0.86**	**0.80**	-0.67	-0.49	**0.81**	**0.58**	**0.73**	-0.50	1.00											
Ga	-0.93	**0.93**	-0.05	-0.56	-0.12	**0.57**	**0.50**	**0.49**	-0.09	-0.49	**0.90**	**0.53**	**0.81**	-0.01	**0.73**	1.00										
Be	-0.59	**0.64**	-0.41	-0.20	-0.34	**0.76**	**0.73**	0.25	-0.46	-0.55	**0.57**	0.19	0.37	-0.43	**0.63**	**0.57**	1.00									
Sn	-0.36	0.38	0.19	-0.30	0.18	0.03	-0.05	0.01	0.30	-0.14	0.31	0.20	0.40	0.19	0.02	0.34	0.10	1.00								
Nb	-0.71	**0.70**	0.25	-0.23	0.12	0.20	0.11	0.23	0.31	-0.46	**0.66**	**0.46**	**0.73**	0.27	0.28	**0.71**	0.34	**0.73**	1.00							
Ta	-0.21	0.21	0.23	0.08	0.12	-0.15	-0.17	0.01	0.35	-0.18	0.10	0.18	0.34	0.26	-0.14	0.10	0.04	**0.82**	**0.69**	1.00						
Y	0.32	-0.37	0.38	0.18	-0.05	-0.68	-0.60	-0.04	0.43	0.31	-0.55	0.04	-0.19	**0.52**	-0.45	-0.41	-0.47	0.10	-0.09	0.33	1.00					
Zn	-0.37	0.37	**0.55**	-0.12	**0.46**	-0.16	-0.28	-0.13	**0.62**	-0.17	0.34	0.20	**0.47**	**0.53**	-0.13	0.44	0.01	**0.73**	**0.82**	**0.66**	-0.09	1.00				
Zr	**0.64**	-0.66	**0.79**	0.40	**0.49**	-0.89	-0.93	-0.62	**0.80**	**0.57**	-0.73	-0.43	-0.56	**0.78**	-0.87	-0.54	-0.64	-0.04	-0.21	0.09	**0.58**	0.18	1.00			
Hf	0.34	-0.36	**0.77**	0.23	0.37	-0.75	-0.80	-0.45	**0.78**	0.32	-0.47	-0.30	-0.27	**0.81**	-0.66	-0.24	-0.44	0.17	0.08	0.27	**0.72**	0.30	**0.87**	1.00		
Th	0.31	-0.34	**0.81**	0.40	0.35	-0.72	-0.76	-0.45	**0.80**	0.34	-0.43	-0.27	-0.17	**0.83**	-0.64	-0.23	-0.38	0.11	0.09	0.26	**0.61**	0.37	**0.85**	**0.90**	1.00	
U	-0.01	-0.02	**0.66**	**0.47**	0.07	-0.39	-0.42	-0.29	**0.61**	0.19	-0.23	-0.11	0.07	**0.64**	-0.34	-0.01	-0.15	0.12	0.26	0.41	**0.53**	0.33	**0.55**	**0.67**	**0.79**	1.00

(0.81), Nb (0.82), Ga (0.85), Y (0.61), Hf (0.59), Th (0.63) and U (0.84); while MnO reflects its residual attributes alongside with Zr by showing positive correlation of 0.70 at $p < 0.05$. TiO_2 equally reveals moderate to high positive correlations with Y (0.54), Zr (0.51), Hf (0.54) and Th (0.63) in the residual profile. These geochemical patterns indicated similarityin the behavior of these relatively immobile HFSEs in weathering environment.

Large ion lithophile elements, though relatively mobile in the Osu residual profile, show high positive correlations amongst each other and with HFSEs. These geochemical patterns are generally revealed in Li-Cs (0.67), Li-Ga (0.81), Li-Sn (0.77), Li-Nb (0.82), Li-Ta (0.48), Li-U (0.74), Cs-Ga (0.56), Cs-Sn (0.48), Cs-Nb (0.62), Cs-Ta (0.59), Cs-Y (0.54), Cs-Th (0.59) and Cs-U (0.51) in the Osu weathering profile. Galium similarly shows high positive correlations with Sn (0.97), Nb (0.90), Ta (0.53) and U (0.95). Tin indicates strong positive correlations with Nb (0.91) and U (0.94) and moderate positive correlations with Ta (0.50). Niobiumhas moderate to high positive correlations with Ta (0.54), Y (0.47), Hf (0.53) and U (0.85). Yttrium showed strong positive correlations with Hf (0.68) and Th (0.73), while Hf-Th (0.66) revealed positive correlation in the matrix of the residual weathering profile of the Osubarren pegmatite.

The correlation matrices for the mineralised pegmatite residual profiles are displayed in Table 4.27 to Table 4.30. The Tables show that SiO_2 is negatively correlated with the basic oxides, indicating the intense leaching of these oxides *vis-à-vis* the relative enhancement of silica during lateritisation processes. The residual attributes of Al_2O_3, Fe_2O_3, TiO_2, MnO, Y, Zr, Th, Hf, Nb, Sn, Ta and U are evident in the positive correlation coefficients resulting from their various element pairs (Table 4.27 – Table 4.30)

P_2O_5 and Zr demonstrate moderate to high positive correlations in the mineralised pegmatite residual profiles (Tables 4.27, 4.29 and 4.30), which can be attributed to therelatively higher modal abundance of zircon and apatite in the parent pegmatites, particularly their enhancements towards the late phase of pegmatite residual melt crystallisation. The enhancement of Zr in the residual profile is especially noteworthy, and

could be possible reason for the high correlations of the duo (P_2O_5 and Zr) in the lateriticprofiles.

High field strength elements, as geochemical element pairs, show consistently high positive correlation among each others, which are revealed in the Nb/Th, Nb/U, Zr/Hf, Zr/Th, Zr/U, Hf/Th, Hf/U, Th/U, Y/Zr, Y/Hf, Y/Th, Y/U, Nb/Ta, Sn/Nb, Sn/Ta pairs (Table 4.27, Table 4.28 and Table 4.30). Nb/Ta, Sn/Nb and Sn/Ta particularly demonstrate peak correlation values among the HFSEs in the mineralised residual pegmatite profiles of Ijero and Ofiki areas. The high positive correlations of the HFSEs of the residual lateritic profiles signify their similar geochemical behavior in weathering environment and the residual enhancement of these elements in the mineralised regolith profiles. These HFSEs (except U) are chemically inert and show congruent behaviour in the secondary geochemical environment (Hallberg, 1984; Braun, 2009; 2012). It is relevant to note that some of the aforelisted elements behave in chemically coherent patterns aselement pairs in magmatic systems (Nb/Ta, Zr/Hf, Th/U), and are observed to be extensively fractionated in rare-element pegmatites resulting in the formation of rare-metal bearing exotic accessory phases (Keppler, 1993; London, 1995; Linnen and Keppler, 1997; Linnen, 1998; 2005; Linnen and Cuney, 2005; Bartels *et al.*, 2010; Linnen *et al.*, 2012; London and Kontak, 2012).

Large ion lithophile elements and HFSEs positively correlate well, as indicated by the bulk geochemical data of the mineralised pegmatite residual profiles (Tables 4.27, 4.28, 4.29 and 4.30), although some LILEs are known to be highly mobile due to their hydrodynamic dispersions in the weathering environment. These geochemical behaviours of LILEs and HFSEs invariably signify the enrichments of these elements in the parent pegmatites.

In general, the LILEs and HFSEs show consistent and moderate to high positive correlation in the barren and mineralised pegmatite-derived weathering profiles of the investigated areas. The high and consistent positive correlations of the HFSEs in the bulk chemical data of the lateritic profiles and their similar geochemical behaviour during lateritisation processes can be explored to determine suitable geochemical ratios

anddiscrimination diagrams to differentiate between rare metal-bearing and barren pegmatite bedrocks underneath lateritic mantles.

4.5.2 Element ratio signatures as geochemical discriminants

Geochemical interrelationships as element ratios are commonly applied in geochemical exploration to discriminate between ore-related and barren geological complexes, predict ore deposit types, and also employed in vectoring toward ore element mineralisations underneath regolith covers (Olade, 1980; Ekwere, 1985; Brand, 1999; Ranasinghe *et al*., 2005; Levitan *et al.,* 2015; Wilkinson *et al.*; 2017).

Element pairs showing consistently high correlations were selected from the correlation matrices (Tables 4.20, 4.21, 4.22, 4.23 and 4.24) of the bulk chemical data of the residual profiles, so as to determine element ratios which most effectively distinguish the pegmatite types from their corresponding weathering profiles. The statistical information obtained from the correlation matrices indicate some subtle semblances in geochemical patterns and strong correlations among certain pegmatite petrogenetically important elements, particularly the LILEs and the HFSEs. The LILEs (Cs, Rb, and Ba) and other labile oxides (Na_2O, K_2O and Li_2O) are strongly depleted in the weathering profiles, as they generally behave as soluble cations and show high susceptibility to local hydrodynamic dispersion. These geochemical characteristics of the LILEs cast some aspersions on their usefulness as element ratios in the geochemical discrimination of the pegmatite types underneath lateritic covers. In this investigation, some HFSEs were employed as element ratios due to their conservative geochemical behaviour in supergene weathering environment (MacLean *et al*., 1997; Zarasvandi *et al*., 2010; 2012). They show similar enrichment (residual) patterns in weathering environment and some of the HFSEs (Ti, Zr, Hf, Th, Ta, and Nb) are largely employed as reference elements to appraise the mass flux of other elements (Hallberg, 1984; Brimhal *et al.*, 1991; Braun *et al.*, 1993, Braun and Pagel, 1994; Gouveia *et al*., 1993; Braun *et al*., 2009; Du, 2012; Du *et al.*, 2012; Braun *et al*., 2012).

A suite of HFSE cations in the investigated residual lateritic profiles, including Zr, Ti, Y, Nb, Ta, Th and U were respectively combined as Zr/Y, Ti/Nb, Zr/Nb, Nb/Ta and Th/U

element ratios, and tested for their geochemical viability in distinguishing between rare metal-bearing and barren pegmatite under lateritic mantles. Other tested element ratios among the HFSEs produce no useful results in the geochemical discrimination of these pegmatite types under lateritic covers. Table 4:31 presents the mean values and ranges of the above highlighted geochemical ratios from their respective whole-rock and residual profile bulk chemical data.

4.5.2.1 Zr/Y element ratio

Variations in zirconium and yttrium are apparent in the investigated whole-rock and residual lateritic profiles of the non-mineralised and mineralised pegmatites. The Osu non-mineralised whole-rock pegmatite has relatively higher Zr (67 ppm) content, when compared to the mineralised pegmatites that indicated 36, 18, 26 and 39 ppm, respectively for the Ijero, Komu, Ofiki and Iwere. The Zr abundances indicated above is a reflection of the modal abundances of zircon in the respective pegmatite types.

The yttrium concentrations are proportionately higher in the mineralised whole-rock pegmatites, relative to the lower contents recorded in the Osu non-mineralised pegmatitewhole-rock samples. Yttrium, as important pegmatite petrogenetic trace element, is generally enhanced towards the late flux-enriched phase of pegmatite crystallisation. As a result, it indicates comparatively higher concentration levels in the mineralised pegmatites. The Zr/Y ratio is, therefore, higher in the non-mineralised pegmatites, but lower in the mineralised pegmatite (Table 4.31).

The constituting horizons of the weathering profiles generally show decreasing Zr/Y trends down the regolith profiles. Zirconium shows late residual concentrations in pegmatite melts, but Y demonstrates particularly higher enhancement in the late residual phase of the mineralised pegmatite. The high Y contents, therefore, generally points to lower Zr/Y (1.2 – 16.6) ratios in the rare metal-bearing pegmatite profile, relative to the higher Zr/Y (9.1-15.9) in the non-mineralised pegmatite profile. Significant amount of Zr is resident in the resistate zircon ($ZrSiO_4$), while monazite (Ce, La, Y, Th)PO_4 show moderate level of Y. Zircon is considered a resistate mineral and it is remarkably stable in

Table 4.31: Zr/Y, Ti/Nb, Zr/Nb, Nb/Ta and Th/U element ratios in whole-rock pegmatite and pegmatite-derived residual profiles of the study areas

		Whole-rock	A-horizon	B-horizon	C-horizon
Zr/Y	OSPP (Barren)	7.5 (1.7 - 14.4)	15.9 (13.3 - 18.2)	13.5 (7.7 - 19.5)	9.1 (6.3 - 12.4)
	IJPP (Mineralsed)	3.5 (0.7 - 7.7)	16.6 (16.6)	10.9 (7.2 - 14.3)	6.7 (4.2 - 10.0)
	KMPP (Mineralised)	2.2 (0.8 - 3.1)	2.2 (1.5 - 3.1)	1.5 (0.6 - 2.6)	1.0 (0.7 - 1.6)
	OFPP (Mineralised)	2.2 (1.0 - 5.5)	17.4 (15.1 - 20.5)	9.6 (4.5 - 16.3)	8.4 (4.6 - 10.7)
	IWPP (Mineralised)	4.2 (0.7 - 12.5)	5.4 (4.7 - 5.9)	4.2 (1.4 - 8.2)	1.2 (0.9 - 1.6)
Ti/Nb	OSPP (Barren)	48.3 (4.3 - 114.5)	176.3 (11.1 - 251.8)	161.6 (129.1 - 253.1)	115.3 (53.6 - 161.1)
	IJPP (Mineralised)	10.4 (1.3 - 45.0)	36.2 (36.2)	34.3 (10.3 - 76.2)	12.9 (0.5 - 27.5)
	KMPP (Mineralised)	2.1 (0.6 - 4.6)	105.2 (4.0 - 299.8)	15.4 (1.6 - 27.1)	8.8 (2.6 - 27.4)
	OFPP (Mineralised)	2.7 (0.8 - 6.3)	90.1 (62.6 - 128.7)	60.4 (24.2 - 126.8)	23.1 (13.5 - 31.4)
	IWPP (Mineralised)	24.6 (0.7 - 102.3)	211.3 (116.7 - 389.7)	74.8 (42.5 - 117.0)	38.2 (18.7 - 46.1)
Zr/Nb	OSPP (Barren)	3.9 (0.5 - 11.1)	16.4 (8.7 - 18.2)	7.3 (4.5 - 13.0)	1.0 (2.1 - 5.6)
	IJPP (Mineralised)	0.5 (0.14 - 10.5)	2.4 (2.4)	1.1 (0.3 - 2.5)	0.2 (0.1 - 1.0)
	KMPP (Mineralised)	0.2 (0.1 - 0.5)	0.4 (0.2 - 0.8)	0.2 (0 - 1.0)	0.2 (0.1 - 2.4)
	OFPP (Mineralised)	0.2 (0.1 - 0.4)	11.5 (7.3 - 16.3)	2.8 (0.8 - 7.1)	1.0 (.05 - 2.1)
	IWPP (Mineralised)	1.4 (0.2 - 7.8)	9.5 (3.1 - 18.8)	2.1 (0.6 - 4.4)	0.7 (0.5 - 1.0)
Nb/Ta	OSPP (Barren)	4.8 (2.3 - 6.4)	6.0 (4.0 - 7.0)	6.1 (4.5 - 14.0)	7.4 (0.3 - 9.5)
	IJPP (Mineralised)	3.1 (1.3 -7.8)	1.2 (1.2)	1.9 (1.1 -3.4)	3.6 (2.7 - 6.0)
	KMPP (Mineralised)	1.5 (0.7 - 3.3)	3.9 (1.6 - 38.7)	3.7 (1.2 - 11.4)	3.0 (1.2 - 4.4)
	OFPP (Mineralised)	0.9 (0.3 - 2.0)	1.9 (1.7 - 2.3)	2.5 (1.4 - 4.0)	1.4 (1.2 - 2.8)
	IWPP (Mineralised)	1.5 (0.7 -3.8)	1.2 (0.8 - 4.0)	1.9 (1.2 - 4.0)	2.5 (1.8 - 4.0)
Th/U	OSPP (Barren)	0.3 (0.1 - 0.7)	0.7 (0.6 -0.8)	0.5 (0.3 - 1.1)	0.3 (0.2 - 3.2)
	IJPP (Mineralised)	1.3 (0.7 - 4.0)	1.3 (1.3)	1.5 (0.8 - 2.5)	1.0 (0.5 - 1.5)
	KMPP (Mineralised)	0.5 (0.3 - 1.0)	3.6 (2.5 -3.5)	3.0 (1.5 - 3.7)	2.4 (1.3 - 2.8)
	OFPP (Mineralised)	0.5 (0.2 -1.0)	1.8 (1.6 - 2.0)	1.9 (1.4 - 3.0)	2.1 (1.7 - 3.0)
	IWPP (Mineralised)	0.5 (0.2 - 1.1)	1.8 (1.0 - 2.6)	1.9 (1.7 -2.3)	1.7 (1.4 - 1.8)

weathering environment because of its exceptional low solubility in aqueous solutions (Nesbitt, 1979).

4.5.2.2 Ti/Nb element ratio

The TiO_2 concentration levels in the Osu non-mineralised and the mineralised pegmatites were noted to be more or less the same, indicating minimal contributions of rutile (TiO_2) and ilmenite ($FeTiO_3$) in the pegmatite types. However, the mineralised pegmatites particularly show higher Nb contents due to the presence of Nb-bearing minerals, such ascolumbite ([Fe, Mn][Nb, Ta]$_2O_6$) and tantalite ([Fe, Mn][Ta, Nb]$_2O_6$); while the non-mineralised pegmatites is characterised by lower Nb concentration. The foregoings result in the elevated Ti/Nb (48.3) ratio in the barren whole-rock pegmatite, but relatively lower Ti/Nb (2.1-24.6) ratios in the mineralised whole-rock pegmatites.

Within the investigated weathering profiles, higher Ti/Nb ratios are generally evident, due to the residual enhancement and non-susceptibility of the Ti-bearing and Nb-bearing accessory phases to secondary chemical alterations. The relatively higher modal abundances of Nb-bearing phases and the lower Ti-bearing discrete phases in the mineralised pegmatites, as well as their non-susceptibility to weathering effects, have largely resulted in the elevated Nb abundances in their respective weathering profiles. The resulting higher Nb contents in the weathering profiles of the mineralised pegmatites have invariably reduced their respective Ti/Nb ratios (Table 4.31). The non-mineralised pegmatite, however, indicates relatively higher Ti/Nb ratios (115.3, 161.6 and 176.3, respectively for the C, B and A-horizons) when compared to the mineralised pegmatite profiles.

4.5.2.3 Zr/Nb element ratio

The Osu non-mineralised pegmatite has been indicated from the previous discussion (section 4.3.4.2.1) to show higher Zr but lower Nb contents relative to the mineralised pegmatites. These have invariably translated to higher Zr/Nb (3.9) ratio in the non-mineralised whole pegmatite samples. On the other hand, the higher Nb and lower Zr contents in the mineralised whole-rock pegmatites have significantly reduced their Zr/Nb (0.2 - 1.4) ratios. These are largely connected to the higher modal mineralogy of Nb-

bearing discrete phases in the mineralised pegmatites.

The Zr/Nb geochemical signatures in the whole-rock samples are significantly enhanced in the weathering profiles of the non-mineralised and mineralised pegmatites (Table 4.31). These Zr/Nb geochemical trends in the weathering profiles could possibly be attributed to the residual chemical character of these rationing elements in weathering environments. The elevated Nb concentration levels in the lateritic profiles of the mineralised pegmatites, have invariably signified reduced Zr/Nb ratios, varying from 0.2 to 11.5; whereas the non-mineralised pegmatite profile reflects higher Zr/Nb (1.0 -16.4) ratio due to its very low Nb contents.

4.5.2.4 Nb/Ta element ratio

The primary lithogeochemical distinctions established amongst the fresh samples of the barren and mineralised pegmatites are evident in their respective Nb/Ta ratios (Table 4:31). These differences are preserved and further amplified in their respective *in situ*-derived lateritic profiles due to the relative immobility of these elements in supergene weathering environment. For instance, the whole-rocksof the Osu non-mineralised pegmatite show higher Nb/Ta (4.8) ratios, while those of the mineralised pegmatites are generally marked by relatively lower Nb/Ta (0.9 – 3.1) ratios.

The Nb/Ta ratio of the barren pegmatite profiles varies between 6.0 and 7.4 within the constituting horizons; whilethe mineralised pegmatite profiles generally showed lower Nb/Ta (1.2 - 3.9) ratios. The above geochemical patterns are consistent with the higher modal abundances of columbo-tantalite-bearing accessory mineral phases in the mineralised pegmatites, which are preserved (due to their relative non-susceptibility to secondary alteration processes) and further enhanced during chemical weathering. It is relevant to remark that the barren pegmatite is lacking in Nb- and Ta-bearing accessory mineral phases, which invariably translated to decreased concentration of these elements in its *in situ*-derivedweathering profiles. Tantalum contents in pegmatites, rather than Nb abundances, are generally accepted as key parameters in distinguishing between pegmatite types and in the estimation of the degree of rare-metal mineralisation in pegmatites (Beus, 1966; 1982; Gordiyenko, 1971; Moller and Morteani, 1987; Linnen, 1998; Morteani *et al*.,

2000; Cerny *et al*., 2005; Linnen and Cuney, 2005; Selway *et al.*, 2005; Kuster, 2009; Kuster *et al*., 2009; Wise and Brown, 2010; Linnen *et al*., 2012; Linnen *et al*., 2014; Melcher *et al*., 2015).

4.5.2.5 Th/U element ratio

Zircon ($ZrSiO_4$) incorporates into its structural lattice, modest amount of other lithophile cations including Hf^{4+}, Th^{4+}, U^{4+}, $Y^{3+}Ti^{3+}$and REE^{3+} (Rollinson, 1993; Harley and Kelly, 2007). Depending on the geological environment, U concentrations generally predominate over Th abundance in zircon. The non-mineralised and mineralised whole-rock pegmatites reflect low Th/U ratios (Table 4.31).

The *in situ*-derived lateritic profiles from the non-mineralised and the mineralised pegmatites indicate elevated Th/U ratios than their corresponding parent rocks. These geochemical patterns reflect the insolubility of thorium and redox-dependent attributes of uraniumin supergene weathering condition, which tend to enhance Th/U ratios with increasing weathering and leaching processes (McLennan *et al*., 1995; Gu *et al*., 2002; Zhang *et al.*, 2013). It is particularly relevant to know that uranium occurs as mobile U^{6+} cation in oxidising surface conditions (Giorgis *et al.*, 2014). The contrast in the geochemical behaviors of Th and U in response to oxidising meteoric water in weathering environment at low pH, invariably results in the increased Th contents but reduced U concentrations within the constituting horizons of the lateritic profiles. The higher Th/U (1.0 –3.6) ratios recorded in the mineralised pegmatite profiles, relative to the lower values (0.3 – 0.7) obtained in the non-mineralised pegmatite profile, are possibly the reflection of the differences in the primary endowment of Th in the respective pegmatite types. These distinct lithogeochemical Th signatures are preserved and better amplified in the respective weathering profiles.

4.5.3 Geochemical discrimination plots

The discriminations of the pegmatite types from the bulk chemical data of their*in situ*-derived weathering profiles were undertaken through the use of binary and ternary discrimination plots. The relatively immobile elements that have consistently high

correlation coefficients, as indicated in their correlation matrices, were employed for this purpose. These essentially include the HFSEs, such as, Ti, Y, Zr, Nb, Ta, Sn, Th and Hf, as well as some lithophile elements among which are Sr, Ba, Rb and Zn. The HFSEs are considered least mobile during weathering, alteration, lateritisation and bauxitisation processes (Floyd and Winchester, 1978; Braun *et al*., 1993; Braun and Pagel, 1994; Braun *et al*., 1998; Butt *et al*., 2000; Gong *et al*., 2011; Xiao *et al*., 2013). The relative abundances of these HFSEs in the respective investigated bedrock pegmatites have been earlier established to differ. These remarkable compositional variations are further preserved, and aptly marked in both the non-mineralised pegmatite and the mineralised pegmatite profiles. This enables the designation of two specific compositional fields, correspondingly typifying the non-mineralised pegmatite profile (NMPP) and the mineralised pegmatite profile (MPP).

4.5.3.1 Binary discrimination plots

Besides the discrimination of the pegmatite types using their relative HFSEs and LILEs abundances and element ratios as geochemical discriminants, binary diagrams were also employed to show certain geochemical trends and to substantiate important correlation relationships among key element pairs. The Y versus Nb bivariate plot (Fig. 4.78) indicated a positive correlation between these element pairs, and aptly separates the residual profiles of the barren and mineralisedprofiles into their respective clusters. The differences in the titanium and niobium contents in the residual profiles of the pegmatitetypes can be inferred from the Ti versus Nb discrimination plot (Fig. 4.79). The mineralised pegmatite profiles indicate enhanced Nb contents, whereas the non-mineralised pegmatite profiles indicate relatively lower Nb concentrations. The Ti versus Nb binary plot (Fig. 4.79) indicates a positive correlation between the two elements, and the pegmatite types are clearly differentiated into their respective fields in the diagram.The compositional variations in Zr and Nb contents in the studied weathering profiles areaptly marked, and amply demonstrated in the Zr-Nb discrimination plot (Fig. 4.80). The mineralised pegmatites show higher Nb contents, but widely varying abundances of Zr, while the non-mineralised pegmatite indicates low Nb but slightly higher Zr

contents.Zirconium versus Nb binary plots revealed positive geochemical relationships among this

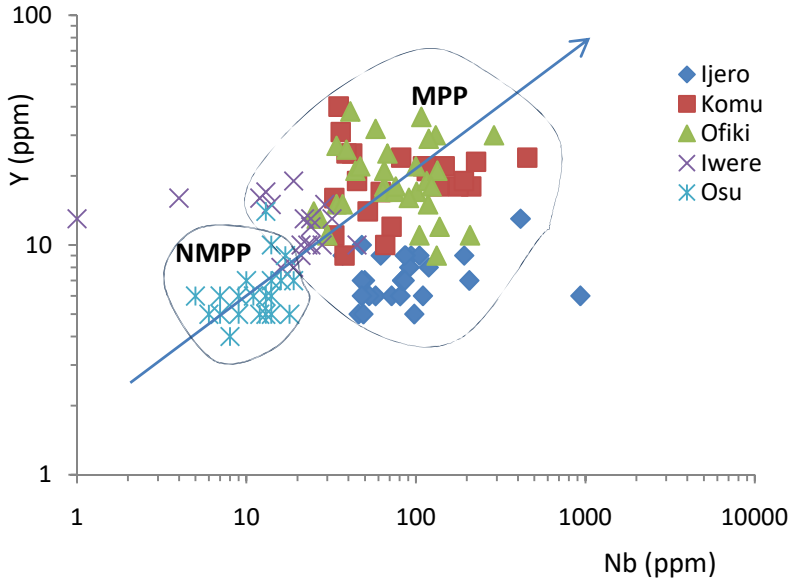

Fig. 4.78: Y vs. Nb bivariate discrimination plot for the residual profiles (MPP = Mineralised pegmatite profile; NMPP = Non-mineralised pegmatite profile)

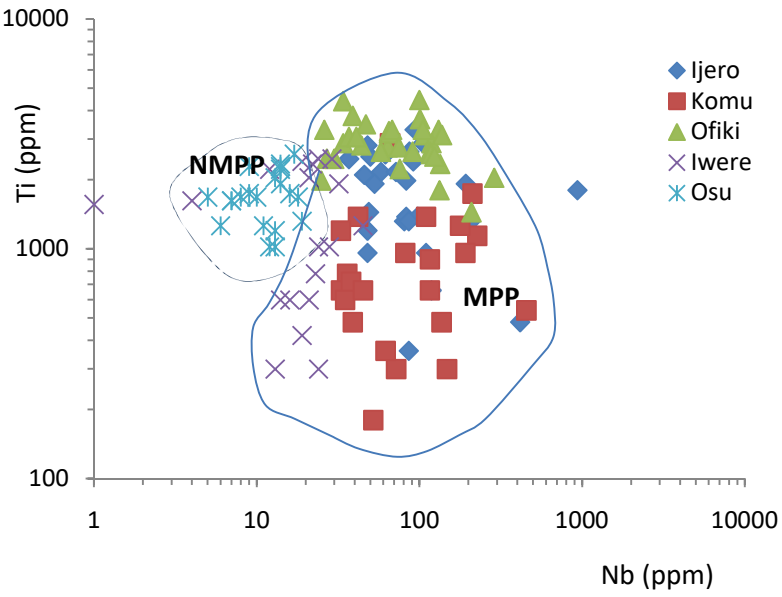

Fig. 4.79: Ti vs. Nb bivariate discrimination plot for the residual profiles (MPP = Mineralised pegmatite profile; NMPP = Non-mineralised pegmatite profile) (modified after Dissanayake and Rupasinghe, 1995)

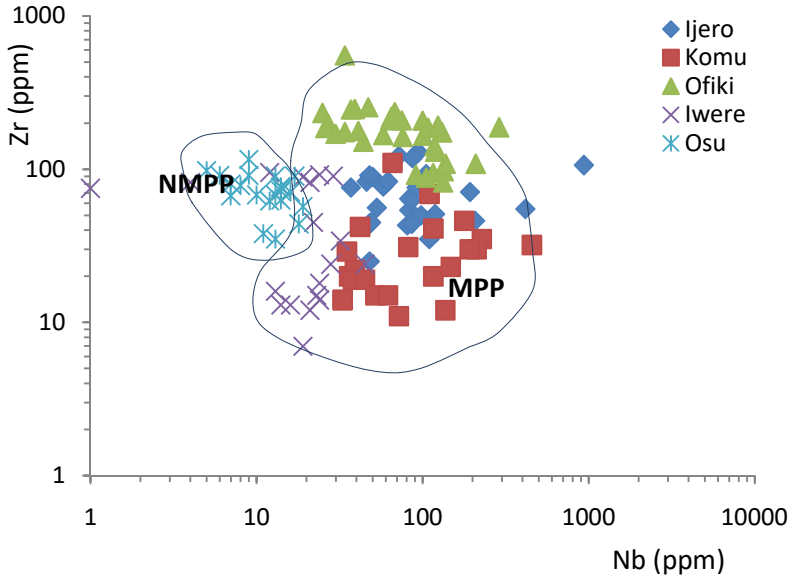

Fig. 4.80: Zr vs. Nb bivariate discrimination plot for the residual profiles (MPP = Mineralised pegmatite profile; NMPP = Non-mineralised pegmatite profile) (modified after Dissanyake 1992)

element pair, and affords the distinction of the weathering profiles of the pegmatite types into their respective fields. The barren and mineralised pegmatite weathering profiles are also readily distinguished into the respective clusters in the Zr-Ta (Fig. 4.81) and Zr-Th (Fig. 4.82) binary plots. These discrimination plots essentially revealedand amplify the disparity in the Ta and Th concentration levels correspondingly in the non-mineralised pegmatite and the mineralised pegmatite profiles. The Zr-Ta and Zr-Th binary plots also showed sympathetic Zr/Ta and Zr/Th relationships within the profiles, which are better amplified in the Zr/Ta versus Zr/Th diagrams (Fig. 4.83).

The above specified plots aptly show the geochemical relationships among element pairs and reflect the similarities in the residual character of these elements in the weathering environment.

4.5.3.2 Ternary discrimination plots

Triangular variation diagrams are generally employed in geochemistry when it is necessary to show simultaneous change between three variables (Rollinson, 1993). They find common applications in petrogenetic and provenance studies, where subtle and inherent geochemical features of rocks are unraveled and utilised for petrogenetic modeling and petrotectonic characterisation (Pearce and Cann, 1973; Pearce *et al*., 1975; Wood *et al*., 1979; Wood, 1980; Nesbitt and Young, 1982; Bhatia and Crook, 1986; Harris *et al*., 1986; Meschede, 1986; Ohta and Arai, 2007; Meunier *et al*., 2013; Zhang *et al*., 2014). In this study, ternary discrimination diagrams of highly correlated HFSEs andselected LILEs, identified using correlation coefficient matrices, were plotted to explore their viability in the discrimination of pegmatite typesfrom their respective *in situ*-derivedlateritic profiles. The diagrams were essentially intended to reveal the varyingprimary geochemical enrichments of rare-elements in the pegmatite bedrocks, which are possibly preserved in the corresponding residual profiles in secondary supergene environment.

The investigated profiles are readily differentiated into their respective separate clusters on the Zr-Nb-Y ternary plot (Fig. 4.84). The diagram shows the non-mineralised pegmatite profiles clustering at Zr-axis, which is a reflection of the higher concentration of zirconium in these profiles, when compared to the mineralised pegmatite profiles. The

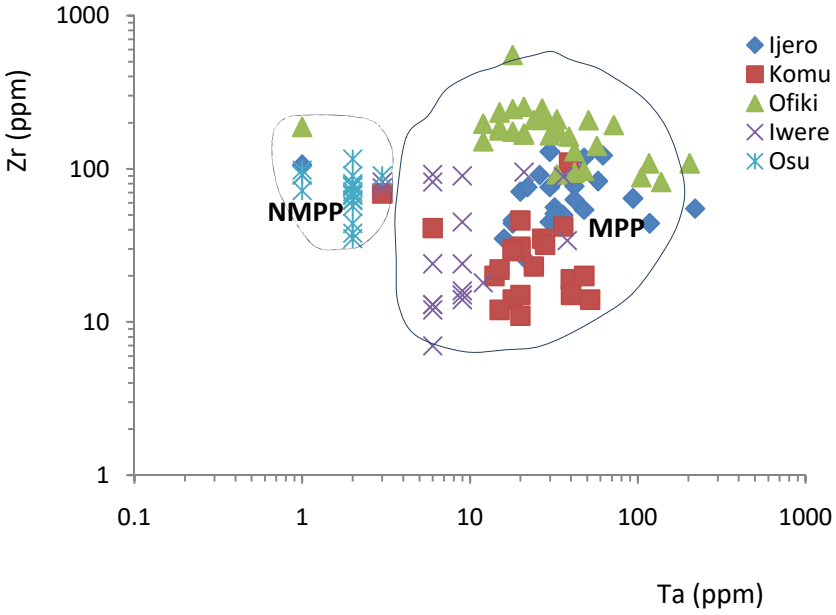

Fig. 4.81: Zr vs. Ta bivariate discrimination plot for the residual profiles (MPP = Mineralised pegmatite profile; NMPP = Non-mineralised pegmatite profile)

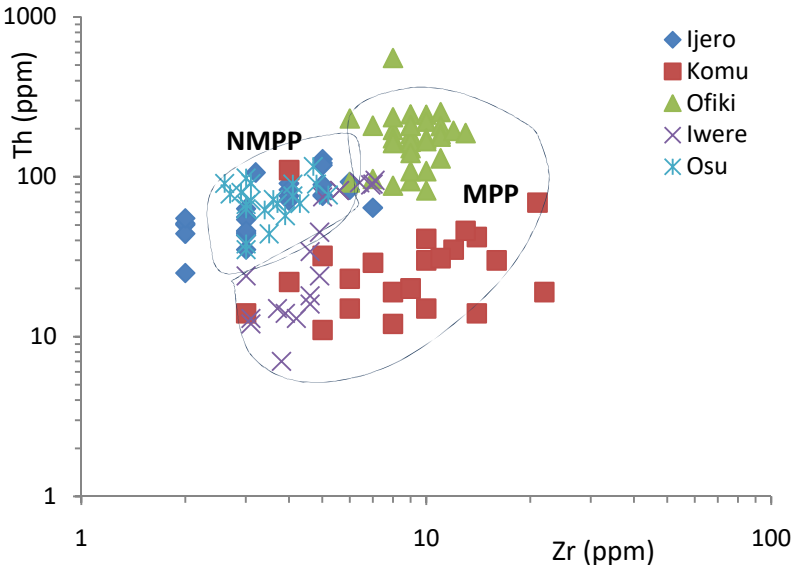

Fig. 4.82: Zr vs. Th bivariate discrimination plot for the residual profiles (MPP = Mineralised pegmatite profile; NMPP = Non-mineralised pegmatite profile)

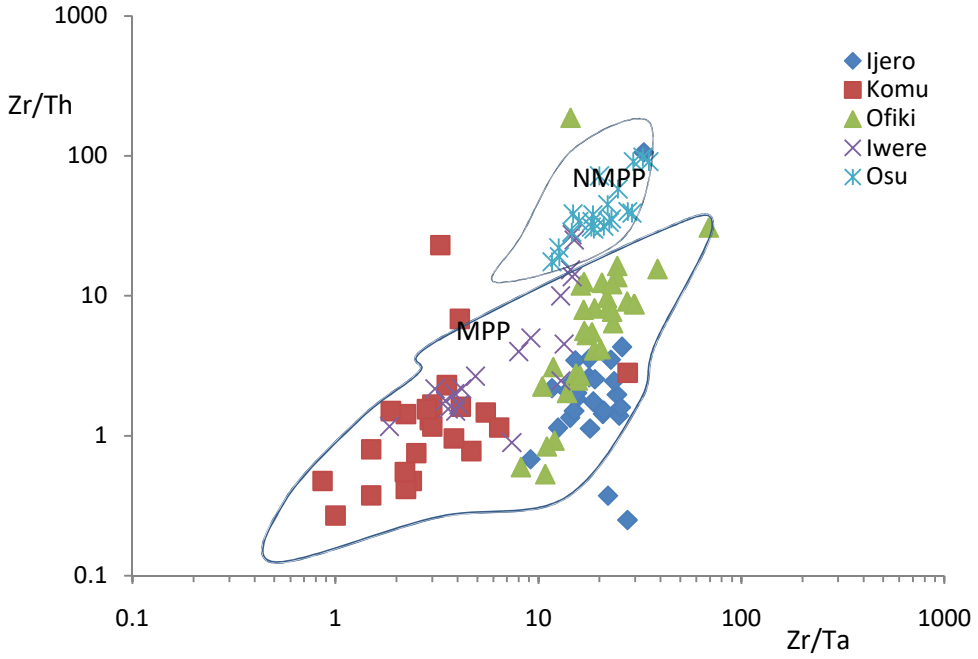

Fig. 4.83: Zr/Ta vs. Zr/Th bivariate discrimination plot for the residual profiles (MPP = Mineralised pegmatite profile; NMPP = Non-mineralised pegmatite profile)

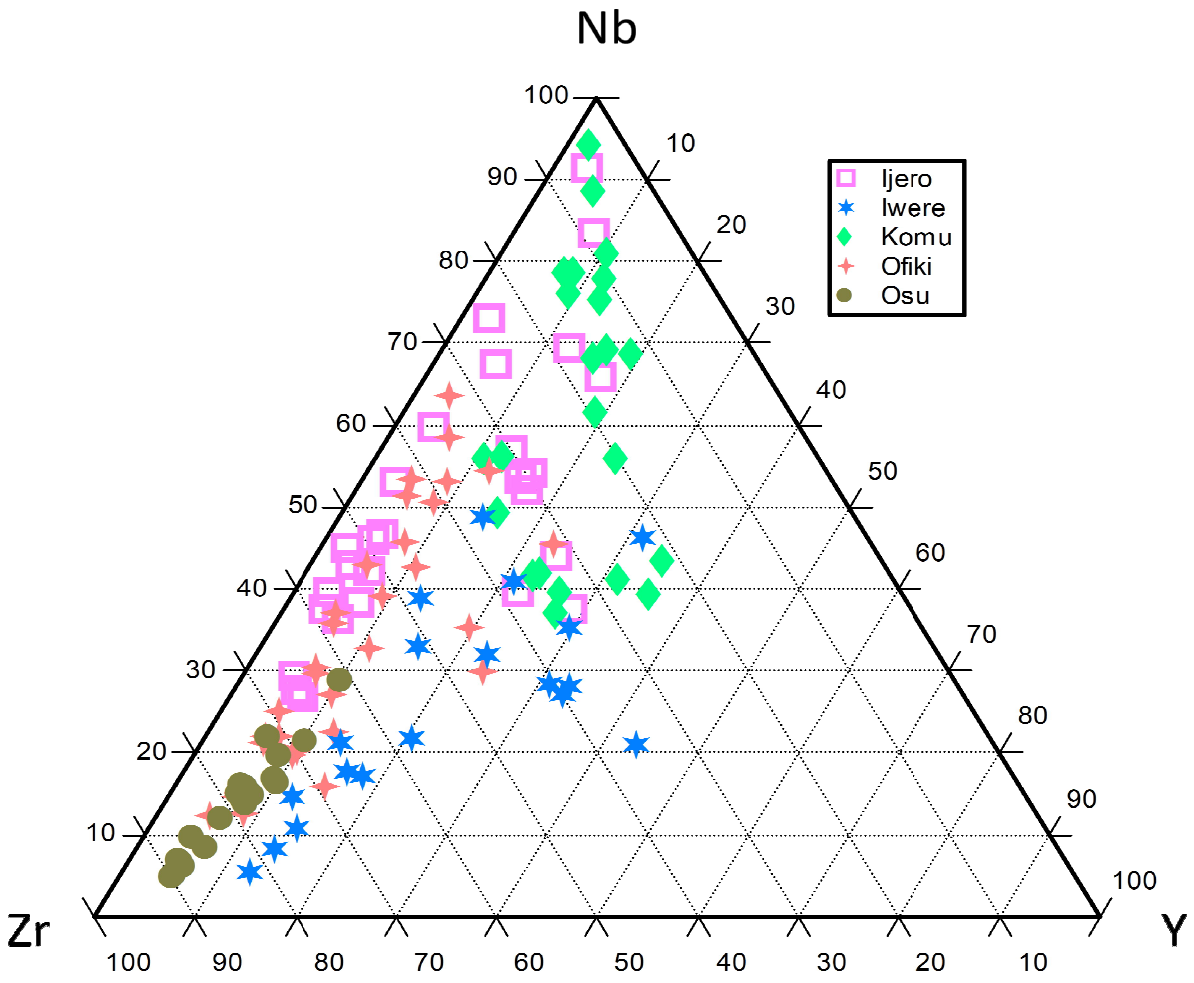

Fig. 4.84: Zr-Nb-Y ternary discrimination plot for the residual profiles

mineralised pegmatite profiles indicate conspicuous geochemical trends towards the Nb-axis of the plot,which is consistent with the enhanced Nb contents in the mineralised pegmatite profiles, relative to the barrenpegmatite profile. The mineralised pegmatite profiles, however, portray a wide spread of sample plots along the Nb-Zr axes, thereby signifying varying geochemical abundances of Nb and Zr among the profiles and within the constituting horizons of the respective mineralised pegmatite profiles (Fig. 4.84). The Zr/10-Nb-Y triangular diagram (Fig. 4.85) with minimised Zr (Zr/10) effect gives moredistinct clusters of the weathering profiles from the barren to the mineralised. The ternary Zr/10-Nb-Ti/300 (Ranasinghe, *et al*., 2005) diagram for the studied profiles grouped the non-mineralised and mineralised pegmatite profiles separately from each other (Fig. 4.86). There are, however, very few overlaps among the lateritic samples derived from the pegmatites. The enhanced Nb contents in the mineralised pegmatite profiles are apparent, as clusters of sample points could be observed towards the Nb-axis of the diagram.

In the Ta-Nb-Sn (Fig. 4.87) ternary plot, the sample points generally cluster away from the Ta and Sn apices. The plot, however, broadly distinguishes the *in situ*-derived residualprofiles of the pegmatite types. The Th-Hf-Ta (Fig. 4.88) triangular variation plot accurately discriminates the profiles of the non-mineralised and mineralised pegmatites into their distinctive fields. The diagram showed the clustering of the mineralised pegmatite profiles towards the Ta-axis, which is consistent with the inherent Ta abundances in the profiles. The Th-Hf-Ta ternary discrimination plot proved to be morepotent as diagnostic tool for identifying rare-element pegmatites underneath lateritic covers.

The Zr/10-Nb-Zn (Ranasinghe *et al.*, 2005) triangular graph (Fig. 4.89) indicated that the mineralised pegmatite profiles distinctly clustering near Nb peak, while the non-

mineralised pegmatite profile is further away from the peak, indicating their very low Nbcontent. The Sr-Ba/10-Rb (Ranasinghe *et al*., 2005) ternary plot of the bulk chemical data of the weathering profiles also showed the clustering of the sample points towards the Rb axis of the diagram (Fig. 4.90).

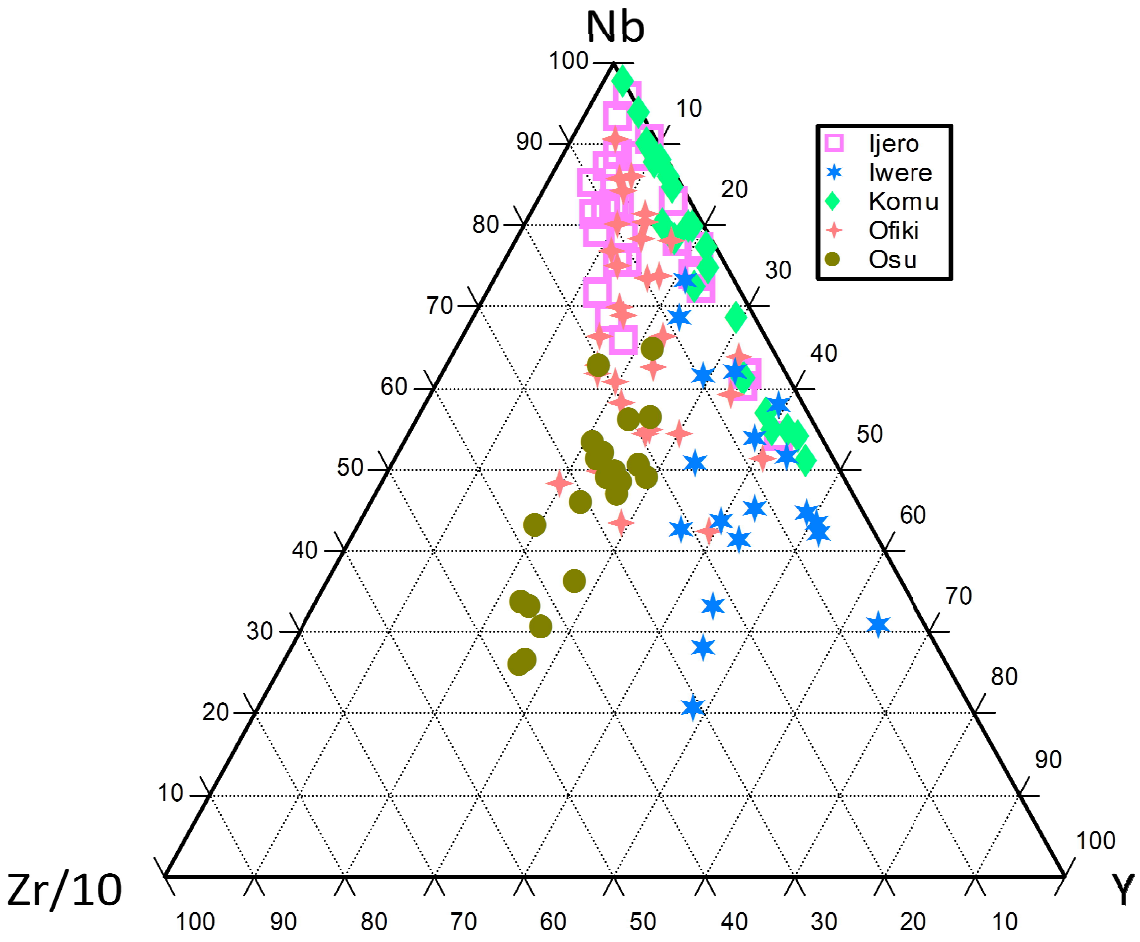

Fig. 4.85: Zr/10-Nb-Y ternary discrimination plot for the residual profiles

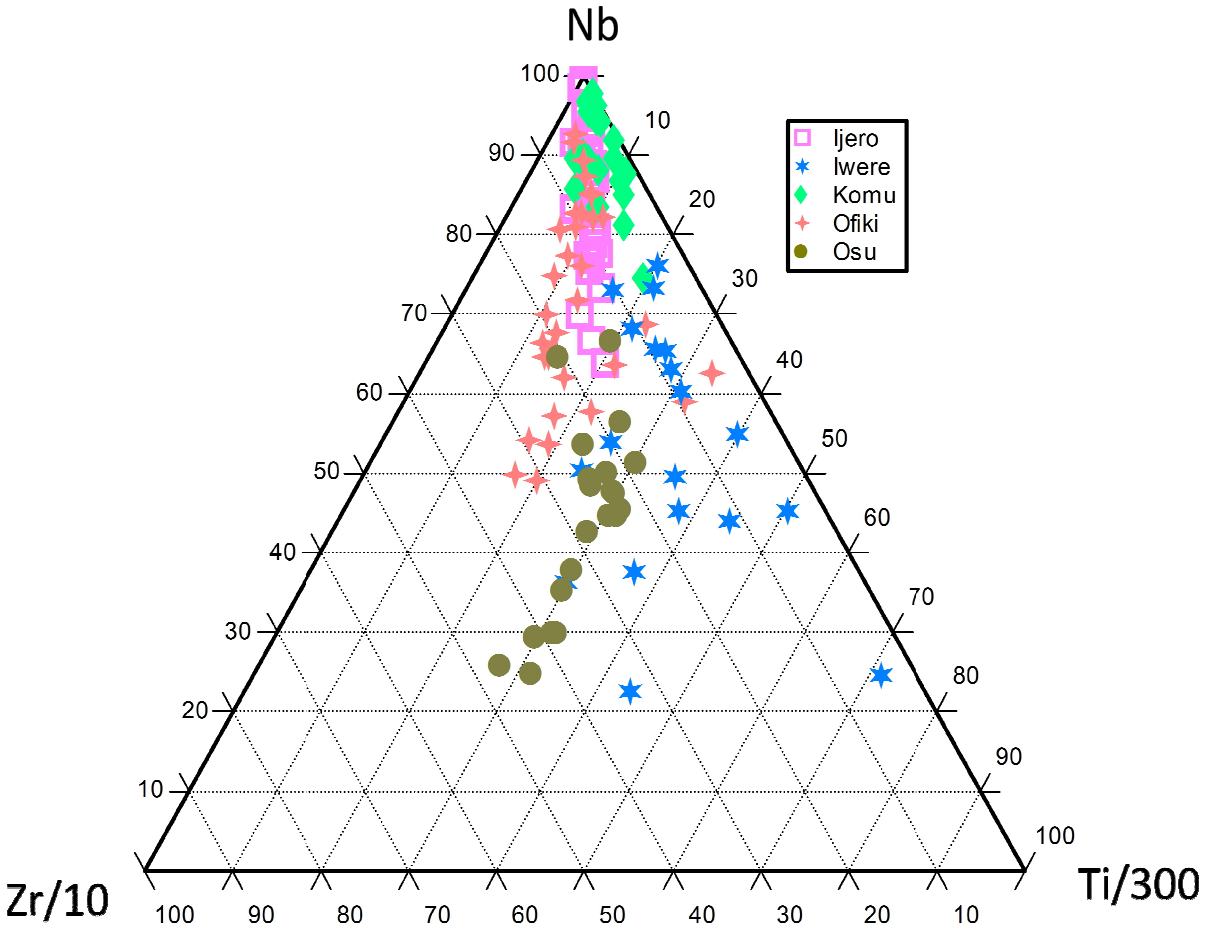

Fig. 4.86: Zr/10-Nb-Ti/300 ternary discrimination plot for the residual profiles (after Ranasinghe *et al*., 2005)

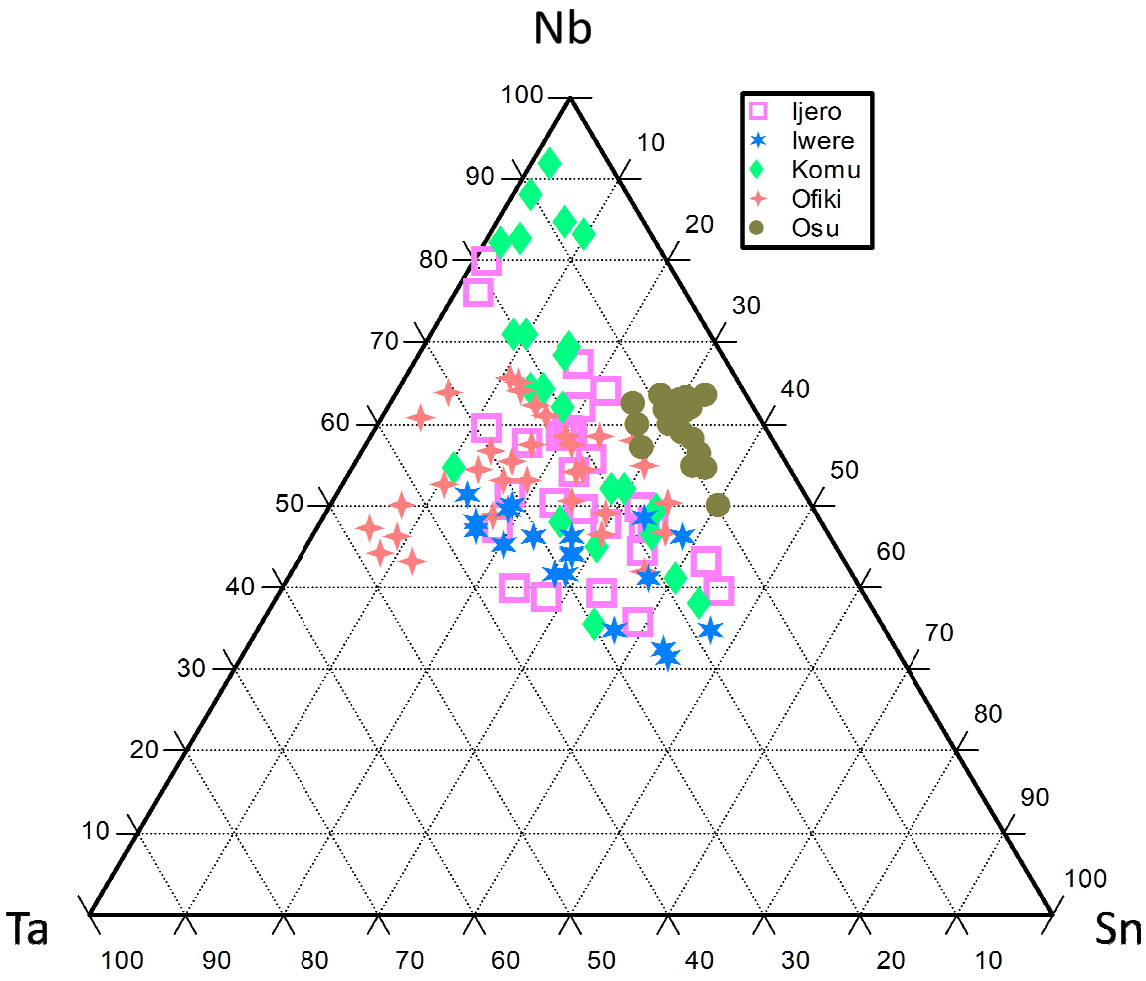
Nb
Ta
Sn
Ijero
Iwere
Komu
Ofiki
Osu
100
90
80
70
60
50
40
30
20
10

Fig. 4.87: Ta-Nb-Sn ternary discrimination plot for the residual profiles

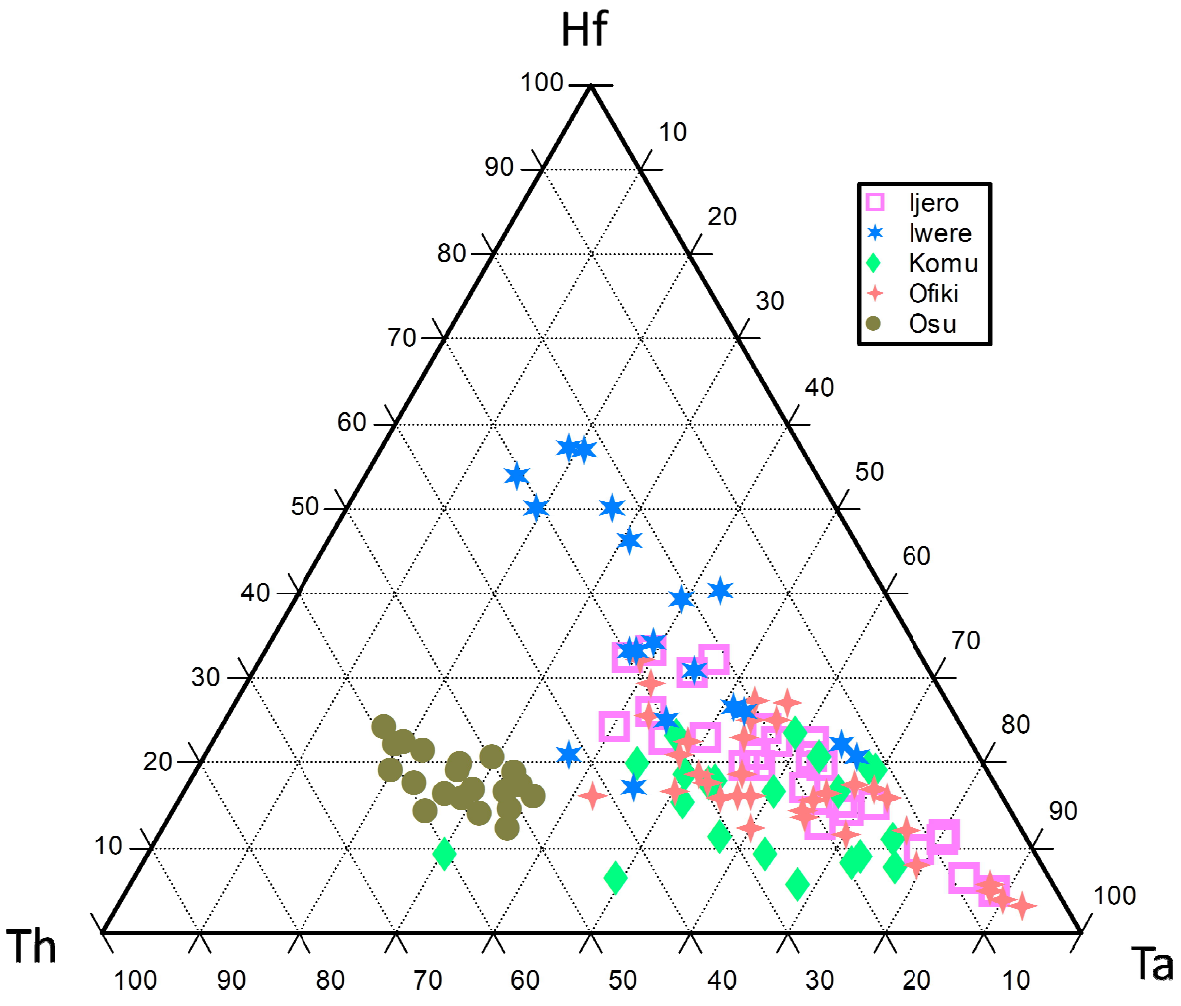

Fig. 4.88: Th-Hf-Ta ternary discrimination plot for the residual profiles

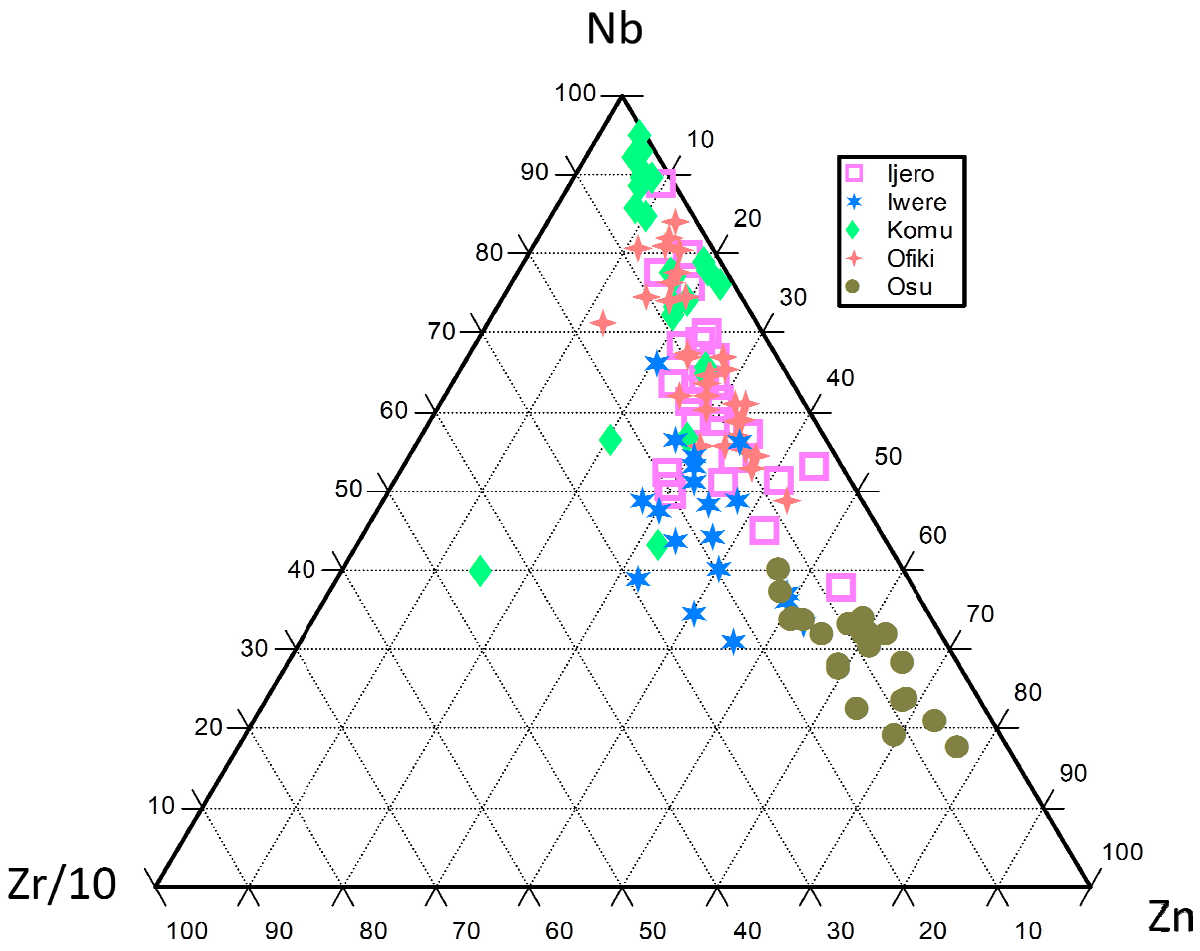

Fig. 4.89: Zr/10-Nb-Zn ternary discrimination plot for the residual profiles (after Ranasinghe *et al*., 2005)

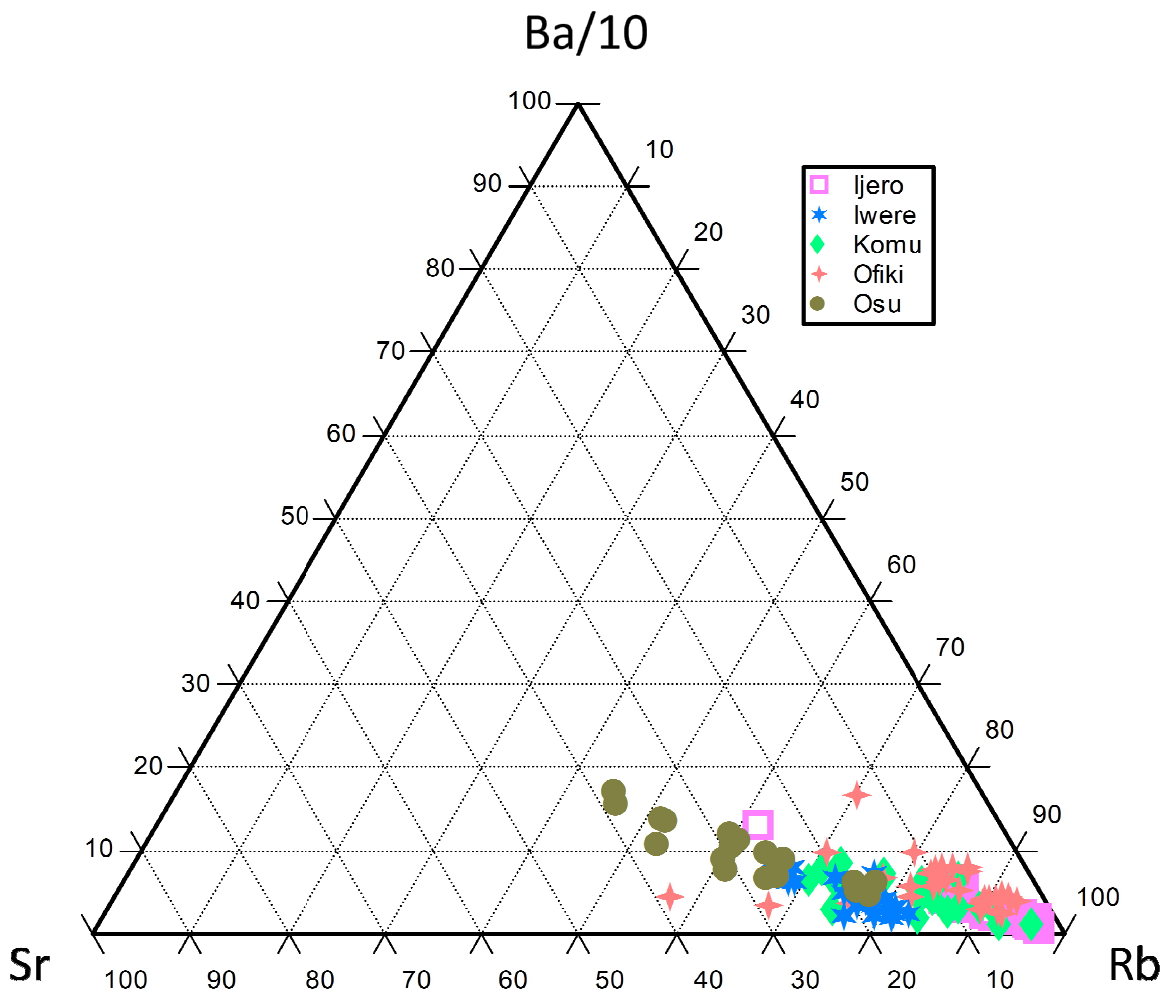

Fig. 4.90: Sr-Ba/10-Rb ternary discrimination plot for the residual profiles (after Ranasinghe *et al*., 2005)

On the whole, it is considered that the clustering of the investigated *in situ*-derived lateritic profile samples into distinct fields, inferably indicates the differences in the primary lithogeochemical signatures of their respective parent rocks. This is invariably a pointer to the remarkable differences in the modal mineralogy and abundances of the accessory mineral phases that host the relatively immobile HFS elements in the respective parent rocks. These mineral phases include ilmenite, sphene, rutile, anatase, zircon, cassiterite

and columbo-tantalite. The relative insusceptibility of these phases tochemical break down in supergene weathering environment could also be adduced for theobserved geochemical patterns (Hallberg, 1984; Brinhall *et al*., 1991; Braun *et al.*, 1993; Gouveia *et al*., 1993; Khider and McQueen, 2005; Du *et al*., 2012).

4.6 Exploration implications of the indicator minerals and the geochemical discriminants in the pegmatite-derived lateritic profiles

Mineralised pegmatites occur together with barren pegmatites within basement rocks, and constituite very small proportion of known pegmatite bodies in any given pegmatite district (Cerny, 1989; London and Kontak, 2012; London and Morgan, 2012). Exploration for rare-element pegmatites are largely hampered by deep weathering of the basement rocks and residual lateritic covers in lateritic terrains. Pegmatite characteristics, their restricted extents, poor outcropping nature, limited alteration haloes and geochemical signatures under covers, which are not easily resolved with imaging techniques, are some of the challenges of pegmatite-hosted mineral exploration.

Indicator minerals, including rutile, magnetite, and schorl in the *in situ*-derived weathering profiles of the mineralised pegmatites and the conspicuous absence of these mineral phases in the barren pegmatite profile, afford the distinction of the rare metal-rich and barren pegmatite bedrocks underneath pegmatite residual profiles. The aforelistedindicator minerals are weathering-resistant and therefore preserved the primary geochemical signatures of the parent pegmatite bedrocks. Rare-element and barren pegmatite bedrocks are marked by distinct relative abundances of HFSEs and LILEs, reflecting varying degrees of pre-enrichments of these lithophile elements in their protoliths and geochemical evolution of these pegmatite types. These distinct primary lithogeochemical signatures are preserved and considerably enhanced in their respective profiles during chemical weathering.

A suite of pegmatite petrogenetic immobile HFSEs, including Nb, Ta, Sn, Y and Th are significantly enhanced in the mineralised pegmatite profiles relative to the barren pegmatite profile, and serve as the best discriminating elements between the pegmatite types under lateritic covers. The observed enhancements of these HFSEs in the studied

weathering profiles are correlatable with their chemical inertness and residual character to hydrodynamic dispersion in supergene weathering environment. The above geochemical attributes of the HFSEs exploited via correlation analysis, were utilised in evolving suitable geochemical ratios and in developing discrimination diagrams for differentiating between rare metal-rich and barren pegmatite profiles. For instance, the mineralised pegmatite profiles indicate low Nb/Ta (0.9 – 3.9) and Zr/Nb (0.2 – 11.5) but high Th/U (0.5 – 3.6) ratios, as opposed to high Nb/Ta (>6.0) and Zr/Nb (1.0 – 16.4) but low Th/U (0.3 – 0.7) in the barren pegmatite profile. The HFSEs abundances in the residual profiles of the pegmatite types also provide suitable diagnostic criteria to distinguish the rare-element bearing and barren pegmatites beneath their respective lateritic profiles via Y-Nb, Ti-Nb, Zr-Nb, Zr-Ta, Zr-Th, and Zr/Th-Zr/Ta bivariate discrimination plots and Zr-Nb-Y, Zr/10-Nb-Y, Zr/10-Nb-Ti/300, Ta-Nb-Sn, Th-Hf-Ta, Zr/10-Nb-Zn and Sr-Ba/10-Rb ternary discrimination diagrams.

It is particularly worth noting that some of the highlighted indicator minerals, including rutile, ilmenite, magnetite, zircon and other refractory accessories, are important carriers of HFSEs (Moller *et al.*, 1988; Berry *et al*., 1999; Linnen and Cuney, 2005; Kuster, 2009; Xiong *et al*., 2011). For instance, beside Nb, Ta and Sn contributions from columbo-tantalite and cassiterite ores from the weathering of the mineralised pegmatite bedrocks, Nb and Ta have been documented to substitute into rutile via columbite-tantalite type substitution (Cerny and Ercit, 1985; Moller *et al*. 1988; Linnen and Keppler, 1997; Linnen and Cuney, 2005), while magnetite has been established as important sinks for Nb and Ta (Linnen and Cuney, 2005). Nb^{5+} (0.64Å), Ta^{5+} (0.64Å) and Sn^{4+} (0.69Ǻ) have common geochemical characteristics and can be preferentially incorporated into the lattice structure of rutile (Fadipe, 1988; Linnen and Cuney, 2005). It is equally important to note that Ti^{4+}(0.61Å) in rutile (TiO_2) also shows similar charge and ionic radius to the aforementioned 'refractory' cations.

The indicator minerals isolated and the geochemical discriminants generated from this study can be optimised with other existing geochemical tools for rare-element pegmatite exploration in any given pegmatite district in a typical lateritic terrain. This integrated technique is hoped to provide a rapid, cost-effective and less invasive approach to

exploring for rare-metal rich pegmatites underneath lateritic profiles, as uneconomic pegmatite prospects can be easily eliminated prior to test drilling and open pit mining. Through this, landscapes in pegmatite mining districts are expected to be better preserved while mining investment capital, labour and time will be profoundly conserved.

CHAPTER FIVE

CONCLUSIONS AND RECOMMENDATIONS

5.1 Conclusions

Barren and rare-element pegmatites occur as intrusive bodies within the basement rocks of southwestern Nigeria which are variedly overlain by deep residual profiles that hinder access to fresh bedrocks of the rare-element pegmatites. These rare-element pegmatites are highly valued for their unusual enrichment in important rare-metals and gem-quality crystals. Residual lateritic profiles above barren and mineralised pegmatites and their parent bedrocks in Osu, Ijero, Komu, Ofiki and Iwere-Ile areas of southwestern Nigeria, were investigated in order to determine the mineralogical indicators and geochemical criteria that can be employed to distinguish between barren and mineralised pegmatites under the lateritic cover.

The pegmatite in Osu area is an extensive outcrop that intruded biotite schist, quartzite/quartz schist, amphibolites and biotite-muscovite granite, while pegmatites of Ijero area are essentially in form of tabular dykes, sheets and veins with the biotite schist. The pegmatites of Komu area are mainly in form of dykes, veins and miarolitic pockets intrusive into banded gneiss, amphibolites and granitic rocks, while pegmatites of Ofiki area are intrusive dykes into biotite granites and those of Iwere-Ile area are intrusive dykes and veins within biotite granites and biotite-hornblende gneiss. Mineralogical data indicated that the Osu pegmatite is the simple, barren type, comprising microcline-perthite, quartz, albite, minor amounts of muscovite, biotite and accessory garnet, schorl, zircon and apatite; whereas the pegmatites of Ijero, Komu, Ofiki and Iwere-Ile areas are mineralised, with accessory constituents of beryl, lepidolite, gem tourmalines, topaz, tantalo-columbite ores, cassiterite, rutile, ilmenite and magnetite, in addition to the common rock-forming minerals highlighted for the barren Osu pegmatite.

Mineralogical composition of the barren pegmatite profile at Osu showed the dominance of quartz, subordinate amounts of persistent muscovite across the horizons, and low quantity of microcline and albite. Kaolinite is relatively enhanced in the horizons, except the A-horizon, of the Osu weathering profile. The mineralogical data of the mineralised pegmatite profiles of Ijero, Komu, Ofiki and Iwere-Ile areas are similar to the Osu pegmatite profile in terms of quartz dominance and low muscovite, microcline and albiteminerals. However, they are distinguished by the presence of minor amounts of schorl, magnetite, rutile and ilmenorutile.

The geochemical data of the whole-rock barren pegmatite of Osu area and the mineralised pegmatites of Ijero, Komu, Ofiki and Iwere-Ile areas revealed that the pegmatites are highly siliceous with SiO_2> 72 wt.%, with average alumina contents ranging between 14.32 and 15.59 wt.%. There are few disparities in the Fe_2O_3, MnO, TiO_2 and P_2O_5 compositions of the pegmatite samples.However, the mineralised pegmatites showed slightly higher concentrations of Na_2O relative to the barren Osu pegmatite. Lithophile trace elements, such as Rb, Cs, Ga, Sn, Nb and Ta in the mineralised pegmatites are higher than those of the barren Osu pegmatite. The mineral-chemical data of the discrete phases of microcline and muscovite indicated low K/Rb, K/Cs and Nb/Ta ratios in the mineralised pegmatites and reflected moderate degree of rare-alkali fractionation and rare-metal enrichment in these pegmatites, while higher ratios of these elements in the barren Osu pegmatite indicated very low chemical fractionation and poor rare-metal potential of the pegmatite. The tantalo-columbite samples from the mineralised pegmatites are essentially of ferrocolumbite to manganocolumbite and ferrotantalite to manganotantalite, indicating variations in melt chemistry or degree of geochemical fractionations of the pegmatite bodies. The presence of Ta-Nb oxides in the mineralised pegmatites of Ijero, Komu, Ofiki and Iwere-Ile, as opposed to their conspicuous absence in the barren Osu pegmatite, also showed geochemical distinctions between these pegmatite types. The degree of rare-alkali fractionation of the pegmatites were better amplified in the K/Rb versus Cs, Ga, and K/Cs versus Na_2O and Ta versus K/Rb plots of the K-feldspars; while the rare-metal mineralisation distinctions between the pegmatite types were further substantiated by the K/Rb versus Rb, Cs, Zn as well as Ta versus Ga, Cs+Rb, Cs, K/Cs, Rb versus Ta and Ta/W versus Cs plots of the muscovite samples. These plots invariably showed that the pegmatite

of Osu area is barren and geochemically poorly evolved, while the pegmatites of Ijero, Komu, Ofiki and Iwere-Ile areas are mineralised and moderately fractioned.

The bulk chemical data of the pegmatite residual profiles generally showed strong depletion, relative to the parent pegmatite bedrocks, of CaO, MgO, Na_2O, K_2O and P_2O_5 and residual accumulation of Al_2O_3, Fe_2O_3, TiO_2 and MnO. Lithium, Rb, Cs, Ba and Sr (LILEs) showed similar geochemical patterns to the depleted oxides, while Nb, Ta, Sn, Y, Zr, Hf, Th and REEs (HFSEs) showed residual accumulation in the weathering profiles relative to the bedrock. Correlations between relevant pegmatite petrogenetic elements showed the geochemical viability of a suite of HFSEs, including Zr, Ti, Y, Nb, Ta, Sn, Th and U as element pairs in deciphering the relative enrichment/depletion patterns in the weathering profiles and in isolating suitable geochemical ratios.

Enrichments of immobile trace elements including Nb, Ta, Sn, Y and Th in the mineralised pegmatite profiles, relative to the barren pegmatite profile, were observed. These are consistent with the rare metal-bearing accessory mineral phases present only in the mineralised pegmatites, as opposed to the barren pegmatite. Similarly, the mineralised pegmatite residual profiles indicated low Zr/Nb (0.2-11.5), Nb/Ta (0.9-3.9) and high Th/U (0.5-3.6) ratios, compared to high Zr/Nb (1.0-16.4), Nb/Ta (>6.0) and low Th/U (0.3-0.7) ratios obtained from the barren pegmatite residual profile.

Pegmatite petrogenetic immobile HFSEs have been used in this study to distinguish between barren and mineralised pegmatite residual profiles. Also, the applications of some HFSEs as suitable geochemical discriminants to isolate rare-metal pegmatite bodies underneath lateritic cover in southwestern Nigeria, has been highlighted. The rare-element pegmatite diagnostic tools highlighted in this study could be used in other tropical zones to complement existing rare-element pegmatite exploration guides, which can be applied prior to test drilling and open pit mining.

5.2 Recommendations

Primary lithogeochemical signatures of the barren and mineralised pegmatites and their *in situ*- derived lateritic profiles have been distinguished in this study. The rare metal-bearing accessory phases in the mineralised pegmatites are believed to be sources of the immobile

HFSEs in their lateritic profiles. The mineral chemistry of these rare metal-bearing phases in the residual weathering profiles, using combined *in situ* analytical techniques including scanning electron microscopy (SEM) and electron microprobe analysis (EMPA) should be investigated to determine chemical alteration and the transitional phases of minerals within the different horizons of the profiles.

Micro-morphological attributes of the HFSE-bearing accessory mineral phases in the lateritic profiles could also be determined, using high resolution imaging techiques, such as, transmission electron microscopy (TEM) and/or nano secondary ion mass spectrometry (NanoSIMS). These will enable adequate geochemical determination of the weathering processes and lateritisation history of the residual pegmatite profiles, which would shed more light on the nature of the immobilisation and/or redistribution of the immobile HFSEs in the rare-metal accessory mineral phases within rare-element pegmatite weathering profiles.

Due to analytical constrain, one barren pegmatite profile was considered in the course of this research. Future work should consider more barren pegmatite profiles together with mineralised pegmatite profiles for the discrimination of bedrock pegmatite mineralisation underneath lateritic profiles.

REFERENCES

Abaa, S. I. 1983. The structure and petrography of alkaline rocks of the Mada Younger Granite Complex, Nigeria.*Journal of African Earth Sciences* 3:107-103.

Acosta-Gongora, P., Gleeson, S. A., Samson, I. M., Ootes, L. and Corriveau, L. 2014. Trace element geochemistry of magnetite and its relationship to Cu-Bi-Co-Au-Ag-U-W mineralization in the Great Bear magnetite zone, NWT, Canada. *Economic Geology* 109:1901-1928.

Adekeye, J. I. D. and Akintola, O. F. 2007. Geochemical features of rare-metal pegmatites in Nassarawa area, central Nigeria. *Journal of Mining and Geology* 43.1:15-21.

Adekoya, J. A. 1988. Precambrian Iron-formation of northwestern Nigeria.*Precambrian Geology of Nigeria*. P. O. Oluyide, W. C. Mbonu, A. E. Ogezi, I. G. Egbuniwe, A. C. Ajibade and A. C. Umeji. Eds. Geological Survey of Nigeria Special Publication.195-210.

Adekoya, J. A. 1993. Proterozoic Maru and Birnin Gwari banded iron-formations northwestern Nigeria. *Journal of Mining and Geology*29.1:63-76.

Adekoya, J. A. 1996. The Nigerian schist belts: age and depositional environment implications from associated banded iron-formation. *Journal of Mining and Geology* 32.1:35-46.

Adekoya, J.A., Kehinde-Phillip, O.O. and Odukoya, A.M. 2003.Geological distribution of mineral resources in southwestern Nigeria.*Prospects for Investment in Mineral Resources of Southwestern Nigeria.*A.A.Elueze. Ed.Nigerian Mining and Geosciences Society Special Publication.1-13.

Adetunji, A. and Ocan, O. O. 2010.Characterization and mineralization potential of pegmatites of Komu area, Oyo State, southwestern Nigeria.*Resource Geology* 60: 87-97.

Adetunji, A. Olarewaju, V. O., Ocan, O. O., Ganev, V. Y. and Macheva, L. 2015. Geochemistry and U-Pb zircon geochronology of the pegmatites in Ede area, southwestern Nigeria: a newly discovered oldest Pan-African rock in southwestern Nigeria. *Journal of African Earth Sciences* 115:177-190.

Adetunji, A. Olarewaju, V. O., Ocan, O. O., Macheva, L. and Ganev, V. Y. 2018. Geochemistry and U-Pb zircon geochronology of Iwo quartz potassic syenite southwestern Nigeria: constraints on petrogenesis, timing of deformation and terrane amalgamation. *Precambrian Research* 307:125-136.

Afifi, A.A., Bricker, O.P. and Chemerys, J.C. 1985. Experimental chemical weathering of various bedrock types at different pH-values- sandstone and granites. *Chemical Geology* 49.1:87-113.

Ajayi, T. R. 1980. On the geochemistry and origin of the amphibolites in Ife-Ilesha area, SW Nigeria.*Journal of Mining and Geology* 17:179-196.

Ajibade, A.C. 1976. Provisional classification and correlation of the schistbelts in northern Nigeria.*Geology of Nigeria.*C. A. Kogbe. Ed. Lagos: Elizabethan Publishing Company. 85-90.

Ajibade, A. C. 1980. Geotectonic evolution of the Zungeru region, Nigeria.*PhD Thesis*, University of Wales, Aberystwyth.xvi+ 303pp.

Ajibade, A. C. and Fitches, W. R. 1988.The Nigerian Precambrian and the Pan-African Orogeny.*Precambrian Geology of Nigeria*. P. O. Oluyide, W. C. Mbonu, A. E. Ogezi, I. G. Egbuniwe, A. C. Ajibade and A. C. Umeji. Eds. Geological Survey of Nigeria Special Publication.45-53.

Ajibade, A.C., Woakes, M. and Rahaman, M.A. 1987.Proterozoic crustal development in the Pan-African regime of Nigeria.*Proterozoic Crustal Evolution.*A. KronerEd.American Geophysical Union Publication: 259-271.

Akintola, O. F. and Adekeye, J. I. D. 2008. Mineralization controls and petrogenesis of the rare metal pegmatites of Nasarawa area, central Nigeria. *Earth Science Research Journal* 12:44-61.

Akoh, J. U., Ogunleye, P. O. and Ibrahim, A. A. 2015. Geochemical evolution of micas and Sn-, Nb-, Ta-mineralization associated with rare metal pegmatite in Angwan Doka, central Nigeria. *Journal of African Earth Sciences* 112:24-36.

Albarede, F. 2003. *Geochemistry: an introduction.* Cambridge: Cambridge University Press.

Alfonso, P., Melgarejo, J. C., Yusta, I. and Velasco, F. 2003. Geochemistry of feldspars and muscovite in granitic pegmatite from the Cap de Creus Field, Catalonia, Spain.*Candian Mineralogist* 41:103-116.

Anand, R. R., 2000. Regolith and geochemical synthesis of the Yandal greenstone belt.*Yandal Greenstne Belt, Regoliths, Geology and Mineralisation.* Phillips, G. N. and Anand, R. R. Eds. Australian Institute of Geoscientists Bulletin 31:79-112.

Anand, R. R. and Paine, M. 2002. Regolith geology of the Yilgarn Craton, Western Australia: implications for exploration. *Australian Journal of Earth Sciences* 49:3-162.

Anderson, J. L., Morrison, J. and Paterson, S. R. 2012. Post-emplacement fluids and pluton thermobarometry: Mount Stuart Batholith, Washington Cascade. *International Geology Review* 54:491-508.

Annor, A. E. 1983. Metamorphism of pelitic rocks in relation to deformation episodes around Okene, Nigeria.*Journal of Mining and Geology* 20:17-24.

Annor, A.E. 1995. U-Pb zircon age for Kabba-Okene granodiorite gneiss: implication for Nigeria's basement chronology. *African Geoscience Review* 2.1:101-105.

Annor, A. E. and Freeth, S. J. 1984. On the origin and thermotectonic history of hypersthene-bearing rocks from the Okene area, Nigeria.*Nigerian Journal of Mining and Geology*21.1-2:73-77.

Anthony, J. W., Bideaux, R. A., Bladh, K. W. and Nicholas, M. C., 2004.*Handbook of Mineralogy,Volume III.*Mineralogical Society of America. Chantilly, Virginia, USA.

Arhin, E. and Nude, P. M. 2009. Significance of regolith mapping and its implications for gold exploration in northern Ghana: a case of Tinga and Kunche. *Geochemistry, Exploration, Environment, Analysis* 9:63-69.

Aristizabal, E., Roser, B. and Yokota, S. 2005. Tropical chemical weathering of hillslope deposits and bedrock source in the Abura Valley, northern Colombian Andes.*Engineering Geology* 81:389-406.

Aromolaran, O. K. 2007. Study of compositional characteristics of pegmatites and associated granitic rocks in parts of the Precambrian Basement Complex of southwestern Nigeria. *M.Sc dissertation*, Department of Geology. University of Ibadan, Nigeria. xii+105p.

Aromolaran, O. K., Elueze, A. A. and Geisler, T. 2017. Nb, Ta and Sn contents and Nb/Ta and Th/U ratios in pegmatite residual profiles as geochemical criteria for distinguishing rare metal-bearing and barren pegmatites under lateritic covers. *Proceedings of the 14th Biennial Meeting of the Society for Geology Applied to Mineral Deposits,* 20-23 August 2017, Quebec City, Canada: 1139-1142.

Averill, S. A. 2001. The application of heavy indicator mineralogy in mineral exploration with emphasis on base metal indicators in glaciated metamorphic and plutonic terrains. Geological Society of London Special Publication 185: 69-81.

Baadsgaard, H., Chaplin, C. and Griffin, W. L. 1984.Geochronology of the Gloserheia pegmatite, Froland, Southern Norway.*Norsk Geologisk Tidsskrift* 64:111-119

Bardossy, G. and Aleva, G.J.J. 1990.*Lateritic bauxites.*Amsterdam: Elsevier.

Bartels, A., Holtz, F. and Linnen, R. L. 2010. Solubility of manganotantalite and manganocolumbite in pegmatite melts. *American Mineralogists* 95:537-544.

Bedard, E., Goulet, A., Sappin, A.A., Makvand, S. and Beaudoin, G. 2017. Chalcopyrite as an indicator mineral to fingerprint mineral deposit types: a preliminary study. *Proceedings of the 14th Biennial Meeting of the Society for Geology Applied to Mineral Deposits,* 20-23 August 2017, Quebec City, Canada: 1115-1118.

Belousova, E. A., Walters, S., Griffin, W. L., and O'Reilly, S. Y. 2001. Trace element signatures of apatite from granitoids of Mount Isa inlier, northwestern Queensland. *Australian Journal of Earth Sciences* 48:603-619.

Belousova, E. A., Griffin, W. L., O'Reilly, S. Y. and Fisher, N. I. 2002. Apatite as an indicator mineral for mineral exploration: trace element compositions and their relationship to host rock types. *Journal of Geochemical Exploration* 76:45-69.

Berry, F., Greaves, C., Helgason, O. and McManus, J. 1999.Synthesis and characterization of tin-doped iron oxides.*Journal of Material Chemistry* 9:233-226

Beus, A. A., 1966. Distribution of tantalum and niobium in muscovite from granitic pegmatites.*Geokhimiya* 10:1216-1220.

Beus, A. A. 1982. Metallogeny of Precambrian rare-metal granitoids.*Revista Brasileira de Geociencias* 12.1-3:410-413.

Bhatia, M. R. and Crook, K. A. W. 1986. Trace element characteristics of greywackes and tectonic discrimination of sedimentary basins. *Contributions to Mineralogy and Petrology* 92:181-193.

Black, R., Caby, R., Moussine-Pouchkine, A., Bayer, R., Bertrand, J. M. L., Boullier, A. M., Fabre, J. and Lesquer, A. 1979.Evidence for late Precambrian plate tectonics in West Africa.*Nature* 278:223-226.

Boutroy, E., Dare, S. A. S., Beaudoin, G., Barnes, S. J., and Lightfoot, P. C. 2014. Magnetite composition in Ni-Cu-PGE deposits worldwide: application to mineral exploration. *Journal of Geochemical Exploration* 145:64-81.

Bouzari, F., Hart, C. J. R., Barker, S. and Bissig, T. 2011. Exploration for concealed deposits using porphyry indicator minerals (PIMs): Application of apatite textures and chemistry. *Proceedings of 25th International Applied Geochemistry Symposium.* 22-26August 2011. Sarja B. Ed. Rovaniemi, Finland: 89-90.

Brand, N.W. 1997.Chemical and Mineralogical characteristics of weathered komatiitic rocks, Yilgarn Craton, Western Australia: discrimination of nickel sulphide bearing and barren komatiites.*PhD Thesis,* University of Western Australia.xxii+373pp.

Brand, N.W. 1999. Element ratios in nickel sulphide exploration: vectoring towards ore environments. *Journal of Geochemical Exploration* 67:145-165.

Brand, N. W. and Butt, C. R. M. 2001. Weathering, element distribution and geochemical dispersion at Mt. Keith, Western Australia: implication for nickel sulphide exploration. *Geochemistry: Exploration, Environment, Analysis* 1:391- 407.

Brand, N. W., Butt, C. R. M. and Hellensten, K. J. 1996. Structural and lithological controls on the formation of the Cawse nickel laterite deposits, Western Australia-implications for supergene ore formation and exploration in deeply weathered terranes. *Australian Institute of Mining and Metallurgy Publication Series* 6/96: 185-190.

Braun, J. J. and Pagel, M. 1994. Geochemical and mineralogical behaviour of REE, Th and U in the Akongo lateritic profile (SW Cameron).*Catena* 21:173-177

Braun, J.J., Pagel, M., Muller, J.P., Bilong, P., Michard, A., and Guillet, B. 1990.Cerium anomalies in lateritic profiles.*Geochimica et Cosmochimica Acta* 51: 4419-4434.

Braun, J.J., Pagel, M., Herbillon, A. and Rosin, C. 1993. Mobilization and redistribution of REEs and thorium in a syenitic lateritic profile: a mass balance study. *Geochimica et Cosmochimica Acta* 57.2:273-299.

Braun, J.J., Viers, J., Dupre, B., Polve, M., Ndam, J. and Muller, J.P. 1998. Solid/liquid REE fractionation in the lateritc system of Goyoum, East Cameroon: the implication for the present dynamics of the soil covers of the humid tropical regions. *Geochimica et Cosmochimica Acta* 62.2:273-299.

Braun, J. J., Descloitres, M., Riotte, J., Fleury, S, Barbiero, L., Boeglin, J. L., Violette, A., Lacarce, E., Ruiz, L., Sekhar, M., Mohankumar, M. S., Subramanian, S.and Dupre, B. 2009. Regolith mass balance inferred from combined mineralogical, geochemical and geophysical studies: Mule hole gneissic watershed, South India. *Geochimica et Cosmochimica Acta*73.4:935-961.

Braun, J. J., Marechal, J. C., Riotte, J., Boeglin, J. P., Bedimo, J. P. B., Ngoupayou, J. R. N. Nyeck, B., Robain, H., Sekhar, M., Audry, S. and Viers, J., 2012. Elemental weathering fluxes and saprolite production rate in a Central African lateritic terrain (Nsimi, South Cameroon). *Geochimica et Cosmochimica Acta*99:243-270.

Brimhall, G. H., Lewis, C. J., Ford, C., Bratt, J., Taylor, G. and Warin, O. 1991. Quantitative geochemical approach to pedogenesis - importance of parent material reduction, volumetric expansion, and eolian influx in lateritization.*Geoderma* 51: 51-91.

Brindley, G. W. and Brown, G. 1980.X-ray diffraction procedures for clay mineral identification.*Crystal structures of clay minerals and their X-ray identification*. G. W. Brindley and G. Brown. Eds. Mineralogical Society of London Monograph 5: 305-359.

Brisbin, W. C. 1986. Mechanics of pegmatite intrusion.*American Mineralogists* 71:644-651.

Broster, B. E., Dickson, M. L. and Parkhill, M. A. 2009. Comparison of humus and till as prospecting materials in areas of thick overburden and multiple ice-flow events: an example from northeastern Brunswick. *Journal of Geochemical Exploration* 103: 115-132.

Brown, J.A. 2004. Mineralogy and geochemistry of beryl and rare-metal-bearing granitic pegmatites in the Kootenay Region of southeatern British Columbia.*British Columbia Geological Survey Geological Fieldwork 2003, Paper 2004*-1:167-184.

Bruguier, O., Dada, S.S. and Lancelot, J.R. 1994. Early Archaean component (>3.5 Ga) within a 3.05 Ga orthogneiss from northern Nigeria: U-Pb zircon evidence. *Earth and Planetary Science Letters* 125:89-103.

Butt, C. R. M. and Zeeegers, H. 1992.Climate, geomorphological environment and geochemical dispersion models.*Handbook of Exploration Geochemistry: Regolith Exploration Geochemistry in tropical and Subtropical Terranes.*C. R. M. Butt and H. Zeeegers. Eds. Amsterdam: Elservier 4: 3-23.

Butt, C. R. M., Lintern, M. J. and Anand, R. R. 2000. Evolution of regoliths and landscapes in deeply weathered terrain — implications for geochemical exploration. *Ore GeologyReviews*16.3-4:167-183.

Caby, R. 1989. Precambrian terrain of Benin-Nigeria and northeast Brazil and the Late Proterozoic South Atlantic fit. *Geological Society of America Special Paper* 230: 145-158.

Caby, R., Bertrand, J. M. L. and Black, R. 1981. Pan-African ocean closure and continental collision in the Hoggar –Iforas segment, Central Sahara.*Precambrian Plate Tectonics.* A. Kroner. Ed. Amsterdam: Elsevier.407-434.

Cameron, E.M., Leybourne, M. I. and Kelley, D. 2002. Exploring for deeply covered mineral deposits: formation of geochemical anomaliesin northern Chile by earthquake-induced surface flooding of mineralized groundwaters. *Geology* 30: 1007-1010.

Cameron, E.M., Hamilton, S.M., Leybourne, M.I., Hall, G.E.M. and McClenaghan, M.B. 2004. Finding deeply buried deposits using geochemistry. *Geochemistry: Exploration, Environment, Analysis* 4.1:7-32.

Cameron, E.M., Leybourne, M.I. and Kelley, D. L. 2005. Exploring for deposits under deep covers using geochemistry. *Society of Economic Geology Newsletter* 63:5-15.

Cameron, E.M., Hamilton, S.M., Leybourne, M.I., Reich, M. and Palacios, C. 2010. Geochemical anomalies in northern Chile as a surface expression of the extended supergene metallogenesis of buried copper deposits. *Geochemistry: Exploration, Environment, Analysis*10:157-169.

Cerny, P. 1982. Anatomy and classification of granitic pegmatites.*Granitic Pegmatites in Science and Industry*. P. Cerny. Ed. Mineralogical Association of Canada Short Course Handbook 8:1-39.

Cerny, P. 1989a.Characteristics of pegmatite deposits of tantalum.*Lanthanides, Tantalum and Niobium.* P. Moller, P. Cerny, and F. Saupe. Eds. Heidelberg:Springer-Verlag.195-239.

Cerny, P. 1989b. Exploration strategy and methods for pegmatite deposits of tantalum: *Lanthanides, Tantalum and Niobium.* P. Moller, P. Cerny, and F. Saupe. Eds. Heidelberg: Springer-Verlag.274-310.

Cerny, P. 1990. Distribution, affiliation and derivation of rare-element granitic pegmatites in the Canadian Shield.*Geologische Rundschau* 79:183-226.

Cerny, P. 1991a. Fertile granites of Precambrian rare-element pegmatite fields: is geochemistry controlled by tectonic setting or source lithologies? *Precambrian Research* 51:429-468.

Cerny, P. 1991b.Rare-element pegmatites.Part I. Anatomy and internal evolution of pegmatite deposits.*Geoscience Canada* 18:49-67.

Cerny, P. 1992. Geochemical and petrogenetic features of mineralization in rare-element granitic pegmatites in the light of current research.*Applied Geochemistry* 7:393-416.

Cerny, P. 2005. The Tanco rare-element pegmatite deposits, Manitoba: Regional context, internal anatomy, and global comparisons. *Rare-Element Geochemistry and Mineral Deposits*.R. L. Linnen and I. M. Samson. Eds. Geological Association of Canada Short Course Notes 17:127-158.

Cerny, P. and Burt, D. M. 1984. Paragenesis, crystallochemical characteristics, and geochemical evolution of micas in granitic pegmatites.*Micas*. S. W. Bailey. Ed. Mineralogical Society of America Review in Mineralogy 13:257-297.

Cerny, P. and Ercit, T. S. 1985. Some recent advances in the mineralogy and geochemistry of Nb and Ta in rare-element granitic pegmatites.*Bulletin Mineralogie* 108:499-532.

Cerny, P. and Erict, T.S. 1989. Mineralogy of niobium and tantalum: crystal chemical relationships, paragenetic aspects and their economic implications. *Lanthanides, Tantalum and Niobium.*P. Moller, P. Cerny and F. Saupe. Eds. Heidelberg: Springer-Verlag.27-79.

Cerny, P. and Erict, T.S. 2005. Classification of granitic pegmatites revisited. *Canadian Mineralogist* 43:185-202.

Cerny, P and Kjellman, J. 1999. The NYF family of granitic pegmatites: simplistic past, fluid present, reformed future. The Eugene E. Foord Memorial Symposium on NYF-type Pegmatites (Denver). *Canadian Mineralogist* 37:799-800.

Cerny, P., Ercit, T.S. and Wise, M. A. 1992. The tantalite-tapiolite gap: natural assemblages versus experimental data. *Canadian Mineralogist* 30:587-596.

Cerny, P., Meintzer, R. E. and Anderson, A. J. 1985. Extreme fractionation in rare-element granitic pegmatites: selected examples of data and mechanisms. *Canadian Mineralogist* 23:381-421.

Cerny, P., London, D. and Novak, M. 2012. Granitic pegmatites as reflections of their sources.*Elements* 8.4:289-294.

Cerny, P., Blevin, P.L., Cunney, M. and London, D. 2005.Granite-related ore deposits.*Economic Geology One Hundredth Anniversary Volume (1905-2005).*J. W. Hedenquist, J. F. H. Thompson, R. J. Goldfarb and J. P. Richards. Eds. Society of Economic Geologists, Colorado, USA: 337-370.

Clark, J. R. 1993. Enzyme-induced leaching of B-horizon soils for mineral exploration in areas of glacial overburden. *Transactions of Institute of Mining and Metallurgy* 102: 19-29.

Clifford, T.N. 1970. The structural framework of Africa. *African magmatism and tectonics.* T. N. Clifford and I. G. Gass.Eds.London: Oliver and Boyd. 1-26.

Colman, S.M. 1982. Chemical weathering of basalts and andesites: evidence from weathering rinds.*U.S. Geological Survey Professional Paper No. 1246*, 51p.

Cooray, P. G. 1972. Note on the charnockite of Ado-Ekiti area, Western State Nigeria. *African Geology.* T. F. J. Dessaugavie and Whiteman, A. J. Eds. Ibadan: Ibadan University Press.45-54.

Cooray, P. G. 1974. Some aspects of the Precambrian of Nigeria: A review. *Journal of Mining and Geology* 8.1-2:17-43.

Cooray, P. G. 1975. A note on the charnockitic rocks of the Otun-Egosi area, Western Nigeria. *Journal of Mining and Geology* 11.1-2:15-25.

Cornelius, M., Robertson, I.D.M., Cornelius, A.J. and Morris, P.A. 2008.Geochemical mapping of the deeply weathered Western Yilgarn Craton of Western Australia, using laterite geochemistry.*Geochemistry: Exploration, Environment, Analysis* 8.3-4:241-254.

Dada, S.S. 1998.Crust-forming ages and Proterozoic crustal evolution in Nigeria; a reappraisal of current interpretations.*Precambrian Research* 87:65-74.

Dada, S. S. 2006. Proterozoic evolution of Nigeria.*The Basement Complex of Nigeria and Its Mineral Resources(A Tribute to Prof. M.A.O. Rahaman).* O. Oshin. Ed. Ibadan: Akin Jinad and Company.29-44.

Dada, S. S., Lancelot, J.R. and Briqueu, L. 1989. Age and origin of annular charnockitic complex of Toro, northern Nigeria: U-Pb and Rb-Sr evidence. *Journal of African Earth Sciences* 9:227-234.

Dada, S. S., Tubosun, I. A., Lancelot, J. R. and Lar, A. U. 1993. Late Archaean U-Pb age for the reactivated basement of northeastern Nigeria.*Journal of African Earth Sciences* 16:405-412.

Dada, S.S., Birck, J.L., Lancelot, J.R. and Rahaman, M.A. 1993. Archaean migmatite-gneiss complex of northcentral Nigeria: its geochemistry, petrogenesis and crustal evolution. *International Colloquium on African Geology, Mbabane, Swaziland:* 97-102.

Dada, S. S., Briqueu, L. and Birck, J. L. 1998. Primodial crustal growth in northern Nigeria: preliminary Rb-Sr and Sm-Nd constraints from Kaduna migmatite-gneiss complex. *Journal of Mining and Geology* 34.1:1-6.

Danbatta, U. A. and Garba, M. L. 2007. Geochemistry and petrogenesis of Precambrian amphibolites in the Zuru schist belt, northwestern Nigeria. *Journal of Mining and Geology* 43.1:23-30

Dare, S. A. S., Barnes, S. J., Beaudoin, G., Meric, J., Boutroy, E. and Potvin-Doucet, C. 2014. Trace elements in magnetite as petrogenetic indicators. *Mineralium Deposita* 49:785-796.

Dequincey, O., Chabaux, F., Clauer, N., Sigmarsson, O., Liewig, N. and Leprun, J. C. 2002. Chemical mobilizations in laterites: evidence from trace elements and ^{238}U-^{234}U- ^{230}Th disequilibria. *Geochimica et Cosmochimica Acta* 66:1197-1210.

Dill, H. G. 2015. Pegmatites and aplites: Their genetic and applied ore geology. *Ore Geology Review* 69:417-561.

Dissanayake, C. B. and Rupasinghe, M. S. 1986. The niobium and yttrium abundance in the sedimentary gem deposits of Sri Lanka. *Journal of Natural Sciences* 14.1:55-74.

Dissanayake, C. B. and Rupasinghe, M. S. 1992. Application of geochemistry to exploration for gem deposits, Sri Lanka. *Journal of Gemmology* 23:165-175.

Du, X. 2012.The occurrence and behaviour of rare earth and associated elements in lateritic regolith profiles in Western Australia.*PhD Thesis*.School of Earth and Environment.The University of Western Australia.xvii+247pp.

Du, X., Rate, A.W. and Gee, M.A.M. 2012.Redistribution and mobilization of titanium, zirconium and thorium in an intensely weathered lateritic profile in Western Australia.*Chemical Geology*330-331: 101-115.

Dupuis, C. and Beaudoin, G. 2011. Discriminant diagrams for iron oxide trace element fingerprinting of mineral deposit types. *Mineralium Deposita* 46:319-335.

Duzgoren-Aydin, N. S., Aydin, A and Malpas, J. 2002. Re-assessment of chemical weathering indices: case study on pyroclastic rocks of Hong Kong. *Engineering Geology* 63:99-119.

Eby, G. N. 1990. The A-type granitoids: A review of their occurrence and chemical characteristics and speculations on their petrogenesis. *Lithos* 26:115-134.

Eby, G. N. 1992. Chemical subdivision of the A-type granitoids: petrogenetic and tectonic implications. *Geology* 20:641-644.

Ekwere, S. J. 1985. Li, F and Rb contents and Ba/Rb and Rb/Sr ratios as indicators of postmagmatic alteration and mineralization in the granitic rocks of the Banke and Ririwai Younger Granite Complexes, Northern Nigeria.*Mineralium Deposita* 20:89-93.

Ekwueme, B.N. and Kroner, A. 1998. Single zircon evaporation ages from the Oban Massif, southeastern Nigeria. *Journal of African Earth Sciences* 26:195-205.

Ekwueme, B. N. and Schlag, C. 1989. Compositions of monazite in pegmatites and related rocks of the Oban Massif, SE Nigeria: implications for economic mineral exploration. *International Geological Correlation Project* (*IGCP) Newsletter/Bulletin 2*.255: 15-20.

Ekwueme, B. N. and Kroner, A. 1993. Preliminary zircon evaporation ages from migmatitic gneisses in Kaduna, northern Nigeria: evidence for early Archaean

(Pre Leonian) event in the Nigeria Basement Complex. *International Geological Correlation Project (IGCP) 280 International Conference,* Salvador, Brazil.

Ekwueme, B. N. and Kroner, A. 1997. Zircon evaporation ages and chemical composition of migmatitic schist in the Obudu Plateau: evidence for Palaeoproterozoic (ca 1789) components in the Basement Complex of southeastern Nigeria. *Journal of Mining and Geology* 33.2:81-88.

Ekwueme, B. N. and Matheis, G. 1995.Geochemistry and economic value of pegmatites in the Precambrian basement southeast Nigeria.*Magmatism in relation to diverse tectonic settings.*R. K. Srivastara and R. Chandra. Eds. New Delhi: Oxford and IBH Publishing Company. 375-392.

Ekwueme, B. N. and Onyeagocha, A. C. 1986.Geochemistry of metasedimentary rocks of Uwet area, Oban massif, southeastern Nigeria.*Geologische Rundschau* 75.2: 411-420.

Ekwueme, B. N., Nyong, E. E. and Peters, S. W. 1995. Geological Excursion Guidebook to Oban Massif, Calabar Flank and Mamfe Embayment, southeastern Nigeria. Calabar: DEC-FORD Publishers Limited.

Elueze, A. A., 1980. Geochemical studies of Proterozoic amphibolites and meta-ultramafites in Nigerian schist belts: Implications for Precambrian crustal evolution. *PhD Thesis.*Department of Geology.University of Ibadan.xix+288p.

Elueze, A.A. 1981a. Geochemistry and petrotectonic setting of metasedimentary rocks of the schist belt of Ilesha area, southwestern Nigeria. *Journal of Mining and Geology* 19.1:194-197.

Elueze, A.A. 1981b. Petrographic studies of metabasic rocks and meta-ultramafites in relation to mineralization in Nigerian schist belts. *Journal of Mining and Geology* 18:31-36

Elueze, A. A. 1982. Mineralogy and chemical nature of meta-ultramafites in Nigerian schist belts.*Journal of Mining and Geology* 19:21-29

Elueze, A. A. 1985. Petrochemical and petrogenetic characteristics of Precambrian amphibolites of the Alawa district, northwest Nigeria. *Chemical Geology* 48:29-41.

Elueze, A. A., 1986. Petrology and gold mineralization of the amphibolite belt Ilesha area, southwestern Nigeria. *Geologie Mijnbouw* 65:189-195.

Elueze, A.A. 1988. Geology of the Precambrian of schist belt in Ilesha area, southwestern Nigeria.*Precambrian Geology of Nigeria*. P. O. Oluyide, W. C. Mbonu, A. E.

Ogezi, I. G. Egbuniwe, A. C. Ajibade and A. C. Umeji. Eds. Geological Survey of Nigeria Special Publication.77-82.

Elueze, A. A. 1992. Rift system for Proterozoic schist belts in Nigeria.*Tectonophysiscs* 209:167-169.

Elueze, A. A., 2000. Compositional appraisal and petrotectonic significance of the Imelu banded ferruginous rock in the Ilesha schist belt, southwestern Nigeria. *Journal of Mining and Geology* 36.1:8-18.

Elueze, A. A. 2002. *Compositional Character: Veritable Tool in the Appraisal of Geomaterials*. Inaugural Lecture, University of Ibadan, Nigeria.

Elueze, A. A. 2003. Laterites: readily exploitable sources of raw materials. *Contributions of Geosciences and Mining to National Development.* A. A. Elueze. Ed. Nigerian Mining and Geosciences Society Special Publication.93-101.

Elueze, A. A. and Akin-Ojo, O. A. 1993.Functional characterization of talc bodies in southwestern Nigeria.*Mineral Wealth* 85:7-114.

Elueze, A. A. and Okunlola, O. A., 2003a. Petrochemical and petrogenetic characteristics of metasedimentary rocks of Lokoja-Jakura schist belt, central Nigeria.*Journal of Mining and Geology 39*:21-27.

Elueze, A. A. and Okunlola, O. A., 2003b.Geochemical features and petrogenetic affinity of Precambrian amphibolites of Burum area, central Nigeria.*Journal of Mining and Geology 39*:71-78.

Elueze, A.A and Aromolaran, O.K. 2009. Compositional characteristics of pegmatites in parts of Oke-Ogun district, southwestern Nigeria. *Book of Abstract of the 45th Annual International Conference of the Nigerian Mining and Geosciences Society (NMGS),* Owerri, Nigeria, 8-13th March, 2009.

Elueze, A.A and Aromolaran, O.K. 2013.Geochemical characteristics and mineralization potential of Precambrian pegmatites in Iwere-Ile area, southwestern Nigeria.*Book of Abstract of the 24th Colloquium of African Geology (CAG24),* Addis Ababa, Ethiopia, 8-14th January, 2013.

Elueze, A.A. and Aromolaran, O.K. 2014. Compositional studies in relation to Ta/Nb enrichment in pegmatites around Ofiki, in Precambrian Basement Complex of southwestern Nigeria. *Journal of Mining and Geology*50:19-29.

Elueze, A.A., Jimoh, A. O. and Aromolaran, O.K. 2015. Compositional characteristics and functional applications of Obajana marble deposit in the Precambrian Basement Complex of central Nigeria. *Ife Journal of Science* 17.3:591-603.

Emofurieta, W. O., 1984. The geochemistry of the Igbetti Granite Complex, Oyo State, Nigeria.*PhD Thesis.*Department of Geology.University of Ife, Ife.xix+370p.

Elueze, A. A. and Emofurieta, W. O. 1995. Field relationships, petrography and geochemistry of mafic units in Igbetti district, southwestern Nigeria, in relation to their origin. *Nigerian Journal of Pure and Applied Sciences* 10:335-346.

Emofurieta, W.O., Olade, M.A. and Ajibade, S.A. 1988. The geochemical distinction between two alkali feldspar types occurring in the Sn-metallogenic belt of southwestern Nigeria. *Journal of Mining and Geology* 24.1-2:9-13.

Ercit, T. S., Cerny, P., Hawthorne, F. C. and McCammon, C. A. 1992. The wodginite group II: Crystal chemistry. *Canadian Mineralogist* 30:613-631.

Ercit, T. S., Wise, M. A. and Cerny, P. 1995. Compositional and structural systematics of the columbite group.*American Mineralogists* 80:613-619.

Ero, K. A. and Ekwueme, B. N. 2009. Mineralization of pegmatites in parts of the Oban massif, southeastern Nigeria: a preliminary analysis. *Chinese Journal of Geochemistry* 28:146-153.

European Commission, 2011.Critical raw materials for the EU.Http://ec.europa.eu/enterprice/policies/raw-materials/files/docs/reports\-b_en.pdf. (Accessed 9 December, 2016).

European Commission, 2014. Report on critical raw materials for the EU. Http://ec.europa.eu/enterprice/policies/raw-materials/files/docs/crm-report-on-critical-raw-materials_en.pdf. (Accessed 6 June,2017).

Evans, A. M. 1993. *Ore Geology and Industrial Minerals*: An Introduction. 3rd Ed. New Jersey: Blackwell Science.

Fabris, A. J.,Keeling, J.L. and Fidler, R. W. 2009.Surface geochemical expression of bedrock beneath thick sediment cover, Curnamona Province, South Australia.*Geochemistry: Exploration, Environment, Analysis* 9.3:237-246.

Fadipe, A. A. 1988. Niobian-tantalian rutiles from some granites-pegmatites in Africa and Malaysia.*Journal of Mining and Geology* 24.1-2:71-77.

Faure, G. 1998. *Principles and Applications of Geochemistry*.2nd Ed. New Jersey: Prentice Hall.

Fedo, C. M., Nesbitt, H. W. and Young, G. M. 1995.Unravelling the effects of potassium metasomatism in sedimentary rocks and paleosols, with implications for paleoweathering conditions and provenance.*Geology* 23:921-924.

Fernando, R., Rupasinghe, M.S. and Dissanayake, C.B. 1996.Application of statistical modelling to gem exploration in sedimentary gem deposits in high grade gneiss terrain.*Journal of Geological Society of Sri Lanka* 6:15-27.

Ferre, E. C., Deleris, J., Bouchez, J. L., Lar, A. U. and Peucat, J. J. 1996. The Pan-African reactivation of contrasted Eburnean and Archaean provinces in Nigeria: Structural and isotopic data. *Journal of Geological Society of London* 153:719-728.

Ferre, E.C., Caby, R., Peucat, J.J., Capdevila, I.R. and Monie, P. 1998. Pan-African postcollisional ferro-potassic granite and quartz-monzonite plutons of eastern Nigeria.*Lithos* 45:255-278.

Fitches, W.R., Ajibade, A.C., Egbuniwe, I.G., Holt, R.W. and Wright, J.B. 1985.Late Proterozoic schist belts and plutonism in NW Nigeria.*Journal of Geological Society London* 142:319-337.

Fletcher, W.K., Dousset, P. E. and Ismail, Y. B. 1987.Elimination of hydraulic effects for cassiterite in a Malaysian stream.*Journal of Geochemical Exploration* 28:385-408.

Floyd, P. A. and Winchester, J. A. 1978.Identification and discrimination of altered and metamorphosed volcanic rocks using immobile elements.*Chemical Geology* 21:29-306.

Foord, E. E., Cerny, P., Jackson, L. L., Sherman, D. M. and Eby, R. K., 1995.Mineralogical and geochemical evolutions of micas from miarolitic pegmatites of the anorogenic pikes- Peak Batholith, Colorado.*Mineralogy and Petrology* 55:1-26

Freyssinet, Ph., Butt, C.R.M., Morris, R. C. and Piantone, P. 2005. Ore forming processes related to lateritic weathering.*Economic Geology One Hundredth Anniversary Volume (1905-2005).*J. W. Hedenquist, J. F. H. Thompson, R. J. Goldfarb and J. P. Richards. Eds. Society of Economic Geologists, Colorado, USA:681-722.

Galeschuk, C.R. and Vanstone, P.J. 2005.Exploration for buried rare-element pegmatites in the Bernic Lake area of southeastern Manotoba.*Rare-Element Geochemistry and Mineral Deposits.*R. L. Linnen and L. M. Samson.Eds. Geological Association of Canada (GAC) Short Course Notes 17:159-173.

Garba, I. 2002. Late Pan-African tectonics and origin of gold mineralization and rare-metal pegmatites in the Kushaka schist belt, northwestern Nigeria. *Journal of Mining and Geology* 38.1:1-12.

Garba, I. 2003. Geochemical discrimination of newly discovered rare-metal bearing and barren pegmatites in the Pan-African (600±150 Ma) basement of northern Nigeria.*Applied Earth Science Transactions of Institute of Mining and Metallurgy B* 112: 287-292.

Garrels, R. M. and Christ, C. L. 1965.Solutions, Minerals, and Equilibrum. New York: Harper and Row.

Glover, A.S., Rogers, W.Z. and Barton, J.E. 2012. Granitic pegmatites: Storehouses of industrial minerals. *Elements* 8.4: 269-273.

Ginsburg, A. I., Timofeyev, I. N. and Feldman, L. G. 1979.Priniples of Geology of the Granitic Pegmatites.Nedra, Moscow, USSR.

Giorgis, I., Bonetto, S., Giustetto, R., Lawane, A., Pantet, A., Rossetti, P., Thomassin, J. and Vinai, R. 2014. The lateritic profile of Balkouin, Burkina Faso: geochemistry, mineralogy and genesis. *Journal of African Earth Sciences* 90:31-48.

Gong, Q., Deng, J., Wang, C., Wang, Z and Zhou, L. 2013. Element behaviours to rock weathering and its implication to geochemical anomaly recognition: a case study on Linglong biotite granite in Jiaodong Peninsula, China. *Journal of Geochemical Exploration* 128:14-24.

Gong, Q. J., Deng, J., Yang, L. Q., Zhang, J., Wang, Q. F. and Zhang, G. X. 2011.Behaviour of major and trace elements during weathering of sericite-quartz schist.*Journal of Asian Earth Sciences*42:1-13.

Goodenough, K. M., Lusty, P. A. J., Roberts, N. M. W., Key, R. M. and Garba, A. 2014. Post-collisional Pan-African granitoids and rare-metal pegmatites in western Nigeria: age, petrogenesis, and the pegmatite conumdrum. *Lithos* 200-201:22-34.

Gordiyenko, V. V. 1971. Concentration of Li, Rb and Cs in potash feldspar and muscovite as criteria for assessing the rare metal mineralization in granitic pegmatites.*International Geology Review* 13:134-142.

Gouveia, M. A., Prudencio, M. I., Figueiredo, M. O., Pereira, L. C. J., Waerenborgh, J. C., Morgado, I., Pena, T. and Lopes, A. 1993. Behaviour of REE and other trace and major elements during weathering of granitic rocks, Evora, Portugal.*Chemical Geology* 107:293-296.

Griffin, W. L. and Ryan, C. G. 1995. Trace elements in indicator minerals: areas selection and target evaluation in diamond exploration. *Journal of Geochemical Exploration*53:311-317.

Griffin, W. L. and Ryan, C. G., O'Reilly, S. Y., Nixon, P. H. and Win, T. T. 1994. Trace elements in garnets from Tanzanian kimberlites: relation to diamond content and tectonic setting. *Diamonds: characterization, Genesis, and Exploration.*H. O. A. Meyer and O. H. Leonardos. Eds. CRPM Special Publication 1B/93: 346-358.

Grigsby, J. D. 1990. Detrital magnetite as a provenance indicator.*Journal of Sedimentary Petrology* 60:940-951.

Grant, N. K. 1970. Geochronology of Precambrian basement rocks from Ibadan, southwestern Nigeria. *Earth and Planetary Science Letters* 10:29-38.

Grant, N. K. 1978. Structural distinction between a metasedimentary cover and an underlying basement in 600 My old Pan-Afican domain in northwestern Nigeria, West African. *Geological Society of American Bulletin* 89:50-58.

Grant, N. K., Hickman, M., Burkholder, F. R., and Powell, J. L. 1972.Kibaran metamorphic belt in the Pan-African domain of West Africa.*Nature (Physical Sciences)* 238:90-91.

Groat, L.A., Giuliani, G., Marshall, D.D. and Turner, D. 2007.Emerald.*Geology of Gem Deposits.*L. A. Groat. Ed. Mineralogical Association of Canada Short Course 37:79-109.

Groat, L.A., Turner, D. and Evans, R. J. 2014. Gem Deposits. *Treatise on Geochemistry*.K. Turekian and H. Holland. Eds. 2nd Ed. Amsterdam: Elservier.595-622.

Gu, X.X., Liu, J.M., Zheng, M.H., Tang, J.X. and Qi, L. 2002. Provenance and tectonic setting of the Proterozoic turbidites in Hunan, south China: Geochemical evidence. *Journal of Sedimentary Research* 72:393-407.

Gubernov, A. P. and Mooney, W. D. 2009.New global geological maps of crustal basement age.*Eos transactions, American Geophysical Union* 90:1569-1583

Hallberg, J. A. 1984. A geochemical aid to igneous rock identification in deeply weathered terrains. *Journal of Geochemical Exploration* 20:1-8.

Hanson, S. L. Simmon, W. B., Webber, K. L., Falster, A. U. and Buchholz, T. 1999. Trace element chemistry of micas in "NYF" and "NY" pegmatites. *Memorial Symposium on NYF-type Pegmatites (Denver)*. E. E. Foord. Ed. *Canadian Mineralogist* 37: 849-852.

Harley, S.L. and Kelly, N.M. 2007. Zircon: Tiny but timely. *Elements* 3.1:13-18.

Harnois, L. 1988. The CIW index: a new chemical index of weathering. *Sedimentary Petrology* 55:319-322.

Harris, N. B. W., Pearce, J. A. and Tindle, A. G. 1986.Geochemical characteristics of collision-zone magmatism.*Collision Tectonics*.M. P. Coward and A. C. Reis. Eds. Geological Society of London Special Publication 19:67-81.

Hatch, G.P. 2012.Dynamics of the global market for rare earths.*Elements* 8.5:341-346.

Hattori, K.H., Hamilton, S., Kong, J. and Gravel, J. 2009.Soil geochemical survey over concealed kimberlites in the Attawapiskat area in northern Canada.*Geochemistry: Exploration, Environment, Analysis* 9.2:139-150.

Henderson,I. H. C. and Ihlen, P. M. 2004. Emplacement of polygeneration pegmatites in relation to Sveco-Norwegian contractional tectonics: examples from southern Norway. *Precambrian Research* 133:207-222.

Hill, R. J. and Howard, C. J. 1987.Quantitative phase analysis from neutron powder diffraction data using the Rietveld method.*Journal of Applied Crystallography*20: 467-474.

Hill, I. G., Worden, R. H. and Meighan, I. G. 2000. Geochemical evolution of a palaeolaterite: the interbasaltic formation, Northern Ireland. *Chemical Geology* 166: 65-84.

Holt, R. W., 1982. The geotectonic evolution of the Anka Belt in the Precambrian Basement complex of northwestern Nigeria.*PhD Thesis.*Open University, Milton Keynes, England.xxii+264p.

Holt, R. W., Egbuniwe, I. G., Fitches, W. R. and Wright, J. B., 1978.The relationship between low grade metamorphic belts, calc-alkaline volcanism and Pan-African Orogeny in northwestern Nigeria.*Geologische Rundschau*67:631-646.

Hurley, P. M., Fairbairn, H. W. and Pinson, W. H. 1966.Continental drift investigations. Massachusetts Institute of Technology 14th Annual Programme Report for 1966: 3-15.

Ibrahim, A. A. 2008. Petrography, geochemistry and origin of banded iron formation of the Kazaure schist belt, northwestern Nigeria. *Journal of Mining and Geology* 44 .1: 13-20.

Ige, O. A. and Asubiojo, O. I. 1991. Trace element geochemistry and petrogenesis of some meta-ultramafites in Apomu and Ife-Ilesa areas of southwestern Nigeria. *Chemical Geology* 91.1:19-32

Iloeje, N. P., 1981. *A New Geography of Nigeria.* Lagos: Longman Nigeria Limited.

Jolliff, B. L., Papike, J. J. and Shearer, C. K. 1986. Tourmaline as a recorder of pegmatite evolution: Bob Ingersoll pegmatite, Black Hills, South Dakota. *American mineralogists* 71:472-500.

Jacobson, R. E. E and Webb, J. S. 1946.*The pegmatites of Central Nigeria.*Geological Survey of Nigeria Bulletin 17, 61p.

Kayode, A. A. 1988. Chemical, zircon typologic and two-pyroxene investigation of the hornblende-granite-acid charnockite contact in Ikere-Ekiti, southwestern Nigeria.*Precambrian Geology of Nigeria*. P. O. Oluyide, W. C. Mbonu, A. E.

Ogezi, I. G. Egbuniwe, A. C. Ajibade and A. C. Umeji. Eds. Geological Survey of Nigeria Special Publication.145-155.

Kehinde-Phillips, O. O. 1991. Compositional variations within lateritic profiles over mafic and ultramafic rock units of the Ilesha schist belt, southwestern Nigeria. *PhD Thesis.*Department of Geology, University of Ibadan.xvii+201p

Kelley, K. D., Eppinger, R. G., Lang, J., Smith, S. M. and Fey, D. L. 2011. Porphyry Cu indicator minerals in till as an exploration tool: Examples from the Giant Pebble Porphyry Cu-Au-Mo deposit, Alaska, USA. *Geochemistry, Exploration, Environment, Analysis* 11:321-334.

Kennedy, W.G. 1964. The structural differentiation of Africa in the Pan-African (± 500 Ma) tectonic episode.Research Institute for African Geology (Leeds). 8th Annual Report: 48-49.

Keppler, H., 1993.Influence of fluorine on the enrichment of high field strength trace element in granitic rocks. *Contributions to Mineralogy and Petrology* 114:479-488.

Khider, K. and McQueen, K. G. 2005.Geochemical discrimination of weathered bedrock in the Hermidale-Byrock region of Western NSW.*Regolith –Ten Years of CRC LEME.* I. C. Roach. Ed. CRC LEME: 170-175.

Kinnaird, J.A. 1984. Constrasting styles of Sn-Nb-Ta-Zn mineralization in Nigeria. *Journal of African Earth Sciences* 2.2:81-90.

Krauskopf, K. B. and Bird, D. K. 1995. *Introduction to Geochemistry.*3rd Ed. New York: McGraw-Hill.

Kroner, A. 1977.The Precambrian of geotectonic evolution of Africa.*Precambrian Research* 4:163-213.

Kroner, A., Ekwueme, B. N. and Pidgeon, R. T. 2001. The oldest rocks in West Africa: SHRIMP Zircon age for Early Archaean migmatitic orthogneiss at Kaduna, northern Nigeria. *Journal of Geology* 109:399-406.

Kuster, D. 1990. Rare-metal pegmatites of Wamba, central Nigeria; their formation in relationship to late Pan-African granites, *Mineralium Deposita* 25:25-33.

Kuster, D. 2009. Granite-hosted Ta mineralization in the Arabian-Nubian Shield: Ore deposit types, tectono-metallogenetic setting and petrogenetic framework. *Ore Geology Reviews* 35:68-86

Kuster, D., Romer, R.L., Tolessa, D., Zerihun, D., Bheemalingeswara, K., Melcher, F and Oberthur, T. 2009. The Kenticha rare-element pegmatite, Ethiopia: internal differentiation, U-Pb age and Ta mineralization. *Mineralium Deposita* 44:723-750.

Kyser, K. 2017. Element migration processes in the near-surface environment and their consequences for exploration. *Proceedings of the 14th Biennial Meeting of the Society for Geology Applied to Mineral Deposits,* 20-23 August 2017, Quebec City, Canada: 1085-1086.

Lapworth, D.J., Knights, K.V., Key, R.M., Johnson, C.C., Ayoade, E., Adekanmi, M.A., Arisekola, T.M., Okunlola, O.A., Backman, B., Eklund, M., Everett, P.A., Lister, R.T., Ridgway, J., Watts, M.J., Kemp, S.J. and Pitfield, P.E.J. 2012. Geochemical mapping using stream sediments in west-central Nigeria: Implications for environmental studies and mineral exploration in West Africa. *Applied Geochemistry* 27:1035-1052.

Levitan, D. M., Zipper, C. E., Donovan, P., Schreiber, M. E., Seal, R. R., Engle, M. A., Chermak, J. A., Bodnar, R. J., Johnson, D. K. and Aylor, J. G. 2015. Statistical analysis of soil geochemical data to identify pathfinders associated with mineral deposits: an example from the Coles Hill uranium deposit, Virginia, USA. *Journal of Geochemical Exploration.* 154:238-251.

Li, C. and Yang, S. 2010. Is chemical index of alteration (CIA) a reliable proxy for chemical weathering in global drainage basins? *American Journal of Science* 310.2: 111-127.

Linnen, R. L. 1998. The solubility of Nb-Ta-Zr-Hf-W in granitic melts with Li and Li+F: constraints for mineralization in rare metal granites and pegmatites. *Economic Geology* 93:1013-1025.

Linnen, R. L. 2005. The effects of water solubility of accessory minerals in granitic melts.*Lithos* 80:267-280.

Linnen, R. L. and Cuney, M. 2005. Granite-related rare-element deposits and experimental constraints on Ta-Nb-W-Sn-Zr-Hf mineralization.*Rare-element Geochemistry and Mineral Deposits Short Course Notes*.R. L.Linnen and I. M. Samson.Eds. Geological Association of Canada Special Publication 17:45-68.

Linnen, R. L. and Keppler, H. 1997. Columbite solubility in granitic melts: consequences for the enrichment and fractionation of Nb and Ta in the Earth'crust. *Contributions to Mineralogy and Petrology* 128:213-227.

Linnen, R.L., Van Lichtervelde, M. and Cerny, P. 2012. Granitic pegmatites as sources of strategic metals.*Elements* 8.4:263-268.

Linnen, R.L., Samson, I.M., Williams-Jones, A.E. and Chakhmouradian, A.R. 2014.Geochemistry of the rare-earth element, Nb, Ta, Hf and Zr deposits.*Treatise*

on Geochemistry. K. Turekian and H. Holland. Eds. 2nd Ed. Amsterdam:Elservier. 543-568.

London, D. 1986a. Formation of tourmaline-rich gem pockets in miarolitic pegmatites. *American Mineralogists* 71:396-405.

London, D. 1986b.Holmquistite as a guide to pegmatite rare-metal deposits.*Economic Geology* 81:704-712.

London, D. 1987. Internal differentiation of rare-element pegmatites: Effects of boron, phosphorus, and fluorine. *Geochimica et Cosmochimica Acta* 51:403-420.

London, D. 1992. The application of experimental petrology to the genesis and crystallization of granitic pegmatites.*Canadian Mineralogist* 30:499-540.

London, D. 1995. Geochemical features of peraluminous granites, pegmatites and rhyolite as sources of lithophile metal deposits. *Magama, Fluids and Ore Deposits*. J. F. H. Thompson. Ed. Mineralogical Association of Canada Short Course Series 23:175-202.

London, D. 2005a.Geochemistry of alkali and alkaline earth elements in ore-forming granites, pegmatites and rhyolites.*Rare Element Geochemistry and Mineral Deposits*. R. L. Linnen and I. M. Samson. Eds. Geological Association of Canada Short Course Notes 17: 17-43.

London, D. 2005b. Granitic pegmatites: an assessment of current concepts and directions for the future. *Lithos* 80:281-303.

London, D. 2008. *Pegmatites*.Canadian Mineralogists Special Publication 10.

London, D. 2009. The origin of primary textures in granitic pegmatites.*Canadian Mineralogist* 47:697-734.

London, D. and Evensen, J. M. 2002.Beryllium in silicic magma and the origin of beryl-bearing pegmatites.*Reviews in Mineralogy and Geochemistry* 50:445-486.

London, D. and Kontak, D. J. 2012. Granitic pegmatites: scientific wonders and economic bonanzas. *Elements* 8 4:257-261.

London, D. and Morgan, G. B. 2012.The pegmatite puzzle.*Elements* 8.4:263-268.

London, D. Morgan, G. B., Babb, H. A. and Loomis, J. L. 1993.Behaviour and effects of phosphorus in the system Na_2O-K_2O-Al_2O_3-SiO_2-P_2O_5-H_2O at 200 Mpa (H_2O).*Contributions to Mineralogy and Petrology* 113:450-465.

London, D. and Morgan, G. B. and Hervig, R. L. 1989. Vapour-undersaturated experiment with Macusani glass + H_2O at 200 MPa, and the internal differentiation of granitic pegmatites. *Contributions to Mineralogy and Petrology* 102.1:1-7.

Mackay, D. A. R. and Simandl, G. J. 2014. Geology, market and supply chain of niobium and tantalum- a review. *Mineralium Deposita* 49.8:1025-1047.

Mackay, D. A. R. and Simandl, G. J. 2015.Pyrochlore and columbite-tantalite as indicator minerals for specialty mineral deposits.*Geochemistry: Exploration, Environment, Analysis* 15.2-3:167-178.

MacLean, W. H., Bonavia, F. F. and Sanna, G. 1997. Argillite debris converted to bauxite during karst weathering: evidence from immobile element geochemistry at the Olmedo Deposit, Sardinia. *Mineralium Deposita* 32:607-616.

Malomo, S., 2004.*National Geological Map of Nigeria, 1:2,000,000*. Nigerian Geological Survey Agency, Abuja, Nigeria.

Mao, M., Rukhlov, A. S., Rowins, S. M., Spence, J. and Coogan, L.A. 2016. Apatite trace element compositions: a robust new tool for mineral exploration. Economic Geology, 111:1187-1222.

Marshall, B. T. and Herman, J. S. 1986. Trace element distribution in soils above deeply weathered pegmatites, Virginia, U.S.A.: implications for exploration. *Applied Geochemistry* 1:681-690.

Martin, R. F. and De Vito, C. 2005. The patterns of enrichment in felsic pegmatites ultimately depend on tectonic setting. *Canadian Mineralogists* 43:2027-2048.

Matheis, G. 1979. The application of geochemical mapping in the tropical environment: an example from Southwest Nigeria. *Natural Resources Development* 16:34-52.

Matheis, G. 1981. Trace-element patterns in lateritic soils applied to geochemical exploration. *Journal of Geochemical Exploration* 15:471-480.

Matheis, G. 1987. Nigerian rare-metal pegmatites and their lithological framework.*Geological Journal* 22:271-291.

Matheis, G. and Caen Vachette, M. 1988. Rb-Sr isotopic study of rare-metal bearing and barren pegmatites in the Pan-African reactivation zone of Nigeria.*Precambrian Geology of Nigeria*. P. O. Oluyide, W. C. Mbonu, A. E. Ogezi, I. G. Egbuniwe, A. C. Ajibade and A. C. Umeji. Eds. Geological Survey of Nigeria Special Publication.291-299.

Matheis G. and Kuster, D. 1989. Geochemical exploration guides for rare-metal pegmatites-examples from Nigeria and Sudan. *Lanthanide, Tantalum and Niobium: Mineralogy, Geochemistry, Characteristics of Primary Ore Deposits, Prospecting, Processing and applications*. P. Moller, P. Cerny and F. Sauge.Ed. Berlin:Springer-Verlag. 321-328.

Mathieu, D., Berrnat, M. and Nahon, D. 1995. Short-lived uranium and thorium isotope distribution in atropical laterite derived from granite (Pitinga River Basin, Amazonia, Brazil): Application to assessment of weathering rate. *Earth and Planetary Science Letters* 136:703-714.

McClenaghan, M. B. 2011. Overview of common processing methods for recovery of indicator minerals from sediments and bedrock in mineral exploration.*Geochemistry: Exploration, Environment, Analysis* 11:265-278.

McClenaghan,M.B., Layton-Matthews,D. and Matile, *G. 2011*.Till geochemical signatures of magmatic Ni–Cu deposits, Thompson Nickel Belt, Manitoba, Canada.*Geochemistry: Exploration, Environment, Analysis* 11.2:145-159.

McCurry, P. 1976. A general review of the geology of the Precambrian to Lower Palaeozoic rocks of northern Nigeria. *Geology of Nigeria.* C. A. Kogbe. Ed. Lagos: Elizabethan Publications.13-37.

McCurry, P. and Wright, J. B. 1977.Geochemistry of calcalkaline volcanic in northwestern Nigeria and a possible Pan-African suture.*Earth and Planetary Science Letter* 37: 90-96.

McDonough, W. F. and Sun, S. S. 1995. The composition of the earth. *Chemical Geology* 120:223-253

McLennan, S.M., Hemming, S.R., Taylor, S.R. and Eriksson, K. A. 1995. Early Proterozic crustal evolution: Geochemical and Nd-Pb isotopic evidence from metasedimentary rocks, southwestern North America. *Geochimica et Cosmochimica Acta* 59:1153-1177.

McMartin, I., Corrivean, L. and Beaudoin, G. 2011. An orientation study of the heavy mineral signature of the NICO Co-Au-Bi deposit, Great Bear magamatic zone, Northwest Territorries, Canada. *Geochemistry: Exploration, Environment, Analysis* 11:293-307.

McQueen, K.G. and Cross, A. J. 1998. Magnetite as geochemical sampling medium: application to skarn deposits. *The State of the Regolith,* Geological Society of Australia Special Publication 20:194-199.

Melcher, F., Graupner, T., Gabler, H., Sitnikova, M., Henjes-Kunst, F., Oberthur, T., Gerdes, A. and Dewaele, S. 2015. Tantalum-(niobium-tin) mineralization in African pegmatites and rare metal granites: Constraints from Ta-Nb oxide mineralogy, geochemistry and U-Pb geochronology. *Ore Geology Reviews* 64:667-719.

Meschede, M. 1986. A method of discriminating between different types of mid-oceanic ridge basalts and continental tholeiites with the Nb-Z-Y diagram.*Chemical Geology* 56:207-218.

Meunier, A., Caner, L., Hubert, F., El Albani, A. and Pret, D. 2013. The weathering intensity scale (WIS): an alternative approach of the chemical index of alteration. *American Journal of Science* 313:113-143.

MMSD, 2012. Nigeria Mineral Projects, Exploration, Development and Exploitation, Federal Republic of Nigeria, Ministry of Mines and Steel Development, Abuja, Nigeria.

Mokhtari, A. R., Cohen, D. R. and Gatehouse, S. G. 2009. Geochemical effects of deeply buried Cu–Au mineralization on transported regolith in an arid terrain. *Geochemistry: Exploration, Environment, Analysis* 9.3:227-236.

Moller, P. and Morteani, G. 1987.Geochemical exploration guide for tantalum pegmatites.*Economic Geology* 82.7:1888-1897.

Moller, P., Dulski, P., Szacki, W., Malow, G. and Riedel, E. 1988.Substitution of tin in cassiterite by tantalum, niobium, tungsten, iron ang manganese.*Geochimica et Cosmochimica Acta* 52:1497-1503.

Moore, D. M. and Reynolds, R. C., Jr. 1997.X-ray diffraction and the identification and analysis of clay minerals. 2nd Ed. Oxford: Oxford University Press.

Morgan, G. B. and London, D. 1987.Alteration of amphibolitic wallrocks around the Tanco rare-element pegmatite, Bernic Lake, Manitoba.*American Mineralogists* 72:1097-1121.

Morgan, G. B. and London, D. 1999. Crystallization of the Little Three layered pegmatite-aplite dike, Ramona district, California. *Contributions to mineralogy and Petrology,* 136:310-330.

Morteani, G. and Gaupp, R. 1989. Geochemical evaluation of the tantalum potential of pegmatites.*Lanthanide, Tantalum and Niobium: Mineralogy, Geochemistry, Characteristics of Primary Ore Deposits, Prospecting, Processing and applications.* P. Moller, P. Cerny and F. Sauge.Eds. Berlin: Springer-Verlag. 303-310.

Morteani, G., Preinfalk, C., Spiegel, W. and Bonalumi A. 1995. The Achala Granitic Complex and the pegmatites of Sierras Pampeanas (Northwest Argentina): a study of differentiation. *Economic Geology* 90:636-647.

Morteani, G., Preinfalk, C. and Horn, A.H. 2000.Classification and mineralization potential of the pegmatites of the Eastern Brazilian Pegmatite Province.*Mineralium Deposita* 35:638-655.

Mumm, A. S., Dart, R. C. and Say, P. 2013. Hematite/maghemite trace element geochemistry in base metal exploration.*Journal of Geochemical Exploration* 124:239-251.

Muotoh, E. O. G., Oluyide, P. O., Okoro, A. U. and Mogbo, O. 1988. The Muro Hills banded iron formation. *Precambrian Geology of Nigeria*. P. O. Oluyide, W. C. Mbonu, A. E. Ogezi, I. G. Egbuniwe, A. C. Ajibade and A. C. Umeji. Eds. Geological Survey of Nigeria Special Publication.219-227.

Nahon, D. and Tardy, Y., 1992. The ferruginous laterites.*Regolith Exploration Geochemistry in Tropical and Subtropical Terrains.*C. R. M. Butt and H. Zeegers. Eds. *Handbook of Exploration Geochemistry* 4:41-55.

Nardi, L.V.S., Formoso, M.L.L., Muller, I.F., Fontana, E., Jarvis, K. and Lamarao, C. 2013. Zircon/rock partition coefficients of REEs, Y, Th, U, Nb, and Ta in granitic rocks: uses for provenance and mineral exploration purposes. *Chemical Geology* 335:1-7.

Nasraoui, M., Toulkeridis, T., Clauer, N. and Bilal, E. 2000. Differentiated hydrothermal and meteoric alteration of the Lueshe carbonatite complex (Democratic Republic of Congo) identified by a REE study combined with a sequential acid-leaching experiment. *Chemical Geology* 165:109-132.

Neiva, A. M. R. 2013. Micas, feldspars and columbite-tantalite minerals from zoned granitic lepidolite-subtype pegmatite at Namivo, Alto Ligonha, Mozambique. *European Journal of Mineralogy* 25:967-985.

Nelson, M.A., Kyser, T. K., Clark, A. H. and Oates, C. 2009. Application of carbon isotope ratios in regolith to the exploration for buried exotic-type copper ore deposits, Collahuasi district, northern Chile. *Geochemistry: Exploration, Environment, Analysis* 9.1:3-8.

Nesbitt, H. W. and Young, G. M. 1982. Early Proterozoic climates and plate motions inferred from major element chemistry of lutites. *Nature* 299:715-717.

Nesbitt, H. W. and Young, G. M. 1984. Prediction of some weathering trends of plutonic and volcanic rocks based on thermodynamic and kinetic considerations. *Geochimica et Cosmochimica Acta* 48.7:1523-1534.

Nesbitt, H. W. and Wilson, R. E. 1992.Recent chemical weathering of basalts.*American Journal of Science*292.10:740-777.

Ng, C. W. W., Guan, P. and Shang, Y. J. 2001.Weathering mechanisms and indices of the igneous rocks of Hong Kong.*Quarterly Journal of Engineering Geology and Hydrogeology* 34:133-151.

Norton, S. A. 1973. Laterites and bauxite formation.*Economic Geology* 68.2:353-361.

Novak, M., Skoda, R., Gadas, P., Krmirek, L. and Cerny, P. 2012. Contrasting origin of the mixed signature in granite pegmatites: examples from the Moldanubian Zone, Czech Republic. *Canadian Mineralogist* 50.4:1077-1094.

Nwabufo-Ene, K. E. and Mbonu, W. C. 1988.The metasedimentary belts of the Nigerian Basement Complex- Facts, fallacies and new frontiers.*Precambrian Geology of Nigeria*. P. O. Oluyide, W. C. Mbonu, A. E. Ogezi, I. G. Egbuniwe, A. C. Ajibade and A. C. Umeji. Eds. Geological Survey of Nigeria Special Publication: 55-67.

Obaje, N G. 2009.*Geology and Mineral Resources of Nigeria*.Heidelberg: Springer-Verlag,

Ocan, O. O. 1991.The petrology of rocks around Idanre area, southwestern Nigeria.*PhD Thesis*.Department of Geology, Obafemi Awolowo University, Ile-Ife.xxii+397p.

Odeyemi, I. B. 1977. On the petrology of the Basement rocks around Igarra, Bendel State, Nigeria.*PhD Thesis*.University of Ibadan, Ibadan.xvii+223p.

Odeyemi, I. B. 1981. A review of the orogenic events in the Precambrian basement of Nigeria, West Africa.*Geologische Rundschau* 70.3: 897-909.

Odeyemi, I. B. 1988. Lithostratigraphy and structural relationships of the Upper Precambrian metasediments in Igarra area, southwestern Nigeria.*Precambrian Geology of Nigeria*. P. O. Oluyide, W. C. Mbonu, A. E. Ogezi, I. G. Egbuniwe, A. C. Ajibade and A. C. Umeji. Eds. Geological Survey of Nigeria Special Publication.111-125.

Odeyemi, I. B., Anifowose, Y. B. and Asiwaju-Bello, Y. A. 1999.Multi-technique graphical analysis of fractures from remote sensing images of basement regions of Nigeria.*Journal of Mining and Geology*38.1:9-21.

Ogezi, A. E. 1977. Geochemistry and geochronology of basement rocks from northwestern Nigeria.*PhD Thesis*.University of Leeds.xxv+295p.

Ogezi, A. E. 1988. Origin and evolution of the Basement Complex of northwest Nigeria in the light of new geochemical and geochronological data.*Precambrian Geology of Nigeria*. P. O. Oluyide, W. C. Mbonu, A. E. Ogezi, I. G. Egbuniwe, A. C. Ajibade and A. C. Umeji. Eds. Geological Survey of Nigeria Special Publication.301-312.

Ogunleye, P. O., Ike, E. C. and Garba, I. 2004. Multivariate statistical analysis of major and trace element data for niobium exploration in the peralkaline granites of the anorogenic ring-complex province of Nigeria.*Journal of Mining and Geology* 40.2:107-117.

Ohta, T. and Arai, H. 2007. Statistical empirical index of chemical weathering in igneous rocks: a new tool for evaluating the degree of weathering. *Chemical Geology*240:280-297.

Ohta, A., Imai, N., Terashima, S. and Tachibana, Y. 2005. Application of multi-element statistical analysis for regional geochemical mapping in central Japan, *Applied Geochemistry* 20:1017-1037.

Okezie, C. N. 1974. 1:2,000,000 Geological Map of Nigeria. Geological Survey of Nigeria.

Okunlola, O.A. 1998. Specialty metal potentials of Nigeria.*Proceedings of the 1st Mining in Nigeria Conference and Workshop, NIMAMOP,* Federal Ministry of Solid Minerals Abuja: 67-90.

Okunlola, O. A., 2001. Geological and compositional investigation of Precambrian marble bodies and associated rocks in Burum and Jakura area, Nigeria.*PhD Thesis*.University of Ibadan, Ibadan.xvi+256p.

Okunlola, O. A. 2005. Metallogeny of tantalum-niobium mineralization of Precambrian pegmatites of Nigeria. *Mineral Wealth* 137:38-50.

Okunlola, O. A and Jimba, S. 2006. Compositional trends in relation to Ta-Nb mineralization in Precambrian pegmatites of Aramoko-Ara-Ijero area, southwestern Nigeria. *Journal of Mining and Geology* 42.2:113-126.

Okunlola, O. A. and Ofonime, B. U. 2006. Geological setting, petrochemical features and ages of rare-metal (Ta-Nb) mineralization of pegmatites of Komu area, southwestern Nigeria.*African Journal of Science and Technology, Science and Engineering Series* 7:96-110.

Okunlola, O. A. and Somorin, E. B. 2006. Compositional features of Precambrian pegmatites of Itakpe area, central Nigeria. *Global Journal of Geological Sciences* 4.2:221-230.

Okunlola, O. A. and Ocan, O. O. 2009.Rare metal (Ta-Sn-Li-Be) distribution in Precambrian pegmatites of Keffi area, central Nigeria.*Natural Science* 7:90-99.

Okunlola, O. A. and Oyedokun, M. O. 2009.Compositional trends and rare-metal (Ta-Nb) mineralization potentials of pegmatites and associated lithologies of Igbeti area, southwestern Nigeria.*RMZ-Materials and Geoenviroment* 56:38-53.

Olade, M. A. 1980. Geochemical characteristics of tin-bearing and tin-barren granites, northern Nigeria.*Economic Geology* 75:71-82

Olade, M. A. and Elueze, A. A. 1979.Petrochemistry of the Ilesha amphibolites and Precambrian crustal evolutions in the Pan-African domain of southwestern Nigeria.*Precambrian Research* 8:303-318.

Olarewaju, V. O. 1981. Geochemistry of the charnockitic and granitic rocks of the Basement Complex around Ado-Ekiti-Akure, southwestern Nigeria.*PhD Thesis*.University of London.xxii+383p.

Olarewaju, V. O. and Rahaman, M. A. 1982.Petrology and geochemistry of Older Granites from some parts of northern Nigeria.*Journal of Mining and Geology*18.1:16-28.

Olarewaju, V. O. 1987. Charnockitic-granite association in SW Nigeria: Rapakivi granite type and charnockitic plutonism in Nigeria. *Journal of African Earth Sciences* 6. 1:67-77.

Olarewaju, V. O. 1988. Petrology and geochemistry of charnockitic and associated granitic rocks of Ado-Ekiti-Akure, southwestern Nigeria.*Precambrian Geology of Nigeria*. P. O. Oluyide, W. C. Mbonu, A. E. Ogezi, I. G. Egbuniwe, A. C. Ajibade and A. C. Umeji. Eds. Geological Survey of Nigeria Special Publication.231-239.

Olarewaju, V. O. 2006. The charnockitic intrusives of Nigeria.*The Basement Complex of Nigeria and Its Mineral Resources (A Tribute to Prof. M.A.O. Rahaman).* O. Oshin. Ed. Ibadan: Akin Jinad and Company.45-70.

Olobaniyi, S. B. and Annor, A. E. 2003. Petrology and age of implication of ultramafic schist in the Isanlu area of Egbe-Isanlu schist belt, southwestern Nigeria. *Journal of Mining and Geology*39.1:1-9.

Olobaniyi, S. B. and Mucke, A. 2011. Chemical composition of chromite and intergrown chlorite in metamorphosed ultramafic rocks (serpentinite and talc schist) of the

Egbe-Isanlu Schist belt, southwest Nigeria: genetic implication. *Journal of Mining and Geology* 47.1:34-42.

Olobaniyi, S. B., Adekeye, J. I. D. and Annor, A. E., 2001.Chemical character of garnets in semipelitic schist and banded iron-formation, in relation to the metamorphic history of the Isanlu area, southwestern Nigeria.*Journal of Mining and Geology*37:1-6.

Oluyide, P. O. and Okunlola, O. A., 1995. Lithostructural setting and emplacement history of Precambrian carbonate deposits, Burum, central Nigeria. *Book of Abstract of the 31st Annual international Conference of the Nigerian Mining and Geosciences Society,* Calabar: 20.

Omada, J. I., Kolawole, M. S. and Odoma, A. N. 2015. Field and petrochemical studies od pegmatites in parts of Lokoja, central Nigeria. *Journal of African Earth Sciences* 101:266-273.

Oversby, V. M. 1975. Lead isotopic study of aplites from the Precambrian basement rocks near Ibadan, southwestern Nigeria. *Earth and Planetary Science Letters* 27:177-180.

Oyawoye, M. O. 1972. The Basement Complex of Nigeria.*African Geology.*T. F. J. Dessauvagie and A. J. Whiteman. Eds. Ibadan: Ibadan University Press. 67-99.

Page, L. R., Northon, J. J., Stoll, W. C., Hanley, J. B., Adams, J. W., Pray, L. C., Steven, T. A., Erickson, M. P., Joralemon, P., Stopper, R. F. and Hall, W. E. 1953. *Pegmatite investigations, 1942-1945. Blach Hills, South Dakota. U.S. Geological Survey Professional Paper* 247.

Papp, J.F. 2013a. Tantalum.U.S. Geological Survey Mineral Commodity Summaries 2013: 162-163

Papp, J.F. 2013b. Niobium (Columbium).U.S. Geological Survey Mineral Commodity Summaries 2013: 110-111.

Parker, A. 1970.An index of weathering for silicate rocks.*Geological Magazine* 107:501-504.

Pearce, J. A. and Cann, J. R. 1973. Tectonic settings of basic volcanic rocks determined using trace element analyses. *Earth and Planetary Science Letters* 19:290-300.

Pearce, J. A. and Norry, M. J. 1979.Petrogenetic implications of Ti, Zr, Y, and Nb variations in volcanic rocks.*Contributions to Mineralogy and Petrology* 69:33-47.

Pearce, T. H., Gorman, B. E. and Birkett, T. C. 1975. The TiO_2-K_2O-P_2O_5 diagram: a method of discriminating between oceanic and non-oceanic basalts. *Earth and Planetary Science Letters* 24:419-426.

Philpotts, A. R. and Ague, J. J. 2009.*Principles of Igneous and Metamorphic Petrology*. Cambridge: Cambridge University Press.

Pichavant, M. 1981. An experimental study of the effect of boron on a water saturated haplogranite at 1kbar pressure: Geological applications. *Contributions to Mineralogy and Petrology* 76:430-439.

Pierson-Wickmann, A.C., Acquilina, L., Martin, C., Ruiz, L., Molenat, J., Jaffrezic, A.and Gascuel-Odoux, C. 2009. High chemical weathering rates in first-order granitic catchments induced by agricultural stress. *Chemical Geology* 265:369-380.

Pisiak, L.K., Canil, D., Lacourse, T. Plouffe, A. and Ferbey, T. 2017. Magnetite as indicator mineral in the exploration of porphyry deposits: a case study in till near the Mount Polley Cu-Au deposits, British Columbia, Canada. *Economic Geology* 112. 4:919-940.

Pollard, P. J. 1995. Geology of rare metal deposits: an introduction and overview. A special issue devoted to the geology of rare metal deposits. *Bulletin of the Society of Economic Geologists*, Economic Geology 90:489-494.

Rahman, A. A. M. S., 1981. Occurrence and mineralogy of bauchite and charnockitic rocks in the Oban Massif, Cross River State, Nigeria.*Journal of Mining and Geology* 18.1:52-59.

Rahaman, M. A. 1976. Review of the basement geology of southwestern Nigeria. *Geology of Nigeria.*C.A. Kogbe. Ed. Lagos: Elizabethan Publications. 39-56.

Rahaman, M. A. 1988. Recent advances in the study of the Basement Complex of Nigeria.*Precambrian Geology of Nigeria*. P. O. Oluyide, W. C. Mbonu, A. E. Ogezi, I. G. Egbuniwe, A. C. Ajibade and A. C. Umeji. Eds. Geological Survey of Nigeria Special Publication.11-43.

Rahaman, M. A. and Ocan, O. O. 1978.On relationships in the Precambrian migmatitic gneisses of Nigeria.*Journal of Mining and Geology*15:23-32.

Rahaman, M. A. and Ocan, O. O. 1988.The nature of granulite facies metamorphism in Ikare area, southwestern Nigeria.*Precambrian Geology of Nigeria*. P. O. Oluyide, W. C. Mbonu, A. E. Ogezi, I. G. Egbuniwe, A. C. Ajibade and A. C. Umeji. Eds. Geological Survey of Nigeria Special Publication.157-163.

Rahaman, M. A. and Lancelot, J. R. 1984. Continental crust evolution in SW Nigeria: Constraints from U-Pb dating of pre-Pan-African gneisses. Rapport d'activite 1980-1984. Documents et Travaux du Centre Geologique et Geophysique de Montpellier II 4:41.

Rahaman, M.A., Emofurieta, W. O. and Caen Vachette, M. 1983. The potassic granite of the Igbetti area: further evidence of the polycyclic evolution of the Pan-African belt in southwestern Nigeria. *Precambrian Research* 22:75-92.

Ranasinghe, P.N., Dissanayake, C. B. and Rupasinghe, M. S. 2005. Application of geochemical ratios for delineating gem-bearing areas in high grade metamorphic terrains.*Applied Geochemistry* 20:1489-1495.

Robb, L. 2005. Introduction to Ore-forming Processes.Oxford: Blackwell Science Limited.

Roda Robles, E., Pesquera Perez, A., Gil, P. P., Torres-Ruiz, J. and de Parseval, P. 2006.Mineralogy and geochemistry of micas from the Pinilla de Fermoselle pegmatite (Zamora, Spain).*European Journal of Mineralogy* 18:369-377.

Roda Robles, E., Keller, P., Pesquera Perez, A. and Fontan, F. 2007. Micas of the muscovite-lepidolite series from Karibib pegmatites, Namibia.*Mineralogical Magazine* 71:41-62.

Rollinson, H. R. 1993.Using Geochemical Data: Evaluation, Presentation, Interpretation. New York: Longman Scientific and Technical.

Roskill, 2013. Tantalum: market outlook to 2016. http://www.roskill.com/reports/minor-and-light-metals/tantalum (accessed 27July 2013).

Rossman, G. R. 2009. The geochemistry of gems and its relevance to gemology: different traces, different prices. *Elements* 5.3:153-162.

Rudnick, R. L. and Gao, S. 2014. Composition of the continental crust.*Treatise on Geochemistry.*K. Turekian and H. Holland. Eds. 2nd Ed. Amsterdam: Elsevier 4:1-51.

Rupasinghe, R.H., Dissanayake, C. B. and Mendis, D. P. J. 1994. Use of indicator minerals in gem exploration: study of granulite terrain of Sri Lanka. *Journal of South East Asian Earth Sciences*9.3:1-6.

Sack, R. O. and Ghiorso, M. S. 1991. Chromian spinels as petrogenetic indicators: thermodynamics and petrological applications. *American Mineralogists* 76:827-847.

Scharer, U., Cosca, M., Steck, A. and Hunziker, J. 1996. Termination of a major strike-slip and differential cooling along the Insubric line (Central Alps): U-Pb, Rb-Sr and $^{40}Ar/^{39}Ar$ ages of cross-cutting pegmatites. *Earth and Planetary Science Letters* 142:331-351.

Schellmann, W. 1983.A new definition of laterite.*Natural Resources and Development* 18: 7-21.

Selway J.B., Breaks, F.W. and Tindle, A. G. 2005.A review of rare-element (Li-Cs-Ta) pegmatite exploration techniques for the Superior Province, Canada, and large worldwide tantalum deposits. *Exploration and Mining Geology*14.1-4:1-30.

Serala, P., Pulkkineu, E., Ojala, V. J. and Peltoniemi-Taivalkoski, A. 2009. Gold exploration using till at Petajalehto, northern Finland.*Geochemistry: Exploration, Environment, Analysis* 9:247-255.

Shearer, C.K., Papike, J.J., Simon, S.B., Laul, J. C. and Christian, R. P. 1984. Pegmatite/wallrock interactions, Black Hills, South Dakota: progressive boron metasomatism adjacent to the Tip Top Pegmatites. *Geochimica et. Cosmochimica Acta* 48:2563-2579.

Shearer, C.K., Papike, J.J. and Laul, J. C. 1985.Chemistry of potassium feldspars from Three Zoned pegmatites, Black Hills, South Dakota: implications concerning pegmatites evolution. *Geochimica et Cosmochimica Acta* 49:663-673.

Shearer, C.K., Papike, J. J. and Simon, S. B. 1986. Pegmatite/wallrock interactions, Black Hills, South Dakota: interaction between pegmatite-derived fluids and quartz-mica schist wallrock. *American Mineralogists* 71.3-4:518-539.

Shelley, D. 1993. Igneous and metamorphic rocks under the microscope: Classification, textures, microstructures and mineral preferred orientations. New York: Chapmanand Hall.

Simmons, S. 2007. Pegmatite genesis: recent advances and areas for future research. *Proceedings of the International Symposium on Granitic Pegmatites:The State of the Art. 6-12th May, 2007,* Martin, T. and Vieira, R. Eds. Porto Portugal: Memorias N.3-6.

Simmons, W. B. 2007. Gem-bearing pegmatites.*Geology of Gem Deposits*. L. A. Groat.Ed. Mineralogical Association of Canada Short Course 37:169-206.

Simmons, W. B. and Webber, K.L. 2008. Pegmatite genesis: state of the art. *European Journal of Mineralogy* 20:421-438.

Simmons, W.B., Webber, K.L., Falster, A. U and Nizamoff, J. W. 2003. Pegmatology: pegmatite mineralogy, petrology and petrogeneis. New Orleans:Rubellite Press.

Simmons, W.B., Pezzotta, F., Shigley, J. E and Beurlen, H. 2012. Granitic pegmatites as sources of coloured gemstones.*Elements* 8.4:281-287.

Singh, B and Cornelius, M. 2006. Geochemistry and mineralogy of the regolith profile over the Aries kimberlite pipe, Western Australia. *Geochemistry: Exploration, Environment, Analysis* 6. 4:311-323.

Skirrow, R.G., Huston, D.L., Mernagh, T. P., Thorne, J. P., Dulfer, H and Senior, A. B. 2013.*Critical Commodities for a High-tech World: Australia's Potential to Supply Global Demand.* Geoscience Australia, Canberra.

Smeds, S. A. 1992. Trace elements in potassium-feldspar and muscovite as a guide in the prospecting for lithium- and tin-bearing pegmatites in Sweden. *Journal of Geochemical Exploration* 42:351-369.

Smith, R. E., Anand, R. R. and Alley, N. F. 1997.Use and implications of palaeoweathering surfaces in mineral exploration.Proceedings of the 4th Decennial International Conference on Mineral Exploration(*Geophysics and Geochemistry at the Millenium).* A. G. Gubins. Ed. Canada: 335-346.

Smith, R. E., Perdrix, J. L. and Davis, J. M. 1987. Dispersion into pisolitic laterite from the Greenbushes mineralized Sn-Ta pegmatite system, Western Australia. *Journal of Geochemical Exploration* 28:251-265.

Smith, R .E. and Singh, B. 2007. Recognizing, in lateritic cover, detritus shed from the Archaean Gossan Hill Cu–Zn–Au volcanic-hosted massive sulphide deposit, Western Australia. *Geochemistry: Exploration, Environment, Analysis* 7.1:71-86.

Solodov, N.A. 1971. Scientific Principles of Perspective Evaluation of Rare-Element Pegmatites.Moscow: Academy of Science.

Sorensen, H. 1992. Minerals for future materials.*Applied Geochemistry* 7:391-392.

Stavrov, O. D., Stolyarov, I. S. and Iocheva, E. I. 1969.Geochemistry and origin of Vekh-Jset granitoid massif in central Ural.*Geochemistry International* 6:1138-1146.

Sun, S. S. and McDonough, W. F., 1989. Chemical and isotopic systematic of oceanic basalts: implications for mantle composition and processes. *Magmatism in the Ocean Basins.*A. D. Saunders and M. J. Norry. Eds. Geological Society of London Special Publication 42:313-145.

Swan, A. R. H and Sandilands, M. 1995. Introduction to Geological Data Analysis.New Jersey: Blackwell Science Limited.

Tantalum-Niobium International Study Centre, 2013a.Tantalum-raw materials and processing.http://tanb.org/tantalum(accessed 17th July, 2013).

Tantalum-Niobium International Study Centre, 2013b.Niobium-raw materials and processing.http://tanb.org/niobium.(accessed 17th July, 2013).

Tardy, Y. 1997.*Petrology of laterites and tropical soil.* Rotterdam: A.A. Balkema/Rotterdam/Brookfield.

Tardy, Y., Boeglin, J. L., Novikoff, A. and Roquin, C. 1993.Petrological and geochemical classification of laterites. Proceedings of the 10th International Clay Conference of the Association Internationale Pour L'etude Des argiles (AIPEA), 18-23, July, 1993, Adelaide, Australia: 481-486.

Taylor, S. R and McLennan, S. M. 1985.The geochemical evolution of the continental crust.*Reviews of Geophysics* 33:241-265.

Taylor, S. R and McLennan, S. M. 1995.*The Continental Crust: Its*Composition *and Evolution- an examination of the geochemical record preserved in sedimentary rocks*. New Jersey:Blackwell Science Limited.

Taylor, C., Taves, R., Ross, M. A., Clark, J. R. and Perrouty, S., 2017.Tungsten-rich rutile as apotential indicator mineral in surficial till for Canadian Malartic-type gold deposits.*Proceedings of the 14th Biennial Meeting of the Society for Geology Applied to Mineral Dpeosits,* 20-23 August 2017, Quebec City, Canada: 1167-1170.

Tkachev, A. V. 2011. Evolution of metallogeny of granitic pegmatites asociated with orogens throughout geologic time.*Granite-Related Ore Deposits.* A. N. Sial, J. S. Bettencourt and C. P. De Campos. Eds. Geological Society of London Special Publication 350:7-23.

Tischendorf, G. 1977. Geochemical and petrographic characteristics of silicic magmatic rocks associated with rare-metal mineralization. *Mineralization Associated with Acid Magmatism.*P. M. Stem,L. Burnol and G. Tischendorf.Eds. Ust Ustav Geol. Prague: 41-98.

Trueman D. L. and Cerny, P. 1982. Exploration for rare-metal granitic pegmatites.*Granitic Pegmatites in Science and Industry.* P. Cerny. Ed. Mineralogical Association of Canada Short Course Handbook8:463-493.

Trumbull, R. B. 1995. Tin mineralization in the Archaean Sinceni rare-element pegmatite fields, Kaapvaal Craton, Swaziland. *Economic Geology* 90:648-657.

Tubosun, I. A., Lancelot, J. R., Rahaman, M. A. and Ocan, O. O., 1984. U-Pb Pan-African ages of two charnockite-granite associations from southwestern Nigeria. *Contributions to Mineralogy and Petrology* 88:188-195.

Turner, D. C. 1983. Upper Proterozoic schist belts in the Nigerian sector of the Pan-African Province of West Africa. *Precambrian Research* 21:55-79.

Umeji, A. C. 1988. The Precambrian of part of SE Nigeria: a magmatic and tectonic study. *Precambrian Geology of Nigeria*. P. O. Oluyide, W. C. Mbonu, A. E. Ogezi, I. G. Egbuniwe, A. C. Ajibade and A. C. Umeji. Eds. Geological Survey of Nigeria Special Publication.69-75.

Umeji, A.C. and Caen-Vachette, M. 1984.Geochronology of Pan-African Nassarawa Eggon and Mkar-Gboko granites, southeast Nigeria.*Precambrian Research* 23: 317-324.

Uribe-Mogollon, C. A. and Maher, K. C. 2017. White phyllosilicates geochemistry-vectoring porphyry ore deposits. *Proceedings of the 14th Biennial Meeting of the Society for Geology Applied to Mineral Deposits,* 20-23 August 2017, Quebec City, Canada: 1171-1174.

Van Breeman, O., Pidgeon, R. T. and Bowden, P. 1975. Age and origin of the Nigerian Mesozoic Granites: Rb-Sr isotopic study. *Contributions to Mineralogy and Petrology* 50:157-172.

Van Breeman, O., Pidgeon, R. T. and Bowden, P. 1977. Age and isotopic studies of some Pan-African Granites from North-central Nigeria.*Precambrian Research* 4:307-319.

Wedepohl, H. 1995. The composition of the continental crust.*Geochimica et Cosmochimica Acta* 59:1217-1239.

Wilkinson, J. J., Baker, M. J., Cooke, D. R., Wilkinson, C. C. and Inglis, S. 2017. Exploration targeting in porphyry Cu systems using propylitic mineral chemistry: a case study of the El Teniente deposit, Chile. *Proceedings of the 14th Biennial Meeting of the Society for Geology Applied to Mineral Deposits,* 20-23 August 2017, Quebec City, Canada: 1111-1114.

Wise, M. A. 1995. Trace element chemistry of lithium-rich micas from rare-element granitic pegmatites. *Mineralogy and Petrology*55:203-215.

Wise, M. A. and Brown, C. D. 2010. Mineral chemistry, petrology and geochemistry of the Sebago granite-pegmatite system, southern Maine, USA.*Journal of Geosciences* 55:3-26.

Woakes, M., Rahaman, M.A and Ajibade, A.C. 1989. Some metallogenetic features of the Nigerian Basement. *Geology of Nigeria.*C.A. Kogbe.Ed.Lagos: Elizabethan Publications. 111-121.

Wood, D. A. 1980. The application of a Th-Hf-Ta diagram to problems of tectonomagmatic classification and to establishing the nature of crustal contamination of basaltic lavas of the British Tertiary volcanic province.*Earth and Planetary Science Letters* 50: 11-30.

Wood, D. A., Tarney, J., Varet, J., Saunders, A. D., Bougault, H., Joron, J. L., Treuil, M. and Cann, J. R. 1979. Geochemistry of basalts drilled in the North Atlantic by IPOD Leg 49: implications for mantle heterogeneity. *Earth and Planetary Science Letters* 42:77-97.

Wood, S. A. 1990. The aqueous geochemistry of the rare-earth elements and yttrium: review of available low-temperature data for inorganic complexes and the inorganic REE speciation of natural waters. *Chemical Geology* 82:159-186.

Wright, J. B. 1970. Controls on mineralization in the older and younger tin fields of Nigeria.*Economic Geologists* 65:945-951.

Wright, J. B. and Ogezi, A. E. 1977.Serpentinite in the basement of northwestern Nigeria.*Journal of Mining and Geology* 14.1:34-37.

Wright, J. B., Hastings, D. A., Jones, W. B. and Williams, H. R. 1985.*Geology and Mineral Resources of West Africa.* London: George Allen and Unwin.

Xianrong, L., Junbo, L., Hong, W. and Peihua, Z. 1999. A survey of ionic conductivity of soil and its significance in prospecting for ore deposits concealed under thick overburden. *Journal of Geochemical Exploration* 66:307-311.

Xiao, W., Hongbing, J., Daojing, L., Zhang, F. and Shijie, W. 2013. Material source analysis and element geochemical research about two types of representative bauxite deposits and terra rossa in western Guangxi, southern China. *Journal of Geochemical Exploration* 133:68-87.

Xiong, X., Keppler, H., Audetat, A., Ni, H., Sun, W. and Li, Y., 2011. Partitioning of Nb and Ta between rutile and felsic melt and the fractionation of Nb/Ta during partial melting of hydrous metabasalt.*Geochimica et Cosmochimica Acta* 75: 1673-1692.

Yang, S., Wang, Z., Guo, Y., Li, C. and Cai, J. 2009. Heavy mineral compositions of the Changjiang (Yangtze River) sediments and their provenance-tracing implication.*Journal of Asian Earth Sciences* 35:56-65.

Zargorskyi, V. Y. E. Makagon, V. M. and Shmakin, B. M. 2003.Systematics of granitic pegmatites.*Russian Geology and Geophysics* 44:422-435.

Zarasvandi, A., Zamanian, H and Hejazi, E. 2010. Immobile elements and mass changes geochemistry at Sar-Faryab bauxite deposit, Zagros Mountains, Iran. *Journal of Geochemical Exploration* 107:77-85.

Zarasvandi, A., Carranza, E. J. M and Ellahi, S. S. 2012. Geological, geochemical and mineralogical characteristics of the Mandan and Deh-now bauxite deposits, Zagros Fold Belt, Iran.*Ore Geology Reviews* 48:125-138.

Zhang, Y., Pe-piper, G and Piper, D. J. W. 2014. Sediment geochemistry as a provenance indicator: unravelling the cryptic signatures of polycyclic sources, climate change, tectonism and volcanism. *Sedimentology*61:383-410.

Zhou, J., Griffin, W. L., Jaques, A. L., Ryan, C. G. and Win, T. T. 1994.Geochemistry of diamond indicator minerals from China.*Diamonds: characterization, Genesis, and Exploration*. H. O. A. Meyer and O.H. Leonardos. Eds. CRPM Special Publication 1B/93: 285-301

Zou, T. R. and Xu, J. G. 1975.The genesis and type-classification of the granite pegmatites.*Geochimica* 9:161-174.

Zou, T.R., Yang, U., Guo, Y. and Ni, Y. 1985. China's crust- and mantle-source pegmatites and their discriminating criteria.*Geochemistry* 4:1-17.

APPENDIX 1

The five classes of Granite Pegmatite

Class	Typical minor elements	Metamorphic host rocks	Relationship to granite	Structural features
Abyssal	U, Th, Zr, Nb, Ti, Y, REE, Mo rarely Be, B; poor (to moderate) mineralization	(upper amphibolite) to) low to high-pressure granulite facies ~400-900MPa ~ 700°-800°C	None (?) (Segregations of anatectic leucosome?)	Conformable to mobilized crosscutting veins
Muscovite	Mineralization absent; micas and ceramic minerals	High pressure, Barrovian amphibolite facies (kyanite-sillimanite) ~500-800MPa ~ 650°-580°C	None (anatectic bodies) to marginal and exterior	Quasiconformable to crosscutting
Muscovite – rare element	Li, Be, Y, REE, Ti, U, Th, Nb>Ta; rarely Li, Be; poor mineralization	Moderate to high pressure, (T) amphibolite facies: ~300-700 MPa ~ 650°-520°C	Interior to exterior; poorly defined	Quasiconformable to crosscutting
Rare-elements	Li, Rb, Cs, Be, Ga, Sn, Hf, Nb-Ta, B, P, F or Be, Y, REE, U, Th, Nb>Ta F; poor to abundant mineralization; gemstock; industrial minerals	Low-pressure, Abukuma amphibolite (to upper greenschist) facies (andalusite-sillimanite); ~200-400MPa, ~ 650°-500°C	Interior to marginal to exterior	Quasiconformable to crosscutting
Miarolitic	Li, Be, B, F, Ta>Nb, or Be, Y, REE, Ti, U, Th, Zn, Nb>Ta, F; poor mineralization; gemstock	Shallow to subvolcanic ~100-200MPa	Interior to marginal	Interior pods and crosscutting dikes

Modified from Cerny and Ercit (2005)

APPENDIX 1 (Continued)

Classification of the Granite Pegmatites of the Rare Element Class

Pegmatite type [feldspar + mica content]	Pegmatite subtype	Geochemical signature	Typical minerals
Rare-earth	Allanite-monazite	(L) REE, U, Th	Allanite, monazite
[KF>plg to ab;bi≥ms]		(P, Be, Nb>Ta)	
	Euxenite	REE, Y, Ti, Zr, Nb>Ta (F,P)	Euxenite, monazite, xenotime, aeschynite
	Gadolinite	Y, (H) REE, Be, Nb>Ta, F	Gadolinite, fergusonite
			(U, Th, Ti, Zr) euxenite, (topaz), (beryl)
Beryl	Beryl-columbite	Be, Nb-Ta (± Sn, B)	Beryl, columbite-tantalite
[Kf>ab;ms>bi]			Beryl, columbite-tantalite, triplite, triphylite
	Beryl-columbite-phosphate	Be, Nb-Ta, P (Li, F, ± Sn, B)	
Complex	Spodumene	Li, Rb, Cs, Be, Ta-Tb	Spodumene, beryl, tantalite
[Kf-ab; ms-lpd]		(Sn, P, F,±B)	(amblygonite), (lepidolite) (pollucite)
	Petalite	Li, Rb, Cs, Be, Ta>Nb	Petalite, beryl, tantalite
		(Sn, Ga, P, F,±B)	(amblygonite), (lepidolite)
	Lepidolite	F, Li, Rb, Cs, Be, Ta>Nb	Lepidolite, topaz, bery,
		(Sn, P, ±B)	Microlite, (pollucite)
	Elbaite	Li, B, Rb, Sn, F	Elbaite, microlite
		(Ta, Be, Cs)	(beryl, tantalite, hambergite)
	Amblygonite	P, F, Li, Rb, Cs, Be, Ta>Nb	Amblygonite, beryl, tantalite
		(Sn, ±B)	(lepidolite), (pollucite)
Albite-spodumene		Li (Sn, Be, Ta-Nb, ±B)	Spodumene, (cassiterite)
[ab>Kf; ((ms))]			(beryl), (tantalite)
Albite		Ta-Nb, Be (Li, ±Sn, B)	Tantalite, beryl (cassiterite)
[ab>>Kf; (ms,lep)]			

Note: underlined = element with economic potential

Modified from Cerny and Ercit (2005)

APPENDIX 1 (Continued)

The Three Petrogenetic Families of the Rare Element Class Granitic Pegmatites[1]

Family	Pegmatite types	Geochemical signature	Associated granites	Granite bulk composition[2]	Source lithologies
LCT	Beryl, complex albite-spodumene Albite Elbaite	Li, Rb, Cs, Be, Sn, Ga, Ta>Nb (B,P,F)	(Synorogenic to late orogenic (to anorogenic); Largely heterogeneous	Peraluminous S, I Or mixed S+I types	Undepleted upper-to middle-crust supracrustals and basement gneisses
NYF	Rare earth	Nb>Ta, Ti, Y, Sc, REE, Zr, U, Th, F	(Syn-, late, post to) mainly anorogenic, in part orogenic; Largely homogeneous	(Peraluminous to) Subaluminous and metaluminous (rarely peralkaline); A and (I) types	Depleted middle to lower crustal granulites, or juvenile granitoids, mantle metasomatized crust
Mixed	Cross-bred LCT and NYF	Mixed	(Postorogenic to) Anorogenic; moderately heterogeneous	Subaluminous to slightly peraluminous	Mixed protoliths or assimilation of supracrustals by NYF granites

[1]**Modified from Cerny and Ercit (2005)**

[2] Definitions: Peraluminous = A/CNK > 1; subaluminous = A/CNK ~1; metaluminous = A/CNK<1 at A/NK>1; subalkaline = A/NK ~ 1; peralkaline = A/NK<1, where A = Al2O3, CNK = CaO + Na2O + K2O, and NK = Na2O + K2O (all in molecular values)

APPENDIX 2

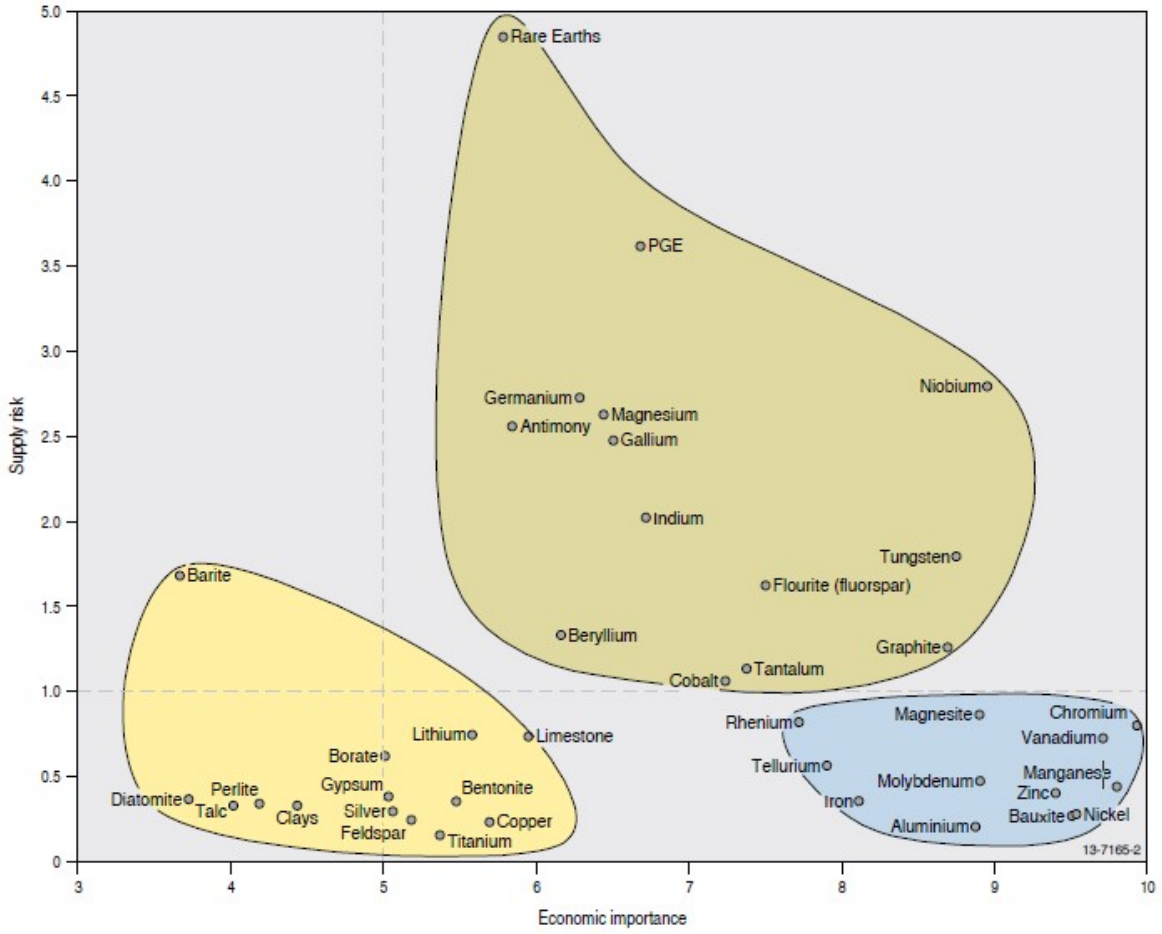

Criticality matrix of selected critical commodities (including metals and non-metals)

(European Commision, 2011)

APPENDIX 3

Chemical Index of Alteration

The Chemical Index of Alteration (Nesbitt and Young, 1982) of the investigated *in situ*-derived pegmatite weathering profiles was evaluated based on the molecular proportions of Al_2O_3, CaO, Na_2O and K_2O. The CIA estimates the gain of the immobile Al_2O_3 relative the major labile oxides in the bulk regolith samples. The formula (Nesbitt and Young, 1982) is:

$$CIA = Al_2O_3/ (Al_2O_3 + CaO^* + Na_2O + K_2O) \times 100 \text{ (molar basis)}$$

Where CaO* is the amount of CaO incorporated in the silicate fraction of the rock.

APPENDIX 4

X-ray diffraction patterns for the *in situ*-derived lateritic profile of non-mineralised pegmatite of Osu area, indicating trends of mineralogical abundances of phases with depth

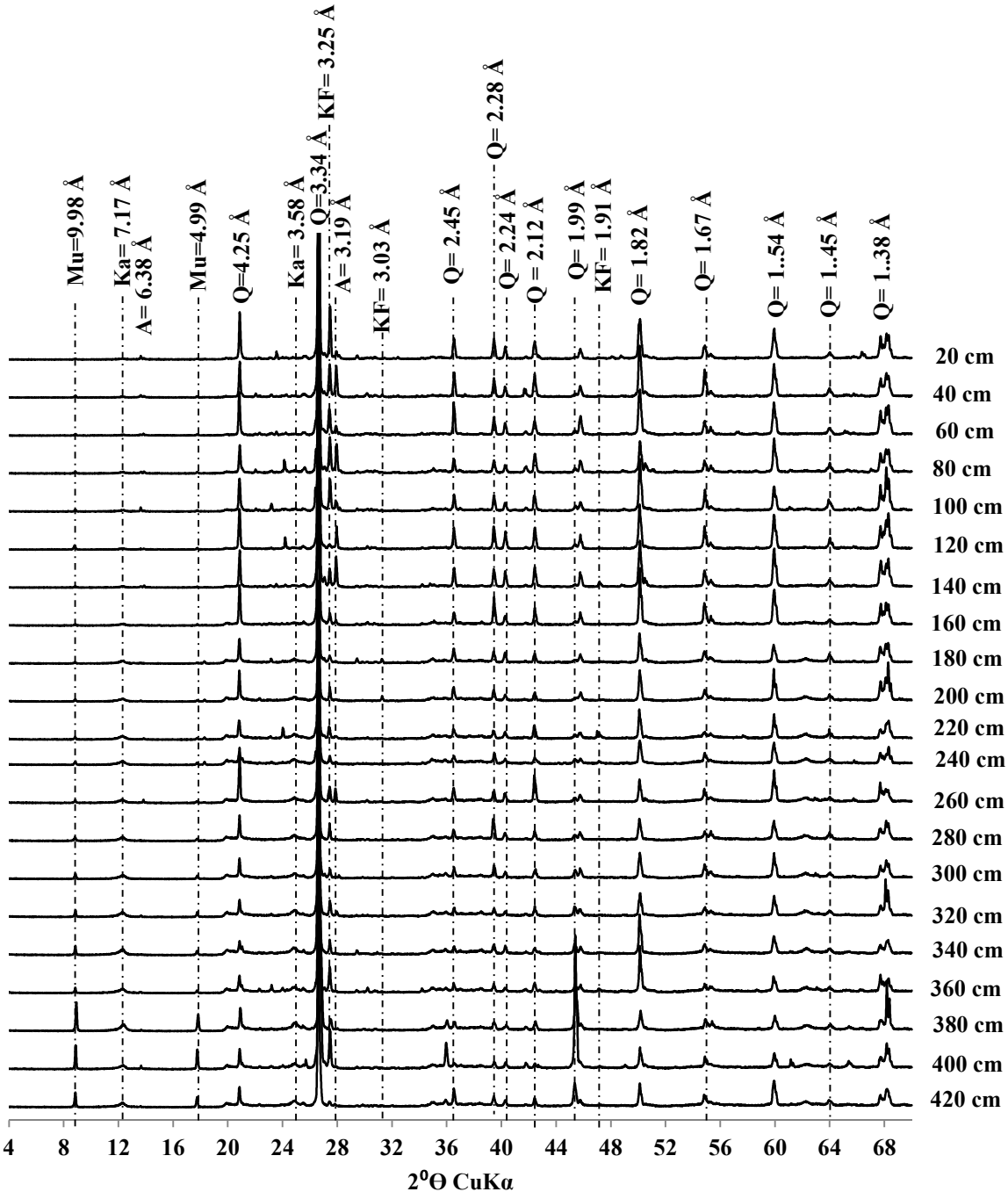

Appendix 4(Continued)

X-ray diffraction patterns for the *in situ*-derived lateritic profile of mineralised pegmatite of Ijero area, indicating trends of mineralogical abundances of phases with depth

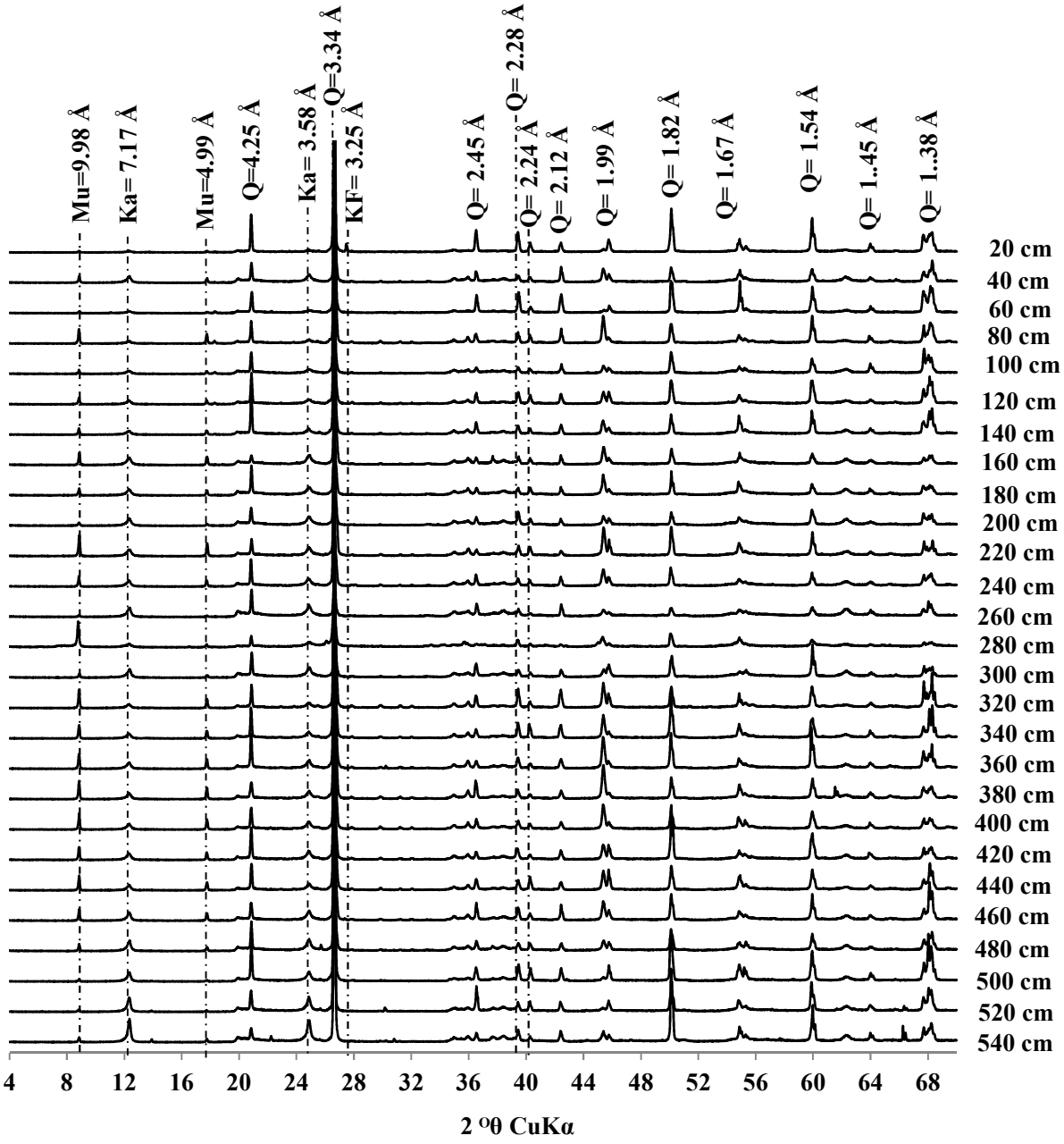

Appendix 4(Continued)

X-ray diffraction patterns for the *in situ*-derived lateritic profile of mineralised pegmatite of Komu area, indicating trends of mineralogical abundances of phases with depth

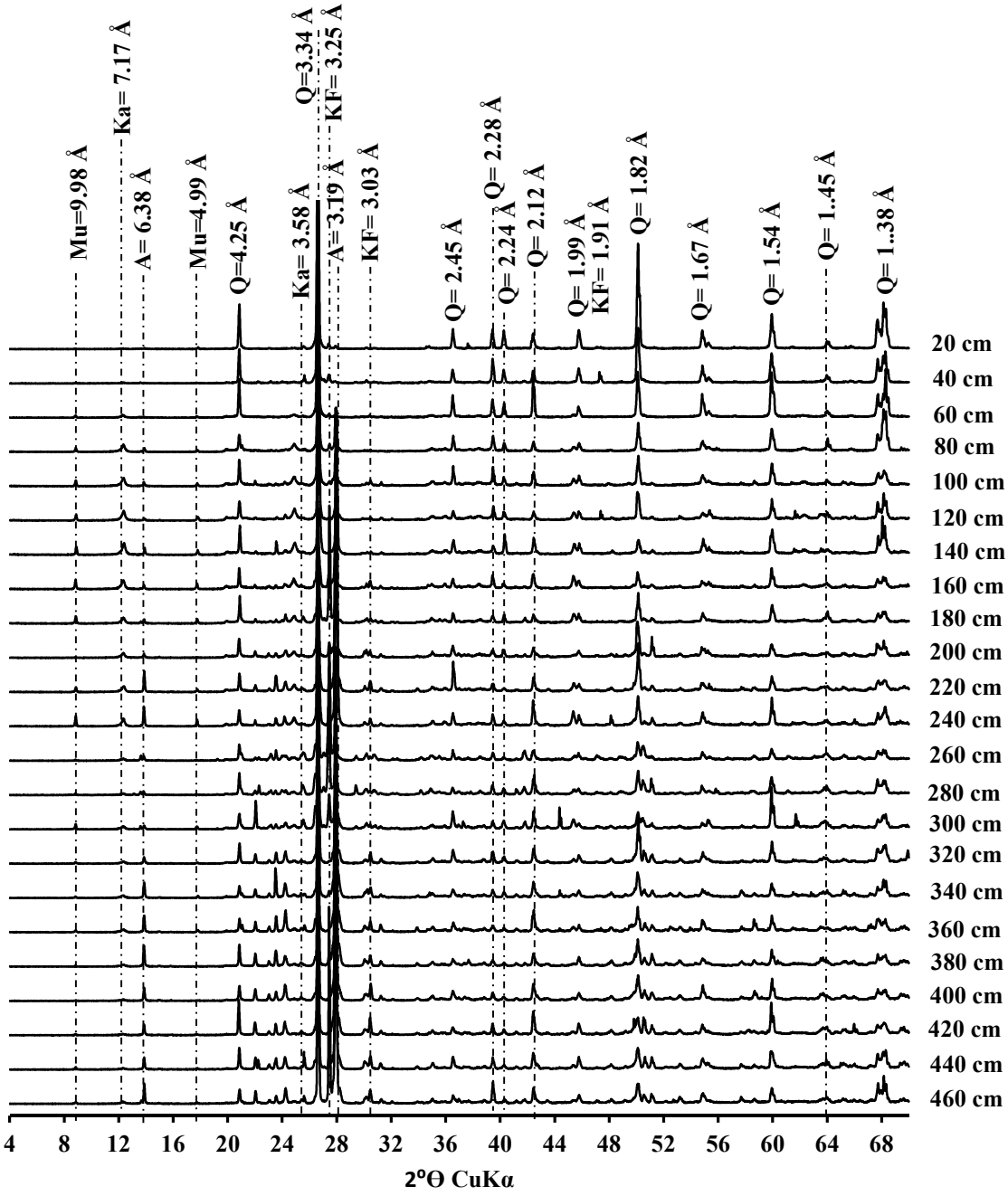

Appendix 4(Continued)

X-ray diffraction patterns for the *in situ*-derived lateritic profile of mineralised pegmatite of Ofiki area, indicating trends of mineralogical abundances of phases with depth

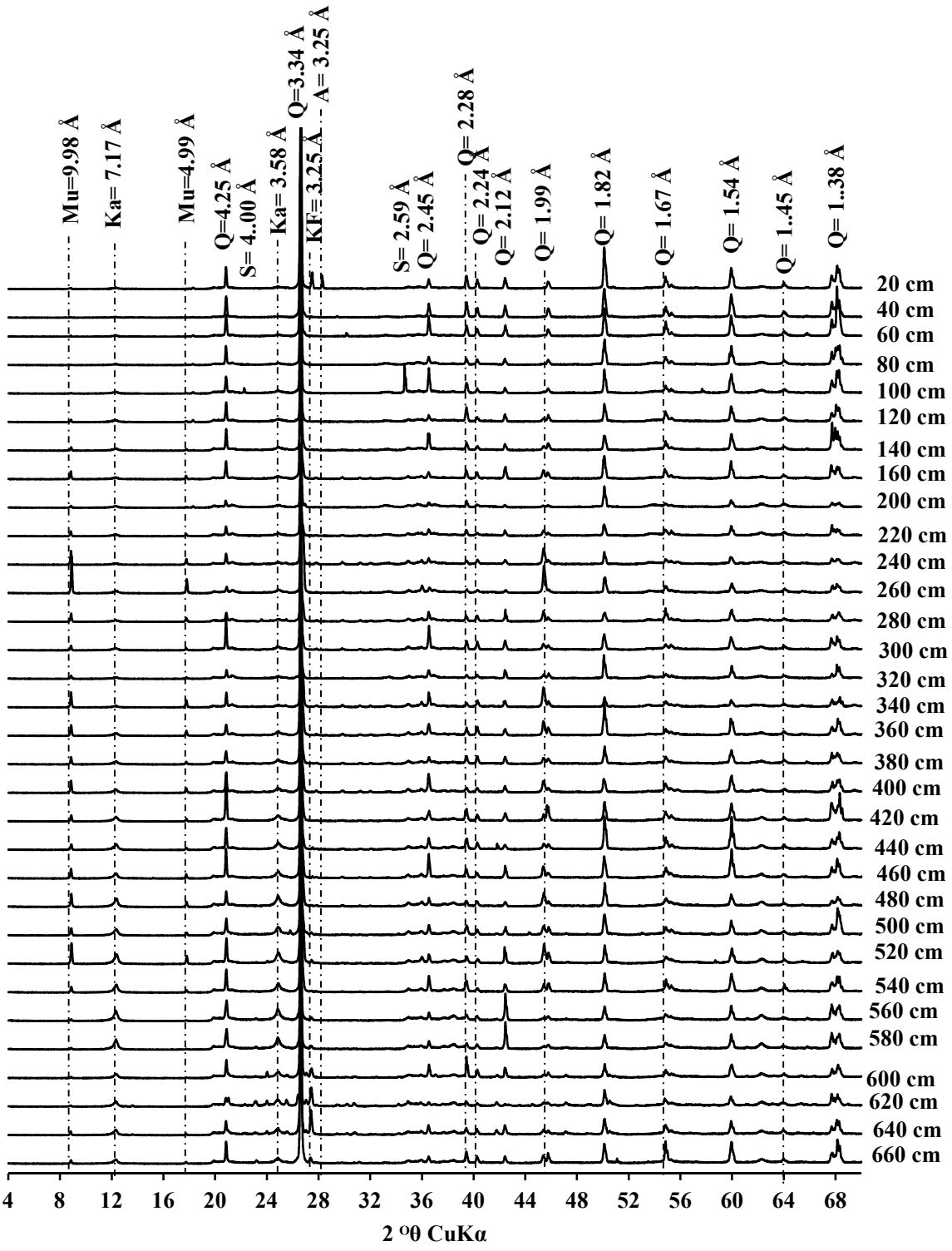

Appendix 4(Continued)

X-ray diffraction patterns for the *in situ*-derived lateritic profile of mineralized pegmatite of Iwere area, indicating trends of mineralogical abundances of phases with depth

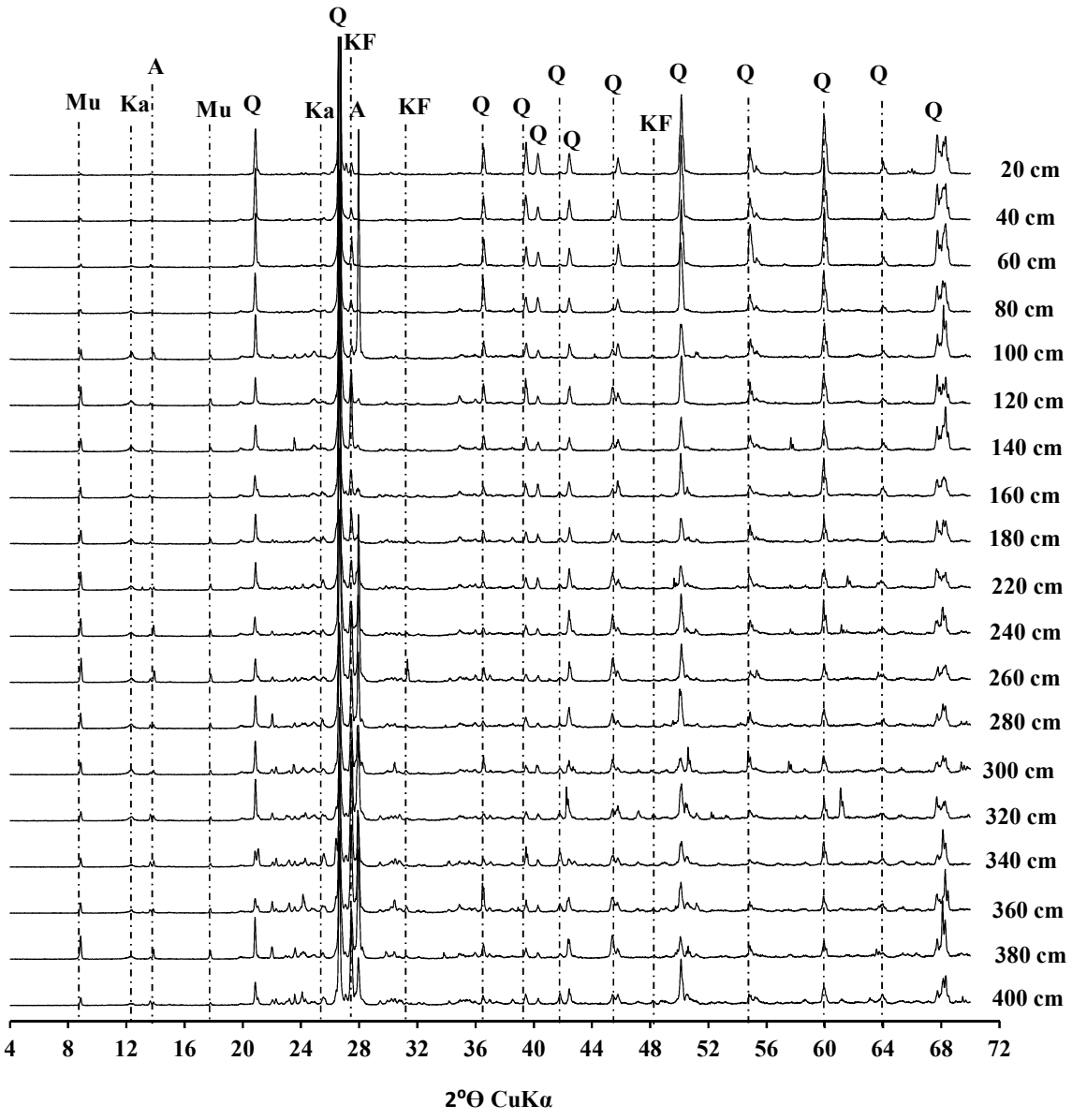

APPENDIX 5

Major and trace element analytical data for the K-feldspar samples of the pegmatites of the study areas

	Ijero Pegmatite							Komu Pegmatite						
	IJK1	IJK2	IJK3	IJK4	IJK5	Mean	Range	KMK1	KMK2	KMK3	KMK4	KMK5	Mean	Range
SiO_2	63.64	64.24	63.49	63.68	63.26	63.66	63.26-64.24	62.35	63.18	63.78	64.62	63.52	63.49	63.25-64.62
TiO_2	0.00	0.01	0.00	0.00	0.01	0.00	0.00-0.01	0.01	0.01	0.009	0.04	0.05	0.02	0.009-0.05
Al_2O_3	18.68	18.28	18.73	18.27	18.60	18.51	18.27-18.73	19.84	18.96	18.34	18.2	18.67	18.80	18.2-19.84
FeO	0.01	0.01	0.02	0.04	0.01	0.02	0.01-0.04	0.007	0.002	0.008	0.001	0.029	0.01	0.001-0.029
MnO	0.01	0.01	0.01	0.00	0.00	0.01	0.00-0.01	0.008	0.01	0.008	0.027	0.03	0.02	0.008-0.03
MgO	0.00	0.00	0.00	0.00	0.00	0.00	0.00-0.00	0.004	0.003	0.004	0.006	0.005	0.00	0.003-0.006
CaO	0.00	0.00	0.00	0.00	0.00	0.00	0.00-0.00	0.03	0.02	0.02	0.02	0.03	0.02	0.02-0.03
Na_2O	1.75	2.06	1.96	1.87	1.78	1.88	1.75-2.06	1.92	1.88	1.92	1.78	1.82	1.86	1.78-1.92
K_2O	16.16	15.82	15.85	16.66	16.42	16.18	15.82-16.66	15.89	15.78	15.68	15.82	16.02	15.84	15.8-16.02
P_2O_5	0.01	0.07	0.03	0.02	0.04	0.03	0.01-0.07	0.03	0.02	0.02	0.02	0.03	0.02	0.02-.03
Total	100.27	100.50	100.10	100.55	100.12	100.31	100.1-100.55	100.089	99.865	99.789	100.534	100.204	100.10	
Trace element														
Li	1440	1164	820	1328	756	1101.60	756-1440	1118	1432	1280	1682	1368	1376	1118-1682
Rb	1120	1326	968	1102	671	1037.40	671-1326	1986	1672	1579	1089	1804	1626	1089-1986
Cs	380	214	351	428	391	352.80	214-428	380	619	830	213	442	496.8	213-830
Ba	273	824	189	411	543	448.00	189-824	612	742	1176	546	1341	883.4	546-1341
Sr	56	239	96	249	158	159.60	56-249	68	253	198	319	113	190.2	68-319
Ga	30	28	33	28	47	33.20	28-47	27	67	49	34	39	43.2	27-67
Be	7	13	12	28	23	16.60	28.0-47	15	9	11	18	28	16.2	9-28
B	20	11	27	14	19	18.20	7.0-28	20	11	27	14	18	18	11-27
Sn	3	2	2	3	6	3.20	11.0-27	3	1	1	2	5	2.4	1.0-5.0
Nb	39	23	31	21	36	30.00	2.0-0.6	34	26	23	41	36	32	23-41
Ta	28	19	26	23	21	23.40	21-39	22	19	28	24	23	23.2	19-28
W	2	1	1	2	1	1.40	19-28	2	1	1	2	2	1.6	1.0-2.0
Y	2	1	1	3	1	1.60	1.0-2.0	2	1	1	2	2	1.6	1.0-2.0
Zn	1	1	2	1	1	1.20	1.0-3.0	2	1	2	1	1	1.4	1.0-2.0
Zr	1	1	2	2	1	1.40	1.0-2.0	1	2	2	1	2	1.6	1.0-2.0
Hf	0.1	0.2	0.2	0.1	0.1	0.14	0.1-.02	0.3	0.3	0.2	0.2	0.1	0.22	0.1-0.2
Th	0.2	0.3	0.8	0.4	0.2	0.38	0.2-.08	0.2	0.2	0.3	0.2	0.2	0.22	0.1-0.2
U	0.2	0.4	1	0.5	0.4	0.50	0.2-1.0	0.3	0.2	0.3	0.3	0.2	0.26	0.1-0.2
K/Ba	491.2	159.31	695.9	336.4	250.9	299.70	159.3-695.9	215.45	176.47	110.64	240.43	99.13	148.77	99.1-240.4
Rb/Sr	20	5.548117	10.08333	4.425703	4.246835	8.86	4.25-20	29.21	6.61	7.97	3.41	15.96	12.63	3.41-29.21
K/Rb	119.73	99	135.87	125.45	203.06	129.44	99.0-129.44	66.39	78.31	82.4	120.55	73.69	80.83	66.39-120.55
K/Cs	352.9	613.43	374.71	323.01	348.47	380.61	323.01-613.43	346.99	211.54	156.76	616.31	300.76	264.54	156.76-616.31
Nb/Ta	1.39	1.21	1.19	0.91	1.71	1.28	0.91-1.71	1.35	1.37	0.82	1.71	1.57	1.4	0.82-1.71
Ta/W	14	19	26	11.5	21	18.3	11.5-26	11	19	29	12	11.5	16.3	11.0-28
Al/Ga	3296.4	3645.29	3004.76	3454.32	2095.06	3099.17	2095.1-3645	3890.1	1498	1981.5	2833.9	2534.3	2548	1498-3890
Zr/Hf	10	5	10	20	10	11	5.0-20.0	3.33	6.66	10	5	10	7	3.33-10.0
Na/K	0.1	0.12	0.11	0.1	0.1	0.1	0.1-0.12	0.11	0.11	0.11	0.1	0.1	0.11	0.1-0.11

APPENDIX 5 (Continued)

	Ofki pegmatite							Iwere-Ile pegmatite						
	OFK1	OFK2	OFK3	OFK4	OFK5	Mean	Range	IWK1	IWK2	IWK3	IWK4	IWK5	Mean	Range
SiO_2	63.79	63.62	63.95	64.04	64.36	63.95	63.62-64.36	63.85	64.02	63.44	64.36	64.01	63.94	63.44-64.36
TiO_2	0.01	0.01	0.01	0.01	0.01	0.01	0.005-0.009	0.002	0.003	0.007	0.05	0.03	0.02	0.02-0.05
Al_2O_3	18.24	18.34	18.56	18.76	19.08	18.60	18.24-19.08	18.73	18.12	18.45	18.86	18.44	18.52	18.12-18.
FeO	0.11	0.03	0.01	0.01	0.01	0.03	0.009-0.112	0.01	0.08	0.012	0.06	0.09	0.05	0.01-0.09
MnO	0.01	0.01	0.01	0.01	0.01	0.01	0.007-0.012	0.01	0.01	0.013	0.03	0.047	0.02	0.01-0.047
MgO	0.00	0.00	0.01	0.00	0.01	0.00	0.003-0.006	0.003	0.008	0.004	0.016	0.03	0.01	0.003-0.03
CaO	0.02	0.01	0.01	0.03	0.03	0.02	0.01-0.03	0.07	0.04	0.016	0.03	0.02	0.04	0.016-0.07
Na_2O	1.56	1.47	1.78	1.82	1.96	1.72	1.47-1.96	1.87	1.92	1.64	1.59	1.43	1.69	1.43-1.92
K_2O	16.43	16.32	15.86	15.46	14.36	15.69	14.36-16.43	15.65	16.04	16.01	15.92	16.2	15.96	15.65-16.2
P_2O_5	0.01	0.01	0.01	0.08	0.19	0.06	0..05-0.19	0.02	0.02	0.008	0.04	0.04	0.03	0.008-0.04
Total	100.18	99.82	100.20	100.22	100.02	100.09	99.815-100.218	100.215	100.261	99.6	100.956	100.337	100.27	99.6-100.96
Li	1168	2871	1018	1445	1778	1656.00	1018-2871	991	2456	1336	2611	1102	1699	991-2611
Rb	2726	3385	2518	2336	3955	2984.00	2336-3955	1722	1552	963	1525	1120	1376	963-1722
Cs	1360	695	1823	1212	734	1164.80	695-1823	1000	358	227	183	398	433	183-1000
Ba	992	778	175	541	1175	732.20	175-1175	239	399	230	810	296	395	230-810
Sr	246	179	58	127	452	212.40	58-452	109	189	226	118	161	161	109-226
Ga	51	48	45	57	53	50.80	45-57	27	32	41	193	56	70	27-193
Be	12	8	10	13	27	14.00	8.0-27	16	28	20	58	36	32	16-58
B	17	38	16	34	23	25.60	16-38	14	21	12	19	31	19	12.0-31
Sn	2	2	4	2	2	2.40	2.0-4.0	2	2	8	4	4	4	2.0-8.0
Nb	32	27	36	34	27	31.20	27-36	17	25	39	32	54	33	17-54
Ta	21	19	26	16	21	20.60	16-26	13	19	27	21	39	24	13-39
W	1.7	0.5	0.5	2	1.3	1.20	0.5-2.0	1	1	2	2	3	2	1.0-3.0
Y	1	3	3	0.5	0.8	1.66	0.5-3.0	2	6	1	2	4	3	1.0-6.0
Zn	1	1	1	2	1	1.20	1.0-2.0	25	15	20	13	19	18	13-25
Zr	0.4	1	1	2	3	1.48	0.4-3.0	2	1	2	3	3	2	1.0-3.0
Hf	0.2	0.2	0.2	0.3	0.2	0.22	0.2-0.03	0.2	0.1	0.1	0.2	0.4	0	0.1-0.4
Th	0.2	0.6	2	0.8	0.7	0.86	0.2-2.0	3	1	3	1	3	2	1.0-3.0
U	0.4	0.6	3	2.3	0.5	1.36	0.4-3.0	2	1	3	2	2	2	1.0-3.0
K/Ba	137.44	174.07	752.04	237.13	101.41	177.77	101.41-752.04	543.36	333.58	577.61	163.09	454.15	336	163.09-577.61
Rb/Sr	11.08	18.91	43.41	18.39	8.75	20.11	8.75-43.41	15.8	8.21	4.26	12.92	6.96	9.63	4.26-15.8
K/Rb	50.01	40.01	52.27	54.92	30.13	43.62	30.13-54.92	75.41	85.76	137.96	86.63	120.02	96.24	75.41-137.96
K/Cs	100.25	194.85	72.19	105.85	162.34	111.75	72.19-194.85	129.86	371.79	585.25	721.88	337.76	305.79	129.86-721.88
Nb/Ta	1.52	1.42	1.38	2.13	1.29	1.55	1.29-2.13	1.31	1.32	1.44	1.52	1.38	1.394	1.31-1.52
Ta/W	12.35	38	52	8	16.15	25.3	8.0-52	13	19	13.5	10.5	13	13.8	10.5-19
Al/Ga	1893.38	2022.75	2183.48	1742.38	1905.84	1949.57	1742.38-2183.48	3672.47	2997.73	2382.3	517.33	1743.2	2263	517.33-3672.47
Zr/Hf	2	5	5	6.67	15	6.734	2-15	10	10	20	15	7.5	12.5	7.5-20
Na/K	0.08	0.08	0.1	0.11	0.12	0.1	0.08-0.12	0.11	0.11	0.09	0.09	0.09	0.08	0.09

APPENDIX 5 (Continued)

	Osu pegmatite						
	OSK1	OSK2	OSK3	OSK4	OSK5	Mean	Range
SiO_2	64.06	64.96	63.73	64.23	64.54	64.30	63.73-64.96
TiO_2	0.005	0.003	0.004	0.008	0.002	0.00	0.002-0.008
Al_2O_3	18.36	18.27	18.78	19.01	18.48	18.58	18.27-19.01
FeO	0.015	0.03	0.015	0.05	0.04	0.03	0.015-0.05
MnO	0.008	0.012	0.009	0.02	0.034	0.02	0.008-0.034
MgO	0.004	0.004	0.004	0.05	0.02	0.02	0.004-0.05
CaO	0.003	0.007	0.009	0.01	0.02	0.01	0.003-0.02
Na_2O	0.86	0.74	0.55	0.69	0.82	0.73	0.55-0.86
K_2O	16.68	16.05	16.42	16.14	16.24	16.31	16.05-16.68
P_2O_5	0.035	0.002	0.035	0.01	0.03	0.02	0.002-0.035
Total	100.03	100.078	99.556	100.218	100.226	100.02	99.56-100.23
Li	45	64	245	53	112	1	45-245
Rb	345	316	452	98	72	257	72-452
Cs	31	26	41	39	27	33	26-41
Ba	65	130	117	141	52	101	52-141
Sr	95	78	131	72	58	87	58-131
Ga	14	13	25	32	18	20	13-32
Be	15	22	16	15	11	16	11.0-22
B	19	33	23	17	29	24	17-33
Sn	2	1	1	1	3	2	1.0-3.0
Nb	14	9	17	22	13	15	9.0-22
Ta	4	2	6	7	3	4	2.0-7.0
W	0.3	0.2	0.5	0.4	1	0	0.2-1.0
Y	1	2	1	1	2	1	1.0-2.0
Zn	2	3	1	1	1	2	1.0-3.0
Zr	1	1	2	2	1	1	1.0-2.0
Hf	0.1	0.2	0.2	0.2	0.1	0	0.1-0.2
Th	0.2	0.2	0.1	0.1	0.2	0	0.1-0.2
U	0.2	0.3	0.2	0.2	0.1	0	0.1-0.2
K/Ba	2129.39	1024.48	1164.56	949.86	2591.53	1340	949.86-2591.53
Rb/Sr	3.63	4.05	3.45	1.36	1.24	2.75	1.24-4.05
K/Rb	401.19	421.46	301.45	1366.65	1871	527	301.45-1366.65
K/Cs	4464.86	5122.42	3323.25	3434.1	4991.09	4125.33	3323.3-5122.4
Nb/Ta	3.5	4.5	2.88	3.14	4.33	3.67	2.88-4.5
Ta/W	13.33	10	12	17.5	3	11.17	3-17.5
Al/Ga	6942.7	7444.18	3976.85	3144.97	5435.17	5388.77	3144.97-7444.18
Zr/Hf	10	5	10	10	10	9	5.0-10
Na/K	0.05	0.04	0.03	0.04	0.05	0.04	0.03-0.05

APPENDIX 6

Calculated cation formulae for the K-feldspar samples of the pegmatites of the study areas

	Ijero pegmatite					Komu pegmatite				
	IJK1	IJK2	IJK3	IJK4	IJK5	KMK1	KMK2	KMK3	KMK4	KMK5
SiO_2	63.64	64.24	63.49	63.36	63.26	62.35	63.18	63.78	64.12	63.52
TiO_2	0.004	0.007	0.003	0.002	0.006	0.01	0.01	0.009	0.04	0.05
Al_2O_3	18.68	18.28	18.73	18.27	18.6	19.84	18.96	18.34	18.2	18.67
FeO	0.01	0.009	0.02	0.04	0.008	0.007	0.002	0.008	0.001	0.029
MnO	0.007	0.006	0.014	0.004	0.004	0.008	0.01	0.008	0.027	0.03
MgO	0.004	0.004	0.004	0.003	0.003	0.004	0.003	0.004	0.006	0.005
CaO	0.002	0.002	0.001	0.001	0.002	0.03	0.02	0.02	0.02	0.03
Na_2O	1.75	2.06	1.96	1.87	1.78	1.92	1.88	1.92	1.78	1.82
K_2O	16.16	15.82	15.85	16.66	16.42	15.89	15.78	15.68	15.82	16.02
Total	100.257	100.428	100.072	100.21	100.083	100.059	99.845	99.769	100.014	100.174
Si	2.9542	2.9721	2.9506	2.9555	2.9487	2.9027	2.9417	2.9682	2.9763	2.9511
Al	1.0221	0.9968	1.026	1.0045	1.0219	1.0887	1.0405	1.006	0.9958	1.0224
Ti	0.0001	0.0002	0.0001	0.0005	0.0002	0.0004	0.0004	0.0003	0.0014	0.0017
Fe	0.0004	0.0003	0.0008	0.0016	0.0003	0.0003	0.0005	0.0003	0.0004	0.0011
Mn	0.0003	0.0002	0.0006	0.0002	0.002	0.0003	0.0004	0.0003	0.0011	0.0012
Mg	0.0003	0.0003	0.0003	0.0002	0.0002	0.0003	0.0002	0.0003	0.004	0.0003
Ca	0.004	0.004	0.005	0.005	0.004	0.0015	0.001	0.001	0.001	0.0015
Na	0.1575	0.1848	0.1766	0.1691	0.1609	0.1733	0.1697	0.1733	0.1602	0.164
K	0.9568	0.9336	0.9395	0.9912	0.9763	0.9436	0.9372	0.9308	0.9367	0.9493
Tot Cation	5.0918	5.0885	5.0944	5.1224	5.1087	5.111	5.0911	5.0805	5.0728	5.0926
Tot Oxy	8.0000	8.0000	8.0000	8.0000	8.0000	8.0000	8.0000	8.0000	8.0000	8.0000
An	0.0045	0.0044	0.0045	0.0045	0.0044	0.0045	0.0904	0.0902	0.0906	0.1339
Ab	14.1317	16.51995	15.8451	15.2039	13.969	15.5141	15.317	15.6758	14.5899	14.7042
Or	85.8638	83.47562	84.1505	84.7917	86.0266	84.4814	84.593	84.2339	85.3196	85.16184
Si+Ti+Al+Fe_3+	4.201	4.194	4.202	4.198	4.194	4.212	4.205	4.2	4.197	4.199
Ca+Na+K	0.93	0.934	0.93	0.927	0.959	0.923	0.925	0.922	0.912	0.93

APPENDIX 6 (Continued)

	Ofiki pegmatite					Iwere-Ile pegmatite				
	OFK1	OFK2	OFK3	OFK4	OFK5	IWK1	IWK2	IWK3	IWK4	IWK5
SiO_2	63.79	63.62	63.95	64.04	64.36	63.85	64.02	63.44	64.36	64.01
TiO_2	0.005	0.008	0.008	0.006	0.009	0.002	0.003	0.007	0.05	0.03
Al_2O_3	18.24	18.34	18.56	18.76	19.08	18.73	18.12	18.45	18.86	18.44
FeO	0.112	0.03	0.01	0.009	0.01	0.01	0.08	0.012	0.06	0.09
MnO	0.012	0.007	0.009	0.01	0.01	0.01	0.01	0.013	0.03	0.047
MgO	0.003	0.004	0.005	0.003	0.006	0.003	0.008	0.004	0.016	0.03
CaO	0.02	0.01	0.01	0.03	0.03	0.07	0.04	0.016	0.03	0.02
Na_2O	1.56	1.47	1.78	1.82	1.96	1.87	1.92	1.64	1.59	0.64
K_2O	16.43	16.32	15.86	15.46	14.36	15.65	16.04	16.01	15.92	16.2
Total	100.172	99.809	100.192	100.138	99.825	100.195	100.241	99.592	100.916	99.507
Si	2.9677	2.9667	2.9641	2.9625	2.9662	2.9576	2.9724	2.9618	2.9596	2.9807
Al	1.0002	1.008	1.041	1.0229	1.0365	1.0226	0.9916	1.0153	1.0223	1.0121
Ti	0.0002	0.0003	0.0003	0.0002	0.0003	0.0007	0.0001	0.0002	0.0017	0.0011
Fe	0.0044	0.0012	0.0004	0.0003	0.0004	0.0004	0.0031	0.0005	0.0023	0.0035
Mn	0.0005	0.0003	0.0004	0.0004	0.0004	0.0004	0.0004	0.0005	0.0012	0.0019
Mg	0.0002	0.0003	0.0003	0.0002	0.0004	0.0002	0.006	0.0003	0.011	0.0021
Ca	0.001	0.0005	0.0005	0.0015	0.0015	0.0035	0.002	0.0008	0.0015	0.001
Na	0.1407	0.1329	0.16	0.1633	0.01752	0.168	0.1729	0.1485	0.1418	0.0578
K	0.975	0.9707	0.9376	0.9122	0.8442	0.9247	0.9499	0.9534	0.9338	0.9622
Tot Cation	5.0899	5.0808	5.0775	5.0636	5.0249	5.0773	5.093	5.0812	5.0653	5.0222
Tot Oxy	8.0000	8.0000	8.0000	8.0000	8.0000	8.0000	8.0000	8.0000	8.0000	8.0000
An	0.0893	0.0452	0.0452	0.138	0.1451	0.3169	0.1769	0.0726	0.1372	0.09134
Ab	12.5993	12.0356	14.565	15.1554	17.1551	15.3203	15.3648	13.4613	13.1605	11.8179
Or	87.3114	87.9191	85.3898	84.7066	82.6998	84.3628	84.4583	86.4661	86.7022	88.0908
Si+Ti+Al+Fe_3+	4.195	4.201	4.202	4.206	4.222	4.203	4.191	4.203	4.204	4.2
Ca+Na+K	0.931	0.921	0.916	0.899	0.853	0.915	0.939	0.919	0.9	0.908

APPENDIX 6 (Continued)

	IWK1	IWK2	IWK3	IWK4	IWK5	OSK1	OSK2	OSK3	OSK4	OSK5
SiO_2	64.85	65.02	64.44	64.36	64.41	64.06	64.96	63.73	64.23	64.54
TiO_2	0.002	0.003	0.007	0.05	0.03	0.005	0.003	0.004	0.008	0.002
Al_2O_3	18.73	18.12	18.45	18.86	18.44	18.36	18.27	18.78	19.01	18.48
FeO	0.01	0.08	0.012	0.06	0.09	0.015	0.03	0.015	0.05	0.04
MnO	0.01	0.01	0.013	0.03	0.047	0.008	0.012	0.009	0.02	0.034
MgO	0.003	0.008	0.004	0.016	0.03	0.004	0.004	0.004	0.05	0.02
CaO	0.07	0.04	0.016	0.03	0.02	0.003	0.007	0.009	0.01	0.02
Na_2O	0.86	0.92	0.64	0.59	0.64	0.86	0.74	0.55	0.69	0.82
K_2O	15.65	16.04	16.01	15.92	16.2	16.68	16.05	16.42	16.14	16.24
P_2O_5	0.02	0.02	0.008	0.04	0.04	0.035	0.002	0.035	0.01	0.03
H_2O*	100.2	100.26	99.6	99.956	99.95	100	100.1	99.56	100.2	100.2
Total										
Si	2.986	3.0009	2.991	2.9762	2.985	2.978	3	2.969	2.967	2.984
Al	1.017	0.9857	1.009	1.028	1.007	1.006	0.995	1.031	1.035	1.007
Ti	5E-04	0.0001	2E-04	0.0017	0.001	2E-04	1E-04	1E-04	3E-04	5E-05
Fe	4E-04	0.0031	5E-04	0.0023	0.004	6E-04	0.001	6E-04	0.002	0.002
Mn	4E-04	0.0004	5E-04	0.0012	0.002	3E-04	5E-04	4E-04	8E-04	0.001
Mg	2E-04	0.0006	3E-04	0.0011	0.002	3E-04	3E-04	3E-04	0.003	0.001
Zn	0	0	0	0	0	0	0	0	0	0
Ca	0.004	0.002	8E-04	0.0015	0.001	1E-04	3E-04	4E-04	5E-04	0.001
Na	0.077	0.0823	0.058	0.0529	0.058	0.078	0.066	0.05	0.062	0.074
K	0.919	0.9443	0.948	0.939	0.958	0.989	0.945	0.976	0.951	0.958
Ba	0	0	0	0	0	0	0	0	0	0
Tot Cation	5.003	5.0194	5.007	5.004	5.018	5.052	5.009	5.028	5.022	5.028
Tot Oxy	8	8	8	8	8	8	8	8	8	8
An	0.346	0.1922	0.079	0.1496	0.097	0.014	0.034	0.044	0.049	0.096
Ab	7.681	8.0027	5.723	5.3241	5.659	7.266	6.546	4.842	0.098	7.12
Or	91.97	91.805	94.2	94.526	94.24	92.72	93.42	95.11	93.85	92.78
$Si+Ti+Al+Fe^{3+}$	4.004	3.9898	4	4.0082	3.997	3.985	3.996	4.001	4.004	3.993
Ca+Na+K	1	1.0286	1.006	0.9934	1.016	1.067	1.012	1.026	1.013	1.032

APPENDIX 6 (Continued)

	IWK1	IWK2	IWK3	IWK4	IWK5	OSK1	OSK2	OSK3	OSK4	OSK5
SiO_2	64.85	65.02	64.44	64.36	64.41	64.06	64.96	63.73	64.23	64.54
TiO_2	0.002	0.003	0.007	0.05	0.03	0.005	0.003	0.004	0.008	0.002
Al_2O_3	18.73	18.12	18.45	18.86	18.44	18.36	18.27	18.78	19.01	18.48
FeO	0.01	0.08	0.012	0.06	0.09	0.015	0.03	0.015	0.05	0.04
MnO	0.01	0.01	0.013	0.03	0.047	0.008	0.012	0.009	0.02	0.034
MgO	0.003	0.008	0.004	0.016	0.03	0.004	0.004	0.004	0.05	0.02
CaO	0.07	0.04	0.016	0.03	0.02	0.003	0.007	0.009	0.01	0.02
Na_2O	0.86	0.92	0.64	0.59	0.64	0.86	0.74	0.55	0.69	0.82
K_2O	15.65	16.04	16.01	15.92	16.2	16.68	16.05	16.42	16.14	16.24
P_2O_5	0.02	0.02	0.008	0.04	0.04	0.035	0.002	0.035	0.01	0.03
Total	100.2	100.26	99.6	99.956	99.95	100	100.1	99.56	100.2	100.2
Si	2.986	3.0009	2.991	2.9762	2.985	2.978	3	2.969	2.967	2.984
Al	1.017	0.9857	1.009	1.028	1.007	1.006	0.995	1.031	1.035	1.007
Ti	5E-04	0.0001	2E-04	0.0017	0.001	2E-04	1E-04	1E-04	3E-04	5E-05
Fe	4E-04	0.0031	5E-04	0.0023	0.004	6E-04	0.001	6E-04	0.002	0.002
Mn	4E-04	0.0004	5E-04	0.0012	0.002	3E-04	5E-04	4E-04	8E-04	0.001
Mg	2E-04	0.0006	3E-04	0.0011	0.002	3E-04	3E-04	3E-04	0.003	0.001
Zn	0	0	0	0	0	0	0	0	0	0
Ca	0.004	0.002	8E-04	0.0015	0.001	1E-04	3E-04	4E-04	5E-04	0.001
Na	0.077	0.0823	0.058	0.0529	0.058	0.078	0.066	0.05	0.062	0.074
K	0.919	0.9443	0.948	0.939	0.958	0.989	0.945	0.976	0.951	0.958
Ba	0	0	0	0	0	0	0	0	0	0
Tot Cation	5.003	5.0194	5.007	5.004	5.018	5.052	5.009	5.028	5.022	5.028
Tot Oxy	8	8	8	8	8	8	8	8	8	8
An	0.346	0.1922	0.079	0.1496	0.097	0.014	0.034	0.044	0.049	0.096
Ab	7.681	8.0027	5.723	5.3241	5.659	7.266	6.546	4.842	0.098	7.12
Or	91.97	91.805	94.2	94.526	94.24	92.72	93.42	95.11	93.85	92.78
$Si+Ti+Al+Fe^{3+}$	4.004	3.9898	4	4.0082	3.997	3.985	3.996	4.001	4.004	3.993
Ca+Na+K	1	1.0286	1.006	0.9934	1.016	1.067	1.012	1.026	1.013	1.032

APPENDIX 7

Major and trace element analytical data for the muscovite samples of the pegmatites study areas

	IJM1	IJM2	IJM3	IJM4	IJM5	Mean	Range		KMM1	KMM2	KMM3	KMM4	KMM5	Mean	Range	
SiO_2	46.15	46.1	45.7	45.5	45.8	45.83	45.5	46.15	45.77	45.64	45.54	45.92	45.61	45.7	45.54	45.92
TiO_2	0.07	0.02	0.01	0.01	0.02	0.026	0.01	0.07	0.13	0.3	0.28	0.06	0.08	0.17	0.06	0.3
Al_2O_3	34.42	34.4	34.5	34.7	34.9	34.6	34.42	34.92	35.72	33.91	33.74	36.54	36.13	35.21	33.74	36.54
FeO	1.71	1.76	1.63	1.67	1.77	1.708	1.63	1.77	0.9	2.99	3.03	0.09	0.11	1.424	0.09	3.03
MnO	0.03	0.06	0.07	0.13	0.14	0.086	0.03	0.14	0.16	0.06	0.05	0.27	0.22	0.152	0.05	0.27
MgO	0.47	0.01	0.02	0.03	0.02	0.11	0.01	0.47	0.01	0.13	0.1	0.03	0.02	0.058	0.01	0.13
CaO	0.01	0.01	0.01	0.02	0.01	0.011	0.01	0.015	0.01	0.01	0.01	0.02	0.01	0.012	0.01	0.02
Na_2O	0.77	0.59	0.56	0.69	0.65	0.652	0.56	0.77	0.66	0.61	0.72	0.72	0.7	0.682	0.61	0.72
K_2O	10.59	10.7	10.6	10.8	10.6	10.66	10.59	10.83	10.51	10.72	10.5	10.45	10.65	10.57	10.45	10.72
Li_2O*	3.68	3.65	3.54	3.49	3.56	3.584	3.49	3.68	3.53	3.53	3.5	3.61	3.52	3.538	3.5	3.61
H_2O*	4.64	4.61	4.59	4.6	4.62	4.612	4.59	4.64	4.61	4.61	4.59	4.68	4.64	4.626	4.59	4.68
Total	102.5	102	101	102	102	101.9	101.2	102.5	102	102.51	102.06	102.39	101.7	102.1	101.7	102.51
Li	1260	2735	1173	2245	3511	2185	1173	3511	697	1697	1241	1742	1436	1363	697	1742
Rb	4068	5067	4299	5267	2761	4292	2761	5267	5632	4708	3313	2848	4548	4210	2848	5632
Cs	1102	959	1429	989	1912	1301	959	1912	1347	998	1913	3127	2749	2027	998	3127
Ba	61	27	89	72	158	81.4	27	158	48	24	41	32	56	40.2	24	56
Sr	80	71	60	139	176	105.2	60	176	30	23	32	24	37	29.2	23	37
Ga	322	226	158	304	383	278.6	158	383	255	138	161	247	262	212.6	138	262
Be	30	34	21	33	37	31	21	37	25	22	28	33	24	26.4	22	33
B	424	362	77	85	420	273.6	77	424	242	163	269	212	192	215.6	163	269
Sn	610	596	143	499	742	518	143	742	183	198	377	263	363	276.8	183	377
Nb	144	189	394	218	406	270.2	144	406	316	406	361	241	158	296.4	158	406
Ta	108	94	206	189	286	176.6	94	286	281	216	332	248	168	249	168	332
W	22	44	40	20	41	33.4	20	44	22	28	42	31	33	31.2	22	42
Y	7	5	3	8	6	5.8	3	8	11	14	19	8	13	13	8	19
Zn	483	789	361	317	634	516.8	317	789	212	232	222	183	267	223.2	183	267
Zr	26	33	28	45	32	32.8	26	45	8	12	15	13	16	12.8	8	16
Hf	4	3	2	3	6	3.6	2	6	1.5	2.2	1.2	2	1.8	1.74	1.2	2.2
Th	2	1	2	1	3	1.8	1	3	2	2	1	2	2	1.8	1	2
U	2	1	2	1	2	1.6	1	2	1	2	2	3	1	1.8	1	3
K/Ba	1504	3428	1033	1304	582	1570	581.9	3428	1897	3870.8	2219.3	2830	1648	2493	1648	3870.8
Rb/Sr	50.85	71.4	71.7	37.9	15.7	49.49	15.69	71.65	187.7	204.7	103.53	118.67	122.9	147.5	103.5	204.7
K/Rb	22.56	18.3	21.4	17.8	33.3	22.67	17.82	33.3	16.17	19.73	27.47	31.8	20.29	23.09	16.17	31.8
K/Cs	83.28	96.5	64.3	94.9	48.1	77.42	48.09	96.51	67.62	93.09	47.57	28.96	33.57	54.16	28.96	93.09
Nb/Ta	1.33	2.01	1.91	1.15	1.42	1.564	1.15	2.01	1.12	1.88	1.09	0.97	0.94	1.2	0.94	1.88
Ta/W	4.91	2.14	5.15	9.45	6.98	5.726	2.14	9.45	12.77	7.71	7.9	8	5.09	8.294	5.09	12.77
Al/Ga	565.9	807	1156	605	483	723.2	482.7	1156	741.6	1300.9	1109.4	783.17	730.1	933	730.1	1300.9
Zr/Hf	6.5	11	14	15	5.33	10.37	5.33	15	5.33	5.45	12.5	6.5	8.89	7.734	5.33	12.5
Na/K	0.06	0.05	0.05	0.06	0.05	0.052	0.045	0.06	0.054	0.049	0.059	0.059	0.056	0.055	0.049	0.059

APPENDIX 7(Continued)

	OFM1	OFM2	OFM3	OFM4	OFM5	Mean	Range		IWM1	IWM2	IWM3	IWM4	IWM5	Mean	Range		OSM1	OSM2	OSM3	OSM4	OSM5	Mean	Range	
SiO_2	45.8	45.97	45.8	45.74	45.67	45.8	45.67	45.97	45.59	46.18	46.17	46.38	45.95	46.05	45.59	46.38	46.14	45.8	46	46.33	46.29	46.1	45.84	46.33
TiO_2	0.09	0.21	0.09	0.02	0.03	0.088	0.02	0.21	0.07	0.23	0.24	0.22	0.21	0.194	0.07	0.24	0.08	0.02	0.23	0.08	0.02	0.09	0.02	0.23
Al_2O_3	33.42	33.24	33.42	34.74	34.33	33.83	33.24	34.74	36.29	32.06	32.88	32.21	32.33	33.15	32.06	36.29	34.92	35.6	33.2	35.3	35.38	34.9	33.19	35.62
FeO	3.58	3.49	3.58	3.52	3.67	3.568	3.49	3.67	0.05	3.75	3.11	3.78	3.71	2.88	0.05	3.78	1.42	1.15	3.33	1.27	1.47	1.73	1.15	3.33
MnO	0.04	0.05	0.04	0.08	0.07	0.056	0.04	0.08	0.2	0.05	0.1	0.04	0.05	0.088	0.04	0.2	0.11	0.01	0.04	0.02	0.01	0.04	0.01	0.11
MgO	0.25	0.41	0.25	0.04	0.02	0.194	0.02	0.41	0.01	0.78	0.56	0.79	0.76	0.58	0.01	0.79	0.51	0.33	0.47	0.52	0.45	0.46	0.33	0.52
CaO	0.01	0.01	0.02	0.01	0.01	0.012	0.01	0.02	0.01	0.01	0.01	0.01	0.02	0.012	0.01	0.02	0.06	0.01	0.02	0.01	0.01	0.02	0.01	0.06
Na_2O	0.61	0.65	0.61	0.62	0.65	0.628	0.61	0.65	0.67	0.53	0.53	0.62	0.61	0.592	0.53	0.67	0.85	0.99	0.7	0.89	0.85	0.86	0.7	0.99
K_2O	10.76	10.74	10.76	10.61	10.47	10.67	10.47	10.76	10.63	10.8	10.9	10.87	10.56	10.75	10.56	10.9	10.31	10.1	10.5	10.55	10.61	10.4	10.07	10.61
Li_2O*	3.58	3.63	3.58	3.56	3.54	3.578	3.54	3.63	3.52	3.69	3.69	3.75	3.62	3.654	3.52	3.75	3.68	3.59	3.64	3.73	3.72	3.67	3.59	3.73
H_2O*	4.6	4.62	4.6	4.65	4.62	4.618	4.6	4.65	4.64	4.59	4.61	4.62	4.59	4.61	4.59	4.64	4.66	4.65	4.62	4.69	4.69	4.66	4.62	4.69
Total	102.7	103	102.8	103.6	103.1	103	102.7	103.6	103.1	102.67	102.8	103.29	102.4	102.9	102.4	103.29	102.7	102	103	103.4	103.5	103	102.3	103.5
µg/g																								
Li	19843	22413	19596	20437	23388	21135	19596	23388	27323	5371	2254	2036	3608	8118	2036	27323	316	346	327	372	905	453	316	905
Rb	6170	6324	5709	6543	5840	6117	5709	6543	2487	4011	2120	4895	3692	3441	2120	4895	364	246	462	129	277	296	129	462
Cs	4379	3672	4906	5638	4868	4693	3672	5638	1656	968	1746	1114	2625	1622	968	2625	37	40	65	39	51	46.4	37	65
Ba	18	24	34	22	17	23	17	34	30	26	15	19	22	22.4	15	30	27	30	107	196	56	83.2	27	196
Sr	12	18	22	36	20	21.6	12	36	11	18	18	16	18	16.2	11	18	17	13	11	6	25	14.4	6	25
Ga	58	112	66	118	60	82.8	58	118	157	220	112	236	116	168.2	112	236	49	54	50	57	97	61.4	49	97
Be	18	28	48	21	35	30	18	48	26	56	17	22	23	28.8	17	56	10	11	28	22	24	19	10	28
B	136	130	68	148	130	122.4	68	148	94	88	75	160	137	110.8	75	160	93	110	104	122	97	105	93	122
Sn	31	32	112	35	114	64.8	31	114	157	65	61	193	98	114.8	61	193	33	21	18	23	36	26.2	18	36
Nb	107	189	304	312	128	208	107	312	310	267	334	128	173	242.4	128	334	21	23	33	10	29	23.2	10	33
Ta	103	132	294	294	136	191.8	103	294	224	187	218	134	98	172.2	98	224	11	16	13	13	19	14.4	11	19
W	205	230	559	224	249	293.4	205	559	44	40	43	31	39	39.4	31	44	11	10	12	11	16	12	10	16
Y	2	2	4	3	4	3	2	4	3	3	3	2	4	3	2	4	8	4	2	7	3	4.8	2	8
Zn	427	160	120	82	210	199.8	82	427	125	113	117	207	135	139.4	113	207	67	79	31	18	47	48.4	18	79
Zr	6	8	3	4	6	5.4	3	8	1	3	3	3	3	2.6	1	3	4	3	2	3	2	2.8	2	4
Hf	0.3	0.2	0.4	0.6	0.5	0.4	0.2	0.6	0.4	0.3	0.2	0.3	0.4	0.32	0.2	0.4	1	0.4	0.5	0.8	0.3	0.6	0.3	1
Th	0.4	0.6	0.2	0.3	0.2	0.34	0.2	0.6	2	1	1	2	2	1.6	1	2	0.2	0.2	0.8	0.6	0.4	0.44	0.2	0.8
U	0.3	0.4	0.1	0.2	0.2	0.24	0.1	0.4	2	2	1	1	1	2	1	2	0.3	0.3	0.8	0.5	0.5	0.48	0.3	0.8
K/Ba	5180	3878	2743	4179	5337	4264	2743	5337	3071	3599.7	6297.3	4957.9	4160	4417	3071	6297.3	3309	2909	854	466.5	1642	1836	466.5	3309
Rb/Sr	514.2	351.3	259.5	181.8	292	319.8	181.8	514.2	226.1	222.8	117.78	305.94	205.1	215.5	117.8	305.94	21.41	18.9	42	21.5	11.08	23	11.08	42
K/Rb	15.11	14.72	16.33	14.05	15.54	15.15	14.05	16.33	37.04	23.33	44.56	19.24	24.79	29.79	19.24	44.56	245.5	355	198	708.7	331.9	368	197.7	708.7
K/Cs	21.29	25.35	19	16.31	18.64	20.12	16.31	25.35	55.63	96.69	54.1	84.56	34.86	65.17	34.86	96.69	2415	2182	2189	2344	2739	2374	2182	2739
Nb/Ta	1.04	1.43	1.03	1.06	0.94	1.1	0.94	1.43	1.38	1.43	1.53	0.96	1.77	1.414	0.96	1.77	1.9	1.44	2.54	0.77	1.53	1.64	0.77	2.54
Ta/W	0.5	0.57	0.53	1.31	0.55	0.692	0.5	1.31	5.09	4.68	5.07	4.32	2.51	4.334	2.51	5.09	1	1.6	1.08	1.18	1.19	1.21	1	1.6
Al/Ga	3050	1571	2681	1559	3029	2378	1559	3050	1224	771.48	1554.2	722.54	1475	1149	722.5	1554.2	3773	3492	3514	3279	1931	3198	1931	3773
Zr/Hf	20	40	7.5	6.67	12	17.23	6.67	40	2.5	10	15	10	7.5	9	2.5	15	4	7.5	4	3.75	6.67	5.18	3.75	7.5
Na/K	0.049	0.05	0.049	0.05	0.053	0.05	0.049	0.053	0.054	0.042	0.042	0.049	0.049	0.047	0.042	0.054	0.07	0.08	0.06	0.07	0.07	0.07	0.06	0.08

APPENDEX 8

Calculated cation formulae for the muscovite samples of the pegmatite of the study areas

	IJM1	IJM2	IJM3	IJM4	IJM5	KMM1	KMM2	KMM3	KMM4	KMM5	OFM1	OFM2	OFM3	OFM4	OFM5
SiO_2	46.15	46.06	45.67	45.5	45.75	45.77	45.64	45.54	45.92	45.61	45.8	45.97	45.8	45.74	45.67
TiO_2	0.07	0.02	0.01	0.013	0.016	0.13	0.3	0.28	0.06	0.08	0.09	0.21	0.09	0.02	0.03
Al_2O_3	34.42	34.44	34.49	34.74	34.92	35.72	33.91	33.74	36.54	36.13	33.42	33.24	33.42	34.74	34.33
FeO	1.71	1.76	1.63	1.67	1.77	0.9	2.99	3.03	0.09	0.11	3.58	3.49	3.58	3.52	3.67
MnO	0.03	0.06	0.07	0.13	0.14	0.16	0.06	0.05	0.27	0.22	0.04	0.05	0.04	0.08	0.07
MgO	0.47	0.01	0.02	0.03	0.02	0.01	0.13	0.1	0.03	0.02	0.25	0.41	0.25	0.04	0.02
CaO	0.01	0.01	0.01	0.015	0.01	0.01	0.01	0.01	0.02	0.01	0.01	0.01	0.02	0.01	0.01
Na_2O	0.77	0.59	0.56	0.69	0.65	0.66	0.61	0.72	0.72	0.7	0.61	0.65	0.61	0.62	0.65
K_2O	10.59	10.68	10.61	10.83	10.61	10.51	10.72	10.5	10.45	10.65	10.76	10.74	10.76	10.61	10.47
Li_2O*	3.68	3.65	3.54	3.49	3.56	3.53	3.53	3.5	3.61	3.52	3.58	3.63	3.58	3.56	3.54
H_2O*	4.64	4.61	4.59	4.6	4.62	4.61	4.61	4.59	4.68	4.64	4.6	4.62	4.6	4.65	4.62
Total	102.54	101.89	101.2	101.708	102.066	102.01	102.51	102.06	102.39	101.69	102.74	103.02	102.75	103.59	103.08
Si	5.96	5.99	5.97	5.94	5.94	5.91	5.94	5.95	5.89	5.90	5.97	5.97	5.97	5.90	5.92
Al iv	2.04	2.02	2.03	2.06	2.06	2.09	2.06	2.05	2.11	2.10	2.03	2.03	2.03	2.10	2.08
∑	8.00	8.00	8.00	8.00	8.00	8.00	8.00	8.00	8.00	8.00	8.00	8.00	8.00	8.00	8.00
Alvi	3.201	3.26	3.289	3.28	3.283	3.351	3.147	3.15	3.414	3.408	3.098	3.06	3.097	3.183	3.168
Ti	0.007	0.002	0.001	0.001	0.002	0.013	0.029	0.028	0.006	0.008	0.009	0.021	0.009	0.002	0.003
Fe	0.185	0.191	0.178	0.182	0.192	0.097	0.326	0.331	0.01	0.012	0.39	0.379	0.39	0.38	0.398
Mn	0.003	0.007	0.008	0.014	0.015	0.018	0.007	0.006	0.029	0.024	0.004	0.006	0.004	0.009	0.008
Mg	0.09	0.002	0.004	0.006	0.004	0.002	0.025	0.019	0.006	0.004	0.049	0.079	0.049	0.008	0.004
Li	1.912	1.908	1.862	1.832	1.861	1.855	1.849	1.84	1.862	1.831	1.875	1.895	1.875	1.847	1.846
∑	5.398	5.37	5.342	5.315	5.357	5.336	5.383	5.374	5.327	5.287	5.425	5.44	5.424	5.429	5.427
Ca	0.01	0.001	0.001	0.002	0.001	0.001	0.001	0.001	0.003	0.001	0.001	0.001	0.003	0.001	0.001
Na	0.193	0.149	0.142	0.175	0.164	0.165	0.154	0.182	0.179	0.176	0.154	0.164	0.154	0.155	0.163
K	1.745	1.77	1.77	1.802	1.757	1.732	1.78	1.75	1.71	1.757	1.788	1.779	1.788	1.746	1.732
∑	1.948	1.92	1.913	1.979	1.922	1.898	1.935	1.933	1.892	1.934	1.943	1.944	1.945	1.902	1.896
OH*	4.000	4.000	4.000	4.000	4.000	4.000	4.000	4.000	4.000	4.000	4.000	4.000	4.000	4.000	4.000
Total	19.337	19.289	19.255	19.295	19.278	19.232	19.318	19.308	19.218	19.221	19.368	19.383	19.368	19.33	19.323
Y total	5.398	5.369	5.342	5.316	5.356	5.335	5.382	5.374	5.327	5.287	5.424	5.439	5.423	5.428	5.427
Xtotal	1.939	1.92	1.913	1.979	1.922	1.897	1.936	1.934	1.891	1.934	1.943	1.944	1.922	1.902	1.896
Al total	5.24	5.275	5.316	5.343	5.343	5.438	5.204	5.198	5.524	5.508	5.131	5.089	5.529	5.282	5.247
Fe/Fe+Mg	0.671	0.99	0.979	0.969	0.98	0.981	0.928	0.944	0.627	0.755	0.889	0.827	0.889	0.98	0.99

APPENDIX 8(Continued)

	Iwere-Ile pegmatite					Osu pegmatite				
	IWM1	IWM2	IWM3	IWM4	IWM5	OSM1	OSM2	OSM3	OSM4	OSM5
SiO_2	45.59	46.18	46.17	46.38	45.95	46.14	45.84	46.03	46.328	46.29
TiO_2	0.07	0.23	0.24	0.22	0.21	0.08	0.02	0.23	0.08	0.02
Al_2O_3	36.29	32.06	32.88	32.21	32.33	34.92	35.62	33.19	35.3	35.38
FeO	0.05	3.75	3.11	3.78	3.71	1.42	1.15	3.33	1.27	1.47
MnO	0.2	0.05	0.1	0.04	0.05	0.11	0.01	0.04	0.02	0.01
MgO	0.01	0.78	0.56	0.79	0.76	0.51	0.33	00.47	0.52	0.45
CaO	0.01	0.01	0.01	0.01	0.02	0.06	0.01	0.02	0.01	0.01
Na_2O	0.67	0.53	0.53	0.62	0.61	0.85	0.99	0.7	0.89	0.85
K_2O	10.63	10.8	10.9	10.87	10.56	10.31	10.07	10.54	10.55	10.61
Li_2O*	3.52	3.69	3.69	3.75	3.62	3.68	3.59	3.64	3.73	3.72
H_2O*	4.64	4.59	4.61	4.62	4.59	4.66	4.65	4.62	4.69	4.69
Total	103.11	102.67	102.8	103.29	102.41	102.74	102.28	102.81	103.39	103.5
Si	5.908	6.027	6.002	6.02	6.007	5.935	5.906	5.98	5.921	5.916
Al iv	2.092	1.973	1.998	1.98	1.993	2.065	2.094	2.02	2.079	2.084
∑	8.0000	8.0000	8.0000	8.0000	8.0000	8.0000	8.0000	8.0000	8.0000	8.0000
Alvi	3.186	2.959	3.04	2.948	2.989	3.229	3.315	3.062	3.238	3.245
Ti	0.007	0.023	0.023	0.021	0.021	0.008	0.002	0.022	0.008	0.002
Fe	0.349	0.409	0.338	0.41	0.406	0.153	0.124	0.362	0.136	0.157
Mn	0.022	0.006	0.011	0.004	0.006	0.012	0.001	0.004	0.002	0.001
Mg	0.002	0.152	0.109	0.153	0.148	0.098	0.063	0.91	0.099	0.086
Li	1.833	1.936	1.927	1.958	1.903	1.904	1.86	1.902	1.917	1.912
∑	5.399	5.485	5.448	5.494	5.473	5.404	5.365	6.262	5.4	5.403
Ca	0.001	0.001	0.001	0.001	0.003	0.008	0.001	0.003	0.001	0.001
Na	0.168	0.134	0.134	0.156	0.155	0.212	0.247	0.176	0.221	0.211
K	1.757	1.798	1.807	1.8	1.761	1.691	1.655	1.747	1.72	1.729
∑	1.926	1.933	1.942	1.957	1.919	1.911	1.903	1.926	1.942	1.941
OH*	4.0000	4.0000	4.0000	4.0000	4.0000	4.0000	4.0000	4.0000	4.0000	4.0000
Total	19.326	19.418	19.39	19.451	19.391	19.314	19.169	19.369	19.342	19.344
Y total	5.399	5.485	5.447	5.494	5.472	5.403	5.365	5.443	5.4	5.403
Xtotal	1.927	1.942	1.942	1.957	1.918	1.912	1.903	1.926	1.942	1.941
Al total	5.279	5.038	5.038	4.928	4.4982	5.294	5.409	5.082	5.317	5.329

APPENDIX 9

pH and Eh data of the *in situ*-derived pegmatite profiles

pH and Eh analyses for the barren pegmatite profile of Osu area

Sample No.	Horizon	Depth (m)	Eh(volts)	pH
A1	A-horizon	0.2	0.291	6.99
A2		0.4	0.264	7.22
A3		0.6	0.261	7.35
A4		0.8	0.270	7.09
A5		1.0	0.276	6.75
A6		1.2	0.278	6.72
A7		1.4	0.270	6.89
A8		1.6	0.264	6.73
B1	B-horizon	1.8	0.272	6.40
B2		2.0	0.279	6.10
B3		2.2	0.275	6.60
B4		2.4	0.255	6.48
B5		2.6	0.247	6.25
B6		2.8	0.258	6.03
B7		3.0	0.240	7.30
B8		3.2	0.252	6.48
B9		3.4	0.251	6.38
B10		3.6	0.246	6.37
B11		3.8	0.243	6.41
C1	C-horizon	4.0	0.203	6.55
C2		4.2	0.287	6.40
Bedrock sample 1			0.910	9.92
Bedrock sample 2			0.111	9.76

APPENDIX 9 (Continued)

pH and Eh analyses for the mineralised pegmatite profile of Ijero area

Sample No.	Horizon	Depth (m)	Eh(volts)	pH
A1	A-horizon	0.2	0.336	4.83
B1	B-horizon	0.4	0.305	4.84
B2		0.6	0.285	5.05
B3		0.8	0.291	4.85
B4		1.0	0.298	4.49
B5		1.2	0.304	4.87
B6		1.4	0.304	4.61
B7		1.6	0.318	4.66
B8		1.8	0.313	4.77
B9		2.0	0.324	4.77
B10		2.2	0.333	5.08
B11		2.4	0.331	4.95
B12		2.6	0.326	4.86
B13		2.8	0.324	4.91
B14		3.0	0.327	4.78
C1	C-horizon	3.2	0.323	5.43
C2		3.4	0.333	5.33
C3		3.6	0.326	4.94
C4		3.8	0.325	5.2
C5		4.0	0.346	5.3
C6		4.2	0.358	4.92
C7		4.4	0.348	5.41
C8		4.6	0.348	4.87
C9		4.8	0.356	4.79
C10		5.0	0.351	4.78
C11		5.2	0.348	4.86
C12		5.4	0.344	4.81
Bedrock sample 1			0.163	9.80
Bedrock sample 2			0.139	9.96

APPENDIX 9 (Continued)

pH and Eh analyses for the mineralised pegmatite profile of Komu area

Sample No.	Horizon	Depth (m)	Eh(volts)	pH
A1	A-horizon	0.2	0.363	6.29
A2		0.4	0.349	6.56
A3		0.6	0.333	6.71
B1	B-horizon	0.8	0.334	6.29
B2		1.0	0.321	6.67
B3		1.2	0.336	6.38
B4		1.4	0.333	6.13
B5		1.6	0.309	6.45
B6		1.8	0.309	6.52
B7		2.0	0.297	6.78
B8		2.2	0.296	6.8
B9		2.4	0.292	6.81
C1	C-horizon	2.6	0.288	6.96
C2		2.8	0.282	7.08
C3		3.0	0.309	6.96
C4		3.2	0.291	6.94
C5		3.4	0.278	7.02
C6		3.6	0.260	7.58
C7		3.8	0.213	9.05
C8		4.0	0.321	6.85
C9		4.2	0.303	6.93
C10		4.4	0.285	7.05
C11		4.6	0.324	6.52
Bedrock sample 1			0.112	10.15
Bedrock sample 2			0.118	9.96

APPENDIX 9 (Continued)

pH and Eh analyses for the mineralised pegmatite profile of Ofiki area

Sample No.	Horizon	Depth (m)	Eh(volts)	pH
A1	A-horizon	0.2	0.269	6.68
A2		0.4	0.274	6.55
A3		0.6	0.242	6.87
A4		0.8	0.256	6.65
A5		1.0	0.312	6.05
B1	B-horizon	1.2	0.342	5.76
B2		1.4	0.328	5.78
B3		1.6	0.332	5.68
B4		1.8	0.346	5.58
B5		2.0	0.358	5.46
B6		2.2	0.356	5.36
B7		2.4	0.342	5.39
B8		2.6	0.357	5.25
B9		2.8	0.363	5.10
B10		3.0	0.366	5.00
B11		3.2	0.367	4.91
B12		3.4	0.345	5.17
B13		3.6	0.399	5.05
B14		3.8	0.406	4.92
B15		4.0	0.395	5.08
B16		4.2	0.404	4.95
B17		4.4	0.407	4.93
B18		4.6	0.405	4.85
C1	C-horizon	4.8	0.405	4.72
C2		5.0	0.403	4.74
C3		5.2	0.413	4.61
C4		5.4	0.416	4.63
C5		5.6	0.422	4.50
C6		5.8	0.416	4.52
C7		6.0	0.415	4.54
C8		6.2	0.415	4.56
C9		6.4	0.435	4.32
C10		6.6	0.418	4.52
Bedrock sample 1			0.130	9.76
Bedrock sample 2			0.124	10.31

APPENDIX 9 (Continued)

pH and Eh analyses for the mineralised pegmatite profile of Iwere area

Sample No.	Horizon	Depth (m)	Eh(volts)	pH
A1	A-horizon	0.2	0.290	6.58
A2		0.4	0.259	6.57
A3		0.6	0.245	6.59
A4		0.8	0.255	6.51
B1	B-horizon	1.0	0.256	6.35
B2		1.2	0.254	6.28
B3		1.4	0.253	6.22
B4		1.6	0.238	6.31
B5		1.8	0.234	6.42
B6		2.0	0.234	6.37
B7		2.2	0.230	6.40
B8		2.4	0.228	6.45
C1	C-horizon	2.6	0.224	6.53
C2		2.8	0.222	6.50
C3		3.0	0.227	6.42
C4		3.2	0.218	6.83
C5		3.4	0.220	6.76
C6		3.6	0.216	7.10
C7		3.8	0.219	7.13
C8		4.0	0.221	7.38
Bedrock sample 1			0.126	9.96
Bedrock sample 2			0.128	9.94